

Synthesis and Biological Evaluation of Natural and Synthetic Ganoderic Acids

Tatiana Jaramillo Forcada, MRes.

Thesis submitted to the University of Nottingham for the degree of Doctor of Philosophy

June 2017

Declaration

This Thesis describes the research conducted in the School of Chemistry and the School of Clinical Sciences, University of Nottingham between October 2010 and July 2014 under the supervision of Prof. Neil R. Thomas, Prof. Sue Watson and Dr. Anna Grabowska. I certify that the research described is original and that any parts of the work that have been conducted by collaboration are clearly indicated. I also certify that I have written all the text herein and have indicated by suitable citation any part of this dissertation that has already appeared in publication.

Signature

Date

Abstract

Ganoderma lucidum also known as lingzhi or mushroom of immortality in East Asia countries, has been known for over 2000 years. Ganoderic acids (GA), which are important secondary metabolites of this mushroom, are highly oxygenated lanostane-type entities with extraordinary pharmacological properties. GA are biosynthesised from lanosterol by a still unknown mechanism.

The synthesis of thirteen GA analogues and the biological evaluation of ten of them against prostate cell-lines is described in this thesis. Analogues with different functionalities at C-3, C-7, C-8, C-9, C-11, C-23, C-24, C-25 and C-26 of the lanostane frame have been synthesised. As functional groups, alcohols, acetates, ketones, carboxylic acids and single and conjugated double bonds have been introduced. For their preparation, aldehyde **89** was formed from commercial lanosterol in up to 47% overall yield over a 3 or 4 step sequence. Wittig olefination, Reformatsky reaction and direct oxidation of aldehyde **89** provided the precursors from which the analogues were achieved. Analogues were prepared after a total of six to eight steps in 7-44% overall yield.

GA and their analogues inhibited the cell viability of prostate cell-lines. However, they were less effective in the inhibition than Taxotere® (docetaxel). Besides, by comparing their IC_{50} values and thus, building a structure activity relationship (SAR) analysis, the most important positions for activity were determined. Interestingly, some of the ganoderic acids, GA-H (**24**), and analogues 3-ketone **108** and 7,11-diketone **146**, were less toxic for the normal prostate cells than for the pre-malignant ones, conferring on them prophylactic activity. It is believed that ketones at C-3, C-7 and C-11 could be responsible for this behaviour.

Ganoderma lucidum is rare in nature. However, due to its great demand, it is now being farmed. For their cultivation sawdust, logs or cork is used. New substrates, otherwise disposed as waste, are being investigated to produce high quality mushrooms, among them oil palm fibres such as mesocarp or empty fruit bunch fibres. Therefore, to unveil new cultivation methods, the triterpene composition of the mushroom grown at different stages, with different substrates or conditions has been assessed and their

biological activity evaluated against prostate cancer cell-lines. Cultivating the mushroom in mesocarp or empty fruit bunch fibres produced similar results to those of sawdust. However, poor ventilated conditions reduced their biological activity against prostate cancer cell-lines. Likewise, it was established that triterpene composition varied during different stages and for different target body parts, their biological activity also varied with age, increasing as the mushroom aged during the 2- to 8-week period studied.

Acknowledgements

First and foremost, I would like to thank my supervisors Prof Neil R. Thomas and Dr Anna Grabowska for their support and guidance through the PhD. They gave me an exciting and rewarding interdisciplinary project to conduct that combined the practice of organic chemistry, cell biology and data analysis. Thus, coming from a chemistry background, I had the opportunity to acquire new skills and discover what cell biology entails and in particular what cancer research involves.

This project has been possible thanks to the unconditional support of the technical and analytical services in chemistry and the friendship and advice of past and present lab-mates in both chemistry and biology labs. To mention some, Dr William Drewe, Dr Sarentha Chetty, Dr Indi Sehmi, Dr Ellie Grimes, Dr Austin Booth, Dr Franzesco Zamberlan, Dr James Krupa, Dr Terry May and Dr Alex Wichlacz from chemistry and Dr María Estévez Cebrero, Dr Luana Sasso, Dr Ahmed Musah-Eroje and Dr Niovi Nicolau from Biology. I would like to extend my gratitude to people from neighbouring labs; Dr Alex Disney, Dr Hao Shao, Dr David Foley, Dr Fabio Rui, Dr Shailesh Mistry and Dr Claudia Valente.

I would also like to thank my collaborators in Malaysia, Dr Surya Mudavasseril Sudheer and her supervisor Prof S. Manickam from the Manufacturing and Industrial Processes Research Division at the University of Nottingham, Malaysia campus and Md Cheng owner of Ganofarm Sendirian Berhad, Malaysia for their open and welcoming approach and for giving us a nice tour for some of the exotic and attractive locations in Malaysia.

Last but not least, I would like to thanks the MRC for financially support both during my project and for travel to Malaysia as well as the University of Nottingham for providing the physical space were to conduct my research. Finally, my family for their unconditional patience and support.

Content

Declaration i

Abstract ii

Acknowledgements iv

Content v

Abbreviations xi

1. Introduction 1

1.1. Medicinal mushrooms 1

1.2. *Ganoderma lucidum* 2

1.3. Ganoderic acids 2

1.4. Prostate cancer 11

1.5. Ganoderic acids for the treatment of cancer 13

1.6. Research objectives 16

2. Synthesis 18

2.1. GA analogue targets 18

2.2. Synthesis of acetoxy-aldehyde **89** 20

2.2.1. Acetylation 21

2.2.2. Direct oxidative cleavage 21

2.2.3. Stepwise oxidative cleavage 25

2.3. Towards the synthesis of methoxy-aldehyde **99** 34

2.3.1. Synthesis of methoxy lanosterol **96** 34

2.3.2. Synthesis of methoxydiol **98** 36

2.3.3. Synthesis of methoxy-aldehyde **99** 37

2.4. Synthesis of precursors derived from aldehyde **89** 37

2.4.1. Wittig olefination 37

2.4.2. Reformatsky reaction 42

2.4.3. Dehomologation 46

2.4.4. Direct oxidation 50

2.5. Synthesis of GA analogues 51

2.5.1. Modification at C-3 52
2.5.2. Modifications at B/C rings 60
2.5.3. Modifications on the side chain 84
2.6. Summary 89

3. Biological Evaluation 94

3.1. Introduction 94
3.2. Optimising the conditions for cell analysis 95
3.2.1. Optimising cell concentration 96
3.2.2. Identifiying a solvent concentration that is non-toxic 97
3.2.3. Variation in PC3 cell viability after drug treatment. Time-course study 100
3.3. Screening of natural and synthetic GA in prostate cells 108
3.3.1. Natural GAs 108
3.3.2. Synthetic GAs 116
3.3.3. Finding the best candidate: Summary 125
3.4. Summary and conclusions 130

4. SAR Analysis 133

4.1. Inhibition of the 5α-reductase and androgen receptor activity 133
4.1.1. Inhibition of the 5α-reductase activity 134
4.1.2. Inhibition of the androgen receptor activity 137
4.2. Inhibition of the cell viability in non-malignant and prostate cancer cell-lines 139
4.3. Summary 147

5. *Ganoderma lucidum* triterpene composition 150

5.1. Molecular weight distribution of triterpenoids 150
5.2. Mass spectral studies 153
5.2.1. ESI-MS profiles of GL extracts 153
5.2.2. Difference in triterpenoid composition over GL growing time 154
5.2.3. GL cultivated under different conditions 156
5.2.4. Solvent effect on the extract composition 157

5.2.5. Determination of the GL composition by LC-MS 159

5.3. Effects of GL extracts on prostate cancer cell viability 176

5.3.1. Effect of GL growing stages 177

5.3.2. Effect of the growing substrate and GL type 178

5.3.3. Effect of the extraction solvent 178

5.4. Summary and conclusions 181

6. Conclusions and Future Work 182

6.1. Conclusions 182

6.1.1. Synthesis 182

6.1.2. Biological evaluation 187

6.1.3. SAR Analysis 193

6.1.4. *Ganoderma lucidum* extracts composition 195

6.2. Future Work 197

7. Experimental 198

7.1. Chemical experiments 198

7.1.1. General methods 198

(a) Reagents, solvents and apparatus preparation 198

(b) Physical characterisation and spectroscopic techniques 198

(c) Chromatographic techniques 199

7.1.2. Synthesis 200

1) Precursors 200

2) Modifications at C-3 216

3) Modifications at rings B-C 220

4) Modifications at the side chain 229

7.2. Biological methods 234

7.2.1. Materials and methods 234

a. Natural and synthetic ganoderic acids (GA) 234

b. Tissue culture 234

i. Cell-lines 234

ii. Cell culture 239

7.2.2. Cell proliferation assay....244
7.2.3. Statistical analysis....244
7.3. *Ganoderma lucidum* extracts....244
7.3.1. Mushroom material....244
7.3.2. Mushroom extractions....245
7.3.3. Mass spectrometry....245
7.3.4. LCMS....246
7.3.5. Mushroom extract stock solution....246
7.3.6. Proliferation assay....246
7.3.7. Statistical analysis....247

8. References....248

Appendix 1....255

Cell concentration standard curves....256
I. Prostate cancer cell-lines....256
(a) PC3....256
(b) PC3M-luc2....258
(c) DU145....258
(d) LNCaP....260
II. Non-malignant cell-lines....262
(a) RWPE1....262
(b) WPE1-NB14....263
(c) WPE1-NB26....263

Appendix 2....265

Time-course study....265
i. Taxotere (**190**)....265
ii. Analogue **108**....266
iii. Analogue **146**....267
iv. Analogue **174**....268

Dose-response curves of natural GAs after 72 h treatment....268
i. GA-H (**24**)....269

ii. GA-T (**11**) 270

Dose-response curves of analogues after 72 h treatment 271

i. Group I 271

ii. Group II 276

iii. Group III 280

Appendix 3 284

Mass Spec data 284

GL 2 weeks 284

GL 4 weeeks 288

GL 6 weeks 293

GL 8 weeks 298

LC-MS data 306

LC-MS Profiles 306

Peak identification 311

Dose-response curves 346

GL 2 weeks 346

GL 4 weeks 348

GL 6 weeks 350

GL 8 weeks 353

Appendix 4 357

Mass fragmentation rules 357

Cleavage of ring A in GA 357

Cleavage of ring B in GA 359

Cleavage of ring C in GA 360

Cleavage of ring D in GA 365

Loss of the methyl group 365

Fragmentation of the side chain 366

Other fragmentation features 374

Appendix 5 375

Triterpenes isolated from GL ordered by molecular weight 375

Appendix 6..... 387

Compound numbering index 387

Abbreviations

Å	Angstroms
α,β-unsat.	α,β-unsaturated
AI	Androgen independent
antisym str	Antisymmetrical stretch
AP-1	Activator protein 1
APCI	Atmospheric Pressure Chemical Ionization
ATCC	American type culture collection
aq. sat. sol.	Aqueous saturated solution
aq. sol.	Aqueous solution
AR	Androgen receptor
AR-LBD	Androgen receptor ligand binding domain
bend	bending
bd	Broad doublet
BOC	*tert*-Butyloxycarbonyl
bs	Broad singlet
bt	Broad triplet
ca	*circa*
CDB	Conjugated double bond
cDNA	Complementary DNA
CK	Cytokeratin
ConA	Concanavalin A

conj	conjugated
COSY	Correlation spectroscopy
d	Doublet
DCC	*N*,*N'*-Dicyclohexylcarbodiimide
DCM	Dichloromethane
DC-STAMP	Dendritic cell - specific transmembrane protein
dd	Doublet of doublets
dddd	Doublet of doublet of doublet of doublets
ddt	Doublet of doublet of triplets
def	Deformations
DEPT	Distortionless Enhancement by Polarization Transfer
DHL	Dehydrolanosterol
DHL-Ac	Dehydrolanosterol acetate
DAD	Diazodicarboxylate
DEAD	Diethylazodicarboxylate
DIAD	Diisopropylazodicarboxylate
DIBAL-H	Diisobutylaluminium hydride
D-M	Dess-Martin
DMAP	Dimethylaminopyridine
DMF	Dimethylformamide
DMP	Dess-Martin periodinane
DMSO	Dimethyl sulfoxide
DNA	Deoxyribonucleic acid

dsDNA	Double stranded DNA
dNTPs	Deoxynucleotide triphosphates
dtd	Doublet of triplet of doublets
DTT	Dithiothreitol
EDC	1-Ethyl-3-(3-dimethylaminopropyl)-carbodiimide
EDTA	Ethylenediaminetetraacetic acid
EGF	Epidermal growth factor
EFB	Empty fruit bunches of oil palm
ESI	Electrospray ionisation
ESI-MS	Electrospray mass spectrometry
eq	Equivalent
FAK	Focal adhesion kinase
FBS	Fetal bovine serum
Fe(PFPP)Cl	*meso*-tetrakis(pentafluorophenyl)porphyrin iron (III) chloride
FT-IR	Fourier transform infrared spectroscopy
Freq.	Frequency
GC-EIMS	Gas chromatography-electron impact mass sprectrometry
GA	Ganoderic acid
GAL	Ganoderal
GenA	Ganoderenic acid
GENONOL	Ganodermenonol
GENON2OL	Ganodermenondiol
GIOL	Ganoderiol

GL	*Ganoderma lucidum*
GLA	Ganolucidic acid
GN2OL	Ganodermanondiol
GN3OL	Ganodermanontriol
GNO	Ganoderone
GNPA	Ganosporenic acid
GOL	Ganoderol
G3OL	Ganodermatriol
GR3OL	Ganoderitriol
h	Hour
HIV	Human Immunodeficiency Virus
HMBC	Heteronuclear Multiple-Bond Correlation spectroscopy
HMG-CoA	3-Hydroxy-3-methyl-glutaryl coenzyme A
hnRNP C	Heterogeneous nuclear ribonucleoprotein C
HOBt	Hydroxybenzotriazole
HRMS	High resolution mass spectra
HSQC	Heteronuclear single-quantum correlation spectroscopy
HPV	Human papillomavirus
J	^{1}H-NMR coupling constant
L2OL	Lucidadiol
LA	Lucidenic acid
LAL	Lucialdehyde
LAN	Lanosterol

LAN-Ac	Lanosterol acetate
LC-MS	Liquid chromatography-mass spectrometry
LDA	Lithium diisopropylamide
LOL	Lucidumol
LonA	4,4,14α-Trimethyl-5α-chol-7,9(11)-dien-3-oxo-24-oic acid
m	Multiplet
MCF	Mesocarp fibre of oil palm
MCC	Mitomycin C
m-CPBA	*meta*-Chloroperbenzoic acid
min	Minute(s)
miRNA	Micro RNA
MMP	Matrix MetalloProteinase
MN	Modal number
MNU	*N*-Methyl-*N*-nitrosourea
mp	Melting point
MS	Mass spectrometry
MTT	Methylthiazolyldiphenyl-tetrazolium bromide
NADPH	Nicotinamide adenine dinucleotide phosphate (reduced form)
NBS	*N*-Bromosuccinimide
NCS	*N*-Chlorosuccinimide
NFATc1	Nuclear factor of activated T cells C1
NF-κB	Nuclear factor-kappaB
NFW	Nuclease free water

NHPI	*N*-Hydroxyphthalimide
NMO	*N*-Methylmorpholine-*N*-oxide
NMR	Nuclear magnetic resonance
NT	Non treated
NOESY	Nuclear Overhouser effect spectroscopy
non-conj	Non-conjugated
Non-mal	Non-malignant
3-oxo-GA-ζ	23*S*-hydroxy-3,7,11,15-tetraoxolanost-8,24*E*-dien-26-oic acid
20OH-LA	20-Hydroxylucidenic acid
OSC	Oxidosqualene-lanosterol cyclase
PAP	Prostatic acid phosphatase
PBS	Phosphate buffer saline
PCa	Prostate cancer
PCC	Pyridinium chlorochromate
PE	Petroleum ether
PINO	Phthalimide *N*-oxyl
PMA	Phosphomolybdic acid
PNB	*para*-Nitrobenzoic acid
PSA	Prostate specific antigen
p-TSA	*para*-Toluene sulfonic acid
Pyr	Pyridine
q	Quartet
RDA	Reverse Diels-Alder

RNA	Ribonucleic acid
r.t.	Room temperature
s	Singlet
SAR	Structure activity relationship
sat	Saturated
sat. aq. sol.	Saturated aqueous solution
SE	Squalene monooxygenase
SF	Serum free
SQS	Squalene synthase
STAT3	Signal transducer and activator of transcription 3
str	Stretching
symm def	Symmetrical deformations
symm str	Symmetrical stretching
t	Triplet
T3P	Propylphosphoric anhydride
TBHP	*tert*-Butylhydroperoxide
TGF	Transforming growth factor
THF	Tetrahydrofuran
TIC	Total ion chromatogram
TLC	Thin layer chromatography
TNF	Tumour necrosis factor
ToF	Time of flight
tq	Triplet of quartets

UV(-vis)	Ultraviolet (visible) light
vs.	Versus

1. Introduction

1.1. Medicinal mushrooms

Fungi play a critical role in the environment. They are not only responsible for the decomposition of organic material, but they also interact symbiotically with other cells, plants and animals either in a positive or negative way. The fungi are classified in four major groups: ascomycetes, basidiomycetes, zygomycetes and chytrids.[1]

It has been estimated that the ratio of fungi to plants on Earth is 10.6 to 1, suggesting that the number of fungi is about 3.5 to 5.1 million. However, the number of known fungi species is considerably lower, currently estimated to be around 99,000 species. Fungi grow in almost all habitats, being more abundant in tropical regions.[2]

The adaptability of fungi to a variety of environments is due mainly to their extensive repertoire of metabolites and their cell wall structure. Many of these products have antimicrobial, antifungal, immunosuppressive or possess cytotoxic activity, which allow them to compete for nutrients, deter predators and communicate with other organisms in the environment.[3]

Humans have been exploiting this ability to their benefit to alleviate their illnesses since ancient times. The oldest book on Oriental medicine, "Shen Nong's Herbal" that explains the medicinal effects of several fungi and dates from 100-200 AD.[4]

The majority of macrofungi belong to the class *Basidiomycetes*, but there are also a few others from the class *Ascomycetes*. Mushrooms are classified in four categories depending on their fruiting body texture. Thus, when the fruiting body is fleshy and edible they are called edible mushrooms; if it has medicinal applications they are referred to as medicinal mushrooms; fruiting bodies that are proven or suspected to be poisonous are named poisonous mushrooms and mushrooms whose properties remain less well defined are categorised into miscellaneous mushrooms.[4,5] Their nutritional and therapeutic interest reside in their composition on polysaccharides, secondary metabolites and enzymes.[6]

A large market has emerged for mushroom nutriceuticals which are derived from either the mycelium or the fruiting body of the mushroom. Their regular intake is said to enhance the immune response of the human body, particularly, they are regarded as dietary supplements with therapeutic effects. These mushroom nutriceuticals are mainly consumed as capsules or tablets.[4,6]

1.2. *Ganoderma lucidum*

Ganoderma lucidum (GL) is one of the most well-known medicinal mushrooms. It has been known for over two millennia in East Asia. Documents describing its applications and uses have been found from the period of the first emperor of China Shih-huang of the Ch'in Dynasty (221-227 BC).[7]

This mushroom has different names in different countries. Thus, it is known as Lingzhi in China, Munnertak, Sachitake or Reishi in Japan, Youngzhi in Korea and Ganoderma in the US.[8]

Bioactive components found in GL preparations include triterpenes, polysaccharides, proteins, unsaturated fatty acids, vitamins and minerals that are thought to be beneficial for the treatment of a variety of ailments.[7-9]

GL is a wood decaying polypore fungus that is rare in nature. Currently, it is being cultivated on sawdust or logs for commercial purposes. However, the cultivation process requires several months and the final mushroom composition is variable. Therefore, a more reliable and rapid method for the production of the bioactive components has been developed, this uses submerged fermentation. Two to three weeks are enough to generate reasonable amounts of polysaccharides and ganoderic acids by this latter method.[7]

1.3. Ganoderic acids

Ganoderic acids (GA) are highly oxygenated C30 lanostane-type triterpenoids. They constitute important components of *G. lucidum* with extraordinary pharmacological properties such as inhibition of histamine release, inhibition of cholesterol synthesis, antihypertensive, antitumour and antihuman immunodeficiency virus (HIV) activities.[10]

All GA have the same common lanostane-type chemical skeleton, differing in the functional groups and side-chain types. According to these differences, GA can be classified into the three structural categories shown in Figure 1.1.

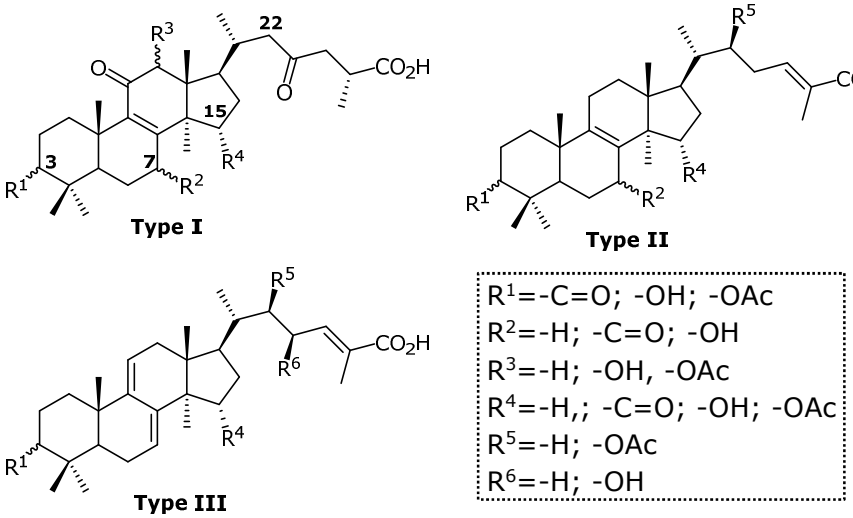
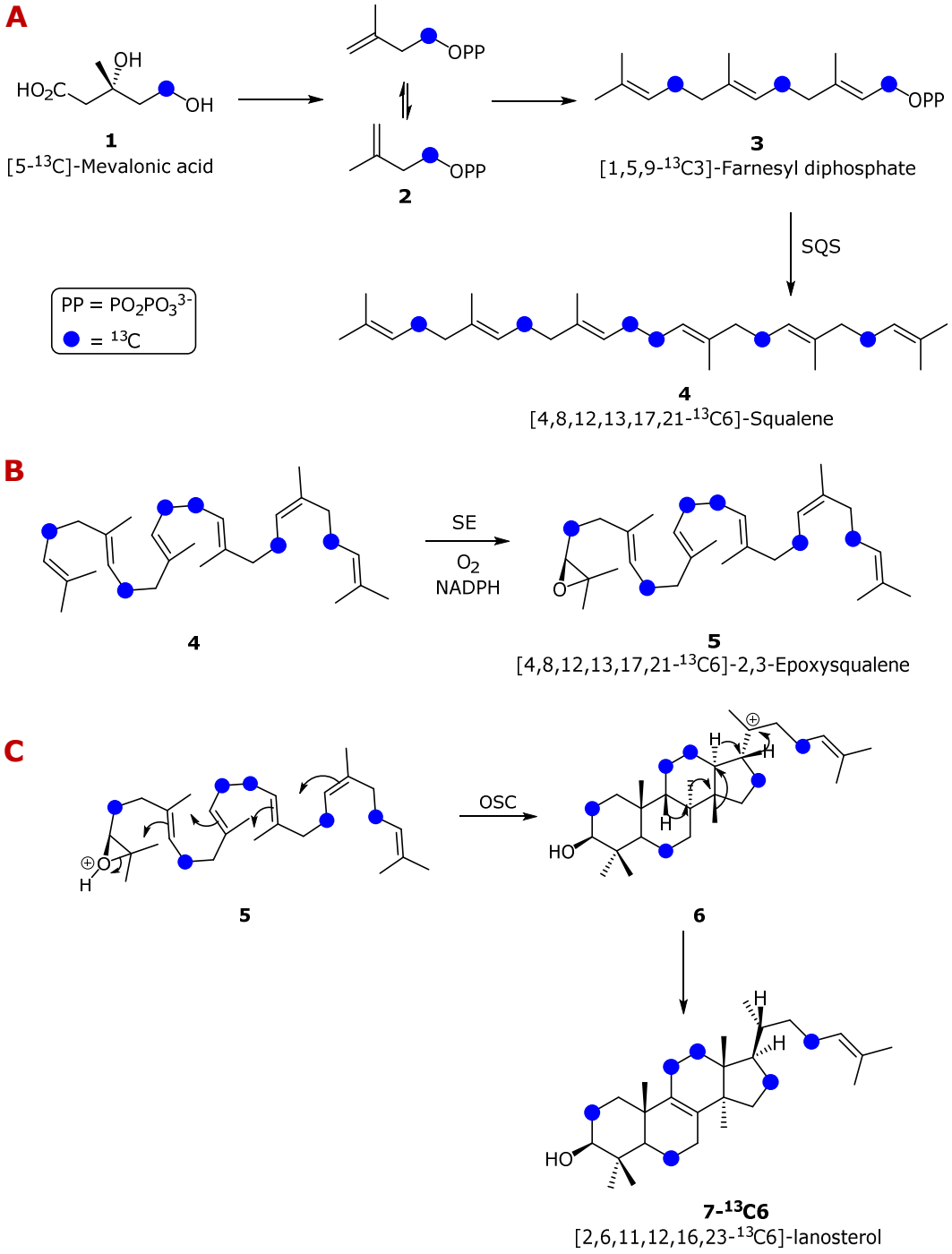


Figure 1.1 Chemical structure of the three different types of ganoderic acids.

Hydroxyl, carbonyl and acetyl groups are commonly observed in the above skeletons, all at positions C-3, C-7, C-15 and C-22. GA's with 3α-substituent are major components of the cultured mycelia of *G. lucidum*. In contrast, in fruiting bodies it is more frequent to encounter 3β-substituted or 3-keto compounds.

Although the biosynthetic pathway of GA is not yet fully understood, early experiments by Shiao with labelled [5-^{13}C]-mevalonate (**1**) suggested that GA are biosynthesised via the mevalonate-isoprenoid pathway (Scheme 1.1). This pathway involves the sequential conversion of farnesyl diphosphate (**3**) to squalene (**4**) catalysed by squalene synthase (SQS) (Scheme 1.1 **A**) and then to 2,3-epoxysqualene (**5**) catalysed by squalene monooxygenase (SE) (Scheme 1.1 **B**). Lanosterol (**7**) is formed by the cyclisation of 2,3-epoxysqualene (**5**) followed by the steroid backbone rearrangement **6** catalysed by lanosterol synthase (LS) (Scheme 1.1 **C**). However, the exact biosynthetic pathway leading to GA, which may include a series of oxidation, reduction and acylation reactions is still unknown (Scheme 1.2).[10-12]

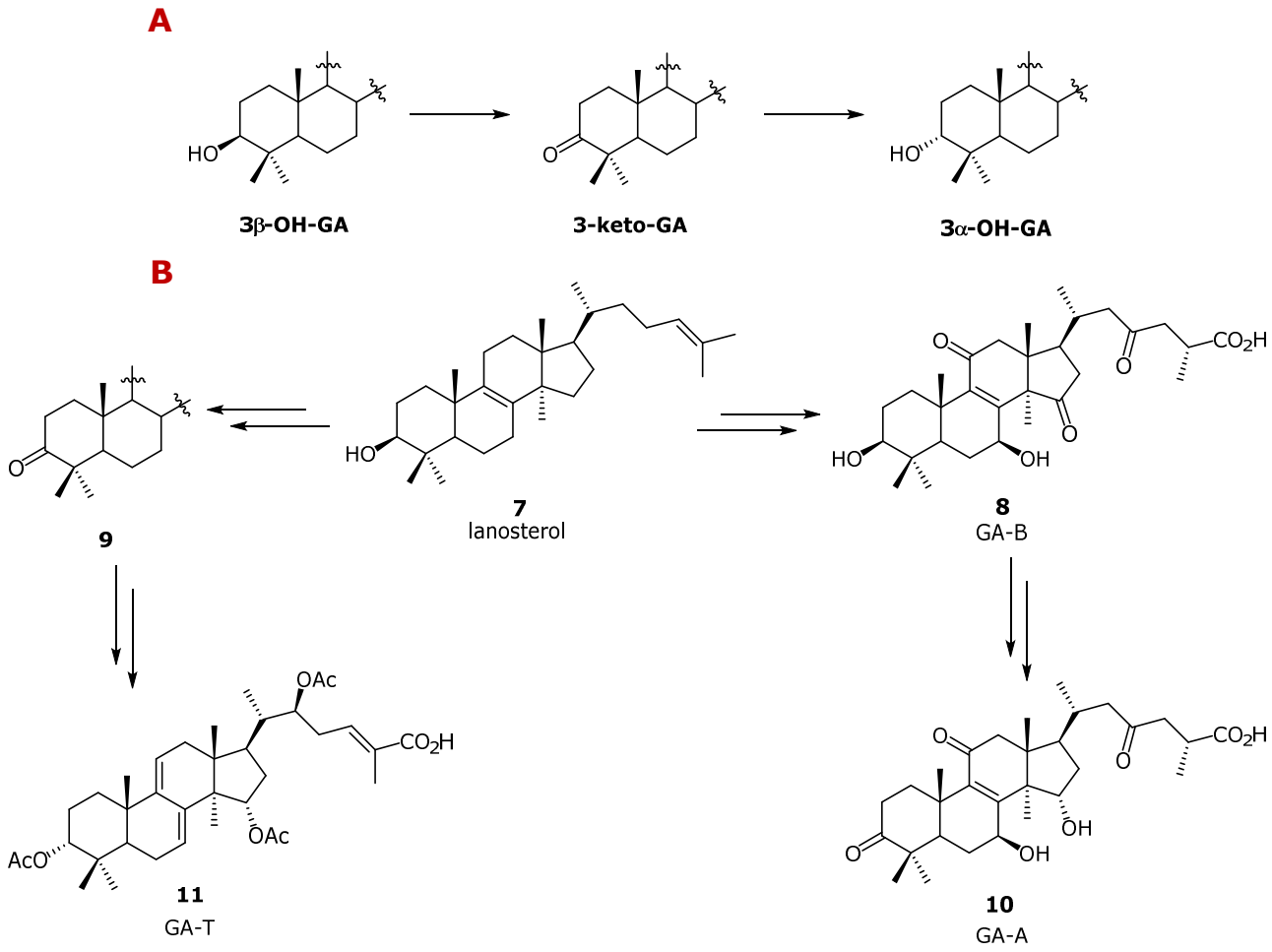


Scheme 1.1 Biosynthesis of lanosterol (**7**) in *Ganoderma lucidum* from [5-^{13}C]-mevalonic acid (**1**). **A** Formation of squalene (**4**) catalysed by squalene synthase (SQS). **B** Formation of 2,3-epoxysqualene (**5**) catalysed by squalene monooxygenase (SE). **C** Formation of lanosterol (**7**) catalysed by 2,3-oxidosqualene-lanosterol cyclase (OSC). Blue dots indicate the position of the ^{13}C carbons.

Triterpenes of *Ganoderma lucidum* regulate different processes within cells. Yue *et al*. found that ganoderma triterpenes induced the expression of fourteen proteins of HELA cells. These proteins have an important role in cell proliferation, cell cycle, oxidative stress and apoptosis.[13] Suppression of

proliferation, inhibition of transcription factors such as activator protein 1 (AP-1), nuclear factor-kappaB (NF-κB) or signal transducer and activation of transcription 3 (STAT-3) , induction of apoptosis, DNA damage and cell cycle arrest are some of the attributable effects of isolated and modified triterpenes.[14]

Furthermore, GA showed antimetastatic activity. They inhibit migration and adhesion by suppressing the focal adhesion kinase (FAK) SRCPaxillin pathway, down regulating genes responsible for cell invasiveness or down-regulation of matrix metalloproteinases (MMP) MMP-2 and MMP-9.[14]



Scheme 1.2 Proposed route for epimerisation at C-3 and pair C-3 - C-15.[12] **A** Interconversion of 3β-OH-GA to 3α-OH-GA through oxidation and reduction process. **B** Formation of GA from lanosterol.

Ganoderma lucidum extracts have also demonstrated anti-inflammatory activity by inhibition of NF-κB and AP-1 signalling pathways.[14]

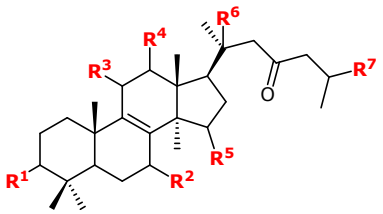
GL triterpenes, most of them GA, have found applications for metabolic diseases, allergies, infections, inflammations, aging or cancer. Table 1.1 correlates the triterpene with their use or application and from Figure 1.2 to Figure 1.8 the triterpene structure is indicated.

Our interest is in discovering GA's and analogues that may have prophylactic or therapeutic activity against prostate cancer.

Application	**Triterpene[10,15,16]**
HIV-1, 2 protease inhibition	GA-B (**8**), GA-C1 (**17**), GA-H (**24**), GA-α (**28**), GLA-A (**29**), GA-β (**34**), GIOL-B (**62**), GIOL-F (**63**), GIOL-A (**65**), GN2OL (**66**), GN3OL (**67**), LOL-B (**68**), 20OH-LA-N (**73**)
Anti-virus	LAL-B (**44**)
Antihypertensive	GA-B (**8**), GA-D (**19**), GA-F (**22**), GA-K (**26**), GA-S (**53**), GA-Y (**59**)
Antihepatotoxic	GA-B (**8**), GNPA-A (**31**), GA-R (**52**), GA-S (**53**)
Aldose reductase inhibition	GA-C2 (**18**), GA-D_f (**20**), 12β-OAc-GenA-H (**47**)
Anti-inflammatory	GA-A (**10**), GA-DM (**32**), GA-F (**22**), GA-T-Q (**57**)
Histamine release inhibition	GA-C (**16**), GA-D (**19**)
Cholesterol synthesis inhibition	GA-Me (**49**), GA-M_f (**50**), GA-Y (**59**)
Amphiphathic effect on platelet aggregation	GA-S (**53**)
Anti-complement	GA-Sz (**56**)
Anti-nociceptive	GA-A (**10**), GA-B (**8**), GA-G (**23**), GA-H (**24**)
Anti-oxidative	GA-A (**10**), GA-B (**8**), GA-C (**16**), GA-D (**19**)
Anti-aging	GA-B (**8**), GA-C2 (**18**), GA-G (**23**)
Neurotrophic activity	MeGA-A (**13**), MeGA-B (**15**), BuGA-H (**25**), GA-S_1 (**55**), GA-T-Q (**57**), GN2OL (**66**), GN3OL (**67**), LonA (**74**), MeGA-A acetonide (**75**)
Neuroprotective	GA-E (**21**)
Anti-obesity	^{t}BuLA-B (**71**)
Hypoglycemic activity	GA-Df (**20**), GOL-B (**64**)
Inhibition of HMG-CoA reductase and acyl CoA acyltransferase	BuGA-B (**14**), 15αOH-GA-S_z (**54**)

Application	Triterpene[10,15,16]
Enhancement of CoA	GA-LM$_2$ (**33**), GA-ε (**37**)
5α-Reductase inhibition	GA-DM (**32**), GA-TR (**58**)
Cell cycle arrest, apoptosis	GA-A (**10**), GA-DM (**32**), GA-Me (**49**), GA-M$_f$ (**50**), GA-S (**53**), GENON2OL (**61**)
Anti-metastatic, anti-invasion	GA-T (**11**)
Anti-tumour activity	GA-A (**10**), GA-AM$_1$ (**12**), GA-B (**8**), GA-D (**19**), GA-F (**22**), GA-K (**26**), GA-DM (**32**)
Cytotoxicity	GA-R (**52**), GA-T (**11**)
Tubulin inhibition	GA-DM (**32**)
Anti-cancer	GA-A (**10**), GA-E (**21**), 7-OEtGA-O (**27**), GLA-B (**30**), GA-γ (**35**), GA-δ (**36**), GA-ε (**37**), GA-ζ (**38**), GA-η (**39**), GA-θ (**40**), 3-Oxo-GA-ζ (**41**), GA-DH (**42**), L2OL (**43**), LAL-B (**44**), LAL-C (**45**), 12βOAc-GenA-H (**47**), GIOL-E (**48**), GA-M$_f$ (**50**), GA-Mk (**51**), GA-S (**53**), GA-Y (**59**), GENONOL (**60**), GENON2OL (**61**), GIOL-F (**63**), GN2OL (**66**), LA-A (**69**), EtLA-A (**70**), LA-N (**72**)

Table 1.1 Correlation of ganoderma triterpene with their use or application.

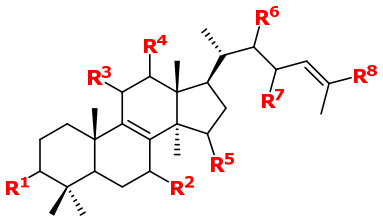


12-31

Nº	Name	R^1	R^2	R^3	R^4	R^5	R^6	R^7
12	GA-AM$_1$	β-OH	-C=O	-C=O	-H	-C=O	-H	*S*-CO$_2$H
13	MeGA-A	-C=O	β-OH	-C=O	-H	α-OH	-H	*R*-CO$_2$Me
14	BuGA-B	β-OH	β-OH	-C=O	-H	-C=O	-H	*R*-CO$_2$Bu
15	MeGA-B	β-OH	β-OH	-C=O	-H	-C=O	-H	*R*-CO$_2$Me
16	GA-C	β-OH	β-OH	-C=O	-H	α-OH	-H	*R*-CO$_2$H
17	GA-C1	-C=O	β-OH	-C=O	-H	-C=O	-H	*R*-CO$_2$H
18	GA-C2	β-OH	α-OH	-C=O	-H	α-OH	-H	*S*-CO$_2$H
19	GA-D	-C=O	β-OH	-C=O	-H	-C=O	-H	*S*-CO$_2$H
20	GA-Df	-C=O	β-OH	β-OH	-H	-C=O	-H	*R*-CO$_2$H
21	GA-E	-C=O	-C=O	-C=O	-H	-C=O	-H	*R*-CO$_2$H
22	GA-F	-C=O	-C=O	-C=O	β-OAc	-C=O	-H	*R*-CO$_2$H
23	GA-G	β-OH	β-OH	-C=O	-OH	-C=O	-H	*R*-CO$_2$H

Nº	Name	R^1	R^2	R^3	R^4	R^5	R^6	R^7
24	GA-H	β-OH	-C=O	-C=O	β-OAc	-C=O	-H	*R*-CO_2H
25	BuGA-H	β-OH	-C=O	-C=O	β-OAc	-C=O	-H	*R*-CO_2Bu
26	GA-K	β-OH	β-OH	-C=O	β-OAc	-C=O	-H	*S*-CO_2H
27	7-OEtGA-O	-C=O	β-OEt	-C=O	-H	-C=O	-OH	*R*-CO_2H
28	GA-α	β-OH	-C=O	-C=O	β-OAc	α-OH	-H	*R*-CO_2H
29	GLA-A	-C=O	-H	-C=O	-H	α-OH	-H	*R*-CO_2H
30	GLA-B	β-OH	-H	-C=O	-H	α-OH	-H	*R*-CO_2H
31	GNPA-A	-C=O	-C=O	-C=O	-C=O	-C=O	-H	*R*-CO_2H

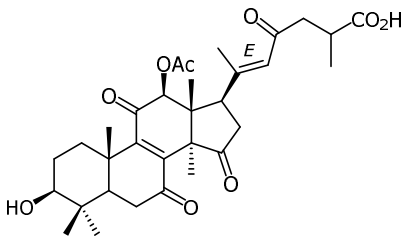
Figure 1.2 Chemical structure of type I GL lanostene triterpene, compounds **12**-**31**. Bu = butyl; Et = ethyl, Me = methyl; GLA = ganolucidic acid; GNPA = ganosporenic acid



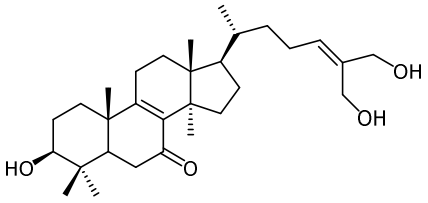
32-46

Nº	Name	R^1	R^2	R^3	R^4	R^5	R^6	R^7	R^8
32	GA-DM	-C=O	-C=O	-H	-H	-H	-H	-H	-CO_2H
33	GA-LM_2	-C=O	-OH	-C=O	-H	-C=O	-H	-OH	-CO_2H
34	GA-β	β-OH	β-OH	-C=O	-H	-C=O	-H	-H	-CO_2H
35	GA-γ	-C=O	β-OH	-C=O	-H	α-OH	-H	*S*-OH	-CO_2H
36	GA-δ	-C=O	α-OH	-C=O	-H	α-OH	-H	*S*-OH	-CO_2H
37	GA-ε	β-OH	β-OH	-C=O	-H	-C=O	-H	*S*-OH	-CO_2H
38	GA-ζ	β-OH	-C=O	-C=O	-H	-C=O	-H	*S*-OH	-CO_2H
39	GA-η	β-OH	β-OH	-C=O	β-OH	-C=O	-H	*S*-OH	-CO_2H
40	GA-θ	β-OH	-C=O	-C=O	β-OH	-C=O	-H	*S*-OH	-CO_2H
41	3-Oxo-GA-ζ	-C=O	-C=O	-C=O	-H	-C=O	-H	*S*-OH	-CO_2H
42	GA-DH	α-OAc	α-OH	-H	-H	-H	*S*-OAc	-H	-CO_2H
43	L2OL	β-OH	-C=O	-H	-H	-H	-H	-H	-CH_2OH
44	LAL-B	-C=O	-C=O	-H	-H	-H	-H	-H	-CHO
45	LAL-C	β-OH	-C=O	-H	-H	-H	-H	-H	-CHO
46	LAL-E	-C=O	β-OH	-C=O	-H	α-OH	-H	-H	-CHO

Figure 1.3 Chemical structure of type II GL lanostene triterpenes. Compounds **32**-**46**. 3-Oxo-GA-ζ = 23*S*-hydroxy-3,7,11,15-tetraoxolanost-8,24*E*-dien-26-oic acid; DOAc-GA = 3α,22β-diacetoxy-7α-hydroxyl-5α-lanost-8,24*E*-dien-26-oic acid; L2OL = lucidadiol; LAL = lucialdehyde.

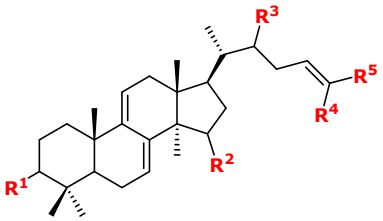


47
12βOAc-GenA-H



48
GIOL-E

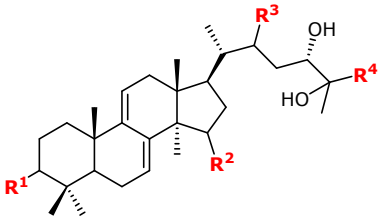
Figure 1.4 Chemical structure of 12β-OAc-GenA-H (**47**) and GIOL-E (**48**). 12βOAc-GenA-H = 12β-acetoxy-3β-hydroxy-7,11,15,23-tetraoxo-lanost-8,20*E*-diene-26-oic acid; GIOL = ganoderiol.



49-64

Nº	**Name**	**R^1**	**R^2**	**R^3**	**R^4**	**R^5**
49	GA-Me	α-OAc	α-OAc	-H	$-CH_3$	$-CO_2H$
50	GA-M_f	α-OAc	α-OH	-H	$-CH_3$	$-CO_2H$
51	GA-Mk	α-OAc	α-OH	-OAc	$-CH_3$	$-CO_2H$
52	GA-R	α-OAc	-H	*S*-OAc	$-CH_3$	$-CO_2H$
53	GA-S	α-OH	-H	*S*-OAc	$-CH_3$	$-CO_2H$
54	15αOH-GA-S_z	-C=O	α-OH	-H	$-CO_2H$	$-CH_3$
55	GA-S_1	-C=O	-H	-H	$-CH_3$	$-CO_2H$
56	GA-Sz	-C=O	-H	-H	$-CO_2H$	$-CH_3$
57	GA-T-Q	-C=O	α-OAc	-H	$-CH_3$	$-CO_2H$
58	GA-TR	-C=O	α-OH	-H	$-CH_3$	$-CO_2H$
59	GA-Y	β-OH	-H	-H	$-CH_3$	$-CO_2H$
60	GENONOL	-C=O	-H	-H	$-CH_3$	$-CH_2OH$
61	GENON2OL	-C=O	α-OH	-H	$-CH_3$	$-CH_2OH$
62	GIOL-B	-C=O	α-OH	-H	$-CH_2OH$	$-CH_2OH$
63	GIOL-F	-C=O	-H	-H	$-CH_2OH$	$-CH_2OH$
64	GOL-B	β-OH	-H	-H	$-CH_3$	$-CH_2OH$

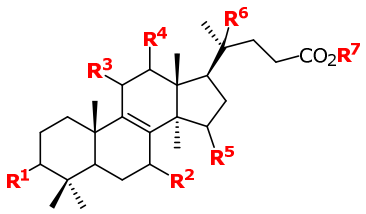
Figure 1.5 Chemical structure of type III GL lanostene triterpene. Compounds **49**-**64**. GENONOL = ganodermenonol; GENON2OL = 15α,26-dihydroxy-5α-lanosta-7,9,24*E*-triene-26-oic acid; GIOL = ganoderiol; GOL = ganoderol.



65-68

Nº	Name	R^1	R^2	R^3	R^4
65	GIOL-A	β-OH	-H	-H	$-CH_2OH$
66	GN2OL	-C=O	-H	-H	$-CH_3$
67	GN3OL	-C=O	-H	-H	$-CH_2OH$
68	LOL-B	β-OH	-H	-H	$-CH_3$

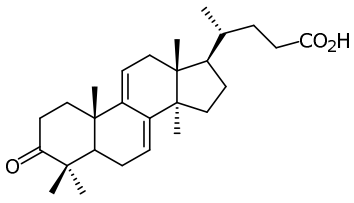
Figure 1.6 Chemical structure of type III GL lanostene triterpene. Compounds **65**-**68**. GIOL = ganoderiol; GN2OL = ganodermanondiol; GN3OL = ganodermanontriol; LOL = lucidumol.



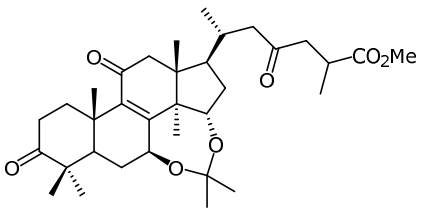
69-73

Nº	Name	R^1	R^2	R^3	R^4	R^5	R^6	R^7
69	LA-A	-C=O	β-OH	-C=O	-H	-C=O	-H	-H
70	EtLA-A	-C=O	β-OH	-C=O	-H	-C=O	-H	-Et
71	^{t}BuLA-B	-C=O	β-OH	-C=O	β-OH	-C=O	-H	-^{t}Bu
72	LA-N	β-OH	β-OH	-C=O	-H	-C=O	-H	-H
73	20OH-LA-N	β-OH	β-OH	-C=O	-H	-C=O	-OH	-H

Figure 1.7 Chemical structure of GL lanostene triterpenes. Compounds **69**-**73**. LA = lucidenic acid; Et = ethyl, ^{t}Bu = *tert*-butyl; 20OH-LA-N = 20-hydroxylucidenic acid N.



74
LonA



75
MeGA-A acetonide

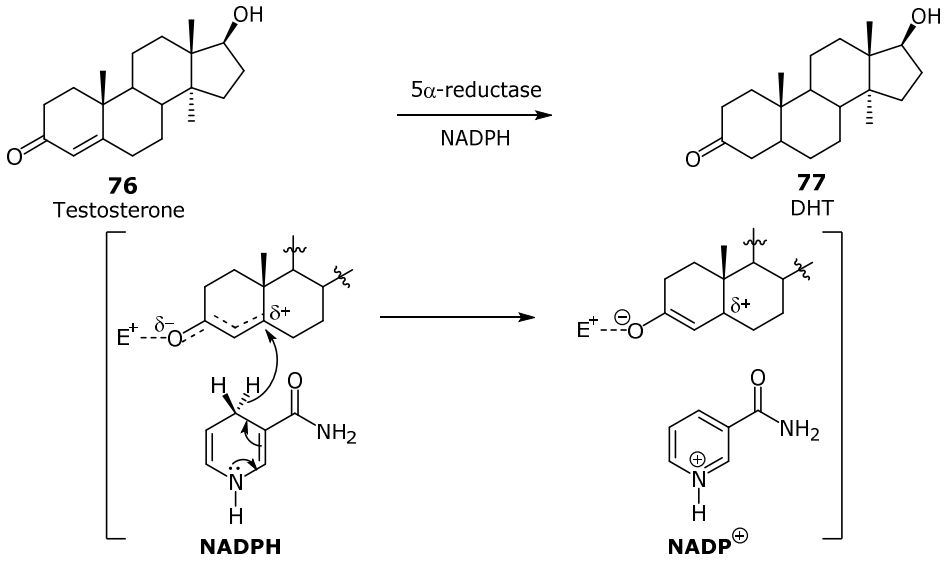
Figure 1.8 Chemical structure of LonA (**73**) and MeGA-A acetonide (**74**). LonA = 4,4,14α-trimethyl-5α-chol-7,9(11)-dien-3-oxo-24-oic acid; Me = methyl.

1.4. Prostate cancer

Prostate cancer (PCa) is the most common cancer in men in the UK.[17] Its incidence depends on several factors, such as, age, diet, family history and ethnic origin.[18] Thus, the elderly are more at risk of suffering from it; diets rich in fruits and vegetables and poor in dairy, alcohol, red meat and saturated fats are preferred for its prevention; having relatives that have had the disease also increases the risk of suffering from it; besides, it is well known that some ethnicities have higher incidence of PCa than others, in particular black men of Caribbean or African origin are at highest risk.[18] The incidence of PCa in Asian countries was reported to be lower a few decades ago. However, currently there is a significant increase due to changing diets and lifestyles. Traditionally, Asian diet has been based more on vegetables and less on both animal protein and high-fat foods. However, this tendency has been reversed in the last few decades due to economic development. This fact together with the genetic differences encountered in Asian populations are thought to have caused the recent increase observed in PCa incidence. It is noteworthy that PCa incidence rates going from 5% in South-Central Asia to 11% in East Asia in 2012 was still much lower than the reported rates for Western countries.[19] All these factors suggest that epigenetic alterations play an important role in prostate carcinogenesis as well as in its progression.[20] Epigenetic modifications include DNA methylation, microRNAs (miRNA) regulation, and histone modifications, such as histone acetylation, deacetylation, and methylation.

The microsomal enzyme steroid 5-α-reductase and the androgen receptor (AR) play a major role in androgen development. 5-α-Reductase catalyses the NADPH-dependent reduction of testosterone (**76**) to dihydrotestosterone (DHT, **77**) (Scheme 1.3).[21] Although both hormones bind to the AR, DHT (**77**) has four to five fold higher affinity for it, therefore effectively becoming its active ligand.[22] After binding, translocation to the nucleus occurs, which activates or represses the target gene expression at the transcriptional level.[23] One interesting component of AR activity is its impact on prostate-specific antigen (PSA) expression, an important marker for PCa. It is believed that there is a correlation between the levels of PSA expression and AR activity. Since its discovery, a PSA screening test has been applied for the early detection of PCa.[24]

Two forms of this enzyme have been identified, 5-α-reductase 1 and 2. 5-α-Reductase 1, which has low affinity for testosterone and basic pH optimum, predominates in tissues such as liver, kidney, brain, lung, skin and in human prostate it is expressed mainly in the epithelial cells, whereas the type 2 isozyme, which shows a high affinity for testosterone and has an acidic pH optimum, is more abundant in genital tissues such as the prostate and is localized mainly in the stromal compartment. Consequently, in advanced PCa, which is characterized by the abnormal proliferation of epithelial cells, type 1 might become the predominant isozyme responsible for androgen metabolism, whilst type 2 isozyme activity remains identical.[21]



Scheme 1.3 Proposed mechanism for the synthesis of dihydrotestosterone (**77**) (DHT) catalysed by 5α-reductase.[21]

It is believed that AR is involved in all stages of prostate tumorigenesis including initiation, progression and treatment resistance. AR is important for the maintenance and development of both normal prostate and PCa cells. Initially PCa is dependent on androgens. Therefore, the first-line therapy relies on androgen deprivation. However, after an average period of 24 months, PCa progresses to an androgen-independent (AI) state with advance metastasis, especially to bones, and high morbidity, that is, suffering from the illness, and mortality, namely, dying from it.[22,25]

The absence of E-cadherin leads to cell detachment and the facilitation of bone metastasis, additionally N-cadherin and cadherin-11 have also been found in prostate cancer cells (*e.g.*, PC3) and are implicated in cancer cell development and metastasis.[24]

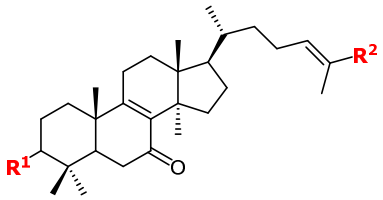
MMPs are also important in metastatic PCa development as they are able to degrade the extracellular matrix allowing for cancer cell invasion. MMP-2 and MMP-9 are of particular importance as they are important biomarkers in PCa. Cancer cell motility is also mediated through upregulation of Ras and Rho synthesis. Ras is a vital component in regulation of cellular proliferation and invasion, whereas Rho is Ras-dependent and is a key promoter of cell motility. Once the cell becomes motile, they are often cleared by the immune system. However, some cells are able to attach to distant sites such as bone through this migratory process.[24]

1.5. Ganoderic acids for the treatment of cancer

The effects of GAs on breast (GA-A (**10**), GA-F (**22**), GA-H (**24**))[26] and lung (GA-Me (**49**), GA-T (**11**))[27-29] cancer cell lines have been well determined. However, much less is known about their effect on prostate cancer. For PCa, studies with GA-DM (**32**)[30,31] has shown it to be effective on either early or advanced PCa cell lines.[24]

GA-DM (**32**) is a lanostane-type triterpene isolated from the *G. lucidum* mushroom that induces cytotoxicity in both androgen dependent and independent PCa cells. It has also been shown that GA-DM (**32**) treatment inhibits both the activity of 5-α-reductase and the conversion of testoterone (**76**) to DHT (**77**). The inhibition of DHT activity possibly occurs due to the conformational similarity in the four-ringed steroidal structures of DHT (**77**) and GA-DM (**32**). GA-DM (**32**) competitively blocks the AR, preventing DHT (**77**) binding and obstructing the normal DHT-mediated signalling pathway.[24] An even more promising effect of GA-DM (**32**) is its inhibition of osteoclastogenesis. Osteoclastogenesis is a significant factor in PCa metastasis and GA-DM (**32**) has shown to limit this process in a pre-osteoclastic cell-line (RAW cell-line). GA-DM (**32**) suppresses the expression of C-Fos and nuclear factor of activated T cells C1 (NFATc1), which leads to the inhibition of dendritic cell - specific transmembrane protein (DC-STAMP) expression and reduces osteoclast fussion.[32] Additionally, metastasis to bone, aided by the RANK ligand binding to the RANK receptor on osteoclast progenitor cells is also inhibited by GA-DM. However, its cytotoxicity to both cancerous and normal cells makes it inadequate as a chemotherapeutic. In order to overcome this issue, nanoparticle conjugated delivery is being investigated to target PCa cells.[24]

A study of the inhibition of osteoclast differentiation on RAW cell-lines with GA-DM (**32**), its methyl derivative MeGA-DM (**78**) and 7-oxo-methylganoderic acid Z (7-oxoMeGA-Z, **80**) (Figure 1.9) showed that in order for the compound to be more active, a carbonyl group in the C-3 position is required and a methyl ester group at C-26 is needed to increase the cell permeability. Thus, whilst GA-DM (**32**) and MeGA-DM (**78**) blocked osteoclast differentiation completely at low concentrations (50 μM and 12.5 μM, respectively), 7-oxoMeGA-Z (**80**) showed only a low inhibitory activity even at 100 μM. From this study, it was also deduced that inhibitory activity is more likely to be due to specific inhibition of differentiation than to cytotoxicity.[32]



32, 43, 78-80

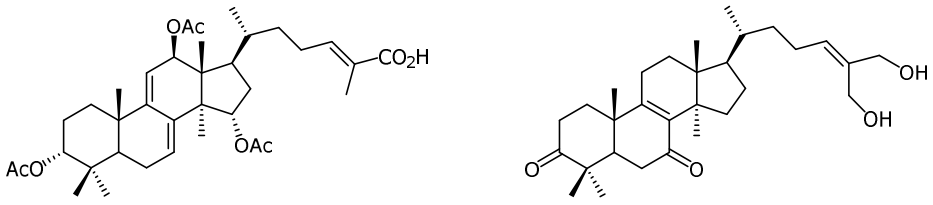
Triterpene		R^1	R^2
Number	**Name**		
32	GA-DM	-C=O	$-CO_2H$
43	L2OL	β-OH	$-CH_2OH$
78	MeGA-DM	-C=O	$-CO_2CH_3$
79	7-oxoGA-Z	β-OH	$-CO_2H$
80	7-oxoMeGA-Z	β-OH	$-CO_2CH_3$

Figure 1.9 Chemical structure of triterpenes used in SAR analysis of osteoclast differentiation and prostate cancer cell proliferation inhibition.

Interestingly, in a previous structure activity relationship (SAR) study of GA's and ganoderic alcohols isolated from *G. lucidum* concluded similar observations as for the one for osteoclast differentiation.[21] In this study, the functional groups required for the inhibition of 5-α-reductase was evaluated. Thus, whilst the following functionalities were essential: carbonyl at C-3 and $\Delta^{24,25}$ unsaturated carboxylic acid in C-26, substitution at C-7, C-11 and lipophilicity of 17β side chain contribute little to enzyme inhibition. A difference with the osteoclast study, the presence of a methyl ester at C-26 dramatically reduced the activity. The most active compounds were GA-TR (**58**), GA-DM (**32**) and GENON2OL (**61**), with GA-TR (**58**) being the most potent followed by GA-DM (**32**).

A SAR analysis with the triterpenes displayed in Figure 1.9 using the prostate cancer cell-line PC3 also revealed that the C-3 ketone and the $\Delta^{24,25}$ α, β-unsaturated carboxylic acid were important for activity. As for osteoclast differentiation, the presence of a methyl ester increased lipophilicity and thus enhanced cell permeability. MeGa-DM (**78**) acted as a pro-drug, although it was detected in the culture medium, after entering the cell, it was entirely metabolised to the active carboxylic acid GA-DM (**32**).[33]

A study of the cytotoxic and anti-angiogenic effects of lanostane triterpenoids from GL performed in three cell-lines, A549 (lung), MCF-7 (breast) and PC3 (prostate) using eighteen triterpenes, revealed five very active inhibitors for PC3. They were in decreasing order of activity: 12βOAc-GA-Me (**81**) > 3-oxo-GIOL-E (**82**) > L2OL (**43**) > LA-A (**69**) > GN2OL (**68**). In this study GA-DM (**32**) was analysed as well. However, contrary to previous results, it appeared as less active than L2OL (**43**). Triterpenes **81** and **82** were newly characterised and their structure is represented in Figure 1.10.[34]

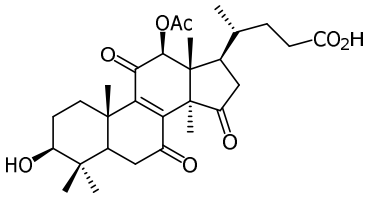


81 12βOAc-GA-Me

82 3-Oxo-GIOL-E

Figure 1.10 Chemical structure of GL triterpenes 12βOAc-GA-Me (**81**) and 3-oxo-GIOL-E (**82**). 12βOAc-GA-Me = 3α,12β,15α-triacetoxy-5α-lanosta-7,9(11),24-tiren-26-oic acid; 3-oxo-GIOL-E = 5α-lanosta-8,24-diene-26,27-dihydroxy-3,7-dione.

Our group was interested in extending the knowledge of the anti-cancer properties of GA for the treatment of PCa. With that aim in mind, GA-B (**8**), -F (**22**), -H (**24**), -K (**26**), -Me (**49**), -T (**11**) and lucidenic acid E2 (LA-E2, **83**) (Figure 1.2, Figure 1.5 and Figure 1.11) were evaluated against WPE1-NB26, DU145 and PC3M prostate cell-lines. Cytotoxicity studies performed with CellTiter-Blue® cell viability assay uncovered that GA-T (**11**) was the most active inhibitor GA.[35]



83
LA-E2

Figure 1.11 Chemical structure of lucidenic acid E2 (**83**) (LA-E2).

GA analogues were synthesised in our group and their biologically activity evaluated against prostate cell lines.[36] From this study it was concluded that having a $\Delta^{24,25}$ α, β-unsaturated carboxylic acid at C-26, and a carbonyl or β-OH at C-3 were important for activity, whereas shortening of the side chain, esterification of the carboxylic acid, increasing the polarity of the side chain with hydroxyl groups or acetylation of the β-OH in C-3 resulted in reduction of activity. On the other hand, the position of the double bond in rings B-C were apparently not affecting the activity. It is worth noting that ketones at C-7 and C-11 reduced the activity.[36] These results were in agreement with some of the observations derived from previous SAR analysis of GA for prostate cancer.[21,32,33]

The GA cell targets are still unknown, nonetheless, studies from our group pointed out to five possible candidates: vimentin, β-tubulin, cytoskeleton 19, heterogeneous nuclear ribonucleoprotein C and enolase α.[35] However, much work is needed in order to achieve a better understanding of the action of GAs in prostate cancer.

1.6. Research objectives

In this thesis, the synthesis of several new GA analogues is described and their inhibitory cell proliferation potential has been evaluated against prostate cancer cell lines with the aim to conduct a SAR analysis and thus, determine which functionalities of the GA are essential for activity.

Figure 1.12 shows a general GA with the three main areas of the molecule to be studied. These three areas comprise ring A, denoted as area **1** and encircled in blue on the drawing; area **2** comprising rings B and C, boxed in red and area **3** that includes the side chain, highlighted in green. The effect on the biological activity of β-hydroxyl, ketone or β-acetate at position C-3 in ring A, changes in the oxidation level and double bond position in rings

B/C and finally, shortening of the side chain length or variations in its oxidation level appear as interesting functionalities to study.

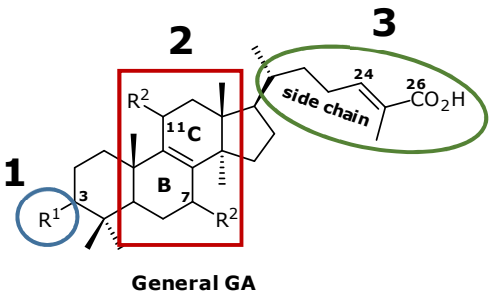


Figure 1.12 General GA with three regions highlighted: **1** (blue), **2** (red) and **3** (green). Functional group modifications in these areas have been performed to evaluate their importance for the biological activity.

The biologically activity of these GA analogues against prostate cancer cell lines has been determined by a variety of proliferation assays, in particular, the MTT assay.

The activity and triterpene composition of GL extracts at different stages of its growth have been studied to determine the optimum harvesting time as well as identify cheaper and more environmentally growing substrates.

2. Synthesis

2.1. GA analogues targets

In this section, the synthesis of ganoderic acid analogues is discussed. The syntheses have been organised according to the area of the molecule being modified. Modifications of the general structure in three key areas have been identified as the most interesting to evaluate. These are C-3 (region 1), the rings B/C (region 2) and the side chain (region 3) (Figure 2.1).

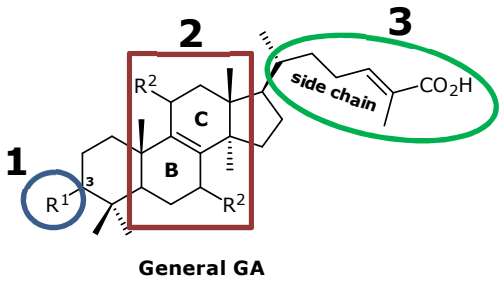
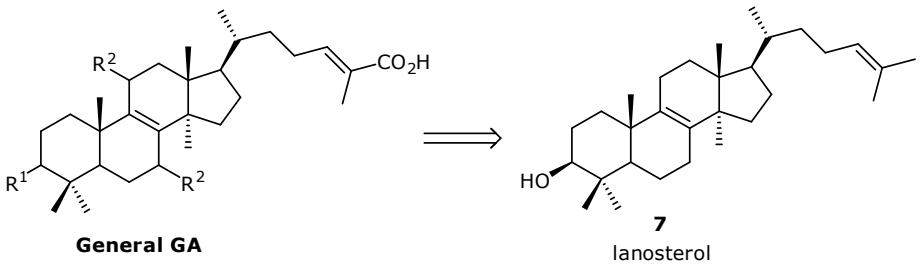


Figure 2.1 Areas of interest for synthetic modification in a generic GA.

In nature, GAs are biosynthesised from lanosterol via the mevalonate pathway. Therefore, commercial lanosterol is a natural starting point for their synthesis (Scheme 2.1). However, commercial lanosterol is sold as a mixture of sterols obtained from the non-saponifiable portion of wool fat from sheep.



Scheme 2.1 Retrosynthesis for GA analogues.

In this mixture, lanosterol (**7**, 5*α*-lanosta-8,24-dien-3*β*-ol) is the major component being 50-60% of the mixture. Other components are dihydrolanosterol (**84**, 5*α*-lanosta-8-en-3*β*-ol) (20-30%) and both agnosterol (**85**, 5*α*-lanosta-7, 9 (11), 24-trien-3*β*-ol) and dihydroagnosterol (**86**, 5*α*-lanosta-7,9 (11)-dien-3*β*-ol) in *ca.* 10% (Figure 2.2).

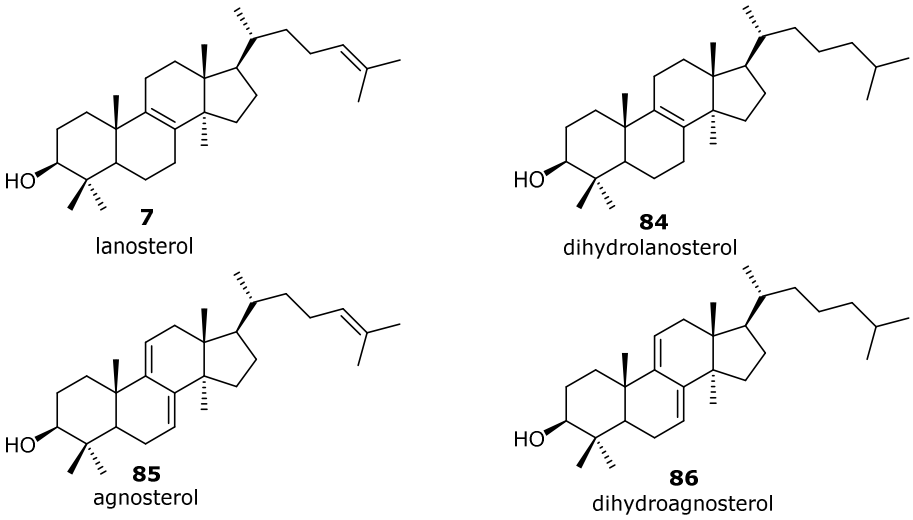
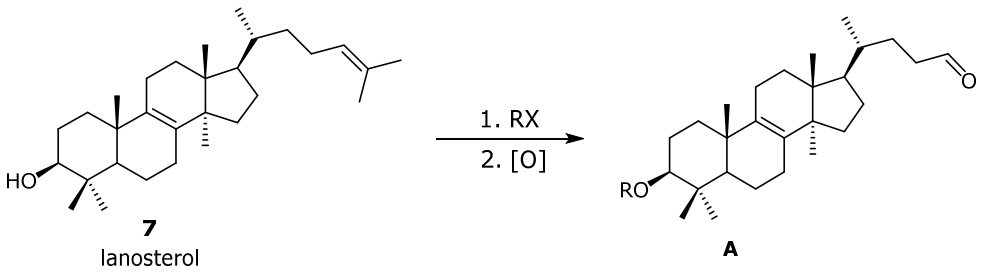


Figure 2.2 Components of commercial lanosterol. Lanosterol (**7**) 50-60%; dihydrolanosterol (**84**) 20-30% and both agnosterols (**85**, **86**) at ca. 10%.

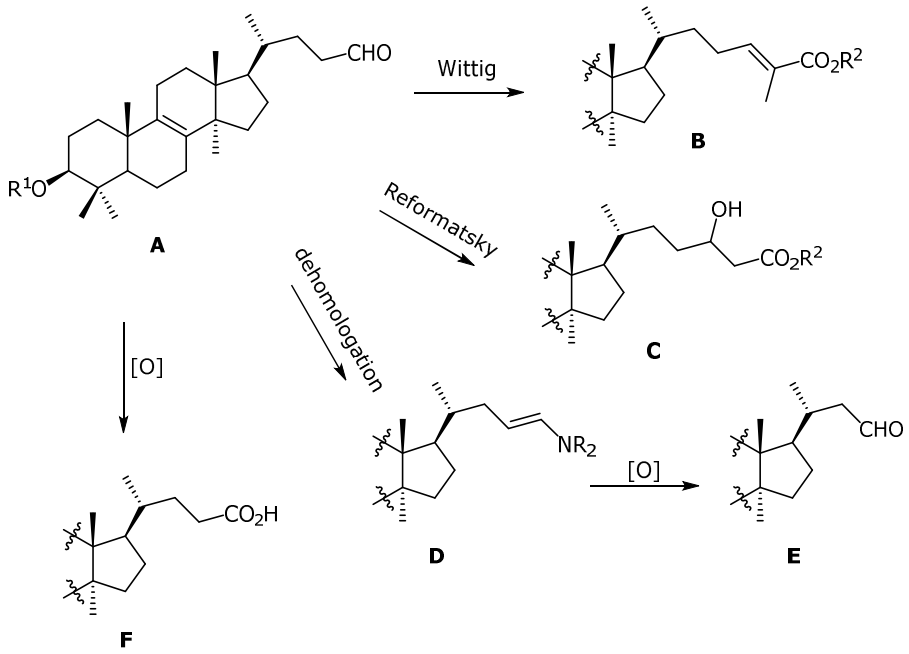
The physical and chemical properties of these four molecules are very similar; as a consequence, their purification by means of physical separation techniques is difficult and tedious.[37] However, separation after chemical modifications seems feasible. Thus, taking advantage of the different reactivity of their side chains, Kavtaradze (2004) and more recently O'Keefee (2015) described methods to separate lanosterol (**7**) from the lanosterol mixture in a non-toxic and efficient manner.[37-39] Hence, lanosterol could easily be isolated after increasing the polarity of its side chain by selective epoxidation or dihydroxylation of the $\Delta^{24,25}$ double bond.

In our pursuit of synthesising GA analogues we were interested in the oxidative cleavage of lanosterol to yield aldehyde **A** after protection at C-3. In this way, we would be able to tackle two problems at once (Scheme 2.2). On the one hand separation of the unwanted impurities, and on the other the synthesis of the most relevant and versatile precursor from which all the analogues are being formed.



Scheme 2.2 Formation of aldehyde **A** from lanosterol (**7**). [O]=oxidation.

Aldehydes are highly electrophilic entities that react quite readily with a variety of nucleophiles. Our intention was to exploit this property in our favour. Thus, attack of aldehyde **A** with carbon nucleophiles such as Wittig or Reformatsky reagents would produce adducts **B** or **C**, respectively, that after additional transformations, could yield the desire GA analogues with different functionalities. In the same way, reactions with secondary amines could allow us to furnish a dehomologated aldehyde **E** after oxidative cleavage of the enamine **D**. Finally, direct oxidation of aldehyde **A** could afford lucidenic acid **F**, lucidenic acids are triterpenoids with a two carbon shorter side chain, the carbonyl group being present at C-24 (Scheme 2.3).

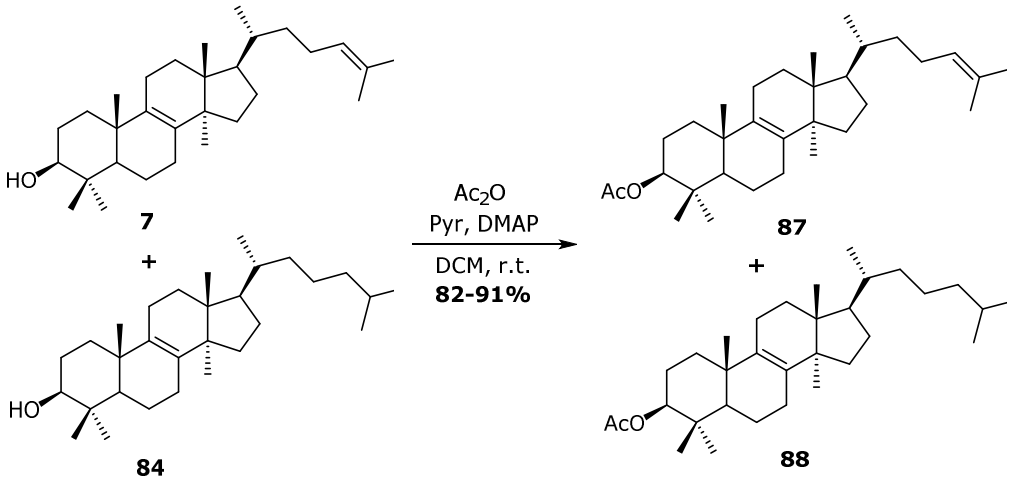


Scheme 2.3 Reactions of aldehyde **A** with different nucleophiles and oxidants.

2.2. Synthesis of acetoxy-aldehyde 89

For the synthesis of our main precursor, two different approaches were followed. In a first attempt, we explored a direct cleavage of the $\Delta^{24,25}$ double bond. However, it turned out to be more efficient to proceed in a stepwise fashion, namely, dihydroxylation followed by oxidative cleavage. In any case, our first step was the protection of the hydroxyl at C-3. Acetate was chosen as protecting group mainly for its easy incorporation and removal.

2.2.1. Acetylation



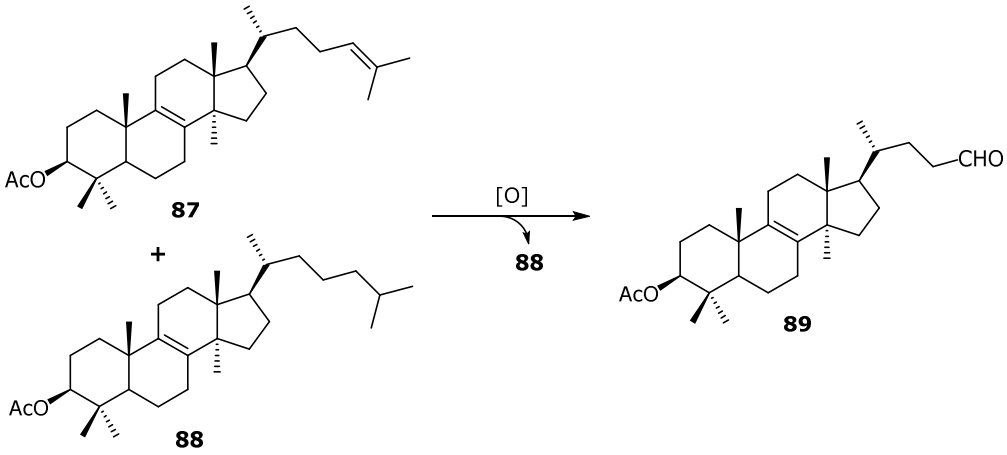
Scheme 2.4 Acetylation of lanosterol mixture. This reaction was performed in excellent yield (82-91%) from acetic anhydride, pyridine and dimethylaminopyridine (DMAP) dissolved in dichloromethane.

The commercial mixture of lanosterols was successfully acetylated using acetic anhydride in the presence of pyridine and dimethylaminopyridine (DMAP) as a catalyst. The reagents were dissolved in dichloromethane and stirred at room temperature for 3 h. Closer control of the end point revealed that the reaction reached completion between 1 h and 2.5 h. Acetylated lanosterols were formed in high yield varying from 82% to 91% (Scheme 2.4). This reaction was carried out on a multi-gram scale (10-40 g) during the course of my PhD.

In the ^{1}H-NMR spectrum, distinctive for the sterol acetates was the appearance of a double doublet peak that integrated for one proton at 4.50 ppm corresponding to the hydrogen at C-3 and a singlet at 2.05 that integrated 3 H, associated with the methyl in the acetate group. The appearance of a peak at 1735 cm^{-1} in the IR confirmed the presence of a carbonyl group in the molecules.

2.2.2. Direct oxidative cleavage

In order to access to our desired aldehyde **89** directly from the mixture of lanosterol acetates, three methods were investigated for the oxidative cleavage: 1. Ozonolysis, 2. Oxidation with sodium periodate with catalysis of ruthenium trichloride and 3. Oxidation with potassium permanganate. Unfortunately, all of them failed to produce reasonable amounts of the desired aldehyde **89** (Scheme 2.5).



Oxidant	Conditions	Yield (%)	Issues
O_3[40, 41]	1. Pyr, DCM, -78 °C 2. Ph_3P, r.t.	0	complex mixture
	1. Pyr, DCM, -78 °C 2. DMS, r.t.	30	
$RuCl_3$-$NaIO_4$[42]	1,2-DCE, r.t.	17	complex mixture
	DCM, r.t.	0	
	$CHCl_3$, r.t.		
	MeCN/water, r.t.		
$KMnO_4/CuSO_4$[43]	DCM/water, r.t.	0	α-ketol

Scheme 2.5 Direct oxidation of the acetylated lanosterol mixture **87** and **88** to produce aldehyde **89**. Oxidants, reaction conditions and isolated yield indicated in table.

Ozonolysis under reductive workup with either triphenylphosphine or dimethylsulfide produced a complex mixture of compounds from which aldehyde **89** was isolated only from the dimethylsulfide reaction in 30% yield.

In view of the poor results that ozone provided, an alternative method was considered. Yang and Zhang developed three protocols for the oxidative cleavage of olefins with catalysis of ruthenium trichloride (3.5 mol%).[42] In the first, Oxone® buffered with bicarbonate in acetonitrile worked well for benzylic olefins but poorly for aliphatic ones. A second protocol was developed for aliphatic olefins that used sodium periodate as the final oxidant, and a heterogeneous solvent system: 1,2-dichloroethane : water 1:1, this system was ideal for di- and tri-substituted aliphatic alkenes, nonetheless it failed for mono-substituted ones. A third method was then developed for these. In this latter protocol, sodium periodate in a

homogenous solvent system consisting of acetonitrile : water 6:1 proved to be satisfactory for the oxidative cleavage of mono-substituted alkenes.

In particular the olefin that we required cleaved is tri-substituted and aliphatic. Therefore, oxidative cleavage with sodium periodate catalysed by ruthenium chloride in a homogeneous or heterogeneous solvent system were evaluated, since, as Yang and Zhang highlighted, Oxone® is able to oxidise aliphatic aldehydes to the corresponding carboxylic acids in neutral conditions.[42,44] The mixture of lanosterol acetates was treated with sodium periodate and ruthenium trichloride as a catalyst. Different heterogeneous solvent systems were investigated, all in the same 1:1 ratio: dichloromethane : water; chloroform : water or 1,2-dichloroethane : water. Cleavage to aldehyde **3** was observed exclusively in the 1,2-dichloroethane system that after purification yielded 17% of **89**. Analysis by mass spectrometry revealed that the other two systems produced an entity with MW 507, which corresponded to the M+Na adduct of $C_{32}H_{52}O_3$ (**90**) (Figure 2.3)., that could be assigned to an epoxide, In all the cases, the reaction did not go to completion; lanosterol acetate (**87**) was also observed in the mixture. When the reaction was carried out in a homogeneous solvent system, acetonitrile : dichloromethane : water 1:1:1, instead of cleavage products, epoxide **90**, diol **91** and α-hydroxy ketone **92** were observed (Figure 2.3). Dichloromethane was added to solubilise the reagents, since they were insoluble in acetonitrile. As pointed out by Yang and Zhang excess of water could be responsible for this behaviour.

A third approach was explored, oxidative cleavage with potassium permanganate adsorbed on copper (II) sulfate. Contrary to the observations of Gareiss and co-workers who reported quantitative yields for their oxidative cleavage of norbornene using those reagents,[43] the mixture of lanosterol acetates was not cleaved in a neutral heterogeneous system. Instead epoxide **90** and α-hydroxy ketone **92** were observed in the mass spectrum.

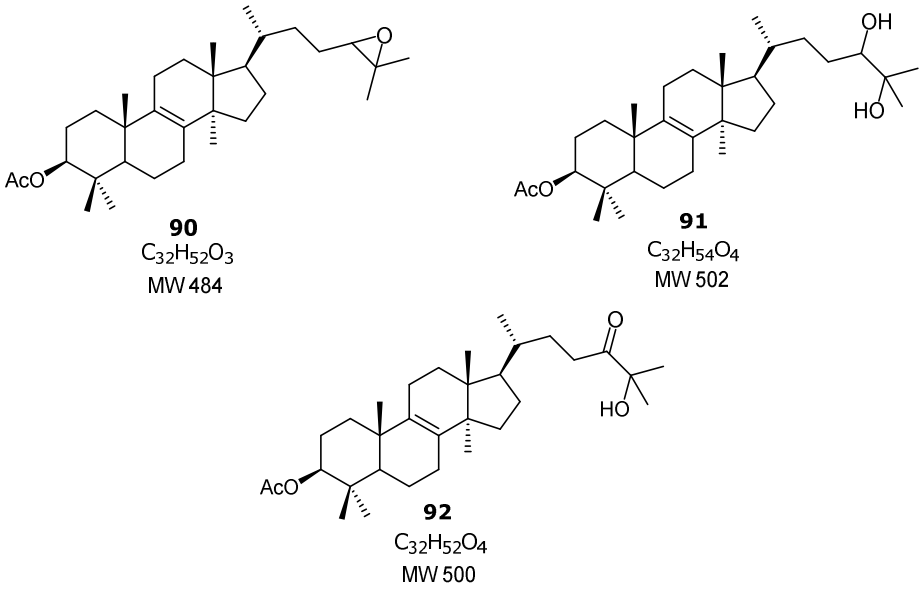
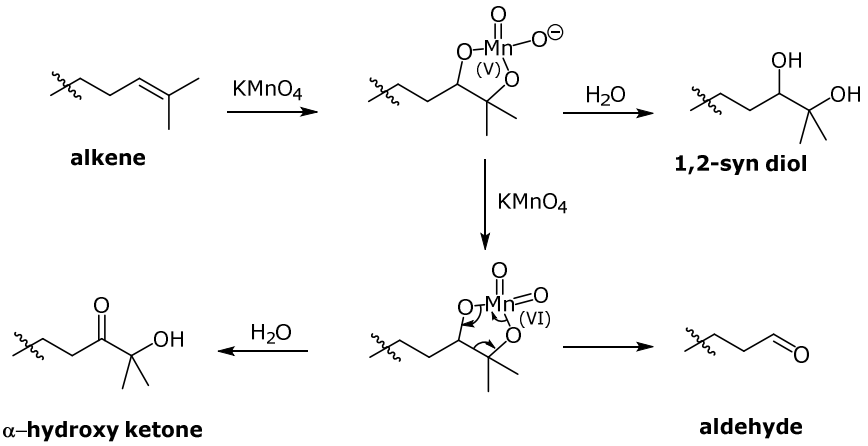


Figure 2.3 Molecular weight and formula for epoxide **90**, diol **91** and α-hydroxy ketone **92**.

Chandrasekaran investigated the oxidation by potassium permanganate by supported copper (II) sulfate.[45] They observed the formation of α-hydroxy ketone, α-diketone, epoxidation and oxidative cleavage of the olefin, depending on the type of alkene reacted. Previous mechanistic studies of alkene oxidation with permanganate suggested that to maximise oxidative cleavage, hydrolysis needed to be minimised (Scheme 2.6).[46,47]



Scheme 2.6 Possible products of the oxidation of an alkene with potassium permanganate.

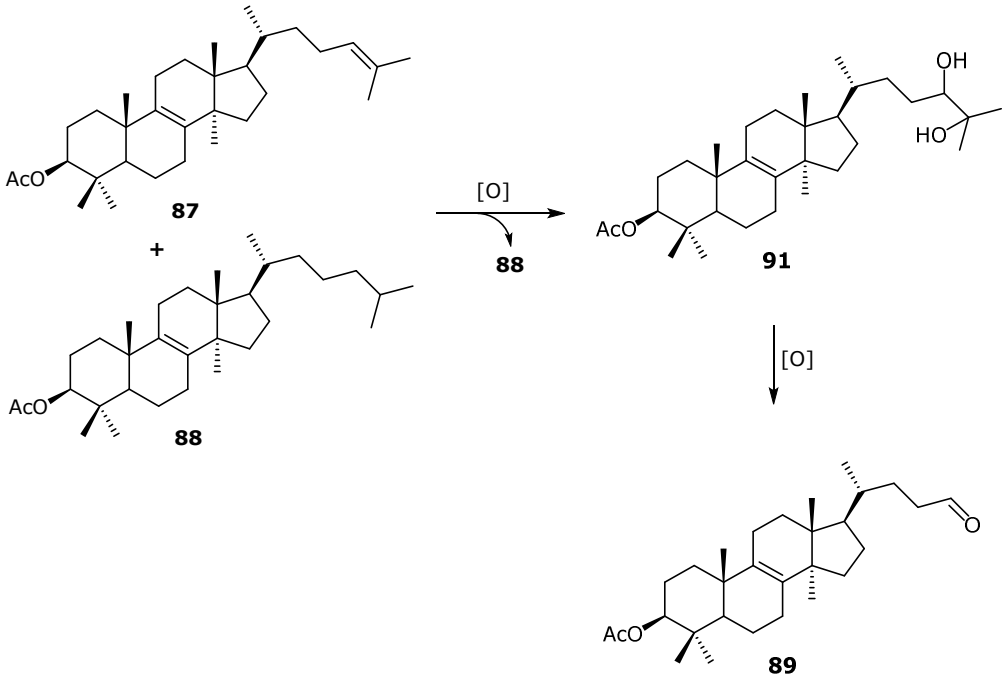
As the direct cleavage seemed inefficient to produce the desired aldehyde, a stepwise approach was investigated.

2.2.3. Stepwise oxidative cleavage

The stepwise approach consisted of a double oxidation, the introduction of 1,2-diol group in the $\Delta^{24,25}$ alkene in lanosterol acetate, followed by oxidative cleavage to furnish the aldehyde **89** (Scheme 2.7).

(a) 1,2-Diol formation

Two methods were envisaged for the 1,2-diol formation: substitution and oxidation with transition metals.



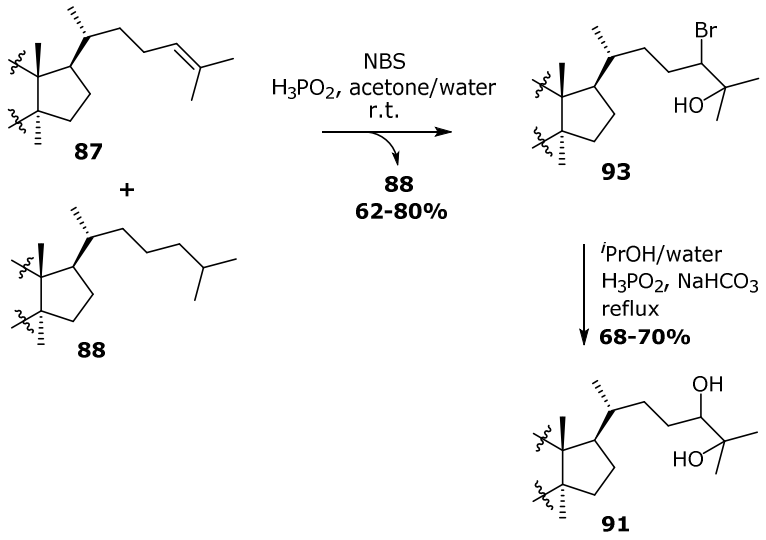
Scheme 2.7 The synthetic strategy for the stepwise oxidative cleavage of lanosterol acetate.

i. By substitution

Kavtaradze, in his attempt to isolate lanosterol from the commercial mixture, devised efficient procedures, both easily scalable and environmentally friendly.[37,38] These methods consisted of the conversion of the $\Delta^{24,25}$ double bond in lanosterol acetate to either the epoxide or hydroxyhalogenated derivative, which after nucleophilic attack were transformed into the 1,2-diol. This route was carried out successfully both stepwise and as a one pot reaction (Scheme 2.8).

Since Kavtaradze reported poor regioselectivity for the epoxidation with 3-chloroperbenzoic acid, only the hydroxybromination was studied. The

reaction was fast, less than 5 minutes were required to reach completion. The reaction was easily followed by naked eye, since the initial yellow solution faded progressively to clear. As a brominating agent, *N*-bromosuccinimide (NBS) was used, the reaction required mildly acidic conditions that were provided by concentrated hypophosphorous acid (50 wt% aq. solution) and the reaction was carried out in acetone : water 49:1 with stirring at room temperature. This reaction was performed from mg up to 17 g scales, with yields varying from 62% to 80%. After purification dihydrolanosterol acetate **88** was recovered from the mixture. The 24-epimeric mixture was purified by two-fold crystallisation with hot hexane. Epimer **93*R*** stayed in solution with 75% purity, giving a ratio of *R*:*S* 3:1 after the first crystallisation, whilst epimer **93*S*** precipitated pure after the second crystallisation. Both epimers were easily identified by ^{1}H-NMR spectroscopy, the signal of 24-H was a doublet of doublets for both, **93*R*** at δ 4.01 ppm (dd, *J* = 9.5, 4.0 Hz, 1H) and **93*S*** at δ 3.96 ppm (dd, *J* = 11.1, 1.9 Hz, 1H).



Scheme 2.8 The Kavtaradze approach route to 1,2-diol **91**. In this approach, the mixture of lanosterol acetate **87** and **88** were reacted with *N*-bromosuccinimide (NBS) with catalysis of hypophosphorous acid at room temperature to form intermediate bromohydroxy lanosterol **93**, which generated the diol **91** after treatment with hypophosphorous acid and a weak base like sodium hydrogen carbonate.

Although Kavtaradze reported X-ray crystallography data for the brominated compounds, no NMR data was provided.[37,38] Therefore, this is the first time that the bromo-hydroxy compounds **93*R*** and **-*S*** has been fully characterised by both ^{1}H- and ^{13}C-NMR.

Hydroxylation was accomplished in isopropanol at reflux. Isopropanol was chosen to afford miscibility with water without nucleophilic competition, which could lead to undesired ethers formation. Three different conditions were investigated (Table 2.1), in the first, the epimeric mixture of **93** was treated with hypophosphorous acid under wet conditions, unfortunately only a low yield (20%) of the 1,2-diol **91** was achieved. The yield was doubled when the reaction was carried out in two successive steps, formation of the epoxide in dry isopropanol with potassium acetate at reflux for two hours, followed by nucleophilic epoxide opening performed in wet isopropanol in the presence of hypophosphorous acid. Much easier and effective was the reaction of the hydroxybromo 24-H epimers **93** in wet isopropanol with phosphorous acid and its sodium salt, formed *in situ* by the addition of sodium hydrogencarbonate, in this latter case, up to 70% yield was obtained. The maximum overall yield achievable over the two steps was 56%.

Reaction type	**Conditions**	**Product**	**Yield (%)**
Hydroxybromination	NBS, H_3PO_2, acetone/water, r.t.	**93**	62-80
Dihydroxylation	(a) ^{i}PrOH, H_2O, H_3PO_2, reflux	**91**	20
	(b) 1.^{i}PrOH, KOAc, reflux 2. ^{i}PrOH-H_2O, H_3PO_2, reflux	**91**	41-42
	(c) ^{i}PrOH, H_2O, H_3PO_2, $NaHCO_3$, reflux	**91**	68-70
One pot	1. NBS, H_3PO_2, acetone/water 2. $NaHCO_3$ 3. ^{i}PrOH, H_2O, H_3PO_2, $NaHCO_3$, reflux	**91**	12-61

Table 2.1 Conditions employed for the formation of 1,2-diol **91**, stepwise and in one pot, according Kavtaradze protocols.[37,38]

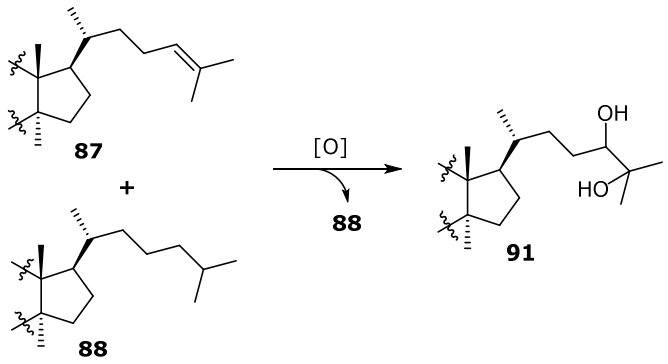
A one pot approach was also considered, hydroxybromination was achieved as per described above. However, after treatment with sodium hydrogen carbonate and evaporation under reduced pressure of the acetone, the crude product was directly redissolved in wet isopropanol with addition of hypophosphorous acid and its sodium salt generated *in situ* with sodium hydrogencarbonate. After purification desired 1,2-diol **91** (12-61%) was

isolated in good yield over the two consecutive steps. The reaction was reproducibly carried out on a multi-gram scale, from 7 g up to 19 g. Separation of the 24-epimers in diol **91** was tedious. Crystallisation was performed with hexane:EtOAc 2:1 dissolving the mixture in hot and allowing to cool down at room temperature, an enriched mixture in epimer *S* precipitated. The best separation was reached after 3-fold crystallisation for epimer **91*S*** (ratio *R*:*S* 1:3.5) and after 12-fold crystallisation for epimer **91*R*** (ratio *R*:*S* 3.3:1), both epimers were achieved with 70% purity. Epimers *R* and *S* were easily detected by ^{1}H-NMR, a triplet at δ 3.34 ppm (t, *J* = 6.1 Hz) for the *R* epimer and a doublet of doublets at δ 3.28 ppm for the *S* epimer (dd, *J* = 9.0, 1.6 Hz).

Despite ^{1}H-NMR peaks being reported previously for **91**, the spectrum was recorded at 100 MHz and no distinction was made for each of the epimers.[48]

ii. By oxidation with transition metals

Formation of the 1,2-diol **91** was also explored by oxidation of the $\Delta^{24,25}$ olefin moiety with the transition metals osmium and ruthenium (Scheme 2.9).



Oxidant	Conditions	Yield (91)%
OsO_4	NMO, 2,6-lutidine, acetone-water, r.t.	Non-isolated[a]
RuO_4	1. $NaIO_4$, $RuCl_3$, H_2O, H_2SO_4, 0 °C 2. EtOAc/MeCN, 0 °C	28

Scheme 2.9 Dihydroxylation of $\Delta^{24,25}$ alkene in lanosterol acetate **87** with transition metals. [a] The crude product from the osmium tetraoxide reaction was used directly in the oxidative cleavage without previous purification.

a. Osmium tetraoxide

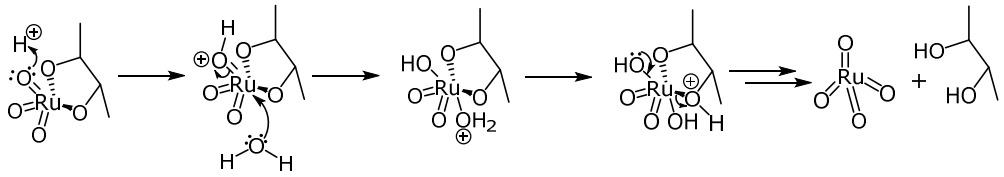
Nicolaou *et al.* in 2010 described a one pot methodology for the oxidative cleavage of olefins by a sequential two step route. In this sequence, the alkene is dihydroxylated with *N*-methylmorpholine-*N*-oxide (NMO), 2, 6-lutidine and catalytic amounts of osmium tetraoxide in wet acetone at room temperature. It is well known that NMO could oxidize some transition metals and therefore it is a preferred stoichiometric oxidant for the transition metal-catalysed oxidations. Oxidative cleavage was successfully accomplished with hypervalent iodine. In particular, Nicolaou claimed that (diacetoxyiodo)benzene proved to be very efficient for the oxidative cleavage of 1,2-diols with the advantage of solubility in organic solvents and the minimization of unwanted by-product formation, such as α-hydroxy keto compounds.[49]

Dihydroxylation under the conditions above described, smoothly produced the 1,2-diol **91**. The reaction was carried out between 100 mg and 9 g of substrate. For the reaction to proceed to completion a reaction time of 30 minutes was required. The reaction end-point was monitored by TLC (SiO_2 ethyl acetate : petroleum ether 2:3) and mass spectrometry. In the MS two peaks were noticed, the appearance of a peak at m/z 525 corresponding to the sodium adduct of MW 502 assigned to the diol **91** (Figure 2.3), as well as the disappearance of lanosterol acetate peak at m/z 491 for the sodium adduct of MW 468. The quantity of osmium tetraoxide added in the reaction seemed essential for a quick transformation. Optimum results were afforded with 2.4 mol%. Reducing this proportion resulted in a dramatic increase in reaction time. Diol **91** was not isolated, but taken directly to the next step without performing any work-up or further purifications.

b. Ruthenium tetraoxide

Plietker and Niggemann studied the conversion of olefins to their corresponding 1,2-diols using catalysis of ruthenium tetraoxide, which was formed *in situ* from catalytic amounts of ruthenium trichloride oxidized with sodium periodate.[50] The optimised conditions for the formation of the *syn* diol involved solution of the reagents in ethyl acetate : acetonitrile : water 3:3:1 at 0 °C with acid catalysis. In contrast to osmium tetraoxide, acid instead of base was required for acceleration of the reaction. A mechanism for the acid catalysed hydrolysis reaction was proposed by Plietker (Scheme

2.10).[50] In this mechanism, activation of the ruthenate ester by protonation at one of the carbonyl oxygens favours nucleophilic attack of a water molecule followed by formation of a dioxo intermediate and proton transfer, which eventually leads to the liberation of the *syn* diol and recovery of the ruthenium tetraoxide. The duration of the reaction was determined to be between two to five minutes, the *syn* diol was obtained in excellent yield varying from 65% to 94%.



Scheme 2.10 Proposed mechanism for the acid accelerated hydrolysis of ruthenate esters to the corresponding 1,2-diol.[50]

The dihydroxylation reaction of the lanosterol acetate mixture **87**-**88** was performed under Plietker conditions. Ruthenium tetraoxide was formed by dissolving sodium periodate in water and diluted sulfuric acid (1M, 13 mol%) followed by cooling and addition of ruthenium trichloride, bright yellow colour developed. Ethyl acetate and acetonitrile were added followed by the lanosterol mixture after five min; the resulting orange-brown slurry was stirred for fifteen minutes. Analysis by mass spectrometry revealed completion at this point. Apparently both the diol **91** and aldehyde **89** were formed. Further mass analysis after work-up showed only m/z 525 associated to the M+Na adduct of diol **91** but none of the aldehyde. However, after chromatography diol **91** was isolated in a disappointing 28% yield. The major product corresponded to a less polar compound with m/z 485, which could correlate to M+1 of the epoxide **90**. Worryingly, none of the dihydrolanosterol acetate **88** was isolated after purification, suggesting that the reaction was not selective for the $\Delta^{24,25}$ alkene.

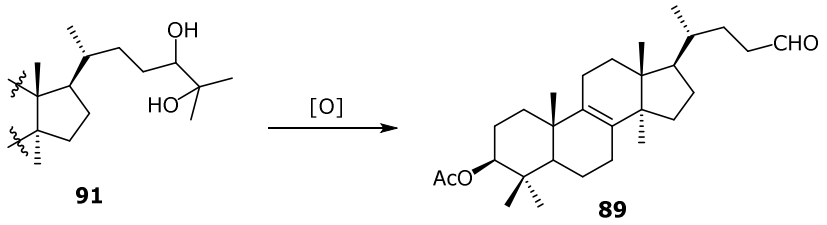
(b) Oxidative cleavage

Two iodine oxidizing agents were investigated: periodic acid and the hypervalent iodine (diacetoxyiodo)benzene.

i. Periodic acid

Oxidative cleavage of diol **91** was effortlessly accomplished following a procedure described by Mori (Scheme 2.11).[51] In this method periodic acid

was dissolved in tetrahydrofuran at 0-5 °C, a solution of alkene in tetrahydrofuran was then added dropwise to the periodic acid solution. Precipitation of iodic acid was indicative of reaction progression, which reached completion after 1 h. Pursuing this method, excellent yields were achieved (77-88%). This reaction was performed from 90 mg to 6 g scale.



91 **89**

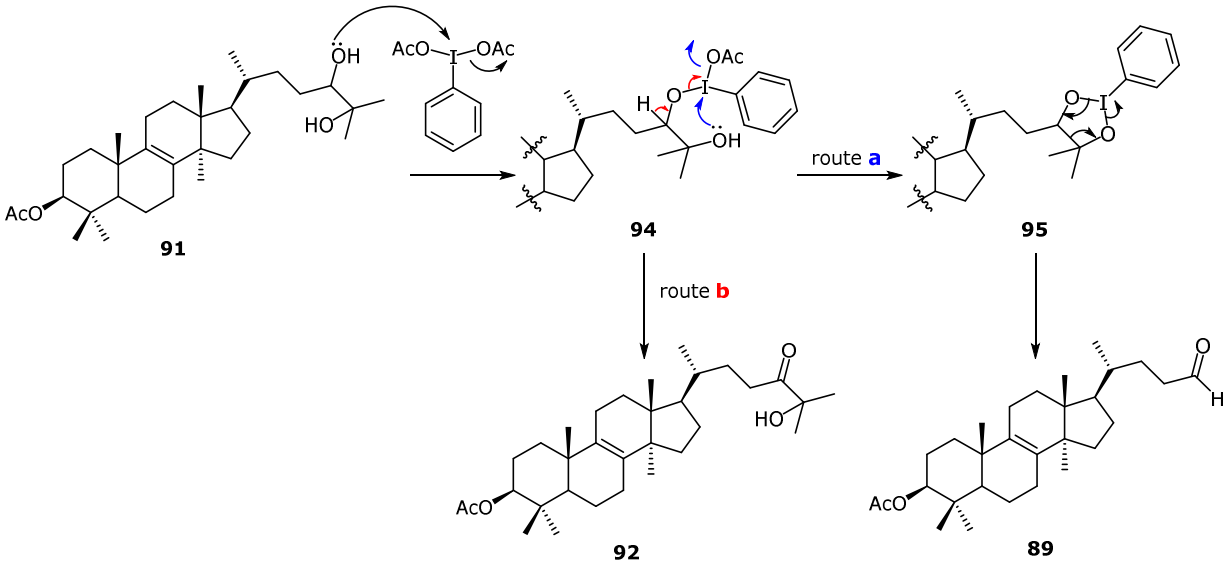
Oxidant	Conditions	% Yield (89)
$HIO_4 \cdot 2H_2O$	THF, 0-5 °C	77-88
$PhI(OAc)_2$	Acetone-water, r.t.	36-59[a]

Scheme 2.11 Oxidative cleavage of 1,2-diol **91** to aldehyde **89**. **a**. This is the overall yield of aldehyde **89** after the two-step reaction from lanosterol acetate (**87**).

ii. (Diacetoxyiodo)benzene

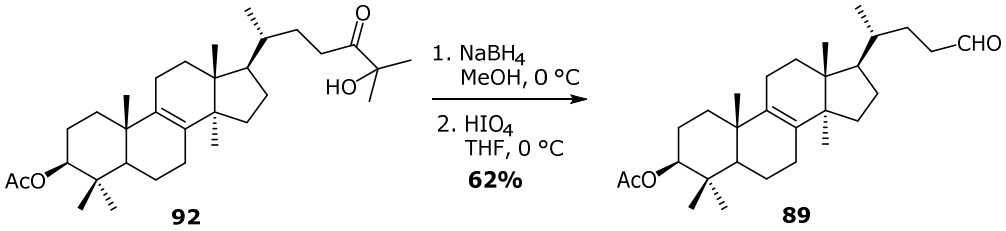
Oxidative cleavage with (diacetoxyiodo)benzene was performed after hydroxylation with osmium tetraoxide. Consumption of diol **91** marked the end of the reaction, which was stablished to be 1 h. The reaction was performed at 100 mg and 9 g scale. The reaction was cleaner at mg scale with a modest isolated yield (59%) over two steps. Nevertheless, scaling up resulted in increased formation of by-products along with a decrease in yield. Aldehyde **91** was isolated in 36% yield, whilst unwanted α-hydroxy ketone **92** (Figure 2.3) was the major product of the reaction being recovered in 58% yield; dihydrolanosterol acetate **88** was isolated after chromatography purification as well.

Formation of both aldehyde **89** and α-hydroxy ketone **92** could be rationalised by the mechanism of the oxidation of alcohols with hypervalent iodine.[52] In this mechanism two scenarios are possible, route a, which is market in blue, and route b that is highlighted in red. in Scheme 2.12. In route a, a pentacyclic iodoether **95** is formed that after disproportion produces aldehyde **89**. However, if the disproportion takes place earlier, at the acyclic iodoether **94**, then the α-hydroxy ketone **92** is formed.



Scheme 2.12 Mechanism for the formation of aldehyde **89** (route a) and α-hydroxy ketone **92** (route b) with (diacetoxyiodo)benzene.[52]

Fortunately, reduction of α-hydroxy ketone **92** with sodium borohydride in methanol at 0 ºC, a procedure described by Takayanagi,[53] followed by oxidative cleavage with periodic acid afforded aldehyde **89** in 62% yield over the two steps (Scheme 2.13), which represented a 21% yield from the mixture **87**-**88**, therefore a total 57% of aldehyde **89** was achieved from the oxidation with osmium tetraoxide when performed at large scale.

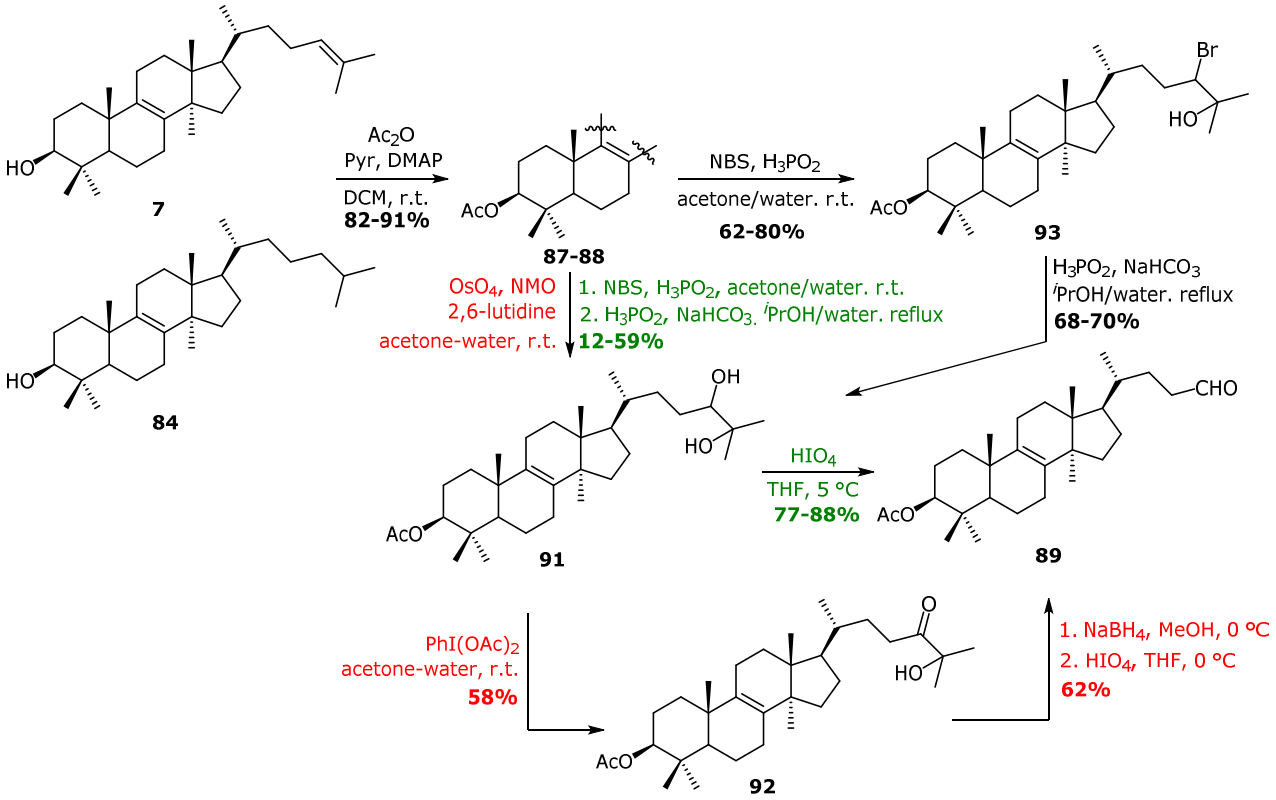


Scheme 2.13 Reduction and oxidative cleavage of α-hydroxy ketone **92** to form aldehyde **89**.[53]

Sato reported the formation of the α-hydroxy ketone **92** as a by-product of the oxidation of **87**.[48] Although they characterised it, the ^{1}H-NMR reported included only the methyl peaks. Thus, this is the first time that α-hydroxy ketone **92** is reported with full ^{1}H- and ^{13}C-NMR spectra.

Detection of aldehyde **89** by mass spectrometry was encumbered due to the formation of (M+Na+MeOH) ions during the mass analysis. Thus, the expected M+Na mass adduct for aldehyde **89** was virtually undetectable, instead a high intensity peak (m/z 497) was observed. Any doubt of the aldehyde **89** formation was dissipated by proton NMR, a broad triplet at

9.77 ppm unmistakably revealed the presence of an aldehyde group in the molecule.



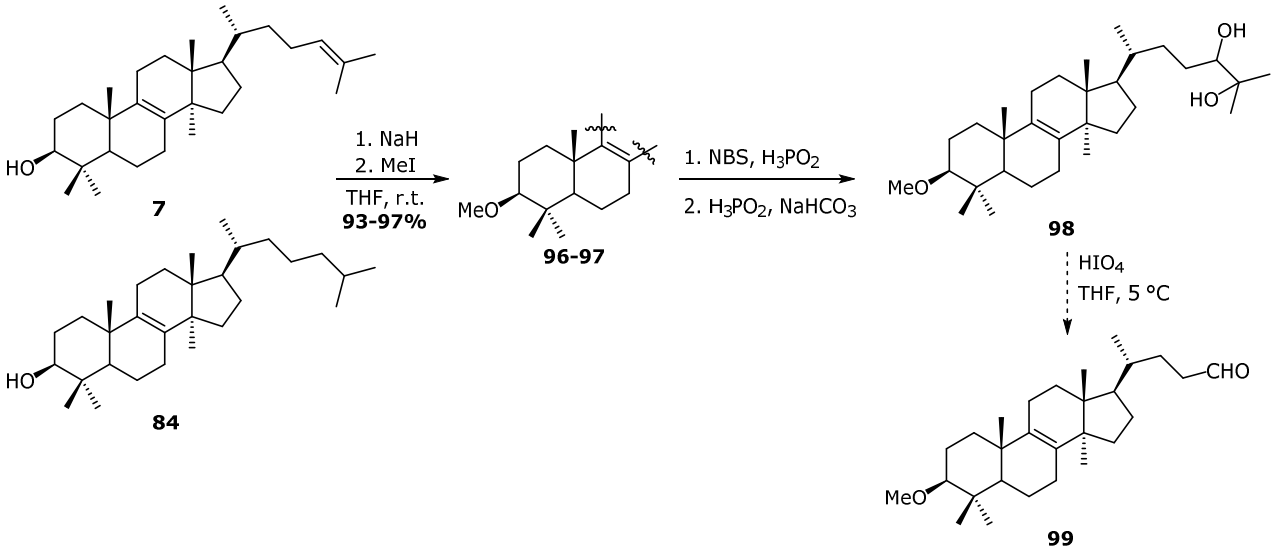
Scheme 2.14 Synthetic routes evaluated for the formation of aldehyde **89** from the commercial lanosterol mixture. In black is the stepwise transformation to diol **91**. In green and red the one-pot transformation to **91**. Black and green routes to the diol **91** were described by Kavtaradze.[37,38] Red route to aldehyde **89** was described by Nicolau.[49]

To summarise, Scheme 2.14 shows the three more efficient routes evaluated in the formation of aldehyde **89**. The routes were colour coded differentiated: black, green and red. The black route corresponds to the stepwise transformation of diol **91**, whilst the other two are one-pot approaches to it. Both black and green routes were described by Kavtaradze[37, 38] and they involved the formation of a bromo-hydroxy derivative **93** prior to the formation of the diol **91**, which after oxidative cleavage with periodic acid yielded aldehyde **89** in excellent yield. The red route was reported by Nicolau[49] and in this case the side chain olefin in **87** is oxidised to the diol **91** with osmium tetraoxide. In this route the oxidative cleavage was performed with (diacetoxyiodo)benzene. However, α-hydroxy ketone **92**, instead of the aldehyde **89**, was the major product formed. Reduction of **92** with sodium borohydride followed by oxidative cleavage

with periodic acid furnished the aldehyde **89** in moderated yield. From these three routes, we have preference for the Kavtaradze routes due to their readily scalability and practicability.

2.3. Towards the synthesis of methoxy-aldehyde 99

To have access to other functionalities around the lanostane frame, an alternative aldehyde was synthesised with a different protecting group at position C-3, the methyl ether protection was chosen. As for aldehyde **89**, the synthesis started with commercial lanosterol, which was first methylated with methyliodide to generate methyl ethers **96** and **97**. For the synthesis of the aldehyde, the one-pot Kavtaradze route was followed.[37] Methyl ether diol **98** was afforded, which eventually led to methoxy-aldehyde **99** after oxidative cleavage with periodic acid (Scheme 2.15). In the next section a fully description of the different steps is given.

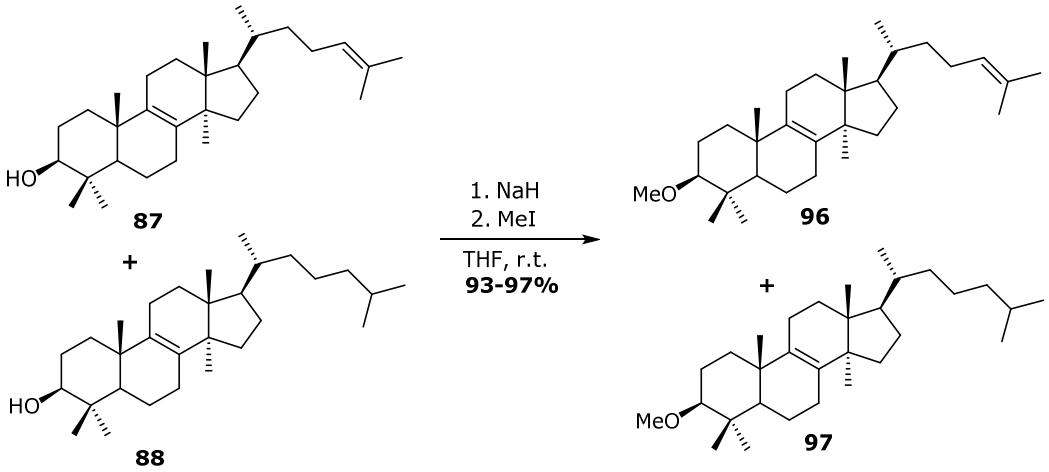


Scheme 2.15 Synthetic route to aldehyde **99** following Kavtaradze procedure.[37] Aldehyde **99** was achieved following a three-step sequence, methylation, diol formation and oxidative cleavage.

2.3.1. Synthesis of methoxy lanosterol 96

Introduction of the C-3 methyl ether was first attempted using a methodology employed by Csuk *et al.* in their synthesis of butelin derivatives.[54] In this approach, the methylation was carried out in dimethylformamide. Sodium hydride and methyl iodide were used for the deprotonation of the hydroxyl group and methylation of the formed alkoxide, respectively. Unfortunately, the lanosterol mixture was insoluble in this solvent and therefore when the other reagents were added no reaction was

observed. A similar approach that used tetrahydrofuran in standard conditions was examined.[55,56] The lanosterol mixture was soluble in this solvent and the reaction produced smoothly the expected methyl ethers **96** and **97** with excellent yields (93-97%) (Scheme 2.16). To reduce the contamination by the mineral oil in sodium hydride, it was washed three times with dry hexane prior to the addition of the lanosterol mixtures. Methoxides **96** and **97** were obtained as a mixture in ratio 1.4:1. This composition was determined by ^{1}H-NMR by comparison of the integration of the mixture **96** and **97** H-3 (1H, 2.68 ppm) and H-24 (0.6H, 5.11 ppm). The signal at 5.11 ppm corresponds to **96** exclusively, while at 2.68 ppm both compounds resonate.



Scheme 2.16 Synthesis of lanosterol methoxide **96** and **97** from lanosterol (**87**) with sodium hydride and methyl iodide in tetrahydrofuran. Methoxide was isolated as a mixture **96**:**97** 1.4:1 in excellent yield.

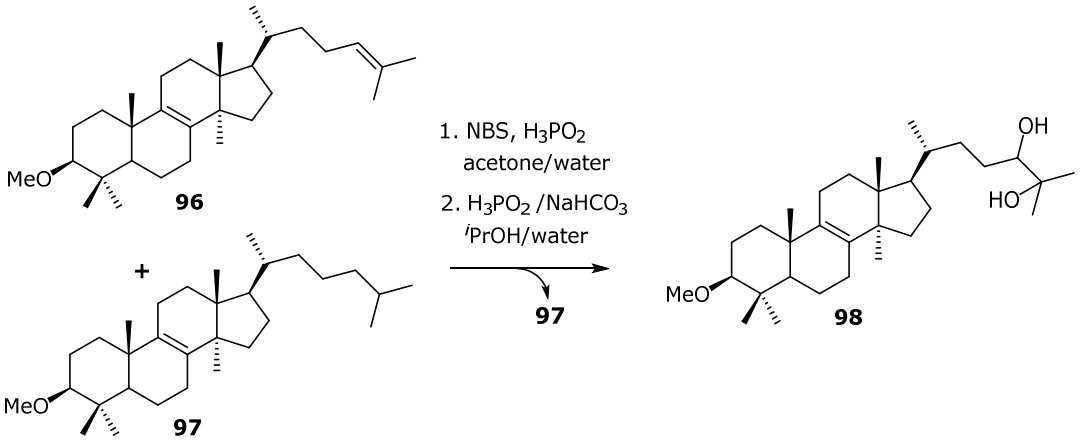
As the molecule lacks chromophoric groups, UV light excitation was not useful for its detection by TLC, the spots were revealed by dipping the TLC plate in a solution of phosphomolybdic acid (PMA). Additionally, these compounds are highly apolar and their mass were not observed in the ESI mass spectrometry, but only by electronic impact mass spectrometry. Their formation was detected by ^{1}H-NMR, the appearance of a singlet at δ 3.37 ppm that integrates for 3H, confirmed the presence of the methyl ether group.

The synthesis of methoxide **96** was reported by Kobayashi *et al.* as a confirmation of the structure of the antileukemic sterol penakerol.[57] However, only mass spectrometry and chromatography retention time data were available for methoxide **97**.[58,59]

2.3.2. Synthesis of methoxydiol 98

For the scale up of the synthesis, the one-pot Kavtaradze method was chosen for the formation of methoxydiol **98** (Scheme 2.17).[37]

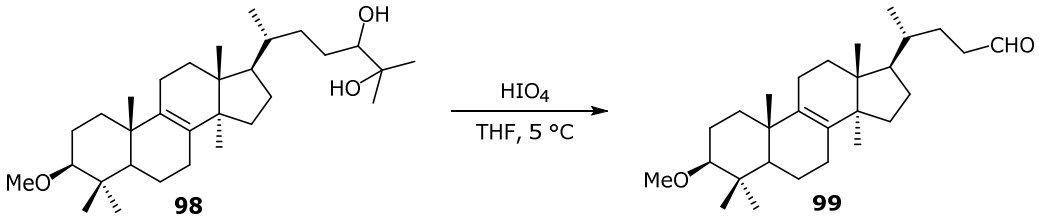
In this methodology, the sequence of two reactions are coupled together: bromination of the $\Delta^{24,25}$ double bond followed by nucleophilic substitution of the bromine. In the first step, bromine is inserted specifically in the $\Delta^{24,25}$ double bond of **96** by *N*-bromosuccinimide (NBS) and aqueous hypophosphorous acid. The end point of the reaction was marked by the solution changing in colour from dark to pale yellow after the addition of the reagents. Less than 5 min. were necessary for this transformation. The nucleophilic substitution reaction was performed in aqueous isopropanol, which was chosen to avoid formation of unwanted ethers.



Scheme 2.17 Formation of methoxydiol **98** following the one-pot route described by Kavtaradze.[37]

The reaction was carried out up to a 15 g scale, using the mixture of methyl ethers **96** and **97**. A mixture of C-24 epimers in a ratio 1:1 was obtained. Methoxydiol **98** was identified by MS, m/z 497 for the sodium adduct of $C_{31}H_{54}NaO_3$, IR gave the characteristic O-H stretching peak for hydroxyls at 3417 cm^{-1} and in the ^{1}H-NMR, two peaks appeared for H-24, one at δ 3.33 ppm (t, *J* = 5.7 Hz) and the other at 3.28 ppm (bd, *J* = 9.9 Hz), each with integration of half a proton corresponding to the mixture of epimers. Due to time constraints, only a portion of the crude product was purified to be able to continue with the next step, the oxidative cleavage. This is the first time that methoxy-diol **98** was reported.

2.3.3. Attempted synthesis of the methoxy-aldehyde 99



Scheme 2.18 Oxidative cleavage of methoxydiol **98** with periodic acid to form methoxy aldehyde **99**.

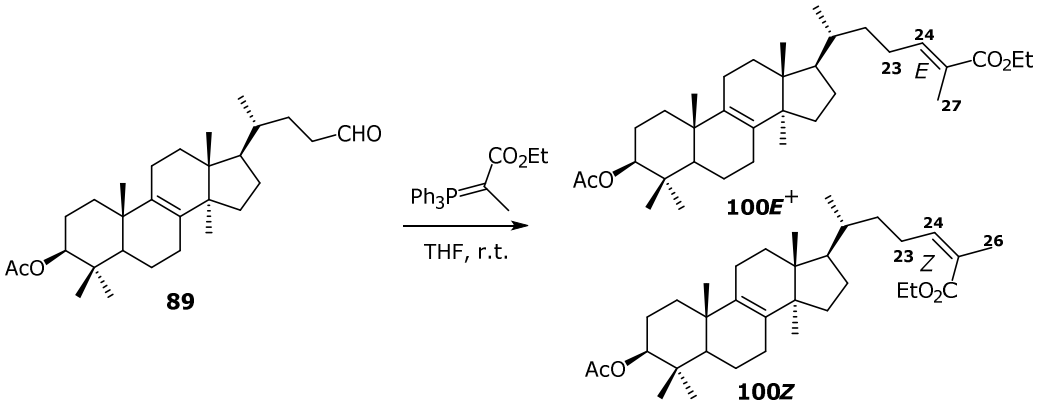
Oxidative cleavage of methoxydiol **98** was carried out using Mori's procedure with periodic acid (Scheme 2.18).[51] Periodic acid was dissolved in tetrahydrofuran and cooled to 5 ºC. A tetrahydrofuran solution of methoxydiol **98** was added dropwise to the cooled periodic acid solution provoking formation of insoluble iodic acid. Full conversion to the methoxy aldehyde **99** was achieved after 1.5 h reaction. Mass spectrometry showed a peak at m/z 437 corresponding to sodium adduct $C_{28}H_{46}NaO_2$ and m/z 432 corresponding to the ammonium adduct $C_{28}H_{50}NO_2$. As for the aldehyde **89**, these peaks showed very weak intensity in the mass spectrum. Unfortunately, due to time constraints no purification was performed on the crude product and therefore no any other additional precursors with a C-3 methoxide was prepared.

2.4. Synthesis of precursors derived from aldehyde 89

The precursors of GA analogues were all synthesised from aldehyde **89**. Different reaction types were considered in order to produce the targeted analogues. Taking into account that aldehydes are reactive species that are readily attacked by nucleophiles, four reactions were envisioned for further development: Wittig olefination, Reformatsky reaction, dehomologation and oxidation.

2.4.1. Wittig olefination

The Wittig olefination is an important reaction in which an aldehyde or ketone reacts with a triphenyl phosphonium ylide to form an alkene and triphenyl phosphine oxide. The stereochemistry of the new double bond depends on the stability of the ylide. Thus, for unstabilised ylides, which are more reactive, the *Z*-alkene predominates. On the contrary, stabilised ylides are more selective to the formation of the *E*-alkene.

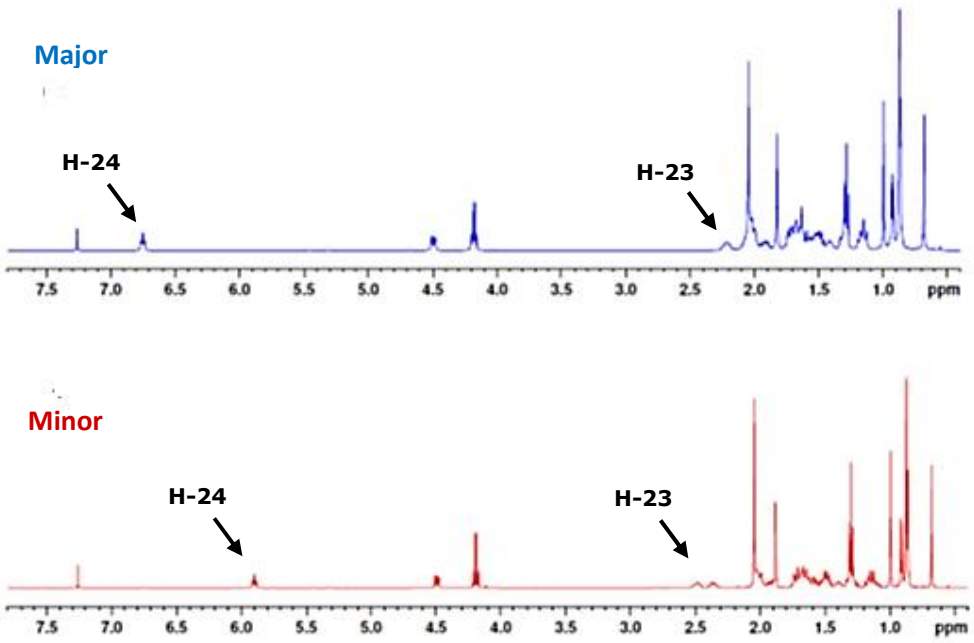


Scheme 2.19 Wittig reaction of aldehyde **89** with (ethoxycarbonylmethyl)-triphenylphosphorane to form *E*- and *Z*-adducts **100*E*** and **100*Z***, respectively.

Our interest was the elongation of the side chain in two carbon units as well as the introduction of an α,β-unsaturated carboxylic group. Hence, a Wittig reaction with (ethoxycarbonylmethyl)-triphenylphosphorane would allow us to reach our goal.

Following a procedure described by Menozzi-Smarrito,[60] aldehyde **89** was treated with (ethoxycarbonylmethyl)-triphenylphosphorane in tetrahydrofuran at room temperature for 16 h. The reaction proceeded smoothly to the formation of the olefin (Scheme 2.19). Analysis by TLC (EtOAc:PE 1:19) revealed two spots with similar polarity and R_f 0.34 and 0.28, respectively. The peaks presented different levels of intensity, whilst the top spot was feint; the bottom one appeared more intense. Mass analysis of each of the spots revealed that both shared the same m/z 549 corresponding to the M+Na adduct for molecular formula $C_{34}H_{54}O_4$ and MW 526. It was expected that both **100*E*** and **100*Z*** were formed. However, as the reaction was performed with a stabilised ylide, it is likely that the *E*-isomer would be much more favoured.

To fully identify the structure of the major and minor isomers, ^{1}H- NMR and NOESY experiments were carried out. The diastereoisomers were easily identified by comparison of their ^{1}H-NMR (Figure 2.4). There are significant differences in their chemical shifts for H-23 and H-24. In the major isomer, H-24 (6.75 ppm) is much deshielded than in the minor one (5.90 ppm). The contrary applies for H-23; minor protons appear at lower field (2.43-2.59 ppm and 2.28-2.42 ppm) than the major ones (2.14-2.29 ppm and 2.06-2.12 ppm).



Isomer	Shift/PPM	
	H-23	H-24
major	2.14-2.29 (m) 2.06-2.12 (m)	6.75 (tq)
minor	2.43-2.59 (m) 2.28-2.42 (m)	5.90 (tq)

Figure 2.4 ^{1}H-NMR for major (blue) and minor (red) isomers in the Wittig reaction. Chemical shifts for H-23 and H-24 for each of the isomers are indicated.

This suggested that H-24 is near an electron-withdrawing group for the major compound, which is the case for H-23 in the minor. Compound **100*E*** has the carbonyl group *syn* to H-24, alternatively **100Z** has H-23 protons *syn* to the carbonyl group.

Further analysis with a NOESY experiment was also carried out to confirm this outcome (Figure 2.5). By comparing the correlations of H-24 for both the minor and major compounds, it was revealed that the number of correlations was different. Thus, the minor isomer presented five correlations for H-24 (2 x H-22, 2 x H-23 and 1 x CH_3) (Figure 2.5 **B**), whereas the major isomer presented only four correlations for this same proton (2 x H-22 and 2 x H-23) (Figure 2.5 **A**). Correlation with the methyl group is expected to happen in the *Z* isomer (Figure 2.6); in consequence, the minor isomer is the *Z* and the major the *E*, as was predicted.

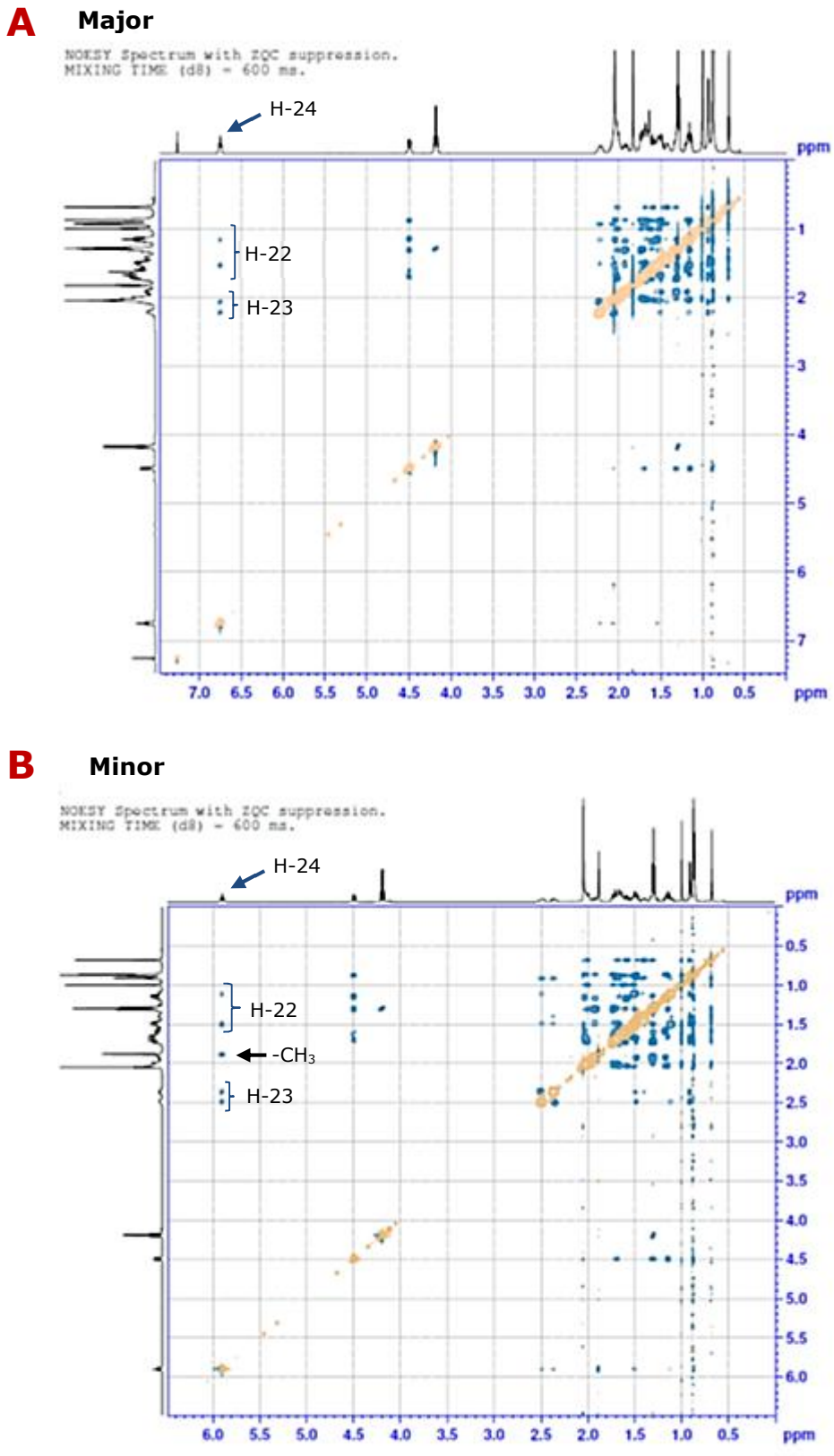


Figure 2.5 NOESY spectra for **A** (major), and **B** (minor) isomers. Correlation of H-24 has been highlighted for each of the isomers.

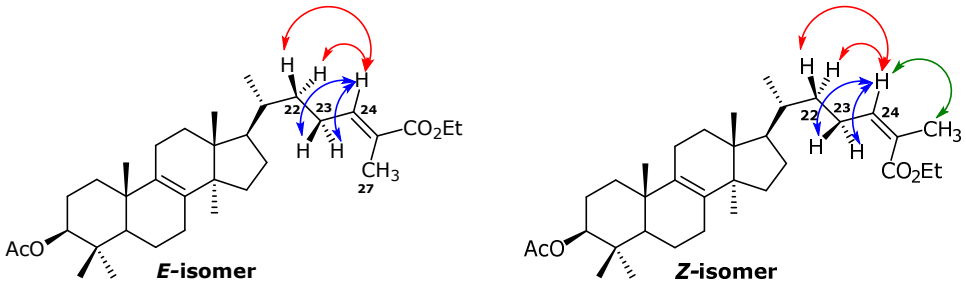
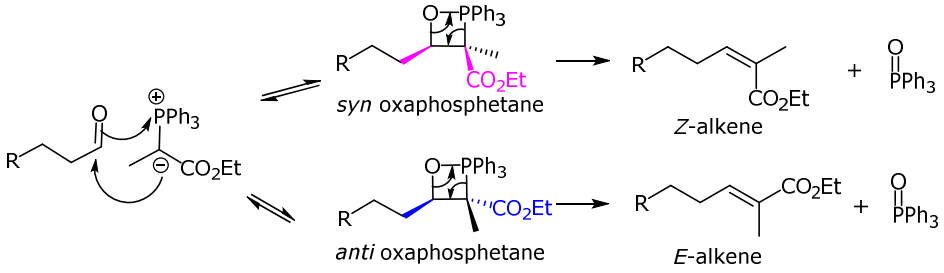


Figure 2.6 NOESY correlations for H-24 expected in *E*- and *Z*-isomers.

The *E* stereoselectivity of the reaction is due to the reversibility of the oxaphosphetane formation step, which in this case, is thermodynamically controlled (Scheme 2.20). The *anti* diastereoisomer is the thermodynamically more stable oxaphosphetane because it has the two bulky groups on opposite sides of the ring. In addition, the rate of the elimination to give the *E*-alkene ought to be significantly faster than the rate of the elimination to give the *Z*-alkene, simply because of steric crowding in their respective transition states. In consequence, the *anti* diastereoisomer produces the *E*-alkene quicker than the *syn* diastereisomer gives the *Z*-alkene. In addition, equilibration of the two oxaphosphetanes via starting material restores the supply of *anti* diastereoisomer, so that almost exclusively *E*-alkene is eventually yielded.



Scheme 2.20 Wittig reaction mechanism explains the selectivity of the reaction.

The Wittig reaction was performed from 60 mg to 2 g scale. After chromatographic purification, **100*E*** was isolated in excellent yield (60-97%), with traces of **100*Z*** were also separated from the reaction mixture (3-5%). These two compounds have not been reported previously, therefore they are novel compounds.

In the protocol two equivalents of phosphorane were employed. We were interested in optimising this quantity and therefore we performed a series of reactions modifiying the stoichiometry of the phosphorane from 1.1 to 2.0 equivalents. It was found that increasing the stoichiometry slightly reduced the *Z*-isomer. Thus, 1.3 equivalents produced 5% of **100*Z***, whilst this

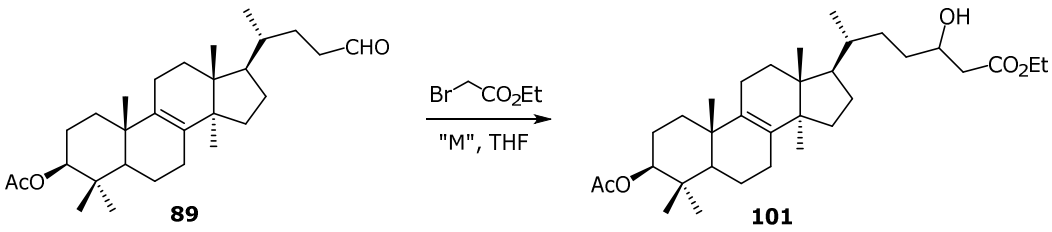
percentage was reduced to 3% with 1.5 equivalents of the phosphorane. In consequence, in our synthesis, the phosphorane loading was reduced to 1.5 equivalents. It is noteworthy that none of **100*Z*** was detected when the reaction was conducted on a very small scale.

Separation of both isomers by column chromatography was tedious, since their polarity was very similar. Hence, combinations of dichloromethane or diethyl ether with petroleum ether or variations on a three solvent system with ethyl acetate, diethyl ether and petroleum ether resulted in overlapping of the two spots. However, good separation was observed with ethyl acetate : petroleum ether 1:19 (ΔR_f = 0.06). Consequently, this latter solvent system was used for both detection and separation.

In summary, the Wittig olefination proceeded in excellent yields to give the desired *E*-isomer **100*E*** accompanied by traces of the *Z*-isomer **100*Z***. ^{1}H-NMR and NOESY experiments were used for the identification of these isomers. Optimisation of the reaction allowed us to reduce the load of the phosphorane in the reaction without compromising the overall yield of the reaction. Additionally, separation of the isomers was achieved when ethyl acetate : petroleum ether 1:19 was used.

2.4.2. Reformatsky reaction

To form analogues with different side chains, aldehyde **89** was reacted under Reformatsky conditions with ethyl bromoacetate to generate the β-hydroxyaceto-ester **101** (Scheme 2.21).



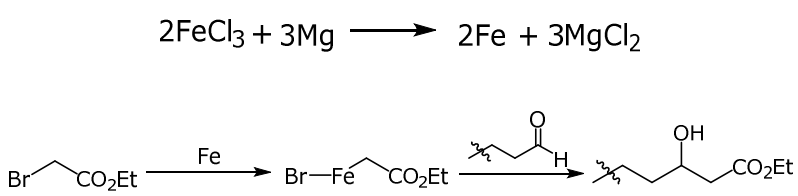
Metal	Conditions	Yield/% (101)
Zn-Cu	Zn, CuCl, H_2SO_4, THF, 45 ºC	n/a
Mg, $FeCl_3$	Mg, $FeCl_3$, THF, r.t.	23-55
In	In, sonication, THF, r.t.	n/a
	In, THF, 60 ºC	13-45

Scheme 2.21 Formation of β-hydroxyester **101** by a Reformatsky reaction. "M"=metal.

A Reformatsky reaction promotes the conversion of an α-haloester and an aldehyde or ketone to a β-hydroxyester. Although in its classic version, zinc metal was used, its scope has been expanded to other metals as well. It is undeniably one of the most useful method for the formation of carbon-carbon bonds characterised by their neutral reaction conditions and absence of *O*-additions; however, when they are compared with those of aldol reactions, two major limitations have been associated with them: lower yields and stereoselectivities. Therefore, it is more common to see them in syntheses that involve subsequent elimination or oxidation steps of the hydroxylated product.[61]

This reaction was attempted using different metals, in our first approach a Zn-Cu couple was used as the activated metal. This was generated *in situ* following a procedure described by Scherkenbeck and Siegel in 2005.[62] In this route zinc metal is combined with copper (I) chloride in the presence of sulfuric acid to form the Zn-Cu couple *in situ*. Addition of the aldehyde and heating at reflux followed by the incorporation of ethyl bromoacetate would generate **101** immediately. Nonetheless, only original aldehyde **89** was recovered in all the attempts, suggesting that the activated Zn-Cu couple may have not been formed.

An alternative procedure using a low valent iron-mediated Reformatsky reaction was attempted.[63] In this procedure iron (III) chloride is activated *in situ* to its low valent form by reduction with magnesium turnings (Scheme 2.22 (1)). This transformation takes place in the presence of the other two reagents, the aldehyde and the ethyl bromoacetate. For the reaction to succeed, insertion of the active metal to the carbon-halogen bond takes place followed by nucleophilic addition to the aldehyde (Scheme 2.22 (2)).



Scheme 2.22 Formation of β-hydroxyester in Reformatsky reaction with low valent metal. (1) Formation of the low valent metal from its salt. (2) Metal insertion to the ethyl bromoacetate and subsequent nucleophilic addition to the aldehyde to form the β-hydroxyester adduct.

The mixture of aldehyde **89**, ethyl bromoacetate, iron chloride and magnesium turnings in tetrahydrofuran produced a large number of products among which the desired β-hydroxyester **101**. Several purification steps were required to isolate it, and due to lack of selectivity, the yield was affected being between 23-55%. The original procedure described by Chattopadhyay used excess of reagents to ensure fast transformation,[63] therefore reducing the stoichiometry might result in a cleaner reaction. However, this latter statement should be investigated further to optimise the reaction conditions.

A third route was explored, this time using an indium mediated Reformatsky reaction. Indium has the advantage that is stable, easy to use and does not require prior-to-use activation. Furthermore, indium mediated reactions can be prepared under Barbier conditions, that is, addition of all the reagents in one pot. Bang *et al*. investigated conditions for an optimal sonochemical Reformatsky reaction with indium.[64] They found that best results in terms of reaction times and conversion were given when indium powder (1 eq.), ethyl bromoacetate (1.5 eq.) and the aldehyde or ketone (1 eq.) were dissolved in dry tetrahydrofuran and sonicated at room temperature for a couple of hours, increasing reaction times or moisture reduced the yield or stopped the reaction. Their conditions gave excellent yields for a variety of substrates including aliphatic and aromatic aldehydes or ketones. Nonetheless, in our hands, the reaction behaved capriciously forming the desired adduct **101** randomly after short (2 h) or long (>6 h) sonication times. In order to verify the efficacy of the reaction, a different aldehyde, furfural and decanal were used, fully conversion to products was observed in these cases.

More recently, Poisson *et al*. described an alternative method for the indium mediated reaction.[65] In their procedure, the aldehyde (1 eq.), indium (1.05 eq.) and ethyl bromoacetate (1.05 eq.) were stirred in tetrahydrofuran at 60 ºC for 6 h, resulting in the formation of the Reformatsky adduct in good to excellent yields. Good toleration of functional groups and chemoselectivity of the reaction was also observed. Applying these conditions, the reaction was more reproducible. However, fully conversion was not achieved and only modest yields of adduct **101** were isolated (13-45%) accompanied by unreacted aldehyde **89** (13-10%). Precursor **101** has not been reported previously, therefore it is a novel compound.

β-Hydroxyester adduct **101** was detected by mass spectrometry m/z 553 corresponding to the sodium adduct $C_{33}H_{54}NaO_5$. ^{1}H-NMR showed peaks for the ethyl ester at 4.17 ppm (q, *J* = 7.1 Hz, 2H) and 1.27 ppm (t, *J* = 7.1 Hz, 3H), H-24 peak as a multiplet at 4.05-3.87 ppm and a pair of doublet of doublets and triplets for H-25. These protons are diastereotopic, a different chemical shift was observed for each of the protons that were labelled H^a and H^b. Additionally, the chemical shift was different for the different *R*- and *S*- epimers. Three coupling constants were measured, a vicinal coupling constant ^3J = 3.1 Hz and two coupling constants around *J* = 9 Hz. According to Karplus's equation (Figure 2.7) a coupling constant of 9 Hz corresponds to a dihedral angle 171°, while the smaller coupling constant corresponds to a dihedral angle of 52°. Geminal coupling constants of methylene groups attached to an electronegative substituent range from 12 Hz to 9 Hz and are only measurable if they are diastereotopic.[66] As this is the case for H-25 and these protons are attached to electronegative groups from both sides H-24 and H-26, it is expected to observe a geminal coupling constant of ^2J = 9 Hz. The integration and the HMQC experiment suggested the pairing of carbon and proton indicated in Table 2.2. However, it is ambiguous to determine the configuration of H-24 with the available data, since the NOESY did not show different correlation in the mixture, interestingly the hydroxyl peak was only observed when the reaction was performed with iron chloride (III)/magnesium. It appeared as a doublet at 2.95 ppm (d, *J* = 4.0 Hz, 0.52H) and 2.89 ppm (d, *J* = 4.0 Hz, 0.48H). Figure 2.8 shows the Fisher projections of epimers *R* and *S*. The ratio of C-24 epimers was 1:1.1 when the reaction was performed with iron chloride (III)/magnesium and 1:1.2 with indium.

Peak/ppm		integration	multiplicity	*J*/Hz	*R*	*S*
Carbon	Proton					
41.6	2.53	0.48	dd	9.4, 3.1	H^b	H^a
	2.37		t	9.2	H^a	H^b
41.3	2.49	0.52	dd	9.4, 3.1	H^b	H^a
	2.41		t	9.2	H^a	H^b

Table 2.2 Correlation carbon-proton in **101**.

To summarise, different methods were explored for the Reformatsky reaction, Zn-Cu couple, iron chloride (III)/magnesium and indium with sonication or conventional heating. Even though formation of product was

observed with iron chloride (III)/magnesium and indium heating at 60 ºC, the isolated yield was only modest (<60%).

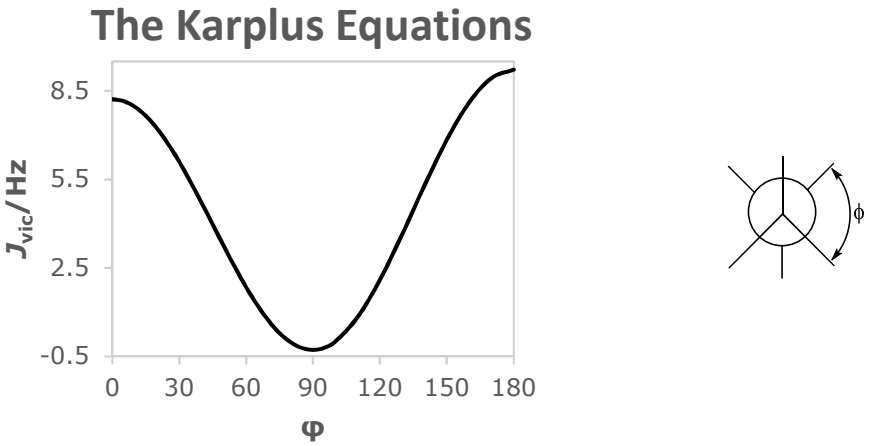


Figure 2.7 Graphical representation of The Karplus equation. Variation of vicinal coupling constant J_{vic} is plotted vs. dihedral angle φ. The maximum values are for the *trans* and *cis* coplanar positions (φ = 180° and 0°) and the minimum values for protons at 90° to each other. The equations used to build the graph are: (1) $0° \geq \varphi \leq 90°$ $J_{vic} = 8.5 \cos^2\varphi - 0.28$; (2) $90° \geq \varphi \leq 180°$ $J_{vic} = 9.5 \cos^2\varphi - 0.28$.[66]

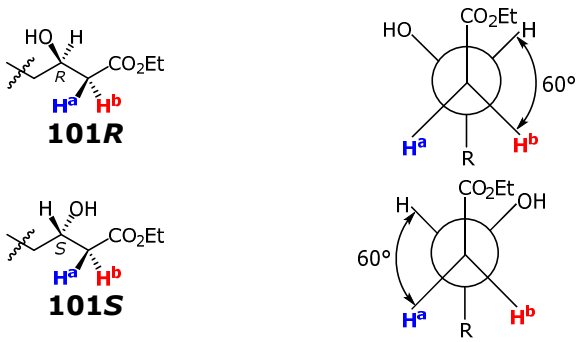
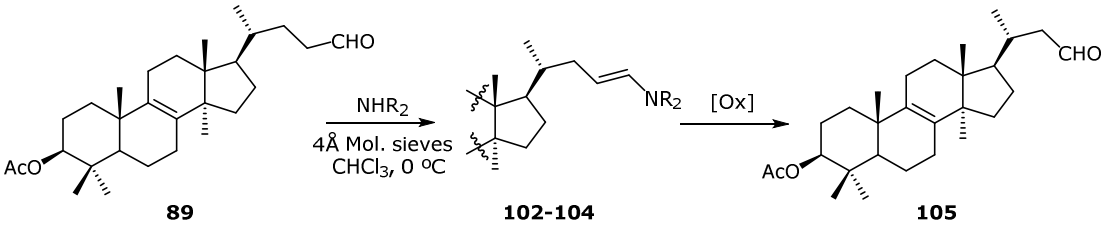


Figure 2.8 Side chain representation of **101*R*** and **101*S*** epimers with their respective Fisher projections. H-25 protons were labelled H^a (blue) and H^b (red).

2.4.3. Dehomologation

For dehomologation of aldehyde **89**, a two-step synthesis was followed. In the first stage, an enamine **102**-**104** was formed that after oxidative cleavage generated the desired dehomologeted aldehyde **105** (Scheme 2.23).



89 **102-104** **105**

Scheme 2.23 Synthesis of dehomologated aldehyde **105**. Two steps were followed, first enamine formation followed by oxidative cleavage. Secondary amines used in the synthesis of the enamine were: dibenzylamine (**102**), pyrrolidine (**103**) and morpholine (**104**).

i. Enamine formation

Standard conditions for the formation of aldehyde enamines normally include the use of either strong acids or bases in refluxing solvents or at room temperature, but with a large excess of the secondary amine and over extended periods of time.[67-70] Bélanger in 2006 presented a mild method claimed as highly efficient in which a chloroform solution of the aldehyde and the secondary amine in nearly stoichiometric quantities were stirred at low temperatures over 4Å molecular sieves, yielding the aldehyde enamine after one hour reaction.[71]

To assess the efficacy of this methodology for aldehyde **89** in the formation of the enamine, three secondary amines were investigated: dibenzylamine, pyrrolidine and morpholine that produced enamine **102**, **103**, and **104**, respectively. In a previous study piperidine was assessed, resulting in no product being formed.[36]

Monitoring the reaction was problematic, since the enamine formed was unstable under atmospheric moisture, hydrolysing quickly to the aldehyde starting material. TLC and MS were therefore useless as detection techniques; in this case, care was needed when recording the proton NMR, which needed to be carried out immediately, since the more time the solution was in the tube, the more hydrolysis was seen in the spectrum, *i.e.*, the same sample analysed at time 0 showed the enamine mixed with little aldehyde, whilst 20 hours later the ratio was reversed, the pick of the aldehyde increased and the one for enamine had almost disappeared (Figure 2.9).

The reaction seemed to proceed better for morpholine than for the other two amines. Additionally, it was easier to follow the progress of the reaction by

NMR because the chemical shift of the morpholine did not overlap with those of the aldehyde or enamine; another point to note is that the morpholine-enamine was a white solid, whilst pyrrolidine and dibenzylamine derivatives were oils.

The reaction was scaled up from 0.11 mmol to 0.68 mmol using morpholine as the enamine. At this scale, two equivalents of the amine were needed to observe a good level of conversion, and the solvent chosen was deuterated chloroform, so that monitoring the reaction by ^{1}H-NMR was easier. The addition of the first equivalent of morpholine resulted in no reaction, but after one hour of having added the second, the reaction reached a 75% conversion (Figure 2.9 **A**) that did not increase further over time. To avoid hydrolysis of the enamine **104**, all the work-up was carried out under a nitrogen atmosphere. No further purifications were performed.

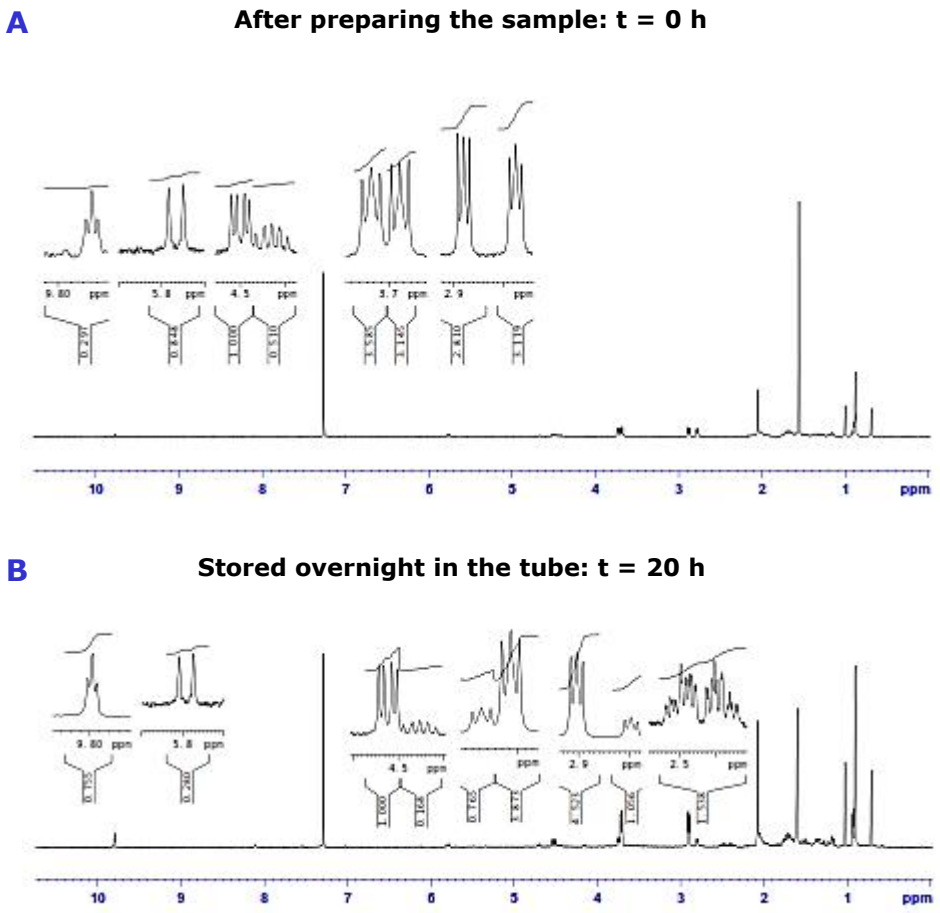
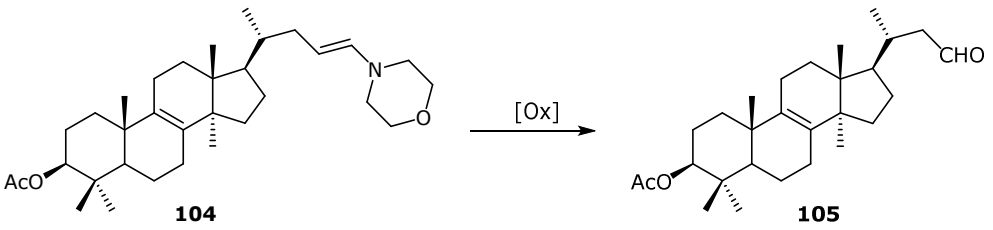


Figure 2.9 ^{1}H-NMR of morpholine-enamine **104**. **A.** t=0 h; **B.** t=20 h. Note change in the integration of aldehyde and double bond $\Delta^{23,24}$ over time.

*ii. Towards the synthesis of dehomologated aldehyde **105**.*

For the formation of aldehyde **105**, the oxidative cleavage of enamine **104** was evaluated under different conditions (Scheme 2.24). In a first approach, a procedure described by Harris was evaluated.[72] They studied the oxidative cleavage of β,β-disubstituted enamines using alumina supported permanganate claiming excellent yields for the series of di-substituted enamines that they examined. However, in order for the reaction to proceed strict anhydrous conditions were required. In our hands, no oxidative cleavage was detected, instead hydrolysis to aldehyde **89** and oxidation to its acid were observed, suggesting wet reagents.



104 **105**

Oxidant	Conditions	Yield
$KMnO_7/Al_2O_3$	Acetone, r.t.	n/a
$NaIO_4$	THF/water, r.t.	n/a
	$CHCl_3$, r.t.	
HIO_4	THF, r.t.	n/a
	$CHCl_3$, r.t.	
$PhI(OAc)_2$	THF, r.t.	n/a

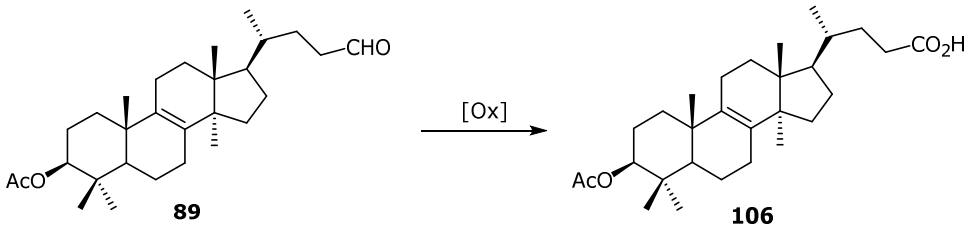
Scheme 2.24 Synthesis of dehomologated aldehyde **105** from enamine **104** by oxidative cleavage.

By chance, Vetelino in 1994 discovered that enamines were cleaved by sodium periodate in aqueous tetrahydrofuran without the assistance of a metal like osmium tetraoxide.[73] In order to assess if enamine **104** could be cleaved under these conditions, a small trial was set up. Periodic acid in tetrahydrofuran was used, instead of periodate. After four hours the reaction showed some of the dehomologated aldehyde **105**. However, after purification dehomologated aldehyde **105** was not isolated pure, but together with aldehyde **89**. It is likely that the starting material was already partially hydrolysed, hence, to succeed with this transformation a one pot reaction including formation of the enamine **104** followed by oxidative cleavage to **105** was envisaged.

For the one pot reaction, three oxidants were investigated: sodium periodate, periodic acid and diacetoxyiodo benzene. The reaction was performed in chloroform with morpholine as the secondary amine at 0 ºC for 5 h. After formation of the enamine, the oxidant was added and the reaction was stirred at room temperature for another 16 h, analysis by MS and ^{1}H-NMR revealed that the major product was the hydrolysed aldehyde **89** for both sodium periodate and periodic acid, whilst no product was identified from diacetoxyiodo benzene.

As hydrolysis was observed as the major product, it was decided to repeat the reaction on a larger scale (2.4 mmol) following a stepwise procedure. This time the enamine formation was performed in fresh distilled dichloromethane using morpholine as the amine. The crude product obtained after filtration and evaporation of the solvent was used directly for the oxidative cleavage reaction that was carried out with sodium periodate in 50% aqueous tetrahydrofuran at room temperature for 1 h. The desired dehomologated aldehyde **105** was observed by MS, m/z 451 for the sodium adduct ($C_{28}H_{44}NaO_3$), accompanied by aldehyde starting material **89**. However, due to time constraints purification of the crude product was not carried out.

2.4.4. Direct oxidation



89 **106**

Oxidant	Conditions	Yield (%)
PCC(2mol%)/HIO_4[74]	MeCN, r.t.	n/a
Oxone®[75]	DMF, r.t.	78

Scheme 2.25 Oxidation of aldehyde **89** to lucidenic acid **106**. Two conditions were studied, catalytic PCC and Oxone®. Better results on the reaction were observed with Oxone® (78%), catalytic PCC formed complex mixtures of compounds difficult to separate.

Many processes have been reported for the oxidation of aldehydes to their corresponding carboxylic acids, most of them are based on transition metals, such as chromium or manganese oxides. Hunsen, in an effort to developed a more environmental friendly method, proposed the used of catalytic pyridinium chlorochromate (PCC) and periodic acid as the terminal oxidant.[74]

He claimed that clean and quantitative conversion to carboxylic acids was achieved for aliphatic, propargylic, vinylic, electron-rich and poor aromatic aldehydes. However, when PCC (2 mol%)/HIO_4 were added to **89**, no reaction was observed after 90 min. Extending the reaction time for 24 h produced complex mixtures among which lucidenic acid **106**. In view of the poor success in forming **106**, a different method was envisaged.

Travis *et al*. described another environmental friendly method that did not use transition metals, instead Oxone® acted as the oxidant.[75] Oxone® is a potassium triple salt containing peroxymonosulfate with formula $2KHSO_5 \cdot KHSO_4 \cdot K_2SO_4$. It is a versatile oxidant that has been used successfully in the oxidation of boron-, nitrogen-, phosphorous- and sulfur-containing compounds, as well as in the epoxidation, oxidative cyclisation and cleavage of olefins.[75] The oxidation reaction of aldehydes to carboxylic acids takes place effortlessly, simply by the mixture of the reagents in dimethylformamide (DMF) at room temperature for 3 h with no rigorous exclusion of air or moisture from the reaction. This procedure produced excellent yields of both aromatic and aliphatic aldehydes with the exemption of electron-rich substrates, which provided primarily the Dakin product. The Dakin oxidation is a redox reaction in which an aldehyde reacts with a peroxide to form a dehomologated alcohol and carboxylic acid following a mechanism similar to the Baeyer-Villiger oxidation. Thus, when equimolar amounts of **89** and Oxone® were combined in DMF for 3 h, excellent yield of the expected lucidenic acid **106** was obtained (78%).

Lucidenic acid **106** was identified by mass spectrometry, sodium adduct m/z 481 corresponding to the formula $C_{29}H_{46}NaO_4$ and by ^{1}H-NMR by the disappearance of the aldehyde triplet peak at δ 9.76 ppm. This compound has been synthesised previously using different oxidation method.[76,77]

2.5. Synthesis of GA analogues

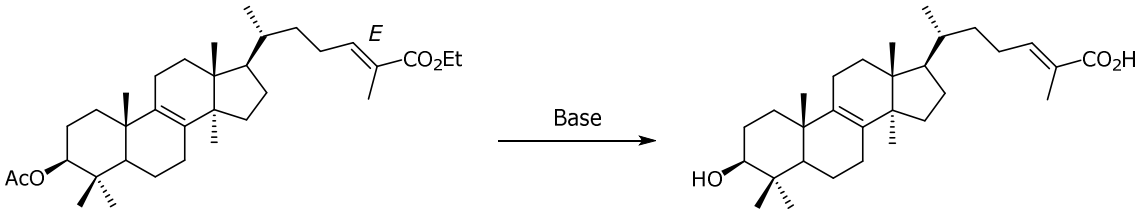
The synthesis has been organised in the three main groups as indicated at the beginning of the chapter: modifications at C-3; rings B/C and on the side chain.

2.5.1. Modification at C-3

Four targets were envisaged with a different functionality at C-3 in ring A: β-hydroxyl group; ketone; β-acetate and α-hydroxyl. All four analogues came from the same precursor, *E*-Wittig adduct **100*E***.

(a) Hydrolysis. Formation of analogue 107

Hydrolysis of Wittig adduct **100*E*** under basic conditions afforded **107** (Scheme 2.26). Initially the hydrolysis was carried out following a procedure described by Kavtaradze with potassium hydroxide in ethanol.[37] However, a more polar by-product was detected by TLC (SiO_2, EtOAc:PE 2:3) that was difficult to remove by standard column chromatography. This side product was formed at all the temperatures studied, from room temperature to 40 ºC and 60 ºC. Thus, different conditions were investigated. Menozzi-Smarrito *et al.* performed the hydrolysis with lithium hydroxide in THF:water 1:1.[59] In this combination of solvents, the reaction proceeded very slowly, formation of product was achieved when an alcohol was added. With ethanol, the lower spot was detected, but the reaction was cleaner and higher yielding with methanol. Therefore, the modified Menozzi-Smarrito procedure using the combination of solvents tetrahydrofuran/methanol/ water 2:1:1 was used to perform this reaction.



100*E* **107**

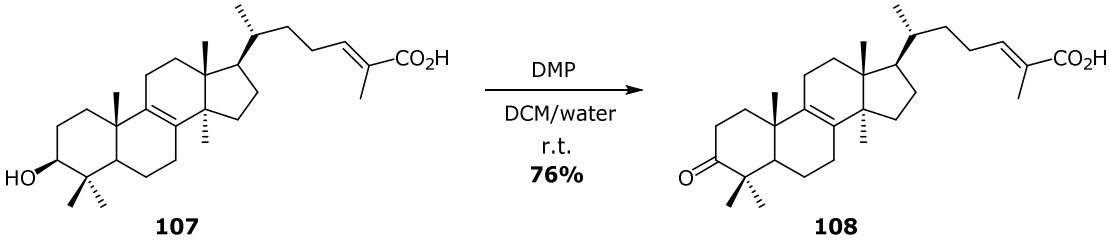
Base	Conditions	Yield (%)
KOH	EtOH, 60 ºC	88[a]
	EtOH, r.t.	50[a]
LiOH	THF/EtOH/water, r.t.	87[a]
	THF/EtOAc/water, 40 ºC	n/a
	EtOH, 40 ºC	n/a
	THF/MeOH/water. r.t.	88-95

Scheme 2.26 Hydrolysis of acetoester **100*E*** in basic condicions. **a.** A lower spot by-product formed when the solvent was ethanol.

Analogue **107** has the same chemical structure as the isolated GA-Z. A previous synthesis of this GA has been described using bio-transformations

with baker's yeast or alternative oxidative methods as the method described in this section.[78,79] Analogue **107** was identified by MS, the peak at m/z 479 corresponding to the sodium adduct of $C_{30}H_{48}NaO_3$ and by ^{1}H-NMR, H-3 upfield shifted to δ 3.24 ppm (dd *J* = 11.6, 4.5 Hz) and disappearance of the peaks for the ethyl ester group in adduct **100*E*** (4.18 ppm (q, *J* = 7.1 Hz, 2H) and 1.29 ppm (t, *J* = 7.1 Hz, 3H)).

(b) C-3 Oxidation. Formation of analogue 108



107 **108**

Scheme 2.27 Synthesis of analogue **108** from Dess-Martin oxidation of **107**.

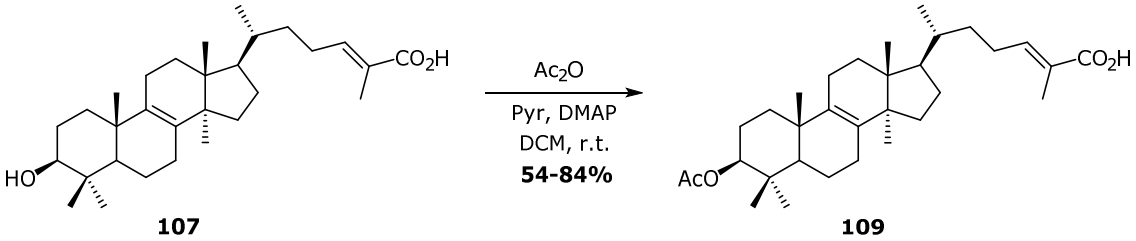
Oxidation of C3 hydroxyl in **107** provided the ketoacid **108**. Different methods have been described for the oxidation of secondary hydroxyls to ketones. The most common ones are Swern, Dess-Martin (D-M) or Jones oxidations. For the oxidation of **107** a D-M oxidation was chosen (Scheme 2.27). Meyer and Schreiber found that the D-M oxidation took place in minutes when 1 eq of water diluted in dichloromethane 1:1000 was added very slowly to a dichloromethane solution of the substrate and Dess-Martin periodinane (DMP).[80] Slow addition of the aqueous dichloromethane was crucial to avoid having a heterogeneous reaction mixture.

When Meyer and Schreiber conditions were applied to **107**, **108** was formed in 30 min with excellent yield (76%). It was identified by MS, m/z 477 corresponding to $C_{30}H_{46}NaO_3$ and in ^{1}H-NMR the absence of the peak for H-3 at δ 3.24 ppm was indicative of the presence of a ketone that was verified in the ^{13}C-NMR, where two carbonyl peaks were present one at δ 218.1 ppm corresponding to the C-3 ketone and the other at 173.4 ppm corresponding to the C-26 carboxylic acid.

Analogue **108** synthesis was reported in a patent,[81] additionally, Zhang evaluated it as anti-HIV agent.[82] However, the reported proton NMR was incomplete and its application as anti-cancer agent has not been previously described.

(c) C-3 Acetylation. Formation of analogue 109

Analogue **109** was afforded in good to excellent yields using the same conditions as previously reported for acetylation of lanosterol, intermediate **87**. The acetylation was carried out using acetic anhydride in the presence of pyridine and dimethylformamide at room temperature. This methodology was used by Kavtaradze *et al*. in their approach to pure lanosterol from the commercial mixture.[37,38]



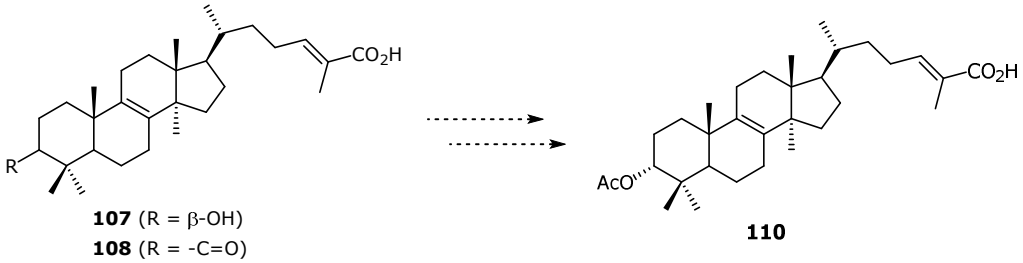
107 **109**

Scheme 2.28 Acetylation of analogue **107** with acetic anhydride, pyridine and dimethylaminopyridine to form aceto-acid **109**.

Analogue **109** was not reported previously. Analogue **109** was identified by MS, a peak m/z 521 corresponding to the sodium adduct $C_{32}H_{50}NaO_4$ was observable and by ^{1}H-NMR, the characteristic chemical shift of H-3 at δ 4.5 ppm (dd, *J*=11.5, 4.5 Hz, 1H) and the singlet peak for the C-32 methyl group at δ 2.05 ppm (s, 3H) were present.

(d) C-3 Inversion. Towards the synthesis of analogue 110

Two approaches were followed for the formation of the 3α-hydroxyl analogue **110**; a stereoselective reduction of a 3-oxo moiety **108** and a C-3 inversion of the 3β-hydroxyl **107** (Scheme 2.29).



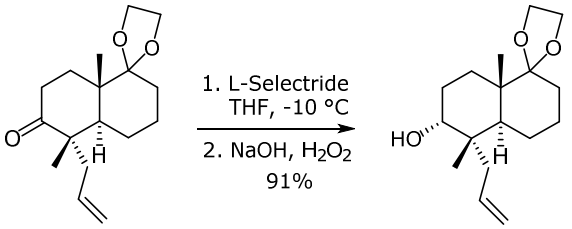
107 (R = β-OH)
108 (R = -C=O)

110

Scheme 2.29 Synthesis of the 3α-hydroxyl analogue **110**. Two routes proposed, a stereoselective reduction from **108** and a C-3 inversion of **107**.

i. Stereoselecive reduction

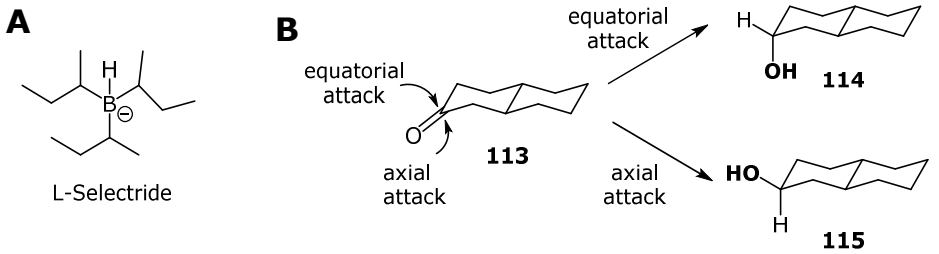
Stereoselective reduction of a 3-oxo compound could produce the α-hydroxyl at this position. Analogue **108** has a ketone at C-3, therefore it was the starting material of choice for exploring this strategy.



111 **112**

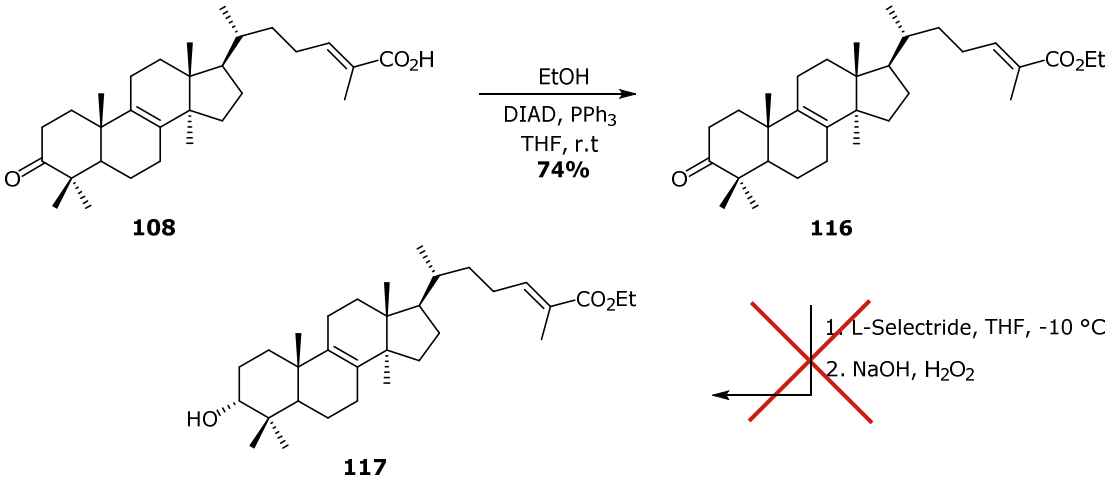
Scheme 2.30 Stereoselective reduction of 3-oxo **111** to the α-hydroxyl **112** by L-Selectride® in a process described by Oguchi *et al*.[83]

Oguchi *et al*. in their synthesis of (-) Candelalides used L-Selectride® to perform a stereoselective reduction of the C-3 carbonyl group of the pure *trans*-decalone **111** to the α-alcohol **112** in excellent yield (Scheme 2.30).[83] L-Selectride® is the commercial name for lithium tri-*sec*-butylborohydride, which is such a bulky borohydride that preferentially attacks equatorially on cyclic systems to produce almost exclusively the α-hydroxyl stereoisomer (Scheme 2.31).



Scheme 2.31 **A**. Chemical structure of L-Selectride®. **B**. Reduction of *trans*-decalone **115** by equatorial or axial attack to form the 3α- or 3β-hydroxyl, **114** and **115** respectively.

The carboxylic acid of **108** was first protected as its ethyl ester, using a Mitsunobu reaction that mirrored a procedure described by Lepore.[84] Analogue **108**, ethanol and triphenylphosphine were dissolved in tetrahydrofuran followed by dropwise addition of diisopropylazo-dicarboxylate and stirring for 1.5 h. Ketoester **116** was recovered in high yield after purification (Scheme 2.32). Analogue **108** was also reacted under the more standard conditions for esterification, ethanol and acid catalysis. However, the starting keto-acid **108** was recovered with no ester being formed.



Scheme 2.32 Synthetic route from ketone **108** to 3α-hydroxyl ester **117**. Carboxylic acid protection as ethyl ester **116** followed by stereoselective reduction with L-Selectride®. Reduction failed to form **117**.

Analogue **116** is a novel compound that was identified by MS, m/z 505 corresponding to the sodium adduct with molecular formula $C_{32}H_{50}NaO_3$ and by ^{1}H-NMR the ethyl group with a quadruplet at δ 4.18 (2H, *J* = 7.1 Hz) and triplet at δ 1.29 (3H, *J* = 7.1 Hz) confirmed the success of the esterification.

Reduction of **116** with L-Selectride using conditions described by Oguchi *et al*. did not produce the expected α-hydroxyester **117**, but the fully reduced molecule **118**. By mass spectrometry a peak at m/z 469 corresponding to the formula $C_{30}H_{54}NaO_2$ and another at m/z 509 corresponding to formula $C_{32}H_{54}NaO_3$ were present. Although one structure fitted with m/z 469, **118**, three possible candidates have m/z 486, **119**-**121** (Figure 2.10).

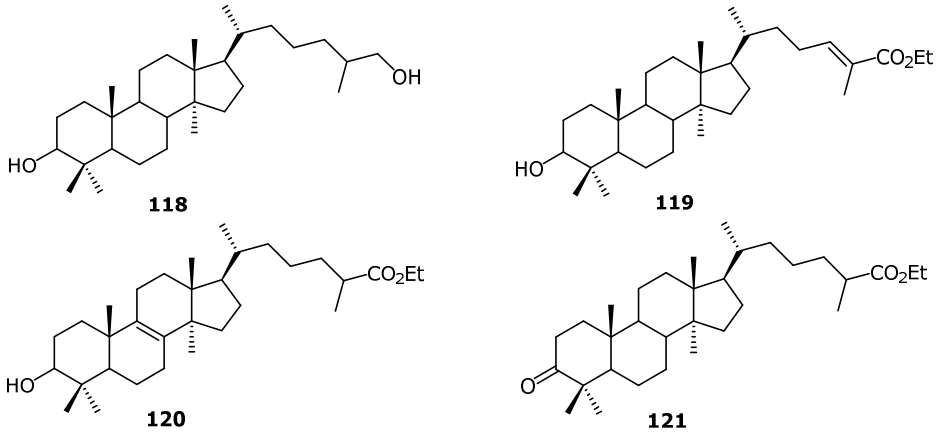


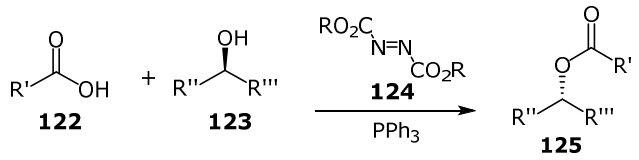
Figure 2.10 Possible products formed after the reduction of **116** with L-Selectride. Compound **118** has molecular formula $C_{30}H_{54}O_2$ and m/z 456; compounds **119-121** have molecular formula $C_{32}H_{54}O_3$ and m/z 486.

L-Selectride® chemoselectivity is similar to that of sodium borohydride, they react well with aldehydes and ketones to form the corresponding alcohols but they rarely react with esters. However, they have a natural tendency to reduce α,β-unsaturated systems. Analogue **116** has an α,β-unsaturated ester, therefore it was reduced by L-Selectride under the conditions used.

As a selective reduction was not appropriate for achieving the expected α-hydroxyl derivative **117**, a different approach was envisaged. In this case an inversion of configuration using a Mitsunobu reaction was studied.

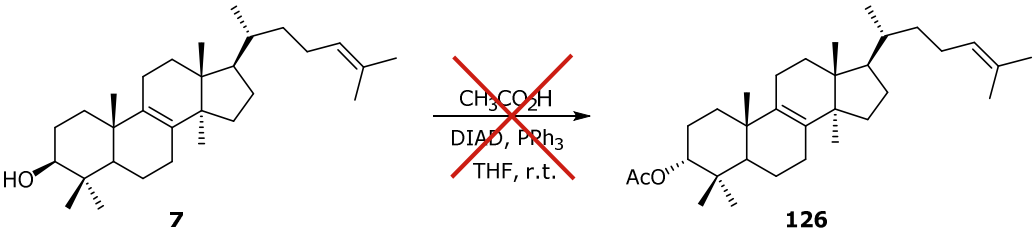
ii. Mitsunobu reaction. Formation of α-acetate **110**

Inversion of configuration of a secondary alcohol is a fundamental operation in synthetic organic chemistry. The Mitsunobu reaction constitutes the classical example for this type of reaction, in which an alcohol is converted to its inverted ester by the action of stoichiometric amounts of a carboxylic acid, a diazodicarboxylate and a phosphine (Scheme 2.33). This reaction was first described in 1967,[85,86] since then, many variations have appeared that try to solve some of the problems associated with it, such as reduction in the amount of by-products formed, reaction times or increasing the reactivity of hinder systems.[87]



Scheme 2.33 Mitsunobu reaction for the inversion of a secondary alcohol. In this reaction a carboxylic acid **122** and an alcohol **123** react with a diazodicarboxylate (DAD) **124** and triphenylphosphine to form the inverted ester of the starting alcohol **125**.

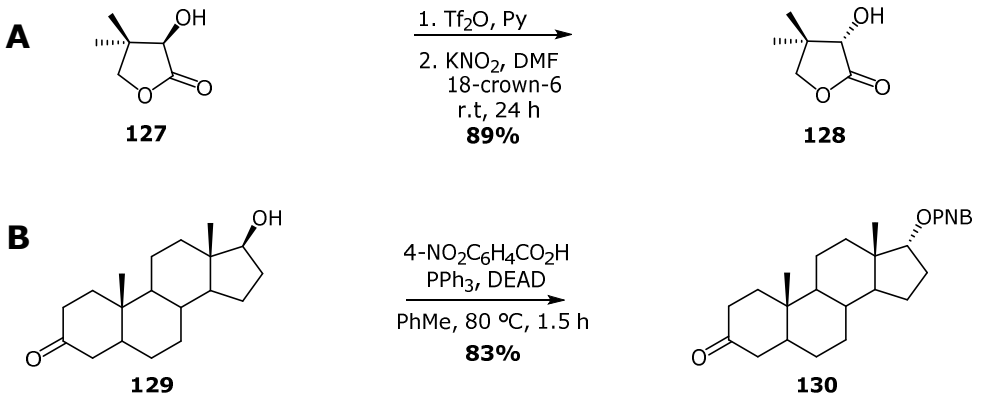
The commercial mixture of lanosterol was reacted under Mitsunobu conditions with acetic acid, diisiopropylazodicarboxylate (DIAD) and triphenylphosphine in tetrahydrofuran at room temperature for 1 h.[84] Mass spectrometry of the reaction mixture at that point revealed formation of triphenylphosphine oxide, but there were no indication of the desired inverted product, therefore the reaction was abandoned.



Scheme 2.34 Mitsunobu reaction of commercial lanosterol with acetic acid, diisopropylazodicarboxylte (DIAD) and triphenylphosphine in thetrahydrofuran at room temperature to form the inverted ester, α-lanosterol acetate. However, the reaction failed to yield the expected product.

Possibly the failure of the reaction in producing α-lanosterol acetate **126** was due to steric hindrance, C-3 hydroxyl in lanosterol is in a neopentyl-like system with two methyl groups at C-4. This type of system has been reported among the poorest candidates for an S_N2 reaction.[88-91] Nonetheless, Moriarty *et al.* succeeded in performing the inversion in two steps.[92] In the first step, a triflate ester of **127** was formed, which was then reacted with a large excess of potassium nitrite in the presence of catalytic amounts of 18-crown-6 ether to form **128** (Scheme 2.35 **A**). Excellent yields were obtained in all the cases studied. Alternatively, Dodge *et al.* managed to invert 17β-steroids by slightly modifying Mitsunobu conditions.[93] In their procedure, androgen **129** was treated with a relatively acidic carboxylic acid such a 4-nitrobenzoic acid in the Mitsunobu reaction. The desired inverted *p*-nitobenzoate ester **130** was achieved in excellent yields (Scheme 2.35 **B**). Unfortunately, due to time constraints none of these approaches were examined.

In an effort to understand the reasons of the failure in the Mitsunobu reaction for steric systems, Anh and co-workers prepared acyloxyphosphonium salts and investigated their fate after reaction with alcohols.[94] They found that deprotonation of the alcohol is not happening from the carboxylate ion but presumably from hydrazide anion **135** (Scheme 2.36 **B**) and that acylation of the alcohol came more likely from the acyloxyphosphonium ion **134** either with retention or inversion of configuration depending on the bulkiness of the alcohol (Scheme 2.36 **C**).



Scheme 2.35 Inversion of configuration of a secondary hindered alcohol. **A** Procedure envisaged by Moriarty *et al*. in which the alcohol **127** is first converted to its triflate and then inverted with potassium nitrite and 18-crown-6 ether, **128**.[92] **B** Mitsunobu modification described by Dodge *et al*.[93] In this process, *p*-nitrobenzoic acid (PNB), triphenyl phosphine and diethylazodicarboxylate (DEAD) reacted with androgen **129** to form the inverted androgen ester **130**.

Apparently, the stability of hydrazide phosphonium ion **133** plays an important role in the success of the Mitsunobu reaction. Hughes and Reamer studied the fate of the Mitsunobu reagents in the absence of alcohol.[95] They found that the stability of **133** is highly dependent on the carboxylate counterion, thus in acetic acid, **133** decomposed fairly quickly, from 15 min in dichloromethane or dimehtylformamide to 8 h in toluene at 2 ºC, nonetheless, the stability improved with increasing acidity of the acid, being very stable with 4-nitrobenzoic acid and chloroacetic acid, for which days where required to observe decomposition at room temperature. This observation suggested that in order for the Mitsunobu inversion to occur, the alcohol must react faster than the carboxylate.

With this information in hand, Ahn proposed a more complete mechanism for the Mitsunobu reaction (Scheme 2.36 **A**-**C**)[94]. In the first stage of the process, the azodicarboxylate reacts with triphenylphosphine to form phosphonium hydrazide **131** that preferencially undergoes proton transfer from the carboxylic acid to give carboxylate and phosphonium ion **133**. At this point, attack of the carboxylate to the phosphonium ion **133** generates acyloxyphosphonium ion **134** and hydrazide anion **135** (Scheme 2.36 **A**). In the second step, deprotonation of the alcohol by hydrazide anion **135** would produce the alkoxide **137** and hydrazide **136** (Scheme 2.36 **B**). Finally, in the last step, alkoxide **137** could either attack at phosphorous or transfer of acyl from acyloxyphosphonium ion **134**. In unhindered alcohols attack at the phosphorous is preferred, which leads to formation of the

phosphonium salt **138** followed by the nucleophilic attack of the carboxylate **132** to generate the inverted ester **125**; on the other hand, for hindered alcohols transfer of acyl could compete with the nucleophilic substitution reaction (Scheme 2.36 **C**). Additionally, more inversion product would be obtained even in hindered systems by increasing the stability of the phosphonium ion **134**. This process competes with the degradation of hydrazide anion **135** either by acyloxyphosphonium ion **134** to generate monoacylated hydrazide **140** or by carboxylic acid **122** to produce the hydrazide **136** and carboxylate **132** that could further react with acyloxyphosphium **134** to form the anhydride **141** (Scheme 2.36 **D**). Presumably, the formation of bisacylated hydrazide **144** is due to the attack of phosphonium hydazide ion **133** to acyloxyphosphonium ion **134** to form monoacylated phosphonium hydrazide **142** and carboxylate **132**. Transfer of phosphorous from **142** to carboxylate **132** generates acyloxyphosphonium ion **134** and monoacylated hydrazide anion **143**. Finally, nucleophilic attack of **143** to the carbonyl **134** will form the bisacylated hydrazide **144** (Scheme 2.36 **E**).[95]

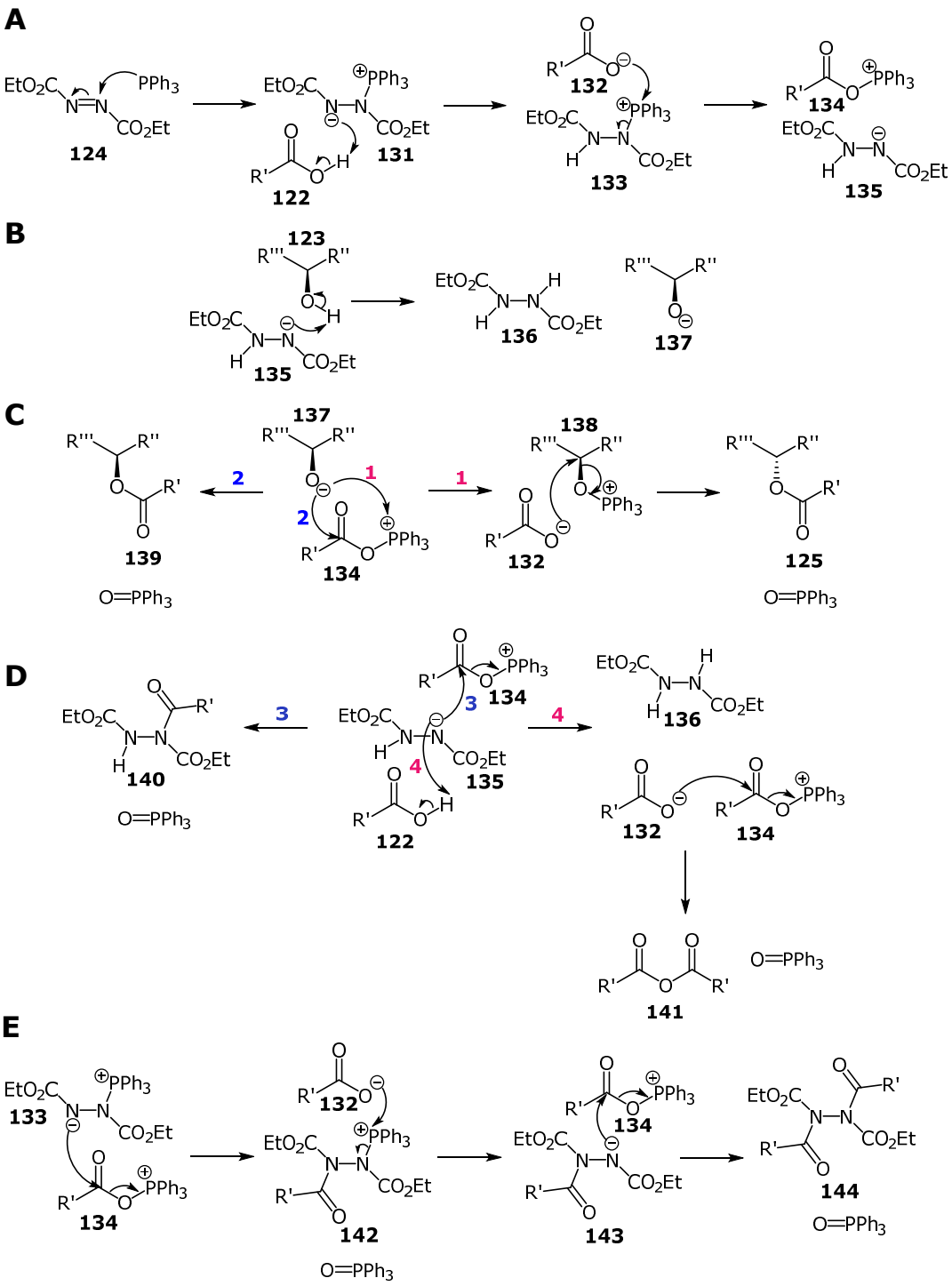
2.5.2. Modifications at B/C rings

Oxidation on rings B/C by incorporation of hydroxyls or ketones at positions C-7 and C-11 and conjugation of the double bond at $\Delta^{7(8),9(11)}$ were considered.

(a) Allylic oxidation

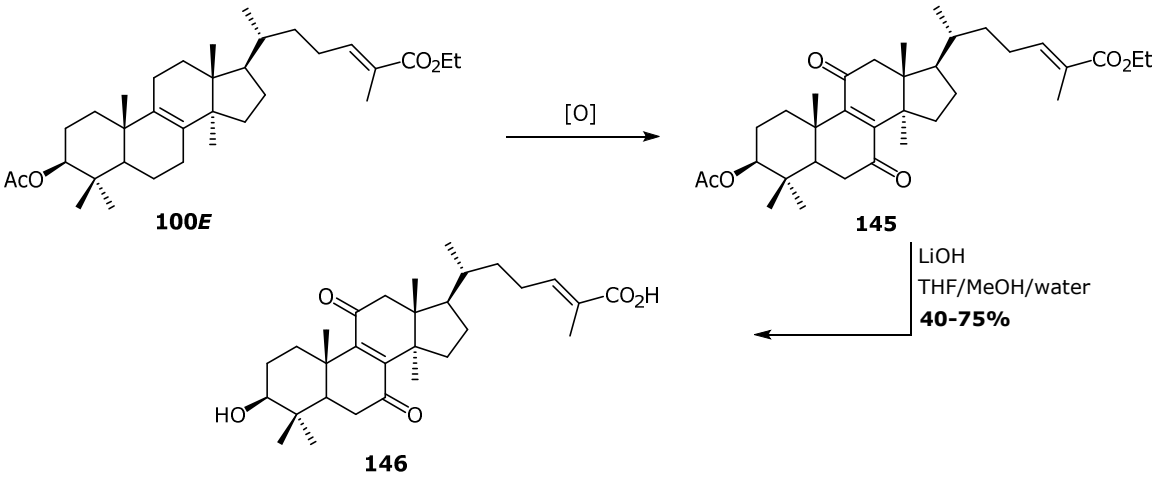
Allylic oxidations are of special interest in Organic Chemistry, since they allow the conversion of alkenes into allyl alcohols or enones. Therefore, they constitute one of the few fundamental method for C-H functionalization.[96]

Classically, these oxidations have been performed with chromium reagents. However, methods employing other metals that readily undergo one-electron redox processes such as manganese, rhodium, iron, copper or cobalt have been developed. Additionally, environmental friendly methods that are metal free have been reported.[96]



Scheme 2.36 Proposed mechanism for the Mitsunobu reaction.[94] Steps **A**, **B** and **C** describe the formation of inverted or retained ester; steps **D** and **E** describe the decomposition of hydrazide anion **135** to form hydrizide **136** and monoacylated hydrizide **140** and the decomposition of hydrazide phosphonium ion **133** in bisacylated hydrizide **144**.

i. Synthesis of analogue **146**



Oxidant	Conditions	Yield
CrO_3	H_2SO_4, acetone, 0-5 ºC	28%
	H_2SO_4, acetone, r.t.	37-58%
t-BuOOH	$RuCl_3$, hexane, r.t.	n/a
	$Rh_2(cap)_4$, DCE, 40 ºC	n/a
	$Fe(PFPP)Cl_3$, MeCN-H_2O, r.t.	41%
m-CPBA	1. $Fe(PFPP)Cl_3$, DCM, -78 ºC 2. $(COCl)_2$, DMSO, DCM, -78 ºC 3. Et_3N, r.t.	28%
$NaClO_2$	NHPI, MeCN-H_2O, 50 ºC	11%

Scheme 2.37 Synthetic route to **146**. Two step reaction consisting on allylic oxidation followed by hydrolysis. Different oxidants were studied for the first step, chromium oxide, *tert*-butylhydroperoxide with different catalysts, 3-chloroperbenzoic acid with *meso*-tetrakis-(pentafluorophenyl)porphyrin iron (III) chloride ($Fe(PFPP)Cl_3$) followed by Swern oxidation and sodium chlorite with *N*-hydroxy-phthalimide. Best yield achieved with chromium oxide at room temperature. Hydrolysis with lithium hydroxide afforded **146** in good yield.

Analogue **146** was synthesised following a two-step synthesis consisting of allylic oxidation of intermediate **100*E*** followed by hydrolysis with lithium hydroxide (Scheme 2.37). For the allylic oxidation leading to **145**, different oxidants were investigated.

a. Allylic oxidation. Synthesis of dioxo aceto-ester **145**

Highlighted in Scheme 2.37 are the different methodologies that were employed for the allylic oxidation of aceto-ester **100*E***. Briefly, the oxidation was performed using different oxidants, chromium trioxide, *tert*-butyl

hydroperoxide (TBHP) with different catalyst, 3-chloroperbenzoic acid in a two-step reaction and sodium chlorite with catalysis of *N*-hydroxy-phthalimide (NHPI).

1. Chromium trioxide

Mazoir developed a method for the allylic oxidation of triterpenes using excess of chromium trioxide in acetone at 0 ºC.[97] Using these conditions no reaction was observed until a few drops of concentrated sulfuric acid were added. The reaction at 0 ºC after 24 h was incomplete, unreacted starting material, monoketone **147** identified by MS m/z 540 corresponding to $C_{34}H_{52}NaO_5$ (Figure 2.11 for structure), and diketone **145** were isolated after chromatographic purification. The yield was improved when the reaction was carried out at room temperature, from 28% at 0 ºC to 37-58% at room temperature. The best yield was achieved when the reaction was worked up after the formation of the monoketone and the crude product reacted with more chromium trioxide. However, the reaction was both very messy, leading to a tedious purification step, and requiring long reaction times (over 24 h). Therefore alternative conditions were investigated.

2. tert-Butylhydroperoxide

Shingate reported a high yielding method for the allylic oxidation of lanosterol derivatives.[98] The allylic oxidation was performed with large excess of *tert*-butylhydroperoxide (TBHP) (70% aq. sol., 10 eq.) with catalysis of ruthenium trichloride (0.5 mol%). When this methodology was applied to precursor **100*E***, using either stoichiometric amounts or large excess of hydroperoxide, the expected diketone **145** was not observed by MS even after extended the reaction time to 7 days; instead monoketone **147** was the major MS peak observed in the stoichiometric reaction whereas with excess of hydroperoxide a mixed peroxide product was detected with m/z 628, **148**, together with the monoketone **147** (Figure 2.11). Shingate also reported the formation of the mixed peroxide intermediate at the beginning of the reaction, they found that extended the reaction time from 2 h to 6 h was enough to reduce its presence and to enhance the formation of the diketone at room temperature and that the time was reduced slightly, to 4 h, when the reaction was carried out at 30-35 ºC.

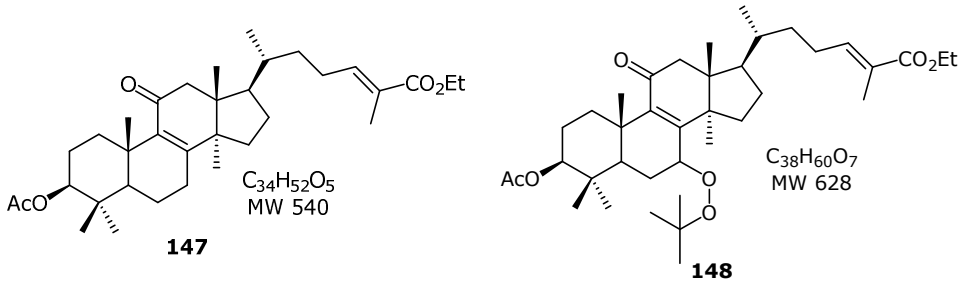
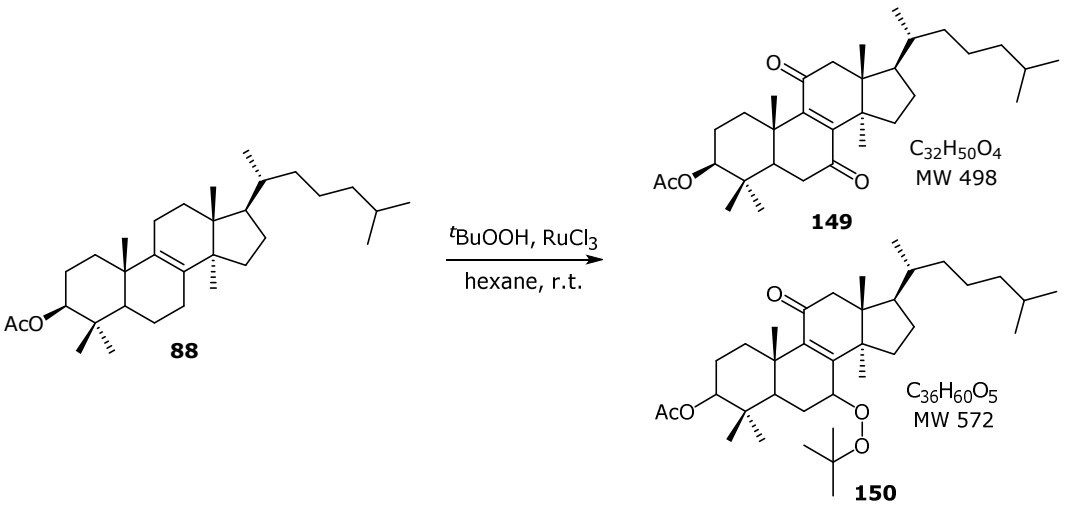


Figure 2.11 Possible mono-ketone **147** and mixed peroxide adduct **148** formed during the allylic oxidation reaction of precursor **100*E*** with TBHP and catalysis of ruthenium trichloride.

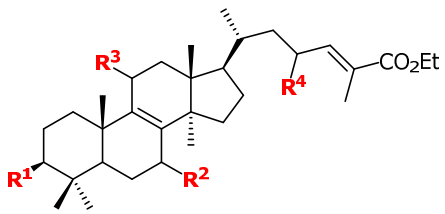
To know if we could repeat the reaction performed as described by Shingate, dehydrolanosterol acetate **88**, the model molecule used by them, was reacted using their conditions for the allylic oxidation with TBHP and ruthenium trichloride. The desired diketone **149** was detected after 5 h reaction with some of the mixed peroxide intermediate **150**. Possibly the better solubility of **88** in hexane influenced the better outcome of the reaction for dehydrolanosterol acetate **88** (Scheme 2.38). Miller solved the solubility issue by performing the allylic oxidation in dichloromethane, reporting excellent yields for this transformation.[99]

Doyle and Choi reported optimal conditions for the allylic oxidation of Δ^5-steroids with TBHP (70% aq. sol.) catalysed by rhodium caprolactamate.[100] In their procedure a load of 4-5 equivalents of TBHP and as little as 0.1-1.0 mol% of rhodium caprolactamate dissolved in 1,2-dichloroethane and performing the reaction at 40 ºC for 20 h were required for the allylic oxidation to occur in high yields. Intermediate **100*E*** was reacted under these conditions monitoring the reaction by MS. After 20 h reaction, MS showed five dominant peaks, m/z 563, 581, 595, 611 and 651. The first and last masses were also observed with ruthenium trichloride and they corresponded to the sodium adduct of the monoketone **147** and keto mixed peroxide **148** (Figure 2.11), the other three peaks might correspond to the sodium adduct of mixed hydroperoxide **152**, keto mixed hydroperoxide **153** and mixed dihydroperoxide **155**, respectively (Figure 2.12), nevertheless, none of the expected diketone **145** was observed.

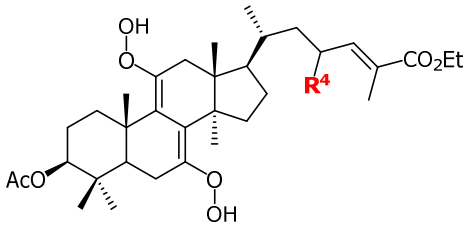


Scheme 2.38 Allylic oxidation reaction of dehydrolanosterol acetate **88** with *tert*-butylhydroperoxide and ruthenium trichloride. Diketone **149** and keto-peroxide **150** were detected by MS after 5 h reaction.

Doyle *et al*. also reported that the allylic oxidation reaction performed better when the reagents were added in two portions, one at the start of the reaction and the other after 16 h.[101] In this way the efficiency of the reaction was maximum, since the two limited factors for this allylic oxidation were overcome. On the one hand, the competition of the oxidation reaction (Scheme 2.39 **A**) with the radical chain decomposition of TBHP (Scheme 2.39 **C**) was bypassed by both increasing the number of equivalents of TBHP and raising the reaction temperature to 40 ºC. On the other hand, the reduction in the concentration of the catalytically active dirhodium species over time was surmounted by addition of the catalyst in two portions, one at the beginning and the other before the end of the reaction. In consequence, after the 22 h reaction more TBHP (2 eq) and rhodium caprolactamate (1 mol%) were added and the reaction was monitored after 5 h (27 h reaction). At that point, m/z 611 and 651 were the most intense peaks. Both peaks might be sodium adducts of mixed peroxides, the first one corresponding to **156** and the latter to **148**. Other masses observed were m/z 563 (**147**), 581 (**152**) and 595 (**153**), all of them detected after 20 h, yet their intensity apparently was decreased over time. In contrast, m/z 553, which might be the sodium adduct of MW 530 (**151**), increased dramatically. There is clearly a progress from monoketone **147** and mono mixed peroxides to the diketone **145** passing through the di mixed peroxides. However, the mass for the diketone **145** was still not present.



151-155



156-157

Compound	R^1	R^2	R^3	R^4	MW
151	-OH	-O-OH	-C=O	-H	530
152	-OAc	-O-OH	-H	-H	558
153	-OAc	-O-OH	-C=O	-H	572
154	-OAc	-C=O	-C=O	-O-OH	586
155	-OAc	-C=O	-C=O	-O-O^{t}Bu	642
156	-	-	-	-H	588
157	-	-	-	-O-O^{t}Bu	676

Figure 2.12 Possible products formed in the allylic oxidation with TBHP with rhodium caprolactamate.

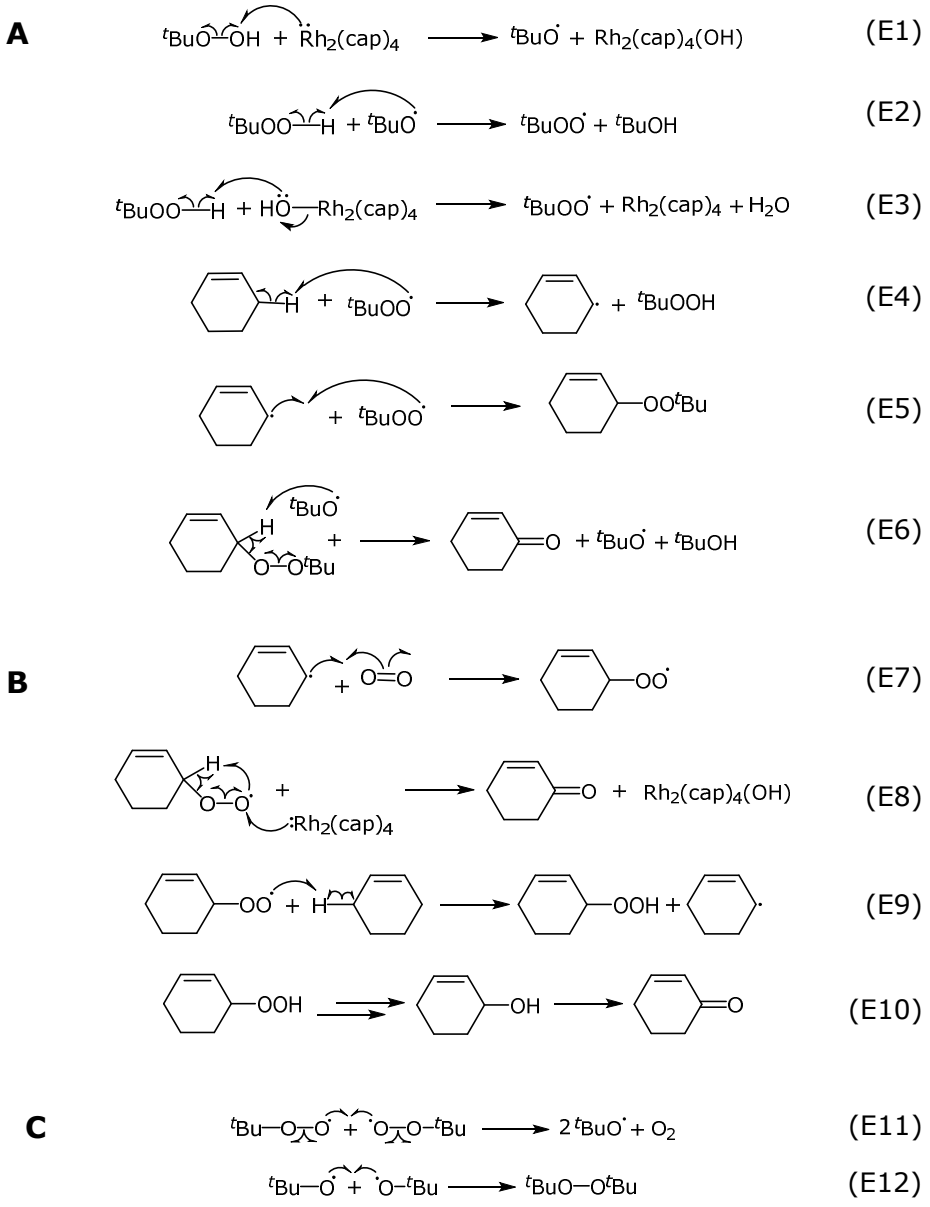
MW	MW+Na	Reaction Time/MS intensity (%)			
		20 h	**27 h**	**48 h**	**5 d**
530	553	38	72	**99**	62
540	563	78	51	-	-
554	577	-	-	43	-
558	581	**100**	86	53	-
572	595	62	53	-	-
586	609	-	-	52	23
588	611	72	**95**	**91**	-
628	651	**87**	**100**	74	-
642	665	-	-	-	**100**
676	699	-	-	45	**80**

Table 2.3 Comparison of the mass intensity detected after 20 h, 27 h, 48 h and 5 d allylic oxidation reaction with TBHP catalysed by rhodium caprolactamate.

The reaction was left ongoing for another day, and after 48 h it was monitored by MS. The two major peaks were m/z 553 and 611, mass of the monoketone **147** disappeared and the mixed peroxide **152** decreased considerably. Three new peaks were detected, m/z 577, 609 and 699. Eventually, the mass of diketone **145** was observed (MW 554), but accompanied of over oxidation products, **152** and **157**. To favour an increase in the diketone **145** the reaction continued for three further days (5 days reaction). However, what was observed was an increase in over

oxidation products m/z 665 (**155**) and 699 (**157**) with complete depletion of the desired diketone **145** peak.

Table 2.3 shows the different masses observed during the oxidation reaction and their MS intensity over time.



Scheme 2.39 Proposed mechanism for the allylic oxidation with TBHP. **A** Allylic oxidation with TBHP catalysed by rodhium caprolactamate. **B** Involvement of oxygen during the allylic oxidation. **C** Decomposition of the *tert*-butylperoxy radical.[101]

In order to understand the process that is taking place during the allylic oxidation reaction, Doyle *et al.* studied the fate of this transformation for α,β-unsaturated carbonyl compounds as substrates having electron-withdrawing substituents are generally less reactive, requiring both greater

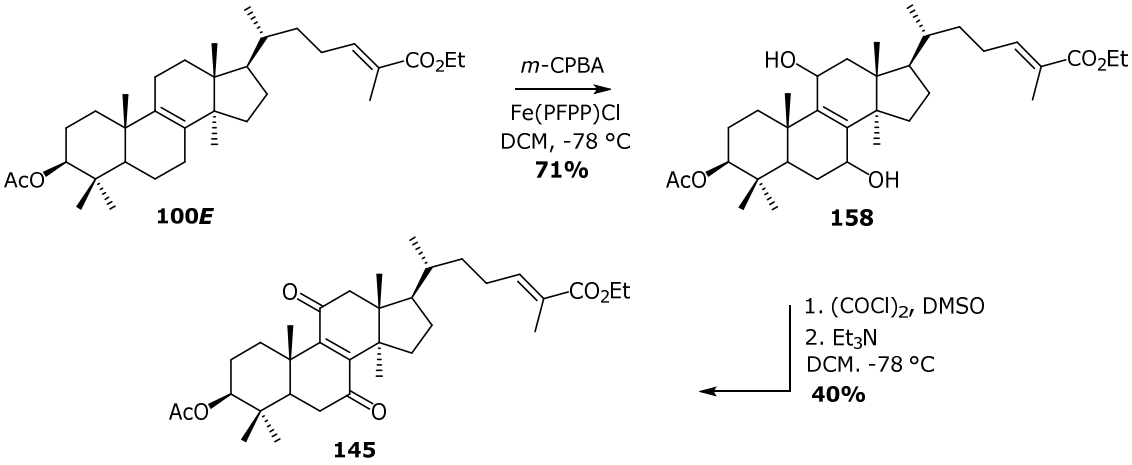
amounts of TBHP and higher catalyst loading to reach completion.[101] They found that the allylic oxidation with TBHP and different catalyst occurs through the same pathway for all the catalyst studied: dirhodium (II) caprolactamate, ruthenium trichloride, cupper (I) iodide or palladium hydroxide, via allyl free radical formation. Scheme 2.39 outlines the mechanistic pathway proposed by Doyle for dirhodium (II) caprolactamate-mediated allylic oxidation using cyclohexene as the model olefinic substrate.

Alternatively, Bandyopadhyay and Awarwala described a method for the C-H activation of cyclohexane and cyclohexene by the use of electronegatively substitututed iron (III) porphyrins such as Fe(PFPP)Cl (*meso-tetrakis* (pentafluorophenyl) porphyrin iron (III) chloride), which constitute a very good model compound for cytochrome P-450 enzymatic oxidation.[102] They claimed that selective allylic hydroxylation of cyclohexene occurred in high yield using TBHP and catalytic amounts of Fe(PFPP)Cl dissolved in 90.9% wet acetonitrile at room temperature and under argon atmosphere for 10 min. However mixed-solvent systems like methanol:dichloromethane 1:2 produced three compounds, the epoxide (50%), the hydroxylate (14%) and the ketone (8%). UV studies suggested the exchange of axial chloro in Fe(PFPP)Cl_3 by hydroxyl in aqueous acetonitrile which acted as the active catalyst for the allylic hydroxylation. Formation of oxo-iron (IV) porphyrin cation radical by TBHP, initiated a radical chain reaction sequence with formation of the allylic hydroxylated product. Interestingly, when the reaction was performed in the presence of oxygen, the ketone was the major product observed. In order to explore this last observation in our pursuit to generate dioxo allylic compound **145**, aceto-ester **100*E*** was reacted under Bandyopadhyay conditions. However, the reagents were not soluble in acetonitrile, therefore dichloromethane was added to assist in the dissolution. A brown biphasic solution was formed which changed colour to brown-green-yellowish after 1 h reaction. Nevertheless, analysis by MS revealed only starting material present after 16 h reaction. At that point, more TBHP and catalyst were added, as well as increasing the proportion of water in the reaction. Monoketone **147**, diketone **145** and mixed peroxide **148** were detected after the addition of 2.2 eq of TBHP, increasing the total equivalents of TBHP to 5.8 and extended the reaction time to six days resulted in increasing the formation of over oxidation products. After purification by column chromatography diketone **145** was isolated in 41% yield.

To summarise allylic oxidation with TBHP seemed very attractive, but the reaction was perturbed by the formation of mixed peroxides, extended reaction times and difficulty in the isolation of the desired product.

3. 3-Chloroperbenzoic acid

Konoike *et al.* described a method for the allylic hydroxylation of hindered alkenes in triterpenes.[103] In their methodology, the allylic hydroxylation was carried out with 3-chloroperbenzoic (*m*-CPBA) acid with catalyst of Fe(PFPP)Cl in dichloromethane at -78 ºC. They reported that the allylic dihydroxylation occurred in good yield for dehydrolanosterol when three equivalents of *m*-CPBA were used in the reaction. Thus, we attempted to form dioxo aceto-ester **145** from precursor **100*E*** by a two-step process, allylic dihydroxylation followed by Swern oxidation (Scheme 2.40).[103, 104] Aceto-ester **100*E*** was reacted with *m*-CPBA (3.2 eq) and Fe(PFPP)Cl_3 (3 mol%) at -78 ºC for 8 h allowing to reach room temperature thereafter, desired dihydroxylated compound **158** was isolated in 71% yield after chromatographic purification. Swern oxidation of **158** generated the di-oxo aceto-ester **145** in modest yield (40%), dihydroxylated aceto-ester **158** (17%) was also recovered after purification. Overall 28% yield over the two steps was afforded.

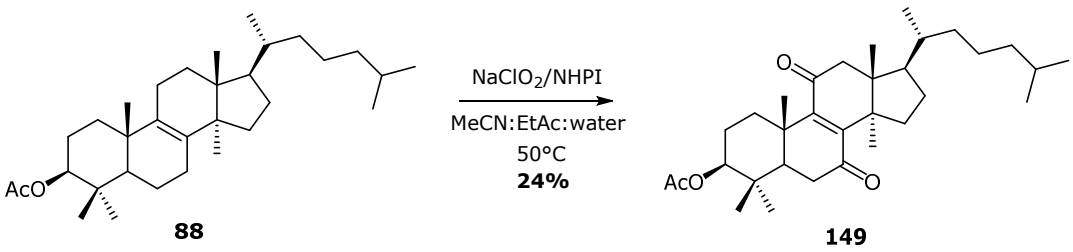


Scheme 2.40 Allylic oxidation of aceto-ester 100*E* following a two-step synthesis. In the first step hydroxylation with *m*-CPBA and Fe(PFPP)Cl formed dihydroxy-aceto-ester **158**;[103] in the second step, Swern oxidation produced the allylic dioxo-aceto ester **145**.[104] *m*-CPBA = 3-chloro-perbenzoic acid; Fe(PFPP)Cl = *meso*-tetrakis(pentafluorophenyl)-porphyrin iron (III) chloride.

4. Sodium chlorite

The development of metal-free oxidations as environmentally friendly processes is of current interest. One such new methodology is the allylic and benzylic oxidation reaction with sodium chlorite developed by Silvestre and Salvador.[105] They described two procedures for this transformation. A combination of sodium chlorite (1.2 equivalents) with TBHP (5 equivalents) in the homogeneous solvent mixture acetonitrile/water 3:1 at 50 ºC or alternatively, sodium chlorite (1.5 equivalents) catalysed by *N*-hydroxyphthalimide (NHPI) (0.1 equivalents) in acetonitrile/water 2:1 or 3:1 at 50 ºC produced the allylic oxidised products in excellent yield and good chemoselectivities. The reaction proceeded via free-radical species by formation of chlorine dioxide radical when sodium chlorite was heated at 50 ºC, which in turn generated *tert*-butylhydroperoxy radical by homolytic cleavage of TBHP in the first process or phthalimide-*N*-oxyl (PINO) radical in the second. These reactive intermediates initiated the allylic hydrogen abstraction, forming the olefin radical which was further oxidised via a radical chain mechanism to the corresponding enone.

In a first attempt of the reaction, dehydrolanosterol acetate **88** and NHPI (0.05 equivalents) were dissolved in a mixture acetonitrile/ethyl acetate/water 2:4:1 as acetonitrile alone failed to dissolve the substrate. However, this solvent system was biphasic (Scheme 2.41). The solution was heated at 50 ºC before the addition of sodium chlorite (1.5 equivalents). The solution became red-brown with little gas evolution which changed to brown and yellow after 3 h. At that point MS showed formation of monoketone **159** as the most intense peak, hydroxyketone **160** and dihydroxyl MW **161** were also detected, but at much lower intensity (Figure 2.13).



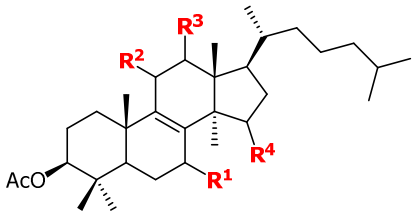
Scheme 2.41 Allylic oxidation of dehydrolanosterol **88** with sodium chlorite and catalysis of *N*-hydroxyphthalimide.

In order to accelerate the formation of the desired diketone, supplementary equivalents of NHPI (0.05 equivalents) and sodium chlorite (0.9 equivalents)

were added. After the addition, the aqueous solution became dark yellow. MS 8 h after the further addition revealed formation of diketone **149**, however, the monoketone **159** was still the most intense peak. Over-oxidation was also taking place, dihydroxyl-diketone **166** was observed in the MS profile.

Eventually, expected diketone **149** was the major peak after a further addition of reagents was performed, NHPI (0.3 equivalents) and sodium chlorite (0.8 equivalents) and the reaction was carried out for another 8 h. Nevertheless, monoketone **159** was still very intense and over-oxidised products **162**, **163**, **164** were detected as well. The reaction was stopped at that point.

Chromatographic purification furnished diketone **149** in poor yield (24%) possibly because of the formation of over-oxidised products. The following compounds were also isolated **159** (3%), **162** (9%), **161** (18%), **164** (13%) and **166** (22%).

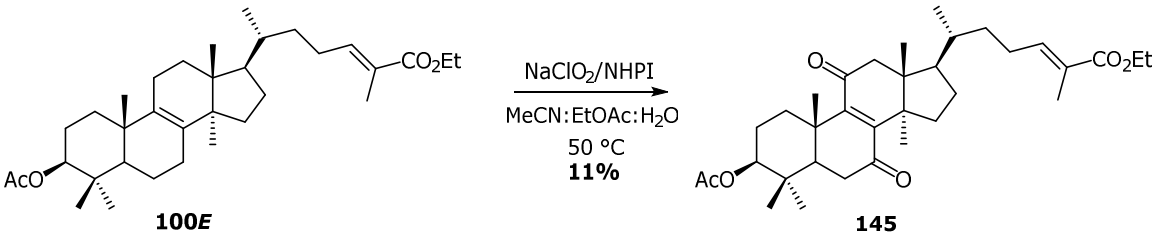


Compound	R^1	R^2	R^3	R^4	MW
159	-H	-C=O	-H	-H	484
160	-OH	-C=O	-H	-H	500
161	-OH	-OH	-H	-H	502
162	-C=O	-C=O	-H	-C=O	512
163	-C=O	-C=O	-H	-OH	514
164	-OH	-C=O	-H	-OH	516
165	-C=O	-C=O	-OH	-C=O	528
166	-C=O	-C=O	-OH	-OH	530

Figure 2.13 Possible compounds formed during the allylic oxidation of dihydrolanosterol **88** with sodium chlorite in catalysis of NHPI. Structure were deduced by HRMS.

The reaction was repeated, this time using aceto-ester **100*E*** as substrate for the allylic oxidation (Scheme 2.42). NHPI (0.1 equivalents) and sodium chlorite (1.5 equivalents) together with **100*E*** were suspended in acetonitrile, a few drops of ethyl acetate and water were also added to assist in the solution of the reagents. The colour of the reaction changed from

yellow to orange-red after heating at 50 ºC. The reddish colour faded after 1 h, becoming yellow. MS after 20 h showed monoketone **147** as the most intense peak (Figure 2.14), aceto-ester **100*E*** and diketone **145** were also detected, though at much less intensity.

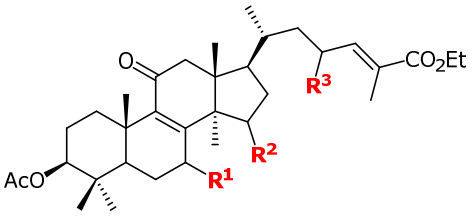


100*E* **145**

Scheme 2.42 Allylic oxidation of **100*E*** with sodium chlorite and *N*-hydroxyphthalimide (NHPI) to form dioxo-aceto-ester **145**.

To force the reaction to the formation of the diketone **145**, more NHPI (0.1 equivalents) and sodium chlorite (0.9 equivalents) were added. This provoked a change in the solution colour from yellow to red, which faded to yellow after 5 min. MS after additional 8.5 h showed complete conversion of **100*E*** to monoketone **147** with increasing proportions of desired diketone **145**, overoxidised products **168**, **169** and **170** were also detected at that point. The reaction continued for 72 h. After chromatographic purification, the following products were isolated: MW **147** (4%), diketone **145** (11%), **168** (15%), **169** (3%), **170** (24%), **172** (15%) and **173** (11%). The other fractions contained mixtures (Figure 2.14).

To summarise, the allylic oxidation reaction with sodium chlorite and catalysis of NHPI produced the monoketone **147** almost exclusively after 20 h reaction. Forcing the conditions to generate the diketone **145** competed with over-oxidation, with dihydroxyketone **170** being the major product after 5 d reaction. Further studies should be carried out to optimise the formation of diketone **145**. Alternatively, Lardy *et al.* described a method for non-metal allylic oxidation using TBHP (6 equivalents) and sodium hypochlorite (2 equivalents) at 2-5 ºC.[106]



147, **167**-**173**

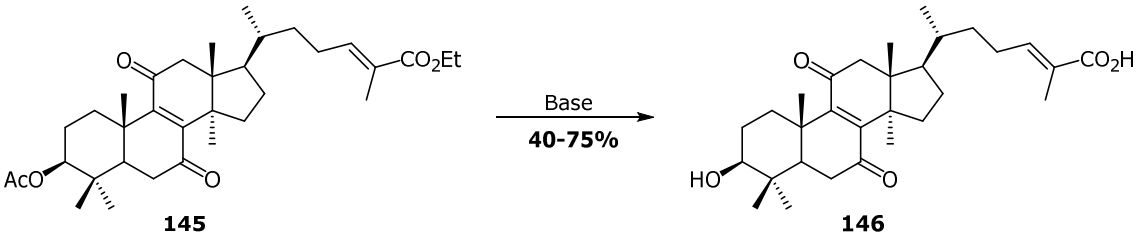
Compound	R^1	R^2	R^3	MW
147	-H	-H	-H	540
167	-OH	-H	-H	556
168	-C=O	-H	-C=O	568
169	-C=O	-H	-OH	570
170	-OH	-H	-OH	572
171	-C=O	-C=O	-C=O	582
172	-C=O	-OH	-C=O	584
173	-C=O	-OH	-OH	586

Figure 2.14 Possible compounds formed during the allylic oxidation of **100*E*** with sodium chlorite in catalysis of NHPI as judged by MS. Structures were deduced by HRMS.

Diketone aceto-ester **145** is a novel compound. It was identified by MS, m/z 577 corresponding to MW 554 and formula $C_{34}H_{50}O_6$ was detected. ^{13}C-NMR revealed four carbonyl carbons at δ 202.4, 201.9, 170.9 and 168.4 ppm, the two first corresponding to the ketones and the two latter to the esters. Deshielding shift in ^{1}H-NMR for H-1β that appeared as doublet of triplets at δ 2.89 ppm (*J* = 13.8, 3.7 Hz, 1H), H-12β as doublet of doublets at δ 2.76 ppm (*J* = 15.9, 1.2 Hz, 1H), H-12α as doublet at δ 2.61 ppm (*J* = 15.8 Hz, 1H) and H-6 at 2.55 – 2.38 ppm (m, 2H).

In conclusion, several methods for the allylic oxidation of aceto-ester **100*E*** were investigated. From classic oxidation with chromium trioxide to metal-free oxidations with sodium chlorite with catalysis of NHPI. None of the methods evaluated were successful in producing clean high yielding reactions, instead 11-58 % yield was achieved for many of them, being the best methodology the classic reaction with chromium trioxide, performing the reaction stepwise, allowing the formation of the monoketone **147** and then reacting the crude product with new oxidant.

b. Hydrolysis. Synthesis of diketone **146**



145 **146**

Base	Conditions	Yield (%)
KOH	EtOH, 60 ºC	61[a]
LiOH	THF/H_2O/EtOH 2:2:1; r.t.	75
	THF/H_2O/MeOH 1:1:1; r.t.	40[b]
	THF/H_2O/MeOH 3:1:1; r.t.	63

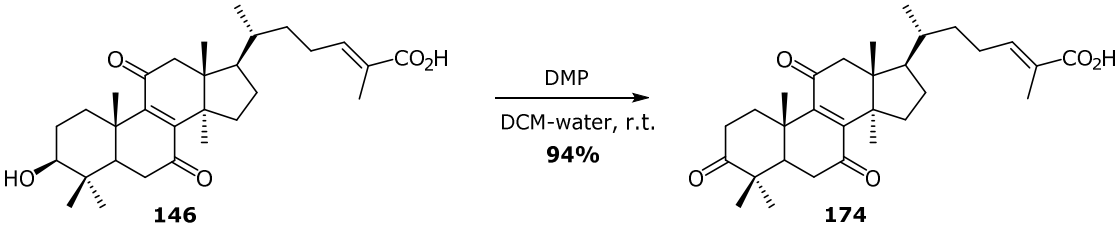
Scheme 2.43 Conditions investigated for the hydrolysis of dioxo aceto-ester **145**. ***a*** Product crude not purified, mixture of two compounds detected by TLC (SiO_2; EtOAc:PE 3:1). ***b*** Unreacted **145** was recovered after purification (56%).

Hydrolysis of **145** under basic conditions produced **146** in modest to excellent yield (40-75%) (Scheme 2.43). As bases, potassium hydroxide and lithium hydroxide were evaluated. With potassium hydroxide in ethanol at 60 ºC,[37] two spots were detected by TLC (SiO_2;EtOAc:PE 3:1) after 3 h reaction, being the product the more polar one. A better outcome was achieved with lithium hydroxide in THF/water/ROH at room temperature, as ROH, ethanol or methanol were considered.[60] In order to enhance the solubility of the base and the substrate, and, hence, the yield of the reaction, it was essential to keep a define ratio of the different solvents. Excellent yield (75%) was achieved with tetrahydrofuran/water/ethanol in 2:2:1 ratio, after 20 h reaction. Experiments with methanol showed incomplete reaction after 16 h and 1:1:1 ratio. The desired hydroxyl-diketo-acid **146** and the starting material **145** were isolated after chromatographic purification in 40% and 56% yield, respectively. Increasing the proportion of tetrahydrofuran helped in the transformation, thus a 3:1:1 solvent ratio furnished 63% of **146** after 22 h reaction. Purification by crystallisation was successful with the mixtures of MeOH:DCM 1:1 and 3:1.

Analogue **146** was recently isolated from the fruiting bodies of *G. resinaceum*.[107] However, this is the first time that a synthetic route to it has been described. Compound **146** was identified by MS, m/z 507 corresponding to the sodium adduct of MW 484 and formula $C_{30}H_{44}O_5$. In addition, the appearance of the H-3 doublet of doublets at lower frequencies

δ 3.28 ppm (dd, *J* = 11.2, 5.1 Hz, 1H) and disappearance of the signal for ethyl at δ 4.18 ppm (q, *J* = 7.1 Hz, 2H) and 1.28 ppm (t, *J* = 7.1 Hz, 3H) and the methyl in the acetate group at δ 2.05 ppm (s, 3H) in the ^{1}H-NMR confirmed that the ester groups were hydrolysed. From the ^{13}C, three carbonyl carbons were found δ 202.5 ppm, 202.3 ppm and 173.0 ppm corresponding the two first to ketones and latter one to a carboxylic acid.

ii. C-3 Oxidation. Synthesis of analogue **174**



Scheme 2.44 Formation of analogue **174** from Dess-Martin oxidation of **146**.

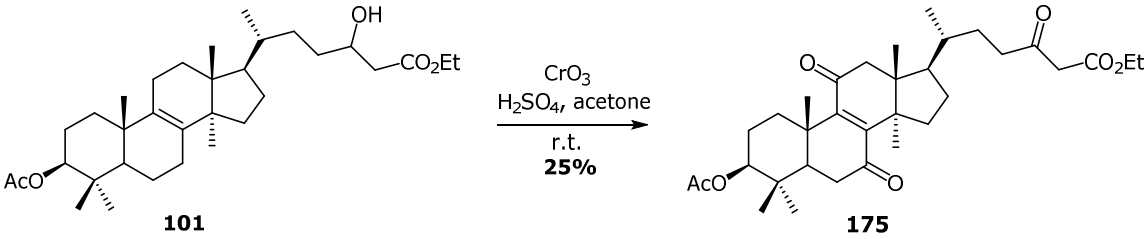
Analogue **174** was formed by Dess-Martin (D-M) oxidation of **146**, following the procedure described by Meyer and Schreiber for the acceleration of the D-M reaction by water (Scheme 2.44).[80] The bright yellow solution of **146** in dichloromethane became cloudy after the addition of the periodinane. Moreover, precipitation was observed after the addition of the mixed solvent DCM/water 1000:1. Nevertheless after 40 min, the reaction reached completion. After chromatographic purification **174** was isolated in excellent yield (94%) as yellow solid. Interestingly, Meyer and Schreiber highlighted that in reactions with water and without excess of DMP, the homogeneity of the reaction was crucial for the oxidation of the substrate. In our case, despite the precipitation almost full conversion was observed. Nonetheless, repeating the reaction on a smaller scale resulted in recovery of the unreacted **146**. Different solvent systems were investigated for the crystallisation; mixtures of DCM:hexane and DCM:MeOH produced an oil, while precipitation was observed with mixtures of EtOAc:hexane.

Direct allylic oxidation of **107** under Mazoir conditions was evaluated for the formation of **174.**[97] The reaction produced a mixture of compounds among them the desired triketone **174**. As the reaction produced complex products, no further investigations were performed based on this route.

Analogue **174** was isolated from the fruiting bodies of *Antrodia camphorata.*[108] Although its chemical structural was elucidated, this is the first time that a synthesis has been reported. Analogue **174** was identified

by MS, a peak at m/z 505 was observed, which corresponded to the sodium adduct of MW 482 and formula $C_{30}H_{42}NaO_5$. Disappearance of the doublet of doublets at δ 3.28 ppm (dd, *J* = 11.2, 5.1 Hz, 1H) corresponding to the hydroxyl at C-3 in **146**, in ^{1}H-NMR and the appearance of four carbonyl groups in ^{13}C-NMR at δ 215.9, 202.1, 201.5 and 173.2 ppm confirmed that **174** has three ketones and a carboxylic acid in its structure.

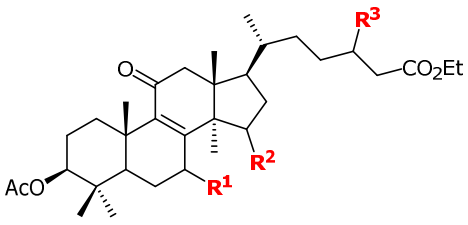
iii. Allylic oxidation. Synthesis of triketo-acetoester **175**



101 **175**

Scheme 2.45 Formation of triketone **175** from allylic oxidation of Reformatsky adduct **101** with chromium (VI) oxide.

Allylic oxidation of Reformatsky adduct **101** using Mazoir conditions produced the expected triketone **175** (Scheme 2.45).[97] The reaction was performed with acidic chromium trioxide, which carried out both processes, oxidising the hydroxyl at C-24 and oxidising the allylic positions C-7 and C-11. Several spots were observed on TLC (SiO_2; Et_2O:PE 2:3). However, the major product corresponded to the desired triketone **175**, although it was isolated after purification in a modest yield, 25%. Two other compounds were eluted after column chromatography and identified by MS, diketone **176** (11%) and tetraketone **177** (traces) (Figure 2.15 for plausible structures).

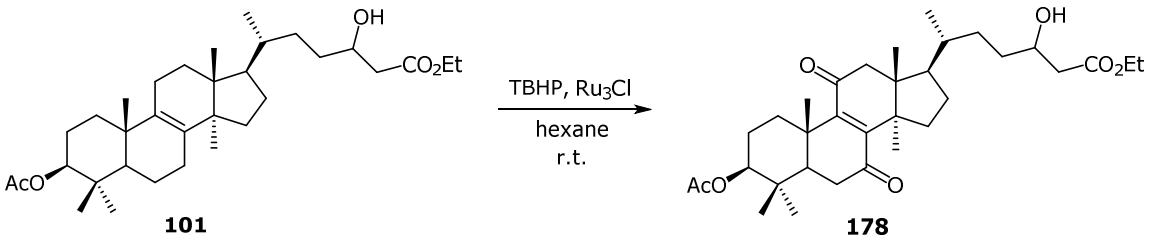


176-177, 179-180

Compound	R^1	R^2	R^3	MW
176	-H	-H	-C=O	542
177	-C=O	-C=O	-C=O	570
179	-C=O	-H	-OH	544
180	-O-O^{t}Bu	-H	-OH	632

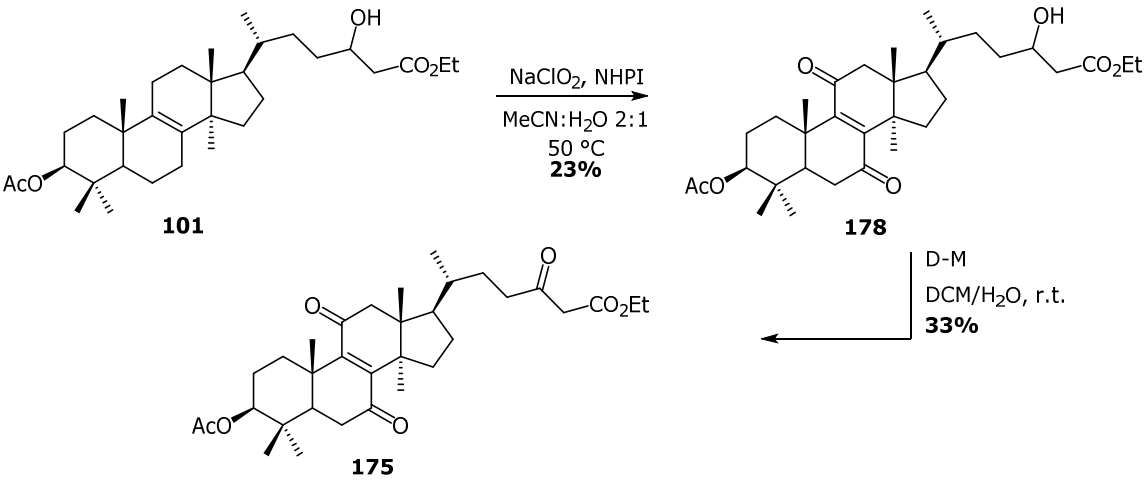
Figure 2.15 Possible minor products formed in the allylic oxidation of **101**.

Two other reaction conditions were evaluated for the formation of **175**. In the first, a Reformatsky adduct **101** was reacted under conditions described by Shingate *et al*., using TBHP (20 eq) and ruthenium (III) chloride for the allylic oxidation (Scheme 2.46).[98] The reaction was stirred at room temperature for 24 h, observing a change in the colour of the solution from dark to grey-green. Unlike the reaction with chromium trioxide, TBHP with ruthenium trichloride did not oxidise the side chain hydroxyl. This observation was noted by Shingate *et al.* as well.[98] Analysis by MS, detected the formation of hydroxy-ketone **179**, hydroxy-diketone **178** and hydroxyl-mixed peroxide **180** (*Figure 2.15*). According to Shingate, improved yields of the diketone were obtained when the reaction was carried out at 40 ºC, therefore increasing the temperature could enhance the formation of the desired diketone product. However, no further optimisation of the reaction conditions were performed.



Scheme 2.46 Allylic oxidation of **101** using TBHP and ruthenium (III) chloride.

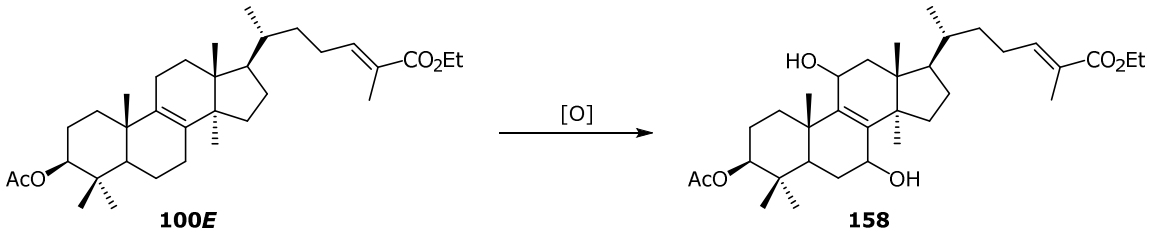
The last approach consisted of reacting hydroxy-aceto-ester **101** with sodium chlorite (1.5 equivalents) and catalysis by NHPI (0.06 equivalents) in acetonitrile:water 2:1 at 50 ºC according to a procedure developed by Silvestre (Scheme 2.47).[105] The suspension became yellow after the addition of NHPI, the colour that faded after the addition of sodium chlorite. MS revealed the hydroxyketone **179** as the most intense peak after 17 hours reaction, very little of the hydroxydiketone **178** was also detected. Further addition of NHPI (0.1 equivalents) and sodium chlorite (2.9 equivalents) and leaving the reaction for an additional 50 h increased the formation of **178**, however, hydroxyketone **179** was still the most intense peak after 34 h. Allowing the reaction to continue for a further 16 h reduced considerably the intensity of hydroxyketone **179** and increased hydroxydiketone **178**. Chromatography purification afforded this latter compound in poor yield (23%). Finally, Dess-Martin oxidation of hydroxydiketone **178** afforded triketone **175** in poor yield (33%).



Scheme 2.47 Formation of triketone **175** following a two-step synthesis; allylic oxidation with sodium chlorite and *N*-hydroxyphthalimide (NHPI) to form **178** followed by D-M oxidation to **175**. D-M = Dess-Martin.

Triketone **175** is a novel compound. It was identified by MS, m/z 579 corresponding to MW 556 and formula $C_{33}H_{48}O_7$ was detected. Five carbonyl carbons appeared on the ^{13}C-NMR spectrum: δ 203.1, 202.3, 201.9, 171.0 and 167.4 ppm. The three first for the three ketones and the two latter for the ester groups. Deshielding of chemical shifts for H-1β, H-6, H-12, H-23 and H-25 in the ^{1}H-NMR, singlet at δ 3.44 ppm (s, 2H, H-25), doublet of triplets at 2.89 ppm (dt, *J* = 13.8, 3.7 Hz, 1H, H-1β), doublet at 2.76 ppm (d, *J* = 15.8, 1.2 Hz, 1H, H-12), doublet at 2.59 ppm (d, *J* = 16.1 Hz, 1H, H-12), δ 2.65 – 2.54 ppm (m, 1H, H-23), 2.54 – 2.42 (m, 3H, H-6, H-23).

(b) Allylic hydroxylation. Synthesis of analogue 158.



Oxidant	Conditions	Yield (%)
TBHP, SeO_2	DCM, r.t.	10
TBHP, Fe(PFPP)Cl	MeCN-H_2O, r.t.	0
m-CPBA, Fe(PFPP)Cl	DCM, -78 ºC	64-71

Scheme 2.48 Synthesis of dihydroxy-aceto-ester **158**. Three approaches were investigated, oxidation with TBHP and selenium oxide and both TBHP and *m*-CPBA with catalysis of Fe(PFPP).

Three approaches were followed for the allylic hydroxylation of aceto-ester **100*E***. Oxidation with TBHP and catalysis of selenium dioxide or Fe(PFPP)Cl and *m*-CPBA and catalysis of Fe(PFPP)Cl.

Selenium dioxide is the classic reagent for performing allylic hydroxylations. However, the formation of reduced forms of selenium, the difficulty of removing colloidal selenium from the products, and the formation of organoselenium by-products led to the development of a more efficient methodology for this transformation. Thus, Sharpless and Umbreit devised a procedure in which catalytic selenium dioxide was used together with TBHP to achieve high yields of the allylic hydroxylated product.[109] The reaction proceeded under mild conditions, 24 h at room temperature, and required 3-4 equivalents of the TBHP for better performance. A smooth reaction was achieved with dichloromethane and one equivalent of water or catalysis by a carboxylic acid. Nevertheless, a higher proportion of selenium oxide was required for unreactive olefins, a powerful system was the combination of 0.5 equivalents of selenium dioxide with two equivalents of the TBHP in dichloromethane at room temperature for 1-2 days without the need of the carboxylic acid catalysis.

Aceto-ester **100*E*** was reacted under Sharpless conditions for allylic hydroxylation: TBHP (2 equivalents) and selenium dioxide (0.5 equivalents) were reacted with **100*E*** in dichloromethane at room temperature (Scheme 2.48). Very little formation of product was detected after 24 h reaction, therefore a large excess of TBHP (8 equivalents) was further added and the reaction was stirred for four days. The work-up was hindered by the appearance of a red-orange precipitate after quenching the reaction with sodium bicarbonate. To facilitate the extraction process the suspension was filtered. The reaction was very messy with several spots to separate. After chromatography purification, expected diol **158** was isolated in very poor yield (29%), monoketone **147** (29%) and unreacted aceto-ester **100*E*** (40%) were recovered, as well. Sharpless highlighted the importance of stopping the reaction at two-thirds completion to avoid competition with over oxidation of the products.

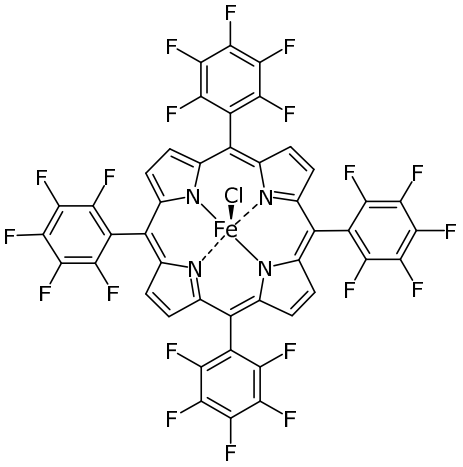


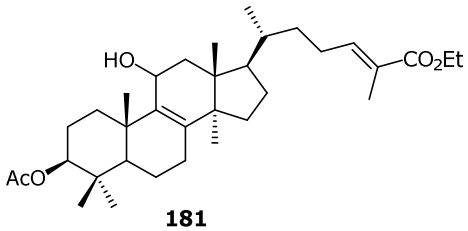
Figure 2.16 Chemical structure of iron (III) perfluorotetraphenylporphyrin chloride (Fe(PFPP)Cl).

In view of the lack of reactivity for the dihydroxylation with selenium dioxide alternatives routes were envisaged. As stated in the section above, both Bandyopadhyay and Konoike described methods for allylic hydroxylations mimicking oxidation with cytochrome P450 by using an electronegative substituted iron porphyrin, Fe(PTTP)Cl as catalyst (Figure 2.16).[102,103] Their approaches differed in the conditions to perform the reaction. Bandyopadhyay used TBHP in acetonitrile-water at room temperature, while Konoike carried it out with 3-chloroperbenzoic acid in dichloromethane at -78 ºC. Both coincided in designating the iron-oxo porphyrin, which is formed during the oxidation of the iron-chloride porphyrin by the peroxide, as the active specie responsible for the hydroxylation.

Aceto-ester **100*E*** was insoluble in acetonitrile, therefore a mixture acetonitrile/dichloromethane 1:1 was used instead. After the addition of Fe(PTPP)Cl the solution became dark purple, which changed to brown-yellow with TBHP (5 equivalents). An inert atmosphere was installed by evacuating the flask and refilling it with nitrogen three times. However, after 5 h the reaction by MS showed monoketone **147** as the major peak, m/z 577, 579 and 651 corresponding to the sodium adducts of diketone **145**, hydroxyketone **167** and mixed peroxide **148** were also detected. After 24 h reaction, the proportions of these peaks were slightly modified, but still there was no signs of the desired dihydroxylated **158**. More TBHP (5 equivalents) was added, and stirring was continued under an inert nitrogen atmosphere. The reaction was stopped after 48 h, at that point, MS showed hydroxyketone **167** as the major peak. Chromatographic purification was

unsuccessful in isolating pure products, instead mixtures were observed when combined fractions were analysed by MS.

Konoike hydroxylation was also assessed for aceto-ester **100*E*** (Scheme 2.48). After dissolving **100*E*** and the catalyst Fe(PTPP)Cl in dichloromethane, the purple solution was cooled to -78 ºC before the addition of the 3-chloroperbenzoic acid. The reaction was performed under inert atmosphere. After 3 h reaction MS showed complete conversion to monohydroxyl **181** with MW 542 (Figure 2.17), some of the dihydroxyl **158** and monoketone **147** were also detected. Therefore, the reaction continued at -78 ºC. After 7 h reaction, the monohydroxyl **181** was still the most intense peak, but dyhydroxyl **158** intensity was increasing. The reaction continued for 3 h at -78 ºC before allowing it to reach very slowly room temperature. After 26 h reaction, MS showed dihydroxyl **158** peak as the most intense. Isolation of dihydroxyl **158** in good yield (64%) was accomplished after chromatographic purification. A slightly better yield (71%) was obtained when the reaction was conducted on a larger scale (6.6X). It turned out that dihydroxylated **158** was very unstable in air at room temperature, it oxidised very readily to the hydroxyketone. However, this transformation was stopped when the product was kept at -20 ºC. This fact, could explained why the reaction failed when performed at room temperature.



181
MW 542

Figure 2.17 Compound **181**. It was formed during the dihydroxylation of **100*E*** under Konoike conditions.[103]

Konoike highlighted the specificity of the allylic hydroxylation with the oxo-iron porphyrin to generate the α-hydroxyl. They rationalized this argument by steric factors, both the olefin and the oxo-iron porphyrin are bulky (Figure 2.16 and Figure 2.18), consequently, the oxo-iron porphyrin abstracts the less hindered allylic hydrogen, that is, the one on the α-side, to generate hydroxyl-iron porphyrin and an allylic radical (E16) which after recombination produces the α-hydroxyl and regenerates the catalyst

(E17).[103] An adaptation of the full proposed mechanism for the allylic hydroxylation with Fe(PTPP)Cl has been depicted in Scheme 2.49. Essentially it is very similar to the one proposed for the allylic oxidation, which was discussed in a previous section.

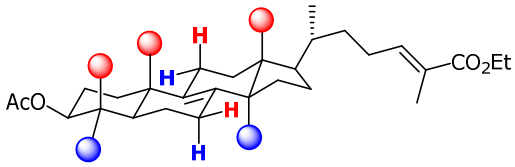
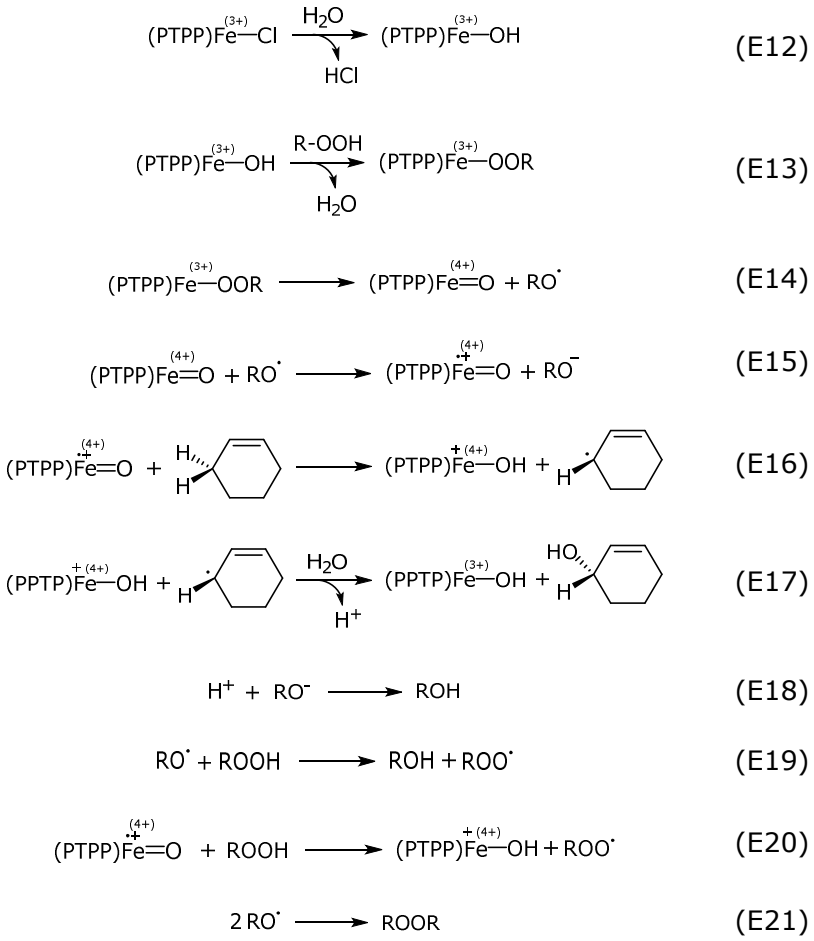


Figure 2.18 Chair conformation of aceto ester **100*E*** that shows the bulkiness of the molecule. Red and blue balls indicate methyl groups on the core rings, the first for the β position and the latter for the α one.

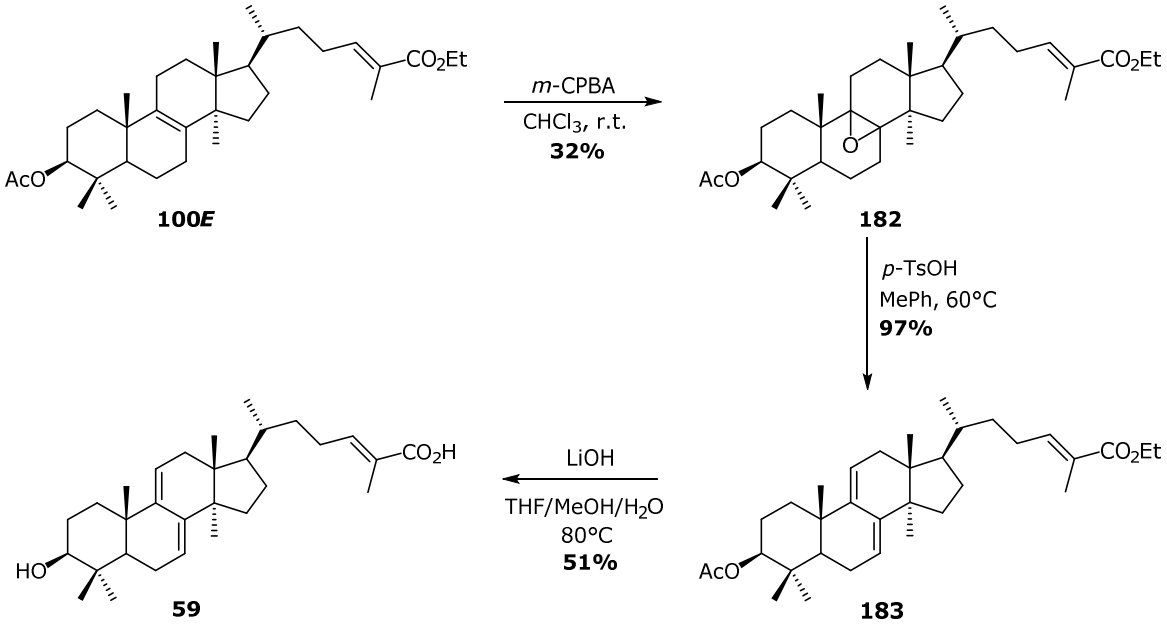


Scheme 2.49 Adaptation of the radical mechanism proposed by Bandyopadhyay for the allylic hydroxylation of olefins.[102] ROOH represents TBHP or *m*-CPBA.

Dihydroxyl-aceto-ester **158** is a novel compound. It was identified by MS, with the peak at m/z 581 corresponding to the sodium adduct of MW 558 and formula $C_{34}H_{54}O_6$ was detected. As predicted by Konoike only one

dihydroxylated compound was formed, positions C-7 and C-11 were assigned in the ^{1}H-NMR to δ 4.38 ppm (dd, *J* = 9.5, 3.8 Hz, 1H, H-11β) and δ 4.26 ppm (t, *J* = 3.1 Hz, 1H, H-7β) and to δ 67.0 ppm (CH) and δ 65.1 ppm (CH) in the ^{13}C-NMR.

(c) Formation of conjugated $\Delta^{7(8),9(11)}$ diene. Synthesis of analogue 59.



Scheme 2.50 Synthetic route for the formation of analogue **59**. Analogue **59** was formed following a route described by Minto *et al.*[104]: epoxidation with 3-chloroperbenzoic acid, ring opening and elimination in mild acidic conditions and finally hydrolysis of the ester groups in basic conditions.

Analogue **59** was synthesised from precursor **100*E*** following a route proposed by Minto *et al.* (Scheme 2.50).[104] This is a three-step synthesis that started with the epoxidation of $\Delta^{8,9}$ in **100*E*** with 3-chloroperbenzoic acid to form intermediate **182**. However, the expected compound **182** (m/z 565 for the M+Na adduct) was afforded only in a modest 32% yield after purification; a more polar compound with MW 558 and formula $C_{34}H_{54}O_6$, which did not present the signal at δ 6.75 ppm for H-24 in the ^{1}H-NMR was also isolated.

Epoxide opening and elimination was achieved by heating at 60 ºC with *para*-toluenesulfonic acid over 1.5 h reaction. Conjugated diene **183** was afforded in excellent yield (97%) after chromatographic purification. It was identified by MS, m/z 525 and 547 for the M+H and M+Na adducts, respectively, were detected. By ^{1}H-NMR two new signals at δ 5.46 ppm (t,

J = 4.3 Hz, 1H) and 5.31 ppm (d, *J* = 5.8 Hz, 1H) appeared corresponding to H-7 and H-11, respectively. Compound **183** has not been synthesised previously, it is therefore novel.

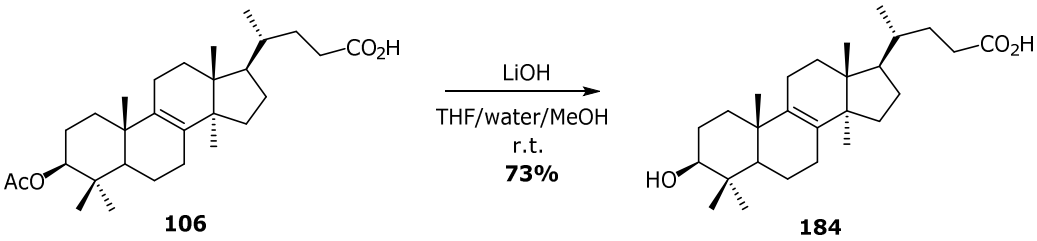
Finally, hydrolysis of **183** to the desired **59** was successful with lithium hydroxide in THF/MeOH/water 2:2:1 at 80 ºC, at room temperature the reaction proceeded very slowly, but increasing it at 80 ºC for 3.25 h resulted in full conversion to product. Purification by column chromatography afforded **59** in modest yield (51%). Different solvents were investigated for the crystallisation, ethyl acetate, and mixtures hexane/EtOAc/MeOH 3:3:1 and EtOAc/MeOH 3:1 resulted ineffective for the formation of crystals. Precipitation was observed after dissolving **59** in the minimum amount of DCM/MeOH followed by addition of hexane and evaporation of some of the dichloromethane with a nitrogen stream.

Analogue **59** known as GA-Y was previously synthesised to prove its chemical structure.[78] This analogue was identified by MS, m/z 455 and 477 corresponding to the M+H and M+Na for MW 454 and formula $C_{30}H_{46}O_3$ were detected. The disappearance of the signal for the methyl from the acetate group at δ 2.05 ppm (s, 3H) and the signals for the ethyl ester group at δ 4.18 ppm (q, *J* = 7.1 Hz, 2H) and δ 1.29 ppm (t, *J* = 7.1 Hz, 3H) in the ^{1}H-NMR were sufficient to assure the hydrolysis of the ester groups.

2.5.3. Modifications on the side chain

We were interested in investigating how the biological activity was affected by modifications on the side chain length, oxidation level and polarity. Therefore, the following series of syntheses were conducted: hydrolysis of precursor **106** to generate lucidenic acid **184**, reduction of the C-26 carboxylic group to form ganodermadiol **183**, hydrolysis of 24,25-diol **91** to afford triol **186** and esterification of analogue **107** to produce **187**.

(a) Hydrolysis of aceto-acid precursor 106. Synthesis of lucidenic acid 182.



106 **184**

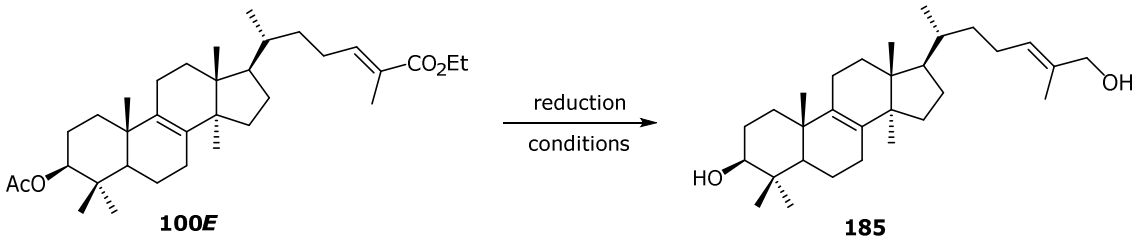
Scheme 2.51 Hydrolysis of aceto-acid precursor **106** with lithium hydroxide to form lucidenic acid **184**.

Hydrolysis of the acetate group in **106** was afforded under basic conditions with lithium hydroxide and a mixture THF/water/MeOH 4:2:1 at room temperature for 16 h (Scheme 2.51).[60] Analogue **184** turned out to be partially insoluble in the solvent mixture and some precipitated from the reaction, in order to recover it, the precipitate was filtered off and combined with the organic layer obtained during the work-up. Eluting solvent for the chromatography purification was investigated. Mixtures of EtOAc:PE from 1:9 to 3:2 were analysed. Better separation on TLC was observed using EtOAc:PE 3:7. After chromatographic purification, the expected **184** was afforded in excellent yield (73%) accompanied of starting aceto-lucidenic acid **106** (16%). Crystallisation from EtOAc:MeOH 3:1 furnished pure **184**.

Analogue **184** is commercially available; however, it is sold as a rare compound at a high price/mg (£84/mg). It has previously been synthesised to study the degradation of the euphol side chain.[110] It was identified by MS, m/z 439 corresponding to the M+Na adduct of MW 416 and formula $C_{27}H_{44}O_3$ was observed. Displacement of H-3 doublet of doublets to higher fields δ 3.16 ppm (dd, *J* = 10.3, 5.8 Hz, 1H) and disappearance of the singlet at δ 2.05 ppm (s, 3H) associated with the methyl in the acetate group, confirmed the hydrolysis of the acetate in **106**. Additionally, the ^{13}C-NMR spectrum showed only one carbonyl C at δ 176.1 ppm.

(b) Ester reduction. Synthesis of ganoderiol 185.

For the formation of ganoderiol **185**, two approaches were followed. Reduction of aceto-ester **100*E*** with either DIBAL or lithium aluminium hydride (Scheme 2.52).

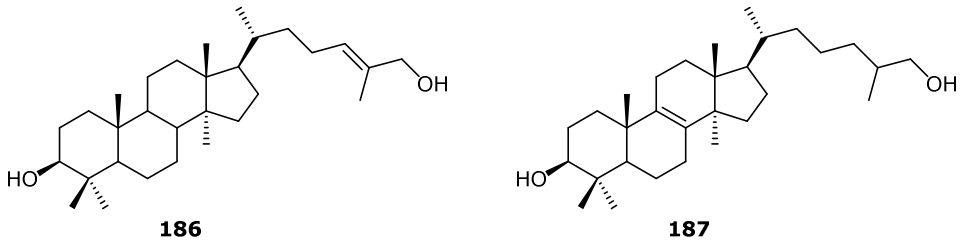


100*E* **185**

Reducing agent	Conditions	Yield (%)
DIBAL-H	DCM, -78 ºC	0
$LiALH_4$	THF, 0 ºC	78

Scheme 2.52 Reduction of aceto-ester **100*E*** to produce ganoderiol **185**. Two reducing agents were assessed, DIBAL-H and lithium aluminium hydride. Whilst the latter afforded **185** in 78% yield, the expected product was not observed with DIBAL-H.

Minto *et al.* used DIBAL-H in their synthesis of ganodermanontriol and their isomers.[104] They achieved excellent yield of the reduced esters carrying out the reaction at -100 ºC coupled with slow addition of the reducing agent. The temperature seemed very important, since in our case, when the reaction was performed at -78 ºC for 55 min, a different product was observed. In the first place, the reaction did not go to completion, and additionally, the formed product was not the expected **185**, but over-reduction was observed. Analysis by MS showed m/z 467 corresponding to MW 444 and formula $C_{30}H_{52}O_2$, Figure 2.19 shows two possible candidates with this molecular weight and formula, **186** and **187**. In view of the difficulties to get the desired product using this method, an alternative route was sought.



186 **187**

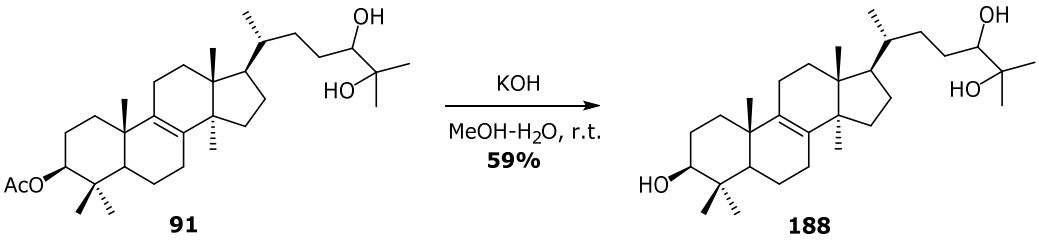
Figure 2.19 Possible products formed during DIBAL-H reduction of **100*E***.

Kato *et al.* described the reduction of esters to alcohols using lithium aluminium hydride.[111] They performed the reaction at room temperature or 0 ºC, depending on the type of ester to reduce. Thus, α,β-unsaturated esters required milder conditions to avoid over-reductions. Using this method, performing the reaction at 0 ºC, **185** was formed after 30 min reaction in excellent yield (78%). After chromatography purification a minor product

(19%) was also detected, this had MW 460 and formula $C_{30}H_{52}O_3$. However, this product was not further characterised and it was assumed to be a starting material impurity.

Ganoderiol **185** was synthesised previously using a different route to study its ability for the inhibition of cholesterol synthesis.[112] It was identified by MS, m/z 465 corresponding to MW 442 and formula $C_{30}H_{50}O_2$ was detected. It is also to note that the highest intensity peak was m/z 425, which corresponded to an elimination product, MW 424 and formula $C_{30}H_{48}O$, this product may have formed in the instrument as both ^{1}H-NMR and ^{13}C-NMR spectra were clean, with no indication of this product on them. In the ^{13}C-NMR, four signals for the olefinic carbons were observed at δ 134.6, 134.5, 134.4 and 127.2 ppm and two signals for the hydroxyl carbons, one secondary and the other primary alcohol, δ 79.1 ppm and 69.2 ppm, respectively. In the ^{1}H-NMR there were three distinctive signals. H-24 chemical shift moved to low frequencies at δ 5.40 ppm (tq, *J* = 7.1, 1.4 Hz, 1H). There was a new singlet at δ 4.00 ppm (s, 2H) corresponding to H-26. Finally, H-3 chemical shift shifted upfield at δ 3.23 ppm (dd, *J* = 11.5, 4.5 Hz, 1H), and no signals for the acetate or ethyl ester were detected.

(c) Hydrolysis of aceto-diol 91. Synthesis of analogue 188



91 **188**

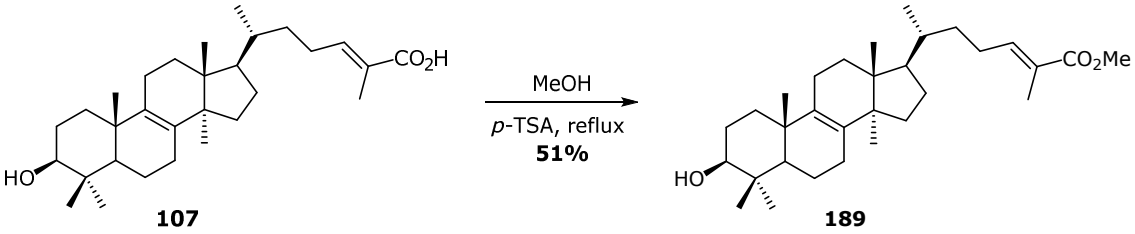
Scheme 2.53 Formation of **186** from hydrolysis of aceto-diol **91** in basic conditions.

The synthesis of analogue **188** was successfully achieved by hydrolysis of aceto-diol **91** under basic conditions (Scheme 2.53).[113] As the base, potassium hydroxide was used. The reaction was carried out in aqueous methanol, which only partially solubilised **91**. Addition of the base provoked a change in colour to yellow. The reaction proceeded for 48 h, at that point the solution became clear. Chromatographic purification afforded both **188** in good yield (59%) and recovered starting aceto-diol **91** (16%).

Analogue **188** was synthesised previously and evaluated for antimicrobial activity.[114] This analogue was identified by MS, m/z 483 corresponding to

MW 460, (M+Na) was detected. ^{13}C-NMR showed no carbonyl groups, only two sp^2 carbons at δ 134.6 ppm and 134.5 ppm; C-3 appeared at δ 79.8 ppm and a different signal for each C-24 epimer was observed, one at δ 79.1 ppm and the other at δ 78.9 ppm; C-25 also resonated at slightly different frequency for each of the epimers, at δ 73.4 ppm and 73.3 ppm. ^{1}H-NMR showed H-3 chemical shift moved to low frequency at δ 3.23 ppm (dd, *J* = 11.5, 4.5 Hz, 1H) and the singlet signal at δ 2.05 ppm was absent, confirming the hydrolysis of the acetate group.

(d) Esterification of 107. Formation of analogue 189



107 **189**

Scheme 2.54 Esterification of **107** to form methyl ester **187**. *p*-TSA = *para*-Toluensulfonic acid

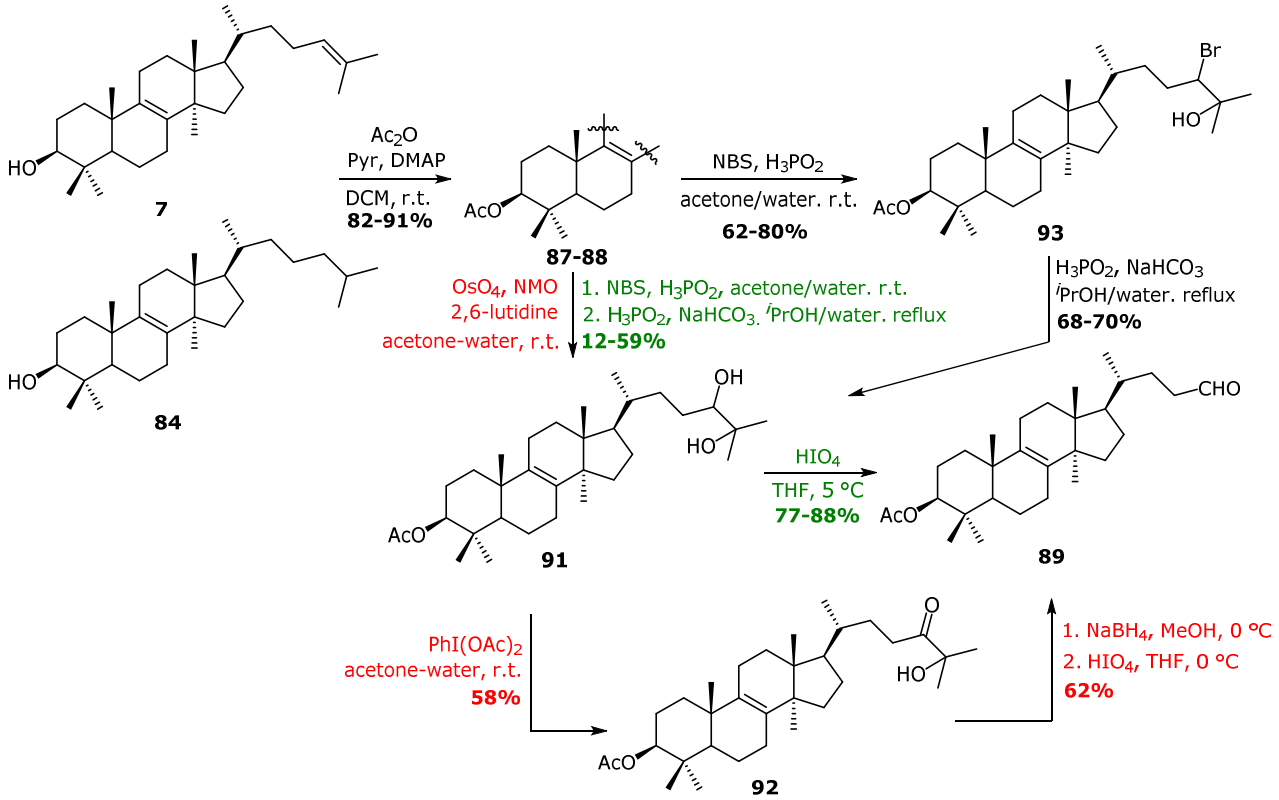
Esterification of **107** to the methyl ester was achieved in moderate yield with *para*-toluenesulfonic acid heating at reflux following a procedure described by Pelliciari *et al* (Scheme 2.54).[115] After 15 h reaction, considerable **107** was still present, suggesting that the reaction reached an equilibrium. In order to break it and favour the formation of the ester, a drying agent, 4Å molecular sieves, was added. However, no progress of the reaction was observed after 24 h of the addition, therefore the reaction was stopped at that point. Chromatographic purification afforded both **189** as a white solid in moderate yield (51%) and recovering of **107** (12%).

Analogue **189** was isolated from *G. lucidum* and synthesised following different routes as the one presented here.[78, 79] It was identified by MS, m/z 493 corresponding to MW 470, (M+Na) was detected. A new peak appeared on ^{1}H-NMR spectrum, a singlet integrating for 3H at δ 3.73 ppm corresponding to the methyl ester. Also ^{13}C-NMR showed 31 carbons, from which eight were methyl groups, the signal at δ 51.8 was assigned to the methyl ester group.

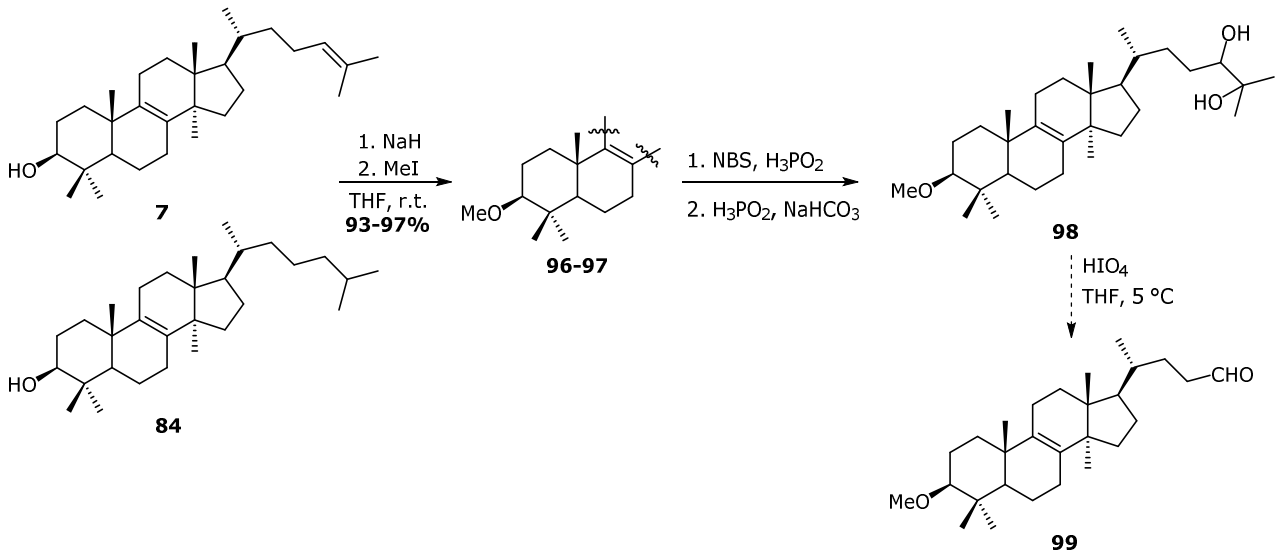
2.6. Summary

The synthesis of several analogues of ganoderic acids has been achieved. The synthetic route started from commercial lanosterol (**7**+**84**) that after three or four steps generated our main precursor, aldehyde **89** (Scheme 2.55). Synthesis of an alternative aldehyde, methoxy-aldehyde **99**, was attempted following the Kavtaradze three-step approach. However, its final purification and characterisation was not accomplished (Scheme 2.56). Further reaction of **89** produced secondary precursors **100** (Wittig), **101** (Reformatsky), **105** (dehomologated aldehyde) and **106** (acid with short side chain) from which our ganoderic acid analogues were derived (Scheme 2.57). The synthesis of the analogues was divided in three groups: analogues that differ at C-3, B/C rings and side chain. From the first group **107**, **108**, **109** and **116** were synthesised (Scheme 2.58), they have β-hydroxyl, ketone and β-acetate groups at C-3, respectively. Compound **116** is the ethyl ester derivative of **109**. Inversion of the C-3 centre was investigated. However, both approaches, selective reduction and Mitsunobu reaction, failed to produce the expected inverted compounds **117** or **110**, respectively. It is envisaged that a Mitsunobu reaction with **107** and 4-nitrobenzoic acid might lead to the formation of **110** in a sequential manner, deprotection of the C-3 PNB group followed by acetylation to form **110**. From the second group, compounds **59**, **145**, **146**, **158**, **174**, and **175** were synthesised. Compounds **145**, **146** and **174** were formed by an allylic oxidation of precursor **100*E*** (Scheme 2.59), while allylic oxidation of **101** lead to **175** (Scheme 2.60). All these compounds have ketones at C-7 and C-11 and differ in C-3 or the side chain, thus, **146** has a β-hydroxyl at C-3, **174** a ketone at that position, **145** has a β-acetate at C-3 and a α,β-unsaturated ethyl ester on the side chain and **175** has a β-acetate at C-3 and a 24-ketone and 26-ethyl ester on the side chain. Although allylic dihydroxylation was successful in forming **158** (Scheme 2.61), this compound was too unstable at room temperature. In consequence no further work was performed with it. Analogue **59** was formed from precursor **100*E*** after a three-step route (Scheme 2.61). It has a diene $\Delta^{7(8),9(11)}$ and a β-hydroxyl at C-3. Analogues **59** and **107** are the synthetic versions of the natural GA-Y and GA-Z, respectively. Finally, in the third group **184**, **185**, **188** and **189** were synthesised (Scheme 2.62). Analogue **184** has a shorter side chain, **185** and **188** do not have carboxylic group on the side

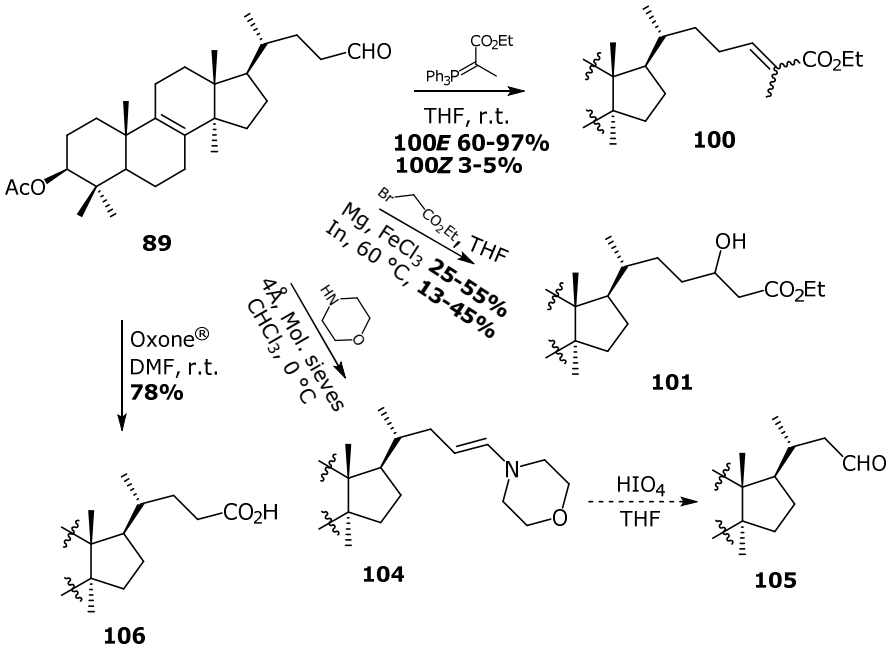
chain; they only have two and three hydroxyls on the structure, respectively. Analogue **189** is the methyl ester of **107**.



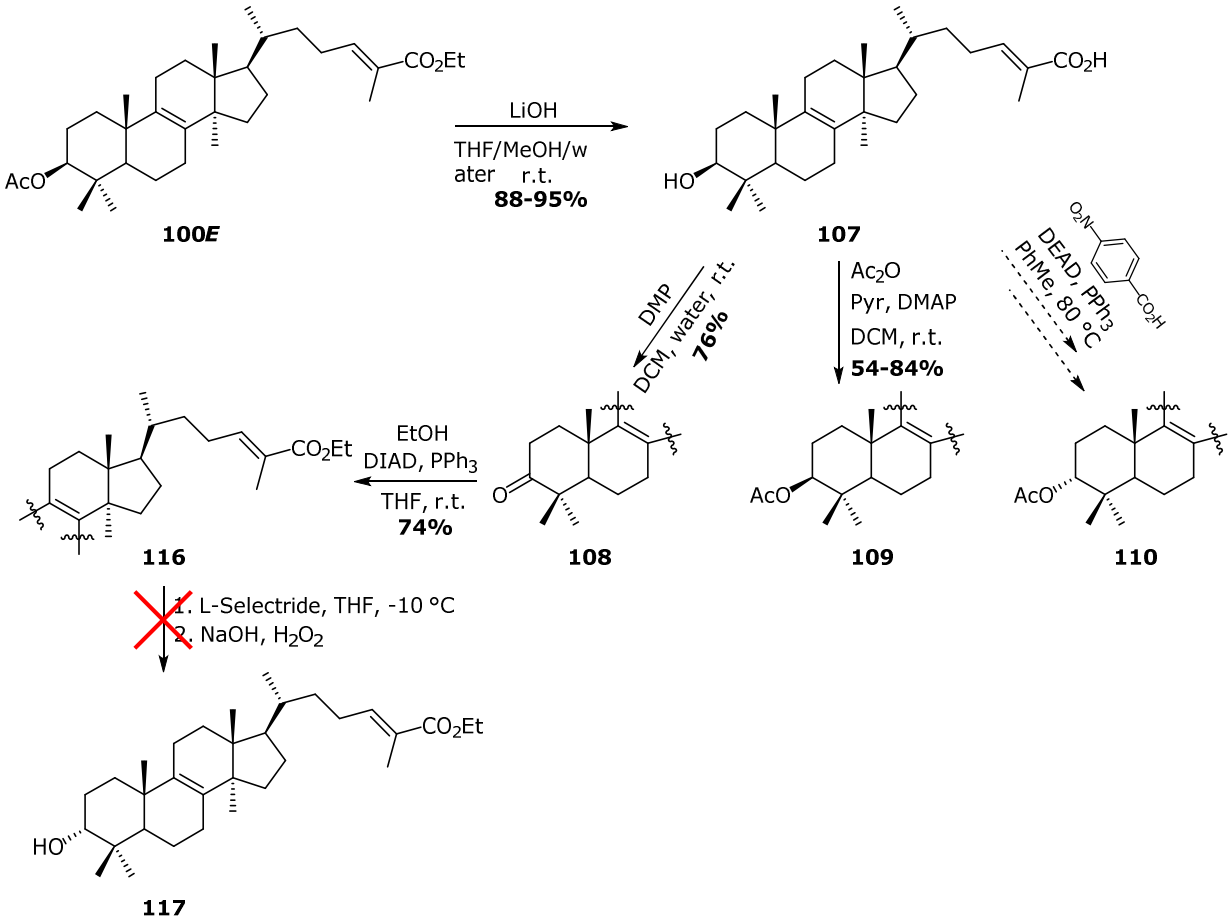
Scheme 2.55 Synthetic routes for the formation of aldehyde **89** from commercial lanosterol (**7**+**84**). Different routes evaluated are colour coded in red, green or black.



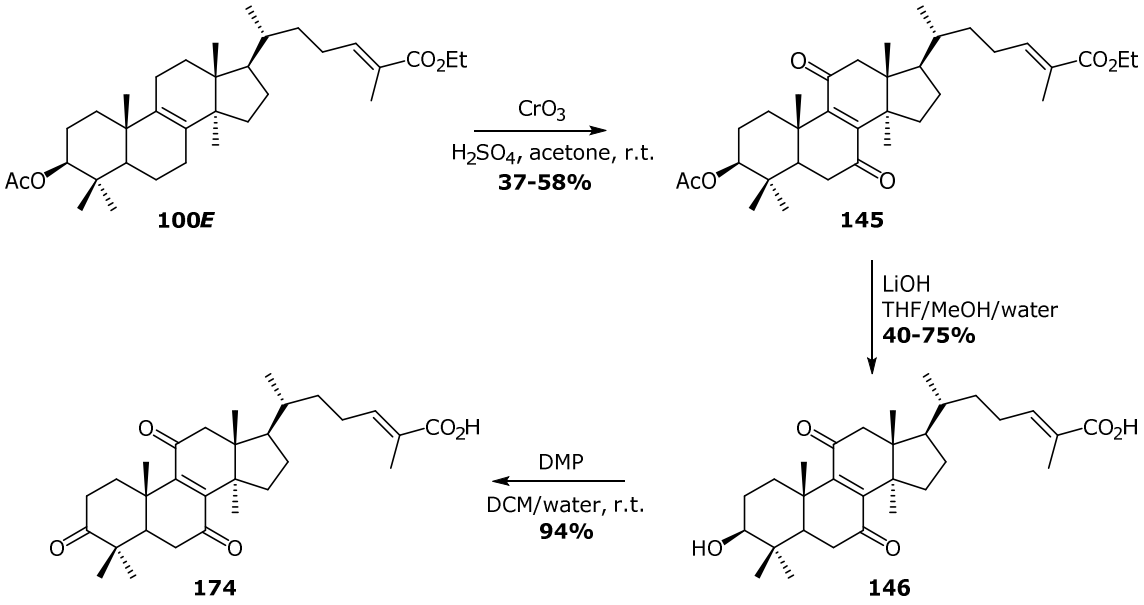
Scheme 2.56 Synthetic route for the formation of methoxy-aldehyde **99**.



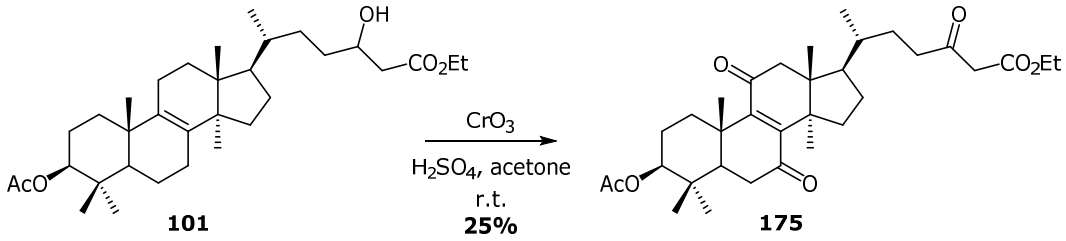
Scheme 2.57 Synthesis of precursors **100**, **101**, **105** and **106**.



Scheme 2.58 Synthetic route for the formation of group I analogues, **107**, **108**, **109**, **110**, **116** and **117**.

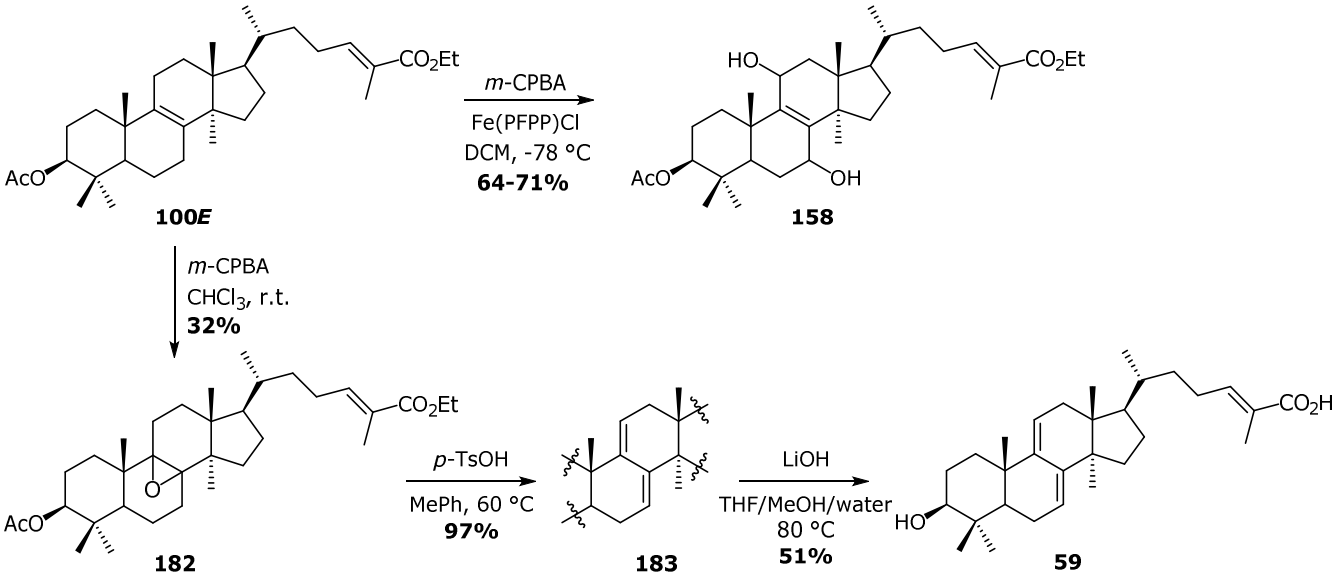


Scheme 2.59 Allylic oxidation of precursor **100*E*** to form group II analogues **146** and **174**.

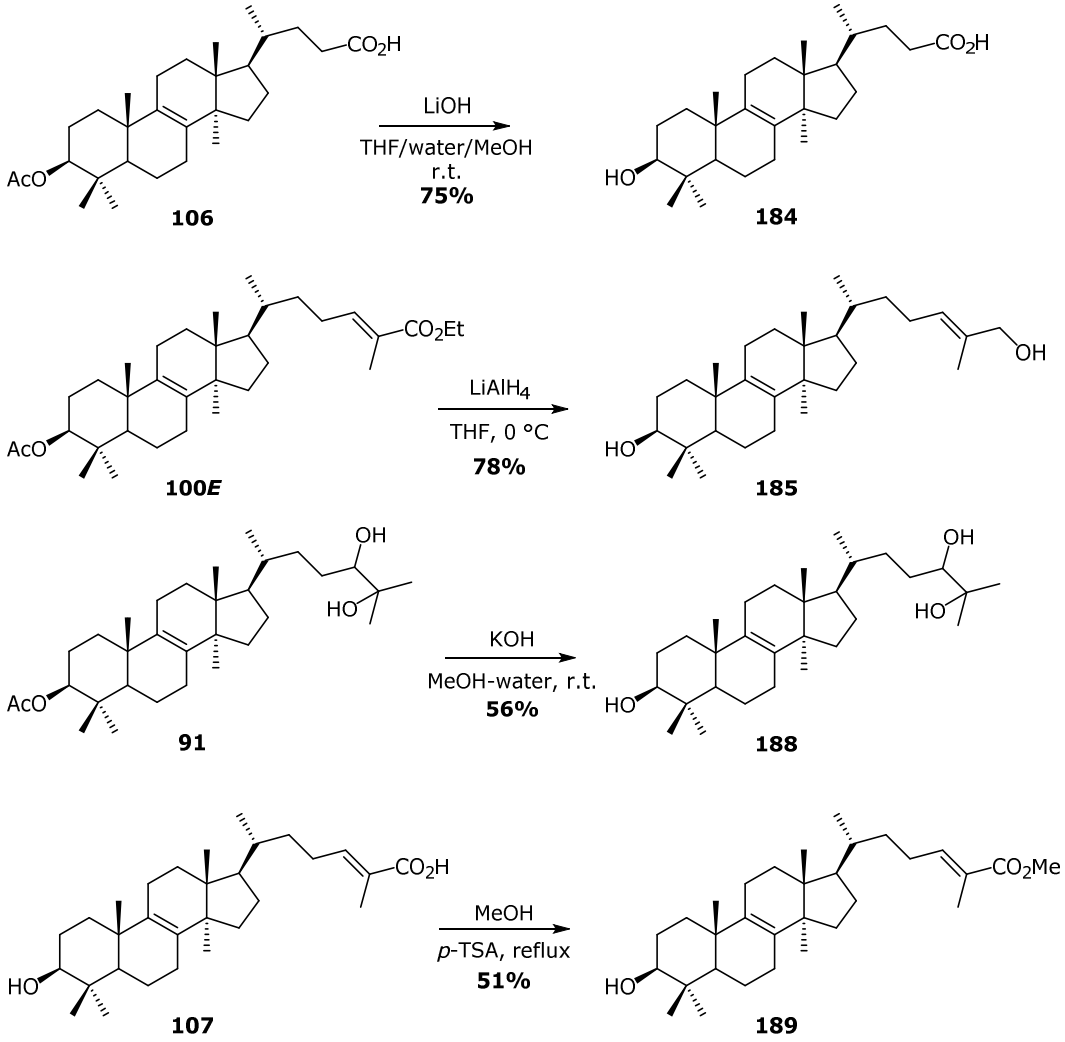


Scheme 2.60 Allylic oxidation of precursor **101** to form group II compound **175**.

Compounds **100**, **101**, **109**, **116**, **145**, **158**, **175** and **183** are novel. The remaining of compounds were either previously synthesised or isolated from the fungus material. However, for many of them, the published data was incomplete and therefore it is reported here for the first time. Likewise, improved synthetic procedures were evaluated and implemented.



Scheme 2.61 Formation of group II analogues. Allylic hydroxylation to prepare allylic diol **158** and double bond conjugation in rings B/C leading to **59**.



Scheme 2.62 Formation of group III analogues **184**, **185**, **188**, **189**.

3. Biological Evaluation

3.1. Introduction

Ganoderma lucidum (GL) has been known for millennia as a health-enhancing medicinal mushroom. Recent analysis of its extracts has shown diverse biological activity *in vitro* and *in vivo* for the treatment of cancerous cells. This activity has been attributed to two major GL components: triterpenes and polysaccharides.[14] Thus, GL triterpene extracts evaluated against the human cervical cancer cell HeLa and the colon cancer cell HT-29 revealed that the triterpenes regulated proliferation, cell cycle, oxidative stress and apoptosis *in vitro*; in addition the extracts reduced tumour growth *in vivo*.[13, 116] Isolated triterpenes, mainly ganoderic acids (GA) have been evaluated against different cancer cell-lines; *i.e.*, breast, lung, cervical, colon, lymphoma or melanoma cancer cells. GA have diverse biological activities that could be cell-line specific.[14] Our research interest was focused on the inhibitory effect of GA analogues in non-malignant and cancerous prostate cell-lines so that a structure-activity relationship could be derived. To evaluate the potency of the analogues, two natural GA were evaluated: GA-H (**24**) and GA-T (**11**). Analogues from group I, II and III that were synthesised in enough quantities were included in our studies. These comprised compounds **107**; **108** and **109** from group I; **59**; **146** and **174** from group II and **184**; **185**; **188** and **189** from group III.

The biological activity of the drugs used in this study was evaluated by the MTT ([3-(4,5-dimethylthiazol-2-yl)-2,5-diphenyl-tetrazolium bromide]) assay. This is a colorimetric assay in which the mitochondrial activity of the cells is quantified spectrophotometrically. Reduction of MTT to formazan by the mitochondria is a process that only takes place in living cells; hence, measuring it gives an estimation of the number of living cells present in the sample.[117]

The parameters IC_{50} and EC_{50} were employed to compare the effect of the different drugs. The IC_{50} was defined as the concentration of inhibitor where the viability was reduced by half; whereas the EC_{50} was defined as the concentration of a drug that gave half-maximal viability. Although they seem very similar, they are not the same. Thus, the first was referred to an absolute value determined by the minimum and maximum controls while the

latter was a relative value defined by the minimum and maximum responses.[118] To facilitate the flow of the discussion all the dose-response curves have been reported in Appendix 2.

For the purpose of our studies, cell-lines were used to mimic the different stages of the PCa progression, thus PCa cell-lines sensitive and insensitive to androgens were employed. PC3 (NCI-60 cell-line), DU145 (NCI-60 cell-line) and LNCaP (Health Protection Agency Culture Collection (HPACC)) are the "classical" PCa cell-lines. They differ in their sensitivity to androgen and molecular marker expression. It is well accepted that PC3 and DU145 make a good model for advanced PCa as these cell-lines are metastatic and insensitive to androgens.[119] Besides, they do not express prostate specific antigen (PSA); human glandular kallikrein 2 (hK2) or androgen receptor (AR).[119] However, immunoblotting studies concluded that both cell-lines express detectable levels of AR mRNA and protein, but they are non-responsive to androgens.[120] On the other hand, LNCaP cell-line is sensitive to androgen and expresses PSA, hK2 and AR, making it ideal as model for earlier stages.[119]

As GAs are being sold as nutraceuticals to enhance general health and for chemoprevention there was also interest in determining the effect of the different GA analogues in normal and pre-malignant cell-lines. In addition, studies in these types of cells could facilitate the evaluation of the toxicity of the analogues. Thus, the normal prostate cell-line RWPE1 and two pre-malignant ones WPE1-NB14 and -NB26 (HPACC) were employed here. RWPE1 was derived from epithelial cells and was immortalised with HPV-18; whereas WPE1-NB14 and -NB26 resulted after exposure of RWPE1 with the carcinogen *N*-methyl-*N*-nitrosourea (MNU) at 100 μg mL^{-1}. All these cell-lines expressed AR, PSA and are responsive to androgens. RWPE1 is non-tumorigenic, whilst the tumorigenicity and invasion increased from WPE1-NB14 to -NB26, being the former non-invasive and the latter highly invasive.[121-123]

3.2. Optimisating the conditions for cell analysis

To perform the assays in the optimal conditions the best cell concentration, solvent to dissolve the drugs and the exposure time were evaluated.

3.2.1. Optimising cell concentration

To identify which cell concentration to plate out, so that a strong signal response would be observed, linear cell concentration standard curves were carried out for all the cell-lines used in this study (Appendix 1). Cell concentrations ranging from about 10^3 to 10^6 cells mL^{-1} were grown for 24, 48 or 72 h. Final cell concentrations were estimated using the MTT assay by plotting the absorbance *vs*. cell concentration and finding the area where linearity correlation applied. As an example, the standard curves for the WPE1-NB14 cell-line are illustrated in Figure 3.1. Curve A represents the total concentration studied, from $7x10^3$ to $4x10^5$ cell mL^{-1}, while in curve B only the linear area is represented. A summary of the best cell concentration range for each of the cell-lines is given in Table 3.1.

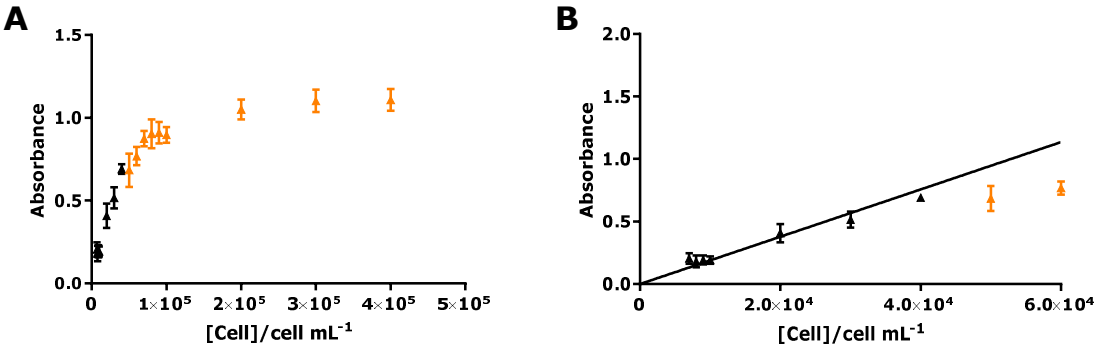


Figure 3.1 Cell concentration standard curve for WPE1-NB14 at 72 h. **A** Absorbance is correlated with the full range of concentrations studied ($7x10^3$ to $4x10^5$ cell mL^{-1}). **B** Expansion of the linear area, correlation with cell densities plotted up to $6x10^4$ cell mL^{-1}.

Cell-line	Cell Concentration/1x10⁴ cell mL⁻¹		
	24 h	48 h	72 h
PC3	2-8	2-7	< 2
PC3M-luc2	-	-	0.8-1
DU145	4-8	4-8	3-4
LNCaP	6-15	4-10	3-4
RWPE1	-	-	3-5
WPE1-NB14	-	-	3-4
WPE1-NB26	-	-	1-2

Table 3.1 Best cell concentrations plated to provide a strong signal response and a linear correlation between cell concentration and readout.

3.2.2. Identifying a solvent concentration that is non-toxic

Different organic solvents are used to dissolve the drugs to treat the cells. Dimethyl sulfoxide (DMSO), useful for dissolving both polar and nonpolar compounds, is one of the most frequently used solvents in both *in vitro* and *in vivo* assays. However, DMSO effects on cells varied from increased membrane permeability to cytotoxicity depending on factors like solvent concentration, type of experiment or cells studied.[124,125] At concentrations below 1% an increased cellular activation was observed while above that concentrations DMSO exerted inhibitory effects, being 1% the critical operational concentration where no effects were detected for some of the cell-lines studied.[126] Alcoholic solvents such as ethanol or methanol have widespread use in extraction of natural products, they have also been used to dissolve compounds for the determination of their biological activity *in vitro* and *in vivo* assays. Nevertheless, they induced loss of function of specific proteins such as ion channels, neurotransmitter receptors, enzymes, and adhesion molecules due to local conformational changes promoted after interaction with their target proteins.[127] Besides, alcohols have been associated with general immunosuppressive effects at concentrations as low as 0.08% W/V and compromised cell viability at concentrations over 0.01 – 5% depending on the cell-line analysed.[126,127]

Previous studies were focus on HeLa and murine breast cancer cells,[124,126] therefore to assess the toxicity of these two types of solvents for cancerous and pre-malignant prostate cell-lines, a study of the effect of the solvent in the reduction of the viability was conducted. The cytotoxicity was determined by using a MTT assay.

i. Dimethyl sulfoxide

DMSO was assessed first and the study was performed only on the cancerous cell-lines, PC3, DU145 and LNCaP. Concentrations of DMSO varying from 0 to 10% V/V were evaluated at 24; 48 and 72 h (Figure 3.2). As mentioned before, the toxicity of the solvent was dependant on the concentration, cell-line type and exposure time. LNCaP was the most sensitive cell-line followed by PC3 and DU145. Increasing the exposure time from 24 to 72 h, reduced the viability for concentrations above 1%. The critical concentration was between 0.5 – 1% as higher concentrations produced a sharp reduction in the viability. However, concentrations over 0.5% were enough to decrease

it below 90%. In view of the high sensitivity of the cell-lines to small quantities of solvent, no further studies were carried out with DMSO.

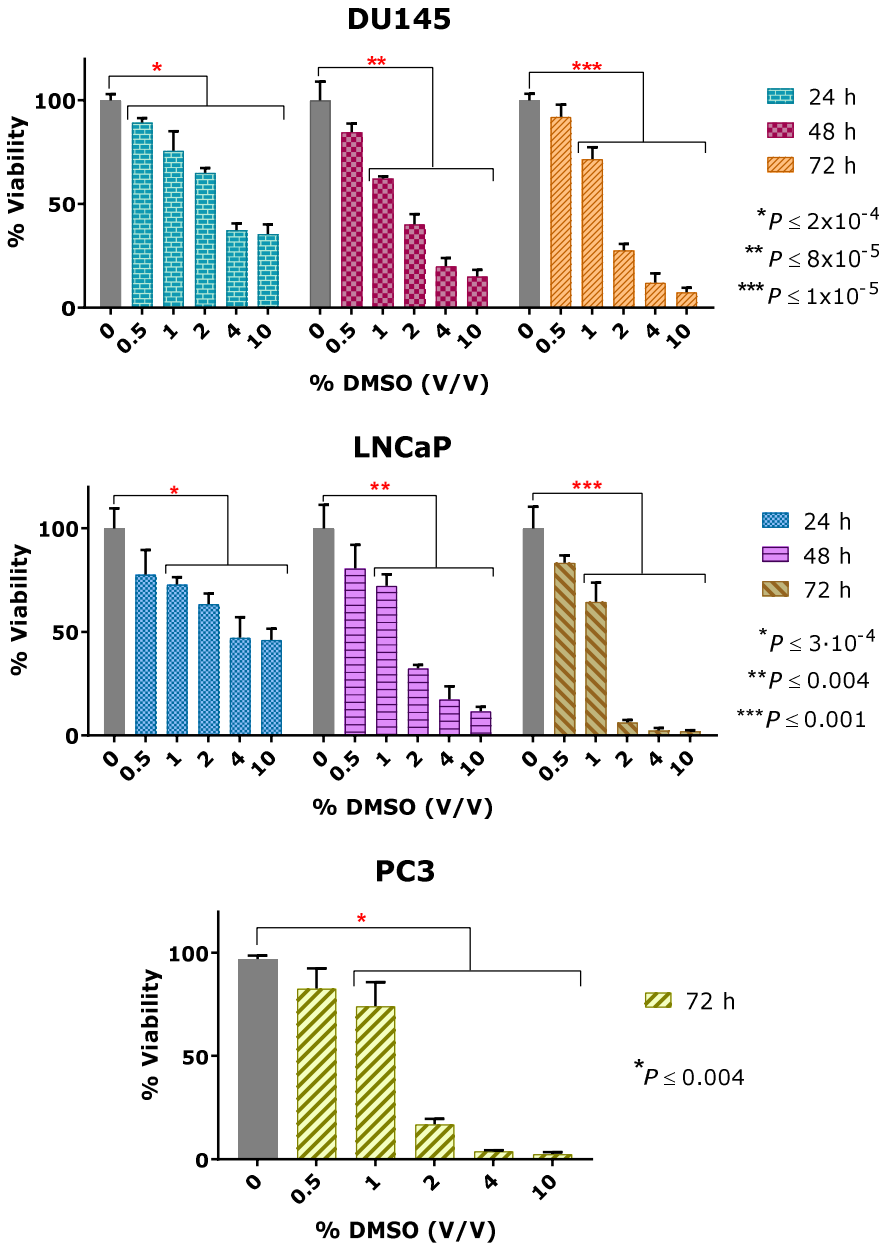


Figure 3.2 Effect of increasing concentrations of DMSO for PC3, DU145 and LNCaP cell-lines at 24 h, 48 h and 72 h exposure. *P* value < 0.01 indicates significantly difference as compared with the control.

ii. Methanol

The same prostate cancer cell-lines as above were used for this experiment. In addition, the effect on the viability of non-malignant cell-lines RWPE1, WPE1-NB14 and -NB26 was also evaluated. Cells were incubated for 72 h

with concentration of methanol varying from 0 to 4% (Figure 3.3 and Figure 3.4).

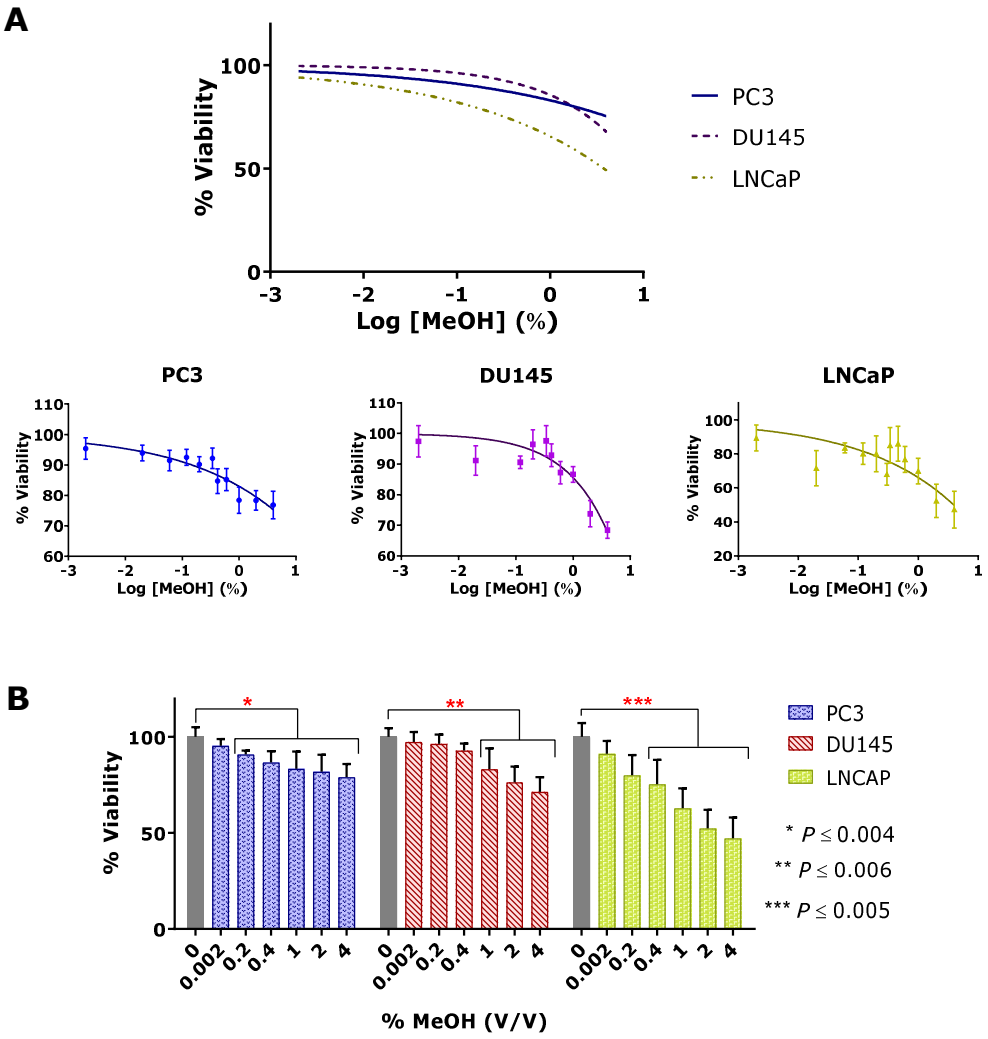


Figure 3.3 Effect of the exposure to 0 to 4% methanol (V/V) for 72 h in the viability of prostate cancer cell-lines PC3, DU145 and LNCaP. **A.** Logarithmic representation. **B.** Bar plots.

For the prostate cancer cell-lines a progressive reduction in the viability was observed from 0.2% methanol (V/V). However, it was less dramatic than for DMSO; thus, at 4% the cell viability was 80%; 70% and 50% for PC3, DU145 and LNCaP, respectively. LNCaP was again the most sensitive cell-line. Interestingly, methanol appeared to be less toxic for non-malignant cell-lines; even at the highest concentration studied, 4% methanol, no significant difference was found when compared with the control (no organic solvent added).

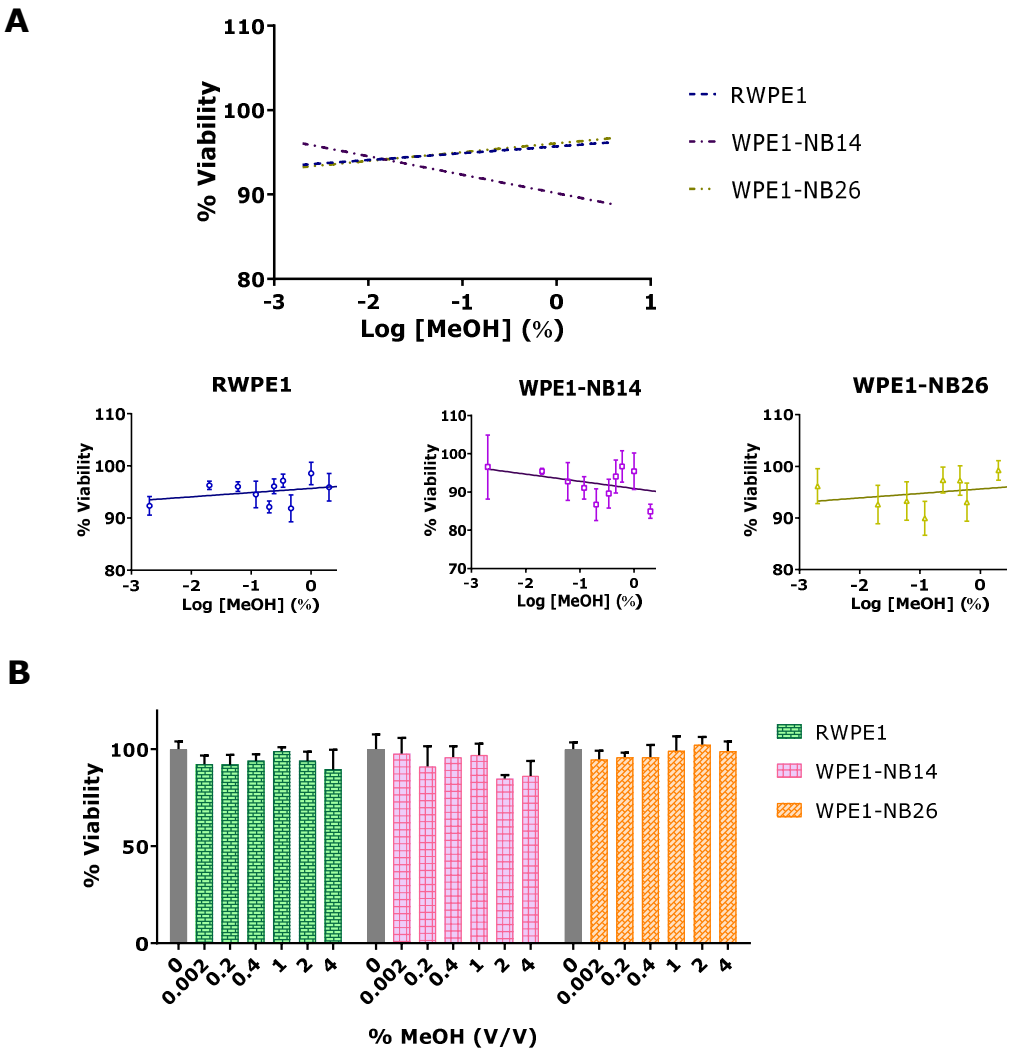


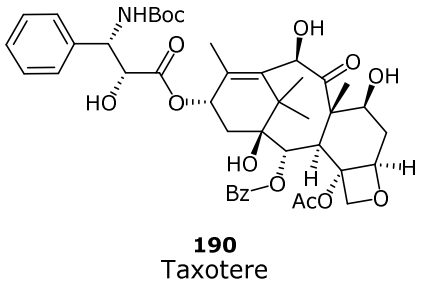
Figure 3.4 Effect of the exposure to 0 to 4% methanol (V/V) for 72 h in the viability of non-maligant cell-lines RWPE1, WPE1-NB14 and -NB26. **A.** Logarithmic representation. **B.** Bar plots.

3.2.3. Variation in PC3 cell viability after drug treatment. Time-course study.

To assess the most appropriate time interval for conducting the experiments, a time-course study was performed. In this experiment, the PC3 cell-line was incubated with increasing drug concentrations at three different times, 24; 48 and 72 h. At the end of the study, cell viability was measured by the MTT assay.

For the time-course experiments, Taxotere (**190**), a drug currently administered to prostate cancer patients, natural ganoderic acid GA-H (**24**) and synthetic analogues **108**, **146** and **174** were used.

i. Effect of Taxotere (190) in the survival of PC3 cell-line



190
Taxotere

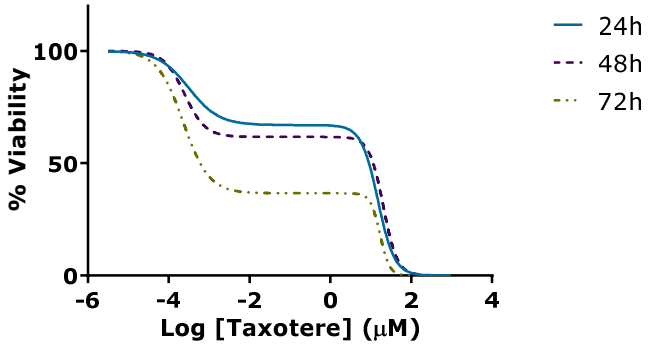
Figure 3.5 Chemical structure of Taxotere (**190**). Ac=acetate; Boc=*tert*-butoxy carbamate; Bz=benzoyl.

Taxotere (**190**) (Teva, UK) (Figure 3.5) is a semisynthetic taxane derived from 10-deacetylbaccatin III, which is extracted from the yew tree. Mechanistically, Taxotere (**190**) stabilises the tubulin heterodimers impairing cell division.[128,129]

Taxotere (**190**) has been used as an effective anti-cancer drug from the mid-90's and it is currently given to patients suffering from breast or metastatic prostate cancer, among other cancer types. However, due to its adverse side effects, it is sometimes preferred to dose in smaller quantities and in combination with other drugs.[130]

We were interested in analysing the effect of Taxotere (**190**) in the PC3 cell-line at different exposure times, 24; 48 and 72 h, to know how its biological activity compares with that of the natural and synthetic GA. For that purpose, PC3 cells were treated with increasing concentrations of Taxotere (**190**) ranging from 0 to 500 μM followed by evaluating its cell viability by the MTT assay at the desired exposure time. Taxotere (**190**) inhibited cell survival in a biphasic manner (Figure 3.6 and Appendix 2-Figure A2-1), therefore the relative EC_{50} values, were determined from the curves.

A variation of the EC_{50} values was noted, while in the first section of the curve the $EC_{50}1$ values were reduced 0.6 times from 24 to 72 h exposure times, in the second, the $EC_{50}2$ values were increased by 1.2 times in that same time span (Figure 3.6 and Figure 3.7). Furthermore, the shape of the curve changed over time. At 24 h the span of the first segment was 33.3%, which increased to 62.7% at 72 h. This increase in the first section of the curve was accompanied by a reduction of the second (Figure 3.8).



EC_{50}	Exposure time		
	24 h	**48 h**	**72 h**
EC_{50}-1/nM	0.415±0.288	0.567±0.186	0.249±0.118
EC_{50}-2/μM	15.9±2.7	19.7±2.5	18.4±4.1

Figure 3.6 Time-course study for Taxotere (**190**). Dose-response curves at 24 h (blue), 48 h (purple) and 72 h (gold) were represented as the mean ± SD of seven independent experiments, each with five or six replicates. PC3 cell-line 8-13x10^4 cell mL^{-1} for the 24 h experiment; 3-8x10^4 cell mL^{-1} for the 48 h experiment and 1-8x10^4 cell mL^{-1} for the 72 h experiment at passages 6 to 24 were used in this study. EC_{50} values in PC3 cells after treatment with taxotere (**190**) for 24 h, 48 h and 72 h.

PC3 cells were very sensitive to Taxotere (**190**), in the nanomolar concentration range for the first phase and in the micromolar for the second one. This toxicity was increased as the exposure time increased from 24 to 72 h.

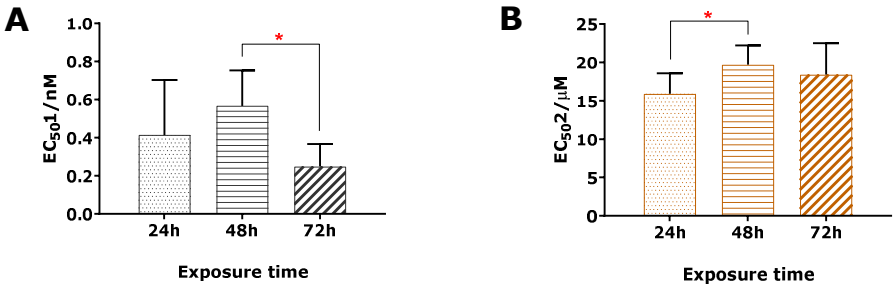
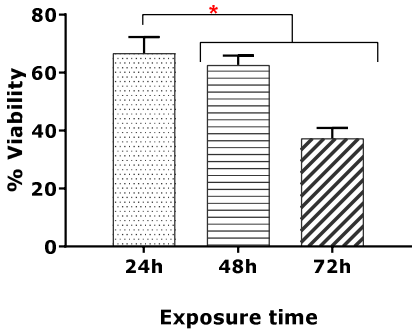


Figure 3.7 Comparison of the the first (grey) and second (orange) phase half effective concentration EC_{50} for the suppression of PC3 cell-line viability by treatment with Taxotere (**190**) for 24 h, 48 h or 72 h. * $P \leq 0.0001$. **A** $EC_{50}1$, **B** $EC_{50}2$.

The dual action of Taxotere (**190**) was reported by Hernández-Vargas *et al*. in a study they conducted with MCF7 and MDA-MB-231 breast cancer cell-lines. They found that Taxotere (**190**) clearly showed two distinct mechanisms of action depending on the drug concentration. At low

concentrations aberrant mitosis was induced followed by necrosis, whereas at high concentrations mitotic arrest was followed by apoptosis.[129]



		% Viability		
		24 h	**48 h**	**72 h**
Middle plateau		66.7±5.5	62.7±3.2	37.3±3.6
Curve span	1st	33.3	37.3	62.7
	2nd	66.7	62.7	37.3

Figure 3.8 Position of the middle plateau and curve span at the different studied times. A statistical difference (*$P \leq 0.004$) was found between 24 h and the other two time-points.

More recently, Bae *et al*. reported the synergistic effect of Taxotere (**190**) and Doxorubicin on refractory prostate cancer. In their study, they used PC3 and DU145 cell-lines as *in vitro* models. As observed in this study and that of Hernández-Vargas, they found that Taxotere (**190**) inhibited both prostate cancer cell-lines in a biphasic manner. Resazurin assay was used in their studies to determine cell viability after 72 h drug exposure. They determined that the half effective concentration for the first phase, $EC_{50}1$, were 0.500 nM for PC3 and 0.392 nM for DU145. However, they were not able to obtain a real effective concentration value for the second one, $EC_{50}2$, due to a precipitation issue they encountered; nonetheless, they gave an estimated value $EC_{50}2$ 92 μM and 104 μM for PC3 and DU145, respectively.[130] These values differ slightly from the ones we found ourselves, but they are still of the same order of magnitude.

In conclusion, Taxotere (**190**) inhibited PC3 viability very efficiently in a biphasic manner, with half effective concentration that varies considerably from the first to the second phase. It is in the nanomolar concentration range for the first and in the micromolar for the second. This biphasic behaviour could be due to a different mechanism of action taking place at different drug concentrations as has been suggested previously.

ii. Effect of GA-H (24) on PC3 cell viability

GA-H (**24**), supplied by Planta Analytica (Danbury, USA), was dissolved in 100% methanol at a stock concentration of 20 mM. Serial dilutions of this stock solution ranging from 0 to 400 μM were added to PC3 cells and incubated for 24; 48; and 72 h followed by analysis of their viability by the MTT assay (Figure 3.9).

Full dose-response curves were not possible to construct because of the low viability reduction observed even at the highest concentration studied. Thus, at 400 μM, the viability of the cells was still over 50% for all the times analysed. However, applying the student *t*-test, it was significantly reduced ($P < 0.01$) at concentrations over 200 μM for both 24 and 48 h and over 40 μM for 72 h. As controls 0.2%, 1% and 2% V/V MeOH at 72 h exposure were used. These concentrations corresponded to the content of methanol in GA-H (**24**) solutions 40 μM, 200 μM and 400 μM, respectively. Analysis of the GA-H (**24**) concentrations with the control revealed no differences at 24 h and 48 h. However, a difference was found at 72 h from GA-H (**24**) 40 μM, indicating that the reduction in the viability at 72 h was due to GA-H (**24**) and that it was only a solvent effect for the other two time-points.

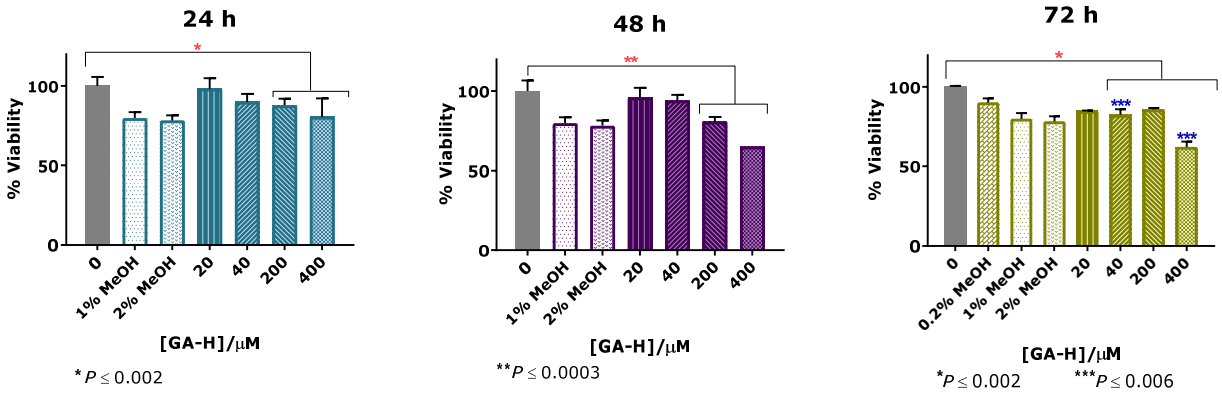


Figure 3.9 Effect of GA-H (**24**) dissolved in methanol on PC3 cells at 24 h (blue), 48 h (purple) and 72 h (gold). PC3 cells were treated with increasing concentrations of GA-H (**24**) ranging from 0 to 400 μM (0, 20, 40, 200 and 400 μM shown). Dilutions were prepared from GA-H (**24**) stock solution in methanol at 20 mM. Significant difference ($P < 0.01$) in the viability was found at concentrations over 200 μM for 24 h and 48 h and over 40 μM for 72 h. Results are the mean ± SD of five replicates for one experiment. PC3 cell-line 1.5×10^5 cell mL^{-1} (24 h), 9×10^4 cell mL^{-1} (48 h) and 2.5×10^4 cell mL^{-1} (72 h) at passage 15 were used in this study.

From this study, it could be concluded that better results could be obtained at 72 h exposure of the drug and that GA-H (**24**) inhibited the viability

poorly, since high concentrations of the GA (> 400 μM) were needed for attaining a 50% inhibition.

When the experiment was repeated by dissolving GA-H (**24**) at a concentration of 400 μM directly in the culture media (RPMI), similar results to the ones observed with methanol were obtained (Figure 3.10); namely, the viability was only poorly inhibited.

In this latter case, no significant difference of the inhibition was found at 24 h exposure, whereas concentrations over 200 μM for 48 h and 40 μM for 72 h were enough to produce a significant reduction of the viability ($P < 0.01$).

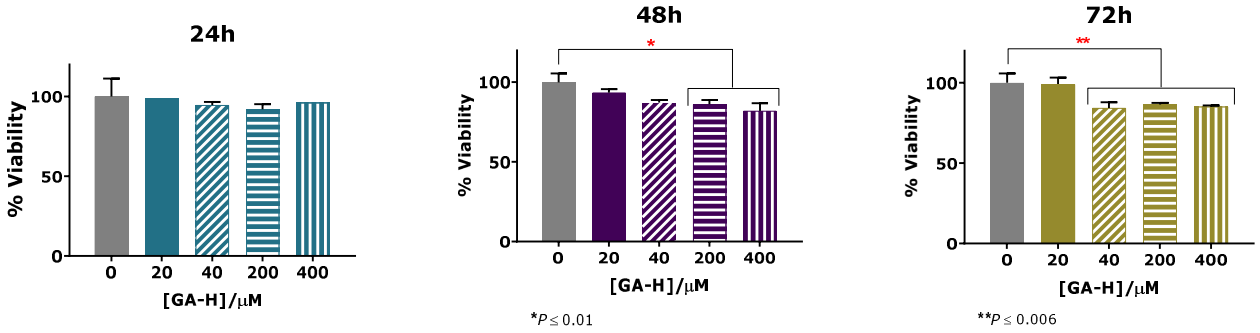


Figure 3.10 Effect of GA-H (**24**) dissolved in RPMI on PC3 cells at 24 h (blue), 48 h (purple) and 72 h (gold). PC3 cells were treated with increasing concentrations of GA-H (**24**) ranging from 0 to 400 μM (0, 20, 40, 200 and 400 μM shown). Dilutions were prepared from GA-H (**24**) solution in RPMI at 400 μM. Significant difference ($P < 0.01$) in the viability was found at concentrations over 40 μM for both 48 h and 72 h. Results are the mean ± SD of five replicates for one experiment. PC3 cell-line $2x10^5$ cell mL^{-1} (24 h), $9x10^4$ cell mL^{-1} (48 h) and $3x10^4$ cell mL^{-1} (72 h) at passage 24 were used in this study.

The lack of toxicity at 24 h and the reduction of viability from a concentration of 40 μM at 72 h exposure was also observed when GA-H (**24**) was dissolved in methanol. However, contrary to the RPMI solution, the methanol one, apparently, did not induced a significant decrease of the viability at 48 h exposure.

To clarify the nature of this difference, a comparison was made between the effect of GA-H (**24**) and methanol on the viability for the three time-points. At both 24 h and 48 h, the comparison was made with 200 μM GA-H (**24**) and 1% methanol, whereas for the 72 h, 40 μM GA-H (**24**) and 0.2% methanol were compared (Figure 3.11). This choice was made based on

previous results showing differences at these specific concentrations. A statistical difference was found at 24 h for the RPMI solution and for both solutions at 72 h. However, no difference was found at 48 h. This indicates that the reduction in viability observed at 24 h was due to the methanol, while at 48 h was due to the GA-H (**24**).

Three main conclusions were derived from these experiments. First, GA-H (**24**) slightly inhibited the PC3 cell-line at high concentrations; second, from the exposure time studied, a better effect was observed after 72 h and finally, although the use of RPMI alone reduced the toxicity effect, methanol was chosen to facilitate the solubility of the different analogues.

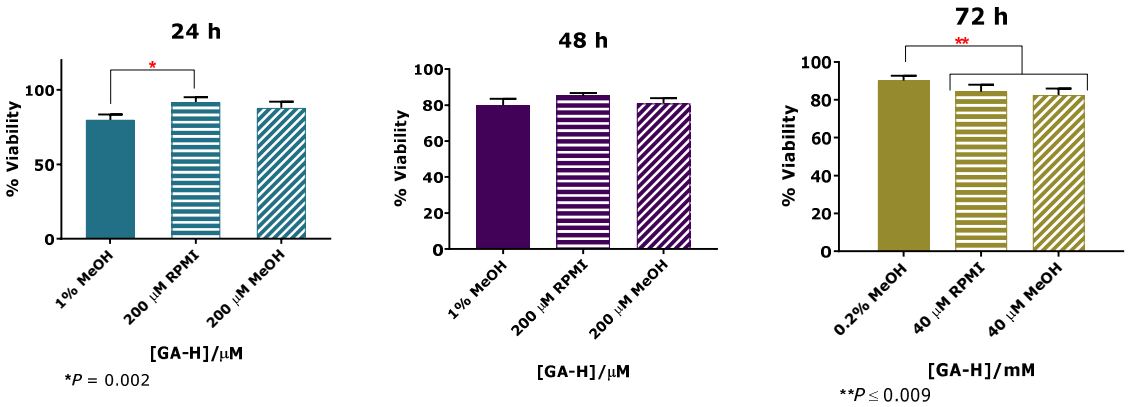
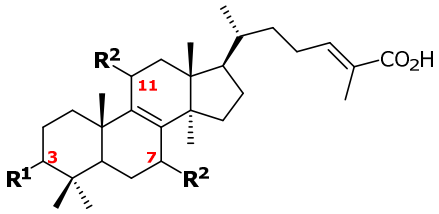


Figure 3.11 Comparison of the reduction in viability for GA-H (**24**) dissolved in RPMI or a mixture RPMI/methanol after 24 h, 48 h and 72 h exposure. For 24 h and 48 h the comparison was made with GA-H (**24**) 200 μM and 1% methanol. A difference ($P < 0.01$) was found for GA-H (**24**) dissolved in RPMI, but not for the RPMI/methanol mixture at 24 h. However, no difference was found for the 48 h exposure. The comparison was made with GA-H (**24**) 40 μM and 0.2% methanol for the 72 h exposure. In this case, GA-H (**24**) dissolved in both RPMI and the mixture RPMI/methanol were significantly different than 0.2% methanol alone.

iii. Effect of GA analogues on PC3 survival.

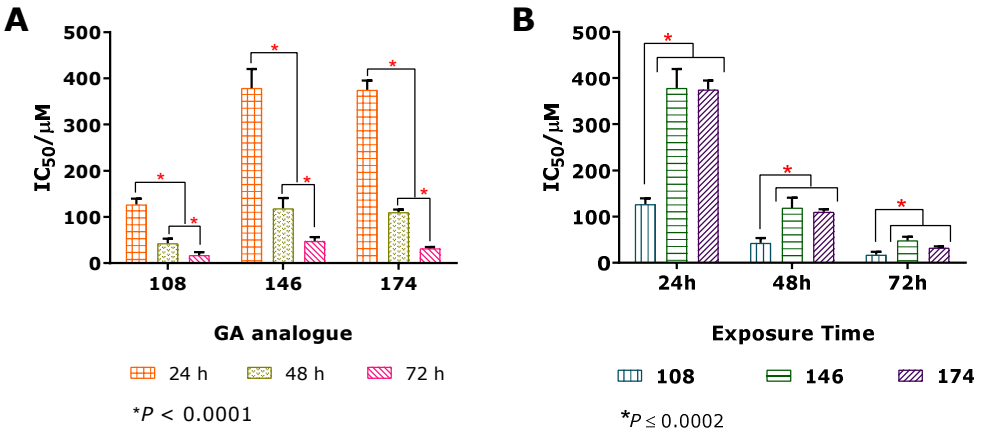
Time-course was also performed with three GA analogues; **108**, **146** and **174** (Table 3.2 for structure). They are different at position C-3 on ring A and at position C-7 and C-11 on rings B and C. Analogues **108** and **174** have a ketone at position C-3 while **146** has a β-hydroxyl group at that position, in addition, **146** and **174** have ketones at positions C-7 and C-11, whilst **108** only has a double bond $\Delta^{8,9}$, that is also present for the other two analogues. The side chain is conserved for all of them.



Analogue	R^1	R^2
108	C=O	H
146	β-OH	C=O
174	C=O	C=O

Table 3.2 Chemical structure of **108**, **146** and **174** highlighting the differences at position C-3 and C-7/C-11.

Solutions of analogues ranging from 0 to 1000 μM were prepared by dilution of the stock solution (20 mM in methanol) with RPMI-1640 media and used for the treatment of PC3 cell-line. Treated plates were harvested at the specified time and analysed. IC_{50} values deduced from the dose-response curves (Appendix 2-Figures A2-2 to A2-4) are indicated in Figure 3.12.



Analogue	IC_{50}/μM		
	24 h	**48 h**	**72 h**
108	127±13	43.2±10.1	17.4±6.7
146	379±41	119±22	48.1±8.5
174	375±20	110±6	32.4±2.6

Figure 3.12 IC_{50} comparison for the inhibition of PC3 cell viability after treatment with analogues **108**, **146** and **174** over 24 h, 48 h and 72 h. **A.** Comparison of the treatment duration. **B.** Comparison of the analogue activity. No statistical difference was found between **146** and **174** IC_{50} values in any of the times studied. Analogue **108** was statistically different to **146** and **174** for all the times studied (*$P \leq 0.0002$). Student *t*-test was applied to determine statistically difference with 99% confidence ($P < 0.01$).

PC3 viability was reduced after treatment with the analogues in a dose-, time- and drug-dependent manner. Thus, for the same analogue IC_{50} values were lower at longer exposure times (Figure 3.12 **A**). However, comparing among the analogues, **108** was the most active, suggesting that the presence of the 7,11-dioxo group dramatically reduced the activity. Alternatively, analogues **146** and **174** behaved very similarly in the inhibition of the cell viability. As they differ exclusively in the oxidation level at C-3, **146** with a β-hydroxyl and **174** with a ketone in that position, it could be derived that having a carbonyl or a hydroxyl at C-3 are equally important for activity (Figure 3.12 **B**).

To conclude, exposure time of 72 h was optimum for the development of the assays. In addition, the drugs evaluated inhibited the viability in a time- and dose-dependent manner, although each in a different way. Taxotere (**190**) was the most active drug, presenting a bifunctional activity; alternatively, GA-H (**24**) was the least active of the group evaluated and finally, the activity of the synthetic analogues was influenced by their substitution pattern. Thus, it was observed that the presence of carbonyl groups at C-7 and C-11 radically reduced the activity and that the oxidation level between hydroxyl and ketone at C-3, did not affect it significatively. As solvent, despite its proven toxicity, methanol was chosen to facilitate the solubility of the analogues.

3.3. Screening of natural and synthetic GA in prostate cells

The behaviour of natural and synthetic GA was evaluated in non-malignant and cancerous prostate cell-lines using the optimised parameters for solvent and time exposure. GA were dissolved in methanol at a stock solution of 20 mM that was diluted in RPMI media to the required concentration for the analysis and the cells were exposed to the different concentration of drugs for 72 h. Cell-lines employed included the normal and non-malignant cell-lines RWPE1, WPE1-NB14 and -NB26 and cancerous cell-lines PC3, PC3M-luc2, DU145 and LNCaP.

3.3.1. Natural GAs

Inhibition of the viability was evaluated for two natural GA, GA-H (**24**) purchased from Planta Analytica (Danbury, USA) and GA-T (**11**) kindly

donated by Dr Jian-Jiang Zhong from Shangai Jiao Tong University (Figure 3.13 for structures). Non-malignant and cancerous prostate cell-lines were used for the analysis.

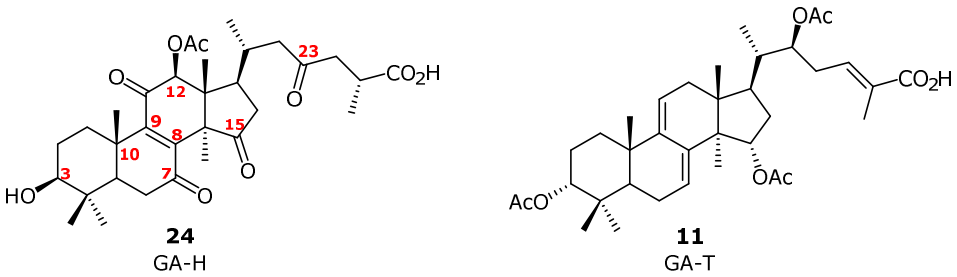


Figure 3.13 Chemical structure of GA-H (**24**) and GA-T (**11**).

These two GAs differ notably in the substitution pattern of all the rings and side chain of the molecule. At C-3, GA-H has a β-hydroxyl group whereas GA-T (**11**) has an α-acetate. GA-T (**11**) has a conjugated double bond system at $\Delta^{7(8),9(11)}$ while GA-H (**24**) has a more complex substitution pattern in this part of the molecule, two allylic ketones, one at C-7 and another at C-11, a β-acetate group at C-12 and a double bond at $\Delta^{8,9}$. At C-15 in ring D there is a ketone for GA-H (**24**) and an α-acetate for GA-T (**11**). Finally, at the side chain, GA-H (**24**) has a ketone at C-23 and a C-26 carboxylic acid, whilst GA-T (**11**) has an acetate at C-22 and a $\Delta^{24,25}$ α,β-unsaturated carboxylic acid.

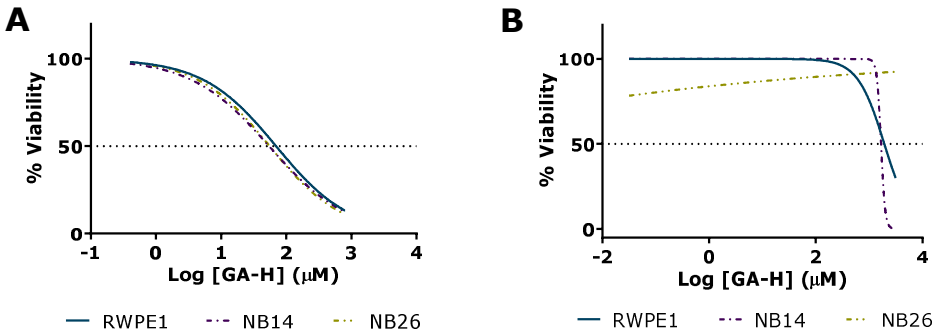
a. GA-H (**24**)

Two independent experiments were carried out with concentrations of GA-H (**24**) ranging from 0 to 2000 μM in non-malignant and cancerous prostate cell-lines.

i. Non-malignant prostate cell-lines treated with GA-H (**24**)

Non-malignant cell-lines RWPE1, WPE1-NB14 and –NB26 were treated with GA-H (**24**) solutions at the concentrations stated above. After analysing the data of each of the two experiments performed, very different results were obtained. In the first experiment IC_{50}s 76 μM, 57 μM and 60 μM were determined for RWPE1, WPE1-NB14 and -NB26, respectively. In the second experiment, no effect of the drug was apparent, with IC_{50} values of 1652 μM and 1658 μM for RWPE1 and WPE1-NB14 being derived from the curve and no effect being observed for the other cell-line, WPE1-NB26 (Figure 3.14 and Appendix 2 Figure A2-5 and A2-6). At that point, no

more GA-H (**24**) was available to repeat the experiment a third time. However, the lack of activity at very high concentrations observed in the second experiment could have been due to contamination of the plate. Alternatively, Fang Lee reported this capricious behaviour with GA-H (**24**) for DU145 and WPE1-NB26 cell-lines, when comparing the activity of commercial GA-H (**24**), with GA-H donated by Prof. Guo from Shangai Research Centre for Modernisation of Traditional Chinese Medicine.[35]



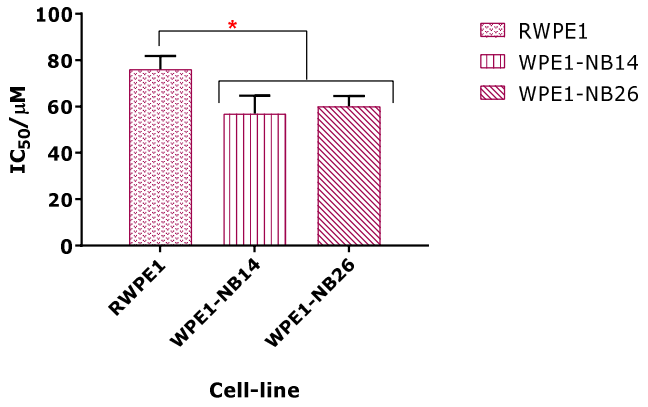
Cell-line		RWPE1	WPE1-NB14	WPE1-NB26
IC_{50}/μM	**A**	76.0±5.8	56.9±7.8	60.1±4.4
	B	1628±155	1672±50	n/a

Figure 3.14 Dose-response curves for non-malignant prostate cell-lines, RWPE1 (blue), WPE1-NB14 (purple) and WPE1-NB26 (gold) treated with GA-H (**24**). IC_{50} values for each of the experiments given. **A.** Experiment 1. **B.** Experiment 2.

Assuming that the first experiment was valid, a comparison of the IC_{50}s for each of the cell-lines revealed that the normal cell-line RWPE1 was slightly more resistant to the inhibition of the viability than both pre-malignant cell-lines WPE1-NB14 and –NB26. Nonetheless, the inhibition was only moderate (Figure 3.15). This has the implication that GA-H (**24**) could be less toxic for normal cells than for pre-malignant cells.

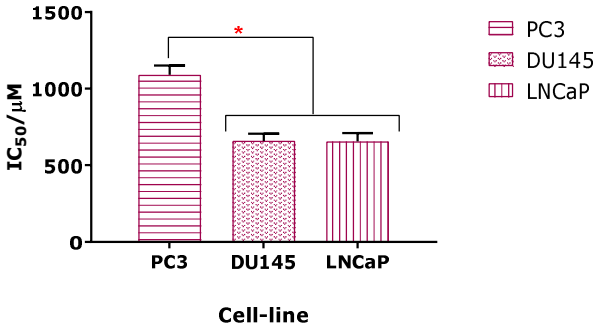
ii. Prostate cancer cell-lines treated with GA-H (**24**)

Prostate cancer cell-lines PC3, DU145 and LNCaP were treated with GA-H (**24**) solutions at the concentrations indicated above. IC_{50} values, calculated from the dose-response curves (Appendix 2 Figure A2-7), were 1090 μM, 659 μM and 657 μM for PC3, DU145 and LNCaP, respectively. These values indicated that GA-H (**24**) had very little effect on the survival of the prostate cancer cell-lines studied. Even though, GA-H (**24**) was 1.6-fold less active for the PC3 cell-line than for the other two cell-lines and its toxic effect in both DU145 and LNCaP was very similar (Figure 3.16).



Cell-line	RWPE1	WPE1-NB14	WPE1-NB26
IC_{50} / µM	76.0±5.8	56.9±7.8	60.1±4.4

Figure 3.15 IC_{50}s comparison among the non-malignant prostate cell-lines, RWPE1, WPE1-NB14 and -NB26 after treatment with GA-H (**24**). Statistically difference with 99% confidence was found between RWPE1 and the other two cell-lines, WPE1-NB14 and –NB26, **P* = 0.0003.



Cell-line	PC3	DU145	LNCaP
IC_{50} / µM	1090±60	659±46	657±53

Figure 3.16 IC_{50}s comparison among the prostate cancer cell-lines, PC3, DU145 and LNCaP after treatment with GA-H (**24**). Statistically difference with 99% confidence was found between PC3 and the other two cell-lines, DU145 and LNCaP, **P* < 0.0001.

Cheng *et al*. determined the cytotoxicity of 43 GAs against HeLa human cervical cancer cells. They found that GA-H (**24**) was not cytotoxic (IC_{50} > 300 µM) against this cell-line.[131] Furthermore, Popovich *et al.* extracted and isolated seven GAs from GL mushroom and evaluated their toxicity against three cancer cell-lines, CaCo-2, Hep G2 and HeLa. They found that GA-H (**24**) was not active for any of the cell-lines studied (IC_{50} > 1.2 mM).[132] These results were in complete agreement with our observations about the lack of activity of GA-H (**24**) against prostate cancer cell-lines. On the other hand, Sliva *et al*. evaluated the bioactivity of three structurally related GAs,

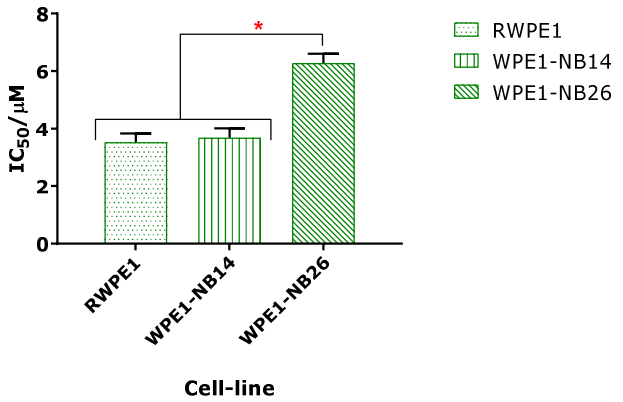
GA-A (**10**), GA-F (**22**) and GA-H (**24**) against the highly invasive breast cancer cell-line MDA-MB-231, they performed the study at three time-points, (24 h, 48 h and 72 h) and evaluated the inhibition of the proliferation relative to the control at three concentrations 100 μM, 250 μM and 500 μM. They found that GA-A (**10**) and GA-H (**24**) inhibited the proliferation of the MDA-MB-232 cell-line in a time- and dose-dependent manner, while GA-F (**22**) was inactive at the concentrations studied. The reduction in the viability was 56% for GA-A (**10**) and 58% for GA-H (**24**) after 72 h exposure time at a 500 μM drug concentration.[26] However, drugs with IC_{50} values over 100 μM are considered poor or non-active. Additionally, GA-H (**24**) and GA-F (**22**) chemical structures shown in the report were mistaken, what they called GA-H (**24**) corresponds to GA-F (**22**) and *vice versa*. Therefore, it is quite likely that the effects that they were claiming for GA-H (**24**) were attributable to GA-F (**22**). If that were the case, GA-H (**24**) would have no activity against breast cancer cell-lines. Regrettably the authors were unable to clarify this point when contacted by us, suggesting a repetition of the experiments is require to resolve this issue.

b. GA-T (**11**)

Solutions of GA-T (**11**) from 0 to 600 μM were used to treat non-malignant and cancerous prostate cell-lines in two or three independent experiments with the following results.

i. Non-malignant prostate cell-lines treated with GA-T (**11**)

Non-malignant prostate cell-lines, RWPE1, WPE1-NB14 and -NB26 were treated with GA-T (**11**) at concentrations ranging from 0 to 200 μM. Dose-response curves provided IC_{50} values 3.53 μM, 3.68 μM and 6.28 μM for each of the cell-lines above mentioned (Annex 2 Figure A2-8). GA-T (**11**) showed high activity for the three cell-lines, with RWPE1 and WPE1-NB14 being the most sensitive, they were 1.4-fold more active than WPE1-NB26 (Figure 3.17). This results indicated that GA-T (**11**) was more toxic to normal cells.



Cell-line	RWPE1	WPE1-NB14	WPE1-NB26
IC_{50} / µM	3.53±0.30	3.68±0.33	6.28±0.32

Figure 3.17 IC_{50} comparison among the non-malignant prostate cell-lines, RWPE1, WPE1-NB14 and -NB26 after treatment with GA-T (**11**). Statistically difference with 99% confidence was found between WPE1-NB26 and the other two cell-lines, WPE1-NB14 and RWPE1, $*P < 0.0001$.

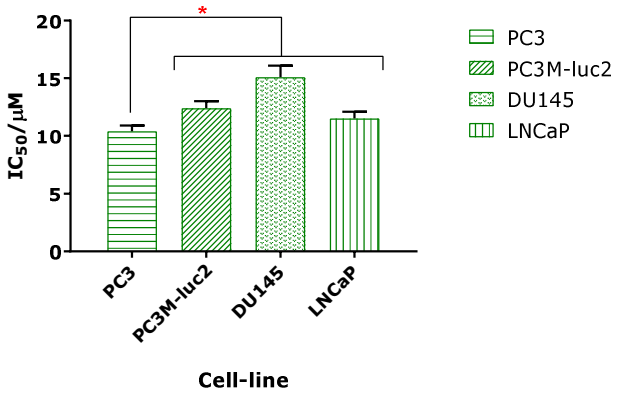
ii. Prostate cancer cell-lines treated with GA-T (**11**)

Prostate cancer cell-lines PC3, PC3M-luc2, DU145 and LNCaP were treated with solutions of GA-T (**11**) ranging from 0 to 600 µM. Non-linear regression analysis provided dose-response curves from where IC_{50} values 10.4 µM, 12.4 µM, 15.1 µM and 11.5 µM for PC3, PC3M-luc2, DU145 and LNCaP, respectively, were calculated (Appendix 2 – Figure A2-9).

GA-T (**11**) was very active for the inhibition of all the prostate cancer cell-lines studied, although the reduction in the viability was between two to four times lower than the inhibition observed for the non-malignant cell-lines. Ordering the cell-lines by activity: PC3 > LNCaP > PC3M-luc2 > DU145, the most sensitive cell was PC3 and the least sensitive DU145 (Figure 3.18).

Zohng *et al*. determined the cytoxicity of GA-T (**11**) for several cancer cell-lines, 95-D (lung), SMMC7721 (liver), KB-A-1 (epidermis), KB-3-1 (epidermis) and HeLa (cervix) and for two normal cell-lines, HLF (lung) and L-02 (liver). They found that GA-T (**11**) inhibited the growth in a dose-dependent manner after 24 h exposure for all the cell-lines studied. However, normal cell-lines were less inhibited than cancer cell-lines. In addition, a different behaviour was found for each of the cell-lines. It was found that lung cancer 95-D was the most sensitive cell-line to GA-T (**11**) with an IC_{50} 46 µM.[29] More recently, whilst they were studying the mechanism of tumour invasion inhibition by GA-T (**11**), they found that it

was very effective for the inhibition of HCT-116 (colon) cell growth, with an IC_{50} 16 μM.[133] Their work concluded that GA-T (**11**) induced apoptosis, G1 phase arrest and upregulation of p53 protein expression, additionally, GA-T was involved in the invasion inhibition by reducing the NF-κB activity.

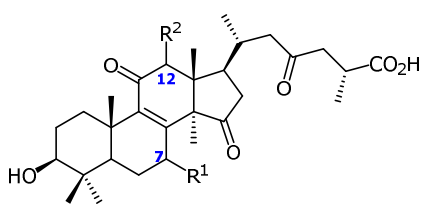


Cell-line	PC3	PC3M-luc2	DU145	LNCaP
IC_{50} / μM	10.4±0.5	12.4±0.6	15.1±1.0	11.5±0.6

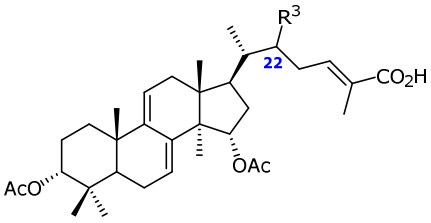
Figure 3.18 IC_{50}s comparison among the prostate cancer cell-lines, PC3, PC3M-luc2, DU145 and LNCaP after treatment with GA-T (**11**). Statistically difference with 99% confidence was found among PC3 with the other three cell-lines, $*P < 0.0001$.

More related to our investigations with prostate cell-lines were the results presented by Fang Lee from Anna Grabowska's group at the University of Nottingham. She investigated the effect of GA type I and III (supplied by Prof Guo, Dr Zhong (Shanghai) and Planta Analytica (Danbury, USA)) in the growth inhibition of non-malignant and cancerous prostate cell-lines. Specifically, WPE1-NB26, PC3M and DU145 cell-lines and GA-B (**8**), GA-H (**24**) and GA-K (**26**) as type I and GA-Me (**49**) and GA-T (**11**) as type III GAs, were used in her study (Figure 3.19). According to her findings, while only a slight difference in activity was observed for type I or type III GA for the prostate cancer cell-lines, the pre-malignant cell-line WPE1-NB26 viability was considerably more inhibited by the type III GA, in both cases, GA-T (**11**) was the most active of the GA family studied.[35] A summary of the IC_{50} values she reported are given in Table 3.3.

To summarise, GA-T (**11**) inhibited the viability of both non-malignant and cancerous prostate cell-lines with IC_{50} values comparable to the ones reported in the literature, being in the low micromolar range.



Type I



Type III

GA	Type I		Type III
	R^1	R^2	R^3
GA-B (**8**)	β-OH	H	-
GA-H (**24**)	C=O	β-OAc	-
GA-K (**26**)	β-OH	β-OAc	-
GA-Me (**49**)	-	-	H
GA-T (**11**)	-	-	(22*R*)-OAc

Figure 3.19 GA used by Fang Lee in her studies with prostate cell-lines.[35]

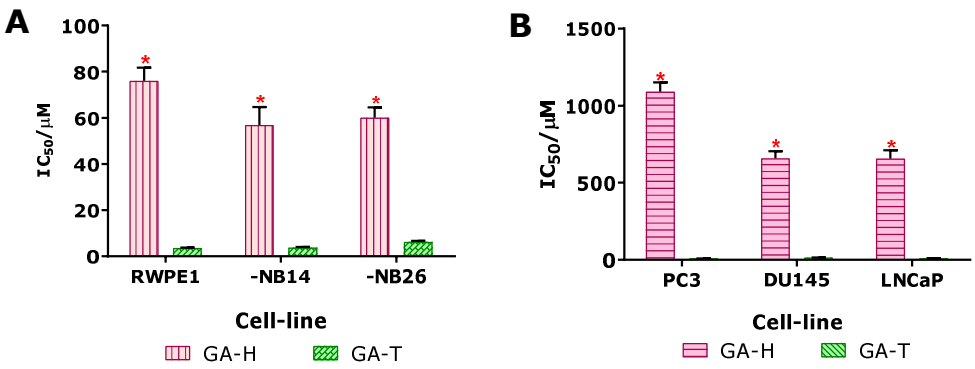
GA	IC_{50}/μM		
	WPE1-NB26	DU145	PC3M
GA-B (**8**)	23.2±2.2	24.9±4.5	-
GA-H (**24**)	22.9±2.3	30.2±1.1	-
GA-K (**26**)	14.2±1.3	23.2±2.8	-
GA-Me (**49**)	0.90±0.17	-	22.6±1.8
GA-T (**11**)	0.42±0.10	-	15.7±2.6

Table 3.3 IC_{50} values for prostate cell-lines after treatment with GA type I or type III. Values were taken from Fang Lee's thesis.[35]

c. Comparison of GA-H (**24**) and GA-T (**11**) activity

GA-H (**24**) and GA-T (**11**) inhibited cell survival differently. GA-H (**24**) inhibited it moderately for the non-malignant prostate cell-lines WPE1-NB14 and -NB26, while it was slightly less active for the normal cell-line, RWPE1. However, it did not supress the viability of the prostate cancer cell-lines. On the contrary, GA-T (**11**) showed high inhibition activity for both types of prostate cell-lines, even though, the IC_{50} values were still not as low as the ones observed for Taxotere (**190**).

A comparison of the IC_{50} values for GA-H (**24**) and GA-T (**11**) is given in Figure 3.20. GA-T (**11**) inhibition potency was 12- to 21-fold higher than GA-H (**24**) for the non-malignant cell-lines and 47- to 107-fold higher for the cancerous cell-lines.



Cell-line		IC_{50}/µM	
		GA-H (24)	**GA-T (11)**
A	RWPE1	76.0±5.8	3.53±0.30
	WPE1-NB14	56.9±7.8	3.68±0.33
	WPE1-NB26	60.1±4.4	6.28±0.32
B	PC3	1090±60	10.4±0.5
	DU145	659±46	15.1±1.0
	LNCaP	657±53	11.5±0.6
	PC3M-luc2	-	12.4±0.6

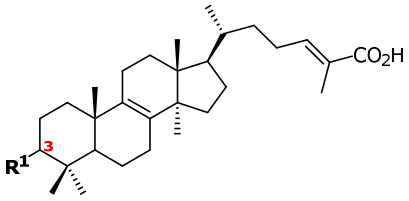
Figure 3.20 IC_{50}s comparison of non-malignant and cancerous prostate cell-lines after treatment with GA-H (**24**) or GA-T (**11**). **A.** Non-malignant cell-lines. **B.** Cancerous cell-lines. Values are represented as mean ± SD. Statistically difference ($P < 0.01$) between GA-H (**24**) and GA-T (**11**) was found for all the cell-lines. *$P < 0.0001$.

3.3.2. Synthetic GAs

Three types of synthetic GA analogues, classified as group I, II and III were evaluated. Group I included analogues with modifications at C-3; group II comprised analogues with modified functionalities at B/C rings and group III contained analogues with different groups on the side chain. The effect in the cell survival was evaluated against non-malignant and prostate cancer cell-lines. However, only analogues from group I and II were evaluated against the non-malignant cell-lines.

a. Group I

The analogues of this group have the same chemical skeleton, differing exclusively at position C-3 (Figure 3.21). Three functionalities were investigated, β-hydroxyl, β-acetate and carbonyl groups.



	107	108	109
R¹	β-OH	C=O	β-OAc

Figure 3.21 Chemical structure of GA analogues belonging to group I, **107**, **108** and **109**.

Analogues **107** and **108** were evaluated against both non-malignant and prostate cancer cell-lines, whereas **109** was only evaluated against prostate cancer cell-lines. Three non-malignant cell-lines were analysed: RWPE1, WPE1-NB14 and –NB26. Prostate cancer cell-lines analysed included PC3, PC3M-luc2, DU145 and LNCaP. Sigmoidal curves were observed for all the cell lines except for the non-malignant cell-lines treated with **107** that generated biphasic curves. (Figure 3.22 and Appendix 2 – Figures A2-10 to A2-14). For this analogue, the EC_{50} of each of the phases was determined.

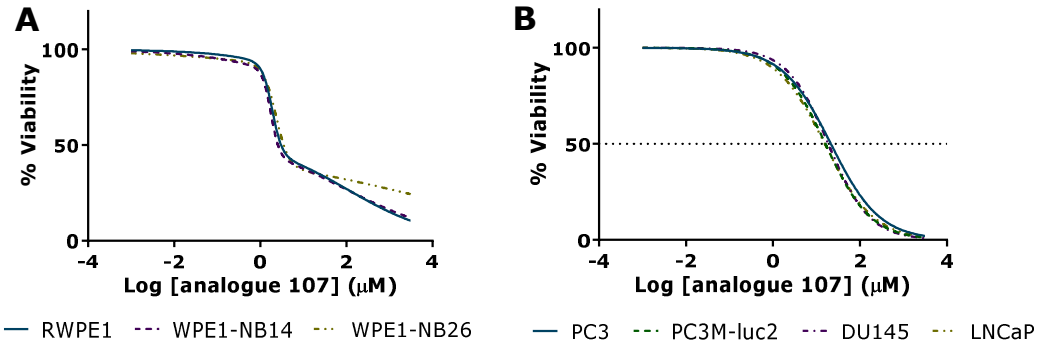
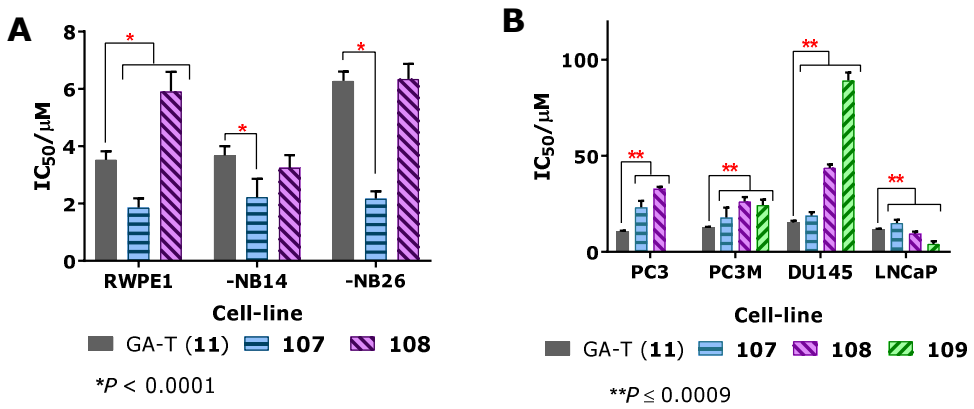


Figure 3.22 Cell-lines treated with analogue **107**. **A.** Non-malignant cell-lines. **B.** Prostate cancer cell-lines. The non-malignant cell-lines followed a biphasic curve whilst the prostate cancer cell-lines followed the typic sigmoidal curve.

Group I analogue EC_{50}/IC_{50} values in non-malignant and prostate cancer cell-lines were compared with the natural GA-T (**11**) using the student *t*-test with 99% confidence (*P* value < 0.01) (Figure 3.23). For the non-malignant cell-lines treated with analogue **107**, the EC_{50} values were determined and they were indicated as 1 and 2, referred to as first and second curve phase, in the table included in that figure.

For the non-malignant cell-lines, analogue **107** was better inhibitor than GA-T (**11**). However, **107** presented a biphasic curve and the comparison

was made only with the first phase that, in this case, represented approximately 65% of the overall curve. Although analogue **108** was less toxic for the normal cell-line than GA-T (**11**), it showed the same level of toxicity for the other non-malignant cell-lines, WPE1-NB14 and –NB26.



Cell-line		EC50-IC50/μM			
		107*	108	109	GA-T (11)
A	RWPE1	*1.* 1.86±0.32 *2.* 259±39	5.92±0.67	-	3.53±0.30
	WPE1-NB14	*1.* 2.22±0.64 *2.* 505±76	3.26±0.44	-	3.68±0.33
	WPE1-NB26	*1.* 2.17±0.26 *2.* 586±67	6.35±0.52	-	6.28±0.32
B	PC3	23.2±3.4	32.9±1.0	-	10.4±0.5
	PC3M	17.9±5.2	26.1±2.4	24.3±2.9	12.4±0.6
	DU145	18.8±1.9	43.7±1.7	89.2±4.2	15.1±1.0
	LNCaP	14.9±1.8	9.60±0.98	4.08±1.51	11.5±0.6

Figure 3.23 Group I GA analogues EC_{50}/IC_{50} values in prostate cell-lines. **A.** Non-malignant cell-lines. **B.** Cancerous cell-lines. *Non-malignant cell-lines treated with analogue **107** data fitted better in a biphasic curve with EC_{50} values indicated as 1 and 2 for each of the segments. For comparisons with this analogue the $EC_{50}1$ was chosen. For all the cell-lines, the activity of the analogues was compared with GA-T (**11**) using the student *t*-test with 99% confidence. * $P < 0.0001$; ** $P \leq 0.0009$.

In contrast, for the prostate cancer cell-lines, a statistical difference was found between GA-T (**11**) and all the analogues in this group. For PC3, PC3M-luc2 and DU145, the analogue IC_{50}s were higher, that is, they were poorer inhibitors than GA-T (**11**). The opposite effect was seen with LNCaP cells. In this cell-line, analogue **108** and **109** were more toxic than GA-T

(**11**). This results suggested that different mechanisms might be occurring for the different cell-lines.

In conclusion, the difference in C-3 functionality was evaluated for non-malignant and prostate cancer cell-lines. For the non-malignant cell-lines, β-hydroxyl and ketone groups at C-3 position reduced the viability differently. Analogue **107** seemed more toxic for all the non-malignant cell-lines. Furthermore, it may have different mechanisms of action for the inhibition at low or high concentrations, since biphasic curves were observed. Contrary to **107**, analogue **108** displayed a sigmoidal dose-response curve. Nonetheless, **108** showed 1.5- to 3-fold less toxicity than **107**, indicating that the β-hydroxyl group at C-3 may be superior at reducing the survival of the non-malignant cell-lines. Besides, it may suggest that hydrogen bonding interactions with the target protein are taking place at that position. It is noteworthy that analogue **108** and GA-T (**11**) despite having very different functional groups around their chemical structure, behaved similarly for the two pre-malignant cell-lines, WPE1-NB14 and –NB26, while **108** was less toxic for the normal cell-line, RWPE1.

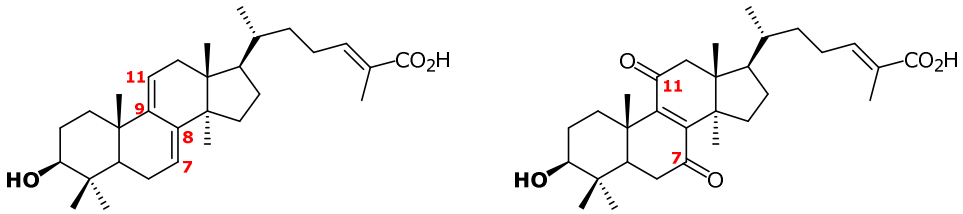
For the cancer cell-lines, the β-hydroxyl group reduced more the viability in the aggressive cell-lines, while the β-acetate enhanced the inhibition of the hormone sensitive cell-line, LNCaP. The effect of the α-acetate group in the more aggressive cell-lines remains to be determined. As GA-T (**11**) has this group and it showed higher activity, it might indicate that the α-acetate enhances the inhibition.

Min *et al*. investigated the cytotoxic and anti-angiogenic effect of various triterpenoids from GL against three cancer cell-lines, A549 (lung), MCF-7 (breast) and PC3 (prostate).[34] In their study they included triterpenoids with α- and β-hydroxyl, ketone or α-acetate groups at position C-3. They reported that the GA with an α-acetate group was the most powerful in the inhibition of the PC3 cell-line, with an IC_{50} 11.5 μM. However, it is difficult to compare the effect of each group individually since their chosen compounds differed at more than one position.

Liu *et al.* synthesised analogues of GA-DM and evaluated their activity against the PC3 cell-line. Their analogues had either C-3 ketone or β-hydroxyl groups. Contrary to our results, they concluded that C-3 ketone was essential for activity.

Additionally, Liu *et al.* determined the effects of ganoderma alcohols on the androgen receptor binding and the survival of LNCaP cells.[134] They selected ganoderma alcohols with either ketone or β-acetate at C-3 for their studies, finding that a ketone group at C-3 inhibited better the androgen receptor and the proliferation of LNCaP. Furthermore, they reported the 5α-reductase inhibitory effect of ganoderma triterpenoids that had either ketone or β-hydroxyl groups at C-3.[21, 135] Once more, triterpenoids with C-3 ketone were more powerful inhibitors. These results were in complete agreement with ours, comparing the IC_{50}s of **107** and **108** (Figure 3.23), **108** with a ketone at C-3 was 1.6-times a better inhibitor than **107** with a β-hydroxyl at that position. However, this is the first time that a comparison in the inhibitory potency among three different groups was performed with LNCaP. From the three functional groups evaluated, it seemed clear that the β-acetate was the most active.

b. Group II



59 **146**

Figure 3.24 Chemical structure of analogues **59** and **146**.

Two analogues belonging to group II were evaluated, **59** with a conjugated double bond system at $\Delta^{7(8),9(11)}$ and **146** with allyl ketones at position C-7 and C-11. Both of these compounds have a β-hydroxyl at C-3 and an α,β-unsaturated carboxylic acid at C-26 (Figure 3.24). Prostate cancer cell-lines were treated with these analogues at concentrations ranging from 0 to 1000 μM, whereas the non-malignant cell-lines were treated with **146** but not with **59**. Although sigmoidal curves were obtained for all the cell-lines, the relative value, EC_{50}, was calculated since the span of the curve was lower than 100%. It varied from 87% to 95% for cell-lines treated with **59**, but more variation was found for cell-lines treated with **146**. For non-malignant cell-lines treated with **146**, the span was reduced from 51% to 38% as the malignancy progressed, while PC3 and DU145 cells inhibited similarly as with analogue **59**, with spans 88% and 96%, respectively (Figure 3.25 and Appendix A2 – Figures A2-15 to A2-17). A comparison of these values for each of the analogues with GA-T (**11**) is found in Figure 3.26.

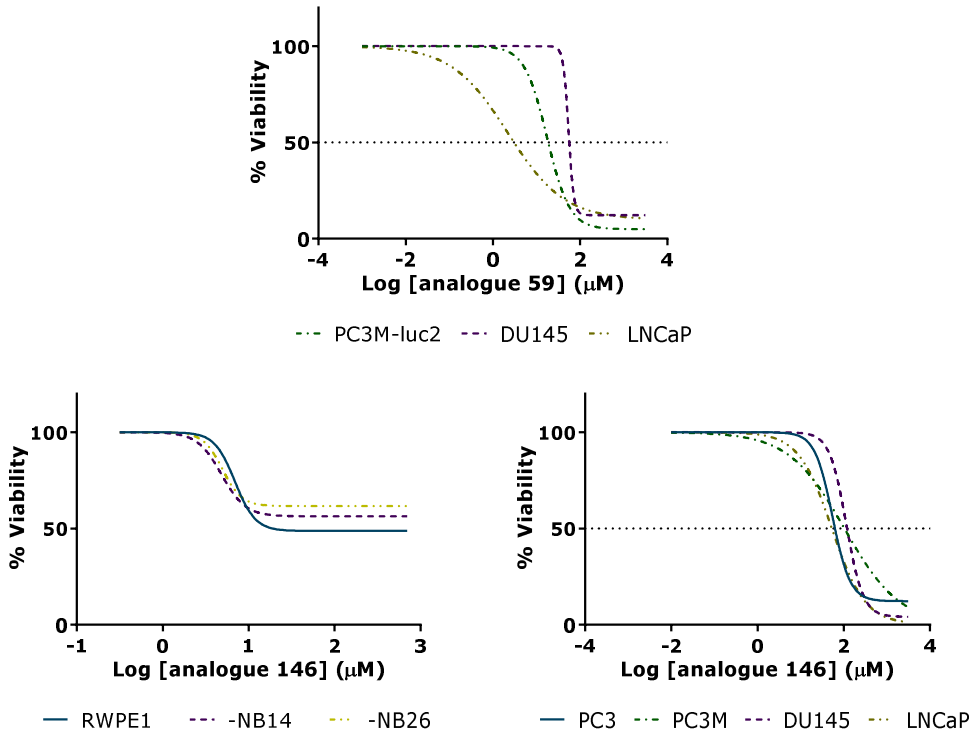
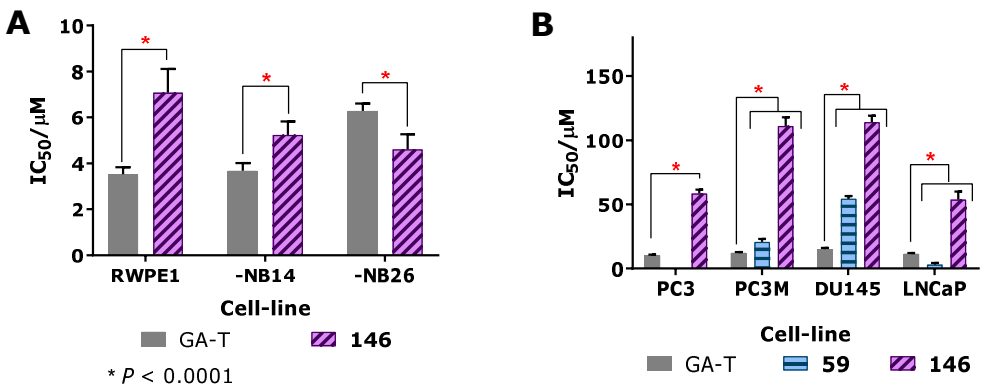


Figure 3.25 Dose-response curves of prostate cell-lines treated with analogues **59** and **146**.

In comparison with GA-T (**11**) in the non-malignant cell-lines, analogue **146** was less toxic for the normal cells, showing increasing toxicity as the malignancy of the cell-line progressed. For the prostate cancer cell-lines, both group II analogues presented EC_{50}/IC_{50} values higher than GA-T (**11**), except for **59** treatment in LNCaP. These results revealed that ketones at positions C-7 and C-11 reduced the activity of all the prostate cell-lines. Furthermore, as both GA-T (**11**) and **59** have the same conjugated double bond system at rings B/C, but GA-T (**11**) was more powerful inhibitor for the more aggressive cell-lines, this indicated that other functionalities around the molecule were playing a more important role for enhancing the reduction in viability.

Similar results were reported by other authors.[34, 35] Both Fang Lee and Min *et al*. analysed the inhibitory activity of a variety of GA for prostate cancer cell-lines. In their studies, they included GA with ketones, hydroxyls or acetate groups around positions C-7, C-11 and C-12. Besides, GA with a conjugated double bond at $\Delta^{7(8),9(11)}$ were also analysed. As for our observations, they concluded that GA with the conjugated double bond system at rings B/C were more powerful inhibitors.



Cell-line		EC50-IC50s/µM		
		59	146	GA-T
A	RWPE1	-	7.08±1.02	3.53±0.30
	WPE1-NB14	-	5.24±0.58	3.68±0.33
	WPE1-NB26	-	4.61±0.65	6.28±0.32
B	PC3	-	58.6±2.8	10.4±0.5
	PC3M-luc2	20.9±2.2	111±7	12.4±0.6
	DU145	54.4±2.1	114±5	15.1±1.0
	LNCaP	3.25±1.24	53.8±6.2	11.5±0.6

Figure 3.26 Group II analogues EC_{50}/IC_{50}s comparison. **A**. Non-malignant cell-lines. **B**. Cancerous cell-lines. . Non-malignant cell-lines treated with analogue **146** showed increased toxicity at increasing malignancy and prostate cancer cell-lines treated with group II analogues were less toxic than GA-T (**11**) for all the cell-lines, except for analogue **59** in LNCaP. *P < 0.0001.

c. Group III

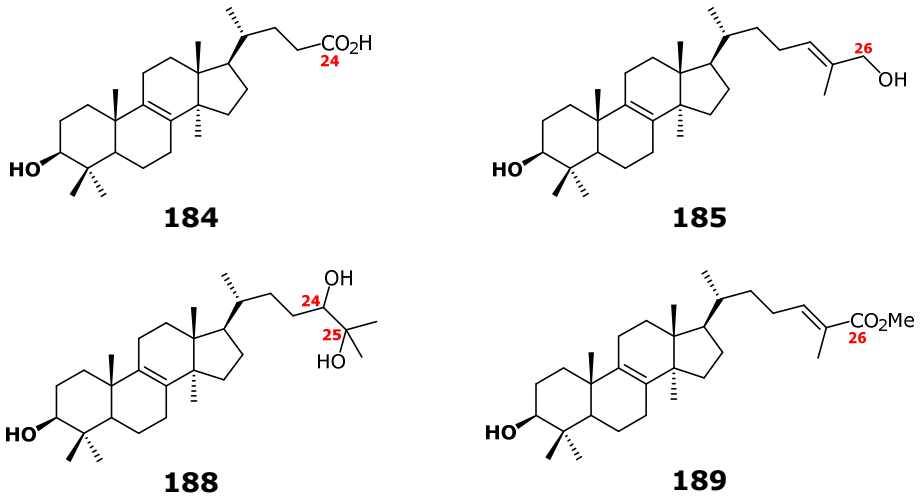
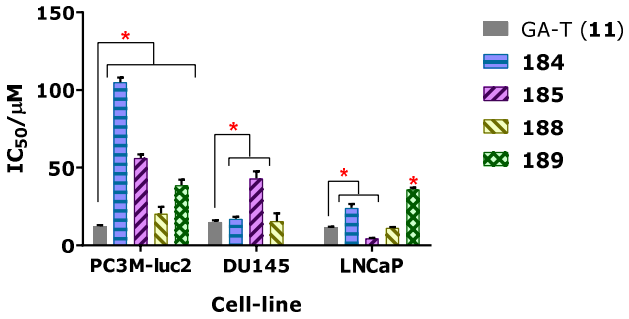


Figure 3.27 Chemical structures of analogues pertaining to group III, **184**, **185**, **188** and **189**.

Group III analogues included compounds with modifications on the side chain, **184**, **185**, **188** and **189** (Figure 3.27). Analogue **184** has a shorter side chain with the carboxylic acid at C-24. Both **185** and **188** have hydroxyls groups on the side chain. Analogue **185** has a primary alcohol at C-26 and a $\Delta^{24,25}$ double bond, while **188** has a 24,25-diol system and two methyl groups at C-25. Analogue **189** has an α,β-unsaturated methyl ester at C-26.

Prostate cancer cell-lines were treated with the above analogues at solutions concentrations ranging from 0 to 2000 μM. Sigmoidal dose-response curves were obtained from a non-linear regression analysis for all the cell-lines. Unfortunately, due to time constraints, the PC3 cell-line was not evaluated for any of the analogues in this group (Appendix A2 – Figures A2-18 to A2-21). A comparison of the IC_{50} values for the other cells is found in Figure 3.28.



	IC_{50}s/μM		
	PC3M-luc2	**DU145**	**LNCaP**
184	105±3	17.0±1.4	24.2±2.4
185	56.3±2.3	43.1±4.4	4.40±0.31
188	20.4±4.4	15.6±5.0	11.3±0.5
189	38.8±3.4	1052±172	36.0±1.2
GA-T (11)	12.4±0.6	15.1±1.0	11.5±0.6

Figure 3.28 IC_{50}s comparison of group III analogues with GA-T (**11**). Statistically a difference was found for all the analogues for all the cell-lines except for **188** in LNCaP. *P < 0.0001. Analogue **189** IC_{50} bar in DU145 was excluded from representation in this graph.

Contrary to the other two groups of analogues that clearly distinguished between the inhibition of hormone sensitive and refractive cell-lines, the inhibition of group III analogues was cell-line dependant, namely, they followed a different pattern for each of the cell-lines. Thus, for LNCaP the IC_{50} values increased in the order **185** < **188** ≈ GA-T (**11**) < **184** < **189**.

Analogue **185** was better than **107** and **188**. Hence, both the alcohol at C-26 and the $\Delta^{24.25}$ double bond appeared as important functional groups for raising the activity in this cell-line, whilst shortening of the side chain length and particularly, esterification were detrimental. Ordering the functionality from higher to lower activity, the complete sequence follows: allylic 26-OH > 24,25-diol > 24-CO_2H > -CO_2Me. In the hormone resistance cell-lines, despite PC3M-luc2 and DU145 coinciding in the best analogue, **188**, the inhibition was different for each of the cell-lines. In PC3M-luc2 the IC_{50} values increased in the order GA-T (**11**) < **188** < **189** < **185** < **184**; whereas in DU145 the order followed was **188** ≈ GA-T (**11**) < **184** < **185** << **189**. Consequently, **188**, with a 24,25-diol functionality and displaying similar activity as GA-T (**11**) was the best inhibitor for DU145, but analogue **188** was a worse inhibitor than GA-T (**11**) for PC3M-luc2, suggesting that the conjugated acid might be better than the 24,25-diol in this cell-line. Thus, ordering the functionality according their activity, it follows: α,β-unsaturated CO_2H > 24,25-diol > -CO_2Me > allylic 26-OH > 24-CO_2H for PC3M-luc2 and 24,25-diol > 24-CO_2H > allylic 26-OH >> -CO_2Me for DU145.

Min *et al.* analysed GA with a variety of side chain features: shorter side chain length, α,β-unsaturated carboxylic acid, allylic alcohols, diols, keto-acids, aliphatic and methyl esters.[34] The most active ones were, starting in decreasing order: allylic 26-OH > 24,25-diol > allylic 26,27-diol > short side chain > α,β-unsaturated CO_2H > CO_2Me. Evidently, these results formed part of the global substitution pattern of the molecule as no isolation of a particular functional group was performed, since in their studies, GA purified from the methanol extracts were used without further modifications. An exhaustive analysis of the functional groups is discussed in next chapter.

More related to our investigations, Fang Lee determined the inhibitory effects of GA with only one variation in their frame.[35] As a result, the isolation of one part of the molecule was achieved. By comparing the IC_{50} of GA-T (**11**) with that of GA-Me (**49**), it was possible to deduce that the presence of a C-22 acetate group in an α,β-unsaturated carboxylic acid side chain enhanced the reduction of the cell survival. As for our observations and that of Min, esterification of the acid group resulted in reduction of the activity. This contrasted with Liu's results with the methyl ester of GA-DM (**78**).[33] The higher activity observed for the ester (IC_{50} 3 μM) was rationalised as a consequence of better cell permeability. They demonstrated that hydrolysis of the ester was occurring inside the cell, and

it was the free acid which acted as the real growth inhibitor. However, this enhancement was only observed when a ketone was at C-3, since the methyl ester was inactive when at that position a hydroxyl was present.

Liu also investigated the effect of the reduction of GA-DM to the 3,26-diol **43** analogue in PC3 cell-line, as for our observations for PC3M-luc2 and DU145 treated with **185**, PC3 cell viability was not inhibited by this analogue.[33] However, it was very effective at inhibiting the LNCaP cell-line and binding to the androgen receptor.[134]

To summarise, the side chain functionality is important for activity. For the androgen-sensitive cell-line, the reduction of a carboxylic acid to the alcohol favoured the binding to the androgen receptor and consequently the growth inhibition of the cell. In the case of the more aggressive cell-lines, the inhibition was cell-line dependent. The highest activity was attributed to the conjugated carboxylic acid in PC3M-luc2 and the 24,25-diol in DU145, respectively.

3.3.3. Finding the best candidate: Summary

GA and their analogues inhibited the survival of both non-malignant and prostate cancer cell-lines. However, the degree of inhibition depends on the substitution pattern of the GA and the type of cell-line. Thus, the lowest IC_{50}s were detected for the non-malignant cell-lines, with slight distinction between the normal and pre-malignant cells. A difference in activity was also found among the more aggressive cell-lines and the hormone sensitive cell-line, LNCaP. For most of the GA and analogues the IC_{50} determined were higher for the prostate cancer cell-lines than for the non-malignant cells.

i. Non-malignant cell-lines

A summary of the IC_{50} values determined for the different natural and synthetic GA in the non-malignant cell-lines is given in Table 3.4. GA-H (**24**) stood out as the least toxic of all the GAs analysed. It displayed less toxicity for the normal cell-line, and moderate activity for the non-malignant cells. Alternatively, although analogue **107** presented a biphasic curve, with a major first phase, it was the most toxic compound being more toxic for the normal cell than for the non-malignant cell-lines. Analogue **146** presented a short span dose-response curve at the studied concentrations. However,

it was less toxic for the normal cell-line, showing increasing toxicity as the malignancy of the cell-lines increases. GA-T (**11**) and analogue **108** had similar activity for the non-malignant cell-lines. Nonetheless, analogue **108** was slightly less toxic for the normal cell-line than GA-T (**11**).

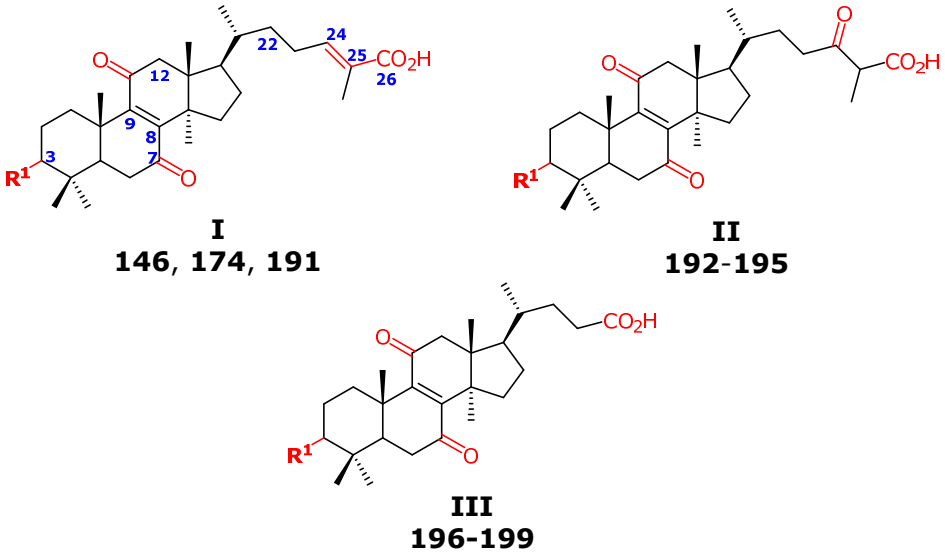
GA	EC_{50}-IC_{50}/μM		
	RWPE1	**WPE1-NB14**	**WPE1-NB26**
GA-H (**24**)	76.0±5.8	56.9±7.8	60.1±4.4
GA-T (**11**)	3.53±0.30	3.68±0.33	6.28±0.32
107*	*1.* 1.86±0.32 *2.* 259±39	*1.* 2.22±0.64 *2.* 505±76	*1.* 2.17±0.26 *2.* 586±67
108	5.92±0.67	3.26±0.44	6.35±0.52
146	7.08±1.02	5.24±0.58	4.61±0.65

Table 3.4 EC_{50}/IC_{50} value after treating non-malignant cell-lines with natural and synthetic GA. Values are given as mean ± SD. * Analogue **107** described biphasic curves with EC_{50} values indicated as 1 and 2.

Previous studies with the non-malignant cell-line WPE1-NB26 treated with GA-B (**8**), GA-F (**22**), GA-H (**24**), GA-K (**26**), GA-Me (**49**), GA-T (**11**) and LA-E2 (**83**) (Figure 3.19 or Appendix 5 for structures and Table 3.3 for IC_{50} values) revealed that the functional groups C-3 and C-7 hydroxyl and C-12 and C-22 acetate were important in reducing cell viability. Additionally, the $\Delta^{7(8),9(11)}$ conjugated double bond dramatically reduced the viability, whereas shortening the side chain resulted in lack of activity at the concentration studied.[35] Further studies with synthetic GA analogues concluded that C-3 β-acetate and ketone were more effective in reducing the survival even for short side chain analogues and that allylic ketones at C-7 and C-11 severely reduced it.[36] However, this is the first time that natural and synthetic GA were evaluated with a normal prostate cell-line. As we were interested in analogues that could be administered as chemo preventive agents, the functionalities should be chosen so that it would be non-toxic for the normal cell-line, RWPE1, but toxic for the pre-malignant cell-lines. Certainly, more studies are needed with the normal cell-line, nevertheless some candidates could be suggested.

Three types of analogues highlighted in Figure 3.29 might be both good candidates for the reduction in the survival of non-malignant cells and, at the same time, they might be less toxic to the normal cell-line. Their selection was based on the available data. All three candidates have allylic ketones at C-7 and C-11, differing at the side chain length and oxidation

level and in the C-3 functional group. From them, analogue **146** is the only one that has been evaluated against the normal and non-malignant cell-lines. However, it is expected that the activity of these analogues decrease in the following order: type I > type II > type III for the same R^1, and within the same analogue type, the activity would be affected by the chosen R^1 group as follows: β-OAc > β-OH > α-OAc > -C=O. Surely, the activity could be tuned further by incorporating C-12 or C-22 acetate groups or C-7 β-hydroxyl instead of having a ketone at this point.



Analogue	Type	R^1
146	I	β-OH
174	I	-C=O
191	I	β-OAc
192	II	β-OAc
193	II	α-OAc
194	II	β-OH
195	II	-C=O
196	III	β-OAc
197	III	α-OAc
198	III	β-OH
199	III	-C=O

Figure 3.29 Chemical structure of analogues with potential anti-proliferation activity for the non-malignant cell-lines. Highlighted in red are the functional groups for each of the studied areas.

ii. Prostate cancer cell-lines

A summary of the IC_{50}s for the natural and synthetic GA analysed against prostate cancer cell-lines is detailed in Table 3.5. None of the analogues

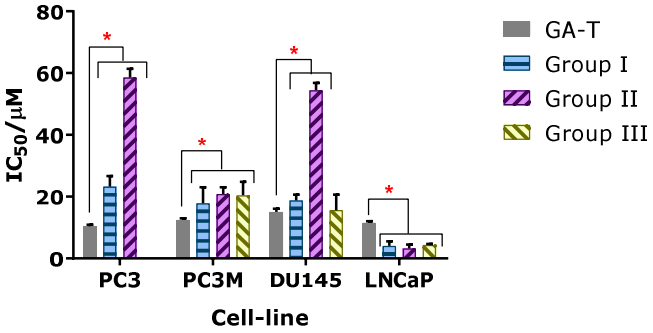
was a better inhibitor than GA-T (**11**) for the more aggressive cell-lines. However, for the hormone sensitive cell-line five analogues reduced the viability more effectively, **108**, **109**, **59**, **185** and **188**. A selection of the best candidate per group is indicated in Figure 3.30. However, PC3 was excluded in the graph for group III as no experiments were performed with that cell-line.

GA	EC_{50}-IC_{50}/μM			
	PC3	**PC3M-luc2**	**DU145**	**LNCaP**
GA-H (**24**)	1090±60	-	659±46	657±53
GA-T (**11**)	10.4±0.5	12.4±0.6	15.1±1.0	11.5±0.6
107	23.2±3.4	17.9±5.2	18.8±1.9	14.9±1.8
108	32.9±1.0	26.1±2.4	43.7±1.7	9.60±0.98
109	-	24.3±2.9	89.2±4.2	4.08±1.51
59	-	20.9±2.2	54.4±2.1	3.25±1.24
146	58.6±2.8	111±7	114±5	53.8±6.2
184	-	105±3	17.0±1.4	24.2±2.4
185	-	56.3±2.3	43.1±4.4	4.40±0.31
188	-	20.4±4.4	15.6±5.0	11.3±0.5
189	-	38.8±3.4	1052±172	36.0±1.2

Table 3.5 EC_{50}/IC_{50}s of natural and synthetic GA in prostate cancer cell-lines. Values are indicated as mean ± SD.

The activity seemed to be affected differently in the different cell-lines, but above all between the hormone refractory cell-lines and the hormone sensitive one. Generally, for all the cell-lines the incorporation of ketones in rings B/C reduced the activity severely. More specifically, for the aggressive cell-lines, the double bond $\Delta^{8,9}$ was more effective at reducing the viability than the conjugated double bond. However, the reverse applied in LNCaP. As for C-3 substitution, α-acetate was the group that reduced the survival the most for the hormone resistant cell-lines, whereas β-acetate was the best for LNCaP. The actual order of activity was cell-line dependent. Thus, the carbonyl was more active in LNCaP, followed by DU145, whilst it was the least active in PC3M-luc2. The side chain functionality that caused a better inhibitory effect was also cell-line dependent. However, the best functionality group for the aggressive cell-lines was the 24,25-diol for DU145 and the conjugated carboxylic acid for PC3M-luc2, while the C-26 hydroxyl was the most effective group for LNCaP.

With this information in hand, analogue candidates could be postulated that maximises the reduction in the viability for the prostate cancer cell-lines. It is anticipated that the binding interactions of these entities with its target would be larger. Two scenarios have been envisaged, one for hormone sensitive cell-lines like LNCaP and the other for the more aggressive, hormone irresponsive cell-lines.



Cell-line	IC_{50}/µM			
	Group I	**Group II**	**Group III**	**GA-T**
PC3	23.2±3.4 (**107**)	58.6±2.8 (**146**)	-	10.4±0.5
PC3M-luc2	17.9±5.2 (**107**)	20.9±2.2 (**59**)	20.4±4.4 (**188**)	12.4±0.6
DU145	18.8±1.9 (**107**)	54.4±4.5 (**59**)	15.6±5.0 (**188**)	15.1±1.0
LNCaP	4.08±1.51 (**109**)	3.25±1.24 (**59**)	4.40±0.31 (**185**)	11.5±0.6

Figure 3.30 IC_{50}s of the best candidate for each group in each cell-line.

Four compounds with potentially high inhibitory activity and binding interactions are given in Figure 3.31 **A**, these are: **110**, **200**, **201** and **202**. All these compounds have an α-substituted at C-3 in addition have the features discussed above on the middle rings and on the side chain.

DU145 viability was less inhibited for **59** in group II than for the compounds of the other two groups, which additionally presented very similar inhibitory activity to that of GA-T (**11**). This suggested that the conjugated double bond system may disrupt both the binding interactions and the growth inhibitory potency, hence from the four proposed compounds in Figure 3.31 **A**, only two: **110** and **201** might be more powerful inhibitors for this cell-line.

As mentioned above, the LNCaP cell-line viability was further reduced for the best analogues in each group than for GA-T. This implied that the β-acetate at C-3, the conjugated double bond at rings B/C and the allylic 26-hydroxyl groups were very important for increasing the inhibition. Figure 3.31 **B** highlights a compound that could potentially behave as a better suppressor of the survival for this cell-line. It is predicted that **203** may display a high affinity for the androgen receptor, as well.

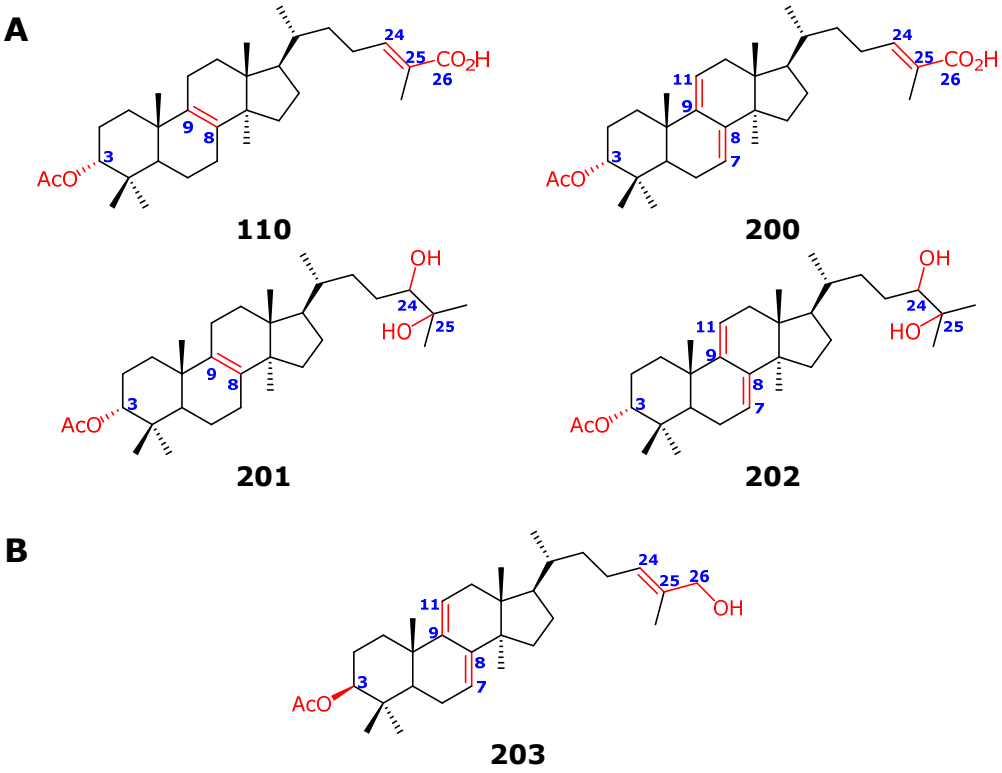


Figure 3.31 Proposed analogues with potentially high inhibitory activity and binding interaction in prostate cancer cell-lines. **A.** Refractory cell-lines. **B.** Hormone sensitive cell-lines.

3.4. Summary and conclusions

Non-malignant and cancerous prostate cell-lines were used for evaluating the reduction of their viability caused by treatment of the cells with natural or synthetic ganoderic acids. The MTT assay was used throughout. To set up the experiments, the best cell concentration for each of the cell-lines studied as well as the cytotoxicity of the vehicle solvent were determined. From the two solvents investigated, dimethyl sulfoxide and methanol, the latter was chosen and the working solution concentrations prepared from a 20 mM stock solution in methanol, which was diluted to the desired concentration with the appropriate media solution. Time-course studies

performed at 24 h, 48 h and 72 h, revealed that the natural and synthetic GA could supress the survival of PC3 cell-line in a time- and dose-dependent manner. GA-H (**24**) and analogues **108**, **146** and **174** were used in these assays. GA-H (**24**) turned out to be a poor inhibitor, while the synthetic analogues were more active. The inhibition potency of these analogues, going from less to more activity, was: **146** ≈ **174** < **108**. This indicated that position C-3 and ketones at rings B/C were important for activity. However, the activity of the GA contrasted with that of Taxotere (**190**), a drug currently being administered to patients with refractory prostate cancer. The IC_{50}s of the former were several orders of magnitude lower, in the micromolar range, than the latter, with EC_{50}s in the nanomolar range. Two natural GA, GA-T (**11**) and GA-H (**24**), were used in the treatment of non-malignant and cancerous cell-lines. The experiments were performed at 72 h, as this time-point provided the best dose-response results. For both types of cell-lines, GA-T (**11**) proved a better inhibitor. Nonetheless, the non-malignant cell-lines were more easily inhibited, which could be rationalised because of their androgen receptor sensitivity. Interestingly, GA-H (**24**) was less toxic for the normal cell-line than for the non-malignant ones. Three analogues, **107**, **108** and **146** were evaluated for the non-malignant cell-lines. Arranging them in order of activity, **107** > **108** > **146**. Although analogue **107** was more active than GA-T (**11**), it presented a characteristic feature that was also observed for Taxotere (**190**): the inhibitory curve was biphasic. Analogue **108** inhibited the cells similarly to GA-T (**11**) except for RWPE1, for which, it was less toxic. These two analogues were much more active than GA-H (**24**). In contrast, analogue **146** was inactive, since the inhibitory curves displayed a very short span that barely caused a reduction of 50% viability. Nonetheless, a clear difference was found between the normal cell-line and the non-malignant ones. As for GA-H (**24**), analogue **146** was less toxic for RWPE1 and the toxicity increased progressively as the malignancy developed. The analogues evaluated for prostate cancer cell-lines were divided in three groups. Group I included analogues with C-3 modifications, **107**, **108** and **109**. The functional groups studied were β-hydroxyl, ketone and β-acetate. The most active of the three was the β-hydroxyl for the more aggressive cell-lines and the β-acetate for LNCaP. Nonetheless, the inhibitory activity was lower than that of GA-T (**11**) except for LNCaP that was more inhibited by some of the analogues than for GA-T (**11**). Group II included analogues **59** and **146**. In this group, the effect of the ketones of the middle rings B/C

was studied. Analogue **146**, with 7,11-diketone groupps, inhibited less the viability. As for group I, a difference was observed between the refractory cell-lines and LNCaP, this latter being much more sensitive to the treatment with **59** than GA-T (**11**). Finally, group III enclosed analogues with modifications on the side chain, **184**, **185**, **188** and **189**. It is worth highlighting that from this group **185** and **188** were the more active, the former for the hormone resistant cell-lines and the latter for LNCaP. Both these analogues have hydroxyls on the side chain, **185** an allylic 26-hydroxyl and **188** a 24,25-diol. With this information in hand, we proposed alternative analogues with potentially more activity than their parents. Thus, analogues **146**, **174** and **191**-**199**, with different C-3 and side chain functionalities and common allylic ketones at C-7 and C-11 may be better inhibitors for the non-malignant cell-lines being less toxic for normal cells, while analogues **110**, **200**-**202** with C-3 α-acetate, either single or double bonds at rings B/C and either α, β-unsaturated carboxylic acid or 24,25-diol side chain could be excellent candidates for the androgen unresponsive cell-lines and analogue **203** with C-3 β-acetate, a conjugated double bond system at rings B/C and an allylic 26-hydroxyl would be more appropriate for LNCaP. The target molecules involved in the observed proliferation remain to be determined. However, previous studies from Liu suggested that these are the androgen receptor and 5α-reductase for the hormone responsive cell-line and α, β-tubulin to the hormone refractory cell-lines.[33,134,135]

4. SAR Analysis

To perform a structure activity relationship (SAR) analysis of the ganoderic acids (GA) in prostate cell-lines, the effect that the different functional groups have in modulating the activity was investigated. In addition to our results, published studies from Liu,[21,33,134] Min[34] and Fang Lee[35] were included in this analysis, since they explored the effects of structurally different GA isolated from *Ganoderma lucidum* mushroom in the same cell-lines. Thus, Liu *et al.* determined that triterpenes with C-3 ketone and hydrophobic 17β-side chain were the better to inhibit the activity of 5α-reductase and the androgen receptor.[21,134] Furthermore, they suggested that α,β-tubulin may be one of the GA targets.[33] Min *et al.* studied the cytotoxic and anti-angiogenic effects of triterpenoids isolated from the mushroom.[34] Fang Lee investigated the effect of the GA in both non-malignant and prostate cancer cell-lines. She identified five putative targets for the GA following proteomic analysis in which these proteins were significantly up or down regulated. These putative targets were: vimentin, β-tubulin, cytokeratin-19, heterogeneous nuclear ribonucleoprotein C (hnRNP C) and enolase α.[35] Prostate cancer cell-lines, PC3, PC3M, DU145 and LNCaP and non-malignant cell-lines RWPE1, WPE1-NB14 and –NB26 were used to performed these studies.

4.1. Inhibition of the 5α-reductase and androgen receptor activity

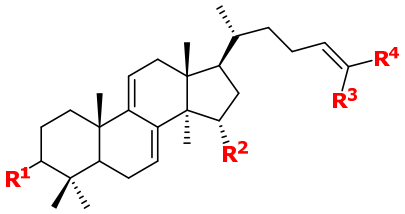
Both 5α-reductase and the androgen receptor play an important role in the maintenance of the prostate gland as well as being involved in prostate cancer progression. 5α-Reductase is responsible for the reduction of testosterone (**76**) to its active form dihydrotestosterone (**77**) (DHT).[21] The androgen receptor regulates transcription in response to androgens, having a higher affinity for DHT (**77**).[134]

4.1.1. Inhibition of the 5α-reductase activity

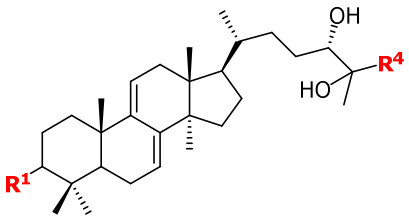
Liu *et al.* studied the inhibitory effect of triterpenes isolated from the fruiting bodies of GL on 5α-reductase activity.[21,135] In their studies, seventeen triterpenes were evaluated, from which three had promising inhibitory effects (Figure 4.1 and Figure 4.2). These compounds were: GA-TR (**58**) > GA-DM (**32**) >> GENON2OL (**61**).

These all have a C-3 ketone and a double bond at $\Delta^{24,25}$. They differ at the substitution pattern of rings B/C/D and the oxidation level at C-26. Thus, GA-TR (**58**) and GENON2OL (**61**) have a conjugated double bond system $\Delta^{7(8),9(11)}$ and a C-15 α-hydroxyl, while GA-DM (**32**) has a double bond $\Delta^{8,9}$ and a C-7 ketone. GA-TR (**58**) and GA-DM (**32**) have a conjugated α,β-unsaturated C-26 carboxylic acid, whereas GENON2OL (**61**) has an allylic 26-hydroxyl.

As GA-TR (**58**) and GA-DM (**32**) were the most active compounds, it could be concluded that the C-3 ketone and C-26 α,β-unsaturated carboxylic acid were essential for activity. 5α-Reductase was remarkably less inhibited by GENON2OL (**61**), as the only difference between GA-TR (**58**) and GENON2OL (**61**) is at C-26. This indicated that the C-26 carboxylic acid was essential for activity. By comparing GA-TR (**58**) and GA-DM (**32**) with their respective methyl esters MeGA-TR (**204**) and MeGA-DM (**78**), it was obvious that esterification of the C-26 carboxylic acid resulted in loss of activity, signalling that ionic or electrostatic interactions with the enzyme might be occurring at that position that were disrupted when the carboxylic acid was methylated. However, what is the case on B/C/D rings? Apparently, despite GA-TR (**58**) and GA-DM (**32**) having very different substitution patterns at these rings, they inhibited 5α-reductase to a similar level. From here it could be deduced that both hydrogen bonding interactions either at C-7 ketone or 15α-hydroxyl and stacking interactions of the double bonds in rings B/C with the enzyme were taking place, and therefore these positions were important for activity.



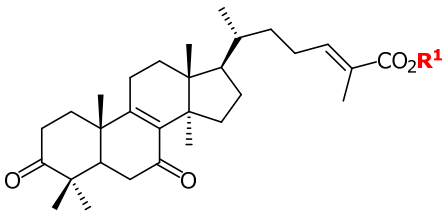
58, **61**, **63**, **64**, **204**, **205**



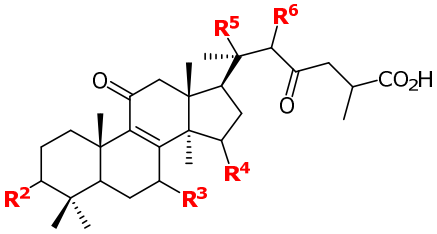
65, **67**, **68**

Triterpene	IC_{50}/μM	R^1	R^2	R^3	R^4
GA-TR (**58**)	8.6[21]	-C=O	α-OH	$-CH_3$	$-CO_2H$
GENON2OL (**61**)	41.9[21,135]	-C=O	α-OH	$-CH_3$	$-CH_2OH$
GIOL-F (**63**)	>300[21]	-C=O	-H	$-CH_2OH$	$-CH_2OH$
GOL-B (**64**)	>300[21]	β-OH	-H	$-CH_3$	$-CH_2OH$
MeGA-TR (**204**)	>50[21]	-C=O	α-OH	$-CH_3$	$-CO_2Me$
G3OL (**205**)	>300[21]	β-OH	-H	$-CH_2OH$	$-CH_2OH$
GIOL-A (**65**)	>300[21,135]	β-OH	-	-	$-CH_2OH$
GN3OL (**67**)	>300[21,135]	-C=O	-	-	$-CH_2OH$
LOL-B (**68**)	>300[135]	β-OH	-	-	$-CH_3$

Figure 4.1 Triterpenes **58**, **61**, **63**-**65**, **67**, **68**, **204**, **205** employed in the 5α-reductase binding studies.[21,135] GA = ganoderic acid; MeGA -= ganoderic acid methyl ester; GENON2OL = 15α,26-dihydroxy-5α-lanosta-7,9,24*E*-triene-26-oic acid; GIOL = ganoderiol; GOL = ganoderol; G3OL = ganodermatriol; GN3OL = ganodermanontriol; LOL = lucidumol.



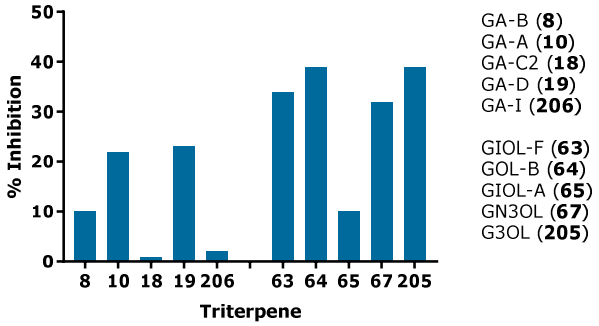
32, **78**



8, **10**, **18**, **19**, **206**, **213**

Triterpene	IC_{50}/μM	R^1	R^2	R^3	R^4	R^5	R^6
GA-DM (**32**)	10.6[21,135]	-H	-	-	-	-	-
MeGA-DM (**78**)	>50[21]	$-CH_3$	-	-	-	-	-
GA-A (**10**)	>300[21,135]	-	-C=O	β-OH	β-OH	-H	-H
GA-B (**8**)	>300[21]	-	β-OH	-C=O	β-OH	-H	-H
GA-C2 (**18**)	>300[21]	-	β-OH	α-OH	α-OH	-H	-H
GA-D (**19**)	>300[21,135]	-	-C=O	-C=O	β-OH	-H	-H
GA-I (**206**)	>300[21]	-	β-OH	-C=O	β-OH	-OH	-H
GenA-A (**213**)	>300[135]	-	-C=O	β-OH	α-OH	$\Delta^{20,22}$	

Figure 4.2 Triterpenes **8**, **10**, **18**, **19**, **32**, **78**, **206**, **213** employed in the 5α-reductase inhibitory activity studies.[21,135] GenA = ganoderenic acid.



GA	% Inhibition	Triterpene	% Inhibition
GA-B (**8**)	10	GIOL-F (**63**)	34
GA-A (**10**)	22	GOL-B (**64**)	39
GA-C2 (**18**)	1	GIOL-A (**65**)	10
GA-D (**19**)	23	GN3OL (**67**)	32
GA-I (**206**)	2	G3OL (**205**)	39

Figure 4.3 Triterpene effect on the inhibition of 5α-reductase activity at concentration 667 μM.[21]

Similarly, from the non-active compounds in Figure 4.1 some information about the effect on the activity due to the functional groups was extracted (Figure 4.3). Hence, GENON2OL (**61**) inhibited the enzyme better than GOL-B (**64**). These two compounds differ at C-3 and C-15, the former having a ketone at C-3 and an α-hydroxyl at C-15, whilst a β-hydroxyl at C-3 and non-substitution at C-15 was encountered in the latter. As GOL-B (**64**) was less active, this suggested that both C-3 ketone and C-15 α-hydroxyl were playing a significant role in the inhibition of the enzyme, possibly behaving as hydrogen acceptor and donor respectively, during the interaction with the enzyme. Likewise, increasing the polarity of the side chain with a C-27 hydroxyl and the absence of a C-15 hydroxyl, as in GIOL-F (**63**) reduced the enzyme activity. However, no difference in activity was found between GOL-B (**64**) and G3OL (**205**), indicating that C-27 substitution was less important for activity than the C-15 α-hydroxyl. Nonetheless, with a more polar C-27 substitution the effect on the activity of C-3 position was reversed, hence the C-3 β-hydroxyl (G3OL (**205**)) inhibited the activity of 5α-reductase more than the C-3 ketone (GIOL-F (**63**)). The double bond $\Delta^{24,25}$ seemed important for activity, as well. Since, increasing the polarity of the side chain with a 24,25-diol system (GN3OL (**67**)) reduced the activity. As observed previously, modifying C-3 ketone by β-hydroxyl (GIOL-A (**65**)) decreased the activity considerably. Reduction of the activity was also observed when the C-26 hydroxyl was replaced by a

methyl (LOL-B (**68**)). Figure 4.4 summarises the effects of the functional groups at the positions above mentioned.

From Figure 4.2, GA with C-11 ketone were less active. These compounds also have a side chain with C-23 ketone and different functionality at C-3, C-7, C-15 and C-20. The presence of C-7 α-hydroxyl (GA-C2 (**18**)) or C-20 hydroxyl (GA-I (**206**)) significantly decreased the activity of the GA (Figure 4.3). However, no difference in activity was found when modifying C-7 from β-hydroxyl (GA-A (**10**)) to ketone (GA-D (**19**)) or when a double bond at $\Delta^{20,22}$ (GenA-A (**213**)) was introduced.

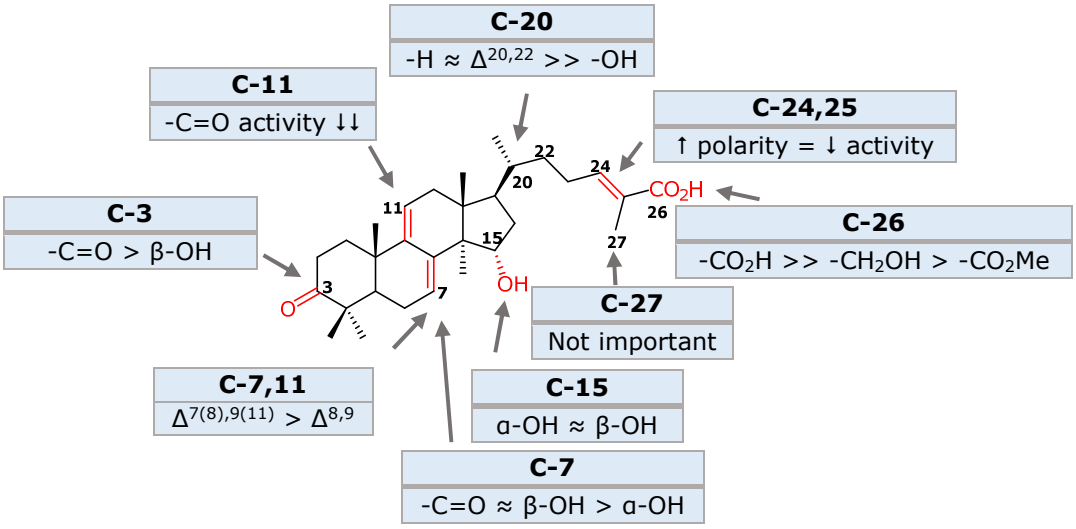


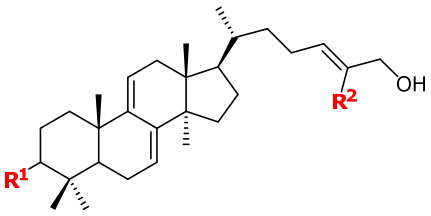
Figure 4.4 SAR analysis for 5α-reductase.

4.1.2. Inhibition of the androgen receptor activity

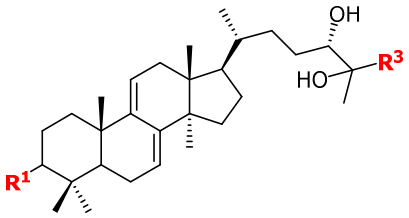
Liu *et al*. studied the inhibitory effect of six ganoderma alcohols in the androgen receptor activity as well as determining their proliferation effect on the prostate cancer cell-line LNCaP.[134] The evaluated ganoderma alcohols are indicated in Figure 4.5. All the compounds of this series have a conjugated double bond $\Delta^{7(8),9(11)}$ in common and differ at C-3 and the functionality of the side chain. According to the saturation on the side chain, the compounds were divided in two main groups. In the first group, there are compounds which are unsaturated at $\Delta^{24,25}$ and a C-26 allylic alcohol. In the second group, there are compounds with a 24,25-diol system and a saturated side chain.

Ganoderma alcohols pertaining to the first group inhibited the androgen receptor more effectively than their counterparts in the second group. Hence, the presence of a double bond at $\Delta^{24,25}$ was essential for increasing

this inhibitory activity. Furthermore, within the same group, *i.e.*, comparing the IC_{50} of GIOL-F (**63**) with G3OL (**205**) or GIOL-A (**65**) with GN3OL (**67**), it was evident that C-3 ketone rather than a hydroxyl was essential for enhancing the inhibition of the androgen receptor activity. Finally, a reduction in the side chain polarity as in GOL-B (**16**) or LOL-B (**68**) had the consequence of enhancing the inhibitory activity. In Figure 4.6 a summary of all these findings has been depicted.



63, **64**, **205**



65, **67**, **68**

Triterpene	IC_{50}/μM	R^1	R^2	R^3
GIOL-F (**63**)	25	-C=O	$-CH_2OH$	-
GOL-B (**64**)	16	β-OH	$-CH_3$	-
G3OL (**205**)	100	β-OH	$-CH_2OH$	-
LOL-B (**68**)	90	β-OH	-	$-CH_3$
GIOL-A (**65**)	470	β-OH	-	$-CH_2OH$
GN3OL (**67**)	400	-C=O	-	$-CH_2OH$

Figure 4.5 Triterpenes **63**-**68**, **205** used for the androgen receptor binding activity studies.[134] GIOL = ganoderiol; GOL = ganoderol; G3OL = ganodermatriol; LOL = lucidumol; GN3OL = ganodermanontriol.

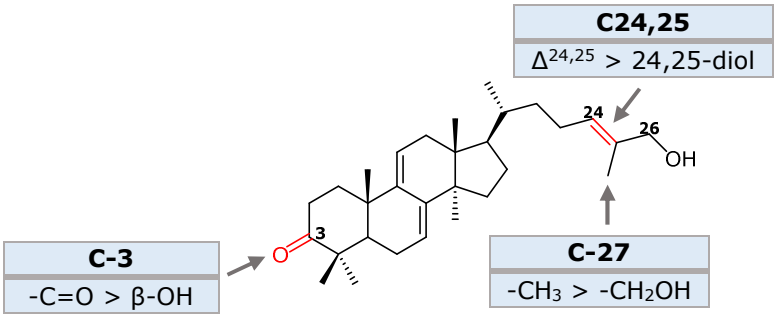
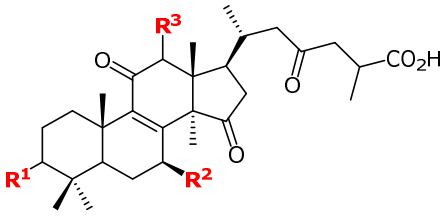


Figure 4.6 SAR analysis of ganoderma alcohols in the inhibition of the androgen receptor.

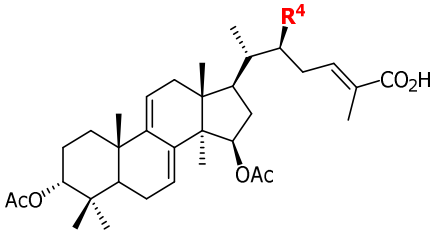
In a comprehensive review Singh *et al.* described in more detail a SAR analysis of the androgen receptor in which steroidal and non-steroidal compounds were assessed.[136] They highlighted the need for a carbonyl at C-3 and a hydroxyl at C-17 for enhancing the inhibitory activity of the receptor. Thus, their observations are consistent with ours.

4.2. Inhibition of the cell viability in non-malignant and prostate cancer cell-lines

The effect of triterpenes, mainly GA, on non-malignant and prostate cancer cell-lines has been reported by several groups.[33-35,134] Fang Lee at Nottingham analysed both natural and synthetic GA in the non-malignant cell-line RWPE1-NB26 as well as in the prostate cancer cell-lines, PC3M and/or DU145.[35] Liu *et al*. included LNCaP and PC3 in their assays.[33,134] This latter cell-line was also employed by Min *et al*. in their research of cytotoxic and anti-angiogenic effects of triterpenes isolated from GL.[34] In chapter 3 of this thesis, a description of the survival effect of GA and their analogues in normal prostate RWPE1 and non-malignant WPE1-NB14 and -NB26 as well as prostate cancer cell-lines PC3, PC3M-luc2, DU145 and LNCaP is given.



8, 22, 24



11, 49

Triterpene	IC$_{50}$/µM		R^1	R^2	R^3	R^4
	Non-mal[1]	PCa[2]				
GA-B (**8**)	23.2±2.2	24.9±4.5[a]	β-OH	β-OH	-H	-
GA-F[d] (**22**)	>1000	>1000	-C=O	-C=O	-H	-
GA-H[c,d] (**24**)	22.9±2.3[c] >1000[d]	30.2±1.1[a,c] >1000[d]	β-OH	-C=O	β-OAc	-
GA-K (**26**)	14.2±1.3	23.2±2.8[a]	β-OH	β-OH	β-OAc	-
GA-T (**11**)	0.42±0.10	15.7±2.6[b]	-	-	-	-OAc
GA-Me (**49**)	0.90±0.17	22.6±1.8[b]	-	-	-	-H

Figure 4.7 Evaluation of functional groups at positions C-3, C-7, C-12 and C-22 in non-malignant and cancerous prostate cell-lines.[35] Triterpenes **8**, **11**, **22**, **24**, **26** and **49** were used in these studies. Non-mal=Non-malignant cell-line, WPE1-NB26; PCa=prostate cancer cell-line; a DU145; b PC3M; c GA from collaborators; d commercial GA from Planta Analytica.

Fang Lee evaluated the effect of seven natural GA: GA-B (**8**), GA-F (**22**), GA-H (**24**), GA-K (**26**), GA-T (**11**), GA-Me (49) and LA-E2 (**83**) plus two synthetic compounds: **106** and **108** (Figure 4.7 and Figure 4.8) in both non-malignant and prostate cancer cell-lines. A large difference in activity was encountered between the more and less substituted GA. Thus, the less substituted GA were better inhibitors for both types of cell-lines. Suggesting

that positions C-7, C-11, C-12, C-22 and C-23 might be important for enhancing the inhibition. Hence, comparing the activity of GA-B (**8**) with GA-K (**26**), the effect of a substitution at C-12 was evaluated. The presence of a β-acetate at that position resulted in an enhancement of the inhibition of both types of cell-lines. However, the effect was larger for the non-malignant cell-line, 1.6- *vs*. 1.1-fold. Likewise, comparing the IC_{50} of GA-H (**24**) with GA-K (**26**), the effect of different functional groups in C-7 was determined. In this case, a β-hydroxyl was better than carbonyl for reducing the IC_{50} value, namely, increasing the inhibition. When comparing GA-Me (**49**) with GA-T (**11**), the effect of C-22 substitution was assessed. A β-acetate group in this position inhibited more efficiently both types of cell-lines. Furthermore, the conjugated double bond $\Delta^{7(8),9(11)}$ was key to increase the toxicity of the GA above all in the non-malignant cell-line, where a significant reduction, up to 55-fold, of the IC_{50} was observed. This enhancement was much more moderate in the prostate cancer cell-lines, where up to 2-fold IC_{50} reduction was observed. It is noteworthy, that both the conjugated double bond in rings B/C and β-acetate in C-22 reduced much more the IC_{50} value than the conjugated double bond alone (GA-T (**11**) *vs*. GA-Me (**49**)).

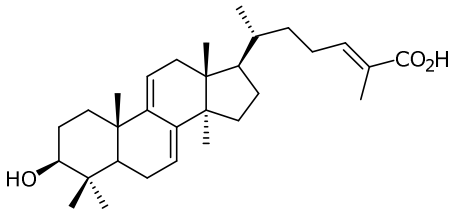
As highlighted in Table 4.1, shortening the length of the side chain, as in lucidenic acid LA-E2 (**83**) (Figure 4.8), had the effect of reducing considerably its activity. However, non-substituted B/C/D rings increased remarkably the inhibition potency for both types of cell-lines (**106**).

Triterpene	**IC_{50}/μM**	
	WPE1-NB26	**DU145**
LA-E2 (**83**)	>1000	>1000
106	56.2±8.5	279±16
108	3.76±0.23	68.5±4.6

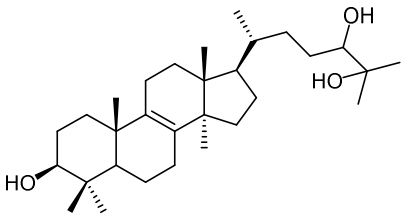
Table 4.1 Evaluation of positions C-3, C-7, C-11, C-12 and C-15 functionalities of triterpenes **83**, **106** and **108** in the non-malignant prostate cell-line WPE1-NB26 and in the prostate cancer cell-line DU145.[35]

A slightly different trend in the inhibitory effect of the GA was noticed for the normal and non-malignant cell-lines analysed: RWPE1, WPE1-NB14 and -NB26 (Figure 4.8, Table 4.2). Thus, some GA were more toxic for the non-malignant cell-lines WPE1-NB24 and -NB26 than for the normal cell-line RWPE1, and this specificity for malignancy would be the ideal trend for a chemo preventive agent. In this line, GA-H (**24**) and **146** followed this

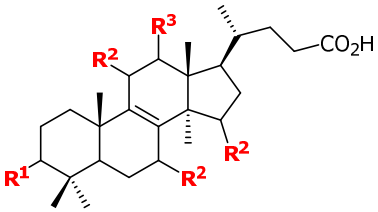
pattern. GA-H (**24**) has ketones at C-7; C-11 and C-15 and on the side chain, while analogue **146** has ketones only at B and C rings. Therefore, the presence of ketones around the rings could favour the differentiation of activity between normal or non-malignant cell-lines.



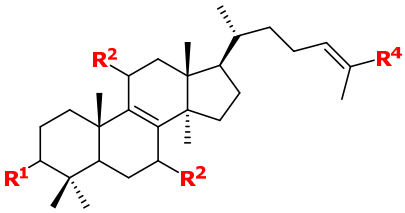
59



188



83, **106**, **184**



107-109, **146**, **185**, **189**

Analogue	R^1	R^2	R^3	R^4
LA-E2 (**83**)	β-OH	-C=O	β-OAc	-
106	β-OAc	-H	-H	-
184	β-OH	-H	-H	-
107	β-OH	-H	-	$-CO_2H$
108	-C=O	-H	-	$-CO_2H$
109	β-OAc	-H	-	$-CO_2H$
146	β-OH	-C=O	-	$-CO_2H$
185	β-OH	-H	-	$-CH_2OH$
189	β-OH	-H	-	$-CO_2Me$

Figure 4.8 Compounds **59**, **83**, **106**-**109**, **146**, **184**, **185**, **188**, **189**.

Liu *et al.* analysed the effect of six ganoderma alcohols in LNCaP: GIOL-F (**63**), GOL-B (**64**), G3OL (**205**), GIOL-A (**65**), GN3OL (**67**) and LOL-B (**68**) (Figure 4.5 and Table 4.3)[134] They found that the three first inhibited the cell growth when cultured with testosterone (**76**) or DHT (**77**) in the order **64** > **63** > **205**. However, the latter three did not produce that effect. The main differences between these two groups are at C-3 and on the side chain. Hence, rearranging the functional groups according to their inhibitory ability, it was revealed that at position C-3, carbonyl > β-OH (GIOL-F (**63**) *vs.* G3OL (**205**)), whilst at the side chain three observations could be made, allylic 26-OH > 24,25-diol (GOL-B (**64**) *vs.* LOL-B (**68**)); 24,25-diol > allylic 26,27-diol (LOL-B (**68**) *vs.* G3OL (**205**)) and 24,25-diol > 24,25,26-triol (LOL-B

(**68**) *vs.* GIOL-A (**65**)). Thus, the functionalities that enhanced the inhibition were: allylic 26-OH > 24,25-diol ≈ allylic 26,27-diol >> 24,25,26-triol.

GA	EC_{50}-IC_{50}/μM		
	RWPE1	**WPE1-NB14**	**WPE1-NB26**
GA-H (**24**)	76.0±5.8	56.9±7.8	60.1±4.4
GA-T (**11**)	3.53±0.30	3.68±0.33	6.28±0.32
107[a]	*1.* 1.86±0.32 *2.* 259±39	*1.* 2.22±0.64 *2.* 505±76	*1.* 2.17±0.26 *2.* 586±67
108	5.92±0.67	3.26±0.44	6.35±0.52
146[b]	7.08±1.02	5.24±0.58	4.61±0.65

Table 4.2 Summary of the EC_{50}-IC_{50} values for the natural and synthetic GA, GA-H (**24**) and GA-T (**11**), **107**, **108** and **146** in non-malignant cell-lines. a Analogue **107** described a biphasic curve with EC_{50} for each segment denoted as 1 and 2. b Values for analogue **146** correspond to the EC_{50}.

From our studies with LNCaP cells, Table 4.4, it was deduced that effectively C-3 carbonyl (**108**) was better than β-hydroxyl (**107**), but β-acetate (**109**) inhibited 2.4-fold more the growth than the carbonyl group (**108**). Besides, **59** with a conjugated double bond $\Delta^{7(8),9(11)}$ was the best inhibitor of all the analogues examined. Alternatively, the addition of ketones on rings B/C, as in **146**, dramatically reduced the inhibition power 3.6-fold compared with **107**. Finally, shortening the side chain (**184**) and esterification (**189**) reduced significantly the inhibitory capacity. However, as indicated by Liu, the presence of hydroxyls on the side chain (**185** and **188**) were preferred to the acid (**107**), the allylic 26-hydroxyl **185** was 2.6- and 3.4-fold stronger towards the inhibition than the 24,25-diol **188** and the conjugated acid **107**, respectively. A summary of the effect of different positions and functional groups in the activity is found Figure 4.9.

Compound	% Cell viability	
	***vs*. testoterone**	***vs*. DHT**
GOL-B (**64**)	59	53
G3OL (**205**)	90	92
GIOL-F (**63**)	81	83
LOL-B (**68**)	103	103
GN3OL (**67**)	94	106
GIOL-A (**65**)	109	108

Table 4.3 Effect of ganoderma alcohols at 40 μM on LNCaP cells. Data obtained from Liu.[134]

GA	EC_{50}-IC_{50}/μM			
	PC3	**PC3M-luc2**	**DU145**	**LNCaP**
GA-H (**24**)	1090±60	-	659±46	657±53
GA-T (**11**)	10.4±0.5	12.4±0.6	15.1±1.0	11.5±0.6
107	23.2±3.4	17.9±5.2	18.8±1.9	14.9±1.8
108	32.9±1.0	26.1±2.4	43.7±1.7	9.60±0.98
109	-	24.3±2.9	89.2±4.2	4.08±1.51
59	-	20.9±2.2	54.4±2.1	3.25±1.24
146	58.6±2.8	111±7	114±5	53.8±6.2
184	-	105±3	17.0±1.4	24.2±2.4
185	-	56.3±2.3	43.1±4.4	4.40±0.31
188	-	20.4±4.4	15.6±5.0	11.3±0.5
189	-	38.8±3.4	1052±172	36.0±1.2

Table 4.4 Summary of the EC_{50}-IC_{50} values of the different GA and analogues evaluated in prostate cancer cell-lines.

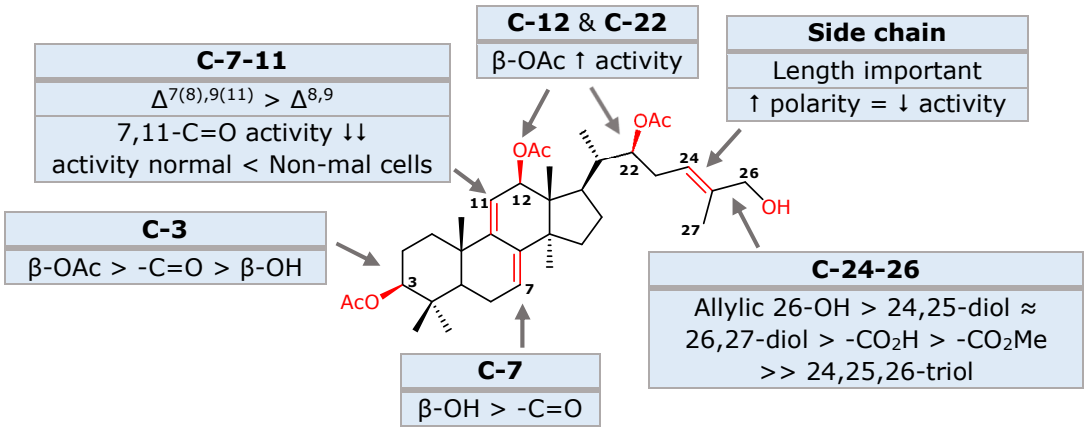
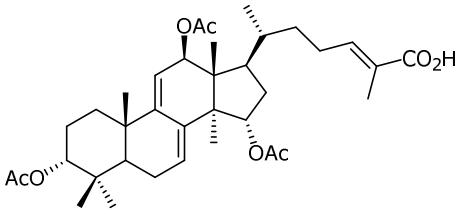


Figure 4.9 SAR analysis for non-malignant cell-lines and LNCaP. Non-mal = non-malignant.

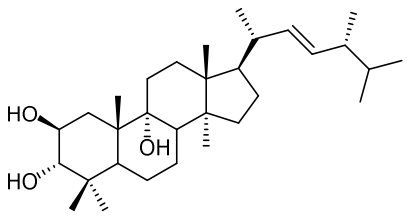
Min *et al.* isolated eighteen triterpenes from the methanol extracts of GL mushroom (Figure 4.10, Figure 4.11 and Figure 4.12).[34] They evaluated their biological activity against three cancerous cell-lines: A549 (lung), MCF7 (breast) and PC3 (prostate). Five of these triterpenes were moderately active for prostate cancer: 12-OAcGA-Me (**81**) > 3-OxoGIOL-E (**82**) > L2OL (**43**) > LA-A (**69**) > GN2OL (**66**).

Apparently, the conjugated double bond $\Delta^{7(8),9(11)}$ (**81**) generated a more suitable inhibitor (Figure 4.10). However, a better picture of the isolated functional group was obtained when comparing the IC_{50} of 3-OxoGIOL-E (**82**) with GIOL-F (**63**) (Figure 4.11). It was evident in that case that the combination $\Delta^{7,8}$ allylic 7-ketone was superior than the conjugated double bond system alone. Besides, the allylic 26-alcohol enhanced the inhibition

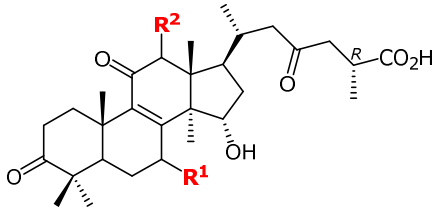
compared with the 24,25-diol (L2OL (**43**) *vs.* GR3OL (**212**)). Nevertheless, the 24,25-diol (GN2OL (**66**)) was preferred to the $\Delta^{24,25}$ α,β-unsaturated 26-carboxylic acid (GA-S_1 (**55**)) or allylic 26,27-diol (GIOL-F (**63**)). Comparing 3-OxoGIOL-E (**82**) with GA-DM (**32**), the allylic 26,27-diol produced a lower IC_{50} than the C-26 α,β-unsaturated carboxylic acid. Esterification with a methyl group increased the IC_{50} value (LA-A (**69**) *vs.* MeLA-A (**207**)) (Figure 4.12). In addition, a shorter side chain (LA-A (**69**)) seemed to inhibit better than a side chain with C-26 α,β-unsaturated carboxylic acid (GA-DM (**32**)). Finally, putting all this information together, the functionality on the side chain could be ranked as follows: allylic 26-OH > 24,25-diol > allylic 26,27-diol > short side chain > C-26 α,β-unsaturated carboxylic acid > C-26 Me-ester. Likewise, the effect at position C-3 was deduced by comparing the IC_{50} of GN2OL (**66**) with GR3OL (**212**). As stated before the conjugated double bond at rings B/C inhibited less than the allylic C-7 ketone, therefore, in view of the lower activity of GR3OL (**212**) with a β-hydroxyl at C-3 compared with GN2OL (**66**) with a ketone at that position, it was concluded that the C-3 ketone produced a much powerful inhibitor.



81
12-OAcGA-Me



214

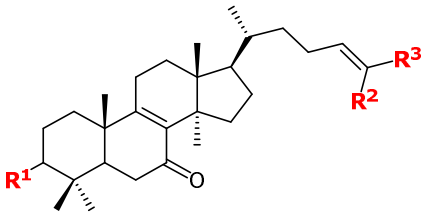


10, **22**

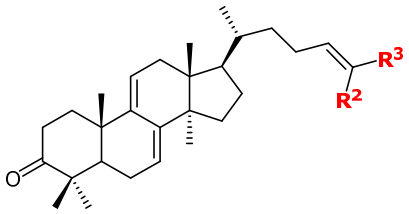
Triterpene	IC_{50}/μM	**R^1**	**R^2**
GA-A (**10**)	>50	β-OH	-H
GA-F (**22**)	>50	-C=O	β-OAc
12-OAcGA-Me (**81**)	11.5±2.3	-	-
214	>50	-	-

Figure 4.10 Evaluation of functional groups at positons C-3, C-7, C-12, C-15 and side chain.[34] For the analysis, triterpenes **10**, **22**, **81**, **214** isolated from GL fruiting bodies were employed.

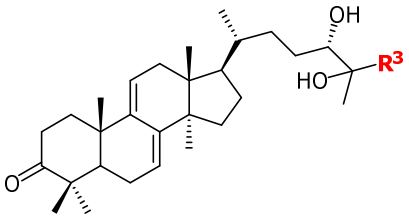
Nevertheless, little can be said about the influence of the different functionalities at positions C-7, C-12, C-15 or C-3 α-acetate and C-23 ketone, since the data provided did not differentiate the strength of their activity.



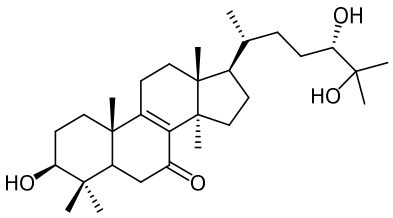
32, **43**, **82**



55, **63**



66-**67**



212

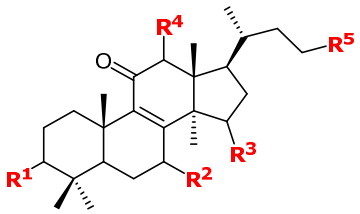
Triterpene	IC_{50}/μM	R^1	R^2	R^3
GA-DM (**32**)	>50	-C=O	$-CH_3$	$-CO_2H$
L2OL (**43**)	32.0±3.2	β-OH	$-CH_3$	$-CH_2OH$
3-OxoGIOL-E (**82**)	21.3±3.1	-C=O	$-CH_2OH$	$-CH_2OH$
GA-S_1 (**55**)	>50	-	$-CH_3$	$-CO_2H$
GIOL-F (**63**)	>50	-	$-CH_2OH$	$-CH_2OH$
GN2OL (**66**)	44.0±5.2	-	-	$-CH_3$
GN3OL (**67**)	>50	-	-	$-CH_2OH$
GR3OL (**212**)	>50	-	-	-

Figure 4.11 Triterpenes isolated from GL fruiting bodies with different C-3 and side chain: **33**, **43**, **55**, **63**, **66**-**67**, **82** and **212**.[34] IC_{50} values obtained from PC3 cells. L2OL = lucidadiol; 3-OxoGIOL-E = 5α-lanosta-8,24-diene-26,27-dihydroxy-3,7-dione; GIOL = ganoderiol; GN2OL = ganodermanondiol; GN3OL = ganodermanontriol; GR3OL = ganoderitriol.

Liu *et al.* examined the activity of GA-DM (**32**) and four analogues (Figure 4.13) in PC3 cell-line.[33] However, some of their findings contradicted the observations of Min. Thus, the effect of GA-DM (**32**) and L2OL (**43**) in PC3 described by Liu were opposite to the effect outlined by Min. Besides, the methyl ester MeGA-DM (**78**) was the most active compound, which was rationalised as the ester possessing better membrane permeability. Comparing L2OL (**43**), 7-OxoGA-Z (**79**) and its methyl ester 7-OxoMeGA-Z (**80**), the order of activity for the allylic C-26 position was $-CO_2Me$ > $-CH_2OH$

> -CO_2H. As for Min, Liu concluded that the C-3 ketone was better than the β-hydroxyl and that the allylic 26-hydroxyl was better than the α,β-unsaturated acid for the inhibition.

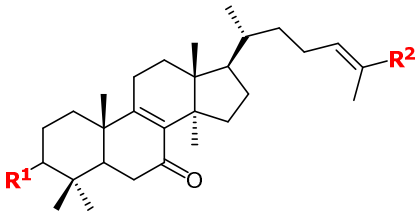
From our studies (Table 4.4), it was identified that the inhibition in the proliferation was cell-line dependent, with major differences between the hormone refractive cell-lines: PC3, PC3M-luc2 and DU145 and the hormone sensitive cell-line LNCaP. Contrary to Liu and Min, our results suggested that GAs with the 3β-hydroxyl was most active towards the inhibition for the aggressive cell-lines. The functionality preference in B/C rings was $\Delta^{8,9}$ (**107**) > conjugated double bond $\Delta^{7(8),9(11)}$ (**59**) > allylic 7,11-diketones (**146**) for PC3M-luc2 and DU145. At the side chain, a shorter one, **184**, was effective exclusively for DU145, the C-26 substitution preference was α,β-unsaturated 26-carboxylic acid (**107**) > 24,25-diol (**188**) > allylic 26-hydroxyl (**185**) for PC3M-luc2, whereas the alcohols inhibited better than the acid for DU145. These observations has been summarised in Figure 4.14.



69, 207-211

Triterpene	IC_{50}/μM	R^1	R^2	R^3	R^4	R^5
LA-A (**69**)	35.0±4.1	-C=O	β-OH	-C=O	-H	-CO_2H
MeLA-A (**207**)	>50	-C=O	β-OH	-C=O	-H	-CO_2Me
LA-C (**208**)	>50	β-OH	β-OH	-C=O	β-OH	-CO_2H
MeLA-C (**209**)	>50	β-OH	β-OH	-C=O	β-OH	-CO_2Me
MeLA-L (**210**)	>50	β-OH	-C=O	-C=O	β-OH	-CO_2Me
MeLA-Q (**211**)	>50	-C=O	β-OH	α-OH	-H	-CO_2Me

Figure 4.12 Triterpenes isolated from GL fruiting bodies: **69**, **207**-**211**.[34] IC_{50} values derived from PC3 cells.



Triterpenes	IC_{50}/μM	% Viability at 50 μM	R^1	R^2
GA-DM (**32**)	40±2	41.2	-C=O	-CO_2H
L2OL (**43**)	>50	55.5	β-OH	-CH_2OH
MeGA-DM (**78**)	3±0.3	30.3	-C=O	-CO_2Me
7-OxoGA-Z (**79**)	>50	70.8	β-OH	-CO_2H
7-OxoMeGA-Z (**80**)	>50	52.6	β-OH	-CO_2Me

Figure 4.13 Triterpenes **32**, **43**, **78**-**80** employed for a SAR analysis of positions C-3 and C-26.[33] IC_{50} values derived from PC3 cells. L2OL = lucidadiol.

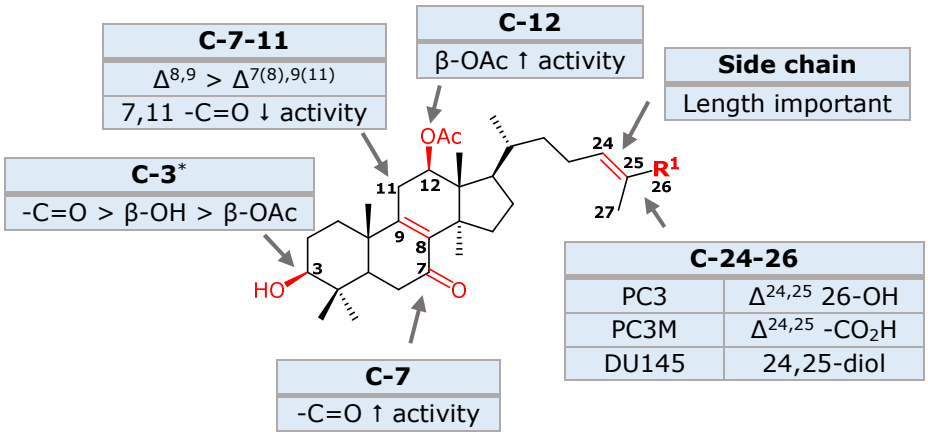


Figure 4.14 SAR analysis of the prostate cancer cell-lines PC3, PC3M-luc2 and DU145. **R^1** varies with the cell-line, the most active functional group is shown. * The activity order reported by Liu[33] and Min[34] for C-3 was -C=O > β-OH, but our results suggested the reverse order β-OH > -C=O.

4.3. Summary

The effect of different GA and analogues in the inhibition of the activity in 5α-reductase, androgen receptor and of prostate cell-lines has allowed to elaborate a SAR analysis (Figure 4.15). Most of the usual substituted positions were evaluated. However, as the analysis was built with data from different sources, some discrepancies were detected. For the enzymes, C-3 ketone was the best functionality. However, more variety was encountered on the cell-lines. Thus, both β-hydroxyl and ketone were reported as the most active functionalities for the hormone-resistant cell-lines while β-acetate was the most powerful for LNCaP. However, no specific studies have

been carried out with the α-hydroxyl or α-acetate for any of them. At rings B/C, $\Delta^{8,9}$ was superior than the conjugated $\Delta^{7(8),9(11)}$ double bond for the hormone-resistant cell-lines, while the reverse applied for the other systems evaluated. The inhibition was enhanced when at position C-7 an allylic ketone was present. However, the 7,11 allylic diketone group reduced the inhibitory activity considerably. Nonetheless, their presence could be beneficial for differentiating between the inhibition of the normal cell-line and the non-malignant ones. Apparently, 12-β-OAc and C-15 -C=O ≈ β-OH ≈ α-OH raised the inhibition potency. However, these are generalisations from the studies with the enzyme as no specific data was available for the cell-lines, therefore further studies should be done to corroborate these observations. Finally, on the side chain, a shorter one was only advantageous for DU145. Ganoderma alcohols proved to be more powerful than the carboxylic acids for the androgen receptor, LNCaP, PC3 and DU145, whilst the $\Delta^{24,25}$ α,β-unsaturated-CO_2H executed a better effect on 5α-reductase and PC3M. Even though, some controversy was observed on PC3, as some authors attributed the methyl ester as better group while others the allylic alcohol. Unsaturation of the side chain was favoured, with the exception of DU145, that was more inhibited by a 24,25-diol. Increasing the polarity of the side chain by increasing the number of hydroxyl groups resulted in a reduction of the inhibitory power of the molecule. The methyl ester was less potent than the free acid, but it contributed to a better permeability to the cell membrane. Still to determine is the effect that C-23 ketone has on the inhibition. All this information suggests that both ends of the molecules were playing a most important role in the inhibition.

5. *Ganoderma lucidum* triterpene composition

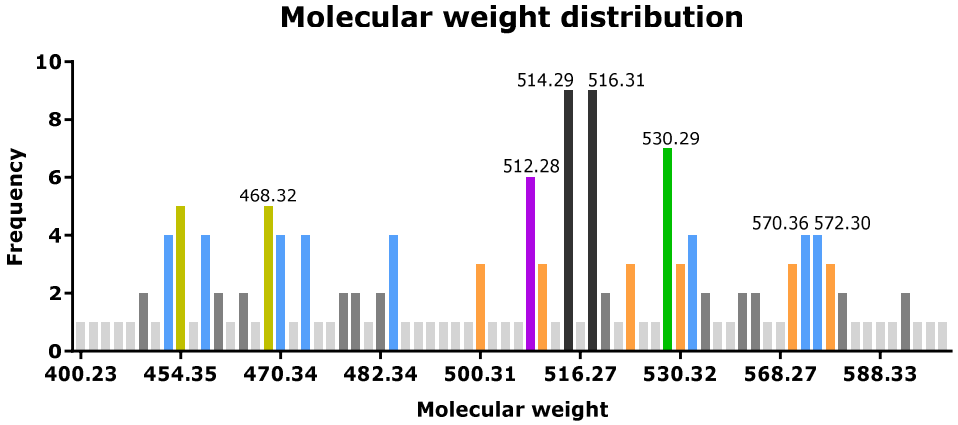
In this chapter, we describe a study on the differences in the triterpene composition of GL extracts over harvesting time and a comparison of the triterpene composition when growing the mushroom on different substrates or under different growing conditions. As substrates, sawdust and oil palm fibres were investigated. Likewise, the triterpene composition of normal fruit body and antler type were compared.

Oil palm fibre is further classified into empty fruit bunch fibre (EFB), shredded EFB fibre, oil palm fruit mesocarp fibre (MSF) and oil palm trunk fibre. EFB, as the name indicates, is the oil palm fruit bunch without the fruit. MSF is the fibre left over after oil extraction of the oil palm fruit.[137] These fibres are currently disposed of as waste. However, to reduce the pollution this causes, alternative applications are being investigated, such as uses as biofuel, soil substrate or compost.

GL antler type is extremely rare in nature; nonetheless, cultivation in farms has facilitated its availability. Its growth is promoted in the dark and in poor ventilated rooms.[138] Traditionally, it has been believed that the antler variety has enhanced the healing properties of GL. Recent publications have confirmed that it has immune-enhancing activities due to its high content of β-D-glucans,[139] as well as inhibiting tumour growth *in vitro* and *in vivo* because of its triterpene content, above all, of ganoderiol F (**63**).[140]

5.1. Molecular weight distribution of triterpenoids

Over 150 triterpenoids have been isolated from GL. A collection of 153 of these are summarised in Appendix 5. Appendix 5 contains the name, molecular formula, molecular weight and structure of triterpenoids from GL, which has been ordered by molecular weight. It becomes evident that many of the triterpenoids are isomers. Table 5.1 shows the molecular weight distribution (each colour represents a molecular weight frequency, 1 = light grey, 2 = grey, 3 = orange, 4 = blue, 5 = gold, 6 = purple, 7 = green and 9 = black). Molecular weights 512, 514, 516, 530 and 570 are the ones that present the largest number of isomers.



Freq.	MF	Exact Mass	Triterpene
1	1. $C_{24}H_{32}O_5$	400.23	Lucidone-B (**282**)
	2. $C_{24}H_{34}O_5$	402.24	Lucidone-A (**215**)
	3. $C_{27}H_{40}O_3$	412.30	LonA (**74**)
	4. $C_{27}H_{40}O_4$	428.29	LA-DM (**217**)
	5. $C_{30}H_{44}O_2$	436.33	GAL-A (**275**)
	6. $C_{30}H_{48}O_2$	440.37	GOL-B (**64**)
	7. $C_{27}H_{36}O_6$	456.25	LA-F (**281**)
	8. $C_{30}H_{50}O_3$	458.38	LOL-B (**68**)
	9. $C_{27}H_{42}O_6$	462.30	LA-M (**277**)
	10. $C_{28}H_{40}O_6$	472.29	MeLA-A (**207**)
	11. $C_{27}H_{38}O_7$	474.26	LA-B (**216**)
	12. $C_{28}H_{42}O_6$	474.30	MeLA-Q (**211**)
	13. $C_{27}H_{42}O_7$	478.29	**276**
	14. $C_{31}H_{48}O_4$	484.36	7-Oxo-MeGA-Z (**80**)
	15. $C_{29}H_{42}O_6$	486.30	EtLA-A (**70**)
	16. $C_{30}H_{46}O_5$	486.33	**266**
	17. $C_{28}H_{42}O_7$	488.28	MeLA-L (**210**)
	18. $C_{28}H_{38}O_7$	490.29	MeLA-C (**209**)
	19. $C_{30}H_{42}O_6$	498.30	**285**
	20. $C_{30}H_{46}O_6$	502.33	GLA-B (**30**)
	21. $C_{30}H_{38}O_7$	510.26	GenA-F (**221**)
	22. $C_{32}H_{46}O_5$	510.33	GA-T-Q (**57**)
	23. $C_{29}H_{38}O_8$	514.26	LA-D (**278**)
	24. $C_{29}H_{40}O_8$	516.27	LA-E2 (**83**)
	25. $C_{32}H_{46}O_6$	526.33	15α-OAc-GLA-E (**267**)
	26. $C_{31}H_{44}O_7$	528.31	MeGA-D (**227**)
	27. $C_{32}H_{48}O_6$	528.35	GA-V (**242**)
	28. $C_{30}H_{42}O_9$	546.28	GA-N (**237**)
	29. $C_{30}H_{44}O_9$	548.30	**258**
	30. $C_{32}H_{46}O_8$	558.32	7-OEtGA-O (**27**)
	31. $C_{32}H_{40}O_9$	568.27	12β-OAc-GenA-F (**272**)
	32. $C_{33}H_{44}O_9$	584.30	MeGA-F (**229**)
	33. $C_{33}H_{46}O_9$	586.31	MeGA-H (**230**)
	34. $C_{33}H_{48}O_9$	588.33	MeGA-K (**231**)
	35. $C_{34}H_{46}O_9$	598.31	EtGA-F (**228**)
	36. $C_{34}H_{46}O_{10}$	614.31	3βOAc-GA-H (**265**)
	37. $C_{34}H_{48}O_{10}$	616.33	**261**
	38. $C_{36}H_{52}O_9$	628.36	BuGA-H (**25**)

Freq.	MF	Exact Mass	Triterpene
2	1. $C_{30}H_{46}O_2$	438.35	GOL-A (**252**), LAL-A (**256**)
	2. $C_{27}H_{38}O_6$	458.27	LA-A (**69**), **279**
	3. $C_{27}H_{40}O_6$	460.28	LA-N (**72**), **280**
	4. $C_{30}H_{50}O_4$	474.37	GIOL-A (**65**), GR3OL-M (**212**)
	5. $C_{27}H_{40}O_7$	476.28	LA-C (**208**), 20OH-LA-N (**73**)
	6. $C_{31}H_{46}O_4$	482.34	MeGA-DM (**78**), MeGA-TR (**204**)
	7. $C_{30}H_{46}O_7$	518.32	GA-C (**16**), GA-C2 (**18**)
	8. $C_{30}H_{46}O_8$	534.32	12βOH-GA-C2 (**257**), GA-L (**235**)
	9. $C_{34}H_{42}O_8$	554.29	**286**, **287**
	10. $C_{34}H_{50}O_6$	554.36	GA-Me (**49**), GA-R (**52**)
	11. $C_{32}H_{46}O_9$	574.31	GA-K (**26**), GA-α (**28**)
	12. $C_{36}H_{52}O_8$	612.37	GA-T (**11**), 12βOAc-GA-Me (**81**)
3	1. $C_{30}H_{44}O_6$	500.31	GA-β (**34**), GLA-A (**29**), GLA-D (**245**)
	2. $C_{32}H_{48}O_5$	512.35	GA-M_f (**50**), GA-S (**53**), GA-X (**251**)
	3. $C_{30}H_{40}O_8$	528.27	12βOH-GA-E (**226**), Elfvingic acid A (**273**), **284**
	4. $C_{31}H_{46}O_7$	530.32	MeGA-A (**13**), MeGA-B (**15**), ^{t}BuLA-B (**71**)
	5. $C_{32}H_{42}O_9$	570.28	GA-F (**22**), 12β-OAc-GenA-H (**47**), 12β-OAc-GenA-D (**224**)
	6. $C_{34}H_{52}O_7$	572.37	BuGA-B (**14**), GA-DH (**42**), GA-W (**243**)
4	1. $C_{30}H_{44}O_3$	452.33	GA-S1 (**55**), GA-SZ (**56**), LAL-B (**44**), 22OxoGOL-A (**253**)
	2. $C_{30}H_{48}O_3$	456.36	GA-Z (**244**), G3OL (**205**), GN2OL (**66**), L2OL (**43**)
	3. $C_{30}H_{46}O_4$	470.34	7-OxoGA-Z (**79**), GIOL-B (**62**), 3-OxoGIOL-E (**82**), GA-Ma (**240**),
	4. $C_{30}H_{48}O_4$	472.36	GA-U (**241**), GIOL-E (**48**), GN3OL (**67**), LOL-A (**256**)
	5. $C_{30}H_{44}O_5$	484.32	GLA-E (**246**),11α-OHGA-DM (**247**), 11β–OHGA-DM (**248**), LAL-E (**46**)
	6. $C_{30}H_{44}O_8$	532.30	GA-G (**23**), GA-I (**206**), GA-η (**39**), MeLA-P (**218**)
	7. $C_{34}H_{50}O_7$	570.36	GA-Mk (**51**), GA-P (**249**), GA-Q (**250**), MeGA-A acetonide (**75**)
	8. $C_{32}H_{44}O_9$	572.30	GA-H (**24**), GenA-K (**223**), **260**, 12β-OAc-GA-D (**264**)
5	1. $C_{30}H_{46}O_3$	454.35	GA-Y (**59**), GIOL-F (**63**), LAL-C (**45**), 15α-G2OL-A (**254**), GNO-A (**268**);
	2. $C_{30}H_{44}O_4$	468.32	GA-DM (**32**), 15αOH-GA-S_z (**54**), GA-TR (**58**), GA-TR_1 (**279**), 22OxoGIOL-F (**255**)
6	$C_{30}H_{40}O_7$	512.28	GA-E (**21**), GenA-D (**220**), GenA-G (**271**), GenA-H (**222**), 3-Oxo-GA-ζ (**41**), GNPA-A (**31**)

Freq.	MF	Exact Mass	Triterpene
7	$C_{30}H_{42}O_8$	530.29	GA-C6 (**233**), GA-M (**236**), GA-O (**238**), GA-θ (**40**), 12βOH-GA-C1 (**225**), 12βOH-GA-D (**263**), 12βOH-GenA-B (**270**)
9	1. $C_{30}H_{42}O_7$	514.29	GA-AM_1 (**12**), GA-C1 (**17**), GA-D (**19**), GA-J (**234**), GA-LM2 (**33**), GA-ζ (**38**), GenA-A (**213**), GenA-B (**219**), **283**
	2. $C_{30}H_{44}O_7$	516.31	GA-A (**10**), GA-B (**8**), GA-B9 (**232**), GA-D_f (**25**), GA-γ (**35**), GA-δ (**36**), GA-ε (**37**), **259**, **269**

Table 5.1 Molecular weight distribution of selected triterpenes. Frequency of triterpenoid molecular formula (MF) and exact mass in a selection of 153 triterpenoids isolated from GL. **BuGA** = butyl ganoderate; ^{t}BULA = *tert*-butyl lucidinate; **EtLA** = ethyl lucidenate; **GA** = ganoderic acid; **GAL** = ganoderal; **GenA** = ganoderenic acid; **GIOL** = ganoderiol; **GLA** = ganolucidic acid; **GNO** = ganoderone; **GN2OL** = ganodermanondiol; **GN3OL** = ganodermanontriol; **GNPA** = ganosporenic acid; **GOL** = ganoderol; **G3OL** = ganodermatriol; **GR3OL** = ganoderitriol; **LA** = lucidenic acid, **LAL** = lucialdehyde; **L2OL** = lucidadiol; **LOL** = lucidumol; **LonA** = 4,4,14α-trimethyl-5α-chol-7,9(11)-dien-3-oxo-24-oic acid; **MeLA** = methyl lucidenate.

5.2. Mass spectral studies

5.2.1. ESI-MS profiles of GL extracts

Mass composition of the crude extracts was determined by application of the sample to an electrospray mass spectrometer (ESI-MS). The system is a time-of-flight mass spectrometer (MS) with mass resolution of 12000 and a working mass range of 50-3000 Da. The mass profiles for each of the samples are included in Appendix 3 (Figures A3-1 to A3-14). Expansion in the area for the expected triterpenoid molecular weights (400-650) was covered. A table with the top twenty mass intensities (Appendix 3; Tables A3-1 to A3-14).

5.2.2. Difference in triterpenoid composition over GL growing time

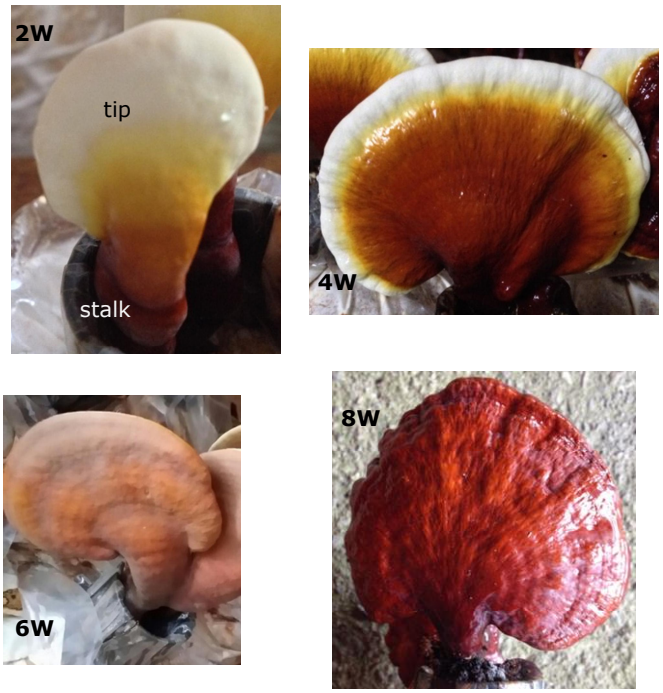
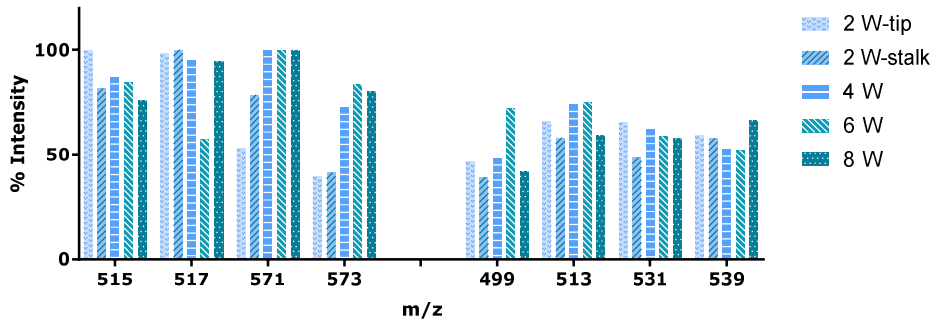


Figure 5.1 Evolution over time of *Ganoderma lucidum*. Pictures of the mushroom correspond to 2-, 4-, 6- and 8-week stages. Pictures were kindly donated by Ganofarm Sendirian Berhad.

Fruiting bodies from GL cultivated in sawdust and harvested at 2-, 4-, 6-, and 8-weeks (Figure 5.1) were supplied dried and chopped by Ganofarm Sendirian Berhad, Malaysia. The tip and stalk of the 2-week old GL differ in colour; being a white tip and brown stalk. To clarify if this differentiation could affect the triterpene composition, the 2-week old sample was separated into tip and stalk portions. The mushrooms were extracted using a Soxhlet apparatus with ethanol as the extracting solvent. The extraction was conducted for 18 h. Evaporation of the solvent left a crude residue, which was analysed by ESI-MS to assess its composition. About 1 mg of the extract sample was dissolved in methanol (1.5 mL), this solution was further diluted (1:10) for MS analysis.



m/z	2 W-tip	2 W-stalk	4 W	6 W	8 W
499	46.9	39.2	48.4	72.0	42.2
513	66.0	58.0	73.9	75.1	59.4
515	**100.0**	81.5	87.1	84.6	76.0
517	98.3	**100.0**	95.1	57.6	94.7
531	65.7	48.6	62.1	58.8	57.7
539	59.3	57.7	52.6	52.3	66.4
571	53.1	78.6	**100.0**	**100.0**	**100.0**
573	39.9	41.4	72.5	83.5	80.3

Table 5.2 Most intense molecular ion peaks over time.

m/z	Adduct	MW	Triterpene
499	M+H	498	**285**
	M+Na	476	**73**; **208**
513	M+H	512	**21**; **31**; **41**; **220**; **222**; **271**
	M+Na	490	**209**
515	M+H	514	**12**; **17**; **19**; **33**; **38**; **213**; **219**; **234**; **283**
537	M+Na		
517	M+H	516	**8**; **10**; **25**; **35**; **36**; **37**; **232**
539	M+Na		
531	M+H	530	**40**; **225**; **233**; **236**; **238**; **263**; **270**
571	M+H	570	**22**; **47**; **224**
593	M+Na		
573	M+H	572	**24**, **223**; **260**; **264**
595	M+Na		

Table 5.3 Triterpenes associated to the most intense peaks.

The profiles were very similar at all of the harvesting times evaluated. Eight molecular ions were predominant in the spectra: 499; 513; 515; 517; 531; 539; 571 and 573. Table 5.2 correlates the molecular ions with the observed relative intensities and Table 5.3 the molecular ion with the possible triterpenes.

5.2.3. GL cultivated under different conditions

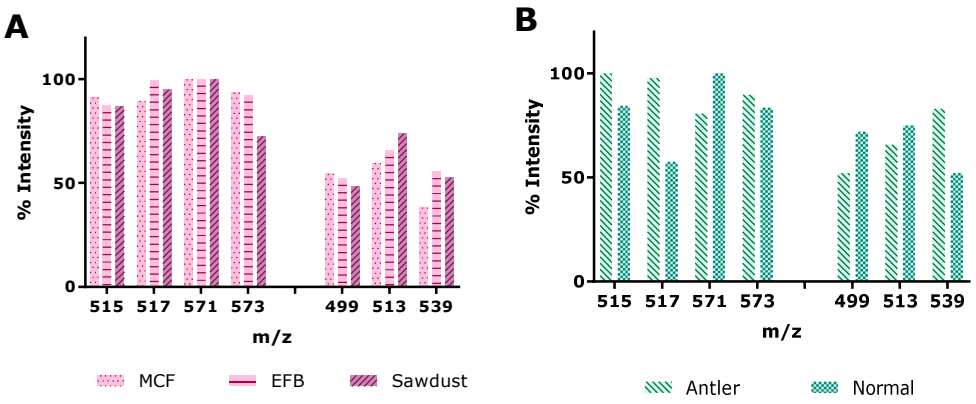
To investigate the effect of the growth substrate on the triterpene distribution in GL, Surya M. Sudheer from Prof. S. Manickam's research group at Manufacturing and Industrial Processes Research Division, Faculty of Engineering, University of Nottingham Malaysia Campus, cultivated the mushroom on two different types of oil palm fibres: mesocarp fibres (MCF) and empty fruit bunch fibres (EFB). Mature fruiting bodies 4-week old were harvested, dried, finely ground and extracted with ethanol at reflux for 18 h; the extracts were analysed by dissolving a portion of them (1 mg) in methanol (1.5 mL) which was further diluted 1:10 for the ESI-MS analysis.

Alternatively, Ganofarm Sendirian Berham, Malaysia, cultivated *Ganoderma lucidum* on sawdust from Malaysian rubber tree under conditions that favoured antler type formation (Figure 5.2). The antler variety was harvested at 6 weeks, dried, chopped and extracted with ethanol at reflux for 18 h. The extract was analysed in the same way as stated above, dissolving a portion in methanol (0.7 mg mL^{-1}) and further diluting (1:10) for the ESI-MS analysis. This technique allowed us to qualitatively estimate the triterpene mass distribution of the extract samples.



Figure 5.2 *Ganoderma lucidum* Antler, 6-week old. Picture kindly donated by Ganofarm Sendirian Berhad, Malaysia.

The more noticeable molecular ions were: 499; 513; 515; 517; 539; 571 and 573 (Table 5.4). The use of oil palm fibres as substrate did not result in an appreciable difference in the mass profile. However, some differences were observed between GL normal and antler type.



m/z	MCF	EFB	Sawdust	Antler	Normal
499	54.4	52.3	48.4	52.1	72.0
513	59.6	65.5	73.9	65.8	75.1
515	91.2	87.3	87.1	**100.0**	84.6
517	89.6	99.4	95.1	97.7	57.6
539	38.2	55.4	52.6	83.1	52.3
571	**100.0**	**100.0**	**100.0**	80.8	**100.0**
573	93.6	92.2	72.5	89.7	83.5

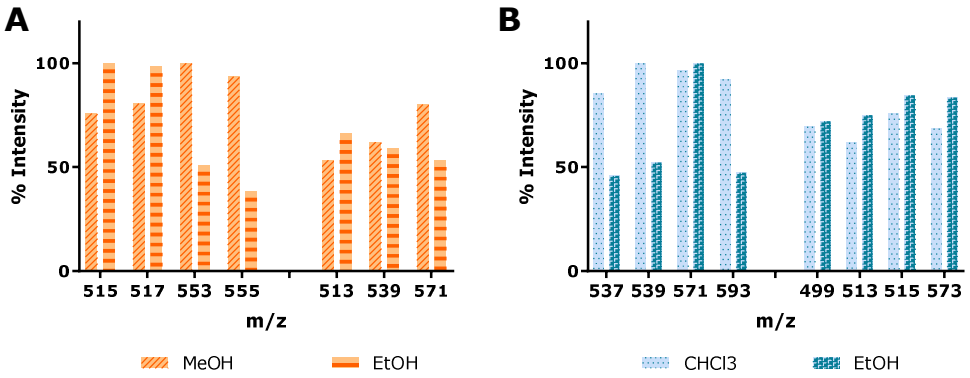
Table 5.4 Most intense peaks for GL grown using: **A.** oil palm fibres or **B.** favouring antler development.

5.2.4. Solvent effects on the extract composition

To determine the potency of the solvent and extraction method GL harvested at 2-, 6- and 8-weeks were extracted with different solvents: ethanol, methanol, dichloromethane, ethyl acetate and water. In addition, differences between Soxhlet extraction with ethanol and sonication with chloroform were evaluated using the 6-week sample. For the 2-week sample methanol and ethanol were compared. Whereas the full range of solvents was used for 8-week sample. At these two latter growing times, Soxhlet extraction was employed.

Molecular ions m/z 499, 513, 515, 517, 531, 537, 539, 553, 555, 571, 573 and 593 were present at different intensities in all the samples (Table 5.5 and Table 5.6). Ethanol, methanol and dichloromethane produced very similar profiles in the 8-week sample, being the opposite for ethyl acetate and water. However, more differences were encountered when the extraction was made with the 2-week sample. In this later case, m/z 553 and 555 intensities were remarkably different for ethanol and methanol. These molecular ions correspond to the sodium adduct of MW 530 and 532, respectively. In the same way, the 6-week sample presented differences

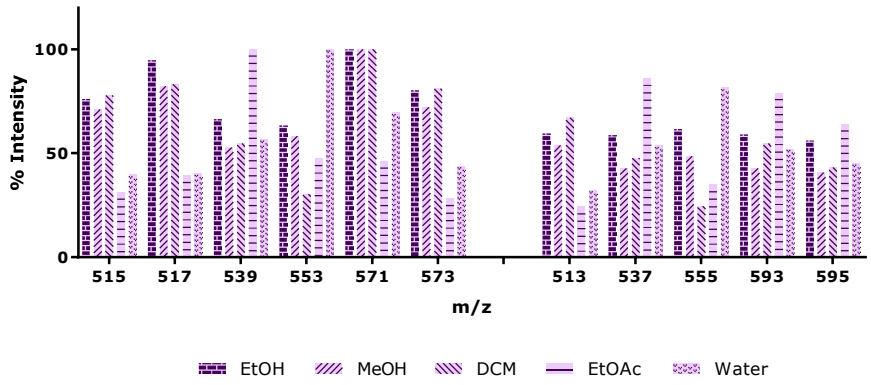
with the molecular ions m/z 537, 539 and 593 which are the sodium adducts of MW 514, 516 and 570, respectively.



m/z	2 W-tip		6 W	
	MeOH	**EtOH**	**$CHCl_3$**	**EtOH**
499	44.8	46.9	69.6	72.0
513	53.2	66.0	61.7	75.1
515	75.8	**100.0**	75.7	84.6
517	80.5	98.3	52.3	57.6
531	49.0	65.7	37.2	58.8
537	44.8	50.0	85.6	45.9
539	62.0	59.3	**100.0**	52.3
553	**100.0**	50.7	59.6	45.1
555	93.4	38.3	40.6	28.9
571	80.0	53.1	96.3	**100.0**
573	40.0	39.9	68.6	83.5
593	28.3	21.2	92.3	47.2

Table 5.5 Differences in composition varying the extraction solvent. **A.** Extractions made in methanol and ethanol for GL tip harvested at 2-weeks. **B.** Extractions made in chloroform and ethanol for GL harvested at 6-weeks.

To summarise, the ESI-MS profiles could indicate which molecular ions were present in the extracts. However, the exact composition could not be determined as the same molecular ion could fit many isomers with the same molecular formula (Table 5.3). Molecular ions m/z 499; 513; 515; 517; 531; 571 and 573 were present in all the extracts at different intensities. To get a more accurate picture of the composition of the extracts LC-MS was performed.



m/z	MeOH	DCM	EtOH	EtOAc	Water
513	53.7	66.9	59.4	24.1	32.4
515	70.9	77.8	76.0	31.1	39.5
517	82.2	83.2	94.7	39.2	40.2
537	42.8	47.6	58.7	85.9	53.6
539	52.7	54.6	66.4	**100.0**	56.6
553	58.2	30.4	63.3	47.4	**100.0**
555	48.5	24.5	61.6	34.7	81.5
571	**100.0**	**100.0**	**100.0**	46.1	69.4
573	72.1	81.0	80.3	28.0	43.9
593	42.7	54.6	58.9	79.0	52.1
595	40.6	43.1	56.1	63.9	45.1

Table 5.6 Comparison of the triterpene extraction with different solvents in GL 8-week samples.

5.2.5. Determination of the GL composition by LC-MS

To compare the different composition of the extracts, the extracts were analysed using LC-MS with an atmospheric pressure chemical ionization interphase (APCI) detector in positive mode. The samples were separated in a SunFire C18 column (4.6 x 150 mm^2; 5 μm) set at 50 °C with a gradient elution of acetonitrile : water containing 0.1% V/V of formic acid during 28 min run. In the total ion chromatogram (TIC) up to 23 peaks were detected (Figure 5.3 and Appendix 3 (Figures A3-15 to A3-20)). However, only a few of these were isolated entities, most of them co-eluted under the conditions used to perform the analysis. Peaks were tentatively assigned considering the observed mass fragmentation together with comparison with the literature data[141-143]. However, as the experiments were performed in positive ion mode, the main fragmentation observed was the loss of series of water molecules (Δm=18) with occasionally loss of the side chain

(Δm=130 or Δm=116). Much more information about the ring substitution pattern could be obtained when the analysis is carried out in the negative mode as fragmentation of the rings and side chain are related with the functional groups attached to the molecule (Table 5.7 and Appendix 4).[142, 143]

GA with a carbonyl at C-23 characteristically loses water and carbon dioxide through a rearrangement process of the side chain (Scheme 5.1 **A**). While the 24,25 α,β-unsaturated side chain loses carbon dioxide directly from the precursor ion (Scheme 5.1 **B**) and the saturated side chains could lose either carbon dioxide directly from the precursor ion or acetic acid (Δm=60) through β-cleavage of the carboxyl group (Scheme 5.1 **C**).[141-143]

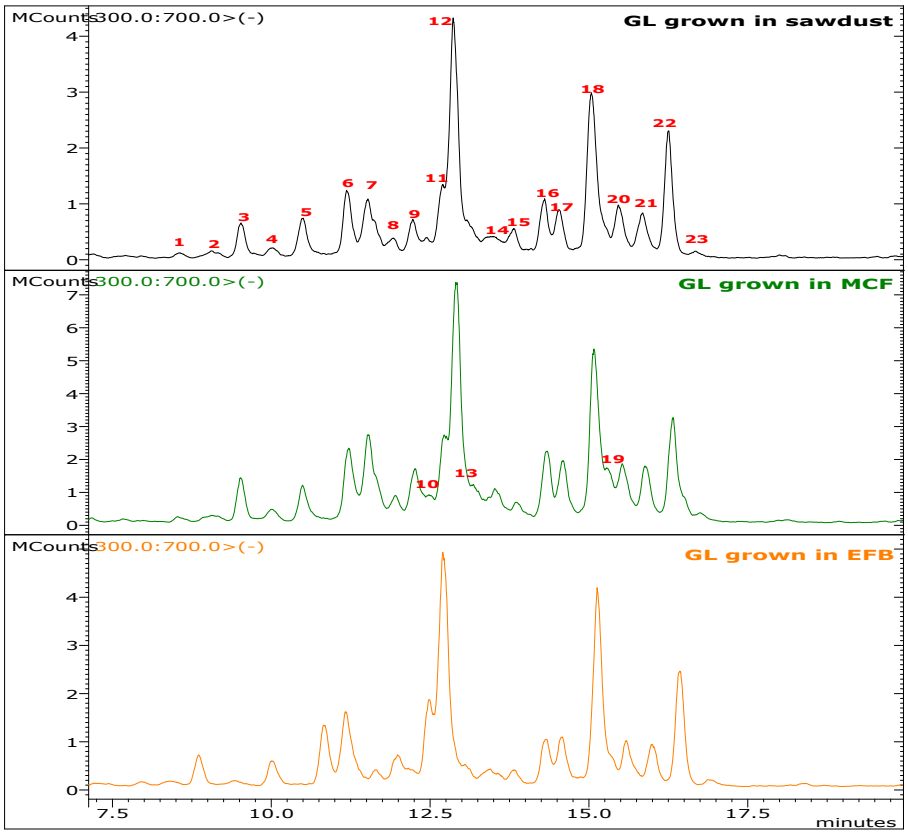
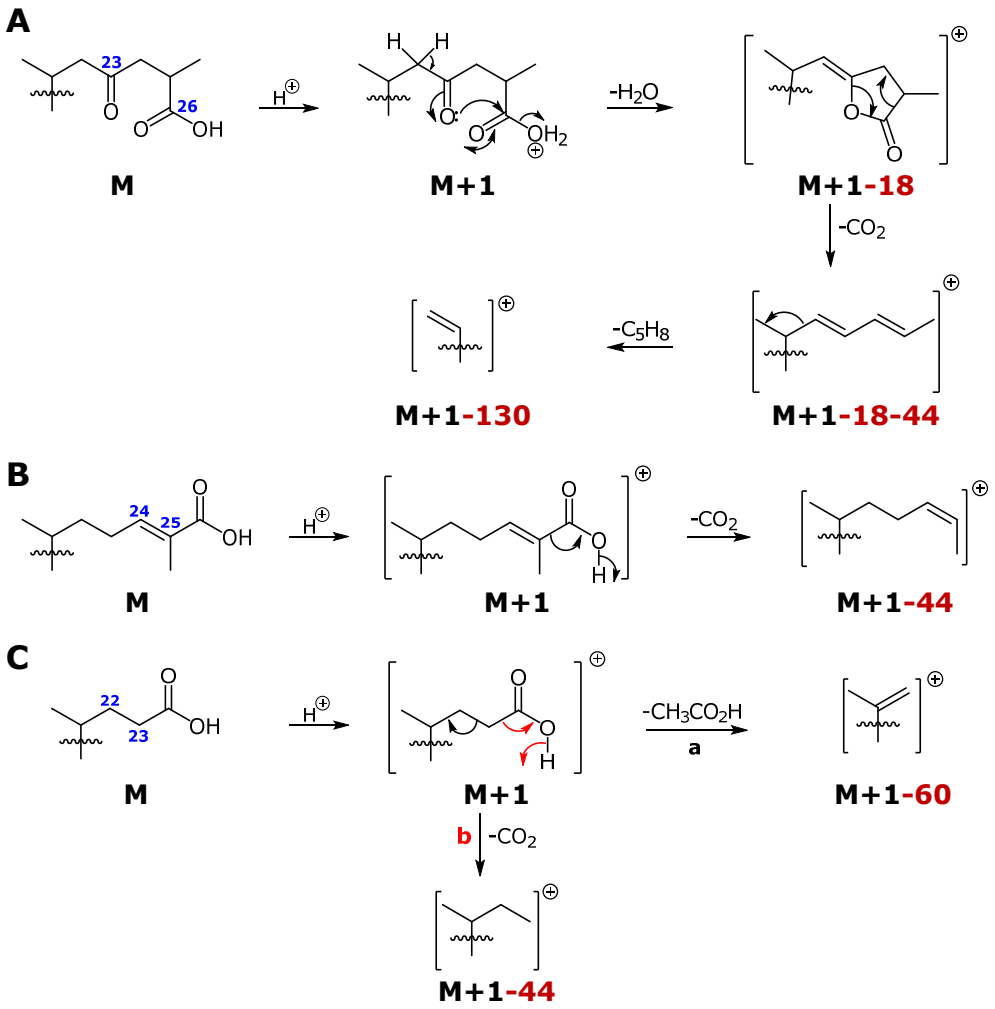


Figure 5.3 Total ion chromatogram (TIC) of GL grown in sawdust, MCF and EFB fibres. The observed 23 peaks were labelled 1-23.



Scheme 5.1 Fragmentation of the side chain. **A** Losing of water, carbon dioxide and side chain in GA containing a C-23 ketone at the side chain. **B** Losing of carbon dioxide in 24,25-unsaturared side chain. **C** Losing of acetic acid (route **a**) or carbon dioxide (route **b**) in unsaturated side chain.

(a) GL harvested at different growing stages

Peak areas were normalised and compared for each of the growing stages (Table 5.8). Two major peaks were found, peaks 12 and 18. Additionally, for some of them, *i.e.*, peaks 11; 21; 22, a correlation between area and age seemed apparent, as the area increased with age. Peak 19 was not present in the 2W extract samples but it was present from the 4W one onwards. The reverse trend was also observed, that is, reduction of the area with age (*i.e.*, peak 13) and on other occasions, after some reduction in area, an increase was observed at later readings (*i.e.*, peak 20).

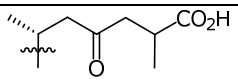
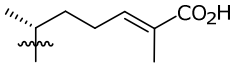
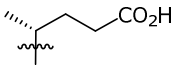
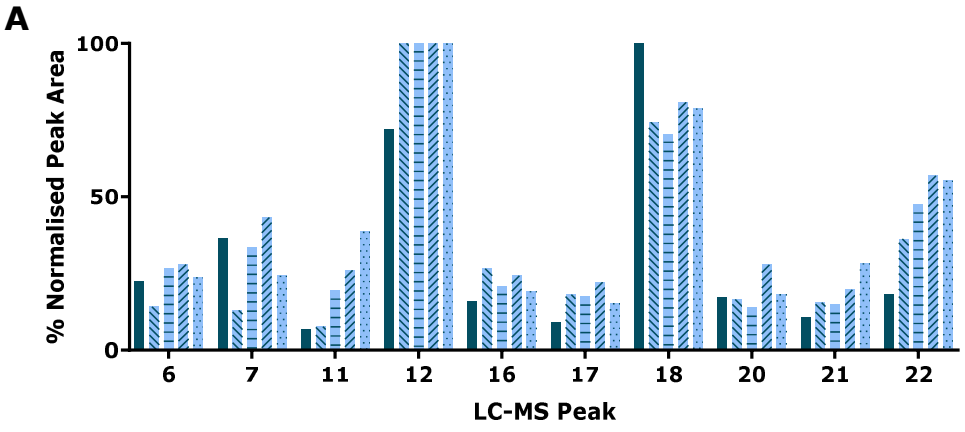
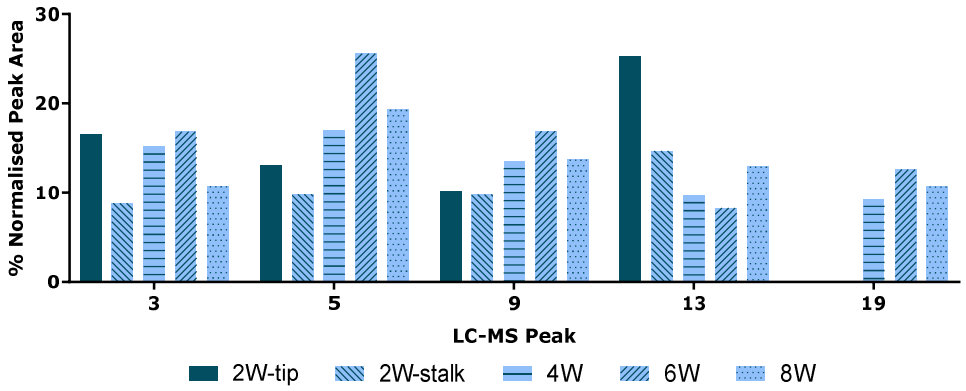
Cleavage	Substitution pattern	Example
Ring A	C-7 = -C=O; C-11 ≠ -C=O	**32**; **79**; **217**; **247**; **248**
Ring B; -CH_4	C-7 = -C=O; C-11 = -OH	**247**; **248**
Ring C	C-7 = -OH; C-15 = -C=O	**17**; **19**
Ring D	Most of the GA, major for C-11 = -C=O	**17**; **19**
n X -CH_3	C-7; C-11 = -C=O or C-7; C-15 = -OH; C-11 = -C=O	**18**; **21**; **22**; **221**; **233**; **234**
H_2O and CO_2		**8**; **10**; **12**; **16**; **17**; **18**; **19**; **20**; **21**; **29**; **30**; **232**; **234**
CO_2		**11**; **33**; **34**; **38**; **40**; **41**; **42**; **49**; **50**; **52**; **57**; **59**; **79**
CO_2 and/or CH_3CO_2H		**69**; **72**; **73**; **74**; **83**; **208**; **216**; **217**; **218**; **278**; **281**
-CH_2CO	C-3 or C-12 = -OAc	**11**; **22**; **24**; **47**; **49**; **51**; **52**
H_2O	C-15 = -OH	**10**; **54**; **58**; **61**; **232**; **234**
n x H_2O in alcohols[a]		**48**; **62**; **64**; **65**; **67**; **68**; **82**; **212**; **239**; **255**

Table 5.7 Observed fragmentation of GL triterpenoids in LC-MS in the negative mode.[142] **a** Alcohols and aldehydes are observed in the positive mode. n = 1, 2, 3.

Even though the separation of the different components was poor, it was evident that the composition in triterpenoids changed slightly with age.



B



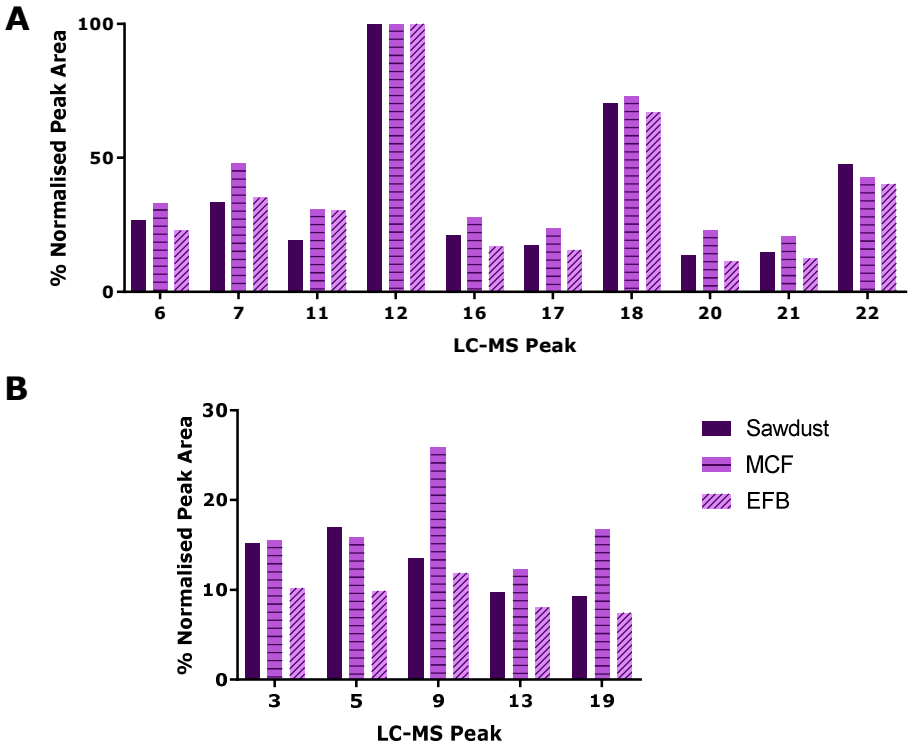
Peak	% Normalised Peak Area				
	2W-tip	2W-stalk	4W	6W	8W
1	1.28	1.69	2.54	2.57	2.07
2	1.69	1.92	4.82	4.70	3.50
3	16.48	8.83	15.16	16.82	10.73
4	3.75	3.00	3.98	8.78	4.85
5	13.08	9.83	17.00	25.59	19.28
6	22.46	14.10	26.64	27.94	23.78
7	36.61	12.96	33.48	43.28	24.29
8	3.86	2.12	6.76	5.85	5.81
9	10.15	9.82	13.54	16.92	13.72
10	2.54	4.10	2.85	6.39	3.20
11	6.63	7.60	19.37	26.07	38.61
12	**71.84**	**100**	**100**	**100**	**100**
13	25.25	14.68	9.71	8.32	12.94
14	2.35	6.20	4.03	13.37	6.21
15	4.02	6.57	6.28	14.40	5.30
16	15.87	26.53	20.86	24.18	19.29
17	8.95	18.16	17.47	22.09	15.38
18	**100**	**74.34**	**70.56**	**80.87**	**78.87**
19	-	-	9.32	12.60	10.71
20	17.13	16.58	13.79	27.77	18.26
21	10.65	15.48	14.68	19.60	28.40
22	18.33	36.30	47.44	56.79	55.27
23	2.41	1.32	1.51	3.55	1.75

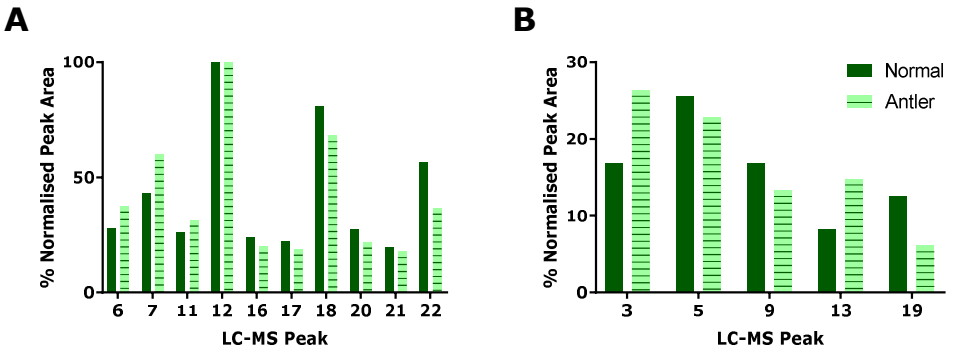
Table 5.8 GL grown at different growing stages. **A** Major peaks. **B** Intermediate peaks.

(b) GL grown in different substrates or conditions

A comparison of the normalised areas of the GL grown on different substrates or under different conditions was performed (Table 5.9). Very

little differences were found in the composition of GL grown in sawdust, MCF or EFB substrates. However, the results suggested that the amount of some of the triterpenes may be enhanced when cultivated in MCF (*i.e.*, peaks 7, 9, 11, 19, 20, 21) while slight reduction in the triterpene content was noted when the mushroom was cultivated in EFB (*i.e.*, peaks 3, 5, 6, 16).





Peak	% Normalised Peak Area				
	Sawdust	MCF	EFB	Normal	Antler
1	2.54	2.33	1.58	2.57	2.09
2	4.82	4.08	1.99	4.70	3.55
3	15.16	15.53	10.21	16.82	26.40
4	3.98	4.69	2.17	8.78	4.29
5	17.00	15.84	9.88	25.59	22.85
6	26.64	33.30	22.96	27.94	37.54
7	33.48	47.84	35.14	43.28	60.03

Peak	% Normalised Peak Area				
	Sawdust	**MCF**	**EFB**	**Normal**	**Antler**
8	6.76	11.02	5.42	5.85	6.23
9	13.54	25.85	11.88	16.92	13.33
10	2.85	5.44	6.95	6.39	7.95
11	19.37	30.88	30.39	26.07	31.60
12	**100**	**100**	**100**	**100**	**100**
13	9.71	12.31	8.046	8.32	14.83
14	4.03	11.07	9.05	13.37	11.42
15	6.28	2.88	5.41	14.40	6.80
16	20.86	27.90	16.86	24.18	19.84
17	17.47	23.52	15.70	22.09	18.94
18	**70.56**	**73.06**	**67.09**	**80.87**	**68.17**
19	9.32	16.76	7.47	12.60	6.11
20	13.79	22.98	11.41	27.77	21.95
21	14.68	20.80	12.46	19.60	17.91
22	47.44	42.74	40.25	56.79	36.73
23	1.51	1.36	1.79	3.55	2.38

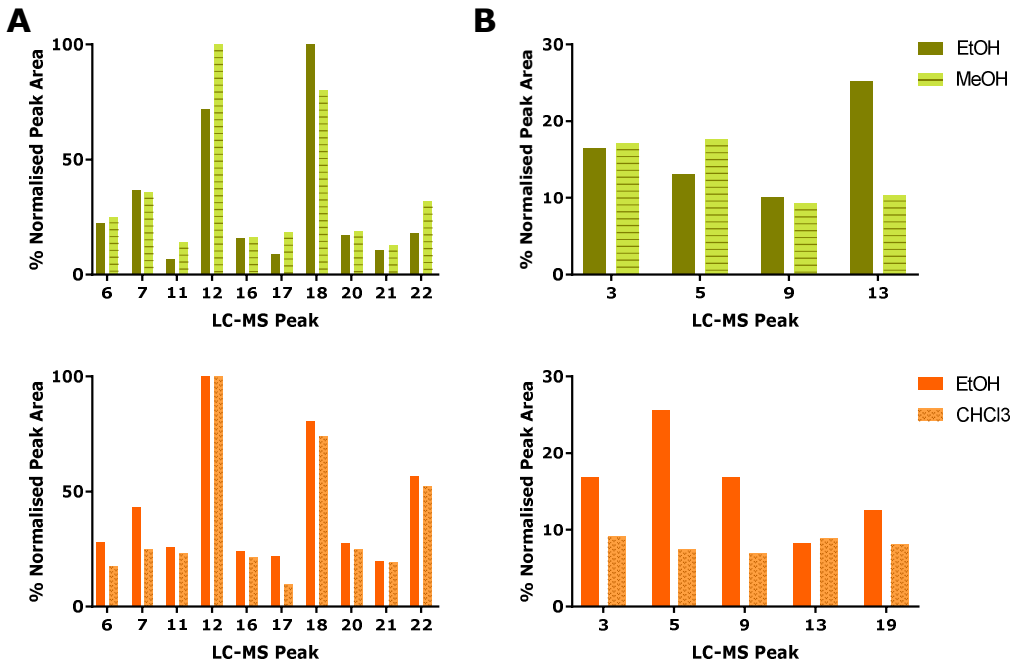
Table 5.9 GL grown in different substrates (sawdust, MCF or EFB) (purple) or conditions (normal and antler types) (green). **A** Major peaks. **B** Intermediate peaks.

More differences were found when comparing the profiles of GL normal and antler. As noted with the different substrates, when the mushroom was grown in the dark and in poor ventilated rooms, both enhancement (*i.e.*, peaks 3, 6, 7, 11, 13) and reduction (*i.e.*, peaks 9, 18, 19, 20, 22) of triterpene content were observed. Thus, there was a predominant increase in the peak area on the first half of the chromatogram, while a reduction was detected on the second half. Therefore, the formation of triterpenes with higher polarity was plausibly preferred in GL antler type.

(c) Effect of the solvent for the extraction of triterpenes in GL

Triterpene composition of GL 2W-tip, 6W (Table 5.10) and 8W (Table 5.11) extracted with different solvents was evaluated. In this study ethanol, methanol, chloroform, dichloromethane, ethyl acetate and water were used for the extraction process. While ethanol and methanol were compared in GL 2W-tip; the extracted power of ethanol and chloroform were compared with the GL 6W samples. Finally, GL 8W samples were extracted with ethanol, methanol, dichloromethane, ethyl acetate and water.

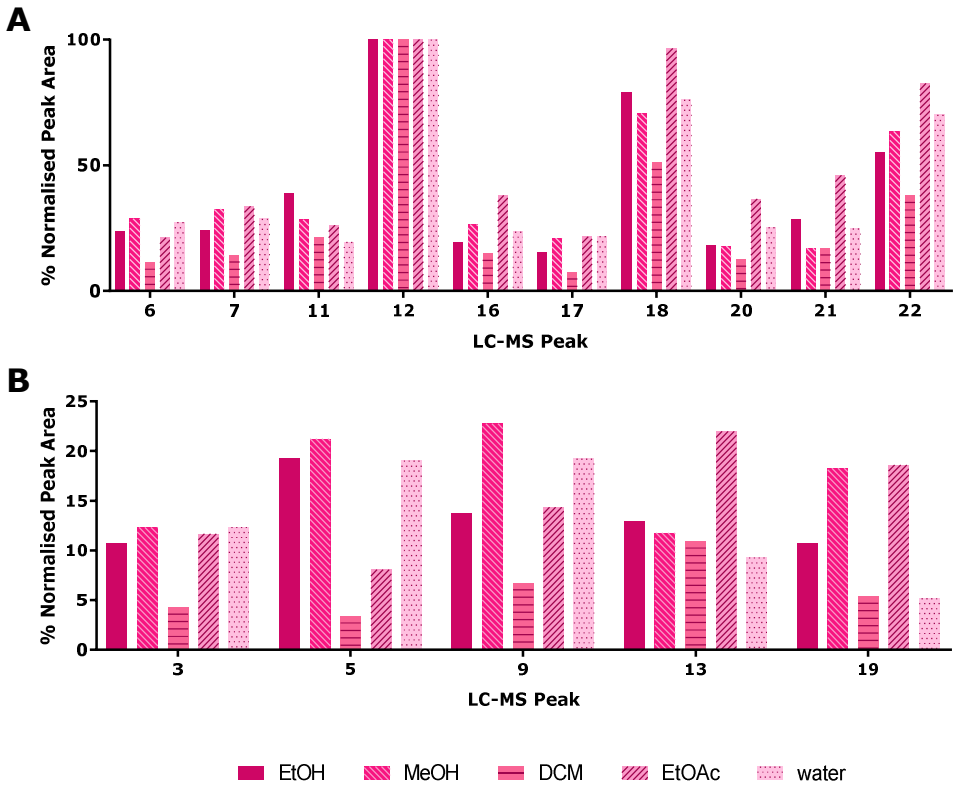
As a rule, ethanol and methanol behaved very similarly, with methanol being slightly more efficient for the extraction. Nonetheless, an enhancement in the area of peaks 13 and 18 was observed with ethanol at both 2W and 8W. Alternatively, chloroform and dichloromethane were slightly less efficient for the triterpene extraction in comparison with ethanol or methanol. Surprisingly, ethyl acetate turned out to be a very good solvent for the extraction of both polar and apolar triterpenes. It was better than dichloromethane and as good as ethanol or methanol for the polar triterpenes with the addition that it was also the best solvent to extract the less polar fraction of triterpenes. Finally, water was also a good solvent for extraction, comparable to ethanol and methanol but not as good as ethyl acetate for the extraction of the less polar triterpenes.



Peak	% Normalised Peak Area			
	2W-tip		6W	
	EtOH	MeOH	EtOH	$CHCl_3$
1	1.28	1.62	2.57	1.88
2	1.69	2.59	4.70	1.54
3	16.48	17.12	16.82	9.16
4	3.75	2.37	8.78	3.09
5	13.08	17.60	25.59	7.49
6	22.46	25.25	27.94	17.86
7	36.61	35.87	43.28	25.09
8	3.86	2.72	5.85	7.66
9	10.15	9.27	16.92	6.98
10	2.54	3.99	6.39	8.20

Peak	% Normalised Peak Area			
	2W-tip		6W	
	EtOH	MeOH	EtOH	$CHCl_3$
11	6.63	14.20	26.07	23.26
12	**71.84**	**100**	**100**	**100**
13	25.25	10.41	8.32	8.93
14	2.35	7.99	13.37	4.27
15	4.02	9.09	14.40	6.01
16	15.87	16.13	24.18	21.45
17	8.95	18.52	22.09	9.67
18	**100**	**80.23**	**80.87**	**74.38**
19	-	-	12.60	8.19
20	17.13	19.07	27.77	25.05
21	10.65	12.94	19.60	19.46
22	18.33	32.05	56.79	52.57
23	2.41	2.41	3.55	5.58

Table 5.10 GL 2W-tip (green) and 6W (orange) extracted with different solvents. **A** Major peaks. **B** Intermediate peaks.



Peak	% Normalised Peak Area (8W)				
	EtOH	**MeOH**	**DCM**	**EtOAc**	**Water**
1	2.07	3.15	1.26	2.37	1.65
2	3.50	3.17	1.13	1.64	1.87
3	10.73	12.33	4.28	11.68	12.37
4	4.85	5.91	1.54	4.01	5.42
5	19.28	21.26	3.39	8.06	19.06
6	23.78	28.73	11.39	21.17	27.41
7	24.29	32.67	14.26	33.72	28.74
8	5.81	11.21	5.88	11.06	4.93
9	13.72	22.77	6.72	14.34	19.25
10	3.20	10.58	7.61	12.63	8.97
11	38.61	28.26	21.12	26.10	19.50
12	**100**	**100**	**100**	**100**	**100**
13	12.94	11.77	10.93	21.98	9.31
14	6.21	11.29	6.48	20.48	15.69
15	5.30	5.16	5.31	13.68	14.35
16	19.29	26.49	14.87	37.95	23.65
17	15.38	21.04	7.50	21.62	21.83
18	**78.87**	**70.60**	**51.00**	**96.56**	**76.11**
19	10.71	18.28	5.36	18.61	5.19
20	18.26	17.86	12.64	36.61	25.39
21	28.40	16.92	17.00	46.04	24.86
22	55.27	63.47	37.98	82.65	70.12
23	1.75	1.52	3.98	12.52	6.13

Table 5.11 GL 8W extracted with different solvents. **A** Major peaks. **B** Intermediate peaks.

In conclusion, the LC-MS could be used to identify differences in the samples. In general, an increase in triterpene content was detected as the mushroom aged. GL grown on MCF showed an increase in some of the triterpenes while EFB trended to reduce the triterpene production. Finally, ethyl acetate was the best solvent for the extraction of both polar and apolar triterpenes.

(d) LC-MS peak identification

Peaks were tentatively identified by comparison of the peaks with the data provided in the literature and the observed fragmentation.[141-143] However, an accurate identification of the peaks was complicated as no standards were used and the fact that most of the triterpenes co-eluted in the same peak. In Table A3-19 (Appendix 3) the complete peak assignment is displayed. A

summary of this table showing possibly the most abundant masses found in each peak is illustrated in Table 5.12.

Peak	Rt/ min	MW	Fragmentation	Assignment
1	8.0	452	365 (7); 361 (4); 323 (23)	GA-S1 (**55**) / GA-S_z (**56**)
		528	529 (29); 511 (4); 485 (3); 475 (8); 467 (9)	**284**
		530	531 (100); 513 (5); 495 (10)	GA-M (**236**) / 12βOH-GA-C1 (**225**) / 12βOH-GA-D (**263**)
		548	531 (100); 513 (5); 467 (9)	**258**
		572	531 (100); 513 (5); 483 (5)	**260**
2	8.6	510	511 (23); 493 (10); 467 (4); 449 (14); 363 (17); 301 (15)	GenA-F (**221**)
		514	515 (100); 497 (3); 481 (8); 473 (43); 467 (4); 439 (27); 437 (5); 383 (41); 301 (15)	GA-AM_1 (**12**); GenA-A (**213**); LA-D (**278**)
		532	533 (17); 515 (100); 497 (3); 467 (4); 437 (2); 425 (10)	GA-I (**206**); GA-G (**23**)
		554	513 (15); 511 (23); 451 (16) 439 (27); 425 (10)	**285**; **286**
		568	569 (11); 553 (26); 509 (13); 467 (4); 437 (2); 301 (15)	12β-OAc-GenA-F (**272**)
		570	571 (4); 553 (26); 511 (23); 481 (8); 467 (4); 449 (14); 437 (2); 347 (3); 301 (15)	12β-OAc-GenA-H (**47**); 12β-OAc-GenA-D (**224**); GA-F (**22**)
		598	515 (100); 511 (23); 467 (4); 451 (16); 301 (15)	EtGA-F (**228**)
3	9.0	516	517 (100); 499 (4); 425 (2)	GenA-C2 (**269**); GA-B (**8**); GA-A (**10**)
		534	517 (100); 499 (4); 425 (2)	12βOH-GA-C_2 (**257**)
4	9.5	474	475 (50); 457 (43); 421 (7); 369 (9); 317 (23)	GR3OL-M (**212**)
		512	513 (75); 481 (6); 465 (5); 437 (5); 423 (3); 421 (7); 407 (1); 337 (3)	GenA-D (**220**); GA-E (**21**) / GNPA-A (**31**); GenA-G (**271**)
		514	515 (47); 497 (41); 481 (23); 479 (18); 473 (19); 461 (10); 453 (3); 437 (5); 423 (3); 409 (33); 379 (51); 317 (23); 311 (22); 305 (8)	**283**; GenA-B (**219**); GA-AM_1 (**12**); GA-C1 (**17**) / GA-D (**19**); GenA-A (**213**); LA-D (**278**); GA-J (**234**)

Peak	Rt/ min	MW	Fragmentation	Assignment
4	9.5	526	527 (67); 485 (1); 423 (3)	15α-OAc-GLA-E (**267**)
		568	569 (100); 551 (1); 465 (5); 437 (5); 421 (7); 317 (30)	12β-OAc-GenA-F (**272**)
		586	587 (20); 569 (100); 545 (11); 527 (67); 511 (26); 483 (9); 465 (5)	MeGA-H (**230**)
5	9.9	510	511 (100); 467 (5)	GenA-F (**221**)
6	10.6	512	513 (100); 495 (14)	GenA-H (**222**); GenA-D (**220**); GA-E (**21**); GenA-G (**271**)
7	11.0	514	515 (48); 497 (100); 479 (3); 471 (4); 355 (2); 303 (1); 303 (1)	**283**; GenA-B (**219**); **287**; GA-C1 (**17**) / GA-D (**19**); GA-J (**234**)
		532	533 (3); 515 (48); 497 (100); 471 (1); 303 (1)	GA-I (**206**); GA-G (**23**)
8	11.4	510	511 (28); 493 (10); 467 (16); 463 (6); 449 (1); 363 (6)	GenA-F (**221**)
		528	529 (100); 511 (28); 467 (16); 363 (6); 319 (4); 307 (3)	**294**; Elfvingic acid A (**273**)
		530	531 (23); 513 (12); 499 (4); 495 (4); 481 (9); 451 (2); 433 (3); 305 (2)	12βOH-GenA-B (**270**); GA-C6 (**233**); GA-M (**236**) / 12βOH-GA-D (**263**); MeGA-B (**15**)
		548	549 (1); 531 (23); 513 (12); 467 (16); 319 (4)	**258**
		570	571 (56); 553 (69); 529 (100); 511 (28); 493 (4); 481 (9); 467 (16); 449 (1); 381 (2); 363 (6)	12β-OAc-GenA-H (**47**); 12β-OAc-GenA-D (**224**); GA-F (**22**)
		572	573 (8); 555 (3); 531 (23); 513 (12); 483 (4); 451 (2); 363 (6); 305 (2)	GenA-K (**223**); GA-H (**24**); **260**
		588	589 (1); 571 (56); 553 (69); 547 (5); 529 (100); 513 (12); 515 (1); 495 (4); 305 (2)	MeGA-K (**231**)
9	11.7	512	513 (100); 495 (4); 481 (3); 477 (2); 465 (3); 451 (2); 437 (1); 433 (3); 403 (2); 331 (2); 325 (2)	GenA-H (**222**); GenA-D (**220**); GA-E (**21**) / GNPA-A (**31**); GenA-G (**271**)

Peak	Rt/ min	MW	Fragmentation	Assignment
9	11.7	530	531 (2); 513 (100); 499 (3); 495 (4); 481 (3); 469 (3); 451 (2); 437 (1); 331 (2); 309 (2)	12βOH-GenA-B (**270**); GA-C6 (**233**); GA-M (**236**) / 12βOH-GA-D (**263**); MeGA-B (**15**)
		548	549 (39); 531 (2); 513 (100); 469 (3); 467 (1); 457 (2); 319 (4)	**258**
		554	555 (24); 513 (100); 511 (3); 469 (3); 451 (2)	**285**; **286**
		572	573 (3); 555 (24); 531 (2); 513 (100); 469 (3); 451 (2); 325 (2)	GenA-K (**223**); GA-H (**24**); **260**
10	11.9	458	459 (70); 441 (5); 423 (4); 385 (1); 303 (3)	LA-A (**69**)
		512	513 (31); 495 (11); 481 (1); 465 (5); 451 (4); 423 (4); 421 (4); 331 (2); 303 (3)	GenA-H (**222**); GenA-D (**220**); GA-E (**21**) / GNPA-A (**31**); GenA-G (**271**)
		530	531 (5); 513 (31); 499 (2); 495 (11); 481 (1); 455 (1); 451 (4); 439 (6); 421 (4); 331 (2); 309 (2); 305 (6); 305 (6); 303 (3)	12βOH-GenA-B (**270**); GA-C6 (**233**); GA-M (**236**); MeGA-B (**15**)
		548	549 (15); 531 (5); 513 (31); 457 (15); 441 (5); 421 (4); 319 (3)	**258**
		554	555 (5); 513 (31); 511 (7); 451 (4); 439 (6); 425 (2); 303 (3)	**285**; **286**
		568	569 (100); 551 (6); 509 (5); 465 (5); 421 (4); 303 (3)	12β-OAc-GenA-F (**272**)
		572	573 (4); 555 (5); 531 (5); 513 (31); 511 (7); 451 (4); 423 (4); 421 (4); 409 (6); 305 (6); 303 (3); 301 (3)	GenA-K (**223**); 12β-OAc-GA-D (**264**); GA-H (**24**); **260**
		574	557 (2); 513 (31); 409 (6); 331 (2)	GA-K (**26**)
		586	569 (100); 545 (3); 527 (1); 465 (5); 331 (2)	MeGA-H (**230**)
11	12.2	570	571 (52); 553 (100); 511 (2); 509 (13); 467 (1); 301 (1)	12β-OAc-GenA-H (**47**); 12β-OAc-GenA-D (**224**); GA-F (**22**)
		588	571 (52); 515 (13); 471 (1)	MeGa-K (**231**)

Peak	Rt/ min	MW	Fragmentation	Assignment
12	12.3	514	515 (100); 497 (3)	GenA-B (**219**); GA-AM$_1$ (**12**); GenA-A (**213**); **287**; GA-C1 (**17**) / GA-D (**19**) / GA-J (**234**)
		532	515 (100); 497 (3)	GA-I (**206**); GA-G (**23**)
		598	515 (100); 511 (2)	EtGA-F (**228**)
13	12.5	498	499 (54); 481 (6); 367 (1)	**285**
		510	511 (27); 493 (5); 467 (3)	GenA-F (**221**)
		512	513 (27); 495 (5); 481 (5); 471 (4); 421 (1); 379 (1); 303 (4)	GenA-H (**222**); GenA-D (**220**); GA-E (**21**) / GNPA-A (**31**); GenA-G (**271**); GA-X (**251**)
		514	515 (100); 497 (31); 481 (6); 479 (4); 473 (8); 471 (4); 467 (3); 455 (2); 453 (9); 443 (2); 435 (2); 379 (2); 321 (1); 317(2); 305 (1); 305 (1); 303 (4)	**283**; GenA-B (**219**); GA-AM$_1$ (**12**); GenA-A (**213**); 297; GA-C1 (**17**) / GA-D (**19**); LA-D (**278**); GA-J (**234**)
		516	517 (4); 499 (54); 483 (1); 481 (6); 475 (3); 471 (4); 467 (3); 455 (2); 445 (1); 413 (5); 329 (2); 303 (4)	**259**; GenA-C2 (**269**); GA-B (**8**); LA-E2 (**83**); GA-A (**10**)
		528	529 (10); 511 (27); 485 (4); 467 (3); 455 (1); 421 (1); 307 (15)	**284**
		530	531 (2); 513 (27); 499 (54); 495 (13); 481 (6); 455 (2); 421 (1); 305 (1); 303 (4)	12βOH-GenA-B (**270**); GA-C6 (**233**) GA-M (**236**) / 12βOH-GA-D (**263**) / 12βOH-GA-C1 (**225**); MeGA-B (**15**)
		532	533 (2); 515 (100); 497 (31); 485 (4); 471 (4); 455 (2); 453 (9); 305 (1); 303 (4);	GA-I (**206**); GA-G (**23**)
		554	555 (8); 513 (27); 511 (27); 303 (4)	**285**; **286**
		572	573 (4); 555 (8); 531 (2); 513 (27); 483 (1); 471 (4); 421 (1); 379 (1); 305 (1); 303 (4)	GenA-K (**223**); GA-H (**24**); **260**

Peak	Rt/ min	MW	Fragmentation	Assignment
13	12.5	574	575 (19); 513 (27); 471 (4); 453 (9)	GA-K (**26**)
		588	571 (11); 529 (10); 515 (100); 471 (4); 453 (9); 305 (1)	MeGA-K (**231**)
		598	527 (1); 515 (100); 511 (27); 467 (3)	EtGA-F (**228**)
14	12.9	510	511 (29); 493 (14); 469 (1); 467 (2); 463 (3); 451 (3); 449 (3); 419 (9)	GenA-F (**221**); GA-T-Q (**57**)
		512	513 (45); 495 (33); 481 (2); 465 (1); 451 (3); 423 (7); 303 (1)	GenA-H (**222**); GenA-D (**220**); GA-E (**21**) / GNPA-A (**31**); GenA-G (**271**)
		514	515 (100); 497 (23); 481 (2); 479 (22); 473 (1); 471 (5); 467 (2); 453 (8); 443 (1); 439 (1); 423 (7); 395 (2); 319 (7); 303 (1)	**283**; GenA-B (**219**); GA-AM$_1$ (**12**); GenA-A (**213**); **287**; GA-C1 (**17**) / GA-D (**19**); LA-D (**278**); GA-J (**234**)
		526	527 (84); 441 (4); 423 (7)	15α-OAc-GLA-E (**267**)
		528	529 (6); 511 (29); 469 (1); 467 (2); 423 (7); 363 (10)	**284**
		530	513 (46); 495 (34); 469 (1); 451 (3); 439 (1); 303 (1); 303 (1)	12βOH-GenA-B (**270**); GA-C6 (**233**); GA-M (**236**) / 12βOH-GA-C1 (**225**) / 12βOH-GA-D (**263**)
		532	533 (2); 515 (100); 497 (23); 471 (5); 453 (8); 303 (1)	GA-I (**206**); GA-G (**23**)
		548	549 (21); 513 (46); 469 (1); 467 (2); 457 (7); 441 (4); 319 (6)	**258**
		554	555 (4); 513 (46); 511 (29); 469 (1); 451 (3); 439 (1); 395 (2); 303 (1)	**285**; **286**
		568	569 (15); 551 (24); 509 (24); 465 (1); 303 (1)	12βOAc-GenA-F (**272**)
		570	571 (3); 553 (17); 511 (29); 481 (2); 467 (2); 449 (3); 303 (1); 303 (1)	12βOAc-GenA-H (**47**); 12βOAc-GenA-D (**224**); GA-F (**22**)
15	13.3	568	569 (1); 551 (2); 509 (100); 465 (4); 437 (2); 421 (6)	12β-OAc-GenA-F (**272**)

Peak	Rt/ min	MW	Fragmentation	Assignment
16	13.7	472	457 (49); 381 (1); 363 (1); 338 (2)	GN3OL (**67**)
		474	475 (2); 457 (49); 329 (5)	GR3OL-M (**212**);
		510	511 (100); 493 (7); 467 (1); 363 (1)	GenA-F (**221**)
		516	475 (2); 457 (49); 329 (5)	LA-E2 (**83**)
		518	483 (1); 457 (49)	GA-C2 (**18**)
		528	529 (16); 511 (100); 467 (1); 455 (1); 363 (1); 336 (1)	**284**
		554	513 (14); 511 (100); 496 (1)	**286**
		570	571 (1); 553 (2); 511 (100); 481 (2); 467 (1); 303 (2)	12β-OAc-GenA-H (**47**); GA-F (**22**)
		598	557 (1); 527 (7); 515 (1); 511 (100); 467 (1); 457 (1); 301 (1)	EtGA-F (**228**)
17	14.0	510	511 (100); 493 (51)	GenA-F (**221**)
		528	529 (2); 511 (100); 479 (2); 453 (2); 438 (1); 435 (1); 421 (2); 423 (1)	**284**; MeGA-D (**227**)
		554	513 (11); 511 (100); 496 (3)	**286**
		568	569 (2); 551 (1); 509 (5); 494 (33); 421 (2); 317 (1)	12β-OAc-GenA-F (**272**)
		570	571 (1); 538 (1); 511 (100); 494 (32); 481 (2)	12β-OAc-GenA-D (**224**); GA-F (**22**)
18	14.5	512	513 (22); 495 (100)	GenA-H (**222**); GenA-D (**220**); GA-E (**21**) / GNPA-A (**31**); GenA-G (**271**)
		530	513 (22); 498 (1); 495 (100)	12βOH-GenA-B (**270**); GA-M (**236**) / 12βOH-GA-C1 (**225**) / 12βOH-GA-D (**263**)
		548	549 (4); 513 (22)	**258**
		554	513 (22); 511 (2); 496 (28)	**286**
		572	513 (22); 496 (28)	GenA-K (**223**)
19	14.7	510	511 (25); 493 (9); 478 (3); 463 (11); 419 (2); 408 (3); 405 (1); 392 (1)	GenA-F (**221**)
		512	513 (100); 495 (74); 481 (1); 480 (2); 471 (1); 465 (7); 451 (3); 437 (2); 436 (2); 410 (2); 379 (2); 337 (6); 303 (1)	GenA-H (**222**); GenA-D (**220**); GA-E (**21**) / GNPA-A (**31**); GenA-G (**271**); GA-X (**251**)

Peak	Rt/ min	MW	Fragmentation	Assignment
19	14.7	528	529 (1); 511 (25); 485 (3); 455 (3); 332 (3); 319 (2)	**284**
		530	513 (100); 498 (1); 495 (74); 481 (1); 455 (3); 451 (3); 437 (2); 436 (2); 408 (3); 305 (2); 305 (2); 303 (1)	12βOH-GenA-B (**270**); GA-C6 (**233**); GA-M (**236**) / 12βOH-GA-C1 (**225**) / 12βOH-GA-D (**263**); MeGA-B (**15**)
		548	549 (10); 513 (100); 455 (3); 425 (2); 305 (2)	**258**
		554	513 (100); 511 (25); 496 (38); 451 (3); 425(2); 395 (4); 303 (1)	**285**; **286**
		568	569 (37); 509 (25); 494 (4); 465 (7); 437 (2); 345 (2); 303 (1)	12β OAC-GenA-F (**272**)
		572	513 (100); 496 (39); 478 (3); 451 (3); 436 (2); 379 (2); 316 (6); 305 (2); 301 (7)	GenA-K (**223**); **260**
		574	557 (3); 513 (10); 498 (1); 471 (1)	GA-K (**26**)
		586	569 (37); 545 (3); 465 (7)	MeGA-H (**230**)
		598	599 (1); 539 (4); 527 (6); 515 (9); 511 (25); 451 (3); 357 (1); 301 (7)	EtGA-F (**228**)
		614	615 (2); 511 (25); 512 (4); 481 (1); 451 (3); 345 (2)	3βOAc-GA-H (**265**)
		616	599 (1); 525 (5); 513 (100); 511 (25); 495 (74); 481 (1); 451 (3)	**261**
20	14.9	510	511 (100); 493 (5); 463 (1); 449 (4); 323 (1)	GenA-F (**221**)
		528	511 (100); 421 (1); 336 (1); 319 (1);	**284**
		546	547 (11); 511 (100); 493 (5);449 (4); 433 (2); 389 (1); 321 (1)	GA-N (**237**)
		570	571 (1); 553 (6); 511 (100); 452 (1)	12β-OAc-GenA-H (**47**); GA-F (**22**)
21	15.3	498	499 (100); 367 (1)	**285**
		534	535 (8); 499 (100)	12βOH-GA-C_2 (**257**)
		570	571 (1); 553 (4); 499 (100); 485 (1); 457 (1)	GA-Mk (**51**) / GA-P (**249**) / GA-Q (**250**)
22	15.7	568	569 (36); 551 (100); 509 (1)	12β-OAc-GenA-F (**272**)
		612	571 (4); 569 (36); 553 (7); 552 (39); 551 (100); 499 (1); 495 (1)	GA-T (**11**)

Peak	Rt/ min	MW	Fragmentation	Assignment
23	16.1	512	513 (100); 495 (7); 465 (6); 437 (5); 421 (3); 410 (16); 303 (2); 303 (2)	GenA-H (**222**); GA-E (**21**)/ GNPA-A (**31**); GenA-G (**271**); GA-X (**251**)
		530	513 (100); 499 (10); 498 (1); 469 (5); 437 (5); 439 (4); 421 (3); 331 (8); 305 (4); 305 (4); 303 (2)	12βOH-GenA-B (**270**); GA-C6 (**233**); MeGA-B (**15**)
		548	549 (16); 513 (100); 469 (5); 441 (3); 421 (3)	**258**
		554	513 (100); 511 (9); 469 (5); 425 (4); 303 (2)	**285**; **286**
		572	513 (100); 478 (3); 469 (5); 421 (3); 331 (8); 315 (14); 305 (4)	GenA-K (**223**); GA-H (**24**)
		574	557 (1); 513 (100); 498 (1); 331 (8)	GA-K (**26**)
		632	603 (7); 559 (7); 515 (4); 514 (52); 513 (100); 511 (7)	BuGA-F (**288**)

Table 5.12 Peak assignment. The most abundant masses are displayed. The assignment was performed considering the mass fragmentation and literature data.[141-143]

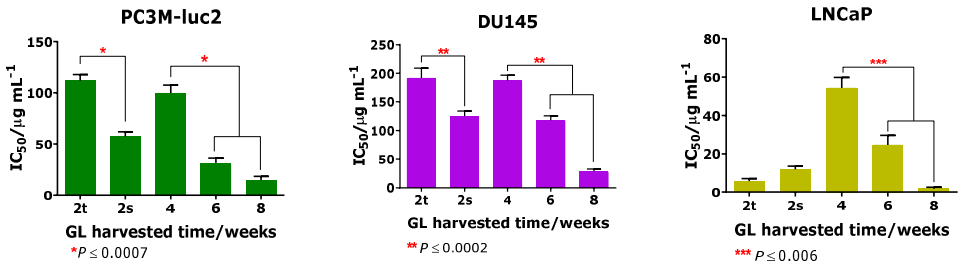
5.3. Effects of GL extracts on prostate cancer cell viability

To determine the ability of the extracts to inhibit the cell viability of the prostate cancer (PCa) cell-lines PC3M-luc2, DU145 and LNCaP, MTT assays were performed. For that purpose, GL extracts at concentrations from 0 to 2000 $\mu g\, mL^{-1}$ were evaluated.

As observed in previous sections, the extracts are complex mixtures of a large number of compounds, therefore the results of the MTT assay could differ significantly from the typical sigmoidal dose-response curves and being an average of the sum of the effect of all the components presents in the sample. Nonetheless, to make a comparison between the samples the data was fitted to sigmoidal curves (Appendix 3 Figures A3-22 to A3-35).

IC_{50} values were defined as the concentration of mushroom extract where the response was reduced by half.

5.3.1. Effect of GL growing stages

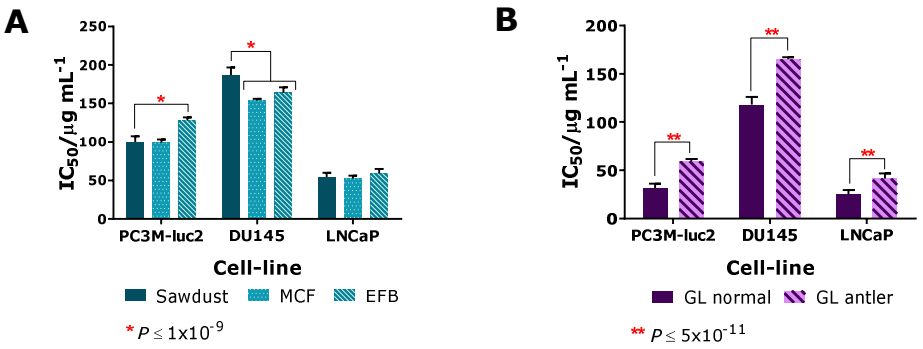


Time/week	IC_{50}/µg mL^{-1}		
	PC3M	**DU145**	**LNCaP**
2 (tip)	112±6	192±17	5.74±1.33
2 (stalk)	57.3±4.8	125±9	11.9±1.8
4	99.8±7.9	187±10	54.4±5.4
6	31.4±4.9	118±8	24.7±4.9
8	14.7±3.8	29.0±3.7	1.77±0.85

Figure 5.4 Comparison of IC_{50}'s for PC3M (green), DU145 (purple) and LNCaP (gold) after treatment with GL harvested at increasing times from 2- to 8- weeks. 2t = 2 weeks (tip); 2s = 2 weeks (stalk). Student t-test was applied to determine significant difference with 95% confidence. $^{*}P \leq 0.0007$; $^{**}P \leq 0.0002$; $^{***}P \leq 0.006$.

Graphs in Figure 5.4 show a significative reduction in the IC_{50}s going from GL harvested from 4- to 8-weeks for all the cell-lines analysed. A distinction was encountered in the GL harvested at 2-weeks, while the tip was significantly less active than the stalk and the 4-week sample for PC3M and DU145 cell-lines, the contrary was observed for LNCaP, thus, the tip was more active than the stalk. In case of the 2-week stalk sample, it inhibited the viability more than the 4-week sample, but less than the 6-week one for PC3M and DU145 and it was more active than the GL harvested at 4- and 6-weeks but comparable to the 2-week tip for LNCaP.

5.3.2. Effect of the growing substrate and GL type



Substrate/Type	IC_{50}/µg mL^{-1}		
	PC3M-luc2	**DU145**	**LNCaP**
Sawdust	99.8±7.9	187±10	54.4±5.4
MCF	99.2±4.0	154±2	52.7±3.6
EFB	128±4	164±7	59.3±5.8
Normal	31.4±4.9	118±8	24.7±4.9
Antler	59.9±2.3	165±2	41.3±5.3

Figure 5.5 Comparison of the IC_{50}s for the different substrates investigated: **A** sawdust, MCF and EFB (blue graph) and **B** the different GL types: normal and antler (purple graph). * $P \leq 1x10^{-9}$, ** $P \leq 5x10^{-11}$.

Inhibition of the cell viability by GL grown on different substrates was cell-line dependent. Thus, no difference in the inhibitory activity were found in LNCaP when comparing the three substrates, but GL grown on MCF and EFB were better inhibitors than GL grown on sawdust for DU145, whereas no significant difference in activity was found in PC3M with GL grown in MCF or sawdust, but the activity was significantly reduced when GL was grown in EFB (Figure 5.5 blue graph).

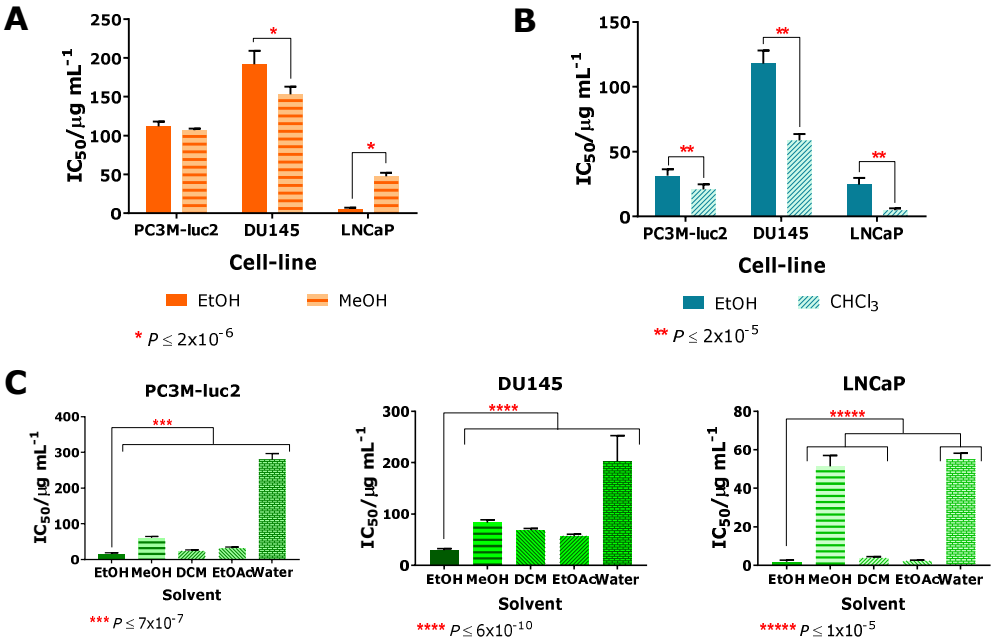
Both GL normal and antler types inhibited the viability of PCa cell-lines. However, GL normal type was a more effective inhibitor compared with GL antler type for all the cell-lines (Figure 5.5 purple graph).

5.3.3. Effect of the extraction solvent

When comparing ethanol and methanol, no significant difference in the IC_{50} values were found for PC3M when treated with the extract of GL tip harvested at 2-weeks but the ethanol extract was better than the methanol one for LNCaP and the reverse was observed for DU145, in this case, the methanol extract was a better inhibitor than the ethanol one (Figure 5.6

orange graph). Whereas for the GL harvested at 8-weeks the ethanol extract was always better than the methanol one (Figure 5.6 green graphs).

Extraction with chloroform produced lower IC_{50}s than the extraction with ethanol for the GL harvested at 6-weeks (Figure 5.6 blue graphs). The contrary was observed for the GL harvested at 8-weeks. In this case, the IC_{50}s of the ethanol extract were lower than the IC_{50}s of the dichloromethane extracts. Indeed, at 8-weeks, ethanol appeared as the best solvent for extraction, while water was the worst. The order of the extract activities regarding the solvent was as follows: ethanol > ethyl acetate > dichloromethane > methanol > water. As for LC-MS, the triterpene content of the extracts differed very slightly for all the solvents, the observed difference in activity may be due not only for this triterpene variation, but also for all the other substances present in the extract, like possibly the major concentration of polysaccharides in the water extract, as despite having essentially the same triterpene content as the ethanol extract, it displayed a much lower activity.



Solvent		$IC_{50}/\mu g\ mL^{-1}$		
		PC3M	**DU145**	**LNCaP**
2 W-t	EtOH	112±6	192±17	5.74±1.33
	MeOH	107±2	153±10	47.6±4.2
6 W	EtOH	31.4±4.9	118±8	24.7±4.9
	$CHCl_3$	59.9±2.3	165±2	41.3±5.3
8 W	EtOH	14.7±3.8	29.0±3.7	1.77±0.85
	MeOH	60.7±3.1	83.0±5.9	51.4±5.6
	DCM	24.2±2.9	68.5±3.0	3.90±0.51
	EtOAc	31.1±3.9	57.3±3.0	2.27±0.33
	Water	280±17	202±51	55±3.3

Figure 5.6 Effect of the extraction solvent in the inhibition of PCa cell viability. **A** GL harvested at 2-weeks (tip) (orange); **B** GL harvested at 6-weeks (blue) and **C** GL harvested at 8-weeks (green). * $P \leq 2x10^{-6}$; ** $P \leq 2x10^{-5}$; *** $P \leq 7x10^{-7}$; **** $P \leq 6x10^{-10}$; ***** $P \leq 1x10^{-5}$.

Liu *et al*. qualitatively determined the GL composition at six different growing stages.[144] They focused their investigation on five triterpenes: GA-A (**10**); GA-D (**19**); GA-DM (**32**); GA-TR (**58**) and G3OL (**205**). In particular, in the amount of GA-DM (**32**) and GA-TR (**58**) at the different stages, as these two GA were the best inhibitors of 5α-reductase. They found that the concentration of these triterpenes varied with the growing stage. Furthermore, the stages with the highest concentration of GA-DM (**32**) and GA-TR (**58**) were also the ones that showed the highest enzyme inhibition, in their case corresponding to stages 4 and 5. This is in complete agreement with our observations. Although only a qualitative analysis was performed in our case, it was identified that the triterpene composition changed with the growing stage, substrate and the extraction solvent.

Liu divided GL at stage 4 into pileus (top) and stipe (stalk) and their composition in the five triterpenes was analysed. Interestingly, the amount of these triterpenes in the stipe was higher than in the pileus making it the most active inhibitor for the enzyme. The higher activity of the stalk was also observed in our experiments, even though it was compared at a lower growing stage. Therefore, this evidence suggested that most of the active components of GL fruiting body were more concentrated in the stalk.

Wang *et al*. studied the effect of the total triterpenoids from GL in PCa cell-lines.[145] They demonstrated that GL total triterpenoids inhibited PCa cell growth and that this inhibition was due to induction of apoptosis and cell

cycle arrest. Consistent with Wang, our studies also suggested that GL total triterpene extract inhibited the cell viability of PCa cell-lines, but that the extent of the inhibition depended on factors such as growing stage, substrate or extraction solvent.

5.4. Summary and conclusions

Mass analysis and the MTT proliferation assay were performed to identify variations in GL composition and biological activity at increasing growing stages (2-, 4-, 6- and 8-week), with the growing substrate (sawdust, MCF or EFB) and the GL type (normal or antler) and with the extraction solvent. For the biological assays, PCa cell-lines were used.

ESI mass analysis revealed the presence of few major triterpenes with m/z 499, 513, 515, 517, 531, 571 and 573 which could correspond to MW 498, 476, 490, 512, 514, 516, 530, 570 and 572. However, little information could be obtained about the real triterpene content. Therefore, LC-MS was performed. In the chromatogram 23 peaks were observed. By comparing the normalised area of the peaks, differences were detected in the triterpene composition of the analysed samples. Thus, different growing stage, substrate, GL type and extraction solvent affected the GL triterpene extract content. In general, the peak area increased with stage; in the order MCF > sawdust > EFB and apparently, ethyl acetate was the best solvent to extract both polar and apolar triterpenes.

Identification of the peaks revealed that the method used for the separation produced the co-elution of most of them. Besides, the lack of standards made the determination of the isomers present in the same peak difficult, although the observed fragmentation was useful to discard some of them.

Inhibition of proliferation was evaluated for each of the extracts using the MTT assay. The assay was performed against three PCa cell-lines: PC3M, DU145 and LNCaP. Data obtained from the experiments where possible, was fitted to sigmoidal curves, above all for LNCaP cell-lines.

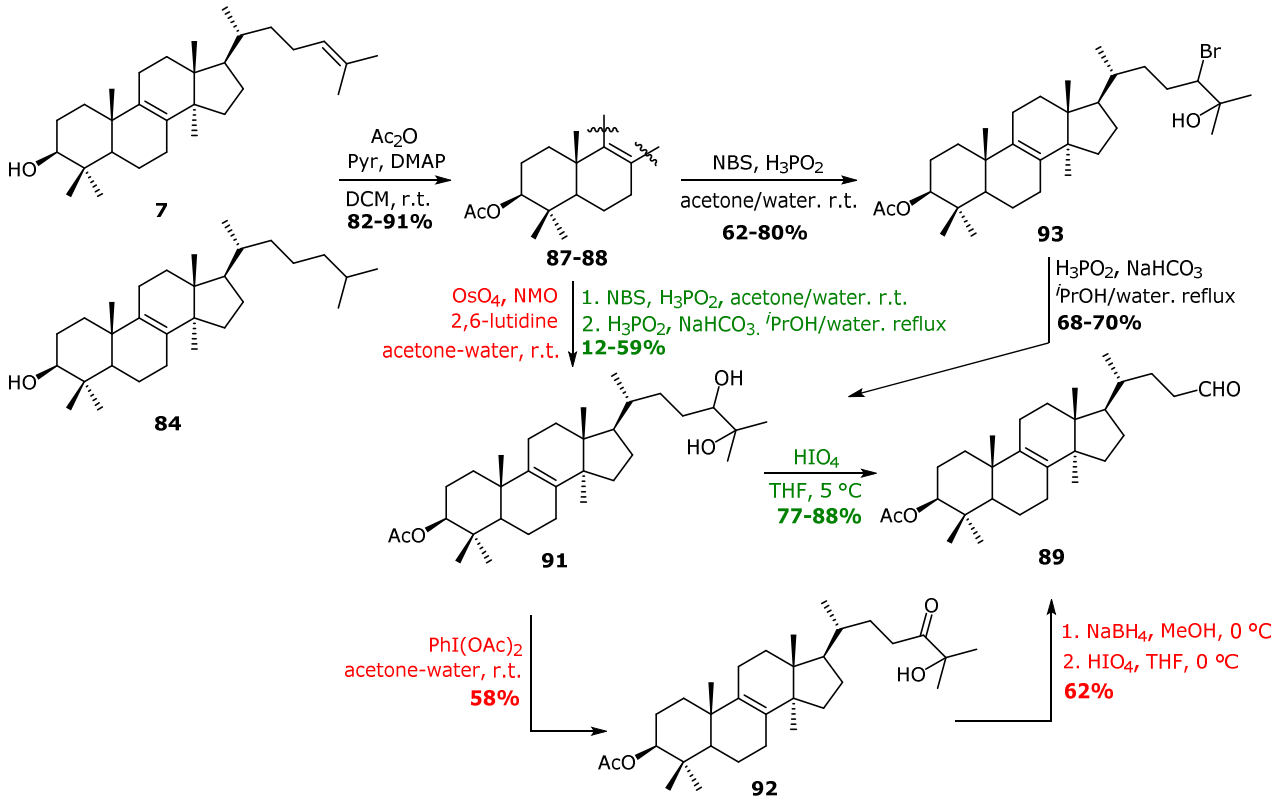
GL total triterpene extract inhibited the cell viability of PCa cell-lines, exhibiting the highest inhibition in the mushroom harvested at 8-weeks, also when separating the stipe from the stalk, it was apparent that the latter was more active. GL antler type was less active than the normal type. Ethanol extract was the most active for the GL harvested at 8-weeks.

6. Conclusions and Future Work

6.1. Conclusions

6.1.1. Synthesis

The synthesis, purification and characterisation of thirteen GA analogues and nine intermediates, eight of which are novel, has been described in this thesis. For their formation, aldehyde **89** was required. Several methods were attempted for the synthesis of this aldehyde. The most successful of which were the step-wise approaches shown in Scheme 6.1.

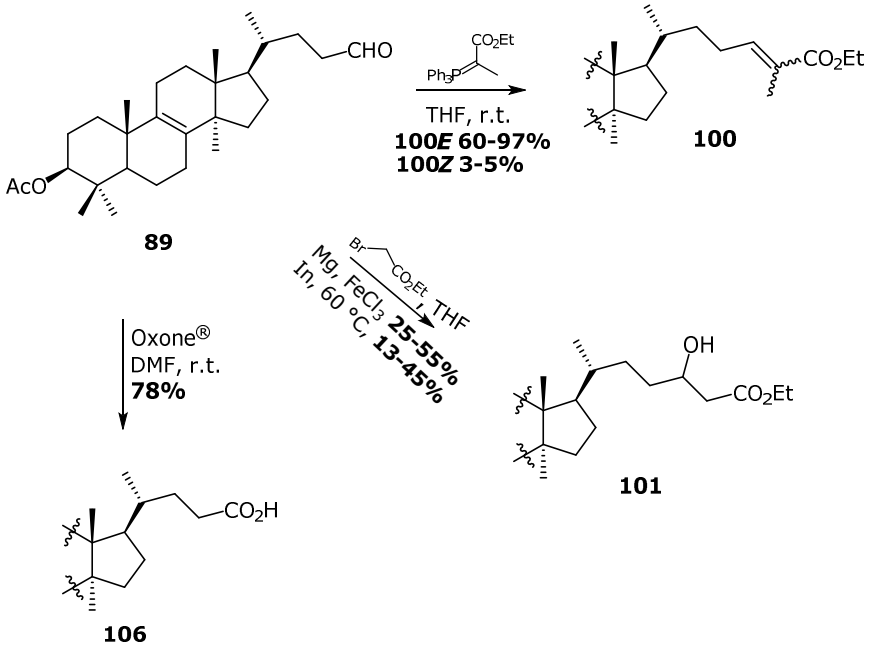


Scheme 6.1 Synthetic routes evaluated for the formation of aldehyde **89** from the commercial lanosterol mixture. In black is the stepwise transformation to diol **91**. In green and red the one-pot transformation to **91**. Black and green routes to the diol **91** were described by Kavtaradze.[37, 38] The red route to aldehyde **89** was described by Nicolau.[49]

In these approaches aldehyde **89** was produced in up to 45-47% overall yield over a 3-4 step sequence. The route started with the acetylation of commercial lanosterol (**7**+**84**), followed by the formation of diol **91**.

Aldehyde **89** was eventually achieved after oxidative cleavage of diol **91** with either periodic acid or (diacetoxyiodo)benzene. However, this latter generated ketol **92** as the major product when the reaction was performed on a large scale. From these three routes, the ones described by Kavtaradze (red or green) were preferred.[37,38]

Wittig olefination, Reformatsky reaction and direct oxidation of aldehyde **89** with Oxone® produced, in good to excellent yield, precursors **100**, **101** and **106**, respectively, (Scheme 6.2). Both adducts **100** and **101** and the oxidation process to form acid **106** are novel in their context.

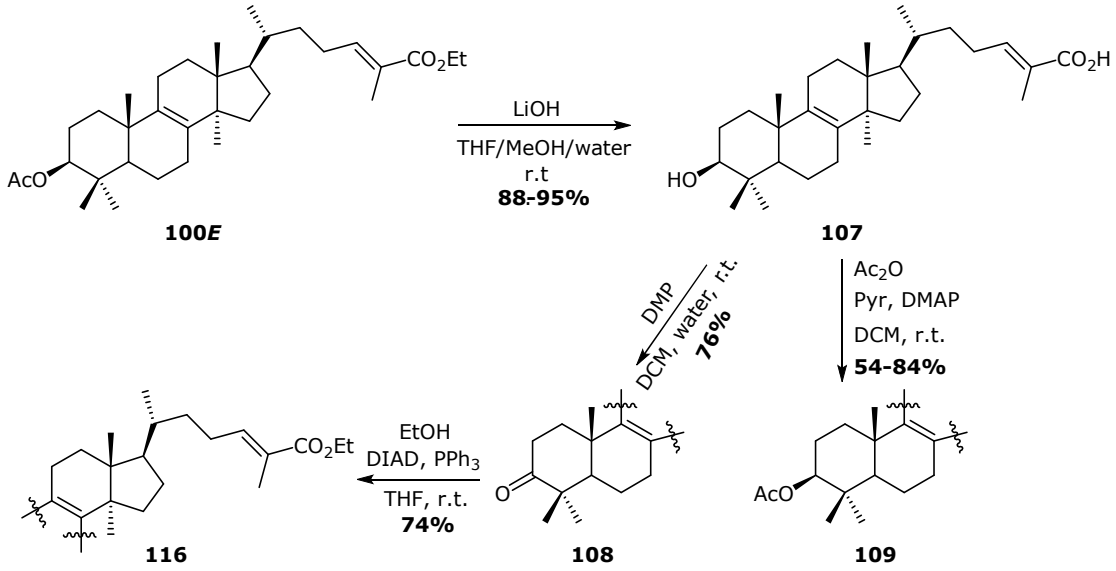


Scheme 6.2 Formation of precursors **100**, **101** and **106** from aldehyde **89**.

The analogues were classified in three groups. Group I included analogues that differ essentially at C-3. Group II has analogues with differences at rings B/C. Finally, group III is composed of analogues with modifications on the side chain.

Analogues from group I were synthesised from Wittig adduct **100*E***. Hydrolysis of this adduct under basic conditions furnished analogue **107** in 88-95% yield. Dess-Martin oxidation and acetylation of **107** generated, in good to excellent yields, analogues **108** and **109**, respectively (Scheme 6.3). Attempts to form analogue **110** by stereoselective reduction of keto ester **116** or Mitsunobu reaction of **107** were unsuccessful. Keto-ester **116** was achieved after esterification of **108** under Mitsunobu conditions in 74%

yield. From these compounds, **109** and **116** are novel, the other two have been previously reported, **107** as the natural GA-Z (**244**)[78,79] and **108** is a patented compound evaluated as an anti-HIV agent.[81,82]

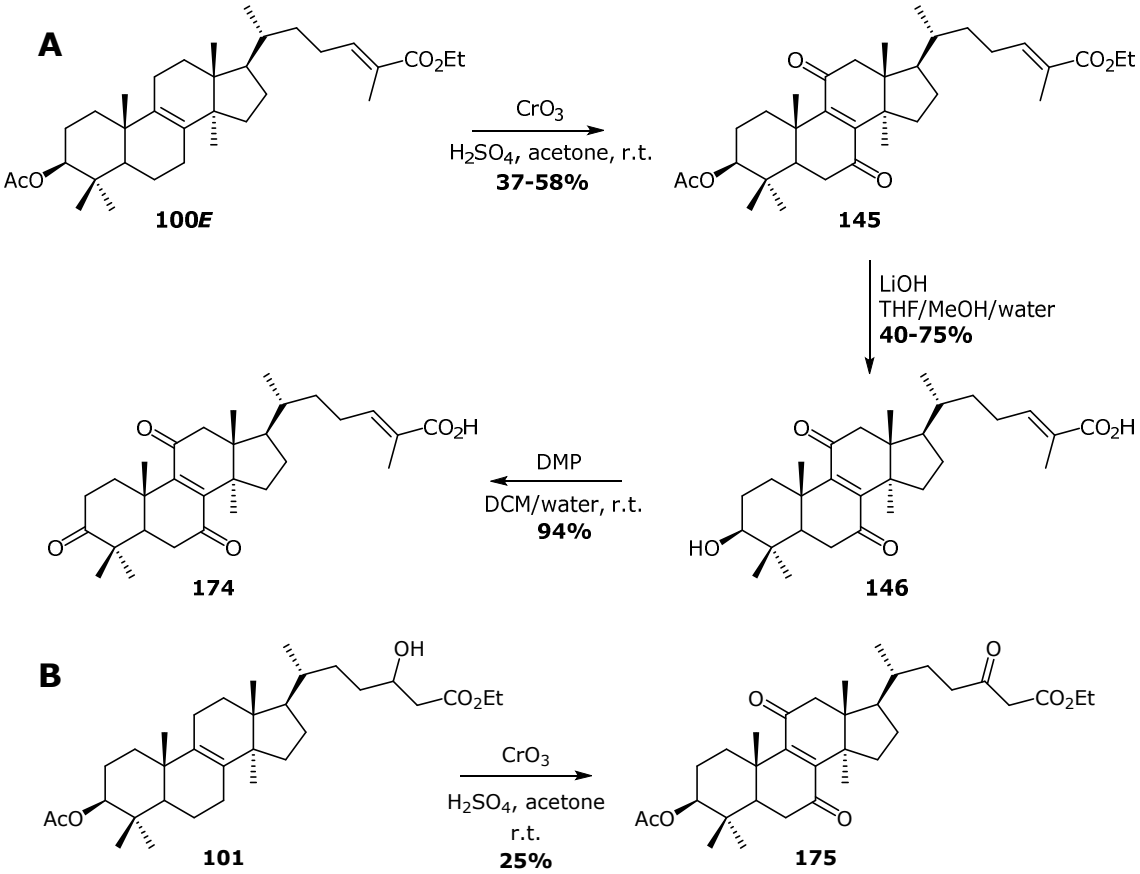


Scheme 6.3 Formation of analogues **107**, **108** and **109**.

For the formation of group II analogues, allylic oxidations and introduction of the diene $\Delta^{7(8),9(11)}$ system were performed. For the allylic oxidation, chromium trioxide, TBHP with different metal catalysis, 3-chloroperbenzoic acid with catalysis of the metalloporphyrin Fe(PFPP)Cl and sodium chlorite with catalysis of *N*-hydroxyphthalimide were all evaluated. However, none of the methods were successful in producing clean high yielding reactions, instead 11-58% yield was achieved for many of them, the best methodology being the classic reaction with chromium trioxide.

Three analogues, **146**, **174** and **175**, were obtained by the allylic oxidation reaction; both **146** and **174** from adduct **100*E*** while **175** was produced from adduct **101**. Thus, **146** was furnished in a two-step process involving allylic oxidation of **100*E*** to give diketone **145** in modest yield (37-58%), followed by hydrolysis of **145** under basic conditions. Analogue **146** was produced in 15-44% overall yield. Analogue **174** was achieved by Dess-Martin oxidation of **146** in excellent yield (94%) (Scheme 6.4 A). Finally, allylic oxidation of adduct **101** gave analogue **175** in 25% yield (Scheme 6.4 B). Compounds **145** and **175** are novel, whilst analogues **146** and **174** were reported as isolated products from the fruiting bodies of *G. resinaceum*

and *Antrodia camphorata*, respectively.[107,108] Nevertheless, this is the first time that they have been synthesised.

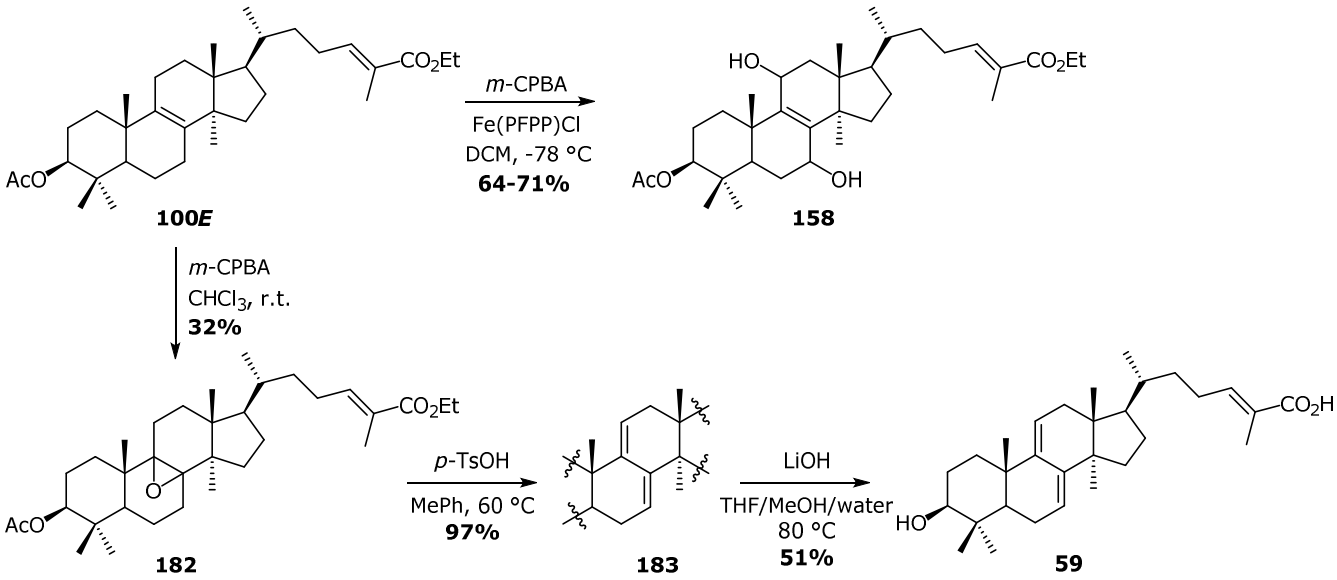


Scheme 6.4 Allylic oxidation. **A** Allylic oxidation of adduct **100*E*** leading to analogue **146** and **174**. **B** Allylic oxidation of adduct **101** to produce analogue **175**.

Allylic dihydroxylation of adduct **100*E*** with 3-chloroperbenzoic acid and catalysis of the metalloporphyrin Fe(PTPP)Cl at -78 ºC successfully gave **158** in good yield (64-71%) (Scheme 6.5). Keeping a low temperature reaction was key as **158** was unstable and oxidised readily at room temperature. Compound **158** is novel.

Analogue **59** with a diene $\Delta^{7(8),9(11)}$ was achieved in 16% overall yield following the three-step process depicted in Scheme 6.5. In this sequence, epoxidation of adduct **100*E*** with 3-chloroperbenzoic acid furnished epoxide **182** in poor yield (32%). Ring opening and elimination of epoxide **182** with *para*-toluenesulfonic acid generated the conjugated diene **183** that after hydrolysis in basic conditions yielded analogue **59**. Analogue **59** has been reported as GA-Y.[78] However, **183** is novel.

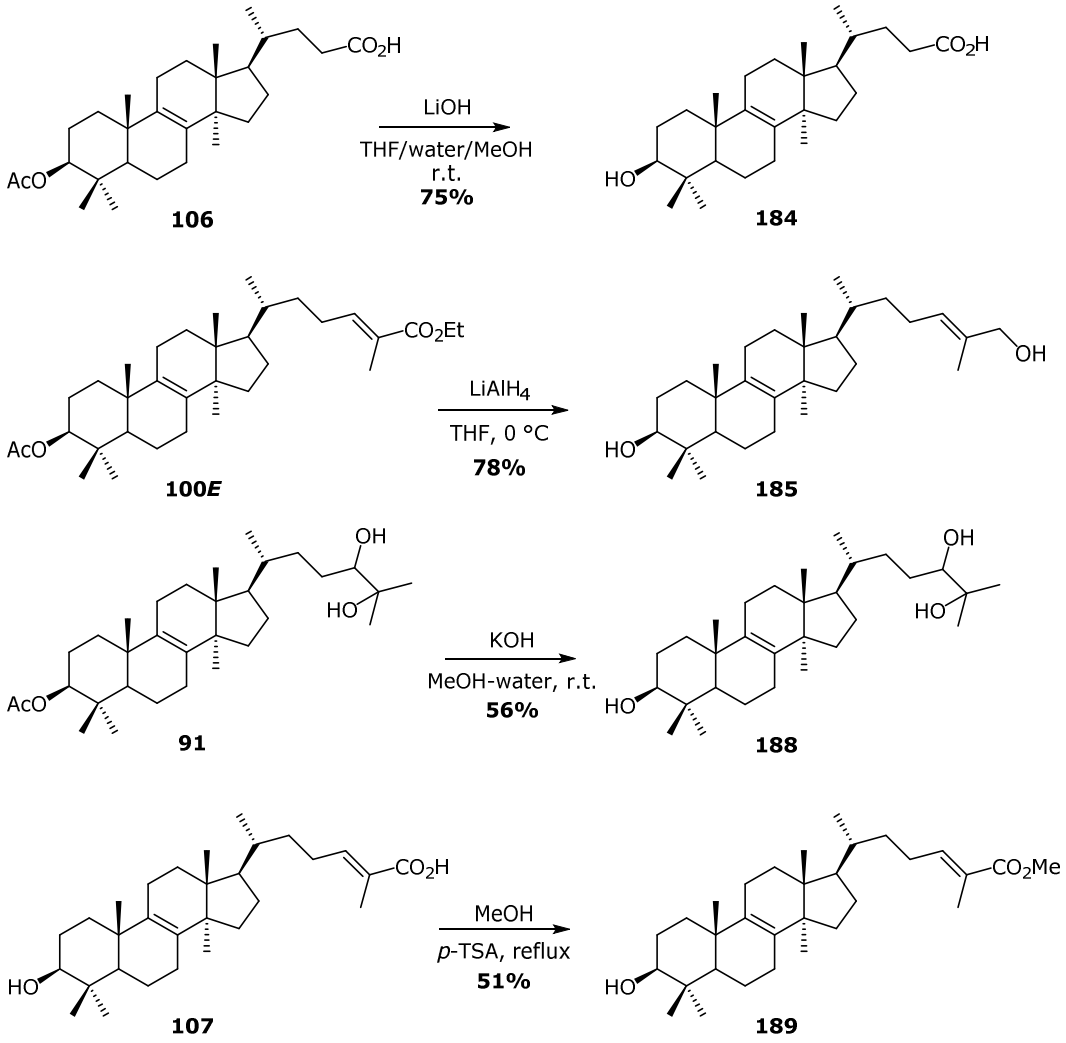
In group III, four analogues were included: **184**; **185**; **188** and **189**. Analogues **184** and **188** were obtained by hydrolysis in basic conditions from **106** and **91**, respectively. Reduction of **100*E*** with lithium aluminium hydride produced analogue **185**. Esterification of analogue **107** in acidic conditions provided analogue **189**. The yields of the different reactions varied between 51-78% (Scheme 6.6). All the analogues of this group were previously reported.[78-79,110,112,114]



Scheme 6.5 Oxidation of **100*E*** to form **158** and analogue **59**.

To conclude, different reaction types were used to accomplish our synthetic goals. From protection as acetyl group to C-C coupling, passing through different kind of oxidations, reductions, substitutions, additions and hydrolysis. Most of the reactions performed in good to excellent yield. The longest route took eight steps to completion, whilst had six steps and an overall yield between 7-44% for the final product.

Compounds **100**, **101**, **109**, **116**, **145**, **158**, **175** and **183** are novel. All the rest were either previously synthesised or isolated from the fungus material. For most of the known compounds, new synthetic procedures were implemented and their characterisation upgraded.



Scheme 6.6 Formation of group III analogues: **184**, **185**, **188**, **189**.

6.1.2. Biological evaluation

Natural GA-H (**24**) and GA-T (**11**) and analogues **59**, **107**, **108**, **109**, **146**, **174**, **184**, **185**, **188** and **189** were employed to conduct SAR analysis. For this purpose, the effect of the GA and their analogues in the viability of prostate cell-lines was evaluated by the MTT assay.

First, PC3 cells were treated with different concentrations of GA-H (**24**) and analogues **108**, **146**, **174** for 24 h, 48 h and 72 h. From these times, exposure at 72 h was the optimum to observed a significant dose-effect. Moreover, the IC_{50} increased in the order **108** < **146** ≈ **174** << GA-H (**24**). As both **146** and **174** have a 7,11-diketone group, whilst they differ only at C-3 oxidation level and GA-H (**24**) additionally has a C-23 ketone. These results suggested that the presence of C-7, C-11, and C-23 ketones

contributed negatively in the activity, whereas having a hydroxyl or ketone at C-3 were both important to enhance it.

Next, normal, non-malignant and cancerous prostate cell-lines were evaluated with the natural GAs, GA-H (**24**) and GA-T (**11**). As observed in the time-course experiment, GA-H (**24**) was a very poor inhibitor for the cancerous cell-lines, with IC_{50} > 500 μM. However, a remarkable difference was discovered among the non-malignant cell-lines. GA-H (**24**) was less toxic for the normal cell-line RWPE1 (IC_{50} = 76 μM) than for the non-malignant cell-lines WPE1-NB14 and -NB26 (IC_{50} = 60 μM). Indicating that GA-H (**24**) may be recommended as a prophylactic for prostate cancer. Nevertheless, these results should be confirmed as lack of GA-H (**24**) prevented us to repeat the experiments. Alternatively, GA-T (**11**) was a much better inhibitor for all the cell-lines analysed. However, it was less active than Taxotere®. Non-malignant cell-lines treated with GA-T (**11**) possessed IC_{50} values around 4-6 μM, whereas for cancerous cell-lines it had higher IC_{50}, with values in the range 10-15 μM. GA-T (**11**) toxicity was the highest for the normal cell-line, IC_{50} = 3.5 μM.

The cell viability of prostate cell-lines was also evaluated for the three groups of analogues. Analogues analysed were: **107**, **108** and **109** from group I; **59** and **146** from group II and **185**, **186**, **188** and **189** from group III. Although both non-malignant and prostate cell lines were employed in the studies, due to time constraints, the non-malignant ones were evaluated only for **107**, **108** and **146**.

Non-malignant cell-lines treated with analogue **107** presented a biphasic dose-response curve. Interestingly, a difference in activity was encountered between the normal cell-line and the two pre-malignant ones. Thus, $EC_{50}1$ and $EC_{50}2$ were the lowest for RWPE1 with values 1.9 μM and 259 μM, respectively, whilst the other two cell-lines had very similar values in the order 2.2 μM and > 500 μM. This behaviour contrasted with the one observed for analogue **108** and **146**. For these analogues, the lowest IC_{50} value was found for the pre-malignant cell-lines WPE1-NB14 (3.3 μM) for **108** and WPE1-NB26 (4.6 μM) for **146**. with the other two cell-lines displaying very similar values in the order of 6.0 μM for **108** and between 5-7 μM for **146**. Therefore, they were behaving as GA-H (**24**), but with a level of toxicity comparable to GA-T (**11**). Both analogues **108** and **146** were less aggressive for the normal cell-line RWPE1, **108** displaying the

highest toxicity at very early pre-malignancy stage, while **146** inhibitory activity increased as pre-malignancy increased: RWPE1 < WPE1-NB14 < WPE1-NB26. Suggesting that the presence of ketones at C-3, C-7 and C-11 were responsible of this behaviour (Table 6.1).

GA	EC_{50}-IC_{50}/μM		
	RWPE1	**WPE1-NB14**	**WPE1-NB26**
GA-H (**24**)	76.0±5.8	56.9±7.8	60.1±4.4
GA-T (**11**)	3.53±0.30	3.68±0.33	6.28±0.32
107	*1.* 1.86±0.32 *2.* 259±39	*1.* 2.22±0.64 *2.* 505±76	*1.* 2.17±0.26 *2.* 586±67
108	5.92±0.67	3.26±0.44	6.35±0.52
146	7.08±1.02	5.24±0.58	4.61±0.65

Table 6.1 EC_{50}-IC_{50} value after treating non-malignant cell-lines with natural and synthetic GA. Values are given as mean ± SD.

For the cancerous cell-lines, the inhibition was cell-line dependant. Hence, a clear distinction was found between the hormone resistant and hormone sensitive cell-lines. LNCaP was the most sensitive cell-line with IC_{50} values around 4-15 μM for group I analogues; 3-54 μM for group II analogues and 4-36 μM for group III analogues, whilst for the more aggressive cell-lines the IC_{50} values were in the order 18-89 μM; 21-115 μM and 16-1000 μM for each group of analogues, respectively (Table 6.2).

GA	EC_{50}-IC_{50}/μM			
	PC3	**PC3M-luc2**	**DU145**	**LNCaP**
GA-H (**24**)	1090±60	-	659±46	657±53
GA-T (**11**)	10.4±0.5	12.4±0.6	15.1±1.0	11.5±0.6
107	23.2±3.4	17.9±5.2	18.8±1.9	14.9±1.8
108	32.9±1.0	26.1±2.4	43.7±1.7	9.60±0.98
109	-	24.3±2.9	89.2±4.2	4.08±1.51
59	-	20.9±2.2	54.4±2.1	3.25±1.24
146	58.6±2.8	111±7	114±5	53.8±6.2
184	-	105±3	17.0±1.4	24.2±2.4
185	-	56.3±2.3	43.1±4.4	4.40±0.31
188	-	20.4±4.4	15.6±5.0	11.3±0.5
189	-	38.8±3.4	1052±172	36.0±1.2

Table 6.2 EC_{50}/IC_{50}s of natural and synthetic GA in prostate cancer cell-lines. Values are indicated as mean ± SD.

Within group I analogues, the IC_{50} increased in the order: **109** < **108** < **107** for LNCaP, whilst the order was inverted for the refractory cell-lines, for

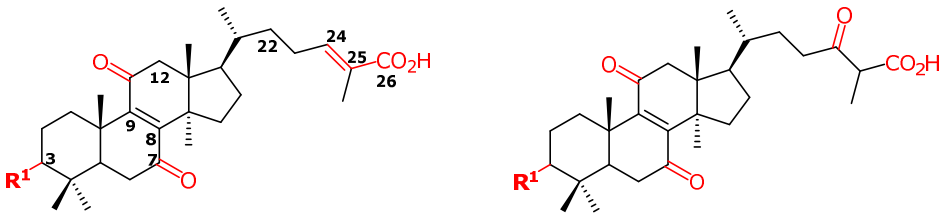
which, the values increased in the order **107** < **109** < **108**. Indicating that the activity was affected when modifying the functionality at C-3, the activity was reduced in the order β-OAc > -C=O > β-OH in LNCaP and in the order β-OH > β-OAc > -C=O in the aggressive cell-lines. GA-T (**11**) IC_{50} had the lowest for the refractory cell-lines, suggesting that the α-acetate may be the best functional group for enhancing the activity in this type of cell-lines.

Group II analogue **59** decreased the cell viability even further in LNCaP cells (IC_{50} = 3.3 μM) where it was 4.6 times more active than **107**. The only difference between them laid on the olefin conjugation at ring B/C, it was concluded that the conjugation of the double bond is essential for activity in this cell-line. However, none of the group II analogues were good inhibitors for the more aggressive cell-lines. Analogue **59** was less active than **107**, but comparable to **108** and **109**. In contrast, analogue **146** was the least active of the analogues, suggesting that conjugation could not be as necessary for the aggressive cell-lines, furthermore ketones at C-7 and C-11 were detrimental, reducing the activity considerably.

Among group III analogues, **185** (IC_{50} = 4.4 μM) was a good candidate for the inhibition of LNCaP. In this cell-line the IC_{50} values increased in the order **185** < **188** ≈ GA-T (**11**) < **184** < **189**. As analogue **185** was better than **107** and **188**, both the alcohol at C-26 and the $\Delta^{24.25}$ double bond appeared as important functional groups for raising the activity, whilst shortening of the side chain length and particularly, esterification dramatically reduced it. Ordering the functionality from higher to lower activity, the complete sequence is as follows: allylic 26-OH > 24,25-diol > 24-CO_2H > -CO_2Me. In the hormone resistant cell-lines, PC3M-luc2 IC_{50} values increased in the order GA-T (**11**) < **188** < **189** < **185** < **184**; whereas in DU145 the order followed was **188** ≈ GA-T (**11**) < **184** < **185** << **189**. Consequently, **188**, with a 24,25-diol functionality and displaying similar activity as GA-T (**11**) was the best inhibitor for DU145, but analogue **188** was worse inhibitor than GA-T (**11**) for PC3M-luc2, suggesting that the conjugated acid might be better than the 24,25-diol in this cell-line. Thus, ordering the functionality according their activity, it follows: α,β-unsaturated CO_2H > 24,25-diol > -CO_2Me > allylic 26-OH > 24-CO_2H for PC3M-luc2 and 24,25-diol > 24-CO_2H > allylic 26-OH >> -CO_2Me for DU145.

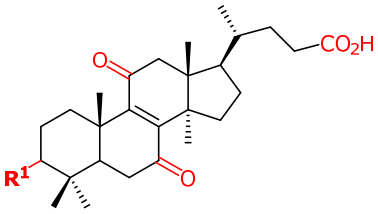
Previous studies with natural and synthetic GA in WPE1-NB26 cell-lines suggested that C-3 ketone or β-acetate, 7-hydroxyl, C-12 and C-22 acetate

and $\Delta^{7(8),9(11)}$ double bond system increased the activity, while shortening of the side chain length and allylic 7,11-diketone reduced it.[35, 36] These results together with ours allowed us to propose three types of analogues with potential enhanced activity for the pre-malignant cell-lines, but being less toxic for the normal one (Figure 6.1). All of them have in common the allylic 7,11-diketone system varying at C-3 and/or side chain functionalities.



I
146, 174, 191

II
192-195



III
196-199

Analogue	Type	R^1
146	I	β-OH
174	I	-C=O
191	I	β-OAc
192	II	β-OAc
193	II	α-OAc
194	II	β-OH
195	II	-C=O
196	III	β-OAc
197	III	α-OAc
198	III	β-OH
199	III	-C=O

Figure 6.1 Chemical structure of analogues with potential anti-proliferation activity for the non-malignant cell-lines. Highlighted in red are the functional groups for each of the studied areas.

Analogously, based on our observations, candidates were proposed that could enhanced the activity of the hormone sensitive and resistant cancerous cell-lines (Figure 6.2). For the more aggressive cell-lines four candidates were selected. These compounds have the common feature of 3α-acetate group with modifications on the double bond system in rings B/C or the side

chain functionality. From these, analogues **110** and **201** could be more effective for DU145, while the four of them might be as good for PC3 and PC3M-luc2. For the hormone sensitive cell-line, one analogue was proposed **203**. It has 3β-acetate, $\Delta^{7(8),9(11)}$ conjugated double bond and allylic 26-hydroxyl groups.

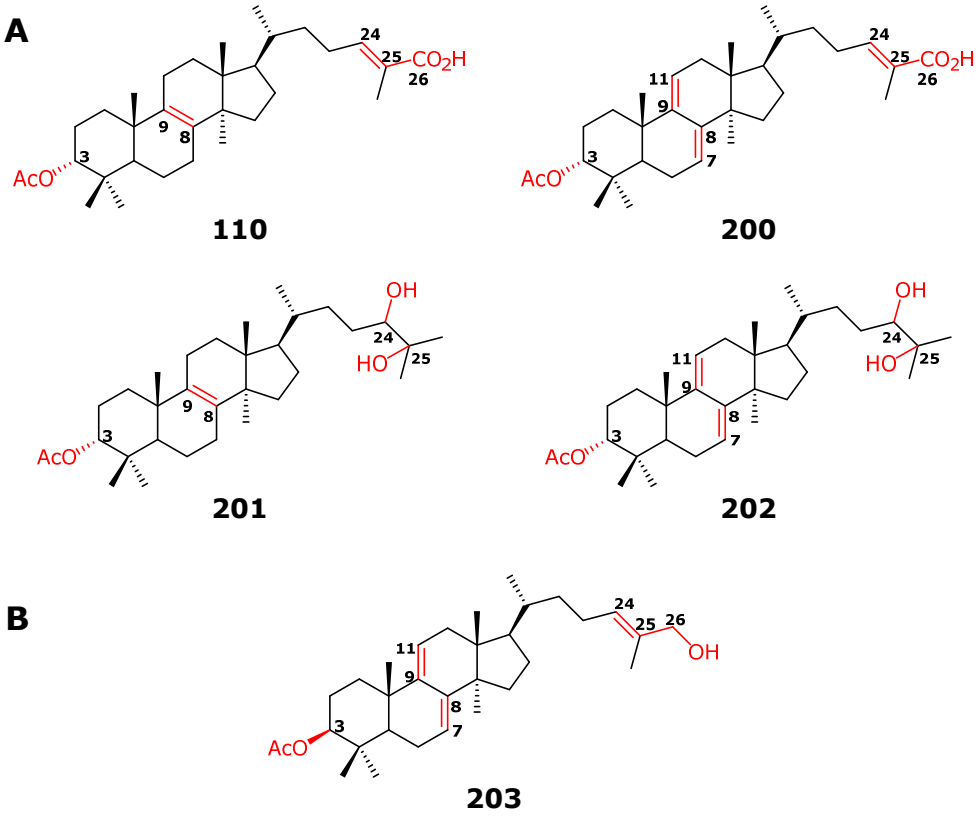


Figure 6.2 Proposed analogues with potentially high inhibitory activity and binding interaction for prostate cancer cell-lines. **A** Best candidates for refractory cell-lines. **B** Best candidate for hormone sensitive cell-lines.

In conclusion, GA and their analogues inhibited in a time- and dose-dependent manner several prostate cancer cell-lines. However, the biological activity observed was cell-line dependent and inferior to that of the activity of Taxotere®. The inhibitory activity decreased from the normal to the more aggressive cell-lines. However, some of the GA and analogues were less toxic to the normal cell-line than to the pre-malignant ones: GA-H (**24**) together with analogues **108** and **146**. The study of the effect that the different functional groups have on the activity, allowed us to rank them according to their strength and to design different analogues that could be more active for each of the cell-line type.

6.1.3. SAR Analysis

Studies with triterpenes and their analogues to determine their activity in 5α-reductase,[21,135] androgen receptor[134] as well as in prostate cell-lines[33,34] allowed us to build a structure activity relationship analysis (Figure 6.3). Most of the positions in the triterpenes frame were investigated. However, as the data were obtained from different sources, some discrepancies were detected.

Functionalities 3-ketone and $\Delta^{24,25}$ α,β-unsaturated 26-carboxylic acid were important for the activity of 5α-reductase. However, more variations in the functional groups could be tolerated on rings B, C, D and in position C-27 without modifying substantially the inhibition. Certainly, that was not the case for all the functionalities. Hence, the effect of C-11 ketone, 7α-hydroxyl, 20-hydroxyl and *E*-$\Delta^{20,22}$ was negative for the inhibition of the enzyme activity, while a C-27 methyl or hydroxyl produced the same effect on its inhibition when a $\Delta^{24,25}$ allylic 26-hydroxyl was present on the side chain.

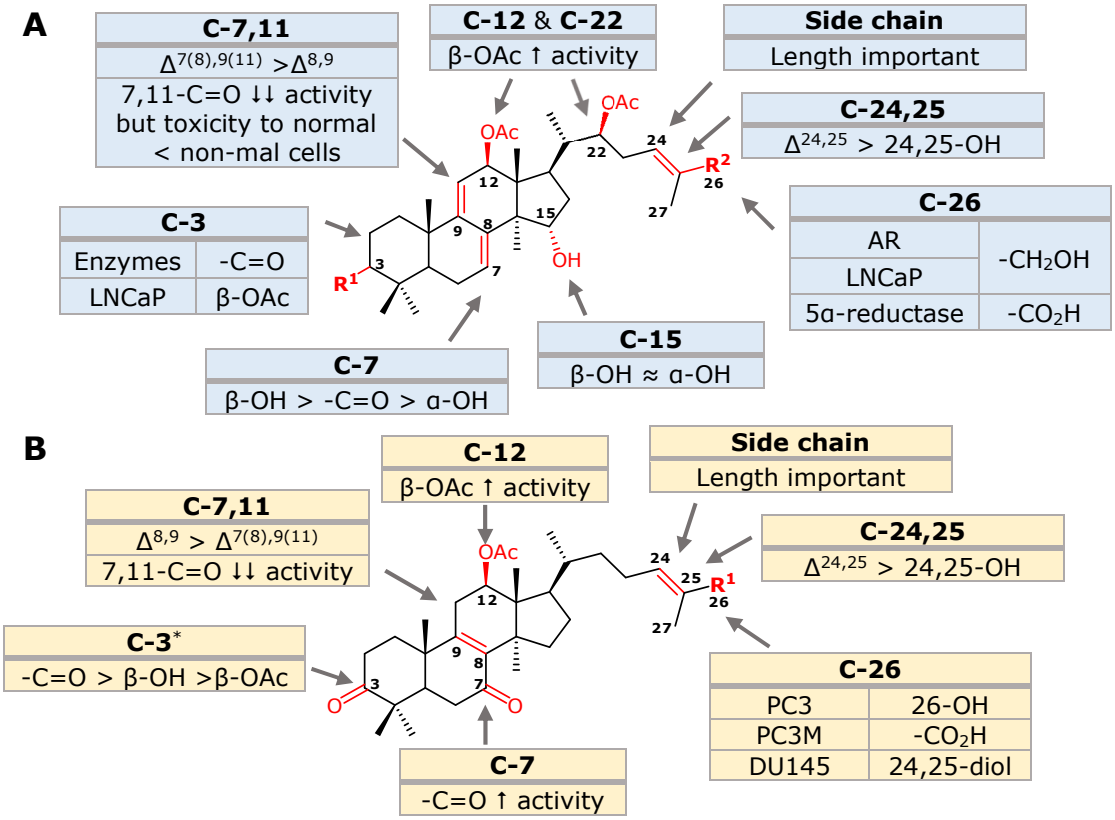


Figure 6.3 SAR analysis of GA and their analogues. **A** 5α-Reductase, androgen receptor, prostate cell-lines RWPE1, WPE1-NB14, -NB26 and LNCaP; **B** prostate cancer cell-lines PC3, PC3M-luc2 and DU145. Non-mal = non-malignant. * Liu[33] and Min[34] reported the activity of 3-ketone > 3β-OH, ours results suggested a reverse order of activity.

Studies on the androgen receptor activity were performed only with ganoderma alcohols,[134] concluding that positons C-3 ketone, $\Delta^{24,25}$ allylic 26-hyhdroxyl and a reduced number of hydroxyls on the side chain were required for enhancing the inhibition of the receptor activity. Contrary to the activity seen with 5α-reductase, modifying the C-27 methyl by a more polar functional group reduced the activity with the androgen receptor.

Although GA and their analogues inhibited the cell viability of both non-malignant and cancerous cell-lines, the inhibition observed differed among them, particularly, the inhibition was always higher for the non-malignant cells and it was reduced with malignancy progression.[35] As a general observation, β-acetate at positions C-12 and C-22 and β-hydroxyl at C-7 increased the inhibition; whereas, allylic 7,11-diketone reduced it considerably. The fact that a different behaviour was encountered for the normal and the two pre-malignant cell-lines when treated with GA or analogues containing the 7,11-diketone functional group, lead us to consider this functionality important for conferring the compounds prophylactic properties.

Although previous studies suggested that having a ketone at C-3 was the most effective functional group for LNCaP,[134] this is the first time that a C-3 β-acetate was included in the evaluation, concluding that this group was a more powerful inhibitor than the ketone. Other functional groups enhancing the inhibition were the conjugated double bond system $\Delta^{7(8),9(11)}$ in rings B/C and the $\Delta^{24,25}$ allylic 26-hydroxyl on the side chain.

The inhibition of the viability was cell-line dependant among the more aggressive cell-lines. Thus, studies on PC3 uncovered that 3-ketone; $\Delta^{8,9}$ allylic 7-ketone and $\Delta^{24,25}$ allylic 26-OH were the best functionalities to enhance the inhibition.[34] However, other authors concluded that the 26-methyl ester was the best functionality on the side chain due to its ability to penetrate the cell membrane.[33] From our results, C-3 β-hydroxyl seemed better than the ketone for the three aggressive cell-lines analysed. The major differences among them were encountered on the side chain, where 24,25-diol performed the best for DU145, $\Delta^{24,25}$ allylic 26-OH did it for PC3 and the $\Delta^{24,25}$ α,β-unsaturated 26-CO_2H was the best for PC3M. It is to note that the side chain length might play a relevant role in the activity. Hence, DU145 and PC3 viability seemed more inhibited by shorter side chains while the longer side chain was preferred for PC3M.

In conclusion, the effect of acetates, hydroxyls, ketones, carboxylic acid, their esters, double bonds and side chain length were evaluated in enzymes, receptors and prostate cell-lines. Although the inhibition was substrate-dependant, it could be generalised that the most relevant positions were at both ends: C-3 and the side chain terminus, all the other areas were much more tolerant to changes in the functionality.

6.1.4. *Ganoderma lucidum* extracts composition

GL at different stages (2-, 4-, 6-, and 8-week old) and grown under different substrates (sawdust, MCF or EFB) or conditions (normal or antler formation) were extracted and the extracts were analysed for determining their composition in triterpenes and their biological activity against prostate cancer cell-lines. As extraction method, Soxhlet extraction and sonication were assessed; while cell viability was evaluated by the MTT assay.

A first estimation of the triterpene composition was made by ESI-MS. Molecular ions m/z 513; 515; 517; 531; 571 and 573 were notoriously the more intense peaks for all the analysed samples. However, little information could be drawn regarding the exact composition, as these molecular ions corresponded to the most abundant isomers, MW 512; 514; 516; 530; 570 and 572.

Next, although LC-MS analysis revealed up to 23 peaks, most of them were co-eluted products. Nevertheless, a comparison of the profiles for each sample revealed that the triterpene composition varies over time as some of the peak areas increased or decreased with age. However, modifying the growing substrate from sawdust to MCF or EFB did not changed considerably the profiles, whereas, prominent variations were encountered for the normal and antler mushroom type, concluding that for the antler variety the production of more polar triterpenes were favoured. Interestingly, apart from the alcohols, the most powerful solvent for performing the extractions was ethyl acetate. Enhanced extraction of both polar and apolar triterpenes was achieved in this solvent. Peaks were tentatively assigned taking into account their fragmentation and the assignment performed in other groups,[141-143] even though the lack of standards and co-elution made it difficult to make accurate assignments.

GL extracts were able to inhibit the cell viability of prostate cancer cell-lines. When comparing the inhibition by stage, it was observed that it increased

with the age of the fungus. Equally, a difference in the inhibition was found between the stalk and the tip of the mushroom, with the stalk being more active than the tip. Among the cell-lines, a different behaviour was encountered for the more aggressive and the hormone sensitive cell-lines. Despite all of them showing the same trend from 4- to 8-weeks, a difference was detected at 2-weeks. Thus, for the LNCaP, the 2-week old sample was almost as good as the 8-weeks one. The tip was more active than the stalk in this cell-line.

With regard to the growing substrate, the effect in the inhibition was cell-line dependent. Hence, no difference among sawdust, MCF or EFB was found for LNCaP, whereas very little variation of the inhibition was detected for the more aggressive cell-lines. For DU145, GL extract grown on MCF or EFB had a lower IC_{50} value than the GL extract grown on sawdust, whilst for PC3M, sawdust and MCF substrates produced a better triterpene combination than EFB. Therefore, growing the mushroom in MCF or EFB may be as good and sometimes better than using sawdust as the substrate.

Comparing the activity of the normal and antler type mushroom, it was noticed that the antler type was slightly less active than the normal for all the cell-lines analysed.

The extraction solvent that achieved the best inhibition results were ethanol and ethyl acetate. The actual order of activity could be stated as ethanol > ethyl acetate > dichloromethane > methanol > water. As the total extracts may contain macromolecules and high- and low-polarity small molecules, like dextran, saccharides, nucleosides and triterpenes;[146] the differences in activity observed for the different solvents could be attributed not only to differences in triterpene composition but also to the different composition on these other substances present in the extracts.

In conclusion, a variation in triterpene content was appreciated as the mushroom aged, this difference resulted in increased activity in the oldest sample. Changing the growing substrate seemed to improve the inhibition of prostate cancer cell-lines and ethyl acetate could be considered as a good solvent to performed the extractions.

6.2. Future Work

Some of the precursors require further characterisation, including the methoxy aldehyde **99** or dehomologated aldehyde **105**. Additionally, scale up of the synthesis of analogues with functionalities at C-12, C-22 and C-23 may be required for comparison with the natural GA activity. Moreover, the synthesis of any of the proposed candidates (Figure 6.1 and Figure 6.2) could bring further information about the activity and confirm our hypothesis. For some other analogues, a different synthetic route was proposed. Thus, analogue **110** could be formed by the procedure reported by Dodge with 4-nitrobenzoic acid.[93] Analogously, it could be interesting to attempt the allylic oxidation with either ruthenium trichloride in dichloromethane or sodium hypochlorite and the chlorination reaction with ammonium chloride and Oxone®.[99, 106, 118]

With regard to the biological evaluation, results shown in this thesis suggested that further studies with the non-malignant cell-lines could be needed to identify other combination of functional groups that could differentiate between the normal and pre-malignant cell-lines, and that could be less toxic for the normal cells.

In relation to the mushroom extracts, other extraction methods could be explored that reduce the extraction time, for instance using microwave heating. In order to identify the peaks accurately, a method should be applied that produces better separation of the products in the mixture,[142, 144] in addition, standards should be used to help in the identification of the peaks. These standards could be obtained from the purification of any of the mushroom material. Furthermore, it could be interesting to study the effect of the extracts in the non-malignant cell-lines and to perform a qualitative analysis of the most active compounds over growing time.

7. Experimental

The experimental section has been divided in three subsections: chemical experiments, biological experiments and *Ganoderma lucidum* (GL) extraction.

7.1. Chemical experiments

7.1.1. General methods

(a) Reagents, solvents and apparatus preparation

Chemicals were purchased from Alfa-Aesar, Fisher Scientific and Sigma-Aldrich and were used without further purification unless otherwise indicated. Analytical and HPLC grade solvents were supplied by Fisher Scientific. When required, these were distilled prior to use according to conventional methods.[147] The distillate was collected in a vessel fitted with a dry seal and stored in the dark. Dichloromethane (DCM) and chloroform were dried overnight and distilled from calcium hydride. The distillate was collected over activated 4Å molecular sieves and stored away from bright light. Molecular sieves were activated by keeping them in the oven at 140 °C. Tetrahydrofuran (THF) was dried by passing it through a column packed with aluminium oxide desiccant 3.2 mm spheres. Anhydrous tetrahydrofuran was purchased from Acrōs Organics. All chemistry reactions were performed in clean, dried glassware kept in an oven at 140 °C for over 16 h. Non-trivial compound names and structures were generated by ChemBioDraw Ultra 14.0.

(b) Physical characterisation and spectroscopic techniques

Melting points were determined using a Stuart Melting point apparatus (SMP3) and are reported without correction. Fourier transform infrared (FT-IR) spectra were recorded in chloroform solution or in potassium bromide discs in the range of 4000-500 cm^{-1} on a Bruker Tensor 27 or on a Nicolet 200 FT-IR, respectively as indicated. Potassium bromide discs were made by finely grinding 1:100 mixture of compound:KBr and pressing the resulting powder at 10 atm under vacuum for few minutes. High resolution mass spectra (HRMS) were recorded on a Bruker MicroToF (time of flight) spectrometer using electrospray ionisation (ESI) or a JEOL AccuTOF GCX

time-of-flight mass spectrometer for gas chromatography-electron impact mass spectrometry (GC-EIMS) as indicated. Specific optical rotation ($[\alpha]_D^T$ where T indicates the temperature of the room in °C) was measured with a sodium lamp at 589 nm in a 50 mm cell using an ADP440 polarimeter, concentrations are expressed in g/100 mL. NMR spectra were recorded in the specified deuterated solvent purchased from Sigma-Aldrich, on a Bruker AV400 (^{1}H-NMR at 400 MHz and ^{13}C-NMR at 100 MHz) or AV500 (^{1}H-NMR at 500 MHz and ^{13}C-NMR at 125 MHz) as indicated. Spectra were processed using Topspin 3.0 or MNova 10.0. All spectra are reported as observed with chemical shifts calibrated to the residual proton and carbon resonance of the solvent peak ($CDCl_3$ δ_H 7.26 ppm, δ_C 77.2 ppm; CD_3OD: δ_H 3.31 ppm, δ_C 49.0 ppm; $(CD_3)_2SO$: δ_H 2.50 ppm, δ_C 39.5 ppm;)[148]. Chemical shifts (δ) are given in ppm and coupling constants (*J*) are in hertz (Hz). Multiplicity abbreviations utilised are: s (singlet), d (doublet), dd (doublet of doublets), dddd (doublet of doublet of doublet of doublets), ddt (doublet of doublet of triplets), dtd (doublet of triplet of doublets), t (triplet), tq (triplet of quartets), q (quartet), m (multiplet), bs (broad singlet), bd (broad doublet), bt (broad triplet). 2D NMR (HMQC) was used for assisting in the integration of overlapping peaks. Compounds were numbered following literature numeration; an example is given in Figure 7.1.[149,150]

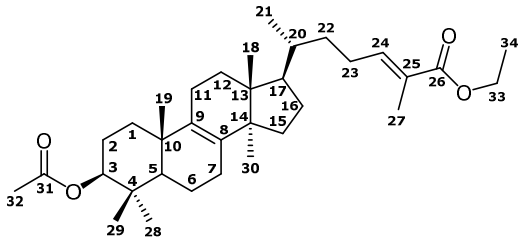


Figure 7.1 General compound numbering.

(c) Chromatographic techniques

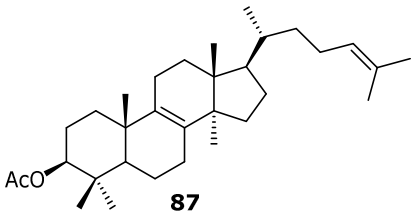
All reactions were monitored by analytical thin layer chromatography (TLC) performed on Merck silica gel 60 F_{254} pre-coated aluminium sheets; they were visualised with both an ultraviolet (UV) lamp (254 nm) and phosphomolybdic acid (PMA). Column chromatography was performed using Sigma-Aldrich silica gel 60Å (40-63 μm).[151]

7.1.2. Synthesis

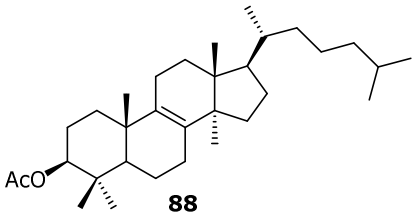
In this section, the synthesis and analytical data of the individual targets is presented. The synthesis was divided into four subsections in line with the discussion chapter. These are: 1) Precursors, 2) Modifications at C-3; 3) Modifications at rings B-C and 4) Modifications at the side chain.

1) <u>Precursors</u>

Lanosterol acetate mixture: [(3*S*,10*S*,13*R*,14*R*,17*R*)-17-[(1*R*)-1,5-dimethylhex-4-enyl]-4,4,10,13,14-pentamethyl-2,3,5,6,7,11,12,15,16,17-decahydro-1*H*-cyclopenta-[α]phenanthren-3-yl] acetate (87) and [(3*S*,10*S*,13*R*,14*R*,17*R*)-17-[(1*R*)-1,5-dimethyl-hexyl]-4,4,10,13,14-pentamethyl-2,3,5,6,7,11,12,15,16, 17-decahydro-1*H*-cyclopenta[α]phenanthren-3-yl] acetate (88)[38]



87



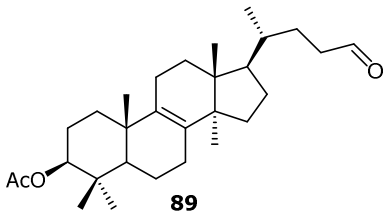
88

Commercial lanosterol (mixture of **7** and **84**, 42 g, 97 mmol, 59% in lanosterol (**7**)), 4-dimethyl-aminopyridine (600 mg, 4.9 mmol) and pyridine (40 mL, 490 mmol) were dissolved in dichloromethame (350 mL), followed by addition of acetic anhydride (16 mL, 168 mmol). The resulting clear solution was stirred at room temperature for 48 h. After work-up, which consisted of dilution of the reaction with dichloromethane (200 mL) and washing sequentially with hydrochloric acid 1M (1 X 200 mL), sodium hydrogen carbonate (aq. sat. sol.) (1 X 200 mL) and water (1 X 200 mL), the organic phase was dried over anhydrous sodium sulfate, filtered and evaporated under reduced pressure. The crude product (a white solid) was purified by column chromatography eluting with Et_2O:PE 1:39. The mixture of lanosterol acetates was furnished as a white powder in excellent yield (42 g, 88 mmol, 91%). The composition of the mixture was estimated to be 59% of **87** by comparing the integration of H-3 and H-24 in the ^{1}H-NMR. The mixture was used directly in the next step without any further purification and the data from that mixture is reported. Dehydrolanosterol acetate **88** was recovered in the following step and reported here separately.

87-**88** R_f 0.31 (mixture) (SiO_2; Et_2O:PE 1:39); mp 116-117 °C; lit.[38] 125-129 °C; ν_{max} (KBr disc)/cm^{-1} 2950 *m* (C-H *str*), 2874 *m* (C-H *str*), 2848 *m* (C-H *str*), 1735 *s* (C=O *str*), 1368 *m* (C-O *str*); ^{1}H NMR (400 MHz, $CDCl_3$) δ 5.10 (dddd, *J* = 8.5, 5.7, 2.8, 1.4 Hz, 0.6H), 4.50 (dd, *J* = 11.5, 4.6 Hz, 1H), 2.05 (s, 3H), 2.09 – 1.94 (m, 4H), 1.96 – 1.81 (m, 1H), 1.68 (d, *J* = 1.7 Hz, 3H), 1.80 – 1.55 (m, 3H), 1.60 (d, *J* = 1.3 Hz, 3H), 1.55 – 1.42 (m, 2H), 1.40 – 1.27 (m, 2H), 1.21 – 1.09 (m, 0.4H), 1.25 (s, 1H), 1.16 (d, *J* = 2.4 Hz, 1H), 1.13 (q, *J* = 3.2 Hz, 1H), 1.00 (s, 3H), 0.91 (d, *J* = 6.4 Hz, 2H), 0.96 – 0.81 (m, 14H), 0.68 (s, 3H); ^{13}C NMR (101 MHz, $CDCl_3$) δ 171.1 (C=O), 134.6 (C=C), 134.4 (C=C), 131.0 (C=C), 125.4 (CH; C=C), 81.1 (CH), 50.7 (CH), 50.5 (CH), 50.0 (C), 44.63 (C), 44.61 (C), 39.7 (CH_2), 38.0 (C), 37.1 (C), 36.64 (CH), 36.61 (CH_2), 36.5 (CH_2), 36.4 (CH), 35.4 (CH_2), 31.1 (CH_2), 31.0 (CH_2), 29.9 (CH_2), 28.4 (CH_2), 28.2 (CH), 28.1 (CH), 26.6 (CH_2), 25.9 (CH_3), 25.1 (CH_2), 24.4 (CH_3), 24.33 (CH_2), 24.26 (CH_2), 23.0 (CH_3), 22.7 (CH_3), 21.5 (CH_3), 21.2 (CH_2), 19.3 (CH_3), 18.9 (CH_3), 18.8 (CH_3), 18.3 (CH_2), 17.8 (CH_3), 16.7 (CH_3), 15.9 (CH_3); HRMS (ESI) m/z ($M^{\cdot}$+Na)$^+$ 491.3862, $C_{32}H_{52}NaO_2$ requires ($M^{\cdot}$+Na)$^+$ 491.3860; (Δ 0.4 ppm); 493.4017, $C_{32}H_{54}NaO_2$ requires ($M^{\cdot}$+Na)$^+$ 493.4016 (Δ 0.2 ppm).

88 R_f 0.17 (SiO_2; DCM:PE 3:7); mp 119-120°C, lit.[37] mp 119-120 ºC (acetone); $[\alpha]_D^{26}$= +55.8° (*c* = 0.88 in $CHCl_3$), lit.[152] $[\alpha]_D^{20}$= +58.5° (*c* = 1.9 in $CHCl_3$); ν_{max} ($CHCl_3$ solution)/cm^{-1} 2920 *w* (C-H *str*). 2890 *w* (C-H *str*), 1711 vs (C=O *str*), 1418 *m* (C-H *def*), 1363 *m* (C-O *str*), 1091 *w* (C-O *str*); ^{1}H NMR (500 MHz, $CDCl_3$) δ 4.50 (dd, *J* = 11.7, 4.5 Hz, 1H), 2.09 – 1.96 (m, 7H), 1.91 (dtd, *J* = 13.5, 9.3, 7.4 Hz, 1H), 1.78 – 1.41 (m, 10H), 1.41 – 1.21 (m, 3H), 1.25 (s, 2H), 1.20 – 1.07 (m, 6H), 1.00 (s, 3H), 0.92 – 0.80 (m, 18H), 0.68 (s, 3H); ^{13}C NMR (125 MHz, $CDCl_3$) δ 171.2 (C=O), 134.6 (C=C), 134.3 (C=C), 81.1 (CH), 50.6 (CH), 49.9 (C), 44.6 (C), 39.7 (CH_2), 37.9 (C), 37.0 (C), 36.63 (CH), 36.59 (CH_2), 35.4 (CH_2), 31.1 (CH_2), 31.0 (CH_2), 29.9 (CH_2), 28.4 (CH_2), 28.2 (CH), 28.1 (CH_3), 26.5 (CH_2), 24.4 (CH_3), 24.31 (CH_2), 24.26 (CH_2), 23.0 (CH_3), 22.7 (CH_3), 21.5 (CH_3), 21.1 (CH_2), 19.3 (CH_3), 18.9 (CH_3), 18.3 (CH_2), 16.7 (CH_3), 15.9 (CH_3); HRMS (ESI) m/z ($M^{\cdot}$+Na)$^+$ 493.4016, $C_{32}H_{54}NaO_2$ requires ($M^{\cdot}$+Na)$^+$ 493.4016 (Δ 0.0 ppm).

[(3*S*,10*S*,13*R*,14*R*,17*R*)-4,4,10,13,14-pentamethyl-17-[(1*R*)-1-methyl-4-oxo-butyl]-2,3,5,6,7,11,12,15,16,17-decahydro-1*H*-cyclopenta[α]-phenanthren-3-yl] acetate (89)



89

Method 1: From diol **91**[51]

A solution of periodic acid (3.2 g, 14 mmol) in tetrahydfrofuran (60 mL) was cooled to 0–5 °C. Diol **5** (5.9 g, 12 mmol) was dissolved in tetrahydrofuran (40 mL) and dichloromethane (25 mL) was added dropwise to the cooled periodic acid solution. The reaction was stirred at 0-5 °C and monitored by TLC (SiO_2; EtOAc:PE 1:9 and 1:4). A white precipitate was formed. After completion, the solvent was evaporated and the crude product was redissolved in ethyl acetate (50 mL) and washed sequentially with water (2 X 50 mL), sodium hydrogen carbonate (sat. aq. sol.) (2 X 50 mL) and brine (1 X 50 mL). The organic phase was then dried over anhydrous sodium sulfate, filtered and evaporated at reduced pressure to give a white powder. The crude product was purified by column chromatography eluting using a solvent gradient of EtOAc:PE 1:9 to 1:1. The title compound, aldehyde **89** (4.6 g, 10 mmol, 88%) was generated as a white powder in excellent yield. Aldehyde **89** was further purified by crystallisation from hexane, yield 61%.

Method 2: One pot oxidation[49]

The mixture of lanosterol acetates **87** and **88** (108 mg, 140 µmol, 62% in **87**) was suspended in a mixture of acetone:water 10:1 (1.25 mL acetone), tetrahydrofuran (1 mL) was added followed by 2,6-lutidine (33 µL; 280 µmol), 4-methylmorpholine *N*-oxide (27 mg, 230 µmol) and osmium tetraoxide 2.5 wt% solution (40 µL, 3.2 µmol). A brown solution was formed. The reaction went to completion after 1 hour of stirring at room temperature. (Diacetoxyiodo)benzene (69 mg, 0.21 mmol) was added. The colour of the solution changed to yellow after three min. Reaction completion was determined to be 1.5 h by TLC (EtOAc:PE 2:3) and MS. The reaction was quenched by the addition of a sodium thiosulfate solution (10 mL). After partitioning the phases, aqueous was extracted with ethyl acetate (3 X 10

mL). The combined organic layers were washed with saturated solution of copper sulfate, dried over sodium sulfate, filtered and evaporated. A dark solid was obtained. Purification by column chromatography eluting with Et_2O:PE 3:17 yielded the title aldehyde **89** (37 mg, 80 μmol, 59%) and dehydrolanosterol acetate **88** (44 mg, 90 μmol).

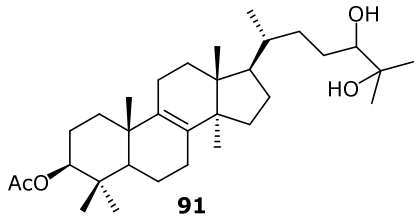
Method 3: Reduction of α-hydroxy ketone **92**.[53]

α-Hydroxy ketone **92** (1.7 g, 3.4 mmol) was dissolved in methanol (10 mL) and cooled to 0 ºC. Sodium borohydride (46 mg, 1.2 mmol) was added in one portion and the reaction was stirred at 0 ºC. A suspension was formed that faded after 6 h reaction, the stirring continued for 18 h. Further addition of sodium borohydride (42 mg, 1.1 mmol) after that time at 0 ºC generated a suspension that cleared after 5 min, but that precipitated thereafter. Monitoring the reaction by TLC (SiO_2 EtOAc:PE 1:4) after 1 h of this extra addition showed the reaction had gone to completion. The solvent was evaporated and the crude product was re-dissolved in tetrahydrofuran (6 mL) and added dropwise over 5 min period to a cooled solution of periodic acid (1.4 g, 6.0 mmol) in tetrahydrofuran (22 mL). A white precipitate started to form almost immediately during substrate addition. The reaction arrived to completion after 1.5 h. The solvent was evaporated and the crude product was re-dissolved in ethyl acetate and water (30 mL each). After phase separation, aqueous layer was extracted with ethyl acetate (3 X 25 mL) and the combined organic phases were washed with sodium hydrogen carbonate (sat. aq. sol.) (2 X 25 mL) and brine (1 X 25 mL), dried over sodium sulfate anhydrous, filtered and evaporated. The crude product was purified by column chromatography eluting Et_2O:PE from 3:37 to 1:3 and changing then to EtOAc:PE 1:19 to 1:1 and finally to 100% ethyl acetate. Aldehyde **89** (939 mg, 2.1 mmol) was isolated with moderate yield (62.0%).

89 R_f = 0.33 (SiO_2; EtOAc : PE 1:9); mp 145-147 ºC, lit.[153] mp 144-147 ºC (acetone); $[\alpha]_D^{26}$= +61.0 (*c* = 0.60 in $CHCl_3$), lit.[153] $[\alpha]_D^{25}$= +58.5° (*c* = 2.4 in $CHCl_3$); ν_{max} ($CHCl_3$ solution)/cm^{-1} 2953 *s* (C-H *str*), 2878 *m* (C-H *str*), 2835 *m* (C-H *str*), 2726 w (CHO), 1721 s (C=O *str*), 1653 *w* (C=C *non-conj*), 1507 m, 1468 *m* (C-H *def)*, 1456 *m* (C-H *def*), 1394 *m* (O-H *bend*), 1373 *m* (CH_3 *sym def*), 1257 *s* (O-H *bend*), 1058 *m* (C-O *str*); ^{1}H NMR (400 MHz, $CDCl_3$) δ 9.76 (t, *J* = 1.9 Hz, 1H), 4.49 (dd, *J* = 11.6, 4.5 Hz, 1H), 2.46 (dddd, *J* = 16.8, 9.7, 5.4, 1.8 Hz, 1H), 2.35 (dddd, *J* = 16.9, 8.9, 6.4, 2.1

Hz, 1H), 2.04 (s, 3H), 2.09 – 1.99 (m, 2H), 2.00 (d, *J* = 18.6 Hz, 2H), 1.98 – 1.87 (m, 1H), 1.81 (dddd, *J* = 13.3, 9.1, 6.3, 2.3 Hz, 1H), 1.76 – 1.55 (m, 6H), 1.54 – 1.39 (m, 3H), 1.38 – 1.23 (m, 3H), 1.26 – 1.16 (m, 2H), 1.14 (dd, *J* = 12.6, 2.3 Hz, 1H), 0.99 (s, 3H), 0.90 (d, *J* = 6.1 Hz, 3H), 0.88 – 0.85 (m, 9H), 0.68 (s, 3H); ^{1}H-NMR lit.[39]; ^{13}C NMR (100 MHz, $CDCl_3$) δ 203.4 (CHO), 171.2 (C=O), 134.5 (C=C), 134.4 (C=C), 81.1 (CH), 50.6 (CH), 50.4 (CH), 49.9 (C), 44.7 (C), 41.3 (CH_2), 37.9 (CH), 37.0 (C), 36.2 (CH), 35.4 (CH_2), 31.1 (CH_2), 30.9 (CH_2), 28.4 (CH_2), 28.3 (CH_2), 28.0 (CH_3), 26.5 (CH_2), 24.4 (CH_2), 24.3 (CH_3), 21.5 (CH_3), 21.1 (CH_2), 19.3 (CH_3), 18.5 (CH_3), 18.2(CH_2), 16.7 (CH_3), 15.9 (CH_3); HRMS (ESI) m/z ($M^{\cdot}$+Na)$^+$ 465.3334, $C_{29}H_{46}NaO_3$ requires ($M^{\cdot}$+Na)$^+$ 465.3339 (Δ 1.0 ppm).

[(3*S*,10*S*,13*R*,14*R*,17*R*)-17-[(1*R*)-4,5-dihydroxy-1,5-dimethyl-hexyl]-4,4,10,13,14-pentamethyl-2,3,5,6,7,11,12, 15,16,17-deca-hydro-1*H*-cyclopenta[a]phenanthren-3-yl] acetate (91)[37,38]



91

Method 1: From lanosterol acetate mixture **87**-**88**.[37]

Lanosterol acetate mixture **87**-**88** (7.7 g, 7.6 mmol in 1, 46%) was dissolved in acetone (390 mL), water (9 mL) and hypophosphorus acid (1.6 mL; 15.44 mmol). *N*-Bromosuccinimide (1.7 g; 9.4 mmol) was added, which resulted in a change of the solution colour from clear to yellow; however, this colour faded after 3 min. The solution was then stirred at room temperature for a further 30 min before the addition of sodium hydrogen carbonate (1.3 g, 15.1 mmol) and evaporation of the solvent at reduced pressure.

The crude product (slurry) was suspended in 2-propanol (195 mL), water (60 mL) and hypophosphorus acid (50 wt% aq. sol.) (4.3 mL, 42 mmol) were added. The resulting suspension was heated at 98 ºC. After 10 min., all of the solid had dissolved and more sodium hydrogen carbonate (2.7 g, 32 mmol) was added. Heating was resumed at 98 ºC for 3 h after which the reaction reached completion. Cooling of the reaction caused solidification of the solution. Therefore, it was diluted with water (200 mL), ethyl acetate (400 mL) and dichloromethane (100 mL). After separation of the phases.

The aqueous layer was extracted with ethyl acetate (2 X 200 mL), the combined organic phases were then washed with water (1 X 100 mL), sodium hydrogen carbonate (aq. sat. sol.; 1 X 100 mL) and brine (1 X 100 mL). The organic layer was then dried over sodium sulfate anhydrous, filtered and evaporated. The residue was purified by column chromatography eluting using a solvent gradient of EtOAc:PE 1:3 to 100% ethyl acetate. This yielded the title diol **91** (2.3 g, 4.6 mmol, 61%) as a mixture of epimers in ratio 1:1.2.

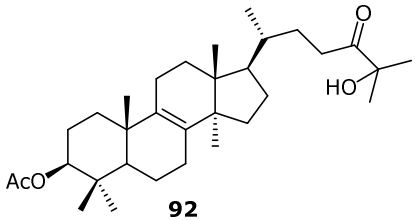
Method 2: From bromo-hydroxy acetate **93**.[38]

Bromohydroxylanosterol acetate (**93**) (13 g, 23 mmol) was suspended in a mixture of isopropanol : water 3:1 (800 mL), hypophosphorus acid (50 wt% aq. sol.) (13 mL, 125 mmol) and sodium hydrogencarbonate (8.4 g, 100 mmol) were added sequentially over 10 min, effervescence was observed. The resulting suspension, which dissolved after 1h, was stirred at reflux for 12 hours. The reaction was cooled to room temperature and the solvent was evaporated at reduced pressure. The slurry residue was diluted in EtOAc:water 1:1 (600 mL). The aqueous phase was then extracted with ethyl acetate (3 X 200 mL), and the combined organic layers were washed with sodium hydrogen carbonate (sat. aq. sol.) (1 X 200 mL) and brine (1 X 200 mL), dried over anhydrous sodium sulfate, filtered and evaporated at reduced pressure to give a pale yellow solid, which was purified by column chromatography eluting using gradient from EtOAc:PE 1:4 to pure ethyl acetate. Diol **93** was isolated as a white powder (8.1 g, 16 mmol, 70%) as a mixture of epimers *R*:*S* 1:1.2. The reported NMRs correspond to the mixture of these epimers, when known, signals were designated *R*, *S* to differentiate epimer **91*R*** from **91*S*** signal.

91 R_f 0.28 (SiO_2; EtOAc:PE 2:3); mp 173-177 °C; lit.[37] 172-175 °C; ν_{max} (KBr disc)/cm^{-1} 3403 *s br* (-O-H *str*), 2964 *s* (C-H *str*), 2949 *s* (C-H *str*), 2876 *m* (C-H *str*), 2839 *w* (C-H *str*), 1721 *s* (C=O *str*), 1260 *s* (O-H *bend*); ^{1}H NMR (400 MHz, $CDCl_3$) δ 4.49 (dd, *J* = 11.5, 4.5 Hz, 1H), 3.34 (t, *J* = 6.1 Hz, 0.5H), 3.28 (dd, *J* = 9.0, 1.6 Hz, 0.6H), 2.04 (s, 3H), 2.10 – 1.97 (m, 4H), 1.98 – 1.88 (m, 1H), 1.80 – 1.55 (m, 7H), 1.55 – 1.44 (m, 2H), 1.44 – 1.23 (m, 3H), 1.21 (s, 3H), 1.18 (d, *J* = 2.1 Hz, 0.4H), 1.15 (s, 4H), 1.13 (d, *J* = 2.4 Hz, 0.6H), 1.00 (s, 3H), 0.91 (d, J_S = 6.4 Hz, 1.4H), 0.90 (d, J_R = 6.2 Hz, 1.3H), 0.87 (bs, 12H), 0.69 (s, 1.8H), 0.68 (s, 1.9H); ^{1}H-NMR lit.[48]; ^{13}C NMR (101 MHz, $CDCl_3$) δ 171.2 (C=O), 134.6 (C=C), 134.4 (C=C),

81.1 (CH), 79.8 (CH), 78.9 (CH), 50.7 (CH), 50.63 (CH), 50.57 (CH), 49.96 (C), 49.94 (C), 44.6 (C), 37.9 (C), 37.0 (C), 36.9 (CH), 36.4 (CH), 35.4 (CH_2), 33.7 (CH_2), 33.3 (CH_2), 31.1 (CH_2), 30.9 (CH_2), 28.9 (CH_2), 28.6 (CH_2), 28.4 (CH_2), 28.3 (CH_2), 28.1 (CH_3), 26.7 (CH_3), 26.5 (CH_2), 24.4 (CH_3), 24.3 (CH_2), 23.4 (CH_3), 23.3 (CH_3), 21.5 (CH_3), 21.1 (CH_2), 19.3 (CH_3), 19.0 (CH_3), 18.7 (CH_3), 18.3 (CH_2), 16.7 (CH_3), 15.9 (CH_3); HRMS (ESI) m/z ($M^{\cdot}$+Na)$^+$ 525.3916, $C_{32}H_{54}NaO_4$ requires ($M^{\cdot}$+Na)$^+$ 525.3914 (Δ 0.2 ppm).

(3*S*,10*S*,13*R*,14*R*,17*R*)-17-((*R*)-6-hydroxy-6-methyl-5-oxoheptan-2-yl)-4,4,10,13,14-pentamethyl-2,3,4,5,6,7,10,11,12,13,14,15,16,17-tetradecahydro-1H-cyclopenta[a]phenanthren-3-yl acetate (92)[49]



92

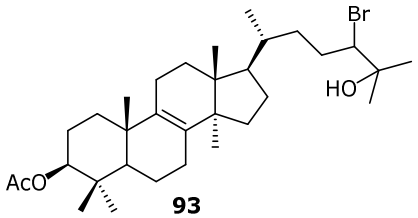
α-Hydroxy ketone **92** was formed as a product of over oxidation during the oxidative cleavage of diol **91** to form aldehyde **89**.

The mixture of lanosterol acetate **87**-**88** (54% pure in **87**) (9.0 g, 10.4 mmol) was suspended in aqueous acetone (93%, 140 mL). Osmium tetraoxide 2.5 wt% in 2-methyl-2-propanol (3.4 mL, 0.271 mmol), 2,6-lutidine (3.5 mL, 29.8 mmol) and 4-methylmorpholine *N*-oxide (2.6 g, 21.6 mmol) were added and the brown suspension was stirred for 30 min at room temperature, monitoring the reaction by TLC (SiO_2, EtOAc:PE 9:11) at that time revealed reaction completion. Diacetoxyiodo benzene (7.1 g, 21.5 mmol) was then added and the stirring continued for 3 h at room temperature. The reaction was quenched with sodium thiosulfate (sat. aq. sol.) (250 mL). After separation of the phases, aqueous phase was extracted with ethyl acetate (3 X 200 mL) and the combined organic layers were washed with copper (II) sulfate (sat. aq. sol.) (2 X 100 mL), filtered and evaporated. The crude product was purified by column chromatography eluting first from Et_2O:PE 1:9 and then using a solvent gradient of EtOAc:PE 3:17 to 1:1. Title compound **92** (3.0 g, 6.0 mmol, 58 %) was isolated as major product of the reaction accompanied by aldehyde **89** (1.6 g,

3.7 mmol, 36%), unreacted diol **91** (1.5 g, 2.3 mmol, 22%) and dehydrolanosterol acetate **88** (4.2 g, 8.9 mmol, 100%).

92 ^{1}H NMR (400 MHz, $CDCl_3$) δ 4.50 (dd, *J* = 11.6, 4.5 Hz, 1H), 2.52 (qdd, *J* = 17.1, 9.5, 5.7 Hz, 2H), 2.05 (s, 3H), 2.22 – 1.86 (m, 6H), 1.86 – 1.55 (m, 6H), 1.55 – 1.44 (m, 1H), 1.39 (s, 3H), 1.38 (s, 3H), 1.46 – 1.31 (m, 2H), 1.35 – 1.21 (m, 2H), 1.21 (dt, *J* = 9.9, 2.2 Hz, 1H), 1.15 (dd, *J* = 12.6, 2.2 Hz, 1H), 1.00 (s, 3H), 1.14 – 0.80 (m, 2H), 0.90 (d, *J* = 6.3 Hz, 3H), 0.88 (s, 9H), 0.69 (s, 3H); ^{1}H-NMR lit.[48]; ^{13}C NMR (101 MHz, $CDCl_3$) δ 215.1 (C=O), 171.1 (C=O), 134.5 (C=C), 134.4 (C=C), 81.1 (CH), 76.3 (C), 50.6 (CH), 50.5 (CH), 50.0 (C), 44.7 (C), 37.9 (C), 37.0 (C), 36.2 (CH), 35.4 (CH_2), 32.7 (CH_2), 31.1 (CH_2), 30.9 (CH_2), 30.3 (CH_2), 28.3 (CH_2), 28.1 (CH_3), 26.70 (CH_3), 26.69 (CH_3), 26.5 (CH_2), 24.4 (CH_3), 24.3 (CH_2), 21.5 (CH_3), 21.1 (CH_2), 19.3 (CH_3), 18.6 (CH_3), 18.2 (CH_2), 16.7 (CH_3), 15.9 (CH_3); HRMS (ESI) m/z ($M^{\cdot}$+Na)$^{+}$ 523.3763, $C_{32}H_{52}NaO_4$ requires ($M^{\cdot}$+Na)$^{+}$ 523.3758 (Δ 1.1 ppm).

[(3*S*,10*S*,13*R*,14*R*,17*R*)-17-[(1*R*)-4-bromo-5-hydroxy-1,5-dimethylhexyl]-4,4,10,13,14-pentamethyl-2,3,5,6,7,11,12,15,16,17-decahydro-1*H*-cyclopenta[a]phenanthren-3-yl] acetate (93)[37,38]



93

The mixture of lanosterol acetates **87** and **88** (17 g, 26 mmol, 59% in **87**) were dissolved in acetone (1.5 L), and hypophosphorous acid (50 wt% aq. sol.) (5.0 mL, 48 mmol) was added followed by *N*-bromosuccinimide (5.6 g, 31 mmol). The reaction was monitored by TLC (SiO_2; dichloromethane) and MS. After 2 minutes the reaction reached completion. The solvent was evaporated and replaced by ethyl acetate (400 mL), washed with sodium thiosulfate (sat. aq. sol.) (6 X 200 mL), dried over anhydrous sodium sulfate, filtered and evaporated under reduced pressure to give a cream powder. The residue was then purified by column chromatography eluting at gradient from DCM:PE 3:7 to DCM:EtOAc 7:3; the first elution separated **88** from the mixture and the second **93**. Title compound **93** (12 g, 21 mmol, 80%) was yielded as a mixture of C-24 epimers in ratio *R*:*S* 1.2:1, which were determined by comparing the integration of H-3 and H-24 in the ^{1}H-NMR.

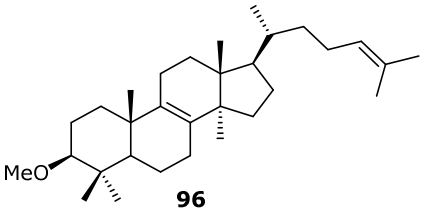
Crystallisation from hexane generated pure epimer **93*S*** as a white solid, while epimer **93*R*** stayed in solution. The maximum purity achieved for **93*R*** was 75% (ratio *R*:*S* 3:1).

This reaction was performed at different scales, from 500 mg to 7.5 g. Mixtures of epimers **93** were achieved in similar yields from 62% to 74%.

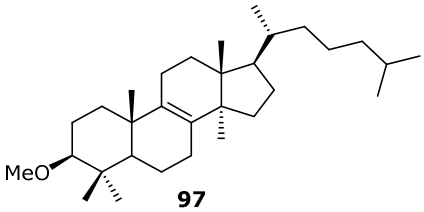
93*R* R_f 0.26 (SiO_2; DCM:PE 4:1); mp 150-153 ºC; lit.[38] 157-159 ºC; ν_{max} (KBr disc)/cm^{-1} 3440 *s*, *br* (-O-H *str*), 2958 *vs* (C-H *str*), 2873 m (C-H *str*), 1721 *vs* (C=O *str*), 1465 *m* (C-H *def*), 1372 s (-CH_3 *sym def*), 1259 *vs* (O-H *bend*), 1031 *m* (C-O *str*), 527 m (C-Br *str*); ^{1}H NMR (500 MHz, $CDCl_3$) δ 4.49 (dd, *J* = 11.7, 4.5 Hz, 1H), 4.01 (dd, *J* = 9.5, 4.0 Hz, 1H), 2.05 (s, 3H), 2.09 – 1.81 (m, 8H), 1.81 – 1.55 (m, 6H), 1.55 – 1.45 (m, 1H), 1.36 (s, 3H), 1.33 (s, 3H), 1.47 – 1.21 (m, 3H), 1.19 (dd, *J* = 12.2, 2.5 Hz, 1H), 1.16 (d, *J* = 2.2 Hz, 1H), 1.13 (d, *J* = 2.2 Hz, 1H), 1.16 – 1.01 (m, 2H), 1.00 (s, 3H), 0.90 (d, *J* = 5.7 Hz, 3H), 0.87 (s, 9H), 0.69 (s, 3H); ^{13}C NMR (126 MHz, $CDCl_3$) δ 171.2 (C=O), 134.5 (C=C), 134.4 (C=C), 81.1 (CH), 72.7 (C), 72.5 (CH), 50.6 (CH), 50.5 (CH), 50.0 (C), 44.6 (C), 37.9 (C), 37.0 (C), 35.7, (CH) 35.4 (CH_2), 35.2 (CH_2), 31.1 (CH_2), 30.9 (CH_2), 30.8 (CH_2), 28.4 (CH_2), 28.0 (CH_3), 26.9 (CH_3), 26.5 (CH_2), 25.8 (CH_3), 24.4 (CH_3), 24.3 (CH_2), 21.5 (CH_3), 21.1 (CH_2), 19.3 (CH_3), 18.5 (CH_3), 18.2 (CH_2), 16.7 (CH_3), 15.9 (CH_3); HRMS (ESI) m/z ($M^{\cdot}$+Na)$^+$ 587.3081, $C_{32}H_{53}BrNaO_3$ requires ($M^{\cdot}$+Na)$^+$ 587.3070 (Δ 1.8 ppm).

93*S* R_f 0.26 (SiO_2; DCM:PE 4:1); mp 168-170 °C, lit.[38] 163-165 °C; ν_{max} (KBr disc)/cm^{-1} 3443 *s*, *br* (-O-H *str*), 2945 *s* (C-H *str*), 2875 *m* (C-H *str*), 2834 *w* (C-H *str*), 1730 *s* (C=O *str*), 1705 *m* (C=O *str*), 776 m (C-Br *str*); ^{1}H NMR (400 MHz, $CDCl_3$) δ 4.50 (dd, *J* = 11.6, 4.5 Hz, 1H), 3.96 (dd, *J* = 11.1, 1.9 Hz, 1H), 2.05 (s, 3H), 2.09 – 1.82 (m, 8H), 1.78 – 1.55 (m, 6H), 1.55 – 1.45 (m, 1H), 1.45 – 1.24 (m, 3H), 1.36 (s, 3H), 1.33 (s, 3H), 1.22 – 1.17 (m, 2H), 1.16 (d, *J* = 2.2 Hz, 1H), 1.13 (d, *J* = 2.2 Hz, 1H),1.06 (ddt, *J* = 16.4, 9.2, 3.7 Hz, 1H), 1.00 (s, 3H), 0.92 (d, *J* = 6.3 Hz, 3H), 0.87 (m, 9H), 0.69 (s, 3H); ^{13}C NMR (101 MHz, $CDCl_3$) δ 171.1 (C=O), 134.6 (C=C), 134.4 (C=C), 81.1 (CH), 73.3 (CH), 72.8 (C), 50.6 (CH), 50.5 (CH), 50.0 (C), 44.6 (C), 38.0 (C), 37.0 (C), 36.7 (CH), 35.8 (CH_2), 35.4 (CH_2), 31.4 (CH_2), 31.1 (CH_2), 30.9 (CH_2), 28.3 (CH_2), 28.1 (CH_3), 26.8 (CH_3), 26.5 (CH_2), 25.9 (CH_3), 24.4 (CH_3), 24.3 (CH_2), 21.5 (CH_3), 21.1 (CH_2), 19.33 (CH_3), 19.25 (CH_3), 18.3 (CH_2), 16.7 (CH_3), 15.9 (CH_3); HRMS (ESI) m/z ($M^{\cdot}$+Na)$^+$ 587.3065, $C_{32}H_{53}BrNaO_3$ requires ($M^{\cdot}$+Na)$^+$ 587.3070 (Δ 0.9 ppm).

(3*S*,10*S*,13*R*,14*R*,17*R*)-3-methoxy-4,4,10,13,14-pentamethyl-17-((*R*)-6-methylhept-5-en-2-yl)-2,3,4,5,6,7,10,11,12,13,14,15,16,17-tetradecahydro-1*H*-cyclopenta[α]phenanthrene (96) and (3*S*,10*S*,13*R*,14*R*,17*R*)-3-methoxy-4,4,10,13,14-pentamethyl-17-((*R*)-6-methylheptan-2-yl)-2,3,4,5,6,7,10,11,12,13,14,15,16,17-tetradecahydro-1*H*-cyclopenta[α]phenanthrene (97)[55,56]



96



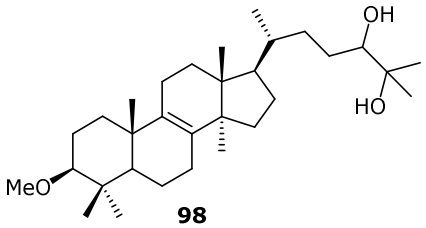
97

Sodium hydride (60% oil dispersion, 2.8 g, 71 mmol) was washed with dry hexane (3 x 10 mL). The hexane washes were removed from the flask with the aid of a syringe. After the third wash, the sodium hydride was dispersed in anhydrous tetrahydrofuran (30 mL).

Commercial lanosterol (mixture of **7** and **84**, 20 g, 47 mmol, 59% in lanosterol (**7**)) was dissolved in tetrahydrofuran (100 mL) and added dropwise to the sodium hydride dispersion over 40 min period. The resulting suspension was stirred for 50 min at room temperature. Methyl iodide (4.5 mL; 71 mmol) was added and the stirred continued at room temperature for 19 h. The suspension became purple after 25 min, however; the colour changed to yellow after 19 h. Completion of the reaction was confirmed by TLC (SiO_2; Et_2O:PE 1:39 and 3:17). The reaction was quenched by the dropwise addition of methanol until cessation of effervescence. The solvent was evaporated and the crude product was redissolved in dichloromethane (400 mL) and water (200 mL). After separating the phases, the aqueous layer was extracted with dichloromethane (1 X 100 mL) and ethyl acetate (2 X 100 mL). The combined organic phases were washed with brine (1 X 100 mL), dried over sodium sulfate anhydrous, filtered and evaporated under reduced pressure. The product crude was purified by column chromatography eluting at gradient from petrol ether to EtOAc:PE 3:97. Lanosterol methoxide **96** was isolated in excellent yield (97%) as a mixture with dihydrolanosterol methoxide **97** in ratio 1.4:1 (**96** and **97**, 20 g; 59% in **96**). The composition of the mixture was determined by comparison of the integration of H-3 and H-24 in ^{1}H-NMR. Reported data refers to the mixture.

96-**97** R_f 0.36 (EtOAc:PE 1:39); mp 116-118 ºC; ν_{max} (KBr disc)/cm^{-1} 2954 *s* (C-H *str*), 2940 *s* (C-H *str*), 2850 *m* (C-H *str*), 2825 *m* (O-CH_3), 1463 *m* (C-H *def*), 1452 *m* (C-H def), 1374 *m* ($C(CH_3)_2$), 1360 *m* (CO-CH_3), 1106 *s* (C-O *str*); ^{1}H NMR (400 MHz, $CDCl_3$) δ 5.11 (tt, *J* = 7.0, 1.4 Hz, 0.6H), 3.37 (s, 3H), 2.68 (dd, *J* = 11.7, 4.2 Hz, 1H), 2.03 (qd, *J* = 8.4, 7.2, 2.8 Hz, 4H), 2.00 – 1.87 (m, 3H), 1.85 (dq, *J* = 13.0, 3.7 Hz, 1H), 1.82 – 1.55 (m, 4H), 1.69 (s, 2H), 1.61 (s, 2H), 1.59 – 1.23 (m, 5H), 1.26 (s, 1H), 1.21 – 1.10 (m, 3H), 1.05 (dd, *J* = 12.6, 2.2 Hz, 1H), 1.10 – 0.98 (m, 1H), 0.99 (s, 6H), 0.92 (d, *J* = 6.3 Hz, 2H), 0.91 – 0.88 (m, 5H), 0.87 (d, *J* = 2.1 Hz, 1H), 0.80 (s, 3H), 0.70 (s, 3H); ^{13}C NMR (101 MHz, $CDCl_3$) δ 134.7 (C=C), 134.5 (C=C), 131.0 (C=C), 125.4 (CH=C), 88.8 (CH), 57.7 (CH_3), 51.1 (CH), 50.7 (CH), 50.6 (CH), 50.0 (C), 44.7 (C), 44.6 (C), 39.7 (CH_2), 39.0 (C), 37.2 (C), 36.6 (CH), 36.5 (CH_2), 36.4 (CH), 35.7 (CH_2), 31.2 (CH_2), 31.0 (CH_2), 29.9 (CH_2), 28.4 (CH_2), 28.2 (CH), 26.7 (CH_2), 25.9(CH_3), 25.1 (CH_2), 24.4 (CH_3), 24.3 (CH_2), 23.0 (CH_3), 22.8 (CH_2), 22.7 (CH_3), 21.2 (CH_2), 19.3 (CH_3), 18.9 (CH_3), 18.8 (CH_3), 18.3 (CH_2), 17.8 (CH_3), 16.3 (CH_3), 15.9 (CH_3); ^{13}C-NMR lit.[57]; HRMS (GC-EIMS) m/z ($M^{\cdot+}$) 440.4041 $C_{31}H_{52}O$ requires 440.4018 (Δ 5.2 ppm), m/z ($M^{\cdot+}$) 442.4181 $C_{31}H_{54}O$ requires 442.4175 (Δ 1.4 ppm).

(6*R*)-6-((3*S*,10*S*,13*R*,14*R*,17*R*)-3-methoxy-4,4,10,13,14-pentamethyl-2,3,4,5,6,7,10,11,12,13,14,15,16,17-tetradecahydro-1*H*-cyclopenta[a]phenanthren-17-yl)-2-methylheptane-2,3-diol (98)[37]



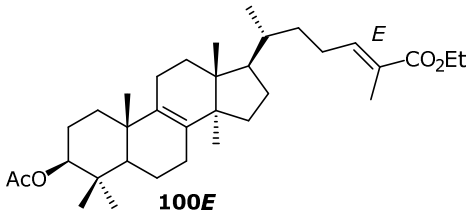
98

A mixture of lanosterol methoxides (**96** and **97**) (15 g; 20 mmol; 59 % in **96**) was suspended in acetone (990 mL), water (22 mL) and hypophosphorus acid 50 wt% aq. sol. (4.0 mL; 38 mmol). *N*-Bromosuccinimide (4.3 g; 24 mmol) was added, an immediate colour change to dark yellow was observed, which faded after 5 min. Sodium hydrogen carbonate (2.7 g; 33 mmol was added and the solvent was evaporated under reduced pressure. The resulting crude product was resuspended in 2-propanol (494 mL), water (152 mL) and hypophosphorus

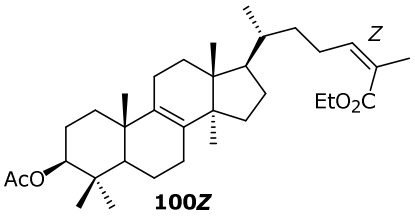
acid (50 wt% aq. sol., 11.0 mL; 106 mmol); more sodium hydrogen carbonate (6.9 g; 83 mmol) was added and the resulting suspension was heated at reflux for 17 h. The heating was stopped and the suspension was allowed to cool to room temperature before work-up. The reaction crude was diluted with ethyl acetate (100 mL) and dichloromethane (200 mL) and it was washed with water (1 X 300 mL); sodium hydrogen carbonate (1 X 200 mL) and brine (1 X 200 mL). Aqueous phase was extracted with ethyl acetate (2 X 200 mL + 3 X 100 mL). The combined organic layers were dried over sodium sulfate anhydrous, filtered and evaporated under reduced pressure. Part of the crude product (6.6 g) was purified by column chromatography eluting using a solvent gradient of EtOAc:PE 1:3 to EtOAc:MeOH 40:1. Title compound methoxydiol **98** (1.1 g; 2.3 mmol) was isolated as a white solid as mixture of epimers in ratio 1:1, which was further purified by precipitation from EtOAc:DCM:hexane 1:2:4. After evaporation of dichloromethane with nitrogen flow, precipitation occurred. Precipitate, a white solid, was filtered and stored. The presented data refers to the mixture of epimers **98*R*** and **98*S***.

98 R_f 0.28 (EtOAc:PE 1:3); mp 154-156 °C; ν_{max} (KBr disc)/cm^{-1} 3417 *s br* (O-H *str*), 2876 *m* (C-H *str*); 1455 *m* (C-H *def*); 1372 *m* (O-H *bend*); 1106 *s* (C-O *str*); ^{1}H NMR (400 MHz, $CDCl_3$) δ 3.36 (s, 3H), 3.33 (t, *J* = 5.7 Hz, 0.5H), 3.28 (bd, *J* = 9.9 Hz, 0.5H), 2.67 (dd, *J* = 11.7, 4.2 Hz, 1H), 2.10 – 1.97 (m, 4H), 1.92 (s, 3H), 1.84 (dd, *J* = 13.2, 3.8 Hz, 1H), 1.81 – 1.52 (m, 6.5H), 1.53 – 1.23 (m, 7H), 1.21 (s, 3H), 1.16 (s, 3H), 1.24 – 1.07 (m, 2H), 1.03 (dd, *J* = 12.6, 2.2 Hz, 1H), 0.98 (s, 6.5H), 0.91 (d, *J* = 6.3 Hz, 1.5H), 0.91 (d, *J* = 6.1 Hz, 1.5H), 0.87 (s, 3H), 0.79 (s, 3H), 0.69 (s, 1.5H), 0.69 (s, 1.5H); ^{13}C NMR (126 MHz, $CDCl_3$) δ 134.7 (C=C), 134.4 (C=C), 88.8 (CH), 79.8 (CH), 78.9 (CH), 73.4 (C), 73.3 (C), 57.7 (CH_3), 51.1 (CH), 50.8 (CH), 50.6 (CH), 49.97 (C), 49.95 (C), 44.67 (C), 44.65 (C), 39.0 (C), 37.2 (C), 36.9 (CH), 36.5 (CH), 35.6 (CH_2), 33.7 (CH_2), 33.3 (CH_2), 31.2 (CH_2), 31.0 (CH_2), 28.9 (CH_2), 28.6 (CH_2), 28.5 (CH_2), 28.3 (CH_2), 28.1 (CH_3), 26.8 (CH_3), 26.7 (CH_3), 26.6 (CH_2), 24.4 (CH_3), 23.4 (CH_3), 23.4 (CH_3), 22.8 (CH_2), 21.2 (CH_2), 19.3 (CH_3), 19.0 (CH_3), 18.7 (CH_3), 18.3 (CH_2), 16.3 (CH_3), 15.9 (CH_3); HRMS (ESI) m/z ($M^{\cdot}$+Na)$^+$ 497.3974, $C_{31}H_{54}NaO_3$ requires ($M^{\cdot}$+Na)$^+$ 497.3965 (Δ 1.8 ppm).

Ethyl (*E*,6*R*)-6-[(3*S*,10*S*,13*R*,14*R*,17*R*)-3-acetoxy-4,4,10, 13,14-pentamethyl-2,3,5,6,7,11,12,15,16,17-decahydro-1*H*-cyclopenta[α]-phenanthren-17-yl]-2-methyl-hept-2-enoate (100*E*) and ethyl (Z,6R)-6-[(3S,10S,13R, 14R,17R)-3-acetoxy-4,4,10,13,14-pentamethyl-2,3,5,6,7,11,12, 15,16,17-decahydro-1H-cyclo-penta[a]-phenanthren-17-yl]-2-methyl-hept-2-enoate (100*Z*)[60]



100*E*



100*Z*

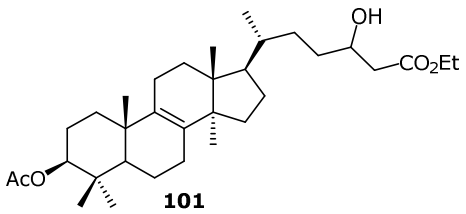
Aldehyde **89** (1.0 g, 2.3 mmol) and (ethoxycarbonylmethyl)triphenylphosphorane (1.2 g, 3.6 mmol) were suspended in tetrahydrofuran (8 mL). This resulted in the formation of a yellow cloudy suspension which was stirred at room temperature for 16 h. The solvent was evaporated at reduced pressure, and the yellow residue was purified by column chromatography eluting with EtOAc:PE 1:19. The title compound **100*E*** (1.18 g, 2.3 mmol, 97%) and its isomer **100*Z*** (45 mg, 0.09 mmol, 3%) where isolated as white solids, in excellent yield for **100*E***.

100*E* R_f = 0.28 (EtOAc : PE 1:19); mp 80-81 ºC; $[\alpha]_D^{26}$= +52.5° (*c* = 0.63 in $CHCl_3$); ν_{max} ($CHCl_3$ solution)/cm^{-1} 3011 *m* (C=CH), 2959 *m* (C-H *str*), 1711 *s* (C=O *str*), 1646 *m* (C=O *α,β-unsat*), 1602 *m* (C=C *str*), 1418 *m* (C-H *def*), 1364 *m* (C-O *str*), 1241 *m* (O-H *bend*), 1145 w (C-O *str*); ^{1}H NMR (400 MHz, $CDCl_3$) δ 6.75 (tq, *J* = 7.3, 1.5 Hz, 1H), 4.49 (dd, *J* = 11.6, 4.5 Hz, 1H), 4.18 (q, *J* = 7.1 Hz, 2H), 2.29 – 2.14 (m, 1H), 2.04 (s, 3H), 2.12 – 1.96 (m, 5H), 1.91 (dddd, *J* = 16.7, 9.4, 6.8, 3.5 Hz, 1H), 1.83 (d, *J* = 1.5 Hz, 3H), 1.79 – 1.57 (m, 7H), 1.60 – 1.42 (m, 3H), 1.49 – 1.34 (m, 1H), 1.37 – 1.22 (m, 2H), 1.29 (t, *J* = 7.1 Hz, 3H), 1.24 – 1.09 (m, 3H), 1.00 (s, 3H), 0.93 (d, *J* = 6.2 Hz, 3H), 0.88 (s, 6H), 0.87 – 0.84 (m, 3H), 0.69 (s, 3H); ^{13}C NMR (101 MHz, $CDCl_3$) δ 171.1 (C=O), 168.5 (C=O), 143.0 (CH=C), 134.6 (C=C), 134.4 (C=C), 127.5 (C=C), 81.1 (CH), 60.5 (CH_2), 50.6 (CH), 50.4 (CH), 50.0 (C), 44.7 (C), 37.9 (C), 37.0 (C), 36.5 (CH), 35.4 (CH_2), 35.1 (CH_2), 31.1 (CH_2), 30.9 (CH_2), 28.3 (CH_2), 28.1 (CH_3), 26.5 (CH_2), 25.8 (CH_2), 24.4 (CH_3), 24.3 (CH_2), 21.5 (CH_3), 21.1 (CH_2), 19.3 (CH_3), 18.7 (CH_3), 18.3 (CH_3), 16.7 (CH_3), 15.9 (CH_3), 14.5 (CH_3), 12.4 (CH_3); HRMS

(ESI) m/z ($M^{\cdot}$+Na)$^+$ 549.3915, $C_{34}H_{54}NaO_4$ requires ($M^{\cdot}$+Na)$^+$ 549.3914 (Δ 0.1 ppm).

100*Z* R_f = 0.31 (EtOAc : PE 1:19); mp 78-79 ºC; $[\alpha]_D^{26}$= +47.5° (*c* = 0.43 in $CHCl_3$); ν_{max} ($CHCl_3$ solution)/cm^{-1} 3011 *m* (C=CH *str*), 2952 *s* (C-H *str*), 2878 *m* (C-H *str*), 1716 *s* (C=O *str*), 1647 *m* (C=O *a,β-unsat*), 1456 *m* (C-H *def*), 1373 *m* (C-H *def*), 1258 *s* (O-H *bend*), 1150 *m* (C-O *str*), 979 *m* (C=CH *oop def*); ^{1}H NMR (400 MHz, $CDCl_3$) δ 5.90 (tq, *J* = 7.3, 1.4 Hz, 1H), 4.49 (dd, *J* = 11.5, 4.5 Hz, 1H), 4.19 (q, *J* = 7.1 Hz, 2H), 2.59 – 2.43 (m, 1H), 2.42 – 2.28 (m, 1H), 2.04 (s, 3H), 2.09 – 1.95 (m, 2H), 2.06 – 1.92 (m, 2H), 1.97 – 1.85 (m, 1H), 1.88 (d, *J* = 1.4 Hz, 3H), 1.78 – 1.58 (m, 7H), 1.60 – 1.41 (m, 3H), 1.50 – 1.34 (m, 1H), 1.30 (t, *J* = 7.1 Hz, 3H), 1.36 – 1.23 (m, 2H), 1.21 – 1.12 (m, 1H), 1.14 (dd, *J* = 12.5, 2.2 Hz, 1H), 1.16 – 1.04 (m, 1H), 1.00 (s, 3H), 0.91 (d, *J* = 6.3 Hz, 3H), 0.88 (s, 6H), 0.86 (d, *J* = 0.9 Hz, 3H), 0.68 (s, 3H); ^{13}C NMR (101 MHz, $CDCl_3$) δ 171.1 (C=O), 168.4 (C=O), 143.6 (CH=C), 134.6 (C=C), 134.4 (C=C), 126.9 (C=C), 81.1 (CH), 60.2 (CH_2), 50.6 (CH), 50.5 (CH), 50.0 (C), 44.7 (C), 37.9 (C), 37.0 (C), 36.6 (CH), 36.1 (CH_2), 35.4 (CH_2), 31.1 (CH_2), 31.0 (CH_2), 28.4 (CH_3), 28.1 (CH_3), 26.8 (CH_2), 26.5 (CH_2), 24.4 (CH_3), 24.3 (CH_2), 21.5 (CH_3), 21.1 (CH_2), 20.9 (CH_3), 19.3 (CH_3), 18.7 (CH_3), 18.3 (CH_2), 16.7 (CH_3), 15.9 (CH_3), 14.5 (CH_3); HRMS (ESI) m/z ($M^{\cdot}$+Na)$^+$ 549.3916, $C_{34}H_{54}NaO_4$ requires ($M^{\cdot}$+Na)$^+$ 549.3914 (Δ 0.3 ppm).

(6*R*)-Ethyl 6-((3*S*,10*S*,13*R*,14*R*,17*R*)-3-acetoxy-4,4,10,13,14-pentamethyl-2,3,4,5,6,7,10,11,12,13,14,15,16,17-tetradecahydro-1*H*-cyclopenta[a]phenanthren-17-yl)-3-hydroxyheptanoate (101)



101

Method 1: Iron (III) chloride/manganese[63]

To a suspension of aldehyde **89** (308 mg; 0.70 mmol), ethyl bromoacetate (154 µL, 13.6 mmol) and iron (III) chloride (362 mg, 2.19 mmol) in tetrahydrofuran (5 mL), magnesium turning (77.8 mg, 3.14 mmol) was added. The final yellow-brown suspension was stirred at room temperature for 18 h, then water (10 mL) and ethyl acetate (10 mL) were added and the

stirring continued for a further 20 min. The suspension was then filtered. To the filtrate hydrochloric acid (1M, aq. sol.) (10 mL) was added. After phase partition, aqueous layer was extracted with ethyl acetate (5 X 10 mL) and combined organic phases were washed with water (1 X 10 mL) and brine (1 X 10 mL), dried over sodium sulfate anhydrous, filtered and evaporated at reduced pressure. The crude product was purified by column chromatography eluting with EtOAc:PE from 1:3 to 2:3. Title β-hydroxyester **101** (203 mg, 0.38 mmol, 55%) was isolated as a white powder in modest yield as mixture with the H-24 epimer (1:1.1) determined by comparing the integration of the hydroxyl group at C-24 in ^{1}H-NMR and the integration of C-25 in ^{13}C-NMR.

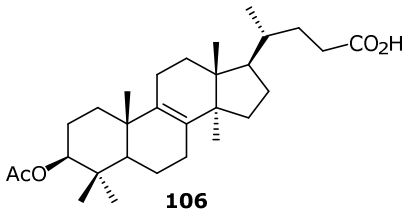
Method 2: Indium[65]

To a suspension of In° (powder, 98 mg; 850 μmol) and aldehyde **89** (333 mg, 750 μmol) in tetrahydrofuran (1.5 mL) was added ethyl bromoacetate (100 μL, 890 μmol). The resulting suspension was stirred at 60 °C for 3.5 h and then cooled to room temperature. The reaction was quenched with hydrochloric acid (1 M aq. sol., 5 mL) and extracted with ethyl acetate (6 X 5 mL). The combined organic layers were washed with brine (1 X 10 mL), dried over sodium sulfate anhydrous, filtered and concentrated under reduced pressure. The crude product was purified by column chromatography eluting with EtOAc:PE 3:17. The hydroxy-acetoester **101** (181 mg, 340 μmol, 45%) was obtained in moderate yield as a mixture of H-24 epimers 1:1.3, determined by integration of the methylene group at C-25 in ^{1}H-NMR. Notation a, b on the ^{13}C-NMR refers to difference in signal frequency for the *R*, *S* epimers, a for the most abundant isomer and b for the minor.

101 R_f 0.35 (EtOAc : PE 1:3); mp 100-102 °C; $[\alpha]_D^{31}$ = +49.6 (*c* = 0.490, $CHCl_3$); ν_{max} ($CHCl_3$ solution)/cm^{-1} 3649 *m* (O-H *str*), 3607 *m* (H-bonded –OH), 2951 *s* (C-H *str*), 2877 *s* (C-H *str*), 2840 *m* (C-H *str*), 1729 *vs* (C=O *str,* ester), 1602 *m* (-CO_2^- *antisym str*), 1467 *m* (C-H *def*), 1456 *m* (C-H *def*), 1394 *m* (-$C(CH_3)_2$ *symm def*), 1373 *s* (-CH_3 *symm def*), 1258 *s* (O-H *bend*), 1027 *m* (C-O *str*); ^{1}H NMR (400 MHz, $CDCl_3$) δ 4.50 (dd, *J* = 11.5, 4.5 Hz, 1H), 4.17 (q, *J* = 7.1 Hz, 2H), 4.05 – 3.87 (m, 1H), 2.95 (d, *J* = 4.0 Hz, 0.52H), 2.89 (d, *J* = 3.9 Hz, 0.48H), 2.53 (dd, *J* = 9.4, 3.1 Hz, 0.48H), 2.49 (dd, *J* = 9.4, 3.1 Hz, 0.52H), 2.41 (t, *J* = 9.2 Hz, 0.52H), 2.37 (t, *J* = 9.2 Hz, 0.48H), 2.04 (s, 3H), 2.10 – 1.94 (m, 4H), 2.00 – 1.84 (m, 1H),

1.81 – 1.33 (m, 12H), 1.38 – 1.21 (m, 2H), 1.27 (t, *J* = 7.1 Hz, 3H), 1.23 – 1.10 (m, 3H), 1.09 – 0.93 (m, 1H), 1.00 (s, 3H), 0.93 – 0.83 (m, 12H), 0.68 (s, 3H); ^{13}C NMR (100 MHz, $CDCl_3$) δ 173.3 (C=O), 171.2 (C=O), 134.6 (C=C), 134.4 (C=C), 81.1 (CH), 68.9 (CH)^a, 68.5 (CH)^b, 60.8 (CH_2), 50.6 (CH), 50.4 (CH)^a, 50.4 (CH)^b, 50.0 (C), 44.6 (C), 41.6 (CH_2)^b, 41.3 (CH_2)^a, 38.0 (C), 37.0 (C), 36.6 (CH)^b, 36.3 (CH)^a, 35.4 (CH_2), 33.4 (CH_2)^a, 33.3 (CH_2)^b, 32.1 (CH_2)^a, 31.9 (CH_2)^b, 31.1 (CH_2), 30.9 (CH_2), 28.3 (CH_2), 28.1 (CH_3), 26.5 (CH_2), 24.4 (CH_3), 24.3 (CH_2), 21.5 (CH_3), 21.1 (CH_2), 19.3 (CH_3), 18.8 (CH_3), 18.3 (CH_2), 16.7 (CH_3), 15.9 (CH_3), 14.3 (CH_3); HRMS (ESI) m/z ($M^{\cdot}$+Na)$^+$ 553.3857, $C_{33}H_{54}NaO_5$ requires ($M^{\cdot}$+Na)$^+$ 553.3863 (Δ 1.1 ppm).

(4*R*)-4-((3*S*,10*S*,13*R*,14*R*,17*R*)-3-acetoxy-4,4,10,13,14-pentamethyl-2,3,4,5,6,7,10,11,12,13,14,15,16,17-tetradecahydro-1*H*-cyclopenta[α]phenanthren-17-yl)pentanoic acid (106)[75]



106

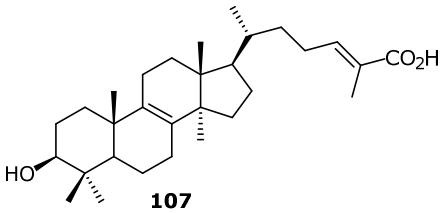
Aldehyde **89** (206 mg, 470 µmol) was suspended in dimethylformamide (5 mL). Oxone® (286 mg, 470 µmol) was added in one portion to the suspension. The reaction was stirred at room temperature and monitored by TLC (EtOAc:PE 1:3), after 3 h the reaction reached completion giving a grey suspension. The reaction was diluted with hydrochloric acid (1M aq. sol.) and ethyl acetate (10 mL each). After separation of the phases, the aqueous layer was extracted with ethyl acetate (2 X 10 mL). The combined organic phases were washed with hydrochloric acid (1M aq. sol., 3 X 10 mL) followed by brine (1 X 10 mL); they were dried over sodium sulfate anhydrous, filtered and evaporated resulting in a yellow crude. This yellow crude was purified by column chromatography eluting at gradient EtOAc:PE from 1:3 to 7:13. The title compound **106** (167 mg, 0.36 mmol, 78%) was obtained in excellent yield as a white powder.

106 R_f 0.09 (EtOAc:PE 1:3); mp 206-208 °C; lit.[154] mp 199-205 ºC; ^{1}H NMR (400 MHz, $CDCl_3$) δ 4.50 (dd, *J* = 11.5, 4.5 Hz, 1H), 2.41 (ddd, *J* = 15.5, 10.1, 5.2 Hz, 1H), 2.27 (ddd, *J* = 15.9, 9.6, 6.5 Hz, 1H), 2.05 (s, 3H), 2.08 – 1.95 (m, 4H), 2.00 – 1.87 (m, 1H), 1.88 – 1.76 (m, 1H), 1.78 – 1.53

(m, 7H), 1.57 – 1.38 (m, 3H), 1.40 – 1.23 (m, 3H), 1.23 – 1.17 (m, 1H), 1.14 (dd, *J* = 12.5, 2.2 Hz, 1H), 1.00 (s, 3H), 0.91 (d, *J* = 5.9 Hz, 3H), 0.88 (s, 6H), 0.87 (s, 3H), 0.69 (s, 3H); ^{1}H-NMR lit.[155]; ^{13}C NMR (101 MHz, $CDCl_3$) δ 180.2 (C=O), 171.2 (C=O), 134.5 (C=C), 134.4 (C=C), 81.1 (CH), 50.6 (CH), 50.4 (CH), 50.0 (C), 44.7 (C), 38.0 (C), 37.0 (C), 36.2 (CH), 35.4 (CH_2), 31.3 (CH_2), 31.2 (CH_2), 31.1 (CH_2), 30.9 (CH_2), 28.2 (CH_2), 28.1 (CH_3), 26.5 (CH_2), 24.4 (CH_3), 24.3 (CH_2), 21.5 (CH_3), 21.1 (CH_2), 19.3 (CH_3), 18.4 (CH_3), 18.3 (CH_2), 16.7 (CH_3), 15.9 (CH_3); ^{13}C-NMR lit.[155]; HRMS (ESI) m/z ($M^{\cdot}$-Na)$^+$ 481.3288, $C_{29}H_{46}NaO_4$ requires ($M^{\cdot}$+Na)$^+$ 481.3288 (Δ 0.0 ppm).

2) <u>Modifications at C-3</u>

(6*R*,*E*)-6-((3*S*,10*S*,13*R*,14*R*,17*R*)-3-hydroxy-4,4,10,13,14-pentamethyl-2,3,4,5,6,7,10,11,12,13,14,15,16,17-tetradecahydro-1*H*-cyclopenta[α]phenanthren-17-yl)-2-methylhept-2-enoic acid (107)[60]



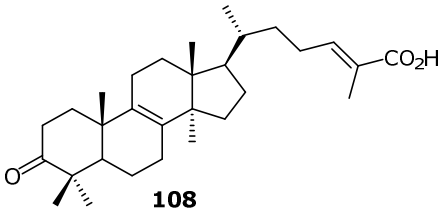
107

Acetoester **100*E*** (213 mg, 0.40 mmol) was suspended in a mixture of THF : MeOH : water 2:1:1 (8 mL). Lithium hydroxide (106 mg; 2.52 mmol) was added and the resulting suspension was stirred at room temperature for 16 h. The reaction was diluted with ethyl acetate and hydrochloric acid (1 M, aq. sol.) (5 mL each). After phase separation, the aqueous phase was extracted with ethyl acetate (3 X 5 mL) and the combined organic layers were washed sequentially with sodium hydrogen carbonate (sat. aq. sol.) (1 X 10 mL) and brine (1 X 10 mL), dried over sodium sulfate anhydrous, filtered and evaporated at reduced pressure. The resulting white crude was purified by column chromatography eluting in EtOAc:PE 7:13. Analogue **107** was furnished as white solid in excellent yield (171 mg; 0.38 mmol; 93%). It was further purified by precipitation from hexane/dichloromethane solution after evaporation of the dichloromethane by nitrogen flow.

107: R_f 0.35 (EtOAc:PE 19:21); mp 157-158 °C; $[\alpha]_D^{26}$ = +60.1 (*c* = 0.69, $CHCl_3$); ν_{max} ($CHCl_3$ solution)/cm^{-1} 3625 *m* (O-H *str*), 3629 *m* (H-*bonded*

OH), 2949 *vs* (-CO_2H O-H *str*), 2876 *s* (C-H *str*), 2840, *m* (C-H *str*), 1723 *vs* (C=O sat. ester *str*), 1686 *s* (C=O CO_2H α,β-unsat), 1644 *m* (C=C α,β-unsat), 1467 *s* (C-H *def*), 1455 *m* (C-H *def*), 1373 s ($C(CH_3)_2$), 1249 *s* (O-H *bend*), 1047 *m* (C-O *str*); ^{1}H NMR (400 MHz, $CDCl_3$) δ 6.90 (td, *J* = 7.5, 1.7 Hz, 1H), 3.24 (dd, *J* = 11.6, 4.5 Hz, 1H), 2.32 – 2.18 (m, 1H), 2.11 (p, *J* = 8.6, 8.1 Hz, 1H), 2.07 – 1.96 (m, 4H), 1.95 – 1.86 (m, 1H), 1.84 (d, *J* = 1.4 Hz, 3H), 1.79 – 1.37 (m, 11H), 1.37 – 1.09 (m, 4H), 1.05 (dd, *J* = 12.6, 2.2 Hz, 1H), 1.00 (s, 3H), 0.98 (s, 3H), 0.93 (d, *J* = 6.1 Hz, 3H), 0.88 (s, 3H), 0.81 (s, 3H), 0.69 (s, 3H); ^{13}C NMR (101 MHz, $CDCl_3$) δ 172.5 (C=O), 145.9 (CH=C), 134.6 (C=C), 134.5 (C=C), 126.6 (C=C), 79.2 (CH), 50.6 (CH), 50.5 (CH), 50.0 (C), 44.7 (C), 39.0 (C), 37.2 (C), 36.5 (CH), 35.7 (CH_2), 35.0 (CH_2), 31.1 (CH_2), 31.0 (CH_2), 28.4 (CH_2), 28.1 (CH_3), 28.0 (CH_2), 26.7 (CH_2), 26.1 (CH_2), 24.4 (CH_3), 21.2 (CH_2), 19.3 (CH_3), 18.7 (CH_3), 18.4 (CH_2), 15.9 (CH_3), 15.6 (CH_3), 12.2 (CH_3); HRMS (ESI) m/z ($M^{\cdot}$-H)$^-$ 455.3544, $C_{30}H_{47}O_3$ requires ($M^{\cdot}$-H)$^-$ 455.3531 (Δ 3.0 ppm).

(6*R*,*E*)-2-methyl-6-((10*S*,13*R*,14*R*,17*R*)-4,4,10,13,14-pentamethyl-3-oxo-2,3,4,5,6,7,10,11,12,13,14,15,16,17-tetradecadydro-1*H*-cyclopenta[α]phenanthren-17-yl)hept-2-enoic acid (108)[80]

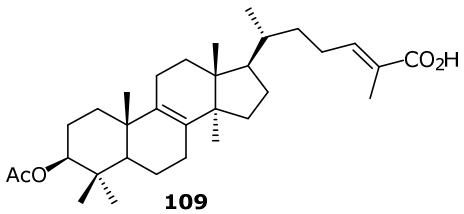


108

Analogue **107** (181 mg, 0.40 mmol) was suspended in dried dichloromethane (6 mL). Dess-Martin periodinane (169 mg, 0.40 mmol) was added and the white suspension was stirred at room temperature. A dispersion of water (10 μL) in dichloromethane (10 mL) was added dropwise to the white suspension. Completion of the reaction was achieved after 15 min. The solvent was evaporated and the resulting syrup was redissolved in ethyl acetate (20 mL) and a mixture of $Na_2S_2O_3$:$NaHCO_3$ (sat. aq. sol.) 1:1 (1 X 20 mL). Column chromatography eluting with EtOAc:PE 7:13 afforded **108** (138 mg; 0.30 mmol; 76%) as a white solid. Analogue **108** was further purified by precipitation from hexane/dichloromethane solution, precipitation occurred after evaporation of dichloromethane with nitrogen flow.

108: R_f 0.24 (EtOAc:PE 7:13); mp 165-166 °C; $[\alpha]_D^{22}$ = +78.8 (*c* = 0.41, $CHCl_3$); ν_{max} ($CHCl_3$ solution)/cm^{-1} 3690 *s* (Free O-H, O-H *str*), 3606 *m* (H-bonded OH), 3444 *m br* (O-H *str*), 3011 *m* (C=CH, C-H *str*), 2953 *m* (C-H *str*), 2879 *w* (C-H *str*), 1699 m (C=O str), 1602 *vs* (CO_2^- *antisym str*), 1420 *w* (CO_2^- *symm str*), 1374 *w* (O-H *bend*), 1242 *m* (C-O *str*); ^{1}H NMR (400 MHz, $CDCl_3$) δ 6.90 (td, *J* = 7.5, 1.5 Hz, 1H), 2.59 (ddd, *J* = 15.6, 11.2, 7.1 Hz, 1H), 2.41 (ddd, *J* = 15.6, 6.8, 3.6 Hz, 1H), 2.33 – 2.18 (m, 1H), 2.18 – 1.87 (m, 7H), 1.84 (d, *J* = 1.4 Hz, 3H), 1.82 – 1.69 (m, 2H), 1.68 – 1.39 (m, 8H), 1.32 (ddd, *J* = 14.6, 7.2, 4.8 Hz, 1H), 1.20 (tdt, *J* = 16.8, 8.6, 3.9 Hz, 2H), 1.12 (s, 3H), 1.09 (s, 3H), 1.07 (s, 3H), 0.94 (d, *J* = 6.2 Hz, 3H), 0.89 (d, *J* = 0.9 Hz, 3H), 0.72 (s, 3H); ^{13}C NMR (101 MHz, $CDCl_3$) δ 218.1 (C=O), 173.4 (C=O), 145.9 (CH=C), 135.4 (C=C), 133.3 (C=C), 126.8 (C=C), 51.4 (CH), 50.5 (CH), 50.1 (C), 47.6 (C), 44.7 (C), 37.1 (C), 36.5 (CH), 36.2 (CH_2), 34.9 (CH_2), 34.8 (CH_2), 31.1 (CH_2), 31.0 (CH_2), 28.3 (CH_2), 26.5 (CH_2), 26.3 (CH_3), 26.0 (CH_2), 24.4 (CH_3), 21.4 (CH_3), 21.2 (CH_2), 19.6 (CH_2), 18.8 (CH_3), 18.7 (CH_3), 16.0 (CH_3), 12.1 (CH_3); Elemental analysis: found C 78.9%; H 10.1%, calcd. for $C_{30}H_{46}O_3$, C 79.3%; H 10.2%; HRMS (ESI) m/z ($M^{\cdot}$+Na)$^+$ 477.3335, $C_{30}H_{46}NaO_3$ requires ($M^{\cdot}$+Na)$^+$ 477.3339 (Δ 0.8 ppm).

(6*R,E*)-6-((3*S*,10*S*,13*R*,14*R*,17*R)*-3-acetoxy-4,4,10,13,14-pentamethyl-2,3,4,5,6,7,10,11,12,13,14,15,16,17-tetradecadydro-1*H*-cyclopenta[α]phenanthren-17-yl)-2-methylhept-2-enoic acid (109)[37,38]



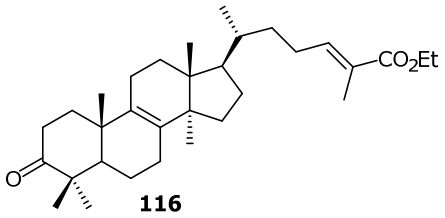
109

Analogue **107** (159 mg, 0.35 mmol), dimethylaminopyridine (2 mg, 16 µmol) and pyridine (150 µL, 1.84 mmol) were dissolved in dichloromethame (14 mL), followed by addition of acetic anhydride (51 µL, 0.54 mmol). The resulting clear solution was stirred at room temperature for 18 h. After that time, the solution was diluted with ethyl acetate (20 mL) and hydrochloric acid (1 M, aq. sol., 10 mL). The layers were separated; the aqueous phase was extracted with ethyl acetate (3 X 10 mL) and the combined organic layers were washed with brine (1 X 10 mL), dried over anhydrous sodium sulfate, filtered and evaporated at reduced pressure. The

resulting white solid crude was purified by column chromatography eluting as a gradient solvent EtOAc:PE starting from 1:4 to 1:1. The title compound, **109** (146 mg; 0.29 mmol; 84%), was furnished as white powder in excellent yield. It was crystallised from DCM/hexane 1:2.

109: R_f 0.37 (EtOAc:PE 3:7); mp 177-181 °C; ν_{max} (KBr disc)/cm^{-1} 3419 *s br* (O-H *str*), 2948 *s* (C-H *str*), 1736 *s* (O-C=O *str*), 1684 *s* (C=O *α,β-unsat*), 1642 *s* (C=O *str*), 1454 w (C-H *def.*), 1427 w (CO_2^- *symm str.*), 1244 m (C-O *str*); ^{1}H NMR (400 MHz, $CDCl_3$) δ 6.90 (td, *J* = 7.6, 1.6 Hz, 1H), 4.50 (dd, *J* = 11.5, 4.5 Hz, 1H), 2.33 – 2.18 (m, 1H), 2.18 – 2.07 (m, 1H), 2.05 (s, 3H), 2.02 (m, 4H), 1.91 (dddd, *J* = 16.6, 9.2, 6.6, 3.6 Hz, 1H), 1.83 (d, *J* = 1.4 Hz, 3H), 1.79 – 1.37 (m, 11H), 1.37 – 1.23 (m, 2H), 1.23 – 1.10 (m, 3H), 1.00 (s, 3H), 0.93 (d, *J* = 6.2 Hz, 3H), 0.88 (s, 6H), 0.87 (s, 3H), 0.69 (s, 3H); ^{13}C NMR (101 MHz, $CDCl_3$) δ 173.4 (C=O), 171.2 (C=O), 146.0 (CH=C), 134.6 (C=C), 134.4 (C=C), 126.7 (C=C), 81.1 (CH), 50.6 (CH), 50.5 (CH), 50.0 (C), 44.7 (C), 38.0 (C), 37.0 (C), 36.5 (CH), 35.4 (CH_2), 34.9 (CH_2), 31.1 (CH_2), 30.9 (CH_2), 28.4 (CH_2), 28.1 (CH_3), 26.5 (CH_2), 26.0 (CH_2), 24.4 (CH_3), 24.3 (CH_2), 21.5 (CH_3), 21.1 (CH_2), 19.3 (CH_3), 18.7 (CH_3), 18.3 (CH_2), 16.7 (CH_3), 15.9 (CH_3), 12.1 (CH_3); HRMS (ESI) m/z ($M^{\cdot}$+Na)$^+$ 477.3599, $C_{32}H_{50}NaO_4$ requires ($M^{\cdot}$+Na)$^+$ 521.3601 (Δ 0.4 ppm).

Ethyl (6*R*,*E*)-2-methyl-6-((10*S*,13*R*,14*R*,17*R*)-4,4,10,13,14-pentamethyl-3-oxo-2,3,4,5,6,7,10,11,12,13,14,15,16,17-tetrahydro-1*H*-cyclopenta[a]phenanthren-17-yl)hept-2-enoate (116)[84]



116

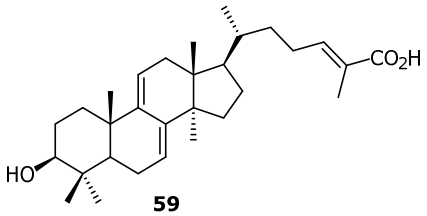
Analogue **108** (175 mg, 0.39 mmol), ethanol (25 µL, 0.43 mmol) and triphenylphosphine (115 mg, 0.43 mmol) were dissolved in tetrahydrofuran (2.5 mL). The dropwise addition of diisopropylazodicarboxylate (90 µL, 0.43 mmol) changed the colour of the solution to yellow. The reaction was stirred at room temperature for 1.5 h, at which point it was monitored by TLC (SiO_2, EtOAc:PE 1:4) confirming completion of the reaction. After evaporation of the solvent, crude product was purified by column chromatography eluting

from Et_2O:PE 1:4 to EtOAc:PE 3:7. The title ketoester **116** (137 mg, 0.28 mmol, 74%) was isolated in excellent yield as a white powder.

116: R_f 0.26 (Et_2O:PE 1:4); mp 168-170 ºC; $[\alpha]_D^{31}$ = +68.2 (*c* = 0.84, $CHCl_3$); ν_{max} ($CHCl_3$ solution)/cm^{-1} 2953 *s* (C-H *str.*), 2878 *s* (C-H *str.*), 1699 *s* (C=O *str.*), 1647 *w* (C=O α,β-unsat *str*), 1458 *m* (C-H *def.*), 1372 *m* (-$C(CH_3)_2$), 1272 *m* (O-H *bend*), 1052 *w* (C-O *str.*); ^{1}H NMR (500 MHz, $CDCl_3$) δ 6.75 (tq, *J* = 7.5, 1.5 Hz, 1H), 4.18 (q, *J* = 7.1 Hz, 2H), 2.58 (ddd, *J* = 15.7, 11.3, 7.2 Hz, 1H), 2.40 (ddd, *J* = 15.7, 6.8, 3.6 Hz, 1H), 2.29 – 2.16 (m, 1H), 2.13 – 2.01 (m, 5H), 2.01 – 1.87 (m, 2H), 1.83 (d, *J* = 1.3 Hz, 3H), 1.80 – 1.66 (m, 2H), 1.67 – 1.53 (m, 6H), 1.55 – 1.37 (m, 2H), 1.39 – 1.24 (m, 1H), 1.29 (t, *J* = 7.1 Hz, 3H), 1.26 – 1.12 (m, 2H), 1.11 (s, 3H), 1.09 (s, 3H), 1.06 (s, 3H), 0.94 (d, *J* = 6.4 Hz, 3H), 0.89 – 0.87 (m, 3H), 0.71 (s, 3H); ^{13}C NMR (126 MHz, $CDCl_3$) δ 218.1 (C=O), 168.5 (C=O), 143.0 (C=CH), 135.4 (C=C), 133.3 (C=C), 127.5 (C=C), 60.5 (CH_2), 51.3 (CH), 50.4 (CH), 50.0 (C), 47.5 (C), 44.6 (C), 37.0 (C), 36.5 (CH), 36.2 (CH_2), 35.1 (CH_2), 34.8 (CH_2), 31.1 (CH_2), 31.0 (CH_2), 28.3 (CH_2), 26.5 (CH_2), 26.3 (CH_3), 25.8 (CH_2), 24.4 (CH_3), 21.4 (CH_3), 21.2 (CH_2), 19.6 (CH_2), 18.8 (CH_3), 18.7 (CH_3), 16.0 (CH_3), 14.5 (CH_3), 12.5 (CH_3); Elemental analysis: found C 79.5%; H 10.4%, calcd. for $C_{32}H_{50}O_3$, C 79.6%; H 10.4%; HRMS (ESI) m/z ($M^{\cdot}$+Na)$^+$ 505.3644, $C_{32}H_{50}NaO_3$ requires ($M^{\cdot}$+Na)$^+$ 505.3652 (Δ 1.7 ppm).

3) <u>Modifications at rings B-C</u>

(6*R*,*E*)-6-((3*S*,10*S*,13*R*,14*R*,17*R*)-3-hydroxy-4,4,10,13,14-pentamethyl-2,3,4,5,6,10,12,13,14,15,16,17-dodecahydro-1*H*-cyclopenta[α]phenanthren-17-yl)-2-methylhept-2-enoic acid (59)[60]



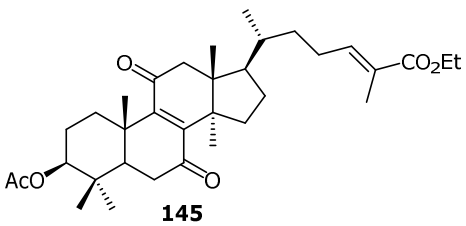
59

Conjugated acetoester **183** (173 mg, 0.33 mmol) was dissolved in THF:MeOH:water 2:2:1 (5 mL). Lithium hydroxide (86 mg, 2.06 mmol) was added and precipitation was observed. The reaction was stirred for 20 h at room temperature. When the reaction was monitored by TLC (SiO_2 EtOAc:PE 1:9 and 1:4), three spots were observed. In order to speed up the reaction

conversion, the temperature was increased to 80 ºC for 3.25 h. After that time, TLC (SiO_2 EtOAc:PE 1:9 and 1:4) and MS confirmed that completion was achieved. In this process, the suspension became yellow-orange. Hydrochloric acid (1M aq. sol., 5 mL) and ethyl acetate (5 mL) were added and work-up proceeded. Aqueous phase was extracted with (6 X 5 mL) and combined organic layers were washed with brine (1 X 5 mL), dried over sodium sulfate, filtered and evaporated at reduced pressure. Reaction crude was purified by column chromatography eluting EtOAc:PE 2:3. Analogue **59** was isolated as a white solid in moderate yield (76 mg; 0.17 mmol; 51%). The compound **59** was repurified by precipitation with hexane from a saturated solution in dichloromethane/methanol to give a white solid.

59 R_f 0.15 (SiO_2; EtOAc:PE 2:3); mp 187-191 ºC; ν_{max} (KBr disc)/cm^{-1} 3428 *br s* (H-bonded -OH), 2930 *m* (C-H *str*), 2881 *w* (C-H *str*), 1639 *m* (*α,β-unsat* C=O), 1372 *w* (-$C(CH_3)_2$), 1262 *m* (O-H *bend*), 1036 *m* (C-O *str*); ^{1}H NMR (400 MHz, MeOD) δ 6.77 (td, *J* = 7.5, 1.6 Hz, 1H), 5.50 – 5.43 (m, 1H), 5.31 (d, *J* = 6.1 Hz, 1H), 3.24 – 3.11 (m, 1H), 2.31 – 2.15 (m, 2H), 2.15 – 2.02 (m, 4H), 2.04 – 1.91 (m, 3H), 1.80 (d, *J* = 1.4 Hz, 3H), 1.72 – 1.50 (m, 5H), 1.49 – 1.23 (m, 3H), 1.17 (dtd, *J* = 13.9, 9.2, 5.0 Hz, 1H), 1.06 (dd, *J* = 10.6, 5.2 Hz, 1H), 0.97 (s, 6H), 0.93 (d, *J* = 6.4 Hz, 3H), 0.87 (s, 3H), 0.85 (s, 3H), 0.56 (s, 3H); ^{13}C NMR (101 MHz, MeOD) δ 171.4 (C=O), 146.7 (C=C), 144.3 (CH=C), 143.2 (C=C), 127.9 (C=C), 121.0 (CH=C), 116.8 (CH=C), 79.1 (CH), 51.6 (CH), 51.0 (C), 50.0 (CH), 44.4 (C), 39.3 (C), 38.5 (CH_2), 38.0 (C), 36.8 (CH), 36.5 (CH_2), 35.5 (CH_2), 32.1 (CH_2), 28.52 (CH_3), 28.50 (CH_2), 27.9 (CH_2), 26.3 (CH_2), 25.9 (CH_3), 23.6 (CH_2), 23.1 (CH_3), 18.7 (CH_3), 16.2 (CH_3), 16.1 (CH_3), 12.4 (CH_3); HRMS (ESI) m/z ($M^{\cdot}$+H)$^+$ 455.3536, $C_{30}H_{47}O_3$ requires ($M^{\cdot}$+Na)$^+$ 455.3520 (Δ 3.5 ppm).

Ethyl (*E*,6*R*)-6-[(3*S*,10*S*,13*R*,14*R*,17*R*)-3-acetoxy-4,4,10,13,14-pentamethyl-7,11-dioxo-2,3,5,6,12,15,16,17-octahydro-1*H*-cyclopenta[α]phenanthren-17-yl]-2-methylhept-2-enoate (145)[171]



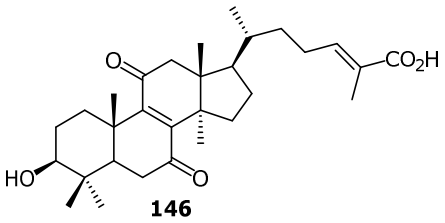
145

The acetoester precursor **100*E*** (401 mg, 0.76 mmol) was suspended in acetone (4 mL). Chromium trioxide (235 mg; 2.33 mmol) was added in one portion, followed by concentrated sulfuric acid (3 drops). The suspension, which became dark brown, was stirred at room temperature. The reaction was monitored by TLC (EtOAc:PE 3:17), after 2-3 h monoketone was detected. More concentrated sulfuric acid (3 drops) and chromium trioxide (79.1 mg, 0.78 mmol) were added, which provoked change in the suspension colour to green. Diketone **145** was detected by MS after 22 h reaction. For the work-up, the suspension was diluted with water (20 mL) and ethyl acetate (20 mL), followed by separation of the phases. The aqueous layer was extracted with ethyl acetate (3 X 10 mL). The combined organic layers were then washed with sodium hydrogen carbonate (sat. aq. sol.) (2 X 10 mL) and brine (2 X 10 mL), dried over anhydrous sodium sulfate, filtered and evaporated. The crude product was purified by column chromatography eluting using EtOAc:PE 3:17. The title diketone **145** (188 mg; 0.34 mmol; 45%) was obtained as a yellow solid.

145: R_f 0.25 (EtOAc:PE 3:17); mp 136-137 ºC; $[\alpha]_D^{24}$ =+72.2 (*c* = 1.05, $CHCl_3$); ν_{max} ($CHCl_3$ solution)/cm^{-1} 3007 *m* (C=CH *str.*), 2974 *m* (C-H *str*), 2875 *m* (C-H *str.*), 1710 *vs* (C=O *str*), 1673 *s* (C=O *a*,*β*-unsat *str*), 1602 *s* (CO_2^- *antisym str*), 1465 *m* (C-H *def*), 1368 *m* (-CH_3 *symm def*), 1274 *m* (O-H *bend*), 1253 *s* (C-O *str.*), 1097 *m* (C-O *str.*), 836 *w* (C=CH *oop def.*); ^{1}H NMR (400 MHz, $CDCl_3$) δ 6.73 (td, *J* = 7.4, 1.5 Hz, 1H), 4.52 (dd, *J* = 11.4, 5.1 Hz, 1H), 4.18 (q, *J* = 7.1 Hz, 2H), 2.89 (dt, *J* = 13.8, 3.7 Hz, 1H), 2.76 (dd, *J* = 15.9, 1.2 Hz, 1H), 2.61 (d, *J* = 15.8 Hz, 1H), 2.55 – 2.38 (m, 2H), 2.28 – 2.18 (m, 1H), 2.14 (ddd, *J* = 15.9, 9.0, 4.4 Hz, 1H), 2.05 (s, 3H), 2.10 – 2.00 (m, 1H), 2.01 – 1.90 (m, 1H), 1.82 (d, *J* = 1.3 Hz, 3H), 1.80 – 1.69 (m, 3H), 1.71 – 1.60 (m, 1H), 1.66 – 1.50 (m, 2H), 1.47 – 1.39 (m, 1H), 1.38 – 1.34 (m, 1H), 1.32 (s, 3H), 1.28 (t, *J* = 7.1 Hz, 3H), 1.36 – 1.23 (m, 1H), 1.26 – 1.08 (m, 1H), 1.16 (d, *J* = 1.0 Hz, 3H), 0.95 (s, 3H), 0.92 (d, *J* = 6.5 Hz, 3H), 0.89 (s, 3H), 0.79 (s, 3H); ^{13}C NMR (101 MHz, $CDCl_3$) δ 202.4 (C=O), 201.9 (C=O), 170.9 (C=O), 168.4 (C=O), 151.9 (C=C), 150.7 (C=C), 142.4 (CH=C), 127.9 (C=C), 79.4 (CH), 60.6 (CH_2), 51.7 (CH_2), 50.3 (CH), 49.13 (C), 49.07 (CH), 47.6 (C), 39.7 (C), 37.9 (C), 36.4 (CH_2), 36.2 (CH), 34.9 (CH_2), 33.9 (CH_2), 32.3 (CH_2), 28.0 (CH_3), 27.5 (CH_2), 26.0 (CH_3), 25.7 (CH_2), 24.1 (CH_2), 21.4 (CH_3), 18.5 (CH_3), 17.7 (CH_3), 16.9 (CH_3), 16.7 (CH_3), 14.4 (CH_3), 12.5 (CH_3); Elemental analysis: found C 73.57%; H 9.22%, calcd. for $C_{34}H_{50}O_6$, C 73.61%; H 9.08%; HRMS

(ESI) m/z ($M^{\cdot}$+Na)$^+$ 577.3505, $C_{34}H_{50}NaO_6$ requires ($M^{\cdot}$+Na)$^+$ 577.3500 (Δ 0.9 ppm).

(*E*,6*R*)-6-[(3*S*,10*S*,13*R*,14*R*,17*R*)-3-hydroxy-4,4,10,13,14-pentamethyl-7,11-dioxo-2,3,5,6,12,15,16,17-octahydro-1*H*-cyclopenta[α]phenanthren-17-yl]-2-methyl-hept-2-enoic acid (146)[60]



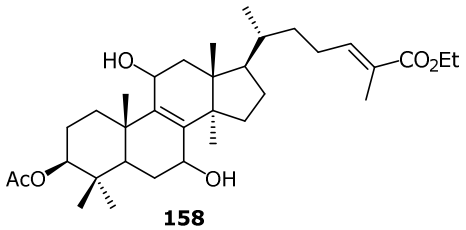
146

The diketone-acetoester **145** (88 mg; 0.16 mmol) was dissolved in THF:MeOH:water (3:1:1) (4 mL) followed by addition of lithium hydroxide (43 mg, 1.02 mmol). An orange solution was formed, which was stirred at room temperature for 22 h. Then, the solution was diluted with ethyl acetate and hydrochloric acid (1 M, aq. sol.) (5 mL each), precipitation and yellow colour in the organic phase were observed. After separation of the two phases, aqueous layer was extracted with ethyl acetate (3 X 5 mL), whilst combined organic layers were washed with sodium hydrogen carbonate (1 X 5 mL) and brine (1 X 5 mL), dried over sodium sulfate anhydrous, filtered and evaporated. The yellow crude product was purified by column chromatography eluting isocratically with EtOAc:PE 11:9. The title compound **146** was afforded in moderate yield as a light yellow solid (48 mg; 99 µmol; 63%). Analogue **146** was further purified by precipitation from MeOH:DCM 3:1.

146 R_f 0.53 (EtOAc:PE 13:1); mp 211-212 ºC; $[\alpha]_D^{24}$ = +97.4 (*c* = 0.48, $CHCl_3$); ν_{max} ($CHCl_3$ solution)/cm^{-1} 3529 *m* (O-H *str*), 2973 *s* (C-H *str*), 2938 *s* (C-H *str*), 2872 *s* (C-H *str*), 1717 *s* (C=O *str*), 1674 *vs* (C=O α,β-unsat *str*), 1466 *m* (C-H *def*), 1425 *m* (C-H *def*), 1252 *m* (C-O *str*), 1065 *m* (C-O str), 980 *m* (C=CH *oop def*); ^{1}H NMR (400 MHz, $CDCl_3$) δ 6.88 (td, *J* = 7.5, 1.7 Hz, 1H), 3.28 (dd, *J* = 11.2, 5.1 Hz, 1H), 2.89 (dt, *J* = 13.7, 3.6 Hz, 1H), 2.75 (d, *J* = 16.1 Hz, 1H), 1H), 2.60 (d, *J* = 15.9 Hz, 1H), 2.55 – 2.42 (m, 2H), 2.26 (dq, *J* = 13.9, 6.3 Hz, 1H), 2.21 – 2.04 (m, 2H), 1.98 (dtd, *J* = 13.5, 9.4, 7.1 Hz, 1H), 1.83 (d, *J* = 1.4 Hz, 3H), 1.79 – 1.63 (m, 4H), 1.58 (dp, *J* = 10.0, 3.7, 3.2 Hz, 1H), 1.52 (dd, *J* = 12.1, 5.2 Hz, 1H), 1.43 (ddt, *J* = 10.2, 6.7, 3.5 Hz, 1H), 1.40 – 1.27 (m, 1H), 1.30 (s, 3H), 1.27 – 1.11

(m, 2H), 1.17 (s, 3H), 1.02 (s, 3H), 0.93 (d, *J* = 6.4 Hz, 3H), 0.88 (s, 3H), 0.80 (s, 3H); ^{1}H-NMR lit[107]; ^{13}C NMR (101 MHz, $CDCl_3$) δ 202.5 (C=O), 202.3 (C=O), 173.0 (C=O), 151.9 (C=C), 150.7 (C=C), 145.3 (CH=C), 127.0 (C=C), 77.8 (CH), 51.8 (CH_2), 50.3 (CH), 49.14 (CH), 49.08 (C), 47.5 (C), 40.0 (C), 39.0 (C), 36.6 (CH_2), 36.2 (CH), 34.7 (CH_2), 34.2 (CH_2), 32.3 (CH_2), 28.0 (CH_3), 27.7 (CH_2), 27.5 (CH_2), 26.0 (CH_3), 25.9 (CH_2), 18.5 (CH_3), 17.7 (CH_3), 17.0 (CH_3), 15.6 (CH_3), 12.2 (CH_3); ^{13}C-NMR lit.[107]; HRMS (ESI) m/z ($M^{\cdot}$+Na) 507.3094, $C_{30}H_{44}NaO_5$ requires ($M^{\cdot}$+Na) 507.3081 (Δ 2.6 ppm).

Ethyl (6*R*,*E*)-6-((3*S*,10*S*,13*R*,14*R*,17*R*)-3-acetoxy-7,11-dihydroxy-4,4,10,13,14-pentamethyl-2,3,4,5,6,7,10,11,12,13,14,15,16,17-tetradecahydro-1*H*-cyclopenta[α]phenanthren-17-yl)-2-methyl-hept-2-enoate (158)[103]



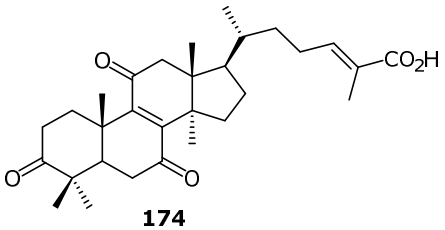
158

Acetoester precursor **100*E*** (57 mg; 0.11 mmol) and *meso*-tetrakis-(tetrafluorophenyl)porphyrin iron (III) chloride (Fe(PFPP)Cl) (6 mg; 5.3 μmol) were dissolved in dichloromethane (2 mL). The solution was cooled to -78 ºC and *meta*-chloroperbenzoic acid (85 mg; 0.34 mmol) was added. The reaction colour became dark, stirring of the reaction continued under nitrogen at room temperature for 24 h. The suspension was diluted with ethyl acetate (5 mL) and quenched with $Na_2S_2O_3$:$NaHCO_3$ (sat. aq. sol.) 1:1. After separation of phases, aqueous phase was extracted with ethyl acetate (3 X 5 mL), whilst combined organic layers were washed with brine (1 X 5 mL), dried over sodium sulfate anhydrous, filtered and evaporated. The product crude was purified by column chromatography eluting at gradient from EtOAc:PE 2:3 to 1:1. The title compound **158** (37 mg; 69 μmol; 64%) was furnished as white powder, this product is very sensitive to air at room temperature, therefore it should be store under nitrogen in the freezer.

158 R_f 0.20 (EtOAc:PE 2:3); ^{1}H NMR (400 MHz, $CDCl_3$) δ 6.74 (td, *J* = 7.4, 1.6 Hz, 1H), 4.57 (dd, *J* = 11.2, 4.1 Hz, 1H), 4.38 (dd, *J* = 9.5, 3.8 Hz, 1H), 4.26 (t, *J* = 3.1 Hz, 1H), 4.18 (q, *J* = 7.1 Hz, 2H), 2.30 (dd, *J* = 14.0, 9.3

Hz, 1H), 2.21 (dt, *J* = 11.2, 6.4 Hz, 1H), 2.14 – 1.94 (m, 2H), 2.05 (s, 3H), 1.83 (s, 3H), 1.92 – 1.61 (m, 9H), 1.61 – 1.48 (m, 3H), 1.44 – 1.21 (m, 2H), 1.28 (t, *J* = 7.1 Hz, 3H), 1.26 (s, 3H), 1.17 (dtd, *J* = 14.2, 9.7, 5.3 Hz, 1H), 1.00 (s, 3H), 0.97 – 0.87 (m, 9H), 0.60 (s, 3H); ^{13}C NMR (101 MHz, $CDCl_3$) δ 171.0 (C=O), 168.5 (C=O), 142.8 (CH=C), 141.9 (C=C), 141.3 (C=C), 127.7 (C=C), 80.6 (CH), 67.0 (CH), 65.1 (CH), 60.5 (CH_2), 51.2 (CH), 50.3 (C), 48.9 (C), 45.0 (CH_2), 44.9 (CH), 38.9 (C), 37.6 (C), 36.4 (CH), 35.0 (CH_2), 34.9 (CH_2), 30.8 (CH_2), 28.8 (CH_2), 28.0 (CH_3), 27.8 (CH_2), 27.2 (CH_3), 25.8 (CH_2), 24.1 (CH_2), 21.4 (CH_3), 19.1 (CH_3), 18.4 (CH_3), 17.3 (CH_3), 16.8 (CH_3), 14.5 (CH_3), 12.5 (CH_3); HRMS (ESI) m/z ($M^{\cdot}$+Na)$^+$ 581.3812, $C_{34}H_{54}NaO_6$ requires ($M^{\cdot}$+Na)$^+$ 581.3813 (Δ 0.2 ppm).

(6*R*,*E*)-2-Methyl-6-((10*S*,13*R*,14*R*,17*R*)-4,4,10,13,14-pentamethyl-3,7,11-trioxo-2,3,4,5,6,7,10,11,12,13,14,15,16,17-tetradecahydro-1*H*-cyclopenta[α]phenanthren-17-yl)hept-2-enoic acid (174)[80]

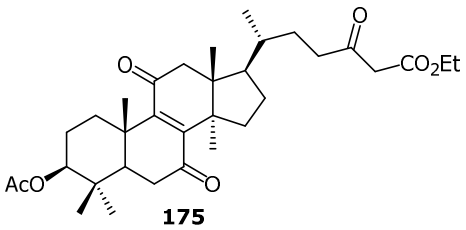


174

Analogue **174** (71 mg; 0.15 mmol) was dissolved in dichloromethane (2 mL). Dess-Martin periodinane (66 mg; 0.16 mmol) was added in one portion, the yellow solution turned cloudy. A mixture of dichloromethane (3 mL) and water (3 µL) was added dropwise, causing precipitation. The reaction was monitored by TLC (SiO_2; EtOAc:PE 1:1), after 40 min it reached completion. The solvent was evaporated under reduced pressure and the resulting crude was redissolved in ethyl acetate (20 mL) and washed successively with $Na_2S_2O_3$:$NaHCO_3$ (sat. aq. sol.) 1:1 (2 X 10 mL), water (1 X 10 mL) and brine (1 X 10 mL). The aqueous phase was extracted with ethyl acetate (5 X 10 mL). The combined organic layers were dried over sodium sulfate anhydrous, filtered and evaporated under reduced pressure. The yellow crude product was purified by column chromatography eluting EtOAc:PE 1:1. The title compound **174** (66 mg; 0.14 mmol; 94%) was isolated in excellent yield as a yellow solid. It was repurified by precipitation from EtOAc/hexane.

174 R_f 0.18 (EtOAc:PE 1:1); mp 163-164 °C; lit[55] 96-98 ºC; $[\alpha]_D^{21}$ = +150.3 (*c* = 0.43, $CHCl_3$); lit.[156] $[\alpha]_D^{25}$ = +13.8 (*c* = 0.004, MeOH); ν_{max} ($CHCl_3$ solution)/cm^{-1} 3691 *vs* (O-H *str*), 3606 *s* (O-H *str*), 3442 *s br* (H-bonded OH), 3008 *m* (C=CH *str*), 2985 *m* (C-H *str*), 1709 *m* (*a,β-unsat* CO_2H, C=O *str*) , 1673 *m* (*a,β-unsat* ketone, C=O str), 1602 *s* (-CO_2^- *antisym str*), 1458 *w* (C-H *def*), 1387 *w* (-$C(CH_3)_2$) , 1241 *s* (O-H *bend*), 1121 *w* (C-O *str*); ^{1}H NMR (400 MHz, $CDCl_3$) δ 6.88 (td, *J* = 7.4, 1.5 Hz, 1H), 2.95 (ddd, *J* = 14.2, 8.5, 6.0 Hz, 1H), 2.74 (dd, *J* = 16.9, 1.2 Hz, 1H), 2.64 (d, *J* = 16.9 Hz, 1H), 2.66 – 2.40 (m, 3H), 2.38 (dd, *J* = 14.3, 2.7 Hz, 1H), 2.33 – 2.20 (m, 2H), 2.21 – 2.06 (m, 2H), 2.06 – 1.92 (m, 1H), 1.83 (d, *J* = 1.4 Hz, 3H), 1.80 – 1.51 (m, 4H), 1.52 – 1.37 (m, 1H), 1.35 (ddd, *J* = 14.7, 11.8, 9.3 Hz, 1H), 1.28 (s, 3H), 1.22 (s, 3H), 1.19 (s, 1H), 1.13 (s, 3H), 1.10 (s, 3H), 0.93 (d, *J* = 6.4 Hz, 3H), 0.82 (s, 3H); ^{1}H-NMR lit.[156]; ^{13}C NMR (101 MHz, $CDCl_3$) δ 215.9 (C=O), 202.1 (C=O), 201.5 (C=O), 173.2 (C=O), 151.7 (C=C), 149.9 (C=C), 145.3 (CH=C), 127.1 (C=C), 51.4 (CH_2), 49.8 (CH), 49.2 (CH), 48.8 (C), 47.0 (C), 46.8 (C), 38.9 (C), 37.2 (CH_2), 36.2 (CH), 35.1 (CH_2), 34.6 (CH_2), 34.2 (CH_2), 32.0 (CH_2), 27.6 (CH_3), 27.5 (CH_2), 26.0 (CH_3), 25.9 (CH_2), 20.5 (CH_3), 18.4 (CH_3), 18.1 (CH_3), 17.0 (CH_3), 12.2 (CH_3); ^{13}C-NMR lit.[156]; HRMS (ESI) m/z ($M^{\cdot}$+Na)$^+$ 505.2937, $C_{30}H_{42}NaO_5$ requires ($M^{\cdot}$+Na)$^+$ 505.2924 (Δ 2.4 ppm).

Ethyl (6*R*)-6-((3*S*,10*S*,13*R*,14*R*,17*R*)-3-acetoxy-4,4,10,13,14-pentamethyl-7,11-dioxo-2,3,4,5,6,7,10,11,12,13,14,15,16,17-tetradecahydro-1*H*-cyclopenta[α]phenanthren-17-yl)-3-oxoheptanoate (175)[97]



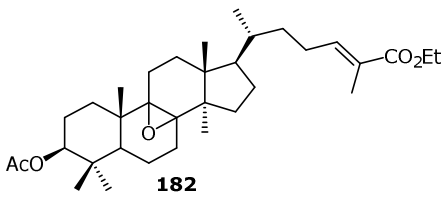
175

Ethyl acetohydroxyester **101** (54 mg; 0.10 mmol) was dissolved in acetone (1 mL). Chromium trioxide (40 mg; 0.40 mmol) and 3 drops of concentrated sulfuric acid were added giving a dark brown suspension, which was stirred at room temperature. After 17 h more chromium trioxide (23 mg) and acetone (2 mL) were added to accelerate the reaction and facilitate the stirring, respectively. After five days stirring at room temperature, the

reaction was worked up. The suspension was diluted with water (10 mL) and this aqueous phase was extracted with ethyl acetate (6 X 10 mL). The combined organic layers were washed with brine (1 X 10 mL), dried over sodium sulfate, filtered and evaporated *in vacuo*. The crude product was purified by column chromatography eluting using a solvent gradient from EtOAc:PE 2:3 to 1:1. The desired triketone **175** (14 mg; 25 µmol; 25%) was obtained as a yellow solid in poor yield.

175 R_f 0.17 (EtOAc:PE 2:3); mp 102-105 ºC; ν_{max} (KBr disc)/cm^{-1} 2978 *s* (C-H *str.*), 1737 *s* (C=O ester *str*), 1716 *s* (C=O ketone *str.*), 1674 *s* (C=O *str. a,β-unsat* ketone), 1465 *m* (C-H *def.*), 1373 *m* (-C(CH_3)$_2$), 1319 *m* (C-O *str.*), 1251 *s* (O-H *bend.*), 1029 *m* (C-O *str.*), 984 *m* (C-H *oop def.* C=C conj with C=O); ^{1}H NMR (500 MHz, $CDCl_3$) δ 4.52 (dd, *J* = 11.6, 4.8 Hz, 1H), 4.19 (q, *J* = 7.1 Hz, 2H), 3.44 (s, 2H), 2.89 (dt, *J* = 13.8, 3.7 Hz, 1H), 2.76 (d, *J* = 15.8 Hz, 1H), 2.65 – 2.54 (m, 1H), 2.59 (d, *J* = 16.1 Hz, 1H), 2.54 – 2.42 (m, 3H), 2.15 (ddd, *J* = 12.8, 9.6, 2.5 Hz, 1H), 2.06 (s, 3H), 2.04 – 1.95 (m, 1H), 1.87 – 1.56 (m, 6H), 1.45 – 1.34 (m, 2H), 1.32 (s, 3H), 1.28 (t, *J* = 7.2 Hz, 3H), 1.32 – 1.19 (m, 2H), 1.16 (s, 3H), 0.95 (s, 3H), 0.90 (s, 3H), 0.87 (d, *J* = 6.5 Hz, 3H), 0.78 (s, 3H); ^{13}C NMR (126 MHz, $CDCl_3$) δ 203.1 (C=O), 202.3 (C=O), 201.9 (C=O), 171.0 (C=O), 167.4 (C=O), 151.8 (C=C), 150.7 (C=C), 79.4 (CH), 61.6 (CH_2), 53.6 (C), 51.7 (CH_2), 50.3 (CH), 49.5 (CH_2), 49.1 (CH), 47.6 (C), 40.2 (CH_2), 39.7 (C), 37.8 (C), 36.4 (CH_2), 35.7 (CH), 33.9 (CH_2), 32.3 (CH_2), 29.5 (CH_2), 28.0 (CH_3), 27.4 (CH_2), 26.0 (CH_3), 24.1 (CH_2), 21.4 (CH_3), 18.5 (CH_3), 17.7 (CH_3), 16.9 (CH_3), 16.7 (CH_3), 14.3 (CH_3); HMRS (ESI) m/z ($M^{\cdot}$+Na)$^+$ 579.3299, $C_{33}H_{48}NaO_7$ requires ($M^{\cdot}$+Na)$^+$ 579.3292 (Δ 1.2 ppm).

Ethyl (6*R*, *E*)-6-((3*S*, 10*S*, 13*R*, 14*R*, 17*R*)-3-acetoxy-4,4,10,13,14-pentamethyltetradecahydro-11*H*-8,9-epoxycyclopenta[*a*]phenanthren-17-yl)-2-methylhept-2-enoate (182)[104]



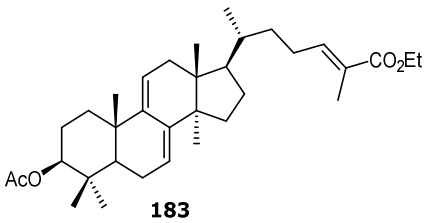
182

To a solution of acetoester precursor **100*E*** (350 mg; 0.67 mmol) dissolved in chloroform (11 mL) was added *meta*-chloroperbenzoic acid (196 mg; 0.66 mmol). The clear solution, which was stirred at room temperature,

became lilac over 20 minutes time and pink after 16 hours. Analysis by TLC (EtOAc:PE 1:19 and 1:9) at that time revealed completion of the reaction. Therefore it was quenched. Sodium hydroxide (159 mg; 3.96 mmol) and sodium sulfate (131 mg; 3.12 mmol) were added, which provoked fading of the pink colour and precipitation. This suspension was filtered off and the filtrate evaporated. Purification by column chromatography eluting with EtOAc:PE 1:9 yielded the title compound **182** in 32% yield (116 mg, 0.21 mmol).

182 R_f 0.28 (SiO_2; EtOAc:PE 1:9); HRMS (ESI) m/z ($M^{\cdot}$+Na)$^+$ 565.3852, $C_{34}H_{54}NaO_5$ requires ($M^{\cdot}$+Na)$^+$ 565.3863 (Δ 2.0 ppm).

Ethyl (6*R*, *E*)-6-((3*S*, 10*S*, 13*R*, 14*R*, 17*R*)-3-acetoxy-4,4,10,13,14-pentamethyl-2,3,4,5,6,10,12,13,14,15,16,17-dodecahydro-1*H*-cyclopenta[*a*]phenanthren-17-yl)-2-methylhept-2-enoate (183)[104]



183

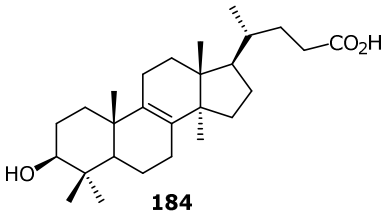
Epoxide **182** (116 mg; 0.21 mmol) was dissolved in toluene (5 mL) forming a clear solution. After addition of *para*-toluenesulfonic acid (5.0 mg; 26 µmol), the reaction was heated at 60 ºC for 1.5 h. Triethylamine solution in toluene (1M, 22 µL) was then added giving a yellow colour and precipitation was observed. The reaction was filtered and evaporated under reduced pressure. The crude product was purified by column chromatography eluting with EtOAc:PE 1:9. The compound **183** was recovered as a white solid in excellent yield (109 mg; 0.21 mmol; 97%).

183 R_f 0.48 (SiO_2; EtOAc : PE 1:9); mp 126-128 ºC; $[\alpha]_D^{23}$ = +76.4 (*c* = 1.06, $CHCl_3$); ν_{max} ($CHCl_3$ solution)/cm^{-1} 2968 *s* (C-H *str*), 2952 *s* (C-H *str*), 2880 *m* (C-H *str*), 1719 *s* (C=O sat ester *str*), 1702 *s* (C=O *α,β-unsat* ester *str*), 1647 *m* (C=C diene), 1602 *m* (C=C diene), 1465 *m* (C-H *def*), 1446 m (C-H *def*), 1393 *m* (-CH_3 *symm def*), 1373 *s* (O-H *bend*), 1258 *s* (O-H *bend*), 1145 *m* (C-O *str*), 1097 *m* (C-O *str*), 978 *m* (C=CH *oop def*), 902 *m* (C=CH); ^{1}H NMR (400 MHz, $CDCl_3$) δ 6.75 (td, *J* = 7.4, 1.5 Hz, 1H), 5.46 (t, *J* = 4.3 Hz, 1H), 5.31 (d, *J* = 5.8 Hz, 1H), 4.51 (dd, *J* = 11.1, 4.8 Hz, 1H), 4.18 (q, *J* = 7.1 Hz, 2H), 2.30 – 2.16 (m, 2H), 2.16 – 2.00 (m, 4H), 2.05 (s, 3H),

2.04 – 1.90 (m, 2H), 1.83 (d, *J* = 1.4 Hz, 3H), 1.78 – 1.65 (m, 2H), 1.66 – 1.47 (m, 4H), 1.45 – 1.34 (m, 2H), 1.36 – 1.22 (m, 1H), 1.29 (t, *J* = 7.1 Hz, 3H), 1.24 – 1.12 (m, 2H), 1.00 (s, 3H), 0.95 (s, 3H), 0.92 (d, *J* = 6.4 Hz, 3H), 0.88 (s, 3H), 0.87 (s, 3H), 0.56 (s, 3H); ^{13}C NMR (101 MHz, $CDCl_3$) δ 171.1 (C=O), 168.5 (C=O), 145.8 (C=C), 142.9 (CH=C), 142.8 (C=C), 127.6 (C=C), 120.1 (CH=C), 116.6 (CH=C), 81.0 (CH), 60.5 (CH_2), 51.0 (CH), 50.5 (C), 49.4 (CH), 43.9 (C), 38.0 (CH_2), 37.8 (C), 37.4 (C), 36.3 (CH), 35.5 (CH_2), 35.0 (CH_2), 31.6 (CH_2), 28.2 (CH_3), 28.0 (CH_2), 25.8 (CH_2), 25.7 (CH_3), 24.4 (CH_2), 23.0 (CH_2), 22.9 (CH_3), 21.5 (CH_3), 18.5 (CH_3), 17.1 (CH_3), 15.8 (CH_3), 14.5 (CH_3), 12.4 (CH_3); HRMS (ESI) m/z ($M^{\cdot}$+Na)$^+$ 547.3752, $C_{34}H_{52}NaO_4$ requires ($M^{\cdot}$+Na)$^+$ 547.3758 (Δ 1.1 ppm).

4) <u>Modification at the side chain</u>

(4*R*)-4-((3*S*,10*S*,13*R*,14*R*,17*R*)-3-hydroxy-4,4,10,13,14-pentamethyl-2,3,4,5,6,7,10,11,12,13,14,15,16,17-tetradecahydro-1*H*-cyclopenta[α]phenanthren-17-yl)pentanoic acid (184)[60]



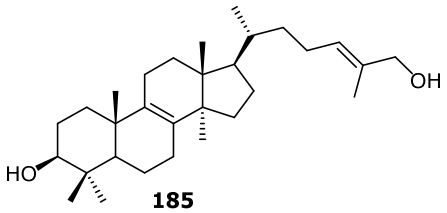
184

Acetolucidinic acid **106** (154 mg; 0.34 mmol) was dissolved in THF:MeOH 1:1 (4 mL). Lithium hydroxide (43 mg; 1.03 mmol) was added in one portion followed by water (1 mL). Precipitation was observed after addition of the base. Further tetrahydrofuran (2 mL) was added to facilitate stirring. This suspension was stirred at room temperature for 16 h. Control of the reaction by TLC (SiO_2 EtOAc:PE 1:1) showed presence of product. The reaction was diluted with hydrochloric acid (1M) and ethyl acetate (5 mL each) and work-up. The aqueous phase was filtered and the filtrate was extracted with ethyl acetate (3 X 10 mL). The combined organic layers were washed with brine (1 X 10 mL), dried over sodium sulfate anhydrous, filtered and evaporated under reduced pressure. The precipitate from aqueous layer was combined with the organic crude and the combined product crude was purified by column chromatography eluting at gradient from EtOAc:PE 3:7 to EtOAc:MeOH 19:1. Two columns were required for the separation of the remaining starting aceto-lucidinic acid **106** (25 mg, 54 µmol, 16%). The compound **184** (103 mg, 0.25 mmol, 73%) was isolated in high yield. The

product was repurified by crystallisation from ethyl acetate/methanol with 81% yield.

184 R_f 0.12 (EtOAc:PE 3:7); mp 245-247 °C; v_{max} (KBr disc)/cm^{-1} 3432 *vs* (O-H *str*), 2964 *vs* (H-bonded –OH), 2941 *vs* (C-H *str*), 2872 *s* (C-H *str*), 2834 *m* (C-H *str*), 1704 *vs* (*sat* -CO_2H)), 1446 *m* (C-H *def*), 1414 *m* (CO_2^- *symm str*), 1369 *s* (O-H *bend*), 1264 *m* (C-O *str*), 1177 *s* (C-O *str*), 1097 *m* (C-O *str*), 1025 *s* (C-O *str*), 997 *m* (C=C), 904 *m* (C=C); ^{1}H NMR (500 MHz, MeOD) δ 3.16 (dd, *J* = 10.3, 5.8 Hz, 1H), 2.35 (ddd, *J* = 15.4, 10.0, 5.3 Hz, 1H), 2.22 (ddd, *J* = 15.5, 9.6, 6.6 Hz, 1H), 2.07 – 1.96 (m, 4H), 1.96 – 1.87 (m, 1H), 1.78 (dddd, *J* = 12.7, 9.5, 6.6, 2.4 Hz, 1H), 1.74 – 1.56 (m, 5H), 1.57 – 1.42 (m, 2H), 1.46 – 1.33 (m, 2H), 1.37 – 1.30 (m, 1H), 1.31 – 1.24 (m, 2H), 1.19 (dddd, *J* = 18.4, 11.3, 9.1, 2.3 Hz, 2H), 1.02 (dd, *J* = 12.6, 2.2 Hz, 1H), 0.97 (s, 3H), 0.96 (s, 3H), 0.89 (d, *J* = 6.3 Hz, 3H), 0.86 (d, *J* = 0.9 Hz, 3H), 0.77 (s, 3H), 0.68 (s, 3H); ^{1}H-NMR lit.[77]; ^{13}C NMR (126 MHz, MeOD) δ 176.1 (C=O), 135.1 (C=C), 134.9 (C=C), 79.1 (CH), 51.1 (CH), 50.8 (CH), 50.4 (C), 45.1 (C), 39.4 (C), 37.6 (C), 36.6 (CH), 36.3 (CH_2), 31.8 (CH_2), 31.7 (CH_2), 31.6 (CH_2), 31.3 (CH_2), 28.6 (CH_2), 28.3 (CH_3), 27.9 (CH_2), 27.0 (CH_2), 24.5 (CH_3), 21.5 (CH_2), 19.5 (CH_3), 18.8 (CH_2), 18.6 (CH_3), 16.1 (CH_3), 15.8 (CH_3); HRMS (ESI) m/z ($M^{\cdot}$+Na)$^+$ 439.3177, $C_{27}H_{44}NaO_3$ requires ($M^{\cdot}$+Na)$^+$ 439.3183 (Δ 1.2 ppm).

(3*S*,10*S*,13*R*,14*R*,17*R*)-17-((*R*,*E*)-7-hydroxy-6-methylhept-5-en-2-yl)-4,4,10,13,14-pentamethyl-2,3,4,5,6,7,10,11,12,13,14,15,16,17-tetradecahydro-1*H*-cyclopenta[α]phenanthren-3-ol (185)[111]



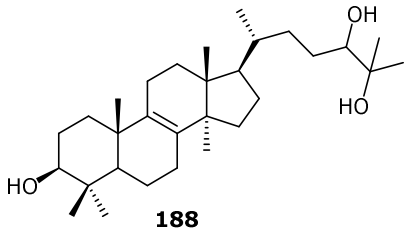
185

The aceto-ester precursor **100*E*** (252 mg, 0.48 mmol) was dissolved in tetrahydrofuran (20 mL) and cooled to 0 ºC. Lithium aluminium hydride powder was added in one portion. At that point, a grey suspension formed and gas evolution were observed. After 30 min reaction, ammonium chloride (aq. sat. sol., 20 mL) was added dropwise at 0 ºC and the stirring continued for another 90 min. Then the reaction was worked-up. The aqueous phase was extracted with ethyl acetate (5 X 10 mL), the combined organic layers were then washed with brine (1 X 5 mL), dried over sodium sulfate

anhydrous, filtered and evaporated. The crude product was purified by column chromatography eluting using a solvent gradient starting from EtOAc:PE 2:3 to 3:1. The title compound **185** (165 mg; 0.37 mmol; 78%) was furnished as a white powder. This sample was further purified by crystallisation from EtOAc:hexane 1:2 (12 mL).

185 R_f 0.51 (EtOAc:PE 9:11); m.p. 149-158 °C; ν_{max} (KBr disc)/cm^{-1} 3427 *vs br* (H-bonded -OH), 2946 *s* (C-H *str*), 2872 *m* (C-H *str*), 1632 *w* (C=C), 1454 *w* (C-H *def*), 1371 *w* (-CH_3 *symm def*), 1028 *w* (C-O *str*); ^{1}H NMR (400 MHz, $CDCl_3$) δ 5.40 (tq, *J* = 7.1, 1.4 Hz, 1H), 4.00 (s, 2H), 3.23 (dd, *J* = 11.5, 4.5 Hz, 1H), 2.25 – 2.07 (m, 1H), 2.07 – 1.97 (m, 4H), 1.96 – 1.85 (m, 2H), 1.67 (s, 3H), 1.79 – 1.50 (m, 7H), 1.55 – 1.32 (m, 4H), 1.34 – 1.12 (m, 3H), 1.13 – 1.01 (m, 2H), 1.00 (s, 3H), 0.98 (s, 3H), 0.92 (d, *J* = 6.3 Hz, 3H), 0.87 (s, 3H), 0.81 (s, 3H), 0.69 (s, 3H); ^{13}C NMR (126 MHz, $CDCl_3$) δ 134.6 (C=C), 134.5 (C=C), 134.4 (C=C), 127.2 (CH=C), 79.1 (CH), 69.2 (CH_2), 50.54 (CH), 50.51 (CH), 50.0 (C), 44.6 (C), 39.0 (C), 37.2 (C), 36.4 (CH), 36.1 (CH_2), 35.7 (CH_2), 31.1 (CH_2), 31.0 (CH_2), 28.4 (CH_2), 28.1 (CH_3), 28.0 (CH_2), 26.6 (CH_2), 24.7 (CH_2), 24.4 (CH_3), 21.1 (CH_2), 19.3 (CH_3), 18.8 (CH_3), 18.4 (CH_2), 15.9 (CH_3), 15.6 (CH_3), 13.8 (CH_3); HRMS (ESI) m/z ($M^{\cdot}$+Na)$^+$ 465.3695, $C_{30}H_{50}NaO_2$ requires ($M^{\cdot}$+Na)$^+$ 465.3703(Δ 1.7 ppm).

(6*R*)-6-((3*S*,10*S*,13*R*,14*R*,17*R*)-3-hydroxy-4,4,10,13,14-pentamethyl-2,3,4,5,6,7,10,11,12,13,14,15,16,17-tetradecahydro-1*H*-cyclopenta[α]phenanthren-17-yl)-2-methylheptane-2,3-diol (188)[113]



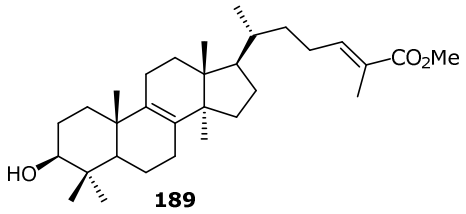
188

Aceto-diol **91** (202 mg; 0.40 mmol) was suspended in methanol (15 mL). Potassium hydroxide (118 mg; 2.08 mmol) was dissolved in water (1 mL) and added to the suspension. After addition of the base, the suspension colour changed to yellow. The reaction was stirred for 48 h, at which point it had formed a clear yellow solution. The reaction was neutralised with hydrochloric acid (1M aq. sol., 2 mL), which caused precipitation. It was then diluted with water (25 mL). The suspension was filtered and the

precipitate was dissolved in ethyl acetate (10 mL), washed with brine (1 X 10 mL), dried over sodium sulfate anhydrous, filtered and evaporated under reducted pressure. The crude product was purified by column chromatography eluting using a solvent gradient from EtOAc:PE 7:13 to EtOAc:PE 9:11. The title compound **188** (108 mg; 0.23 mmol; 59%) was isolated in moderate yield as colourless solid. The product was re-purified by precipitation from a mixture hexane/DCM/EtOAc with 79% yield.

188 R_f 0.15 (EtOAc:PE 7:13); mp 168-172 °C; lit.[114] 153-158 °C (methanol); ν_{max} (KBr disc)/cm^{-1} 3434 *vs br* (H-bonded -OH), 2947 *s* (C-H *str*), 1633 *w* (C=C), 1453 *w* (C-H *def*), 1371 *w* (C-O *bend*), 1076 *w* (C-O *str*); ^{1}H NMR (400 MHz, $CDCl_3$) δ 3.34 (t, *J* = 6.2 Hz, 0.4H), 3.28 (dd, *J* = 10.2, 1.8 Hz, 0.6H), 3.23 (dd, *J* = 11.5, 4.5 Hz, 1H), 2.02 (ddt, *J* = 11.5, 7.6, 3.5 Hz, 4H), 1.93 (ddd, *J* = 17.1, 10.8, 6.8 Hz, 1H), 1.81 – 1.63 (m, 7H), 1.64 – 1.54 (m, 2H), 1.54 – 1.45 (m, 2H), 1.45 – 1.30 (m, 2H), 1.21 (s, 3H), 1.31 – 1.10 (m, 3H), 1.16 (s, 3H), 1.05 (dd, *J* = 12.6, 2.2 Hz, 1H), 1.02 (s, 1H), 1.00 (s, 3H), 0.98 (s, 3H), 0.91 (d, *J* = 6.3 Hz, 2H), 0.91 (d, *J* = 6.1 Hz, 1H), 0.88 (s, 3H), 0.81 (s, 3H), 0.70 (s, 1H), 0.69 (s, 2H); ^{1}H-NMR lit.[114]; ^{13}C NMR (101 MHz, $CDCl_3$) δ 134.6 (C=C), 134.5 (C=C), 79.8 (CH), 79.1 (CH), 78.9 (CH), 73.4 (C), 73.3 (C), 50.7 (CH), 50.58 (CH), 50.55 (CH), 49.97 (C), 49.95 (C), 44.7 (C), 44.6 (C), 39.0 (C), 37.2 (C), 36.9 (CH), 36.5 (CH), 35.7 (CH_2), 33.7 (CH_2), 31.2 (CH_2), 31.0 (CH_2), 28.9 (CH_2), 28.3 (CH_2), 28.1 (CH_3), 28.0 (CH_2), 26.73 (CH_3), 26.70 (CH_3), 26.65 (CH_2), 24.4 (CH_3), 23.4 (CH_3), 23.3 (CH_3), 21.2 (CH_2), 19.3 (CH_3), 19.0 (CH_3), 18.4 (CH_2), 15.9 (CH_3), 15.6 (CH_3); HRMS (ESI) m/z ($M^{\cdot}$+Na)$^+$ 483.3795, $C_{30}H_{52}NaO_3$ requires ($M^{\cdot}$+Na)$^+$ 483.3809 (Δ 2.9 ppm).

Methyl (6*R*,*E*)-6-((3*S*,10*S*,13*R*,14*R*,17*R*)-3-hydroxy-4,4,10,13,14-pentamethyl-2,3,4,5,6,7,10,11,12,13,14,15,16,17-tetradecahydro-1*H*-cyclopenta[α]phenanthren-17-yl)-2-methylhept-2-enoate (189)[115]



189

Analogue **107** (173 mg; 0.38 mmol) was dissolved in methanol; *para*-toluene sulfonic acid (7.7 mg; 40 µmol) was added. The resulting

suspension was heated at reflux for 36 h. In order to help with the formation of product, molecular sieves 4 Å (1.00 g) were added. The reaction was filtered and evaporated under reduced pressure. The crude product was purified by column chromatography eluting at gradient from EtOAc:PE 3:17 to 1:1. The title compound **189** (91 mg; 0.19 mmol; 51%) and starting material **107** (21 mg; 0.05 mmol; 12%) were isolated as white solids. The sample was further purified by crystallisation from hexane (8 mL) with 59% yield.

189 R_f 0.26 (EtOAc:PE 1:4); mp 118-120 °C; lit.[78] 123-125 °C; ν_{max} (KBr disc)/cm^{-1} 3443 *s br* (H-bonded O-H), 2946 *s* (C-H *str.*), 2875 *m* (C-H *str.*), 1714 *m* (*a,β-unsat* -CO-O), 1695 *m* (*a,β-unsat* –CO_2H), 1644 *w* (*a,β-unsat* –C=O), 1438 *w* (C-H *str.*), 1371 *w* (O-H *bend.*), 1276 *w* (C-O *str.*), 1141 *w* (C-O *str*); ^{1}H NMR (400 MHz, $CDCl_3$) δ 6.76 (td, *J* = 7.4, 1.6 Hz, 1H), 3.73 (s, 3H), 3.23 (dd, *J* = 11.5, 4.5 Hz, 1H), 2.21 (ddd, *J* = 18.5, 9.3, 4.8 Hz, 1H), 2.13 – 1.97 (m, 5H), 1.91 (dtd, *J* = 13.5, 9.2, 7.5 Hz, 1H), 1.83 (d, *J* = 1.4 Hz, 3H), 1.79 – 1.53 (m, 8H), 1.54 – 1.37 (m, 3H), 1.36 – 1.28 (m, 1H), 1.28 – 1.21 (m, 1H), 1.21 – 1.08 (m, 2H), 1.04 (dd, *J* = 12.6, 2.2 Hz, 1H), 1.00 (s, 3H), 0.98 (s, 3H), 0.93 (d, *J* = 6.2 Hz, 3H), 0.87 (s, 3H), 0.81 (s, 3H), 0.69 (s, 3H); ^{13}C NMR (101 MHz, $CDCl_3$) δ 168.9 (C=O), 143.4 (CH=C), 134.6 (C=C), 134.5 (C=C), 127.2 (C=C), 79.1 (CH), 51.8 (CH_3), 50.54 (CH), 50.46 (CH), 50.0 (C), 44.7 (C), 39.0 (C), 37.2 (C), 36.5 (CH), 35.7 (CH_2), 35.1 (CH_2), 31.1 (CH_2), 31.0 (CH_2), 28.3 (CH_2), 28.1 (CH_3), 28.0 (CH_2), 26.6 (CH_2), 25.8 (CH_2), 24.4 (CH_3), 21.1 (CH_2), 19.3 (CH_3), 18.7 (CH_3), 18.4 (CH_2), 15.9 (CH_3), 15.6 (CH_3), 12.5 (CH_3); HRMS (ESI) m/z ($M^{\cdot}$+Na)$^+$ 493.3659, $C_{31}H_{50}NaO_3$ requires ($M^{\cdot}$+Na)$^+$ 493.3652 (Δ 1.4 ppm).

7.2. Biological methods

7.2.1. Materials and methods

a. Natural and synthetic ganoderic acids (GA)

GA-H (>95%) was purchased from Planta Analytica (Danbury, USA); GA-T (99%) was provided by Dr Jian-Jiang Zhong from Shangai Jiao Tong University. All synthetic ganoderic acids were prepared as indicated in the synthesis part of this chapter. GAs stock solution were dissolved in 100% methanol to a final concentration of 20 mM and diluted with appropriate growing medium (RPMI or keratinocyte) to give the desired stock solution (400 -1800 μM).

b. Tissue culture

i. Cell-lines

Prostate cell-lines PC3, PC3M, DU145, LNCaP, RWPE1, WPE1-NB14 and -NB26 were used in this study. A brief description of each cell-line follows.

I. Prostate cancer cell-lines

(a) PC3

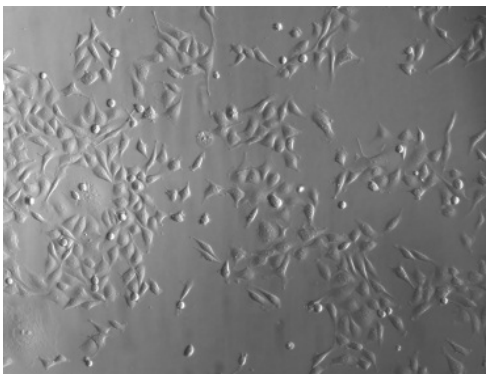


Figure 7.2 PC3 cell-line. Picture was taken from a 24 well plate well after 24 h of seeding. Wells were supplied with $5x10^4$ cells (passage 16) suspended in 500 μL RPMI 1640.

PC3 is an epithelial cell-line that was derived from a lumbar vertebral metastasis in a 62-year-old white man. The cells are fast growing, with a doubling time of 33 hours, and their growth is not stimulated by growth factors. They are aneuploidal (58 chromosomes at passage 30).

Furthermore, they express cytokeratin (CK) 5, 8 and 18, but not AR, PSA, or hK2.[119]

(b) PC3M-luc2

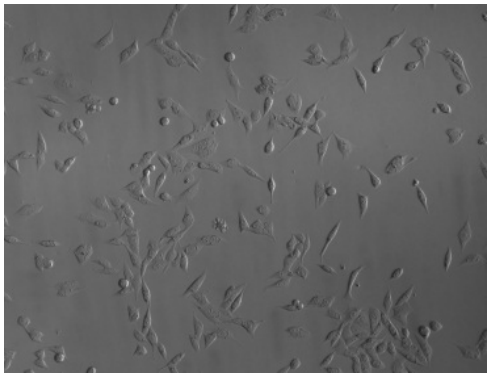


Figure 7.3 PC3M-luc2a cell-line. Picture was taken from a 24 well plate well after 24 h of seeding. Wells were supplied with $5x10^4$ cells (passage 53) suspended in 500 μL RPMI 1640.

PC3M was derived from a PC3 xenograft. Compared with PC3, PC3M has a more aggressive phenotype. PC3M-luc2 is the luciferase expressing version of PC3M cell-line. They express normal levels of prostatic acid phosphatase (PAP), CK 8 and 18 and fail to express CK 5 and 15. As with any PC3 cell-line, they do not express AR, PSA or hK2.[119]

(c) DU145

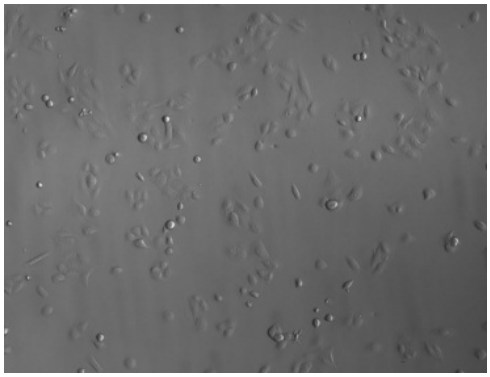


Figure 7.4 DU145 cell-line. Picture was taken from a 24 well plate well after 24 h of seeding. Wells were supplied with $5x10^4$ cells (passage 19) suspended in 500 μL RPMI 1640.

DU145 are epithelial cells derived from a tumour mass extirpated from the brain of a 69-year-old white man with PCa and lymphocytic leukaemia. This cell-line expresses CK-7, 8, 18, 19 and low levels of PAP, but it not expresses CK-5, 14, AR, PSA, hK2 nor neuroendocrine markers. This is also a fast

growing cell-line, with a doubling time of 34 hours. The number of chromosomes at passage 57 varied from 46 to 143 with modal number (MN) 64.[119]

(d) LNCaP

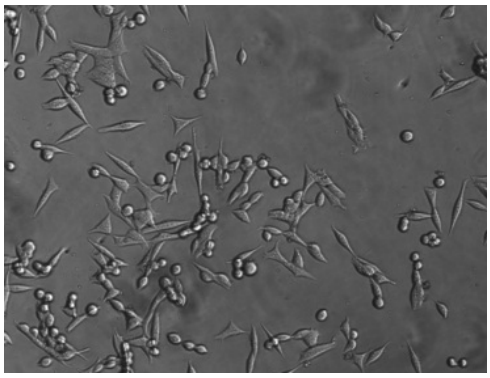


Figure 7.5 LNCaP cell-line. Picture was taken from a 24 well plate well 72 h of seeding. Wells were supplied with $5x10^4$ cells (passage 11) suspended in 500 μL RPMI 1640.

LNCaP cells were isolated from a lymph node metastatic lesion of a 50-year-old white man. These cells are semi-adherent with doubling growing times of 60 hours. LNCaP cells detach at high densities as sheets, making cell counts unreliable. Besides, trypsinization of cells results in cell clumps, also burdening the counting. However, this problem may be sorted by vigorous pipetting after trypsinization. They grow well in medium containing fetal bobine serum (FBS) at concentrations of 2.5% to 10%. Lower amounts result in delayed doubling times.

The karyotype of this type of cells is highly aneuploidal (33 to 91 chromosomes) with an MN of 76 to 91. LNCaP express PSA, AR, CK-8, 18, but they do not express CK-5, 14. Interestingly, AR has a T877A mutation that results in a promiscuous response to androgens.[119]

Characteristic	**Cell-line**			
	PC3	**PC3M-luc2**	**DU145**	**LNCaP**
Androgen sensitivity	No	No	No	Yes
PSA/hK2/AR	No	No	No	RNA+protein
CKs + other markers	5, 8, 18	PAP, 8, 18	PAP, 7, 8, 18, 19	8, 18
Doubling time	33		34	60
Derivation	Vertebrae	PC3	Brain	Lymph node

Table 7.1 Prostate cancer cell-lines used for biological evaluation of GAs.

II. Non-cancerous and pre-malignant cell-lines

(a) RWPE-1

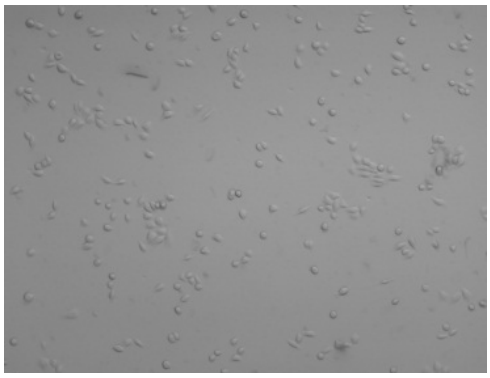


Figure 7.6 RWPE1 cell-line. Picture was taken from a 24 well plate well after 24 h of seeding. Wells were supplied with $5x10^4$ cells (passage 57) suspended in 500 μL keratinocyte medium.

The normal RWPE-1 cell-line was derived from ephithelial cells taken from the peripheral zone of a non-neoplastic adult human prostate in a 54-year-old white man. The cells were immortalized with human papilloma virus (HPV) 18. This cell-line shows typical polygonal, epithelial morphology; strong positive cytoplasmic staining for CK-8 and 18, as well as being responsive to androgens (149%); whilst nuclear staining of AR and cytoplasmic staining of PSA were observed after administration of the synthetic androgen mibolerone, no staining was noted in the absence of this androgen. RWPE-1 is a slow growing cell-line with average doubling time of 120 h. It is sensitive to growth factors for growing stimulation 150% (epithelial growth factor (EGF)) or inhibition 63% (transforming growth factor-β (TGF-β)). However, it fails to display anchorage independent growth; invasive ability (1%) or formation of tumours in nude mice. This is an aneuploid human line composed of two cell populations, one with MN 45 and the other 51 chromosomes.[121-123]

(b) WPE1-NB14

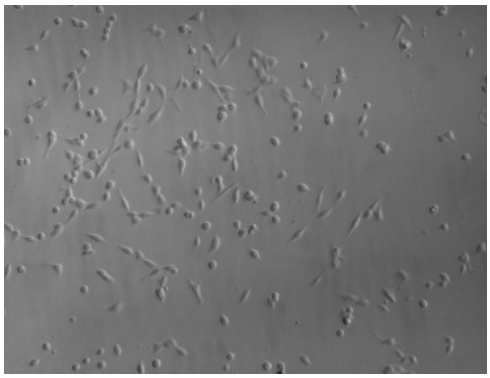


Figure 7.7 WPE1-NB14 cell-line. Picture was taken from a 24 well plate well after 24 h of seeding. Wells were supplied with $5x10^4$ cells (passage 35) suspended in 500 μL keratinocyte medium.

WPE1-NB14 was derived from RWPE1 by treating the latter cell-line with carcinogen *N*-methyl-*N*-nitrosourea (MNU) at a concentration of 100 g/mL. Cells were stablished after the second generation of tumours. This cell-line has a slightly elongated epithelial morphology and, as its parent, it expresses CK-8 and 18; it is sensitive to androgens (AR located in nucleus but heterogeneous and PSA in cytoplasm). Compared with RWPE-1, this cell-line grows faster with a doubling growing time of 45 h. It is sensitive to growth factors for growth and inhibition; EGF stimulated the proliferation by 139% whilst FGB-β inhibited it by 40%. This cell-line has the ability to form colonies in 1.85% efficiency. It is slightly more aggressive than its parent with 30% invasiveness. In addition, it forms less differentiated tumours.[121,122]

(c) WPE1-NB26

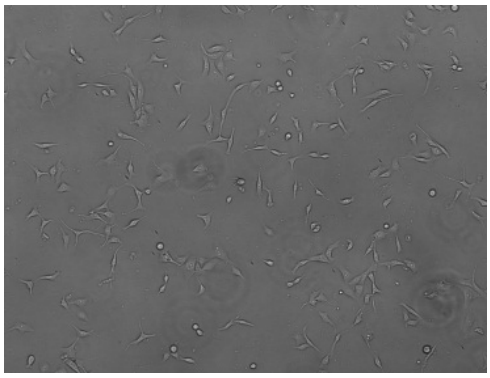


Figure 7.8 WPE1-NB26 cell-line. Picture was taken from a 24 well plate well after 24 h of seeding. Wells were supplied with $5x10^4$ cells (passage 19) suspended in 500 μL keratinocyte medium.

WPE1-NB26 were derived in the same way as WPE1-NB14. This cell-line shows an elongated epithelial morphology, expresses CK-8 and 18 and it is responsive to androgens (AR detected in nucleus and PSA in cytoplasm). It has doubling growing times of 40 h and although it is sensitive to growth factors, the response is lower than its parent or WPE1-NB14. Thus, its growth is stimulated 122% by EGF and inhibited 33% by TGF-β, both at concentration 10 ng ml^{-1} and compared to untreated control. WPE1-NB26 cell-line presents the highest colony forming efficiency (2.58%) and invasion ability (95%). Its invasion capacity is comparable to DU145 (100%). Besides, it forms poorly differentiated tumours with invasive characteristics.[121,122]

Characteristic	RWPE1	WPE1-NB14	WPE1-NB26
Ck 8, 18	+	+	+
AR	+	+[a]	+
PSA	+	+	+
Doubling time/h	120	45	40
EGF stimulation[b]	150	139	122
TGF-β inhibition[b]	40	40	33
% CFE	0	1.85	2.58
% Invasion (DU145 100%)	1	30	95

Table 7.2 General characteristic of normal and pre-malignant cell-lines. [a] Heterogeneous nuclear staining; [b] Effect at [growth factor]=10 ng mL^{-1} compared with untreated control; CFE=colony forming efficiency.

ii. Cell culture

Prostate cancer cell-lines were cultivated in RPMI-1640 medium (Sigma-Aldrich) containing 10% fetal bovine serum (FBS) and 2 mM L-glutamine (Sigma-Aldrich). Non-cancerous prostate cell-lines were maintained in keratinocyte-serum free medium with 2.5 μg Epidermal Growth Factor and 25 mg Bovine Pituitary Extract (Invitrogen, Paisley, UK).

All the tissue culture work was performed in a Class II safety cabinet, which was sterilised with Distel before and after use. Sterile techniques were used throughout.

The cells were incubated at 37 °C in humidified 5 % v/v CO_2 conditions, grown for a maximum of two months and monitored monthly for mycoplasma contamination.

i. Cell-line maintenance

1. Frozen cell recovery

A frozen cell aliquot (1 mL vial) from the -80 °C freezer or liquid nitrogen bank was defrosted in a water bath at 37 °C for 1-2 minutes, followed by immediate vial transfer to a universal tube containing 19 mL of medium. The universal tube containing the cell suspension was centrifuged in a Heraeus Mega 16 Centrifuge (Thermo Scientific) at 8497 *g* (5000 rpm) or a Harrier 15/80 (MSE) at 6708 *g* (5000 rpm). The medium was aspirated and the pellet vortexed before and after re-suspension in fresh medium (2 mL). The whole of this new cell suspension was pipetted in to a T75 cm^2 flask (Corning, Fisher Scientific, UK) and diluted with media (11 mL). The flask was incubated at 37 °C for 16 h to allow cell attachment to the bottom of the flask. Cells were monitored on daily basis; if the flask was less than 70% confluent, the medium was changed; otherwise cells were split. The flask was labelled with the resuscitating and monitoring date, cell-line name, passage and final medium volume.

2. Freezing cells

In order to keep a stock of cells with low passage, an aliquot of cells were re-frozen after resuscitating them. A harvested sub-confluent flask (70-80% confluence) was treated as indicated in the subculture routine for recovering the cells as pellet. The pellet was vortexed and re-suspended in a medium with 10% DMSO (1 mL). The cell suspension was immediately transferred to a cryogenic vial which was labelled with the cell-line name, passage and date and placed in a -80 °C freezer. At that temperature the cells decayed considerably after 4 months storage.

3. Subculture routine

Cells were monitored daily to check cell morphology and cell density. Cells were harvested and sub-cultured at 70-80% confluence in T75 cm^2 flasks, when a large number of cells were needed T225 cm^2 flasks were used instead. Every 48 h, flasks exhibiting a greater than 70-80% confluence

were split to reduce cell number. However, if the confluence was lower than 70% the medium was changed.

a) Re-feeding (<70% confluence)

The media was aspirated from the flask using a sterile Pasteur pipette attached to a vacuum line. New growth media (13 mL for T75 cm^2; 4 mL for T25 cm^2 or 33 mL for T225 cm^2) was pipetted into the flask very gently through the opposite wall of the flask where cells laid to avoid cell detachment. The flask was then placed in the incubator.

b) Splitting (>70% confluence)

The media was aspirated using a sterile Pasteur pipette attached to a vacuum line. Phosphate buffered saline solution (PBS) (3 mL for T75 cm^2; 1 ml for T25 cm^2 or 9 mL for T225 cm^2) was added and the flask was gentle swung so that the media was washed off the flask, the PBS was removed from the flask with the aid of a sterile pipette and trypsin (Sigma-Aldrich) or 0.025% sterile solution of ethylendiaminetetraacetic acid (EDTA) (4 mL for T75 cm^2; 2 ml for T25 cm^2 or 12 mL for T225 cm^2) was added. EDTA was preferred for LNCaP cell-line. The flask was incubated at 37 °C for 5-10 min, after removing it from the incubator; the flask was gently tapped to detach all the cells. The cell suspension was pipetted with a sterile pipette and returned to the flask passing it through the wall where the cells were attached, this process was repeated twice. Following this, the cell suspension was transferred to an universal tube. Finally the flask was washed twice with fresh media (6 mL for T75 cm^2; 3 ml for T25 cm^2 or 12 mL for T225 cm^2). This second media was combined with the trypsin cell suspension. The universal container was centrifuged in a Heraeus Mega 16 Centrifuge (Thermo Scientific) at 8497 *g* (5000 rpm) or a Harrier 15/80 (MSE) at 6708 *g* (5000 rpm) for 5 min. The supernatant solution was aspirated; the pellet was vortexed before and after being re-suspended in media (3-5 mL depending on cell-line). 1 mL (~1-2x10^6 cell mL^{-1} for T75 cm^2, 0.5x10^6 cell mL^{-1} for T25 cm^2 or 4x10^6 cell mL^{-1} for T225 cm^2) of this cell suspension was transferred to a new flask and the flask was re-fed with media (12 mL for T75 cm^2, 3 mL for T25 cm^2 or 32 mL for T225 cm^2). The flask was placed in the incubator at 37 °C.

ii. Cell counting

(a) Sample preparation

The pellet obtained as indicated in the splitting process was re-suspended in 8-10 mL of growing media and the cell suspension was passed through a syringe attached to a green 21 gauge 50 mm (2 inch) length sterile hypodermic needle (Becton Dickinson BD Microlance 3), the suspension was transferred gently from the syringe to the walls of the universal tube, this process was repeated 3-4 times to break any cell lump. A 1:1 mixture of trypan blue (50 μL) and cell suspension (50 μL) was placed in an Eppendorf tube. This mixture was properly homogenised by pipetting up and down several times. Four sample mixtures were prepared in this manner.

(b) Haemocytometer

Cells were counted using a Haemocytometer, which was prepared as follows. A cover slip was placed over the two chambers of the Haemocytometer making sure that it was well adhered to the surface (Newton's rings were visible). Eventually, each chamber was filled in with a small amount of the trypan/cell suspension mixture, a different Eppendorf was used for each chamber. As four samples were prepared, four counts were made.

(c) Cell count

The Haemocytometer is a glass slide containing two chambers each with a 3 X 3 grid (Figure 7.9 **A**). Each of the squares, labelled A-I has a surface area A = 1 mm^2 and volume V = 0.1 mm^3. The middle square, E (Figure 7.9 **B**), consists of a triple line 5 X 5 grid, each of which subdivided in a 4 X 4 grid. Counts were mainly performed in the E grid having the microscope set at 10X. Cells were counted bottom to top, starting from square 25 to 1 in zigzag. Cells outside the borders, touching the bottom or the left sides and cells crossing the middle line of the square were disregarded from the count. Figure 7.9 **C** shows a grid with counted cells, yellow dots represent the excluded cells; blue dots are dead cells, and the brown dots with numbers are the counted cells.

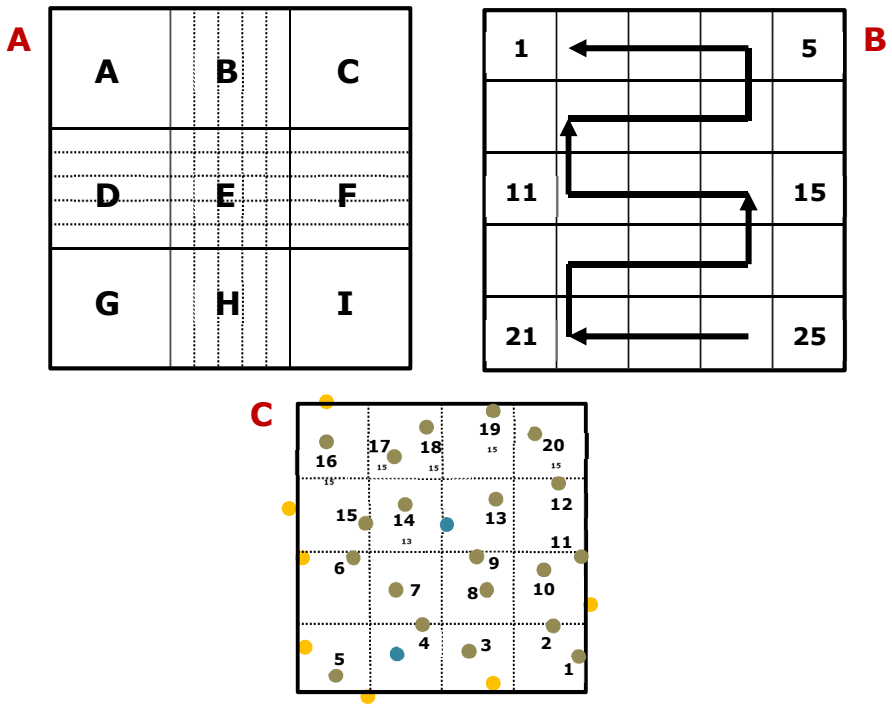


Figure 7.9 Haemocytometer for cell counting. **A.** Haemocytometer full counting chamber consisting of a grid with nine squares, labelled A-I, each square with a total area A = 1.0 mm^2 and volume V = 0.1 mm^3. **B.** Expansion of square E, subdivided in 25 smaller squares, cells counted from bottom to top in zigzag, starting at square 25. **C.** Cells counted, blue dots represent dead cells and yellow ones are the cells to disregard from counting.

Cell concentration was calculated according to equation E1:

$$[Cell] = \frac{number\ of\ cells}{number\ of\ squares \cdot volume \cdot dilution\ factor} \qquad \text{(E1)}$$

Where number of cells is the mean of four counts, the number of squares is the number of squares that were counted in the chamber, which in this case is 1, since only square E was counted; each square has a volume of V = 0.1 mm^3 = $1x10^{-4}$ mL and the sample was diluted 1:2, so the dilution factor is ½. Reordering E1 results:

$$[Cell] = number\ of\ cells\ x\ 2x10^4 \qquad \text{(E2)}$$

Cell concentration has dimensions of cells mL^{-1}.

Likewise, the cell viability was calculated according equation E3:

$$\%Viability = \frac{Number\ of\ viable\ cells}{Total\ number\ of\ cells}\ 100 \qquad \text{(E3)}$$

Viability is defined as the number of viable cells divided by the total number of cells multiplied by 100. Where the number of viable cells is the mean of the four counts and the total number of cells is the sum of the number of viable cells plus the mean of the dead cells in the four counts.

7.2.2. Cell proliferation assay

All the proliferation assay were performed with methylthiazolyldiphenyl-tetrazolium bromide (MTT, Sigma-Aldrich). Assays were carried out in 96-microtitre well plates (Corning, Fisher Scientific, UK). Each well was filled in with 100 μL of cell suspension and plates were incubated at 37 °C for over 16 h to allow for cell adherence. Plates were monitored under the microscope for well uniformity. The medium was aspirated and 200 μL of increasing concentrations of natural or synthetic GA ranging from 0 up to 2000 μM was platted to treat the cells. Each GA dilution was replicated five or six times. Non-treated cells were included as control. Plates were incubated at 37 °C for 24h, 48 h or 72 h, as indicated. After the required exposure time, 50 μL MTT solution (1 $\mu g \cdot mL^{-1}$) was added to each well and the plate was incubated for 4 h at 37 °C. The culture medium was aspirated and replaced by DMSO (75 μL). The plates were read on a MRX Revelation at 550 nm.

7.2.3. Statistical analysis

Inhibition curves were generated with GraphPad Prism 7.0 software. The blank was deducted from absorbance values generated from the instrument, when the blank was not directly on the plate, an average blank of A=0.047±0.006 was considered. Top and bottom plateaus were constrained to 100 and 0, respectively. Equation chosen was the best fit between log(inhibition) vs response variable slope (4 parameters) and biphasic. Data is presented as the mean±SD of at least three independents experiments unless otherwise stated.

7.3. *Ganoderma lucidum* extracts

7.3.1. Mushroom material

Fruiting bodies of *Ganoderma lucidum* (Fr.) P. Karst cultivated on sawdust from rubber tree plantation (Malaysia), were supplied dried and chopped by the Ganofarm Sendirian Berhad firm (Malaysia). They supplied mushrooms

2, 4, 6 and 8 weeks old as well as an "antler" variety 6 weeks old. Two week samples were split into tip and stalk.

Mature fruiting bodies of *Ganoderma lucidum* (Fr.) P. Karst cultivated on oil palm fibres such as empty fruit bunch fibre (EFB) and mesocarp fibre (4 weeks old), were supplied dried and finely ground by Surya M. Sudheer from Prof. S. Manickam research group at Manufacturing and Industrial Processes Research Division, Faculty of Engineering, University of Nottingham Malaysia Campus. Samples were kept at 0 °C.

7.3.2. Mushroom extraction

Two methods were used for the extraction of the mushrooms, Soxhlet and sonication.

(a) Soxhlet extraction

Approximately 12 g of dry mushroom sample was weighted out and inserted in a 33 X 100 mm^2 Soxhlet thimble; 300 mL of solvent was added in a round bottom flask and the system was heated at reflux for 16h. After which time, the solvent was evaporated at reduced pressure and the crude extract was transferred to a vial, dried at high vacuum and kept in the fridge at 0 °C. About 0.5-1.0 g of extract was obtained. Solvents used for extraction were ethanol, methanol, dichloromethane, ethyl acetate and water.

(b) Sonication

Six-week old dry mushroom (12 g) was suspended in a 250 mL round bottom flask containing chloroform (100 mL). The flask was sonicated in a Kerry KC3 ultrasonic bath for 2 h at room temperature, after which time, the coloured solution was filtered and replaced with new solvent, the sonication process was repeated three times. The combined filtrates were evaporated under reduced pressure leaving a yellow crude residue.

7.3.3. Mass spectrometry

The mushroom extracts were analysed with a Bruker micrOTOF (time of flight) Open Access instrument, which was operated in flow injection mode, using 50% MeOH:water as eluent. The system is a Time-of-Flight mass spectrometer with a mass resolution of 12000 and a working mass range of 50-3000 Da.

The Open Access system operates by firstly injecting a solution of sodium formate (10 nM) followed by injection of the sample (1 μL) 30 s thereafter, so that mass calibration is assured in each sample.

7.3.4. LCMS

LC-MS was performed on a Varian Pro Star HPLC equipped with a binary solvent delivery system, autosampler and coupled with a Varian 310 MS detector. A SunFire C18 column (4.6 x 150 mm^2; 5 μm) set at 50 °C; was applied for all the analysis. The mobile phase consisted of 0.1% (V/V) aqueous formic acid (A) and 0.1% formic acid (V/V) in acetonitrile (B). Elution was at gradient as stated below (Table 7.3):

T/min.	0	15	21	25	25.01	28
%B	30	55	95	95	30	30

Table 7.3 LC-MS gradient conditions.

The flow rate was 0.8 mL min^{-1}, with multichannel UV detection set at 210 nm and 254nm and MS with positive ion detection scanning at 300-700 m/z.

7.3.5. Mushroom extract stock solution

Mushroom extract stock solution (20 mL) of 2000 μg mL^{-1} were prepared by weighing out 40 mg of sample, which was dissolved in 100% methanol (1 mL) and sonicated for 3 min. This solution was diluted with RPMI-1640 (19 mL) containing 10% FBS and 2 mM *L*-glutamine.

7.3.6. Proliferation assay

Cell viability was evaluated against three prostate cancer cell-lines: PC3M-luc2, DU145 and LNCaP by using the MTT assay. Briefly, 100 μL of cell suspension at concentrations $4.5x10^4$ cells mL^{-1} for both DU145 and LnCAP cell-lines and $3.0x10^4$ cells mL^{-1} for PC3M were plated in 96 well plates. Plates were incubated for 24 h to allow cells to attach to the well, RPMI medium was aspirated and replaced by 200 μL of RPMI with mushroom extract at concentrations ranging from 0 to 2000 μg mL^{-1}, every concentration was replicated six times. Plates with mushroom extracts were incubated at 37 ºC for 72 h, 50 μL MTT (1 mg·mL^{-1}) solution in PBS was then dispensed in each well and the plates incubated for 4h. The medium was

aspirated and replaced by 75 μL DMSO, plates were vigorously shacken before reading using a MRX Revelation plate reader at 550 nm.

7.3.7. Statistical analysis

Inhibition curves were generated with GraphPad Prism 7.0 software. An average blank (A=0.047±0.006) was deducted from the absorbance. Top and bottom plateaus were constrained to 100 and 0, respectively. The data was fitted to a sigmoidal curve using the 4-parameter equation and the calculated values are presented as the mean±SD of at least two independents experiments unless otherwise stated.

8. References

1. J. E. Galagan, M. R. Henn, L. J. Ma, *et al.*, *Genome Res.*, *15*, **2005**, 1620-1631.
2. M. Blackwell, *Am. J. Bot.*, *98*, **2011**, p. 426-438.
3. M. B. Quin, C. M. Flynn and C. Schmidt-Dannert, *Nat. Prod. Rep.*, *31*, **2014**, 1449-1473.
4. V. E. C. Ooi, *Medicinally important fungi*, *Mushr. Sci., 15*, **2000**, 41-51.
5. I. Ferreira, J. A. Vaz, M. H. Vasconcelos, *et al.*, *Anticancer Agents Med. Chem.*, *10,* **2010**, 424-436.
6. S. P. Wasser, *Int. J. Med. Mushrooms*, *12,* **2010**, 1-16.
7. R. Wagner, D. A. Mitchell, G. L. Sassaki, *et al.*, *Food Technol. Biotechnol.*, *41*, **2003**, 371-382.
8. R. Russell and M. Paterson, *Phytochemistry*, *67*, **2006**, 1985-2001.
9. X. W. Zhou, J. Lin, Y. Z. Yin, *et al*., *Am. J. Chin. Med.*, *35*, **2007**, 559-574.
10. J. W. Xu, W. Zhao, *et al*., *Appl. Microbiol. Biot.*, *87*, **2010**, 457-466.
11. L. A. Shi, A. Ren, D. S. Mu, *et al*., *Appl. Microbiol. Biot.*, *88*, **2010**, 1243-1251.
12. M. S. Shiao, *Chem. Rec.*, *3*, **2003**, 172-180.
13. Q.-X. Yue, F.-B. Xie, S.-H. Guan, *et al.*, *Cancer Sci.*, *99*, **2008**, 1461-1470.
14. S. Cheng and D. Sliva, *Integr. Cancer Ther.*, *14*, **2015**, 249-257.
15. Q. Xia, H. Z. Zhang, X. F. Sun, *et al*., *Molecules*, *19*, **2014**, 17478-17535.
16. B. S. Gill, P. Sharma, R. Kumar, *et al*., *Tumor Biol*., *37*, **2016**, 2789-2804.
17. M. Mistry, D. M. Parkin, A. S. Ahmad, *et al.*, *Brit. J. Cancer*, *105*, **2011**, 1795-1803.
18. P. Kheirandish and F. Chinegwundoh, *Brit. J. Cancer*, *105*, **2011**, 481-485.
19. R. Chen, S. Ren, C P C Consortium, *et al*., *Asian J. Urol.*, *1*, **2014**, 15-29
20. C. Jeronimo, P. J. Bastian, A. Bjartell, *et al*., *Eur. Urol.*, *60*, **2011**, 753-766.
21. J. Liu, K. Kurashiki, K. Shimizu, *et al*., *Bioorg. Med. Chem.*, *14*, **2006**, 8654-8660.
22. Y. Niu, T. M. Chang, S. Yeh, *et al.*, *Oncogene*, *29*, **2010**, 3593-3604.
23. S. Bayraktar, *Open Prost. Cancer J.*, *3*, **2010**, 47-56.

24. B. M. Johnson, B. P. Doonan, F. F. Radwan, *et al.*, *Open Prost. Cancer J., 3*, **2010**, 78-85.
25. E. M. Wilson, *Ther. Adv. Urol.*, *2*, **2010**, 105-117.
26. J. Jiang, B. Grieb, A. Thyagarajan and D. Sliva, *Int. J. Mol. Med., 21*, **2008**, 577-584.
27. G. Wang, J. Zhao, J. Liu, *et al*., *Int. Immunopharmacol.*, *7*, **2007**, 864-870.
28. N.-H. Chen, J.-W. Liu and J.-J. Zhong, *J. Pharmacol. Sci.*, *108*, **2008**, 212-216.
29. W. Tang, H.-W. Liu, W.-M. Zhao, *et al*., *Life Sci.*, *80*, **2006**, 205-211.
30. J. Liu, J. Shiono, K. Shimizu, *et al.*, *Bioorg. Med. Chem. Lett.*, *19,* **2009**, 2154-2157.
31. I. Miyamoto, J. Liu, K. Shimizu, *et al.*, *Eur. J. Pharmacol.*, *602*, **2009**, 1-7.
32. J. Liu, J. Shiono, Y. Tsuji, *et al*., *Open Bioactive Compound. J.*, *2*, **2009**, 37-42.
33. J. Liu, K. Shimizu, A. Tanaka, *et al*., *Sci. Rep.*, *2*, **2012**, 905.
34. N. Van Thu, T. Nguyen The, C. To Dao, *et al*., *Phytochem. Lett.*, *12*, **2015**, 69-74.
35. Y. Fang Lee, Doctor of Philosophy thesis, University of Nottingham, **2011**.
36. D. Wallock, Master of Research thesis, University of Nottingham, **2010**.
37. L. K. Kavtaradze, M. Manley-Harris and B. K. Nicholson, *Steroids*, *69*, **2004**, 697-700.
38. L. K. Kavtaradze, M. Manley-Harris and B. K. Nicholson, *Steroids*, *69*, **2004**, 227-233.
39. R. O'Keeffe, O. Kenny, N. P. Brunton, *et al.*, *Bioorg. Med. Chem.*, *23*, **2015**, 2270-2280.
40. J. S. Liu and Y. Tao, *Tetrahedron*, *48,* **1992**, 6793-6798.
41. W. R. Bartlett, W. S. Johnson, M. S. Plummer, *et al*., *J. Org. Chem., 55*, **1990**, 2215-2224.
42. D. Yang and C. Zhang, *J. Org. Chem.*, *66*, **2001**, 4814-4818.
43. P. C. Gareiss, P. B. Palde, R. D. Hubbard, *et al*., *Eur. J. Org. Chem.*, *1*, **2007**, 53-61.
44. T. C. Zheng and D. E. Richardson, *Tetrahedron Lett.*, *36,* **1995**, 833-836.
45. S. Baskaran, J. Das and S. Chandrasekaran, *J. Org. Chem.*, *54,* **1989**, 5182-5184.
46. D. G. Lee and T. Chen, *J. Am. Chem. Soc.*, *111*, **1989**, 7534-7538.
47. F. Freeman, C. O. Fuselier, C. R. Armstead, *et al.*, *J. Am. Chem. Soc.*, *103*, **1981**, 1154-1159.
48. Y. Sato and Y. Sonoda, *Chem. Pharm. Bull.*, *29*, **1981**, 356-365.

49. K. C. Nicolaou, V. A. Adsool and C. R. H. Hale, *Org. Lett.*, *12*, **2010**, 1552-1555.
50. B. Plietker and M. Niggemann, *Org. Lett.*, *5*, **2003**, 3353-3356.
51. K. Mori, T. Ohtaki, H. Ohrui, D. R. Berkebile, *et al*., *Biosci. Biotechnol. Biochem.*, *68*, **2004**, 1768-1778.
52. M. Uyanik and K. Ishihara, *Chem. Commun.*, **2009**, 2086-2099.
53. H. Takayanagi, S. Sugiyama and Y. Morinaka, *J. Chem. Soc. Perkin Trans. 1*, **1995**, 751-756.
54. R. Csuk, A. Barthel, S. Schwarz, *et al.*, *Bioorg. Med. Chem. 18*, **2010**, 2549-2558.
55. A. L. Howard, J. L. Liu, G. A. Elmegeed, *et al.*, *Arch. Biochem. Biophys.*, *521*, **2012**, 43-50.
56. A. Rahier, M. Taton and P. Benveniste, *Eur. J. Biochem.*, *181*, **1989**, 615-626.
57. J. F. Cheng, J. Kobayashi, H. Nakamura, *et al*., *J. Chem. Soc. Perkin Trans. 1*, **1988**, 2403-2406.
58. D. R. Idler, L. M. Safe and S. H. Safe, *Steroids*, *16*, **1970**, 251-262.
59. R. B. Clayton, *Nature*, *190*, **1961**, 1071-1072.
60. C. Menozzi-Smarrito, C. E. Riera, C. Munari, *et al*., *J. Agric. Food Chem.*, *57*, **2009,** 1982-1989.
61. R. Ocampo and W. R. Dolbier, *Tetrahedron*, *60*, **2004**, 9325-9374.
62. T. Scherkenbeck and K. Siegel, *Org. Process Res. Dev.*, *9*, **2005**, 216-218.
63. A. Chattopadhyay and A. K. Dubey, *J. Org. Chem.*, *72*, **2007**, 9357-9359.
64. K. Bang, K. Lee, Y. K. Park, *et al*., *Bull. Korean Chem. Soc.*, *23*, **2002**, 1272-1276.
65. T. Poisson, M. C. Belhomme and X. Pannecoucke, *J. Org. Chem.*, *77*, **2012**, 9277-9285.
66. W. Kemp, *Organic Spectroscopy*, Palgrave, New York, Third edn., **1991**.
67. W. A. White and H. Weingarten, *J. Org. Chem.*, *32*, **1967**, 213-214.
68. G. Stork, J. Szmuszkovicz, R. Terrell, *et al*., *J. Am. Chem. Soc.*, *85*, **1963**, 207-222.
69. K. C. Brannock, C. A. Kelly, R. D. Burpitt, *et al*., *J. Org. Chem.*, *29*, **1964**, 801-812.
70. N. L. Allinger, J. C. Graham and B. B. Dewhurst, *J. Org. Chem.*, *39*, **1974**, 2615-2617.
71. G. Belanger, M. Dore, F. Menard, *et al*., *J. Org. Chem.*, *71*, **2006**, 7481-7484.
72. C. E. Harris, W. Chrisman, S. A. Bickford, *et al.*, *Tetrahedron Lett.*, *38*, **1997**, 981-984.
73. M. G. Vetelino and J. W. Coe, *Tetrahedron Lett.*, *35*, **1994**, 219-222.

74. M. Hunsen, *Synthesis-Stuttgart*, **2005**, 2487-2490.
75. B. R. Travis, M. Sivakumar, G. O. Hollist, *et al*., *Org. Lett.*, *5*, **2003**, 1031-1034.
76. R. K. Thaper, A. Y. Zykov, Y. N. Bubnov, *et al*., *Synthetic Commun.*, *23*, **1993**, 939-947.
77. J. Hasserodt, K. D. Janda and R. A. Lerner, *J. Am. Chem. Soc.*, *122*, **2000**, 40-45.
78. J. O. Toth, B. Luu and G. Ourisson, *Tetrahedron Lett.*, *24*, **1983**, 1081-1084.
79. J. Bujons, R. Guajardo and K. S. Kyler, *J. Am. Chem. Soc.*, *110*, **1988**, 604-606.
80. S. D. Meyer and S. L. Schreiber, *J. Org. Chem.*, *59*, **1994**, 7549-7552.
81. Y. Watanabe, K. Soda, K. Kamigori, T. Miyoshi,. Jpn. Kokai Tokkyo Koho **1990**, 5 pp. JP 02167295. Application: JP 87-299041 19871127.
82. H. J. Zhang, G. T. Tan, V. D. Hoang, *et al*., *J. Nat. Prod.*, *66*, **2003**, 263-268.
83. T. Oguchi, K. Watanabe, K. Ohkubo, *et al*., *Chem. Eur. J.*, *15*, **2009**, 2826-2845.
84. S. D. Lepore and Y. He, *J. Org. Chem.*, *68*, **2003**, 8261-8263.
85. O. Mitsunobu and M. Yamada, *Bull. Chem. Soc. Jpn.*, *40*, **1967**, 2380-2382.
86. O. Mitsunobu, M. Yamada and Mukaiyam.T, *Bull. Chem. Soc. Jpn.*, *40*, **1967**, 935-939.
87. K. C. K. Swamy, N. N. B. Kumar, E. Balaraman, *et al.*, *Chem. Rev.*, *109*, **2009**, 2551-2651.
88. I. Dostrovsky and E. D. Hughes, *J. Chem. Soc.*, **1946**, 157-161.
89. I. Dostrovsky and E. D. Hughes, *J. Chem. Soc.*, **1946**, 161-164.
90. I. Dostrovsky and E. D. Hughes, *J. Chem. Soc.*, **1946**, 164-165.
91. I. Dostrovsky and E. D. Hughes, *J. Chem. Soc.*, **1946**, 166-169.
92. R. M. Moriarty, H. Zhuang, R. Penmasta, *et al.*, *Tetrahedron Lett.*, *34,* **1993**, 8029-8032.
93. J. A. Dodge and C. W. Lugar, *Bioorg. Med. Chem. Lett.*, *6*, **1996**, 1-2.
94. C. J. Ahn, R. Correia and P. DeShong, *J. Org. Chem.*, *67*, **2002**, 1751-1753.
95. D. L. Hughes and R. A. Reamer, *J. Org. Chem.*, *61*, **1996**, 2967-2971.
96. V. Weidmann and W. Maison, *Synthesis-Stuttgart*, *45*, **2013**, 2201-2221.
97. N. Mazoir, A. Auhmani, M. Daoubi, *et al*., *Synthetic Commun.*, *37*, **2007**, 1289-1299.

98. B. B. Shingate, B. G. Hazra, D. B. Salunke, *et al*., *Tetrahedron Lett.*, *52*, **2011**, 6007-6010.

99. R. A. Miller, W. J. Li and G. R. Humphrey, *Tetrahedron Lett.*, *37*, **1996**, 3429-3432.

100. H. Choi and M. P. Doyle, *Org. Lett.*, *9*, **2007**, 5349-5352.

101. E. C. McLaughlin, H. Choi, K. Wang, *et al*., *J. Org. Chem.*, *74*, **2009**, 730-738.

102. A. Agarwala and D. Bandyopadhyay, *Chem. Commun.*, **2006**, 4823-4825.

103. T. Konoike, Y. Araki and Y. Kanda, *Tetrahedron Lett.*, *40*, **1999**, 6971-6974.

104. E. M. Kennedy, S. J. P'Pool, J. H. Jiang, *et al.*, *J. Nat. Prod.*, *74*, **2011**, 2332-2337.

105. S. M. Silvestre and J. A. R. Salvador, *Tetrahedron*, *63*, **2007**, 2439-2445.

106. P. Marwah, A. Marwah and H. A. Lardy, *Green Chem.*, *6*, **2004**, 570-577.

107. X. R. Peng, J. Q. Liu, Z. H. Han, *et al.*, *Food Chem.*, *141*, **2013**, 920-926.

108. H. C. Huang, C. C. Liaw, H. L. Yang, *et al*., *Phytochemistry*, *84*, **2012**, 177-183.

109. M. A. Umbreit and K. B. Sharpless, *J. Am. Chem. Soc.*, *99*, **1977**, 5526-5528.

110. M. Audouin and J. Levisalles, *Tetrahedron*, *39*, **1983**, 2799-2802.

111. N. Kato, H. Takeshita, H. Kataoka, *et al.*, *J. Chem. Soc. Perkin Trans. 1*, **1989**, 165-174.

112. B. L. Song, N. B. Javitt and R. A. DeBose-Boyd, *Cell Metab.*, *1*, **2005**, 179-189.

113. I. S. Levina, L. E. Kulikova, A. V. Kamernitsky, *et al.*, *Russ. Chem. Bull.*, *54*, **2005**, 2664-2670.

114. B. B. Shingate, B. G. Hazra, D. B. Salunke, *et al.*, *Tetrahedron*, *69*, **2013**, 11155-11163.

115. A. Gioiello, P. Sabbatini, E. Rosatelli, *et al*., *Tetrahedron*, *67*, **2011**, 1924-1929.

116. A. Thyagarajan, A. Jedinak, H. Nguyen, *et al*., *Nutr. Cancer*, *62*, **2010**, 630-640.

117. T. Mosmann, *J. Immunol. Methods*, *65*, **1983**, 55-63.

118. J. L. Sebaugh, *Pharm. Stat.*, *10*, **2011**, 128-134.

119. R. E. Sobel and M. D. Sadar, *J. Urology*, *173*, **2005**, 342-359.

120. F. Alimirah, J. M. Chen, Z. Basrawala, *et al*., *Febs Lett.*, *580*, **2006**, 2294-2300.

121. R. E. Sobel and M. D. Sadar, *J. Urology*, *173*, **2005**, 360-372.

122. M. M. Webber, S. T. A. Quader, H. K. Kleinman, *et al*., *Prostate*, *47*, **2001**, 1-13.

123. D. Bello, M. M. Webber, H. K. Kleinman, *et al.*, *Carcinogenesis*, *18*, **1997**, 1215-1223.

124. E. Simsek, E. A. Aydemir, N. Imir, *et al.*, *Neuropeptides*, *53*, **2015**, 37-43.

125. E. N. Fossum, M. J. Lisowski, T. A. Macey, *et al*., *Brain Res.*, *1204*, **2008**, 53-58.

126. M. Timm, L. Saaby, L. Moesby, *et al.*, *Cytotechnology*, *65*, **2013**, 887-894.

127 O. Desy, D. Carignan, M. Caruso, *et al.*, *Toxicol. Sci.*, *117,* **2010**, 303-313.

128. D. Guenard, F. Guerittevoegelein and P. Potier, *Accounts Chem. Res*., *26*, **1993**, 160-167.

129. H. Hernandez-Vargas, J. Palacios and G. Moreno-Bueno, *Oncogene*, *26*, **2007**, 2902-2913.

130. E. Tsakalozou, A. M. Eckman and Y. Bae, *Biochem. Res. Int.*, 2012, **2012**, 832059-832059.

131. C. R. Cheng, Q. X. Yue, Z. Y. Wu, *et al.*, *Phytochemistry*, *71*, **2010**, 1579-1585.

132. W. Ruan, A. H. H. Lim, L. G. Huang, *et al.*, *Nat. Prod. Res.*, *28*, **2014**, 2264-2272.

133. N. H. Chen, J. W. Liu and J. J. Zhong, *Pharmacol. Rep.*, *62*, **2010**, 150-163.

134. J. Liu, K. Shimizu and R. Kondo, *Fitoterapia*, *81*, **2010**, 1067-1072.

135. J. Liu, K. Kurashiki, K. Shimizu, *et al*., *Biol. Pharm. Bull.*, *29*, **2006**, 392-395.

136. S. M. Singh, S. Gauthier and F. Labrie, *Curr. Med. Chem.*, *7*, **2000**, 211-247.

137. H. C. Trading, Oil Palm Fibre, http://www.hoongchan.com/, (accessed 14Aug2014, 2014).

138. P. Mcintosh, *Ganoderma lucidum*, the Reishi Mushroom, https://suite.io/philip-mcintosh/2y0f2v4, (accessed 14Aug14, 2014).

139. M. Kohguchi, T. Kunikata, H. Watanabe, *et al.*, *Biosci. Biotech. Bioch.*, *68*, **2004**, 881-887.

140. J. J. Gao, A. Hirakawa, B. S. Min, et al., *J. Nat. Med.*, *60*, **2006**, 42-48.

141. Y. Qi, L. L. Zhao and H. H. Sun, *Front. Pharmacol.*, *3,* **2012**.

142. C. R. Cheng, M. Yang, Z. Y. Wu, *et al*., *Rapid Commun. Mass Sp.*, *25*, **2011**, 1323-1335.

143. M. Yang, X. M. Wang, S. H. Guan, *et al.*, *J. Am. Soc. Mass Spectrom.*, *18*, **2007**, 927-939.

144. J. Liu, K. Kurashiki, A. Fukuta, *et al*., *Food Chem.*, *133*, **2012**, 1034-1038.

145. T. Wang, Z. P. Xie, Z. S. Huang, *et al.*, *J. Huazhong Univ. Sci. Technol. Med. Sci.*, *35*, **2015**, 736-741.

146. Z. Qian, J. Zhao, D. Li, *et al*., *J. Sep. Sci.*, *35*, **2012**, 2725-2734.

147. D. D. Perrin and W. L. F. Armerego, *Purification of laboratory chemicals*, Pergamon Press, Oxford, **1988**.

148. H. E. Gottlieb, V. Kotlyar and A. Nudelman, *J. Org. Chem.*, *62*, **1997**, 7512-7515.

149. IUPAC, *J. Am. Chem. Soc.*, *82*, **1960**, 5575-5584.

150. IUPAC-IUB, *Definive Rules for Nomenclature of Steroids*, Butterworths, London, **1971**, 285-322.

151. W. C. Still, M. Kahn and A. Mitra, *J. Org. Chem.*, *43*, **1978**, 2923-2925.

152. L. Ruzicka, R. Denss and O. Jeger, *Helv. Chim. Acta*, *28*, **1945**, 759-766.

153. D. H. R. Barton, G. Mellows, D. A. Widdowson, *et al*., *J. Chem. Soc. C*, **1971**, 1142-1148.

154. J. M. Bernassau and M. Fetizon, *Synthesis-Stuttgart*, **1975**, 795-796.

155. I. G. Reshetova, R. K. Tkhaper, A. V. Kamernitskii, *et al*., *B. Acad. Sci. USSR Ch+, 39,* **1990**, 607-609.

156. H. C. Huang, C. C. Liaw, H. L. Yang, *et al*., *Phytochemistry*, *84*, **2012**, 177-183.

157. A. Mehta, Ultraviolet-Visible (UV-Vis) Spectroscopy – Derivation of Beer-Lambert Law, http://pharmaxchange.info/press/2012/04/ultraviolet-visible-uv-vis-spectroscopy-%E2%80%93-derivation-of-beer-lambert-law/, (accessed 9 Dec 2015, **2015**).

158. A. Mehta, Ultraviolet-Visible (UV-Vis) Spectroscopy – Limitations and Deviations of Beer-Lambert Law, http://pharmaxchange.info/press/2012/05/ultraviolet-visible-uv-vis-spectroscopy-%E2%80%93-limitations-and-deviations-of-beer-lambert-law/, (accessed 9 Dec 2015, **2015**).

159. J. L. Rios, I. Andujar, M. C. Recio *et al*, *J. Nat. Prod.*, *75*, **2012**, 2016-2044.

160. Á. Trigos and J. Suárez Medellin, *Rev. Mex. Micol.*, *34*, **2011**, 63-83.

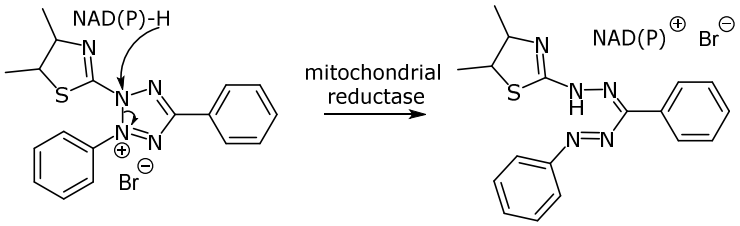
Cell concentration standard curves

According to Lambert-Beer law the concentration of a solution is directly proportional to its absorbance following equation 1, where A is the absorbance of the solution, ε correspond to its molar absorptivity expressed in L mol^{-1} cm^{-1}, b is the path length expressed in cm and c is the concentration of the solution expressed in mol L^{-1}.[157]

$$A = \varepsilon bc \qquad (1)$$

However, the linearity of the Beer's law is limited by chemical and instrumental factors at high concentrations.[158] Therefore it is imperative to construct a standard curve to determine the concentration range where the linearity is follow.

The MTT assay is a colorimetric assay based on the formation of formazan in living cells by NAD(P)H-dependant oxidoreductase enzymes (Scheme A1-1). This formation is thought to be directly proportional to the cell viability. However, as it depends on the metabolic activity of the cell, the amount of MTT reduced could vary in different cell-lines. Thus, cell-lines that are rapidly dividing will produce more formazan compared with those cell-lines with a low metabolic rate.



Scheme A1-1 Formation of formazan by reduction of MTT by mitochondrial reductase.

Formazan is a purple dye, which concentration in solution is determined by measuring its absorbance. A linear correlation between the concentration of formazan in the sample and the absorbance is observed at concentrations that follows the Lambert-Beer law. Furthermore, taking into account that the formazan formed is proportional to the number of living cells in the sample, a determination of the cell concentration could be assessed indirectly by measuring the absorbance of the formazan in the sample. This

is the principle of the MTT assay and the one used to measure the toxicity of the ganoderic acids evaluated in this study.

I. Prostate cancer cell-lines

Linear correlation curves were elaborated for PC3, DU145 and LNCaP at three times, 24 h; 48 h and 72 h. Cell suspension was dispensed (100 µL/well) at increasing concentrations in 96-well plates. Each cell concentration was replicated five times. After attachment of the cells (16 h), the media was aspirated and replaced for fresh one (200 µL/well). Plates were incubated for 24 h, 48 h and 72 h followed by evaluation of the proliferation by the MTT assay. A graph correlating the absorbance *versus* cell concentration was plotted for each of the studied times. Conversely, PC3M-luc2 cell concentrations were replicated six times, and the study performed exclusively at 72 h.

(a) PC3

The experiment was performed with PC3 cells at passage 19 and 99% viability. Dilutions of parent concentration ($1x10^6$ cell mL^{-1}) ranging from $2x10^4$ to $7x10^5$ cell mL^{-1} were prepared, plated in 96-well plates and incubated for 24h, 48 h and 72 h.

i. 24 h

At 24 h there was a linear correlation between absorbance and cell concentration at concentrations lower than $1x10^5$ cell mL^{-1}; from that concentration a plateau was reached with absorbance 2.0 (Figure A1-1).

ii. 48 h

A linear correlation was observed at 48 h for cell concentrations below $9x10^4$ cell mL^{-1}. Higher cell concentrations reached a plateau with absorbance 1.5. (Figure A1-2).

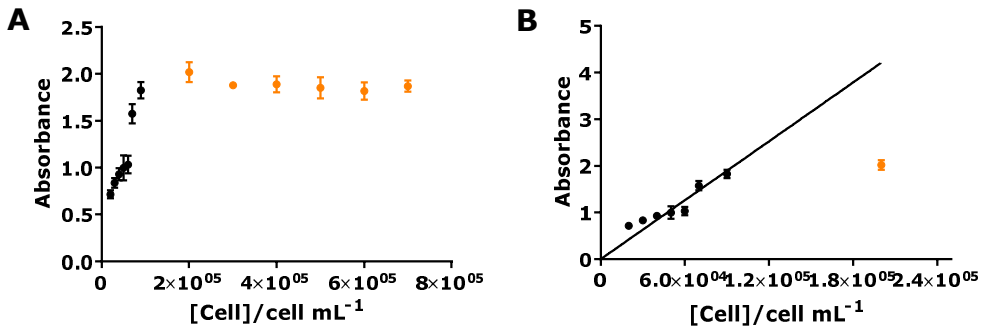


Figure A1-1 Cell concentration standard curve for PC3 cells at 24 h. **A** Absorbance is correlated with the full range of concentrations studied ($2x10^4$ to $7x10^5$ cell mL^{-1}). **B** Expansion of the linear area, correlation with cell concentrations was plotted up to $2x10^5$ cell mL^{-1}. Orange dots indicate non-lineal trend.

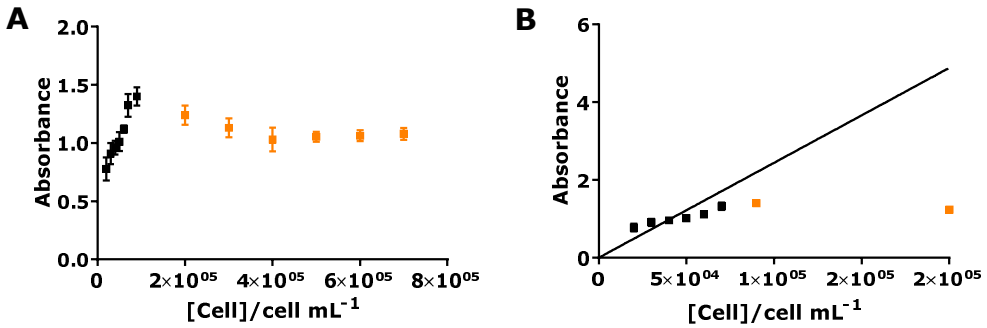


Figure A1-2 Cell concentration standard curve for PC3 at 48 h. **A** Absorbance is correlated with the full range of concentrations studied ($2x10^4$ to $7x10^5$ cell mL^{-1}). **B** Expansion of the linear area, correlation with cell concentrations was plotted up to $2x10^5$ cell mL^{-1}. Orange squares indicate non-lineal trend.

iii. 72 h

No linear correlation was observed for the experiment carried out at 72 h, the lowest cell concentration analysed ($2x10^4$ cell mL^{-1}) was already in a plateau with absorbance 2.0. Interestingly, at concentrations over $1x10^5$ cell mL^{-1} there were a decrease in the absorbance signal to 1.5 (Figure A1-3).

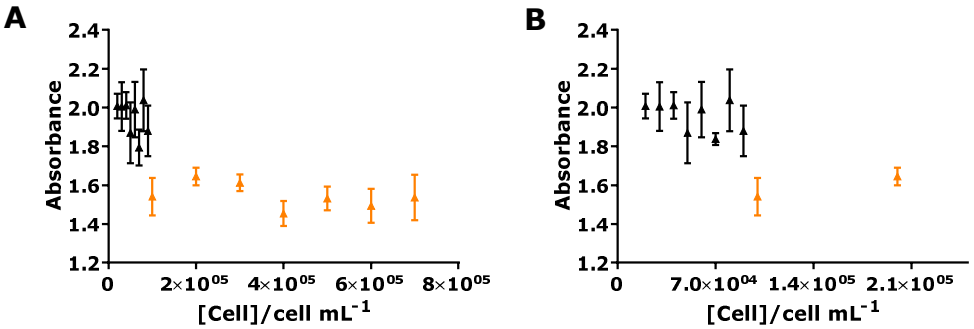


Figure A1-3 Cell concentration standard curve for PC3 at 72 h. **A** Absorbance is correlated with the full range of concentrations studied ($2x10^4$ to $7x10^5$ cell mL^{-1}). **B** Expansion of the linear area, correlation with cell concentrations plotted up to $2x10^5$ cell mL^{-1}. Orange triangles indicate reduction in absorbance.

(b) PC3M-luc2

PC3M-luc2 cells at passage 44 and 92% viability were used for this experiment. Cell concentrations ranging from $1x10^3$ cell mL^{-1} up to $4x10^5$ cell mL^{-1} were prepared. Plates were incubated for 72 h. Linearity was observed for concentrations lower than $1x10^4$ cell mL^{-1}, for higher concentrations a plateau at absorbance 1.0 was reached (Figure A1-4).

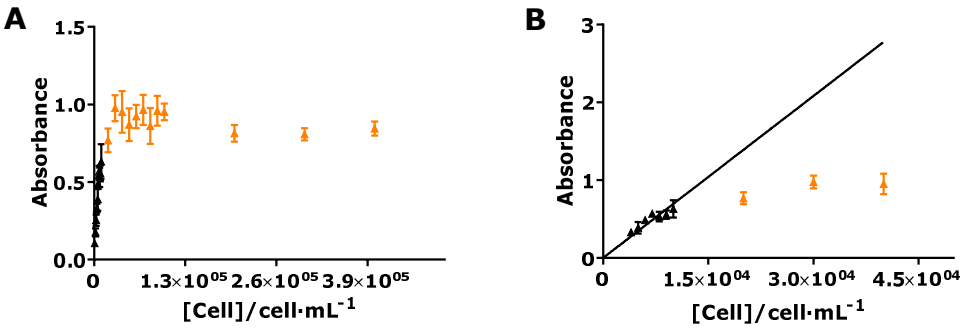


Figure A1-4 Cell concentration standard curve for PC3M at 72 h. **A** Absorbance is correlated with the full range of concentrations studied ($4x10^3$ to $4x10^5$ cell mL^{-1}). **B** Expansion of the linear area, correlation with cell concentrations was plotted up to $4x10^4$ cell mL^{-1}. Orange triangles denote the non-lineal trend.

(c) DU145

DU145 cells at passage 17 and viability 97% were used in this experiment. Cell concentrations ranging from $1x10^4$ cell mL^{-1} to $1x10^6$ cell mL^{-1} were dispensed in 96-well plates and incubated for 24 h, 48 h and 72 h.

i. 24 h

Linearity was observed for cell concentrations below $1x10^5$ cell mL^{-1}. Higher cell concentrations reached a plateau with absorbance 2.0 (Figure A1-5).

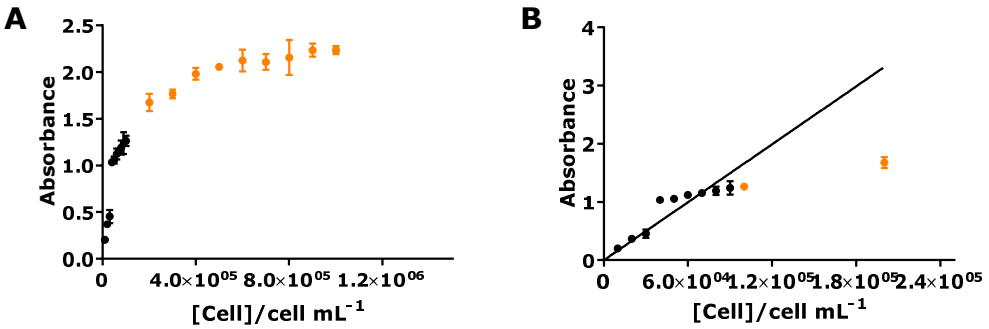


Figure A1-5 Cell concentration standard curve for DU145 at 24 h. **A** Absorbance is correlated with the full range of concentrations studied ($1x10^4$ to $1x10^6$ cell mL^{-1}). **B** Expansion of the linear area, correlation with cell concentrations plotted up to $2x10^5$ cell mL^{-1}. Orange dots refer to non-lineal trend.

ii. 48 h

Linearity was observed at 48 h incubation for cell densities below $8x10^4$ cell mL^{-1}. At higher concentrations, a plateau was reached with absorbance 1.5 (Figure A1-6).

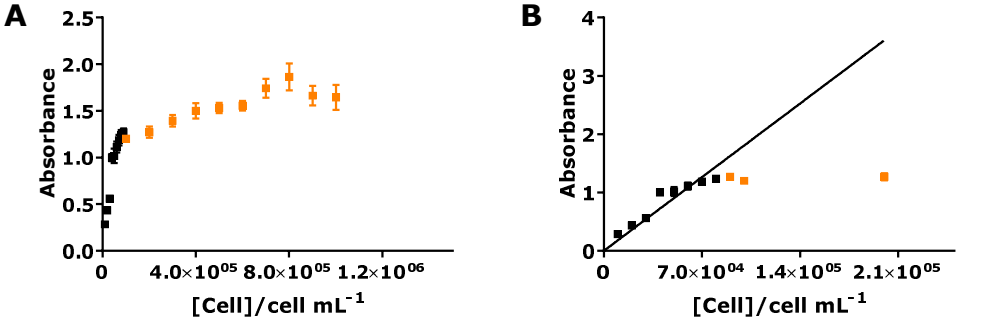


Figure A1-6 Cell concentration standard curve for DU145 at 48 h. **A** Absorbance is correlated with the full range of concentrations studied ($1x10^4$ to $1x10^6$ cell mL^{-1}). **B** Expansion of the linear area, correlation with cell concentrations plotted up to $2x10^5$ cell mL^{-1}. Orange squares indicate non-lineal trend.

iii. 72h

Lineal correlation was observed for cell concentrations below $8x10^4$ cell mL^{-1}. Higher cell concentrations reach a plateau with absorbance 1.8 (Figure A1-7).

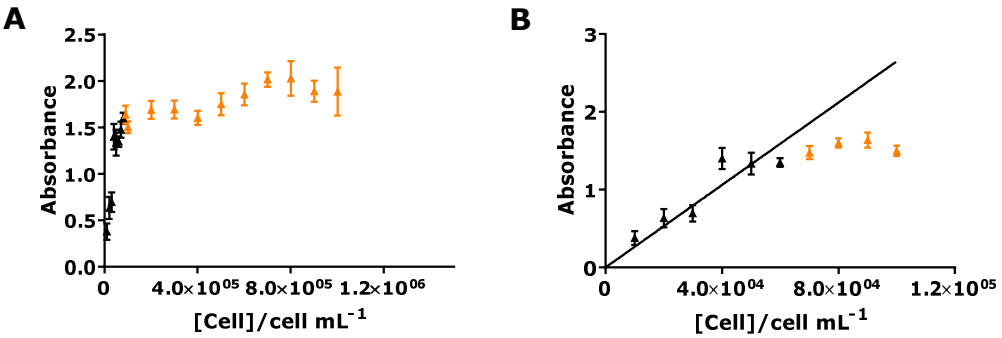


Figure A1-7 Cell concentration standard curve for DU145 at 72 h. **A** Absorbance is correlated with the full range of concentrations studied ($1x10^4$ to $1x10^6$ cell mL^{-1}). **B** Expansion of the linear area, correlation with cell concentrations was plotted up to $1x10^5$ cell mL^{-1}. Orange triangles show non-lineal correlation.

(d) LNCaP

LNCaP cells passage 13 and viability 81% were used for the experiment. Cell concentration ranging from $1x10^4$ to $5x10^5$ cell mL^{-1} were prepared, dispensed in 96-well plates and incubated for 24 h, 48 h and 72 h.

i. 24 h

At 24 h, linear correlation was found in cell concentrations up to $2x10^5$ cell mL^{-1}. Higher cell concentrations showed a plateau at absorbance 2.0 (Figure A1-8).

ii. 48 h

At 48 h linearity was detected for cell densities lower than $1x10^5$ cell mL^{-1}. At higher cell concentrations, the response is a plateau at absorbance 1.7 (Figure A1-9).

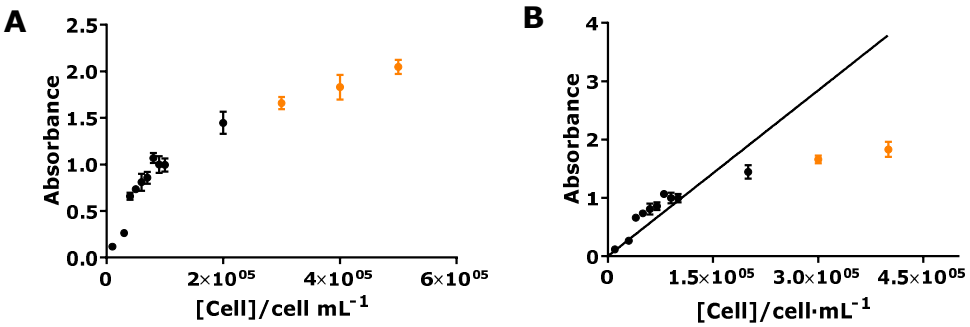


Figure A1-8 Cell concentration standard curve for LNCaP at 24 h. **A** Absorbance is correlated with the full range of concentrations studied ($1x10^4$ to $5x10^5$ cell mL^{-1}). **B** Expansion of the linear area, correlation with cell densities plotted up to $4x10^5$ cell mL^{-1}. Orange dots indicate non-lineal correlation.

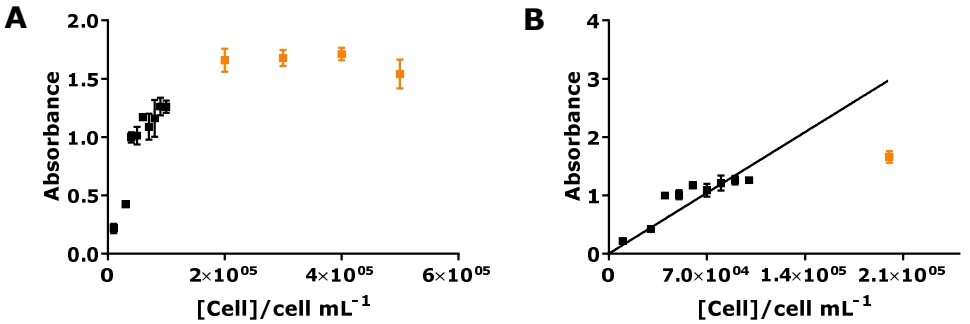


Figure A1-9 Cell concentration standard curve for LNCaP at 48 h. **A** Absorbance is correlated with the full range of concentrations studied ($1x10^4$ to $5x10^5$ cell mL^{-1}). **B** Expansion of the linear area, correlation with cell concentrations was plotted up to $2x10^5$ cell mL^{-1}. Orange squares indicate non-lineal correlation.

iii. 72 h

At 72 h a lineal correlation between cell concentration and absorbance was detected at concentrations under $1x10^5$ cell mL^{-1}. A higher concentrations, the response was a plateau at absorbance 2.2 (Figure A1-10).

In summary, linear correlations were found at all the times and cell-lines studied with the exception of PC3 cell-line at 72 h. The best cell concentrations to use would be those that show absorbance between 0.8-1.2, in that way the linearity could be assured as well as maintaining an excellent signal. Table A1-1 highlights the interval of concentration to dispense in 96-well plates when platting 100 µL/well for each of the cell-lines studied at 24 h, 48 h and 72 h.

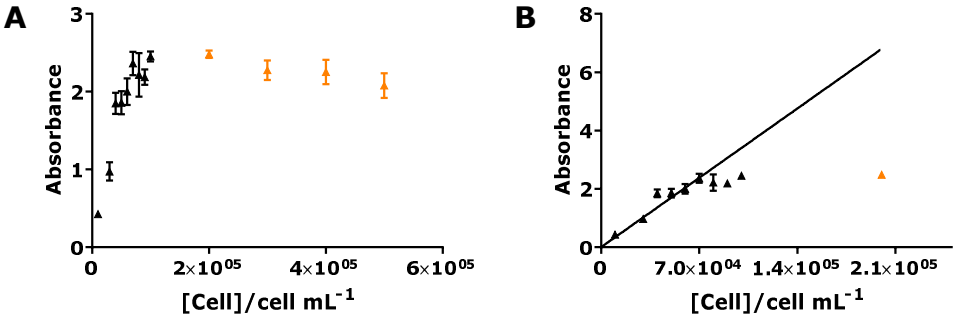


Figure A1-10 Cell concentration standard curve for LNCaP at 72 h. **A** Absorbance is correlated with the full range of concentrations studied ($1x10^4$ to $5x10^5$ cell mL^{-1}). **B** Expansion of the linear area, correlation with cell concentrations was plotted up to $2x10^5$ cell mL^{-1}.

Cell-line	Cell concentration/$1x10^4$ cell mL^{-1}		
	24 h	**48 h**	**72 h**
PC3	2-8	2-7	< 2
PC3M	-	-	0.8-1
DU145	4-8	4-8	3-4
LNCaP	6-15	4-10	3-4

Table A1-1 Cell concentration interval for cancerous cell-lines used in this study at 24 h, 48 h and 72 h. This interval satisfies linearity correlation and excellent signal response.

II. Non-malignant cell-lines

Normal prostate cell-line RWPE1 and pre-malignant cell-lines WPE1-NB14 and -NB26 standard curves were elaborated by representing increasing cell concentrations ranging from $7x10^3$ to $6x10^5$ cell mL^{-1} *versus* absorbance. Each cell concentration (100 µL/well) was replicated six times in 96-well plates. The cells were allowed to attach (16 h) before aspirating and changing the media (200 µL/well). Plates were then incubated for 72 h. MTT proliferation assay was employed to determine the final cell concentration. Representation of the absorbance, to which the blank was subtracted, against initial cell concentration gave curves with a lineal zone.

(a) RWPE1

Two experiments were carried out, in the first, RWPE1 cells passage 59 and viability 94% were used, in the second, cells with passage 66 and viability 86% were platted. Representation of the different cell concentration dilutions against absorbance gave a graph with linearity at concentrations

below $5x10^4$ cells mL^{-1}. Higher concentrations formed a plateau at absorbance 1.5 (Figure A1-11).

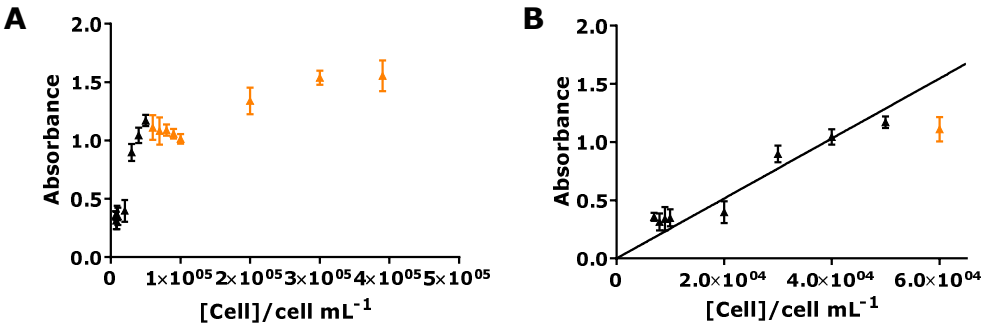


Figure A1-11 Cell concentration standard curve for RWPE1 at 72 h. **A** Absorbance is correlated with the full range of concentrations studied ($7x10^3$ to $3.9x10^5$ cell mL^{-1}). **B** Expansion of the linear area, a correlation with cell concentrations was plotted up to $6x10^4$ cell mL^{-1}.

(b) WPE1-NB14

Two experiments were performed, in the first, WPE1-NB14 at passage 33 and viability 91% were used; in the second, cells at passage 40 and viability 86% were platted. Linearity correlation with absorbance was found in cell concentrations below $4x10^4$ cell mL^{-1}. Higher concentrations formed a plateau at absorbance 1.1 (Figure A1-12).

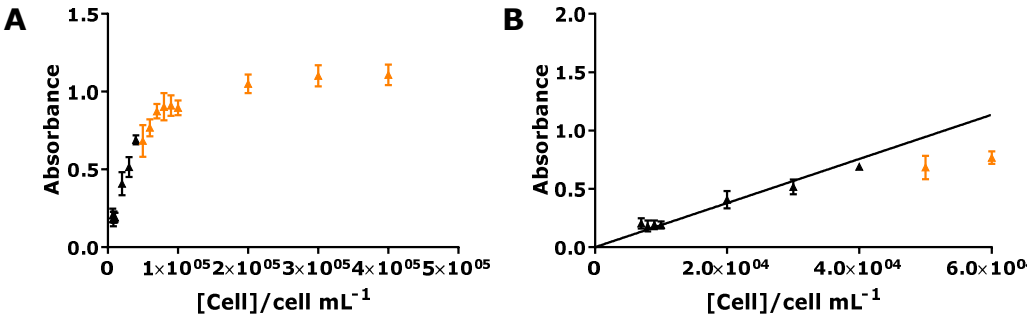


Figure A1-12 Cell concentration standard curve for WPE1-NB14 at 72 h. **A** Absorbance is correlated with the full range of concentrations studied ($7x10^3$ to $4x10^5$ cell mL^{-1}). **B** Expansion of the linear area, correlation with cell concentrations plotted up to $6x10^4$ cell mL^{-1}.

(c) WPE1-NB26

Two experiments were carried out, in the first, WPE1-NB26 cells at passage 21 and viability 91% were used; in the second, cells at passage 27 and viability 93% were platted. Linearity correlation was found for

concentrations lower than $2x10^4$ cell mL^{-1}. At higher concentrations, a plateau was reached at absorbance 1.2 (Figure A1-13).

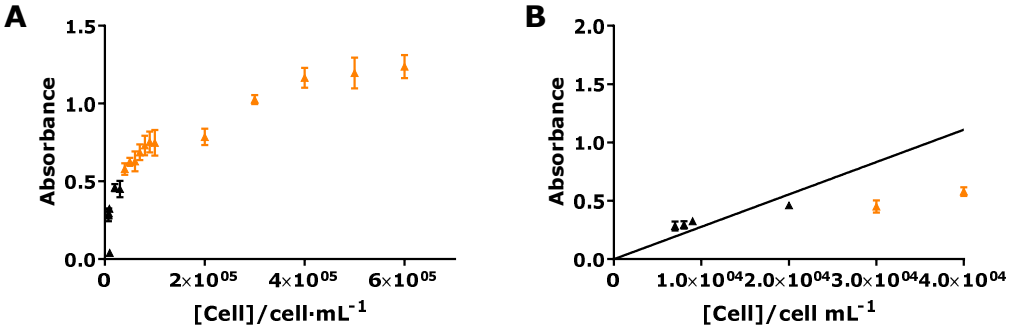


Figure A1-13 Cell concentration standard curve for WPE1-NB26 at 72 h. **A** Absorbance is correlated with the full range of concentrations studied ($7x10^3$ to $6x10^5$ cell mL^{-1}). **B** Expansion of the linear area, correlation with cell concentrations was plotted up to $4x10^4$ cell mL^{-1}.

In summary, all the cell-lines showed a linear correlation between the concentration and the absorbance. In this set of experiments the plateau was reached at absorbance slightly above 1. Best cell concentrations to use are those in the linear area with absorbance in the range 0.7-.0.9. Table A1-2 highlights this optimum range.

	Cell-line		
	RWPE1	**WPE1-NB14**	**WPE1-NB26**
[Cell]/1x10⁴ cell mL⁻¹	3-5	3-4	1-2

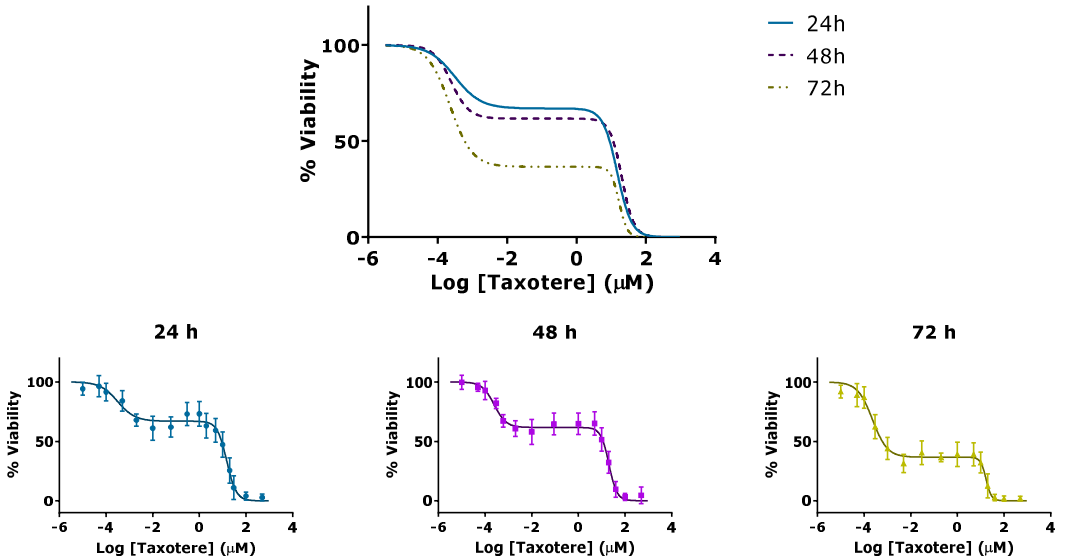
Table A1-2 Cell concentration interval for pre-malignant cell-lines used in this study at 72 h. This interval satisfies linearity correlation and best signal response.

Dose-response curves of natural and synthetic GA are documented in this section.

Time-course study

Dose-response curves of Taxotere (**190**) and analogues **108**, **146** and **154** at 24; 48 and 72 h are represented below.

i. Taxotere (**190**)



$EC_{50}1$=0.415±0.288 nM
$EC_{50}2$=15.9±2.7 µM

$EC_{50}1$=0.567±0.186 nM
$EC_{50}2$=19.7±2.5 µM

$EC_{50}1$=0.249±0.118 nM
$EC_{50}2$=18.4±4.1 µM

Figure A2-1 Time-course study for Taxotere (**190**). Dose-response curves at 24 h (blue), 48 h (purple) and 72 h (gold) were represented as the mean ± SD of seven independent experiments, each with five or six replicates. PC3 cell-line 8-13x10^4 cell mL^{-1} for the 24 h experiment; 3-8x10^4 cell mL^{-1} for the 48 h experiment and 1-8x10^4 cell mL^{-1} for the 72 h experiment at passages 6 to 24 were used in this study.

ii. Analogue **108**

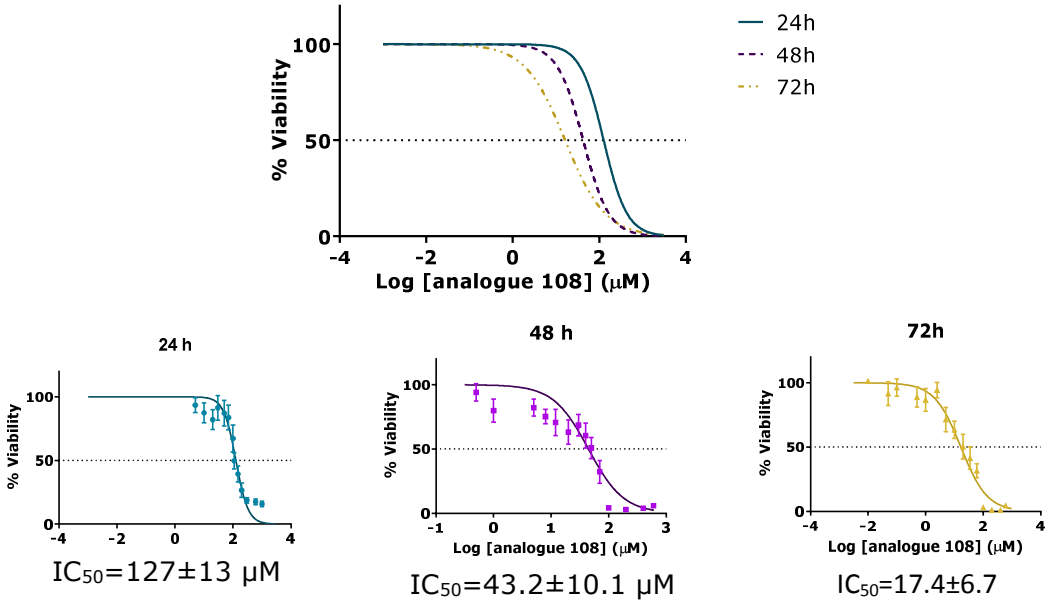


Figure A2-2 Time-course study for **108**. Inhibition curves at 24 h (blue), 48 h (purple) and 72 h (gold) were represented as the mean ± SD of five or six replicates for five independent experiments. PC3 cell-line $1.3x10^5$, $1x10^5$ and $9x10^4$ cell mL^{-1} for the 24 h experiment; $8.5x10^4$, $2.5x10^4$ and $3x10^4$ cell mL^{-1} for the 48 h experiment and $2.8x10^4$, $1.5x10^4$ and $1.2x10^4$ cell mL^{-1} for the 72 h experiment at passages 21, 27 and 24, respectively were used in this study.

iii. Analogue **146**

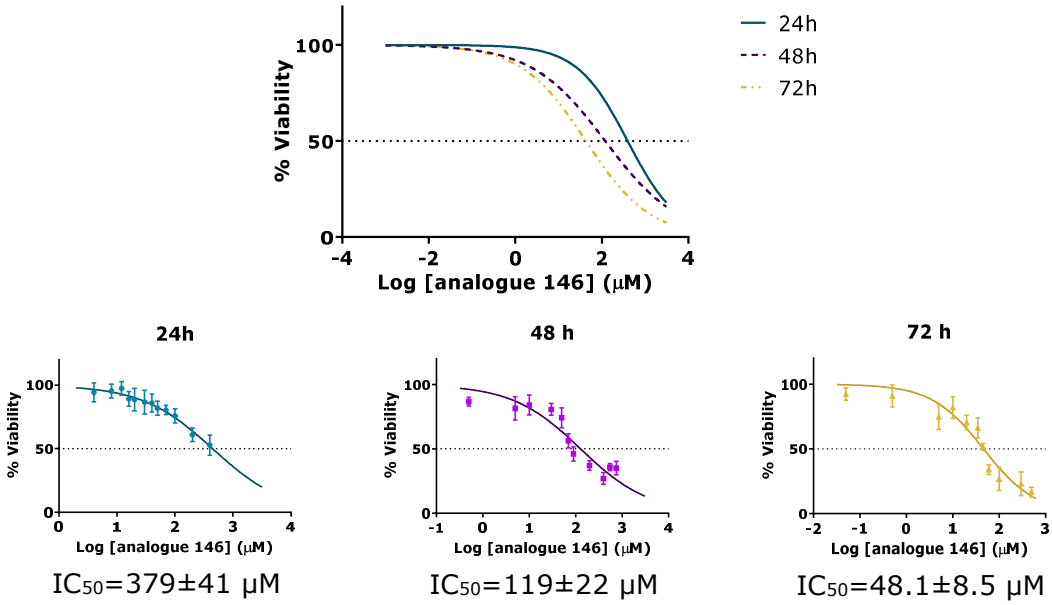


Figure A2-3 Time-course study for **146**. Inhibition curves at 24 h (blue), 48 h (purple) and 72 h (gold) were represented as the mean ± SD of two independent experiments, each with five replicates. PC3 cell-line $1.3x10^5$ and $9x10^4$ cell mL^{-1} for the 24 h experiment; $8.5x10^4$ and $2.5x10^4$ cell mL^{-1} for the 48 h experiment and $2.8x10^4$ and $1.3x10^4$ cell mL^{-1} for the 72 h experiment at passages 23 and 29, respectively were used in this study.

iv. Analogue **174**

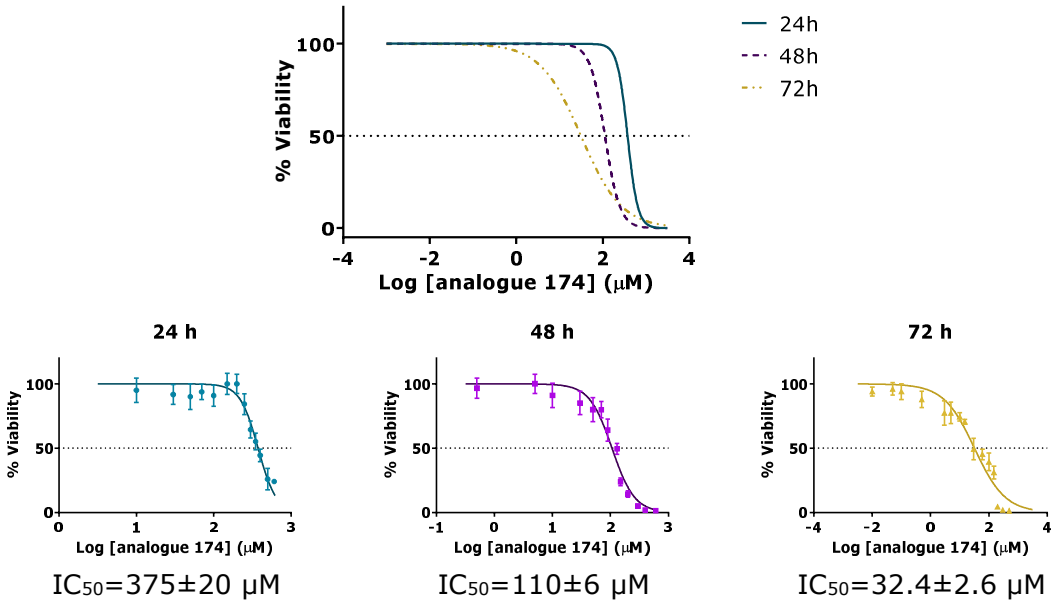


Figure A2-4 Time-course study for **174**. Inhibition curves at 24 h (blue), 48 h (purple) and 72 h (gold) were represented as the mean ± SD of two independent experiments, each with five replicates. PC3 cell-line $1.3x10^5$ and $9x10^4$ cell mL^{-1} for the 24 h experiment; $8.5x10^4$ and $2.5x10^4$ cell mL^{-1} for the 48 h experiment and $2.8x10^4$ and $1.3x10^4$ cell mL^{-1} for the 72 h experiment at passages 23 and 29, respectively were used in this study.

Dose-response curves of natural GAs after 72 h treatment

Dose response curves of non-malignant prostate cell-lines, RWPE1; WPE1-NB14 and -NB26 and cancer cell-lines PC3; PC3M-luc2; DU145 and LNCaP after treatment with GA-H (**24**) and GA-T (**11**) for 72 h are represented below. For GA-H (**24**), no treatment was performed on PC3M-luc2 cells due to lack of sample.

i. GA-H (**24**)

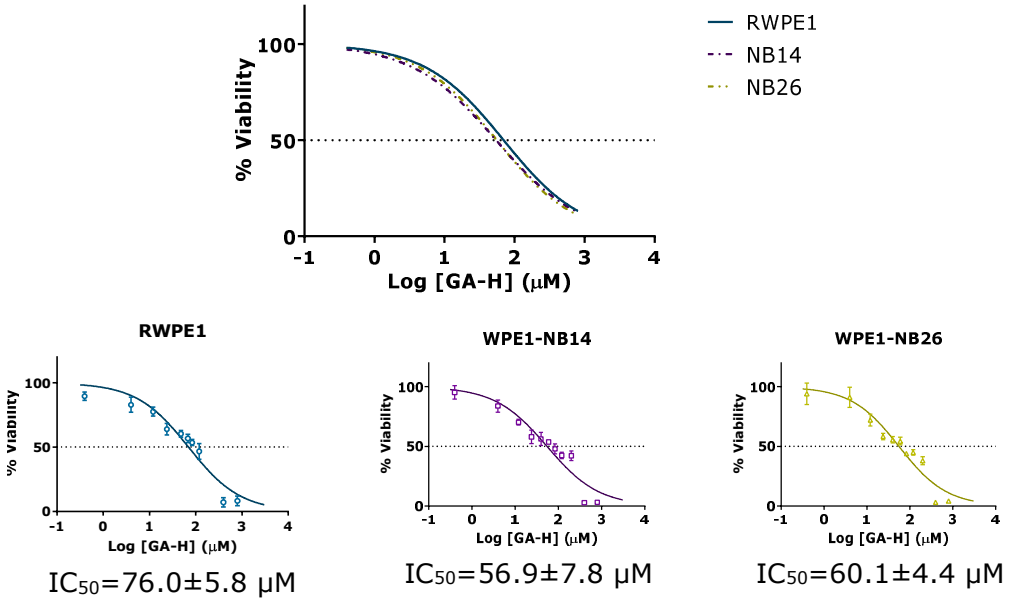


Figure A2-5 Dose-response curves for non-malignant prostate cell-lines, RWPE1 (blue), WPE1-NB14 (purple) and WPE1-NB26 (gold) treated with GA-H (**24**) [experiment 1]. Cells were treated with GA-H (**24**) ranging from 0 to 800 μM and seeded as follow: RWPE1 $2.8x10^5$ cell mL^{-1} at passage 66, WPE1-NB14 $3x10^5$ cell mL^{-1} at passage 34 and WPE1-NB26 $3x10^5$ cell mL^{-1} at passage 21.

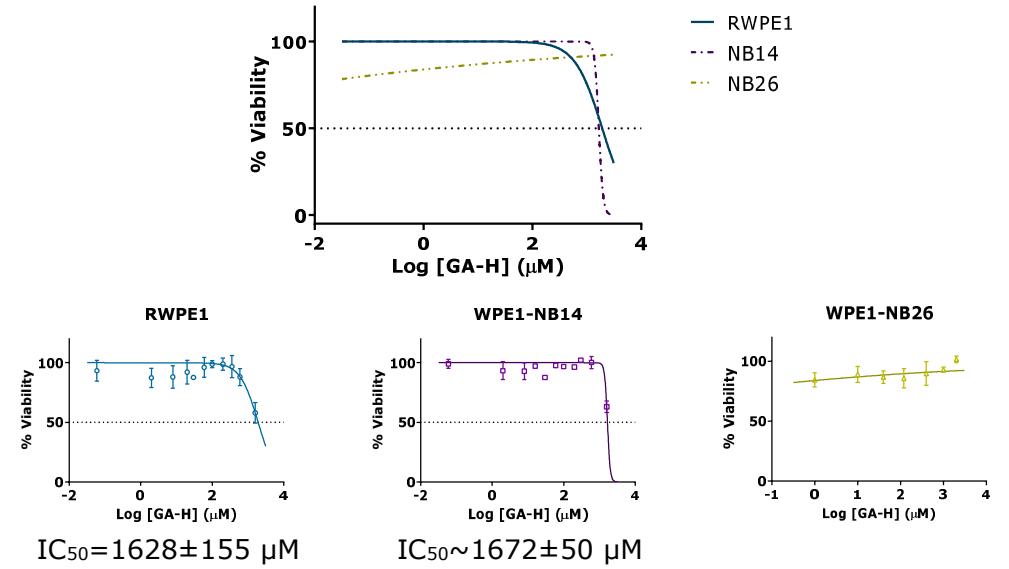


Figure A2-6 Dose-response curves for non-malignant prostate cell-lines, RWPE1 (blue), WPE1-NB14 (purple) and WPE1-NB26 (gold) treated with GA-H (**24**) [experiment 2]. Cells were treated with GA-H (**24**) from 0 to 2000 μM and seeded as follow: RWPE1 $2.6x10^5$ cell mL^{-1} at passage 74, WPE1-NB14 $2.4x10^5$ cell mL^{-1} at passage 44 and WPE1-NB26 $2.8x10^5$ cell mL^{-1} at passage 26.

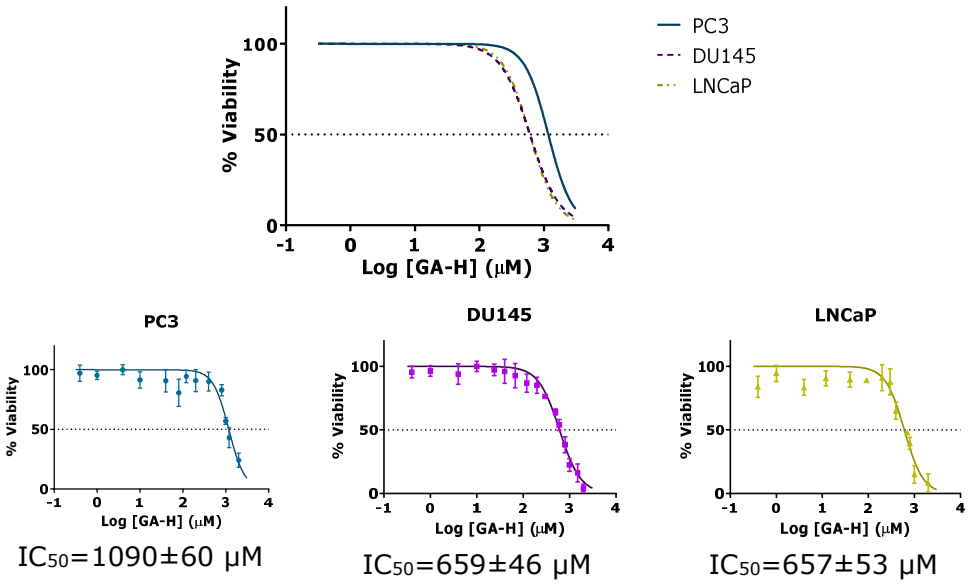


Figure A2-7 Dose-response curves for prostate cancer cell-lines, PC3 (blue), DU145 (purple) and LNCaP (gold) treated with GA-H (**24**) from 0 to 2000 μM. Curves are the mean of two experiments each with six replicates. PC3 was seeded at $1.5x10^4$ cell mL^{-1}, DU145 and LNCaP were seeded at $3.5x10^4$ cell mL^{-1}.

ii. GA-T (**11**)

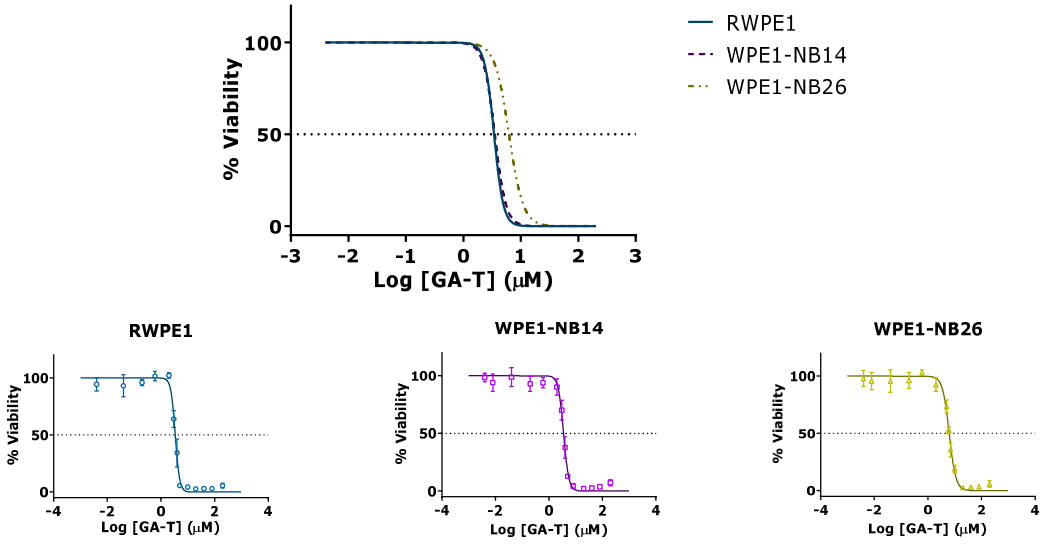


Figure A2-8 Dose response curves for non-cancerous cell-lines, RWPE1 (blue), WPE1-NB14 (purple) and WPE1-NB26 (gold) treated with GA-T (**11**) from 0 to 200 μM. Curves are the mean of two experiments each with six replicates. Plates were seeded as follow: RWPE1 $2.8x10^5$ cell mL^{-1} at passage 66, WPE1-NB14 $3x10^5$ cell mL^{-1} at passage 34 and WPE1-NB26 $3x10^5$ cell mL^{-1} at passage 21 for experiment 1 and RWPE1 $2.6x10^5$ cell mL^{-1} at passage 74, WPE1-NB14 $2.4x10^5$ cell mL^{-1} at passage 44 and WPE1-NB26 $2.8x10^5$ cell mL^{-1} at passage 26 for experiment 2. IC_{50} values are indicated as mean ± SD.

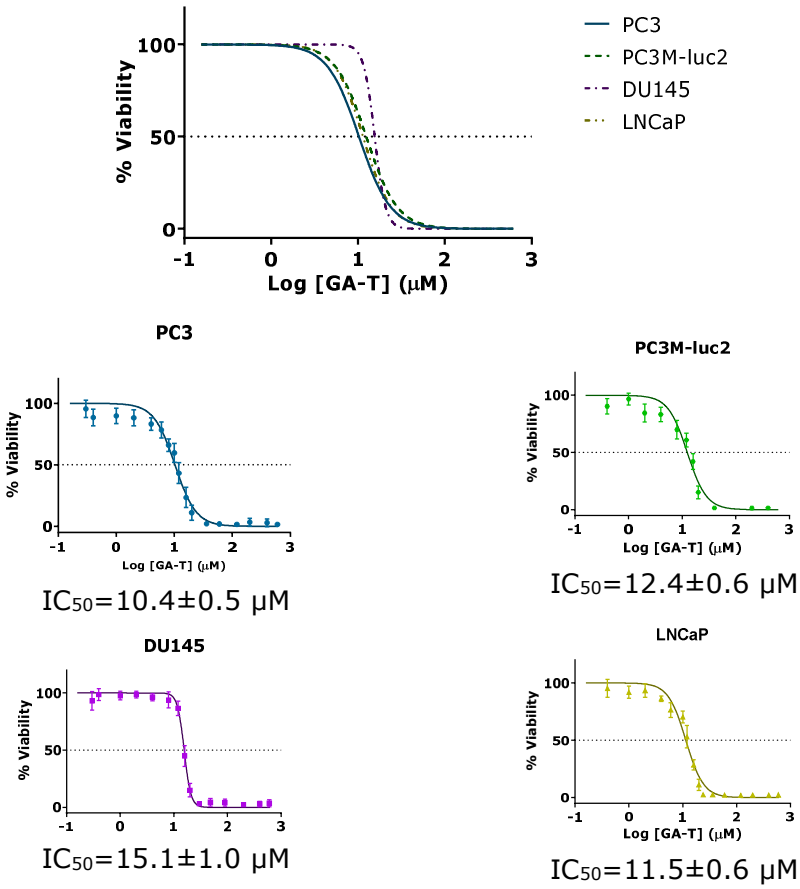


Figure A2-9 Dose-response curves for prostate cancer cell-lines, PC3 (blue), PC3M-luc2 (green), DU145 (purple) and LNCaP (gold) treated with GA-T (**11**) from 0 to 600 μM. Curves are the mean of two or three experiments each with six replicates. Plates were seeded as follows: PC3 at $1.5x10^4$ cell mL^{-1}; PC3M-luc2 at $3x10^4$ cell mL^{-1} and both DU145 and LNCaP at $3.5x10^4$ cell mL^{-1}. IC_{50} values are indicated as mean ± SD.

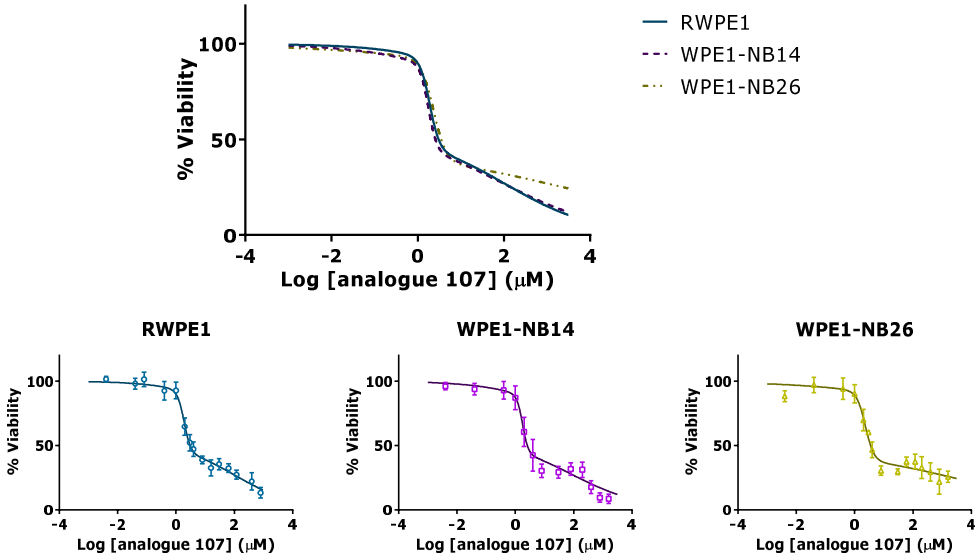
Dose-response curves of analogues after 72 h treatment

The analogues were classified in three groups.

i. Group I

To this group pertains analogues **107**; **108** and **109**. Assays with non-malignant and prostate cancer cell-lines were performed with **107** and **108**. For analogue **109**, assays were performed only with prostate cancer cell-lines.

(a) Analogue **107**



$EC_{50}1$=1.86±0.32 μM
$EC_{50}2$=259±39 μM

$EC_{50}1$=2.22±0.64 μM
$EC_{50}2$=505±76 μM

$EC_{50}1$=2.17±0.26 μM
$EC_{50}2$=586±67 μM

Figure A2-10 Dose-response curves for non-cancerous cell-lines, RWPE1 (blue), WPE1-NB14 (purple) and WPE1-NB26 (gold) treated with **107** from 0 to 1600 μM. Curves are the mean of three experiments each with six replicates. Plates were seeded as follow: RWPE1 $2.8x10^5$ cell mL^{-1} at passage 66 and $2.6x10^5$ cell mL^{-1} at passage 68 and 74, WPE1-NB14 $3x10^5$ cell mL^{-1} at passage 35 and 37 and $2.4x10^5$ cell mL^{-1} at passage 44 and WPE1-NB26 $3x10^5$ cell mL^{-1} at passage 21 and 23 and $2.8x10^5$ cell mL^{-1} at passage 30. Biphasic curves fitted better to the data. EC_{50} values for each of the phases are indicated as mean ± SD.

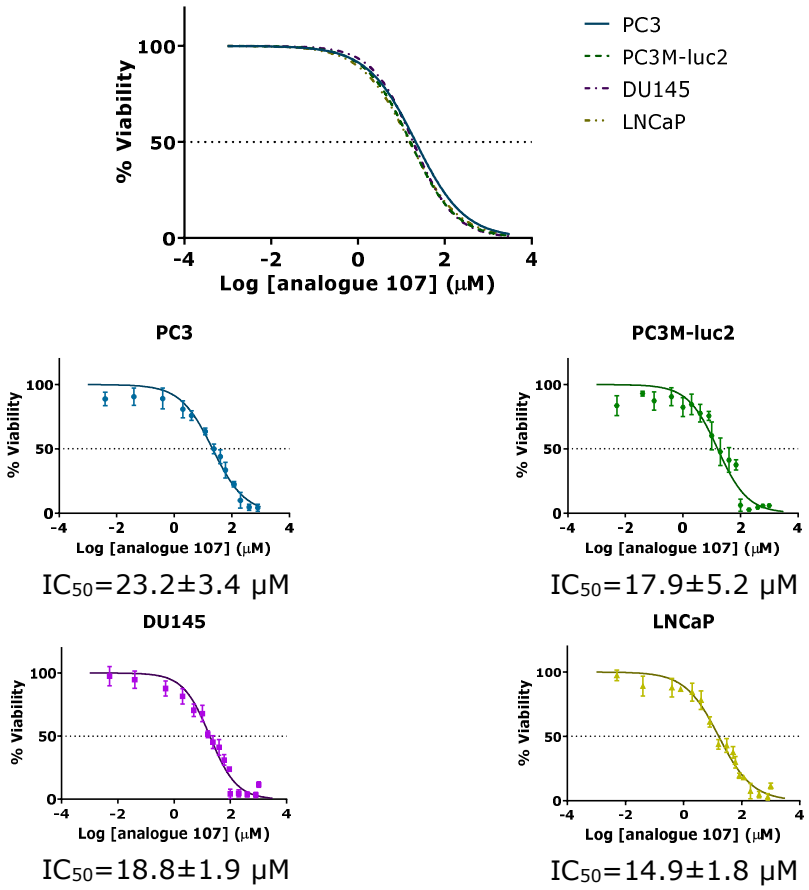
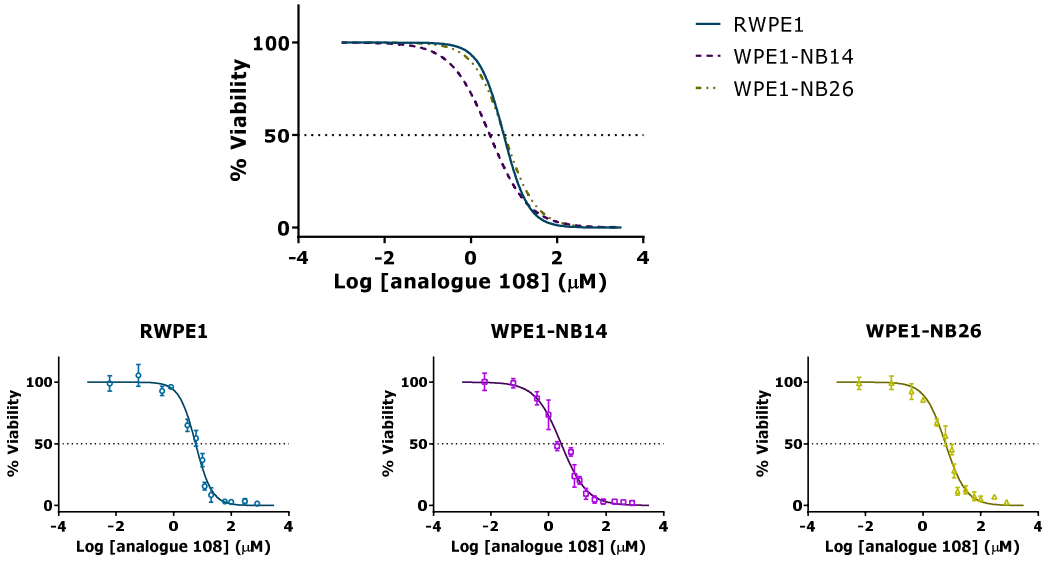


Figure A2-11 Dose response curves for prostate cancer cell-lines, PC3 (blue), PC3M-luc2 (green), DU145 (purple) and LNCaP (gold) treated with **107** from 0 to 1000 μM. Curves are the mean of at least three experiments each with six replicates. Plates were seeded as follow: PC3 at 1.5×10^4 cell mL^{-1}; PC3M-luc2 at 3×10^4 cell mL^{-1} and both DU145 and LNCaP at 3.5×10^4 cell mL^{-1}. IC_{50} values are indicated as mean ± SD.

(b) Analogue **108**



IC_{50}=5.92±0.67 μM IC_{50}=3.26±0.44 μM IC_{50}=6.35±0.52 μM

Figure A2-12 Dose-response curves for non-malignant cell-lines, RWPE1 (blue), WPE1-NB14 (purple) and WPE1-NB26 (gold) treated with **108** from 0 to 800 μM. Curves are the mean of three experiments each with six replicates. Plates were seeded as follow: RWPE1 $2.5x10^5$-$2.6x10^5$ cell mL^{-1}, WPE1-NB14 $2x10^5$-$3x10^5$ cell mL^{-1} and WPE1-NB26 $2.6x10^5$-$3x10^5$ cell mL^{-1}. IC_{50} values are indicated as mean ± SD.

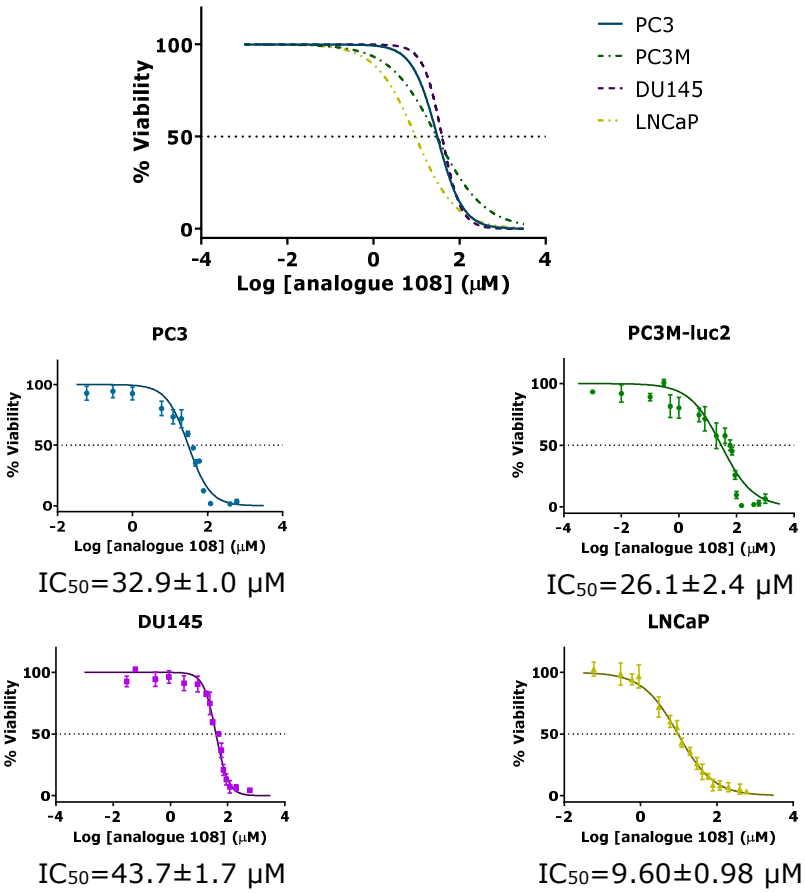
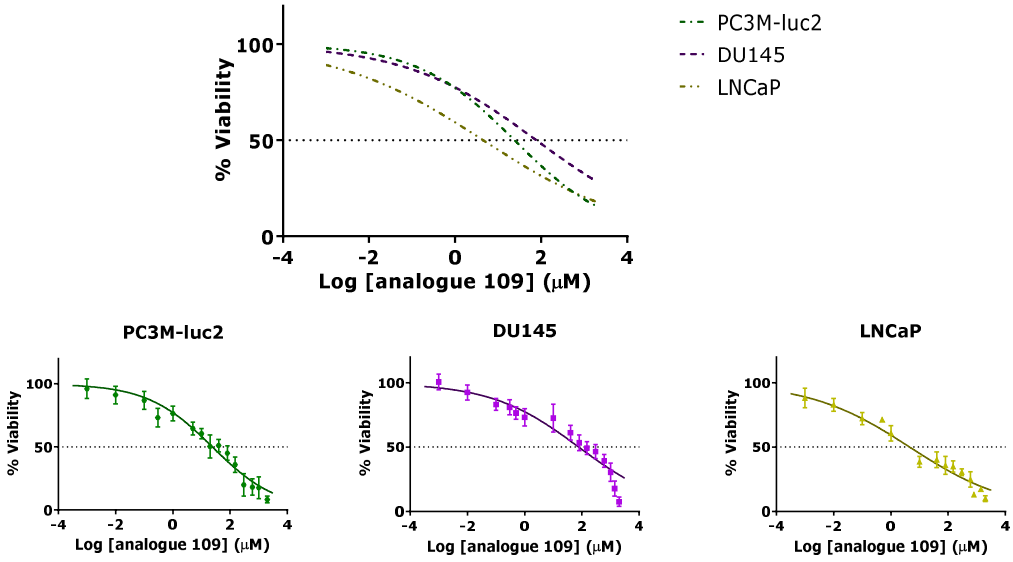


Figure A2-13 Dose-response curves for prostate cancer cell-lines, PC3 (blue), PC3M-luc2 (green), DU145 (purple) and LNCaP (gold) treated with **108** from 0 to 1000 μM. Curves are the mean of two, three or four experiments each with six replicates. Plates were seeded as follows: PC3 at 1.5×10^4 cell mL^{-1}; PC3M-luc2 at 3×10^4 cell mL^{-1} and both DU145 and LNCaP at 3.5×10^4 cell mL^{-1}. IC_{50} values are indicated as mean ± SD.

(c) Analogue **109**



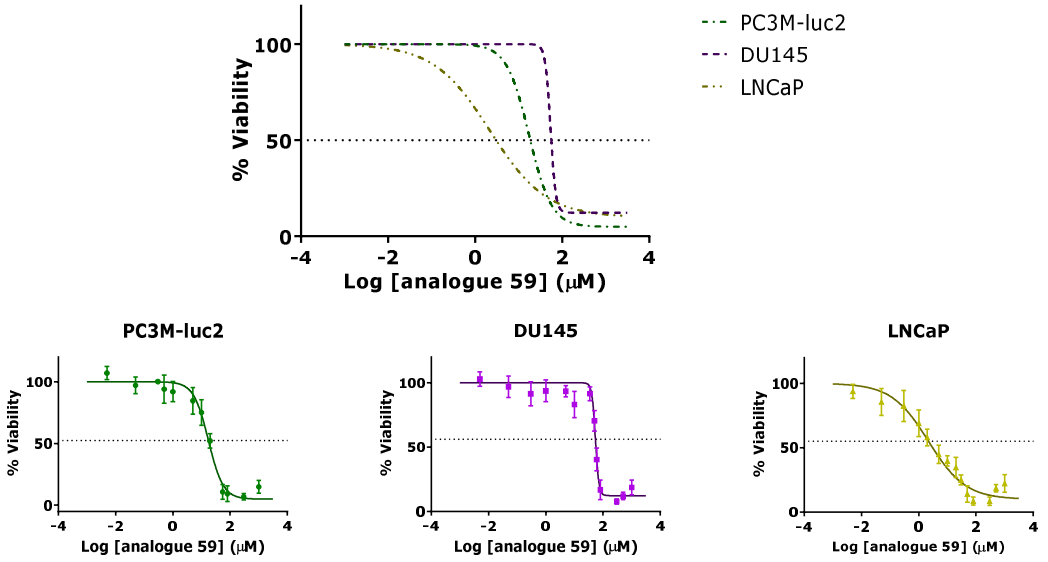
IC_{50}=24.3±2.9 μM IC_{50}=89.2±4.2 IC_{50}=4.08±1.51 μM

Figure A2-14 Dose-response curves for prostate cancer cell-lines, PC3M-luc2 (green), DU145 (purple) and LNCaP (gold) treated with **109** from 0 to 2000 μM. Curves are the mean of at least two independent experiments each with six replicates. Plates were seeded as follows: PC3M-luc2 at $3x10^4$ cell mL^{-1} and DU145 and LNCaP at $4.5x10^4$ cell mL^{-1}. IC_{50} values are indicated as mean ± SD.

ii. Group II

Two analogues, **59** and **146** are enclosed in this group. Experiments with non-malignant cell-lines were performed only with **146**.

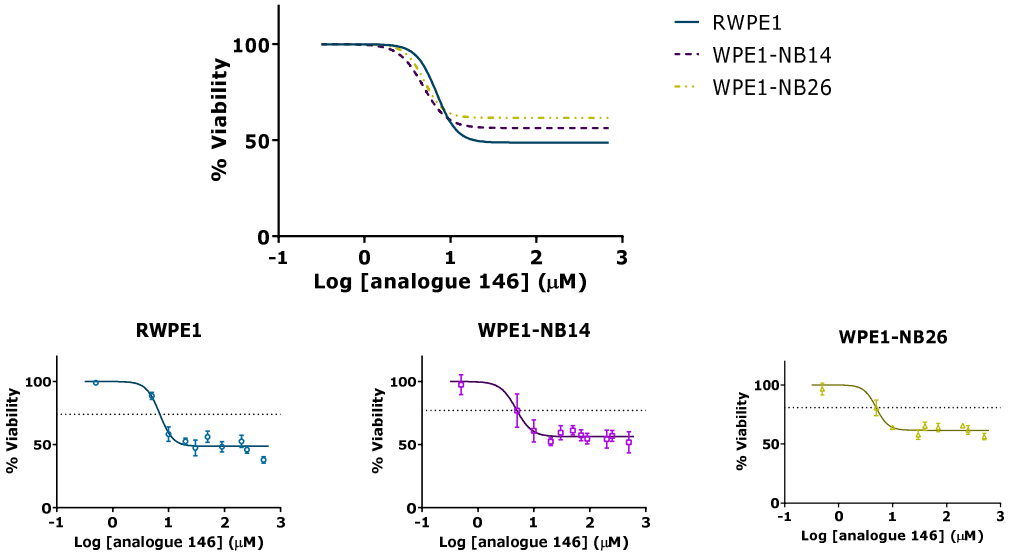
(a) Analogue **59**



EC_{50}=20.9±2.2 μM EC_{50}=54.4±2.1 μM EC_{50}=3.25±1.24 μM

Figure A2-15 Dose-response curves for prostate cancer cell-lines, PC3M-luc2 (green), DU145 (purple) and LNCaP (gold) treated with analogue **59** from 0 to 1000 μM. Curves are the mean of three experiments each with six replicates. Plates were seeded as follows: PC3M-luc2 at $3x10^4$ cell mL^{-1} and DU145 and LNCaP at $4.5x10^4$ cell mL^{-1}. EC_{50} values are indicated as mean ± SD.

(b) Analogue **146**



EC_{50}=7.08±1.02 μM EC_{50}=5.24±0.58 μM EC_{50}=4.61±0.65 μM

Figure A2-16 Dose-response curves for non-malignant cell-lines, RWPE1 (blue), WPE1-NB14 (purple) and WPE1-NB26 (gold) treated with **146** from 0 to 500 μM. Curves are the mean of one independent experiment with six replicates. Plates were seeded as follow: RWPE1 $2.5x10^5$ cell mL^{-1}, WPE1-NB14 $2x10^5$ cell mL^{-1} and WPE1-NB26 $2.6x10^5$ cell mL^{-1}. EC_{50} values are indicated as mean ± SD.

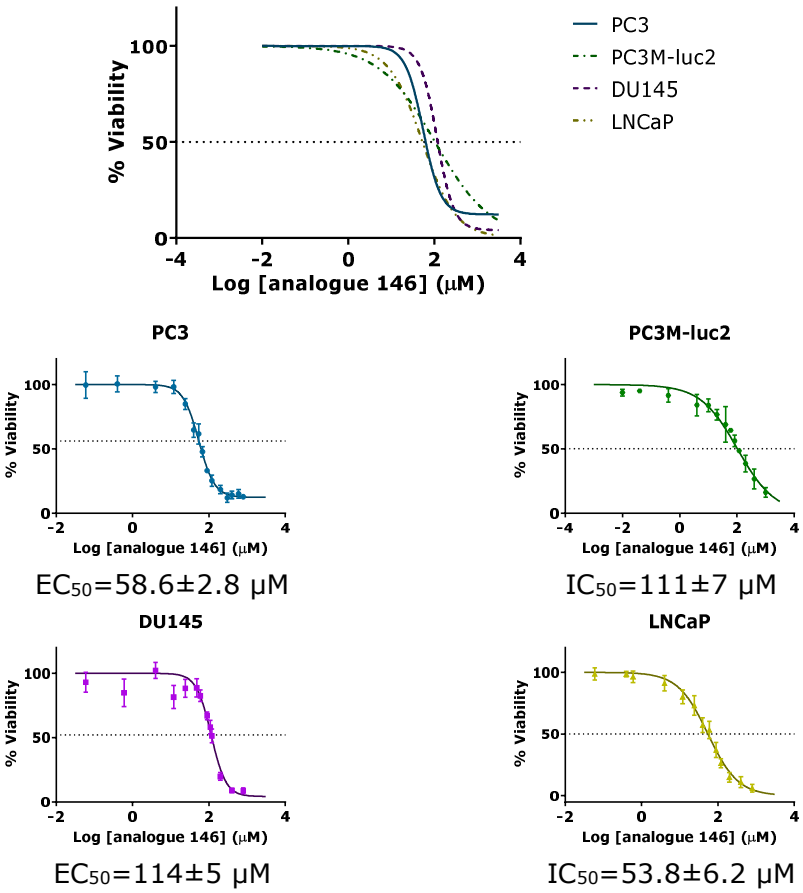


Figure A2-17 Dose-response curves for prostate cancer cell-lines, PC3 (blue), PC3M-luc2 (green), DU145 (purple) and LNCaP (gold) treated with analogue **146** from 0 to 1000 μM. Curves are the mean of two experiments each with six replicates. Plates were seeded as follows: PC3 at $1.3x10^4$-$1.5x10^4$ cell mL^{-1}; PC3M-luc2 at $3x10^4$ cell mL^{-1}, DU145 at $3.5x10^4$-$3.8x10^4$ cell mL^{-1} and LNCaP at $3.5x10^4$-$4x10^4$ cell mL^{-1}. EC_{50}/IC_{50} values are indicated as mean ± SD.

iii. Group III

To this group pertain analogues **184**; **185**; **188** and **189**. Experiments were only performed with prostate cancer cell-lines for this group.

(a) Analogue **184**

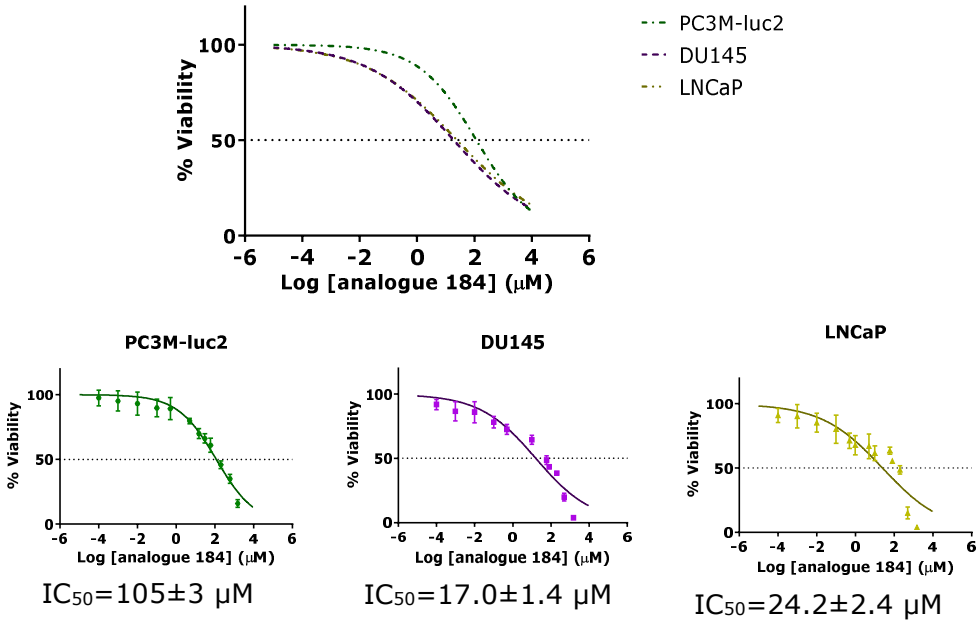
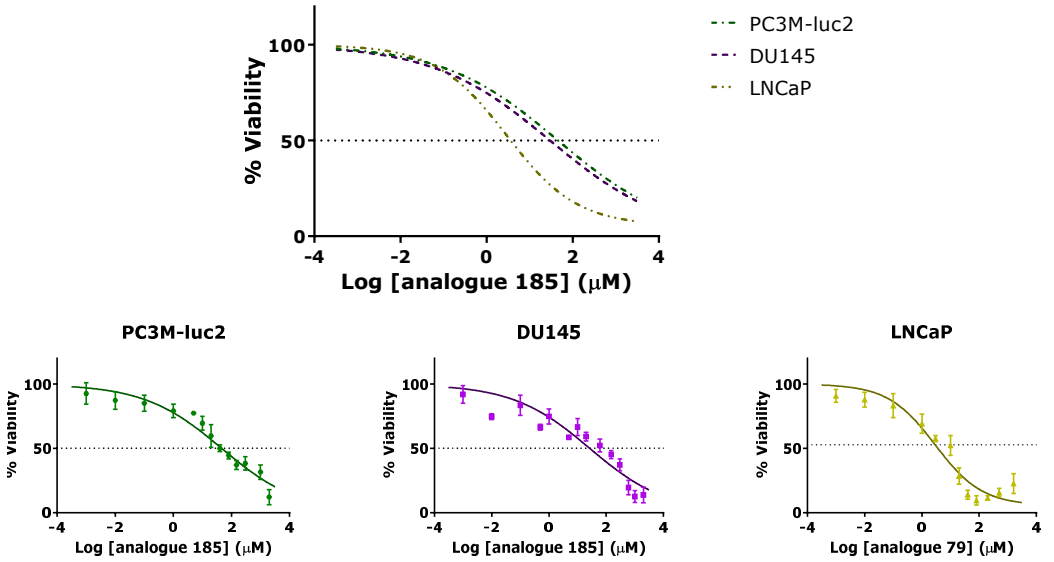


Figure A2-18 Dose-response curves for prostate cancer cell-lines, PC3M-luc2 (green), DU145 (purple) and LNCaP (gold) treated with **184** from 0 to 1500 μM. Curves are the mean of two experiments each with six replicates. Plates were seeded as follows: PC3M-luc2 at $3x10^4$ cell mL^{-1} and DU145 and LNCaP at $4.5x10^4$ cell mL^{-1}. IC_{50} values are indicated as mean ± SD.

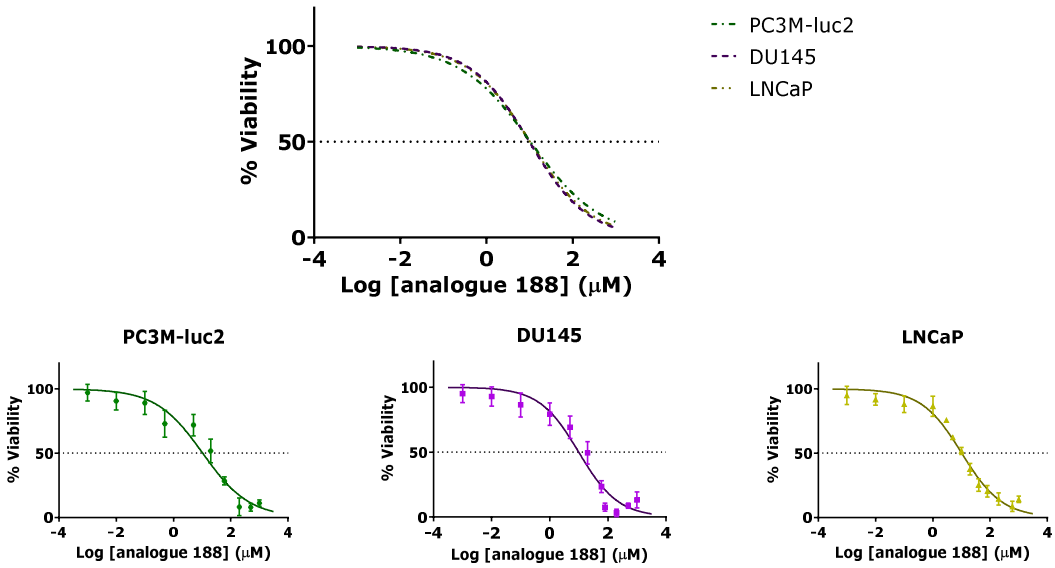
(b) Analogue **185**



IC_{50}=56.3±2.3 μM IC_{50}=43.1±4.4 μM EC_{50}=4.40±0.31 μM

Figure A2-19 Dose-response curves for prostate cancer cell-lines, PC3M-luc2 (green), DU145 (purple) and LNCaP (gold) treated with **185** from 0 to 2000 μM. Curves are the mean of two experiments each with six replicates. Plates were seeded as follows: PC3M-luc2 at $3x10^4$ cell mL^{-1} and DU145 and LNCaP at $4.5x10^4$ cell mL^{-1}. Ec_{50}/IC_{50} values are indicated as mean ± SD.

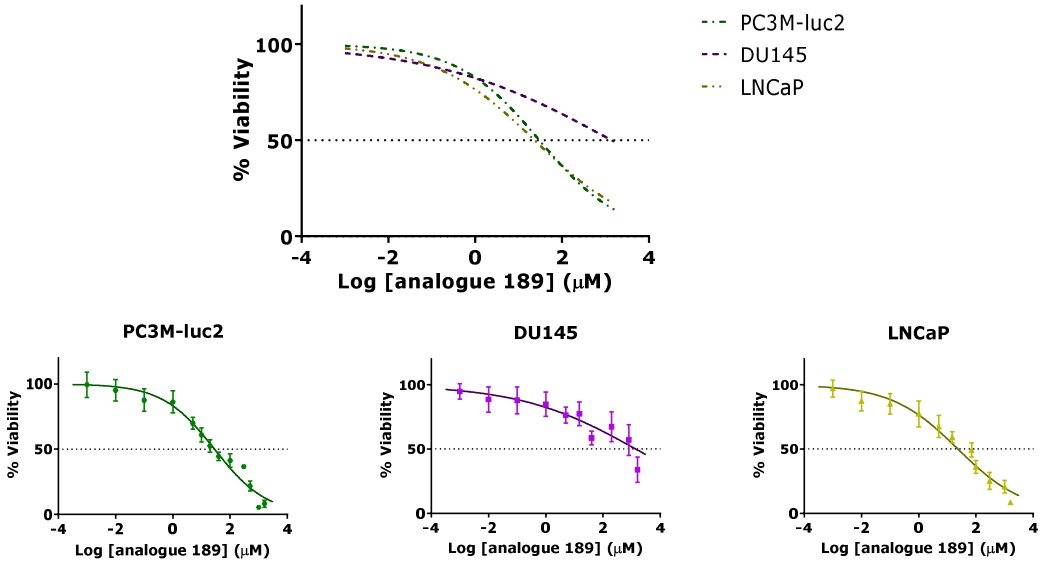
(c) Analogue **188**



IC_{50}=20.4±4.4 μM IC_{50}=15.6±5.0 μM IC_{50}=11.3±0.5 μM

Figure A2-20 Dose-response curves for prostate cancer cell-lines, PC3M-luc2 (green), DU145 (purple) and LNCaP (gold) treated with **188** from 0 to 1000 μM. Curves are the mean of at least two experiments each with six replicates. Plates were seeded as follows: PC3M-luc2 at $3x10^4$ cell mL^{-1} and DU145 and LNCaP at $4.5x10^4$ cell mL^{-1}. IC_{50} values are indicated as mean ± SD.

(d) Analogue **189**



IC_{50}=38.8±3.4 μM IC_{50}=1052±172 μM IC_{50}=36.0±1.2 μM

Figure A2-21 Dose-response curves for prostate cancer cell-lines, PC3M-luc2 (green), DU145 (purple) and LNCaP (gold) treated with **189** from 0 to 1600 μM. Curves are the mean of three independent experiments each with six replicates. Plates were seeded as follows: PC3M-luc2 at $3x10^4$ cell mL^{-1} and DU145 and LNCaP at $4.5x10^4$ cell mL^{-1}. IC_{50} values are indicated as mean ± SD.

Mass spec footprint, their associated mass/triterpene correlation, LC/MS traces and dose-response curves for prostate cancer cell-lines are being documented in this section.

Mass Spec data

Ganoderma lucidum harvested at progressive growth times spanning from 2 to 8 weeks were analysed. The mushroom was grown in sawdust and extracted in ethanol unless otherwise stated.

GL 2 weeks

At 2 weeks, the harvested mushroom was split in tip and stalk and analysed separately.

Tip

Extractions were carried out in ethanol and methanol for this sample.

Extraction in ethanol

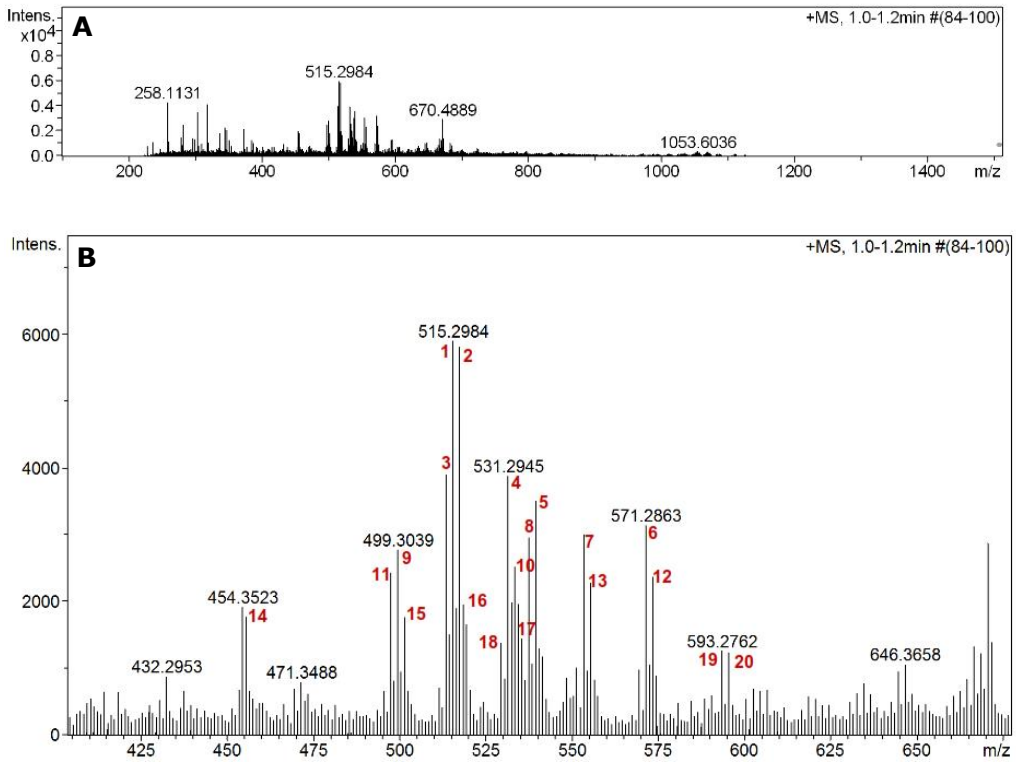


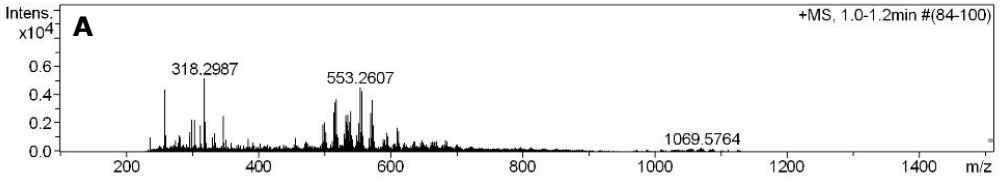
Figure A3-1 MS profile of the ethanol extract of GL tip harvested at 2 weeks. **A**. Full MS spectrum; **B**. expansion m/z 400-675, red figures show the order of signal intensity.

Entry	%I	m/z	Adduct	Triterpene
1	100.0	515.2984	M+H	**12**; **17**; **19**; **33**; **38**; **213**; **219**; **234**
2	98.3	517.3127	M+H	**8**; **10**; **35**; **36**; **37**; **232**
3	66.0	513.2871	M+H	**21**; **41**; **220**; **222**
			M+Na	**209**
4	65.7	531.2945	M+H	**40**; **225**; **233**; **236**; **238**
5	59.3	539.2959	M+Na	**8**; **10**; **35**; **36**; **37**; **232**
6	53.1	571.2863	M+H	**22**; **47**; **224**
7	50.7	553.2709	M+Na	**40**; **225**; **233**; **236**; **238**
8	50.0	537.2832	M+Na	**12**; **17**; **19**; **33**; **38**; **213**; **219**; **234**
9	46.9	499.3039	M+Na	**208**
10	42.5	533.3114	M+H	**23**; **39**; **206**; **218**
			M+Na	**57**
11	41.1	497.2896	M+Na	**216**
12	39.9	573.3038	M+H	**24**, **223**
13	38.3	555.2847	M+Na	**23**; **39**; **206**; **218**
14	29.8	455.3534	M+H	**45**; **59**; **63**; **254**
15	29.7	501.3237	M+H	**29**, **245**
16	27.9	519.3272	M+H	**18**
17	24.2	535.2943	M+Na	**21**; **41**; **220**; **222**
18	23.2	529.2824	M+H	**226**
19	21.2	593.2762	M+Na	**22**; **47**; **224**
20	20.8	595.2885	M+Na	**24**, **223**

Table A3-1 Top 20 masses found in ethanol extract of GL tip harvested at 2 weeks. Possible adduct and related triterpene given. Compound numeration is found in Appendix 5.

For this sample four masses have the highest intensity: m/z 515, 517, 513 and 531, which correspond to the molecular weight M+1 for all of them. Additionally, m/z 513 could also be the M+Na adduct of MW 490. Only for these four masses 24 possible GA could be present.

Extraction in methanol



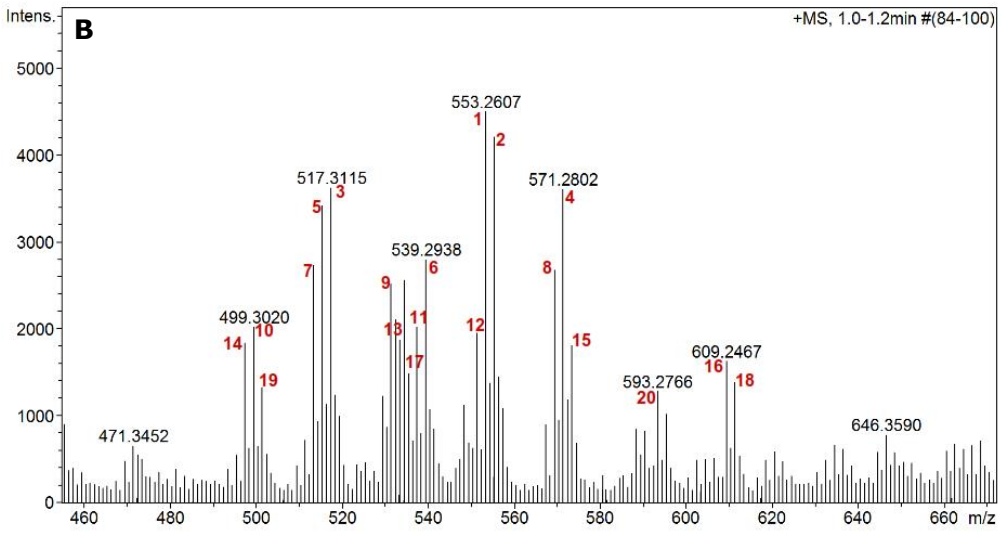


Figure A3-2 MS profile of the methanol extract of GL tip harvested at 2 weeks. **A**. Full MS spectrum; **B**. expansion M/z 460-670.

Entry	%I	%I Norm	m/z	Adduct	Triterpene
1	87.7	100.0	553.2607	M+Na	**40**; **225**; **233**; **236**; **238**
2	81.9	93.4	555.2719	M+Na	**23**; **39**; **206**; **218**
3	70.6	80.5	517.3115	M+H	**8**; **10**; **35**; **36**; **37**; **232**
4	70.2	80.0	571.2802	M+H	**22**; **47**; **224**
5	66.5	75.8	515.2978	M+H	**12**; **17**; **19**; **33**; **38**; **213**; **219**; **234**
6	54.4	62.0	539.2938	M+Na	**8**; **10**; **35**; **36**; **37**; **232**
7	53.2	60.7	513.2843	M+H	**21**; **41**; **220**; **222**
				M+Na	**209**
8	52.1	59.4	569.2554	M+Na	**237**
9	49.0	55.9	531.2958	M+H	**40**; **225**; **233**; **236**; **238**
10	39.3	44.8	499.3020	M+Na	**208**
11	39.3	44.8	537.2844	M+Na	**12**; **17**; **19**; **33**; **38**; **213**; **219**; **234**
12	37.9	43.2	551.2522	M+Na	**226**
13	36.3	41.4	533.3109	M+H	**23**; **39**; **206**; **218**
				M+Na	**57**
14	35.7	40.7	497.2887	M+Na	**216**
15	35.1	40.0	573.3030	M+H	**24**, **223**
16	31.6	36.0	609.2467	M+Na	**230**
17	28.8	32.8	535.3093	M+H	**235**
				M+Na	**21**; **41**; **220**; **222**
18	26.9	30.7	611.2596	M+Na	**231**
19	25.8	29.4	501.3212	M+H	**29**, **245**
20	24.8	28.3	593.2766	M+Na	**22**; **47**; **224**

Table A3-2 Top 20 masses found in the methanol extract of GL tip harvested at 2 weeks. Possible adduct and related triterpene given. Compound numeration is found in Appendix 5.

For this sample, the intensity was normalised so that comparisons were facilitated.

Extraction with methanol produced five intense peaks: m/z 553, 555, 517, 571 and 515, the two first corresponding to the M+Na and the rest to the M+H adducts. Potentially 26 GA could be included in these five masses.

Stalk

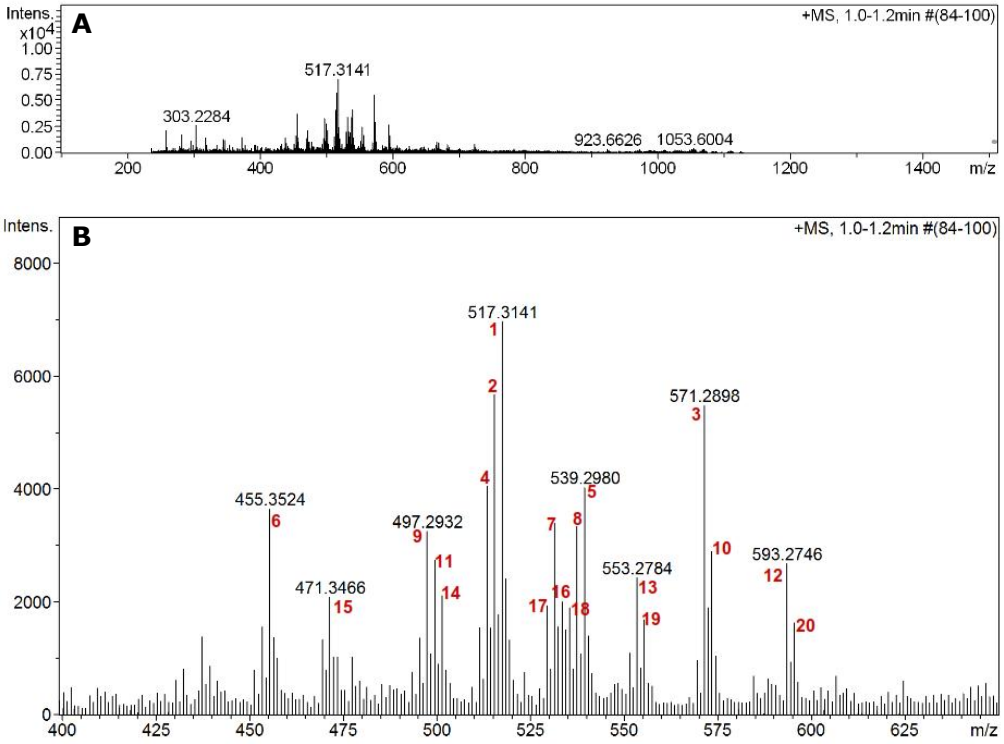


Figure A3-3 MS profile for the ethanol extract of GL stalk harvested at 2 weeks. **A**. Full MS spectrum; **B**. expansion m/z 400-650.

The four most distinctive masses are: m/z 517; 515; 571 and 513, which could be the M+H adduct of all of them. Additionallly, for m/z 513 the M+Na adduct could also be present.

Entry	%I	m/z	Adduct	Triterpene
1	100.0	517.3141	*M+H*	**8**; **10**; **35**; **36**; **37**; **232**
2	81.5	515.2987	*M+H*	**12**; **17**; **19**; **33**; **38**; **213**; **219**; **234**
3	78.6	571.2898	*M+H*	**22**; **47**; **224**
4	58.0	513.2898	*M+H*	**21**; **41**; **220**; **222**
			M+Na	**209**
5	57.7	539.2980	*M+Na*	**8**; **10**; **35**; **36**; **37**; **232**
6	52.3	455.3524	*M+H*	**45**; **59**; **63**; **254**
7	48.6	531.2971	*M+H*	**40**; **225**; **233**; **236**; **238**
8	47.7	537.2852	*M+Na*	**12**; **17**; **19**; **33**; **38**; **213**; **219**; **234**
9	46.6	497.2932	*M+Na*	**216**
10	41.4	573.3041	*M+H*	**24**, **223**
11	39.2	499.3056	*M+Na*	**208**
12	38.3	593.2746	*M+Na*	**22**; **47**; **224**
13	34.7	553.2782	*M+Na*	**40**; **225**; **233**; **236**; **238**
14	30.2	501.3238	*M+H*	**29**, **245**
15	29.8	471.3466	*M+H*	**79**
16	28.6	533.3128	*M+H*	**23**; **39**; **206**; **218**
			M+Na	**57**
17	27.7	529.2833	*M+H*	**226**
18	27.2	535.3060	*M+H*	**235**
			M+Na	**21**; **41**; **220**; **222**
19	24.1	555.2901	*M+Na*	**23**; **39**; **206**; **218**
20	23.3	595.2891	*M+Na*	**24**, **223**

Table A3-3 Top 20 masses found in the ethanol extract of GL stalk harvested at 2 weeks. Possible adduct and related triterpene given. Compound numeration is found in Appendix 5.

GL 4 weeks

Ganoderma lucidum grown in sawdust, mesocarp fibres (MCF) and empty fruit bunches fibres (EFB) were harvested at 4 weeks. The extraction of these samples was performed in ethanol.

Sawdust

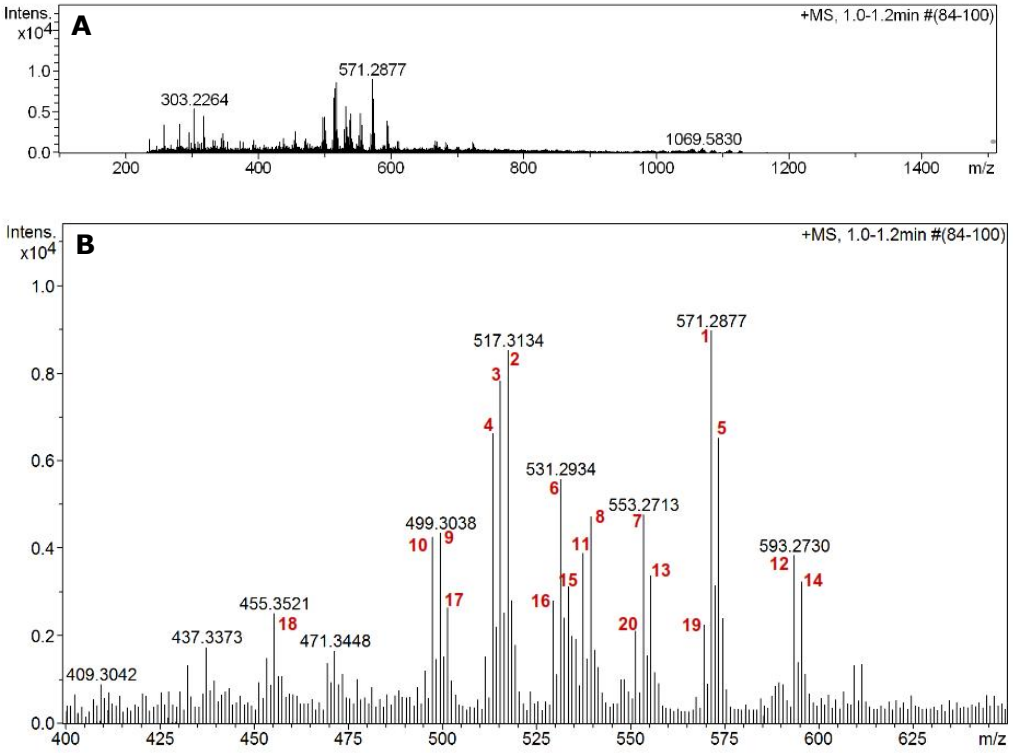


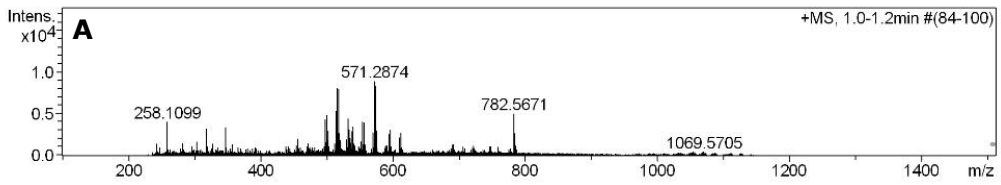
Figure A3-4 MS profile of the ethanol extract of GL harvested at 4 weeks. **A**. Full MS spectrum; **B**. expansion M/z 400-650.

Six masses were the most intense, m/z 571, 517, 515, 513, 573 and 531, which corresponded to the M+H adduct. Additionally, m/z 513 could also correspond to the M+Na adduct.

Entry	%I	m/z	Adduct	Triterpene
1	100.0	571.2877	M+H	**22**; **47**; **224**
2	95.1	517.3134	M+H	**8**; **10**; **35**; **36**; **37**; **232**
3	87.1	515.2979	M+H	**12**; **17**; **19**; **33**; **38**; **213**; **219**; **234**
4	73.9	513.2847	M+H	**21**; **41**; **220**; **222**
			M+Na	**209**
5	72.5	573.3048	M+H	**24**, **223**
6	62.1	531.2934	M+H	**40**; **225**; **233**; **236**; **238**
7	53.1	553.2713	M+Na	**40**; **225**; **233**; **236**; **238**
8	52.6	539.2961	M+Na	**8**; **10**; **35**; **36**; **37**; **232**
9	48.4	499.3038	M+Na	**208**
10	47.3	497.2922	M+Na	**216**
11	43.2	537.2824	M+Na	**12**; **17**; **19**; **33**; **38**; **213**; **219**; **234**
12	42.7	593.2730	M+Na	**22**; **47**; **224**
13	37.5	555.2845	M+Na	**23**; **39**; **206**; **218**
14	36.0	595.2886	M+Na	**24**, **223**
15	34.7	533.3094	M+H	**23**; **39**; **206**; **218**
			M+Na	**57**
16	31.0	529.2821	M+H	**226**
17	29.3	501.3230	M+H	**29**, **245**
18	27.9	455.3521	M+H	**45**; **59**; **63**; **254**
19	25.0	569.2657	M+Na	**237**
20	23.4	551.2608	M+Na	**226**

Table A3-4 Top 20 masses found in the ethanol extract of GL grown in sawdust and harvested at 4 weeks. Possible adduct and related triterpene given. Compound numeration is found in Appendix 5.

Mesocarp fibres (MCF)



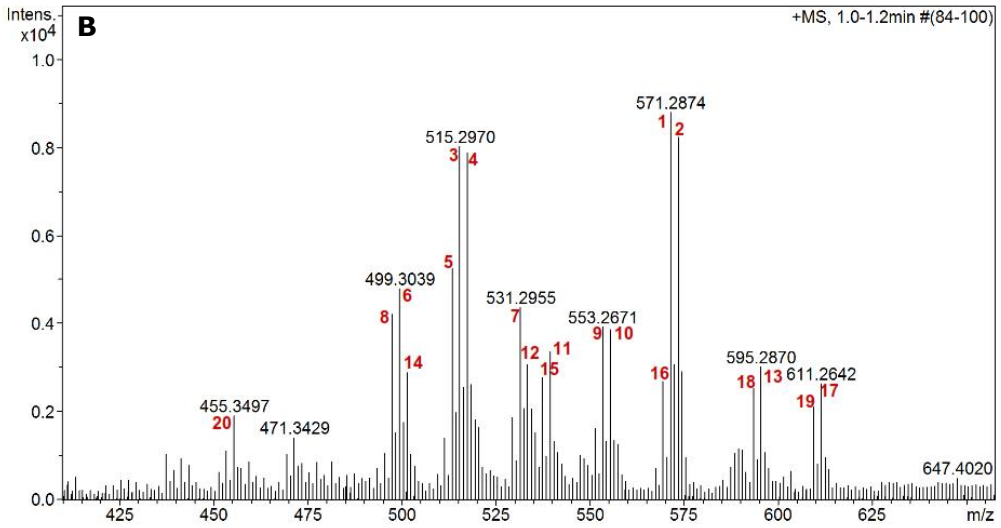


Figure A3-5 MS profile of the ethanol extract of GL grown in MCF and harvested at 4 weeks. **A**. Full MS spectrum; **B**. expansion m/z 400-655.

Entry	%I	m/z	Adduct	Triterpene
1	100.0	571.2874	M+H	**22**; **47**; **224**
2	93.6	573.3052	M+H	**24**, **223**
3	91.2	515.2970	M+H	**12**; **17**; **19**; **33**; **38**; **213**; **219**; **234**
4	89.6	517.3114	M+H	**8**; **10**; **35**; **36**; **37**; **232**
5	59.6	513.2859	M+H	**21**; **41**; **220**; **222**
			M+Na	**209**
6	54.4	499.3039	M+Na	**208**
7	49.6	531.2955	M+H	**40**; **225**; **233**; **236**; **238**
8	47.9	497.2898	M+Na	**216**
9	44.5	553.2671	M+Na	**40**; **225**; **233**; **236**; **238**
10	43.8	555.2793	M+Na	**23**; **39**; **206**; **218**
11	38.2	539.2978	M+Na	**8**; **10**; **35**; **36**; **37**; **232**
12	34.7	533.3114	M+H	**23**; **39**; **206**; **218**
			M+Na	**57**
13	34.2	595.2870	M+Na	**24**, **223**
14	32.7	501.3206	M+H	**29**, **245**
15	31.5	537.2832	M+Na	**12**; **17**; **19**; **33**; **38**; **213**; **219**; **234**
16	30.5	569.2622	M+Na	**237**
17	29.8	611.2693	M+Na	**231**
18	28.6	593.2758	M+Na	**22**; **47**; **224**
19	23.8	609.2503	M+Na	**230**
20	21.6	455.3497	M+H	**45**; **59**; **63**; **254**

Table A3-5 Top 20 masses found in the ethanol extract of GL grown in MCF and harvested at 4 weeks. Possible adduct and related triterpene given. Compound numeration is found in Appendix 5.

GL grown in MSF showed four most intense masses: m/z 571, 573, 515 and 517 corresponding all of them to the M+H adduct. Potentially 19 GA could be included in these four masses.

Empty fruit bunch fibres (EFB)

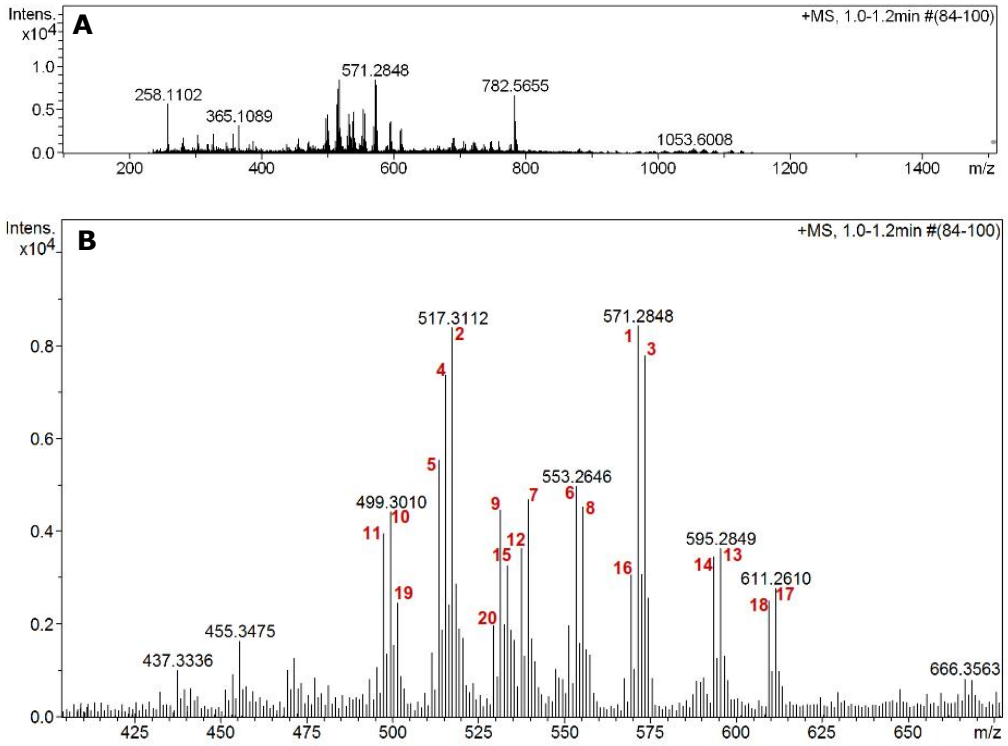


Figure A3-6 MS profile of the ethanol extract of GL grown in EFB and harvested at 4 weeks. **A**. Full MS spectrum; **B**. expansion m/z 400-675. Compound numeration is found in Appendix 5.

Five most intense masses were found: m/z 571; 517; 573; 515 and 513. All of them the M+H adduct. Besides, m/z 513 could be associated to the M+Na adduct.

Entry	%I	m/z	Adduct	Triterpene
1	100.0	571.2848	M+H	**22**; **47**; **224**
2	99.4	517.3112	M+H	**8**; **10**; **35**; **36**; **37**; **232**
3	92.2	573.3018	M+H	**24**, **223**
4	87.3	515.2957	M+H	**12**; **17**; **19**; **33**; **38**; **213**; **219**; **234**
5	65.5	513.2844	M+H	**21**; **41**; **220**; **222**
			M+Na	**209**
6	58.8	553.2646	M+Na	**40**; **225**; **233**; **236**; **238**
7	55.4	539.2952	M+Na	**8**; **10**; **35**; **36**; **37**; **232**
8	53.5	555.2769	M+Na	**23**; **39**; **206**; **218**
9	52.8	531.2924	M+H	**40**; **225**; **233**; **236**; **238**
10	52.3	499.3010	M+Na	**208**
11	46.9	497.2894	M+Na	**216**
12	43.0	537.2815	M+Na	**12**; **17**; **19**; **33**; **38**; **213**; **219**; **234**
13	43.0	595.2849	M+Na	**24**, **223**
14	40.8	593.2718	M+Na	**22**; **47**; **224**
15	38.4	533.3077	M+H	**23**; **39**; **206**; **218**
			M+Na	**57**
16	36.2	569.2584	M+Na	**237**
17	32.8	611.2610	M+Na	**231**
18	29.6	609.2449	M+Na	**230**
19	29.0	501.3189	M+H	**29**, **245**
20	23.3	529.2797	M+H	**226**

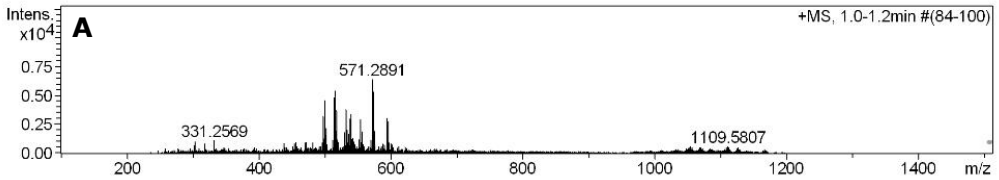
Table A3-6 Top 20 masses found for the ethanol extract of GL grown in EFB and harvested at 4 weeks. Possible adduct and related triterpene given. Compound numeration is found in Appendix 5.

GL 6 weeks

GL harvested at 6 weeks was extracted using ethanol and sonication with chloroform. In addition, GL antler variety was harvested at this time and extracted with ethanol.

Extraction in ethanol

GL (normal)



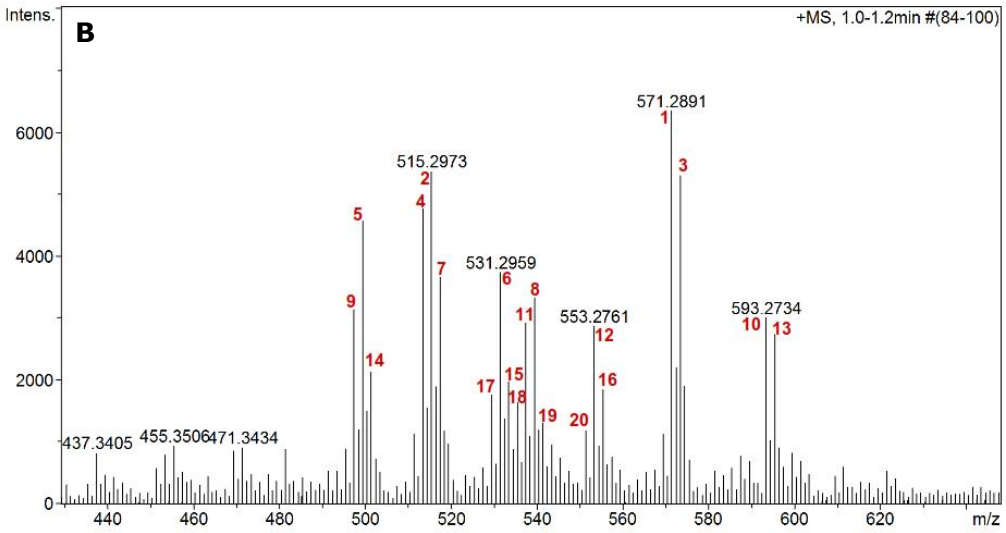


Figure A3-7 MS profile for the ethanol extract of GL harvested at 6 weeks. **A**. Full MS spectrum; **B**. Expansion m/z 430-640. Figures in red refer to signal intensity.

Entry	%I	m/z	Adduct	Triterpene
1	100.0	571.2891	M+H	**22**; **47**; **224**
2	84.6	515.2973	M+H	**12**; **17**; **19**; **33**; **38**; **213**; **219**; **234**
3	83.5	573.3067	M+H	**24**, **223**
4	75.1	513.2866	M+H	**21**; **41**; **220**; **222**
			M+Na	**209**
5	72.0	499.3064	M+Na	**208**
6	58.8	531.2959	M+H	**40**; **225**; **233**; **236**; **238**
7	57.6	517.3132	M+H	**8**; **10**; **35**; **36**; **37**; **232**
8	52.3	539.2966	M+Na	**8**; **10**; **35**; **36**; **37**; **232**
9	49.3	497.2907	M+Na	**216**
10	47.2	593.2734	M+Na	**22**; **47**; **224**
11	45.9	537.2843	M+Na	**12**; **17**; **19**; **33**; **38**; **213**; **219**; **234**
12	45.1	553.2761	M+Na	**40**; **225**; **233**; **236**; **238**
13	42.9	595.2874	M+Na	**24**, **223**
14	33.3	501.3205	M+H	**29**, **245**
15	31.0	533.3100	M+H	**23**; **39**; **206**; **218**
			M+Na	**57**
16	28.9	555.2892	M+Na	**23**; **39**; **206**; **218**
17	27.6	529.2857	M+H	**226**
18	25.6	535.2787	M+Na	**21**; **41**; **220**; **222**
19	20.5	541.3119	M+Na	**18**
20	18.5	551.2647	M+Na	**226**

Table A3-7 Top 20 masses found in the ethanol extract of GL harvested at 6 weeks. Possible adduct and related triterpene given. Compound numeration is found in Appendix 5.

Five masses were the most remarkable: m/z 571; 515; 573; 513 and 499. These are the M+H adduct of the four first masses and the M+Na adduct of m/z 513 and 499.

GL antler type

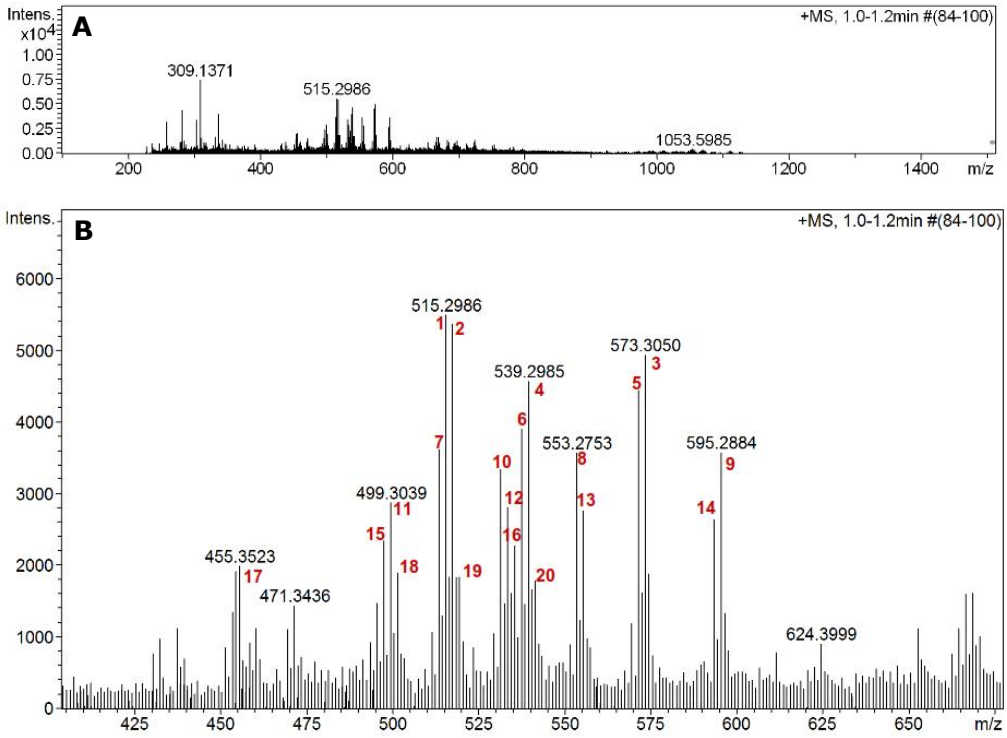


Figure A3-8 MS profile of the ethanol extract of GL antler variety harvested at 6 weeks. **A**. Full MS spectrum; **B**. expansion m/z 400-675.

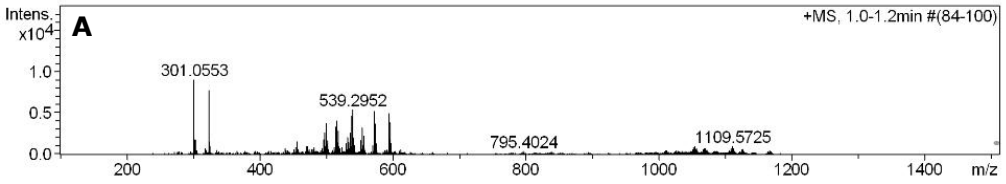
To be able to compare with the other samples and since the 100% peak did not corresponded to any of the interesting masses, intensities were normalised to the most intense peak in the full list of masses (m/z 515); this normalised intensity percentage is given in Table A3-8 along with the other percentages.

The five masses with highest intensity are: m/z 515; 517; 573; 539 and 571. These are the M+H adducts except for m/z 539 that is the M+Na adduct.

Entry	%I	%I norm	m/z	Adduct	Triterpene
1	74.6	100.0	515.2966	M+H	**12**; **17**; **19**; **33**; **38**; **213**; **219**; **234**
2	72.9	97.7	517.3138	M+H	**8**; **10**; **35**; **36**; **37**; **232**
3	66.9	89.7	573.3050	M+H	**24**, **223**
4	62.0	83.1	539.2985	M+Na	**8**; **10**; **35**; **36**; **37**; **232**
5	60.3	80.8	571.2893	M+H	**22**; **47**; **224**
6	53.0	71.0	537.2861	M+Na	**12**; **17**; **19**; **33**; **38**; **213**; **219**; **234**
7	49.1	65.8	513.2877	M+H	**21**; **41**; **220**; **222**
				M+Na	**209**
8	48.4	64.9	553.2753	M+Na	**40**; **225**; **233**; **236**; **238**
9	48.4	64.9	595.2884	M+Na	**24**, **223**
10	45.3	60.7	531.2965	M+H	**40**; **225**; **233**; **236**; **238**
11	38.9	52.1	499.3039	M+Na	**208**
12	38.0	50.9	533.3133	M+H	**23**; **39**; **206**; **218**
				M+Na	**57**
13	37.3	50.0	555.2904	M+Na	**23**; **39**; **206**; **218**
14	35.6	47.7	593.2773	M+Na	**22**; **47**; **224**
15	31.7	42.5	497.2941	M+Na	**216**
16	30.8	41.3	535.3075	M+H	**235**
17	26.9	36.1	455.3523	M+H	**45**; **59**; **63**; **254**
18	25.7	34.5	501.3223	M+H	**29**, **245**
19	24.8	33.2	519.3302	M+H	**18**
20	24.1	32.3	541.3177	M+Na	**18**

Table A3-8 Top 20 masses found in the ethanol extract of GL antler variety harvested at 6 weeks. Possible adduct and related triterpene given. Compound numeration is found in Appendix 5.

Extraction by sonication in chloroform



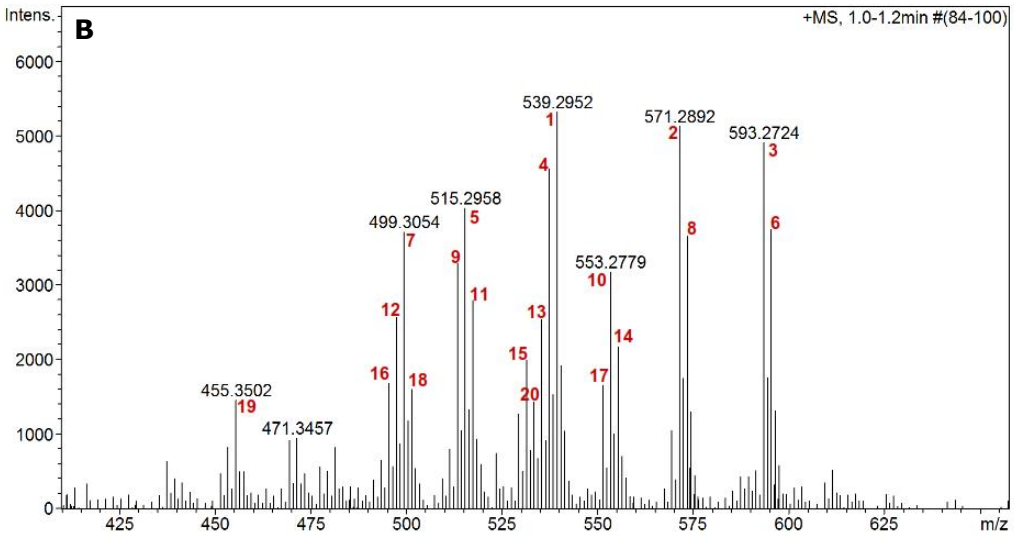


Figure A3-9 MS profile of the chloroform extract of GL harvested at 6 weeks. **A**. Full MS spectrum; **B**. Expansion M/z 400-650.

Entry	%I	% I Norm	m/z	Adduct	Triterpene
1	59.6	100.0	539.2952	M+Na	**8**; **10**; **35**; **36**; **37**; **232**
2	57.4	96.3	571.2892	M+H	**22**; **47**; **224**
3	55.0	92.3	593.2724	M+Na	**22**; **47**; **224**
4	51.0	85.6	537.2808	M+Na	**12**; **17**; **19**; **33**; **38**; **213**; **219**; **234**
5	45.1	75.7	515.2958	M+H	**12**; **17**; **19**; **33**; **38**; **213**; **219**; **234**
6	41.9	70.3	595.2868	M+Na	**24**, **223**
7	41.5	69.6	499.3054	M+Na	**208**
8	40.9	68.6	573.3050	M+H	**24**, **223**
9	36.8	61.7	513.2902	M+H	**21**; **41**; **220**; **222**
				M+Na	**209**
10	35.5	59.6	553.2779	M+Na	**40**; **225**; **233**; **236**; **238**
11	31.2	52.3	517.3123	M+H	**8**; **10**; **35**; **36**; **37**; **232**
12	28.7	48.2	497.2917	M+Na	**216**
13	28.3	47.5	535.2719	M+Na	**21**; **41**; **220**; **222**
14	24.2	40.6	555.2903	M+Na	**23**; **39**; **206**; **218**
15	22.2	37.2	531.2946	M+H	**40**; **225**; **233**; **236**; **238**
16	18.7	31.4	495.3394	M+Na	**67**; **241**; **256**
17	18.5	31.0	551.2686	M+Na	**226**
18	17.8	29.9	501.3196	M+H	**29**, **245**
19	16.2	27.2	455.3502	M+H	**45**; **59**; **63**; **264**
20	15.9	26.7	533.2962	M+H	**23**; **39**; **206**; **218**
				M+Na	**57**

Table A3-9 Top 20 masses found in the chloroform extract of GL harvested at 6 weeks. Possible adduct and related triterpene given. Compound numeration is found in Appendix 5.

Peaks were normalised to the highest intense peak within the m/z peaks of interest for facilitating the comparison. Both percentages of intensity are shown in Table A3-9.

Eight masses ranked the highest intensity: m/z 539; 571; 593; 537; 515; 595; 499; 573. Three masses corresponded to the M+H adduct, m/z 571; 515 and 573, all the rest corresponded to the M+Na.

GL 8 weeks

GL harvested at 8 weeks was extracted with a variety of solvents: ethanol, methanol, dichloromethane, ethyl acetate and water.

Extraction in ethanol

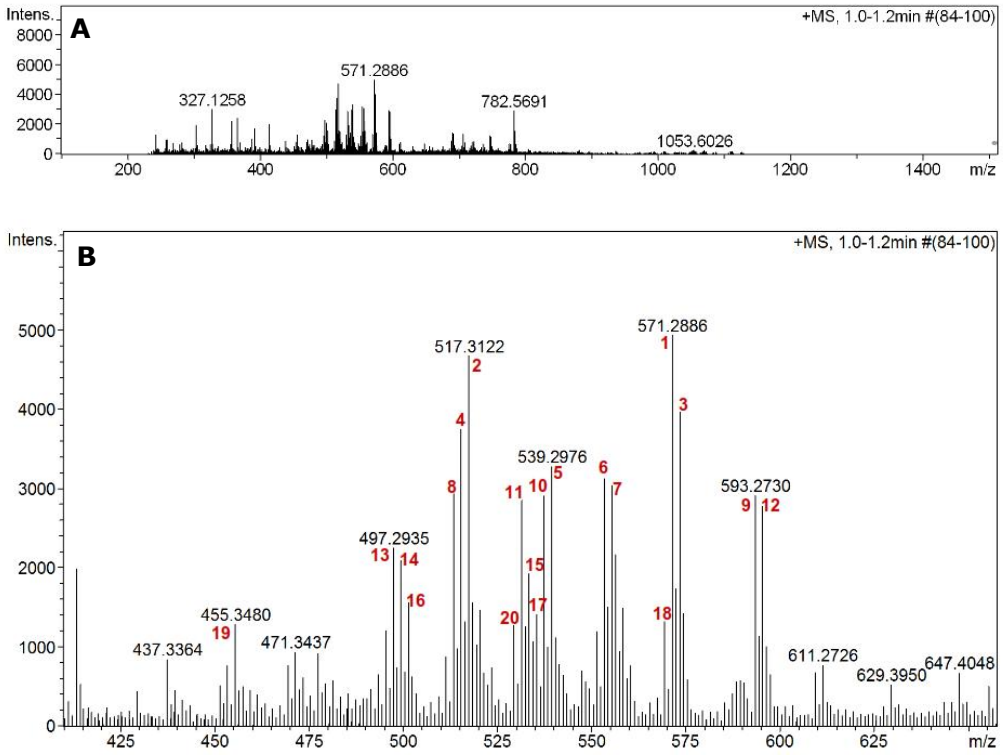


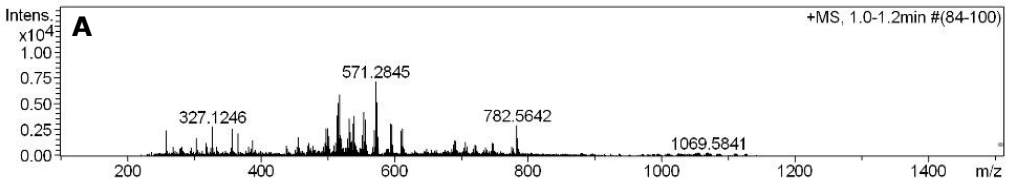
Figure A3-10 MS profile of the ethanol extract of GL harvested at 8 weeks. **A**. Full MS spectrum; **B**. Expansion m/z 400-655. Figures in red refer to signal intensity from 1 to 20.

The five most intense peaks are: m/z 571, 517, 573, 515, 539. The four first corresponding to the M+H adduct and the last one to the M+Na adduct.

Entry	%I	m/z	Adduct	Triterpene
1	100.0	571.2886	M+H	**22**; **47**; **224**
2	94.7	517.3122	M+H	**8**; **10**; **35**; **36**; **37**; **232**
3	80.3	573.3037	M+H	**24**, **223**
4	76.0	515.2977	M+H	**12**; **17**; **19**; **33**; **38**; **213**; **219**; **234**
5	66.4	539.2976	M+Na	**8**; **10**; **35**; **36**; **37**; **232**
6	63.3	553.2740	M+Na	**40**; **225**; **233**; **236**; **238**
7	61.6	555.2770	M+Na	**23**; **39**; **206**; **218**
8	59.4	513.2869	M+H	**21**; **41**; **220**; **222**
			M+Na	**209**
9	58.9	593.2730	M+H	**22**; **47**; **224**
10	58.7	537.2822	M+Na	**12**; **17**; **19**; **33**; **38**; **213**; **219**; **234**
11	57.7	531.2948	M+H	**40**; **225**; **233**; **236**; **238**
12	56.1	595.2872	M+Na	**24**, **223**
13	45.4	497.2935	M+Na	**216**
14	42.2	499.3039	M+Na	**208**
15	38.8	533.3090	M+H	**23**; **39**; **206**; **218**
			M+Na	**57**
16	31.4	501.3195	M+H	**29**, **245**
17	28.4	535.2876	M+Na	**21**; **41**; **220**; **222**
18	26.6	569.2664	M+Na	**237**
19	26.0	455.3480	M+H	**45**; **59**; **63**; **254**
20	25.7	529.2827	M+H	**226**

Table A3-10 Top 20 masses found in ethanol extract of GL harvested at 8 weeks. Possible adduct and related triterpene given. Compound numeration is found in Appendix 5.

Extraction in methanol



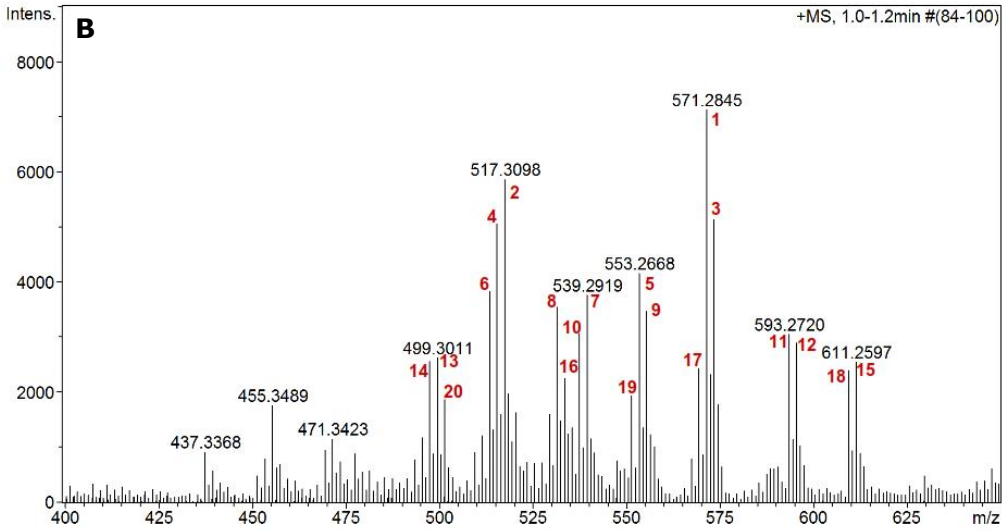


Figure A3-11 MS profile of the methanol extract of GL harvested at 8 weeks. **A**. Full MS spectrum; **B**. expansion M/z 400-650.

Entry	%I	m/z	Adduct	Triterpene
1	100.0	571.2845	M+H	**22**; **47**; **224**
2	82.2	517.3098	M+H	**8**; **10**; **35**; **36**; **37**; **232**
3	72.1	573.3041	M+H	**24**, **223**
4	70.9	515.2976	M+H	**12**; **17**; **19**; **33**; **38**; **213**; **219**; **234**
5	58.2	553.2668	M+Na	**40**; **225**; **233**; **236**; **238**
6	53.7	513.2839	M+H	**21**; **41**; **220**; **222**
			M+Na	**209**
7	52.7	539.2919	M+Na	**8**; **10**; **35**; **36**; **37**; **232**
8	49.7	531.2931	M+H	**40**; **225**; **233**; **236**; **238**
9	48.5	555.2758	M+Na	**23**; **39**; **206**; **218**
10	42.8	537.2788	M+Na	**12**; **17**; **19**; **33**; **38**; **213**; **219**; **234**
11	42.7	593.2720	M+Na	**22**; **47**; **224**
12	40.6	595.2862	M+Na	**24**, **223**
13	36.7	499.3011	M+Na	**208**
14	35.8	497.2916	M+Na	**216**
15	35.7	611.2597	M+Na	**231**
16	34.7	533.3027	M+H	**23**; **39**; **206**; **218**
			M+Na	**57**
17	34.0	569.2604	M+Na	**237**
18	33.5	609.2459	M+Na	**230**
19	27.0	551.2570	M+Na	**226**
20	26.1	501.3204	M+H	**29**, **245**

Table A3-11 Top 20 masses found in the methanol extract of GL harvested at 8 weeks. Possible adduct and related triterpene given. Compound numeration is found in Appendix 5.

Four masses predominate: m/z 571, 517, 515, 573 all of which corresponded to the M+H adduct.

Extraction in dichloromethane

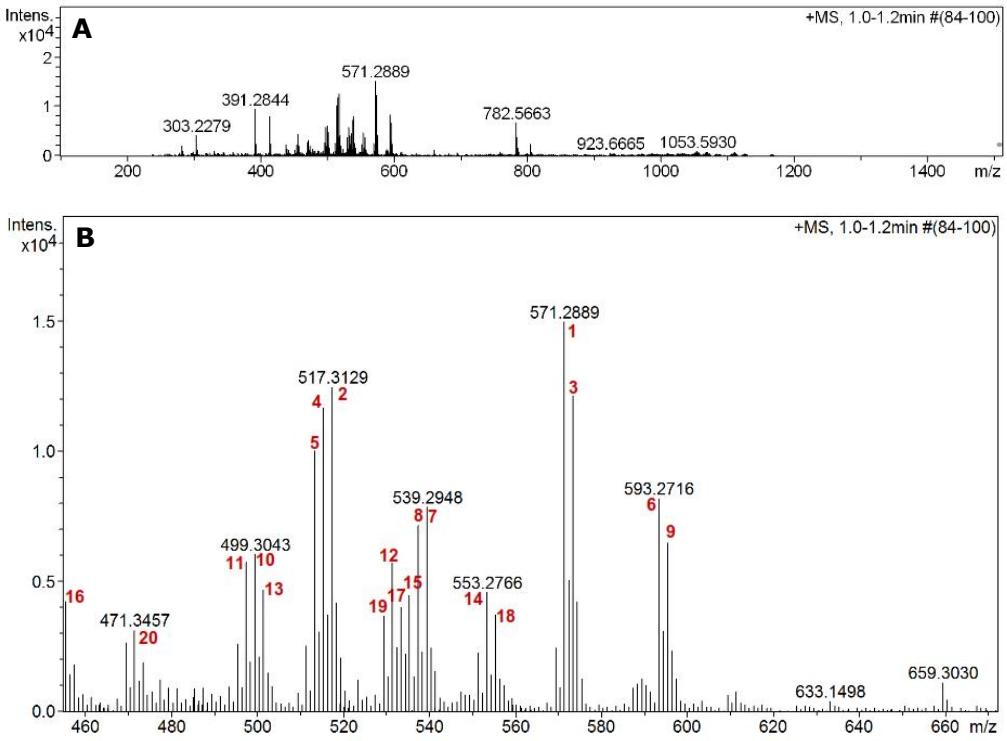


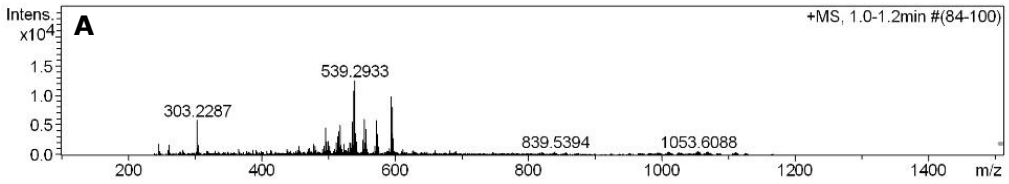
Figure A3-12 MS profile of the dichloromethane extract of GL harvested at 8 weeks. **A**. Full MS spectrum; **B**. Expansion M/z 450-600 and C. expansion M/z 600-800.

Five masses showed the highest intensity: m/z 571; 517; 573; 515 and 513. These are all M+H adducts, with the exception of m/z 513 that could also be the M+Na adduct.

Entry	%I	m/z	Adduct	Triterpene
1	100.0	571.2889	M+H	**22**; **47**; **224**
2	83.2	517.3129	M+H	**8**; **10**; **35**; **36**; **37**; **232**
3	81.0	573.3061	M+H	**24**, **223**
4	77.8	515.2984	M+H	**12**; **17**; **19**; **33**; **38**; **213**; **219**; **234**
5	66.9	513.2884	M+H	**21**; **41**; **220**; **222**
			M+Na	**209**
6	54.6	593.2716	M+Na	**22**; **47**; **224**
7	52.3	539.2948	M+Na	**8**; **10**; **35**; **36**; **37**; **232**
8	47.6	537.2795	M+Na	**12**; **17**; **19**; **33**; **38**; **213**; **219**; **234**
9	43.1	595.2868	M+Na	**24**, **223**
10	40.1	499.3043	M+Na	**208**
11	38.1	497.2940	M+Na	**216**
12	38.0	531.2940	M+H	**40**; **225**; **233**; **236**; **238**
13	31.2	501.3213	M+H	**29**, **245**
14	30.4	553.2766	M+Na	**40**; **225**; **233**; **236**; **238**
15	29.6	535.2748	M+Na	**21**; **41**; **220**; **222**
16	28.2	455.3526	M+H	**45**; **59**; **63**; **254**
17	26.6	533.3043	M+H	**23**; **39**; **206**; **218**
			M+Na	**57**
18	24.5	555.2897	M+Na	**23**; **39**; **206**; **218**
19	24.2	529.2825	M+H	**226**
20	20.6	471.3457	M+H	**79**

Table A3-12 Top 20 masses found in the dichloromethane extract of GL harvested at 8 weeks. Possible adduct and related triterpene given. Compound numeration is found in Appendix 5.

Extraction in ethyl acetate



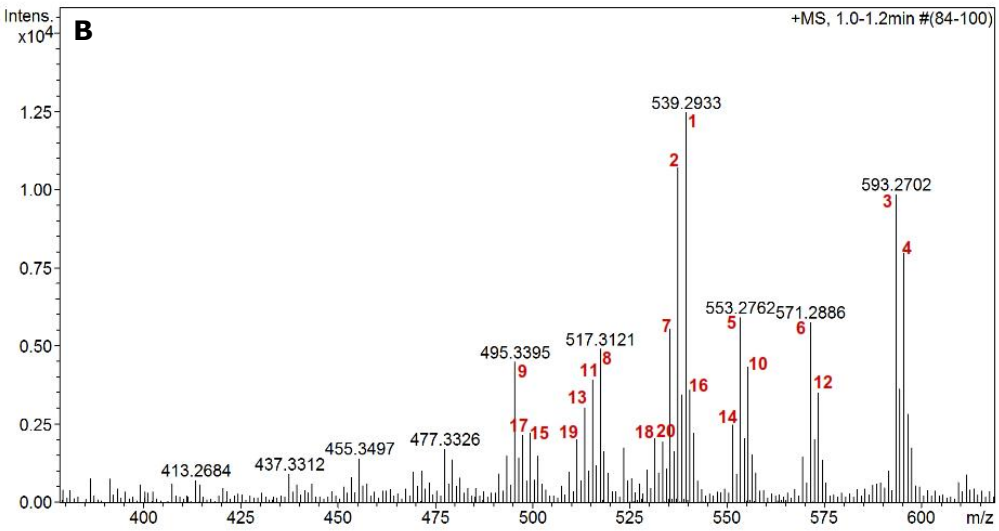


Figure A3-13 MS profile of the ethyl acetate extract of GL harvested at 8 weeks. A. Full MS spectrum; B. expansion M/z 380-615 and C. expansion M/z 600-800.

Entry	%I	m/z	Adduct	Triterpene
1	100.0	539.2933	M+Na	**8**; **10**; **35**; **36**; **37**; **232**
2	85.9	537.2790	M+Na	**12**; **17**; **19**; **33**; **38**; **213**; **219**; **234**
3	79.0	593.2702	M+Na	**22**; **47**; **224**
4	63.9	595.2860	M+Na	**24**, **223**
5	47.4	553.2762	M+Na	**40**; **225**; **233**; **236**; **238**
6	46.1	571.2886	M+H	**22**; **47**; **224**
7	44.4	535.2696	M+Na	**21**; **41**; **220**; **222**
8	39.2	517.3121	M+H	**8**; **10**; **35**; **36**; **37**; **232**
9	35.8	495.3395	M+Na	**67**; **241**; **256**
10	34.7	555.2924	M+Na	**23**; **39**; **206**; **218**
11	31.1	515.2969	M+H	**12**; **17**; **19**; **33**; **38**; **213**; **219**; **234**
12	28.0	573.3048	M+H	**24**, **223**
13	24.1	513.3160	M+H	**21**; **41**; **220**; **222**
			M+Na	**209**
14	19.8	551.2718	M+Na	**226**
15	17.6	499.3040	M+Na	**208**
16	17.6	541.3063	M+Na	**18**
17	17.1	497.3139	M+Na	**216**
18	16.2	531.2922	M+H	**40**; **225**; **233**; **236**; **238**
19	16.0	511.3223	M+H	**57**
20	15.4	533.2893	M+H	**23**; **39**; **206**; **218**
			M+Na	**57**

Table A3-13 Top 20 masses found in the ethyl acetate extract of for GL harvested at 8 weeks. Possible adduct and related triterpene given. Compound numeration is found in Appendix 5.

Four masses were found with the highest intensity: m/z 539; 537; 593 and 595. All of them as M+Na adducts.

Extraction in water

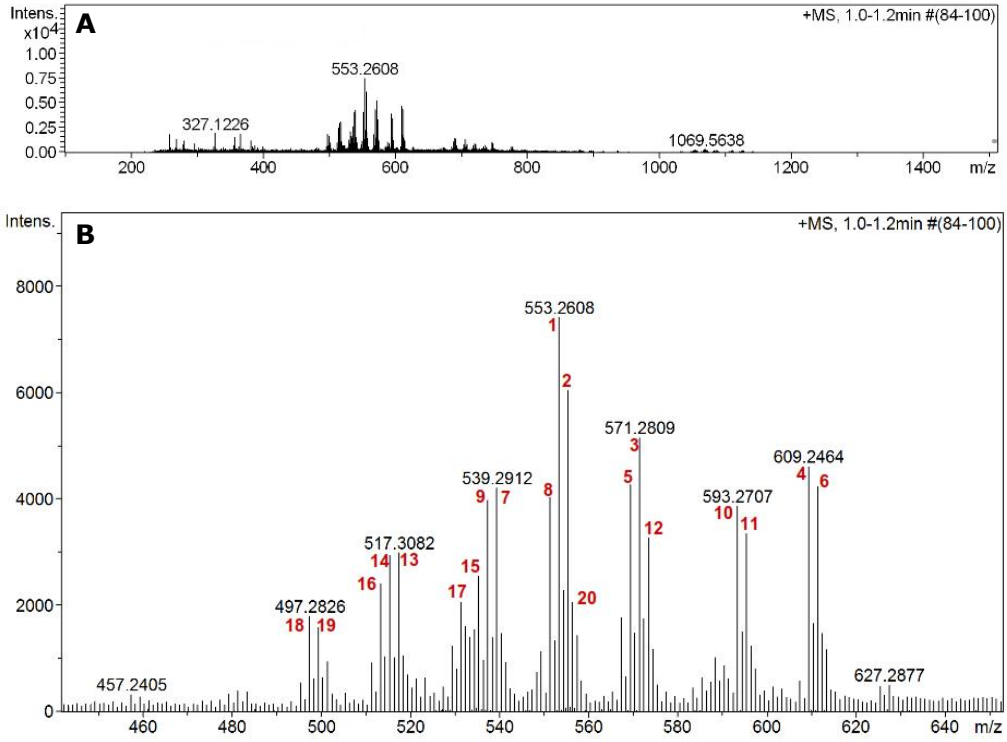


Figure A3-14 MS profile of the water extract of GL harvested at 8 weeks. **A**. Full MS spectrum; **B**. expansion M/z 440-650.

The four masses with highest intensity in the mass spec were: m/z 553; 555; 571 and 609. All of which attributed to the M+Na adduct except for m/z 571 that may be the M+H adduct.

Entry	%I	m/z	Adduct	Triterpene
1	100.0	553.2608	M+Na	**40**; **225**; **233**; **236**; **238**
2	81.5	555.2738	M+Na	**23**; **39**; **206**; **218**
3	69.4	571.2809	M+H	**22**; **47**; **224**
4	62.2	609.2464	M+Na	**230**
5	57.4	569.2566	M+Na	**237**
6	57.1	611.2601	M+Na	**231**
7	56.6	539.2912	M+Na	**8**; **10**; **35**; **36**; **37**; **232**
8	54.3	551.2464	M+Na	**226**
9	53.6	537.2775	M+Na	**12**; **17**; **19**; **33**; **38**; **213**; **219**; **234**
10	52.1	593.2707	M+Na	**22**; **47**; **224**
11	45.1	595.2851	M+Na	**24**, **223**
12	43.9	573.3022	M+H	**24**, **223**
13	40.2	517.3082	M+H	**8**; **10**; **35**; **36**; **37**; **222**
14	39.5	515.2942	M+H	**12**; **17**; **19**; **33**; **38**; **213**; **219**; **234**
15	34.2	535.2685	M+Na;	**21**; **41**; **220**; **222**
16	32.4	513.2819	M+H	**21**; **41**; **220**; **222**
			M+Na;	**209**
17	27.2	531.2919	M+H	**40**; **225**; **233**; **236**; **238**
18	24.1	497.2826	M+Na	**216**
19	21.1	499.2969	M+Na	**208**
20	19.2	557.2864	M+Na	**235**

Table A3-14 Top 20 masses found in the water extract of GL harvested at 8 weeks. Possible adduct and related triterpene given. Compound numeration is found in Appendix 5.

LC-MS data

The extracted GL were also analysed by LC-MS. The profiles were grouped by growing stage, substrate, GL type and extraction solvent. A table with the normalised peak area and graphs of the major and medium area size peaks was included.

LC-MS Profiles

i. GL harvested at different growing stages

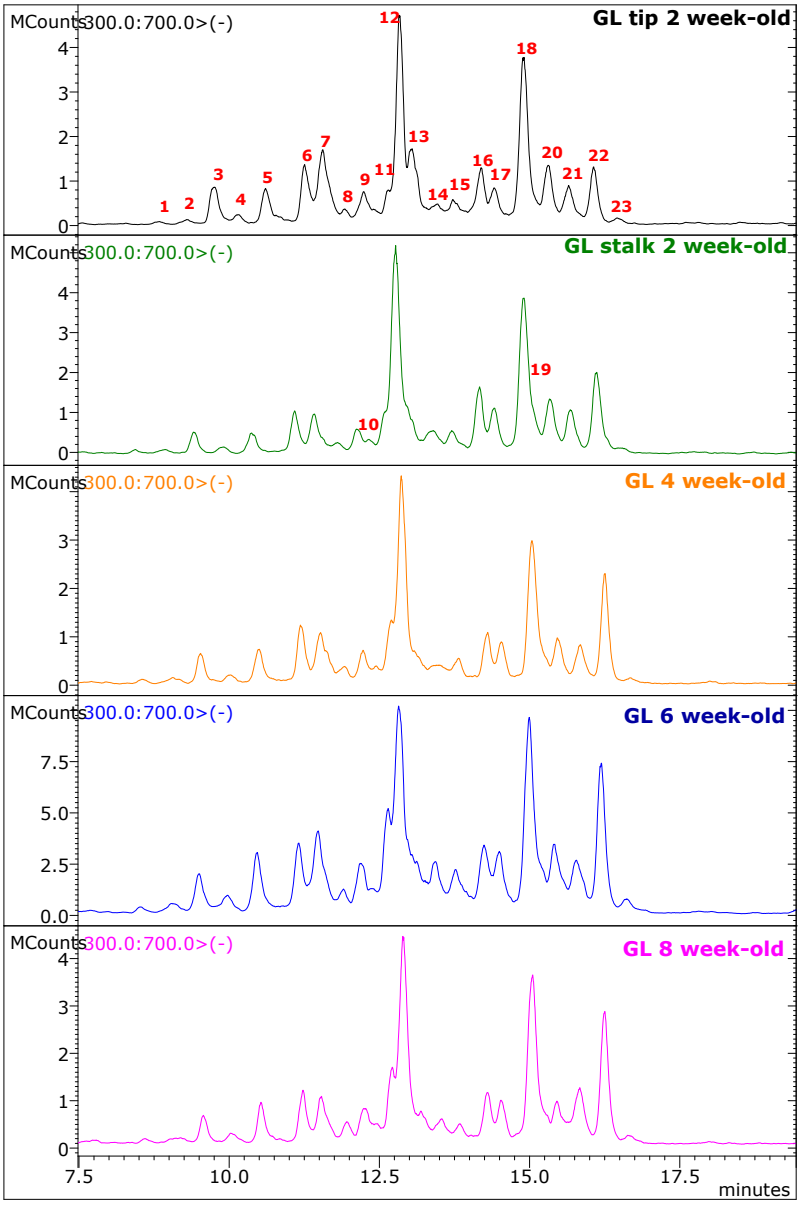


Figure A3-15 LC-MS profile for the ethanol extract of GL harvested at different times, from 2 to 8 weeks.

ii. GL grown in different substrates

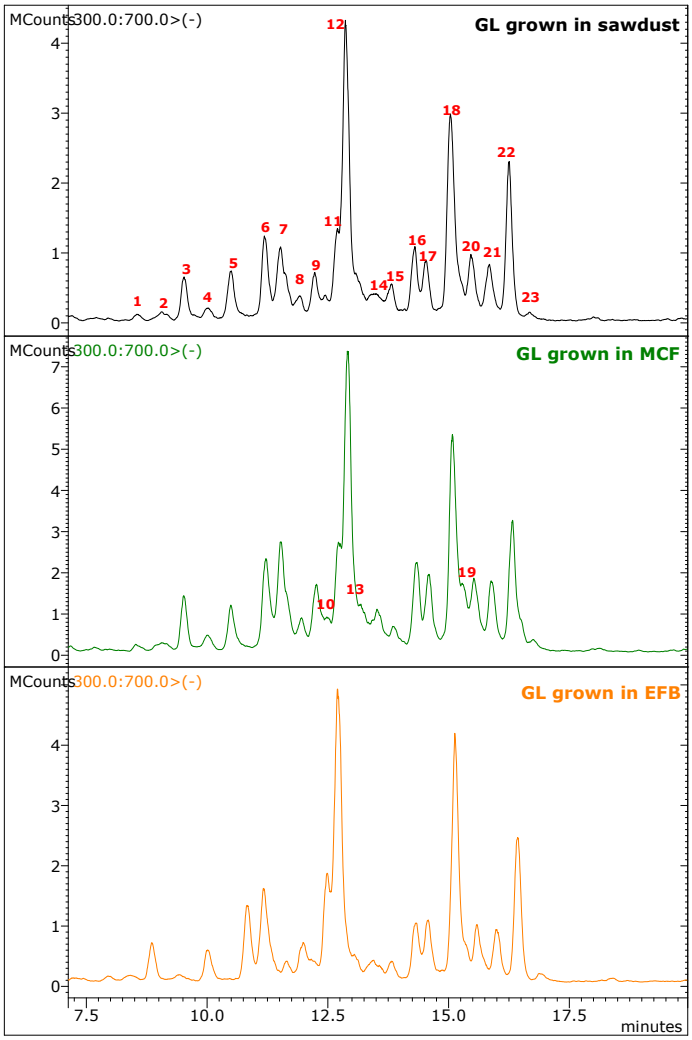


Figure A3-16 LC-MS profile for the ethanol extract of GL grown in different substrates: sawdust (red), MCF (green) and EFB (orange).

iii. Different GL types

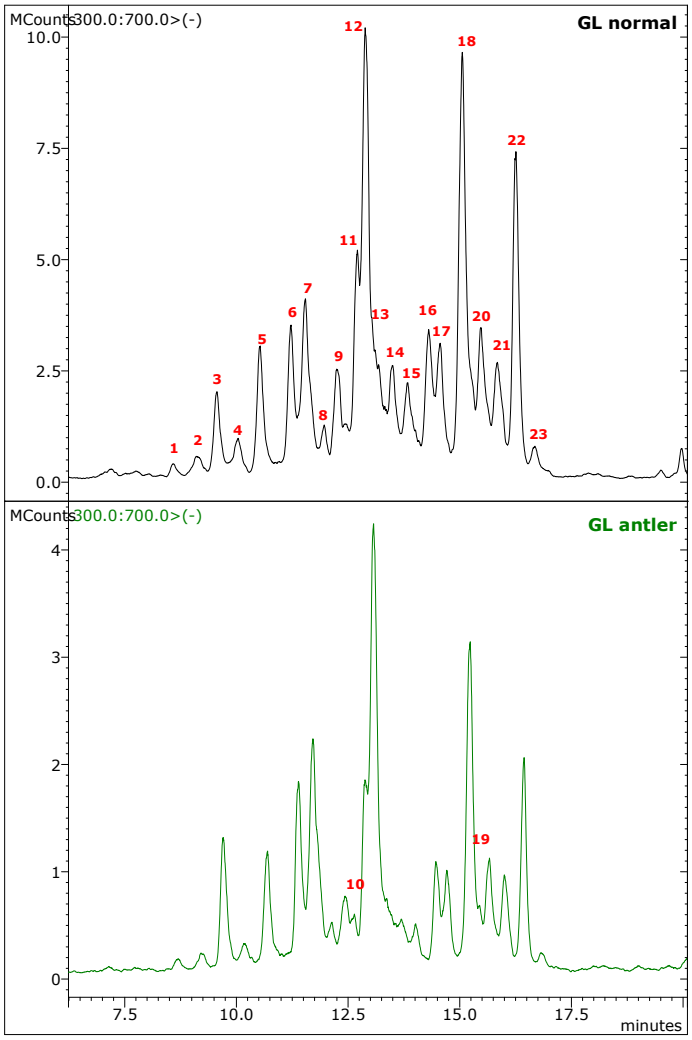


Figure A3-17 LC-MS profile for the ethanol extract of different types of GL: normal (black) and antler (green).

iv. Extraction solvent

GL tip harvested at 2-weeks

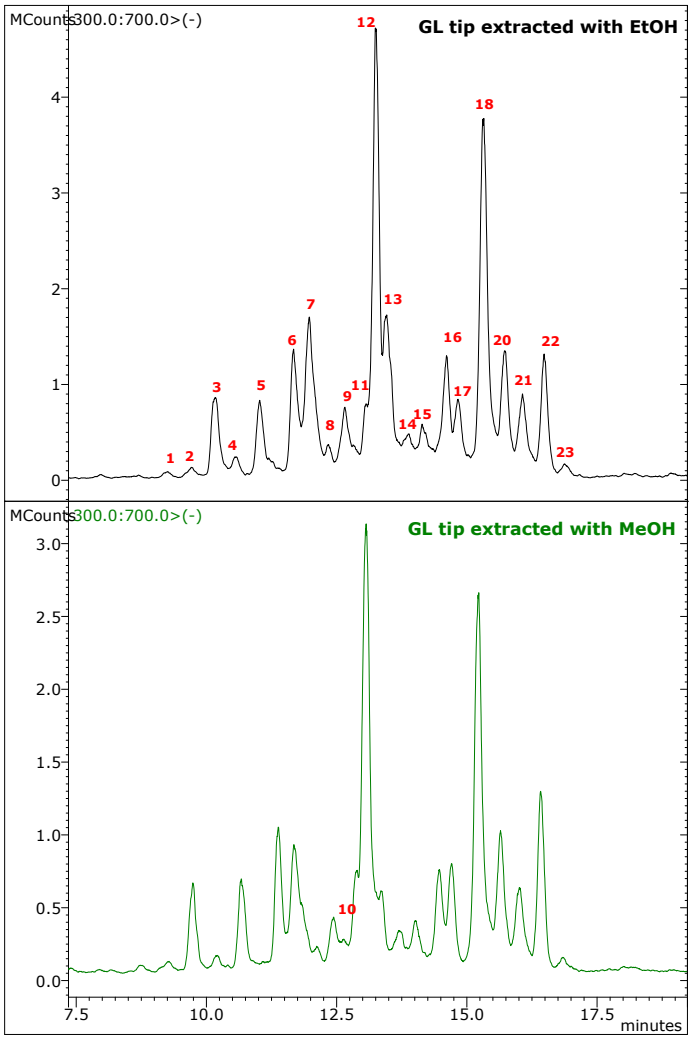


Figure A3-18 LC-MS traces of the ethanol (black) and methanol (green) extracts of GL tip harvested at 2 weeks.

GL harvested at 6 weeks

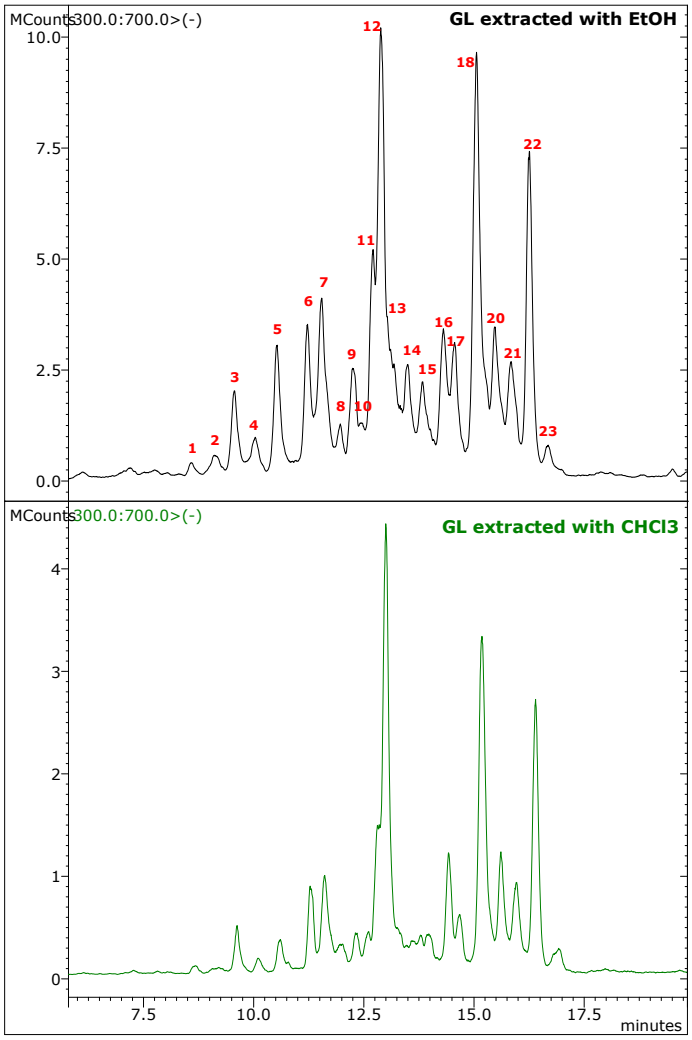


Figure A3-19 LC-MS traces of the ethanol (black) and chloroform (green) extracts of GL harvested at 6 weeks.

GL harvested at 8 weeks

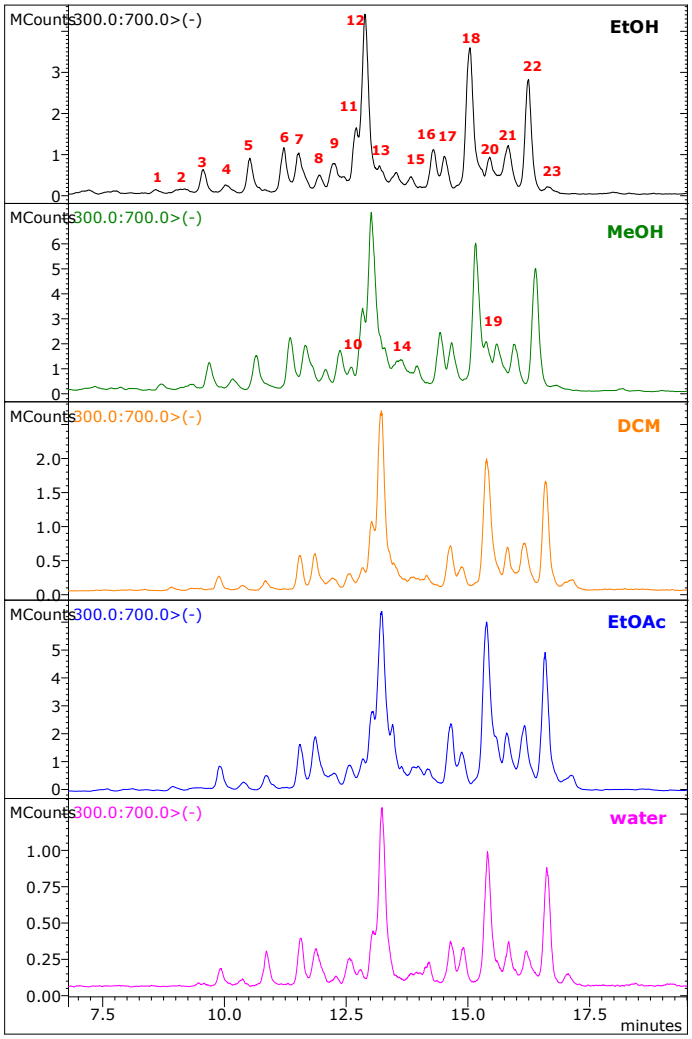
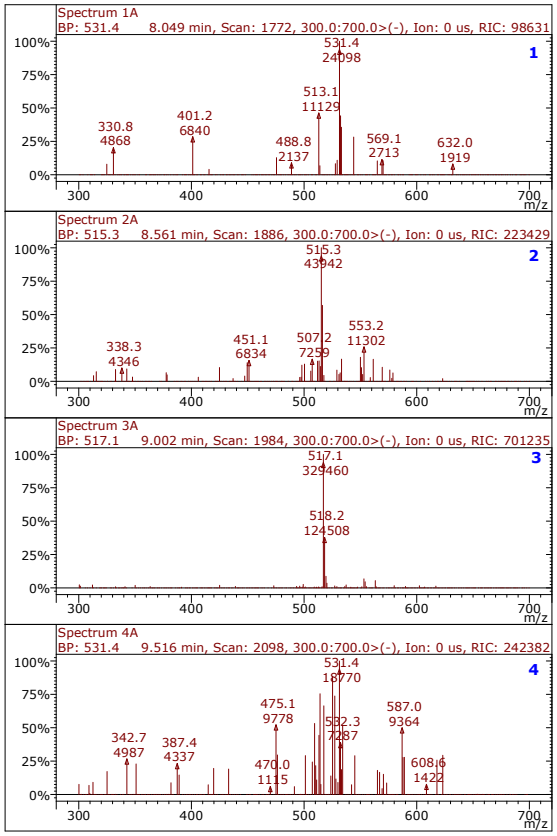
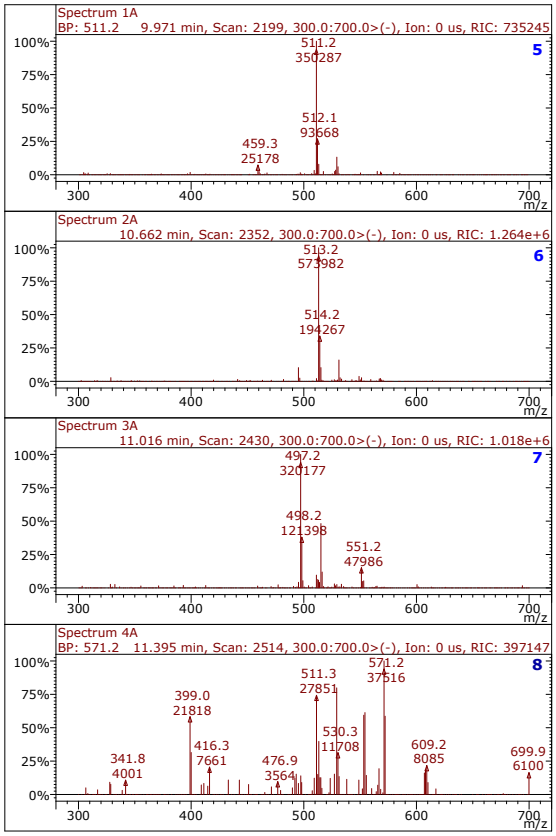


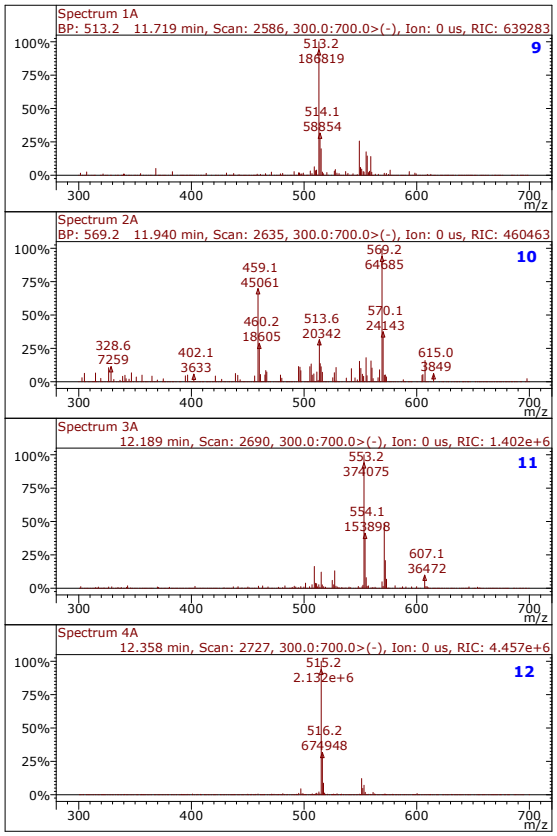
Figure A3-20 LC-MS traces of the ethanol (black), methanol (green), dichloromethane (orange), ethyl acetate (blue) and water (purple) extracts of GL harvested at 8 weeks.

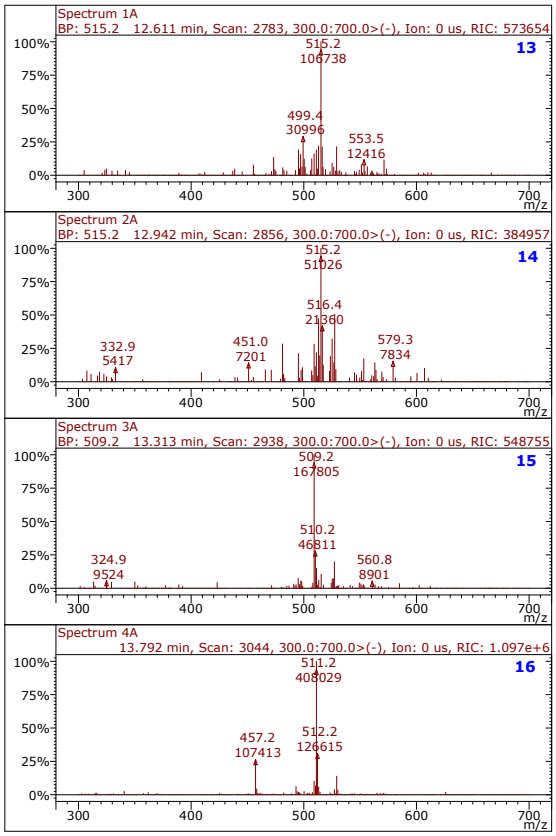
Peak identification

GL harvested at 4 weeks was used as reference for the identification of the different peaks. The mass profile of each of the peaks has been depicted in Figure A3-21.


Spectrum 1A
BP: 531.4 8.049 min, Scan: 1772, 300.0:700.0>(-), Ion: 0 us, RIC: 98631
1
531.4 24098
513.1 11129
401.2 6840
330.8 4868
488.8 2137
569.1 2713
632.0 1919
Spectrum 2A
BP: 515.3 8.561 min, Scan: 1886, 300.0:700.0>(-), Ion: 0 us, RIC: 223429
2
515.3 43942
553.2 11302
451.1 6834
507.2 7259
338.3 4346
Spectrum 3A
BP: 517.1 9.002 min, Scan: 1984, 300.0:700.0>(-), Ion: 0 us, RIC: 701235
3
517.1 329460
518.2 124508
Spectrum 4A
BP: 531.4 9.516 min, Scan: 2098, 300.0:700.0>(-), Ion: 0 us, RIC: 242382
4
531.4 18770
475.1 9778
587.0 9364
582.3 7287
342.7 4987
387.4 4337
470.0 1115
608.6 1422
100%
75%
50%
25%
0%
300
400
500
600
700
m/z


Spectrum 1A
BP: 511.2 9.971 min, Scan: 2199, 300.0:700.0>(-), Ion: 0 us, RIC: 735245
5
511.2 350287
512.1 93668
459.3 25178
Spectrum 2A
10.662 min, Scan: 2352, 300.0:700.0>(-), Ion: 0 us, RIC: 1.264e+6
6
513.2 573982
514.2 194267
Spectrum 3A
11.016 min, Scan: 2430, 300.0:700.0>(-), Ion: 0 us, RIC: 1.018e+6
7
497.2 320177
498.2 121398
551.2 47986
Spectrum 4A
BP: 571.2 11.395 min, Scan: 2514, 300.0:700.0>(-), Ion: 0 us, RIC: 397147
8
571.2 37516
511.3 27851
399.0 21818
530.3 11708
609.2 8085
416.3 7661
699.9 6100
341.8 4001
476.9 3564
100%
75%
50%
25%
0%
300
400
500
600
700
m/z


Spectrum 1A
BP: 513.2 11.719 min, Scan: 2586, 300.0:700.0>(-), Ion: 0 us, RIC: 639283
9
513.2 186819
514.1 58854
Spectrum 2A
BP: 569.2 11.940 min, Scan: 2635, 300.0:700.0>(-), Ion: 0 us, RIC: 460463
10
569.2 64585
459.1 45061
570.1 24143
513.6 20342
460.2 18605
328.6 7259
402.1 3633
615.0 3849
Spectrum 3A
12.189 min, Scan: 2690, 300.0:700.0>(-), Ion: 0 us, RIC: 1.402e+6
11
553.2 374075
554.1 153898
607.1 36472
Spectrum 4A
12.358 min, Scan: 2727, 300.0:700.0>(-), Ion: 0 us, RIC: 4.457e+6
12
515.2 2.132e+6
516.2 674948
100%
75%
50%
25%
0%
300
400
500
600
700
m/z


Spectrum 1A
BP: 515.2 12.611 min, Scan: 2783, 300.0:700.0>(-), Ion: 0 us, RIC: 573654
13
515.2 106738
499.4 30996
553.5 12416
Spectrum 2A
BP: 515.2 12.942 min, Scan: 2856, 300.0:700.0>(-), Ion: 0 us, RIC: 384957
14
515.2 51026
516.4 21360
579.3 7834
451.0 7201
332.9 5417
Spectrum 3A
BP: 509.2 13.313 min, Scan: 2938, 300.0:700.0>(-), Ion: 0 us, RIC: 548755
15
509.2 167805
510.2 46811
560.8 8901
324.9 9524
Spectrum 4A
13.792 min, Scan: 3044, 300.0:700.0>(-), Ion: 0 us, RIC: 1.097e+6
16
511.2 408029
512.2 126615
457.2 107413
100%
75%
50%
25%
0%
300
400
500
600
700
m/z

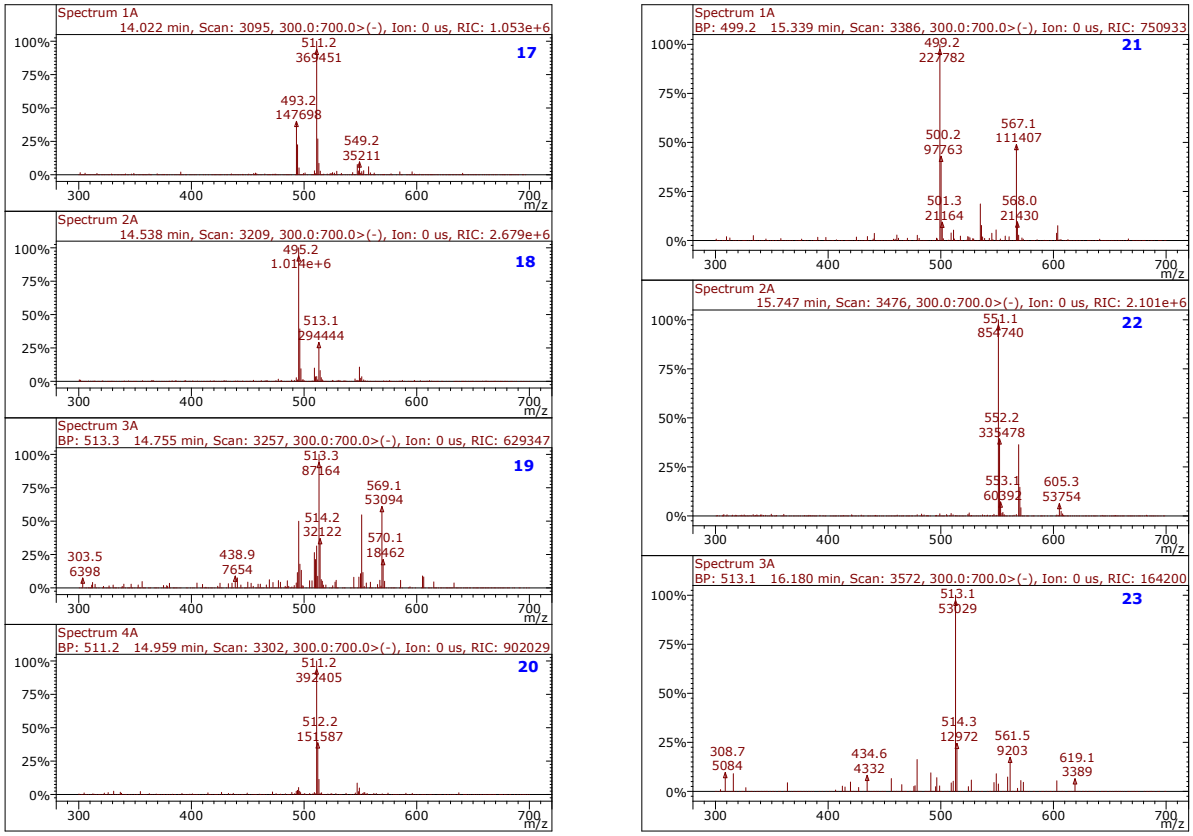


Figure A3-21 Mass profile of the different LC-MS peaks. The profiles were taken from GL 4W grown in sawdust. The spectra were numbered 1-23.

Peaks were tentatively assigned comparing the fragmentation pattern observed with the one given in the literature.[141-143]

Peak	R_t/min	MW	Fragmentation	Assigment
1	8.0	452	365 (7; M+1-44); 361 (4; M+1-44-16-32); 323 (23; M+1-44-32-54)	GA-S1 (**55**) / GA-S_z (**56**)
		460	401 (3; M+1-60); 399 (18; M+1-18-44); 387 (7; M+1-44-30); 365 (6; M+1-2x18-16)	LA-N (**72**)
		462	403 (13; M+1-60); 401 (3; M+1-18-44); 365 (6; M+1-3x18-44); 349 (6; M+1-3x18-60)	LA-M (**277**)
		484	485 (3; M+1); 467 (9; M+1-18); 387 (7; M+1-98)	11α-OH-GA-DM (**247**) / 11β-OH-GA-DM (**248**)
		510	511 (4; M+1); 467 (9; M+1-44); 323 (1; M+1-32-156)	GenA-F (**221**)
		512	513 (5; M+1); 495 (10; M+1-18); 325 (22; M+1-30-158)	GA-E (**21**) / GNPA-A (**31**)

Peak	R_t/min	MW	Fragmentation	Assigment
1	8.0	514	515 (5; M+1); 473 (10; M+1-42); 467 (9; M+1-18-30); 365 (7; M+1-18-16-116); 351 (6; M+1-18-44-42-60)	GenA-A (**213**); LA-D (**278**)
		516	517 (8; M+1); 475 (9; M+1-42); 371 (8; M+1-44-42)	LA-E2 (**83**)
		528	529 (29; M+1); 511 (4; M+1-18); 485 (3; M+1-44); 475 (8; M+1-3x18); 467 (9; M+1-18-44)	**284**
		530	531 (100; M+1); 513 (5; M+1-18); 495 (10; M+1-2x18)	GA-M (**236**) / 12βOH-GA-C1 (**225**) / 12βOH-GA-D (**263**)
		532	515 (5; M+1-18); 485 (3; M+1-18-30); 403 (13; M+1-130); 349 (6; M+1-3x18-130)	GA-I (**206**)
		548	531 (100; M+1-18); 513 (5; M+1-2x18); 467 (9; M+1-2x18-16-30)	**258**
		570	511 (4; M+1-18-42); 467 (7; M+1-18-44-42); 351 (4; M+1-18-42-30-130)	GA-F (**22**)
		572	531 (100; M+1-42); 513 (5; M+1-18-42); 483 (5; M+1-18-42-30)	**260**
		584	585 (4; M+1); 511 (4; M+1-42-32); 467 (9; M+1-42-32-44); 399 (18; M+1-42-32-44-68)	MeGA-F (**229**)
		598	515 (5; M+1-14-28-42); 511 (4; M+1-46-42); 467 (9; M+1-46-44-42)	EtGA-F (**228**)
2	8.6	400	401 (14; M+1); 383 (41; M+1-18)	Lucidone-B (**282**)
		460	425 (10; M+1-2x18); 387 (14; M+1-44-30); 369 (6; M+1-18-44-30)	LA-N (**72**)
		468	425 (10; M+1-44); 371 (2; M+1-98); 327 (5; M+1-44-98)	GA-DM (**32**)
		478	449 (14; M+1-30); 387 (14; M+1-18-30-44); 371 (2; M+1-18-30-60); 369 (6; M+1-2x18-14-60)	**276**
		484	467 (4; M+1-18); 449 (14; M+1-2x18); 425 (10; M+1-60); 387 (14; M+1-98); 347 (3; M+1-138); 327 (5; M+1-44-16-98); 313 (4; M+1-44-30-98)	11α-OH-GA-DM (**247**) / 11β-OH-GA-DM (**248**)

Peak	R_t/min	MW	Fragmentation	Assigment
2	8.6	498	451 (15; M+1-18-30); 437 (2; M+1-18-44); 369 (6; M+1-130)	**285**
		510	511 (23; M+1); 493 (10; M+1-18); 467 (4; M+1-44); 449 (14; M+1-18-44); 363 (17; M+1-32-116); 301 (15; M+1-210)	GenA-F (**221**)
		512	513 (15; M+1); 495 (11; M+1-18); 481 (8; M+1-2x16); 451 (16; M+1-18-44); 437 (2; M+1-32-44); 421 (48; M+1-18-44-30)	GenA-H (**222**); GenA-D (**220**); GA-E (**21**) / GNPA-A (**31**); GenA-G (**271**)
		514	515 (100; M+1); 497 (3; M+1-18); 481 (8; M+1-18-16); 473 (43; M+1-42); 467 (4; M+1-18-30); 439 (27; M+1-44-32); 437 (5; M+1-18-60); 383 (41; M+1-16-116); 301 (15; M+1-16-42-156)	GA-AM_1 (**12**); GenA-A (**213**); LA-D (**278**)
		516	517 (4; M+1); 481 (8; M+1-2x18); 467 (4; M+1-18-2x16); 457 (4; M+1-60); 451 (16; M+1-2x18-30); 437 (2; M+1-2x18-44); 387 (13; M+1-130); 383 (41; M+1-18-44-30-42); 371 (2; M+1-42-44-60); 369 (6; M+1-130-18); 347 (3; M+1-14-156); 327 (5; M+1-130-60); 301 (15; M+1-216)	**259**; GenA-C2 (**269**); LA-E2 (**83**); GA-A (**10**)
		528	529 (8; M+1); 511 (23; M+1-18); 481 (8; M+1-18-30); 467 (4; M+1-18-44); 437 (2; M+1-18-30-44); 421 (48; M+1-18-44-30-16); 363 (16; M+1-18-30-32-44-42)	**284**; Elfvingic acid A (**273**)
		530	531 (5; M+1); 513 (15; M+1-18); 497 (3; M+1-18-16); 481 (8; M+1-18-32); 451 (16; M+1-2x18-44); 439 (27; M+1-18-44-30); 421 (48; M+1-2x18-44-30); 401 (14; M+1-130); 383 (41; M+1-18-130)	GA-C6 (**233**); MeGA-B (**15**)
		532	533 (17; M+1); 515 (100; M+1-18); 497 (3; M+1-2x18); 467 (4; M+1-2x18-30); 437 (2; M+1-2x18-60); 425 (10; M+1-18-44-16-30)	GA-I (**206**); GA-G (**23**)

Peak	R_t/min	MW	Fragmentation	Assigment
2	8.6	534	517 (4; M+1-18); 425 (10; M+1-2x18-44-30); 387 (14; M+1-18-130); 327 (5; M+1-18-130-60)	12βOH-GA-C_2 (**257**)
		548	531 (5; M+1-18); 513 (15; M+1-2x18); 467 (4; M+1-2x18-30-16); 457 (4; M+1-18-30-44); 421 (48; M+1-3x18-30-44)	**258**
		554	513 (15; M+1-42); 511 (23; M+1-44); 451 (16; M+1-18-44-42) 439 (27; M+1-42-44-30); 425 (10; M+1-130)	**285**; **286**
		568	569 (11; M+1); 553 (26; M+1-16); 509 (13; M+1-60); 467 (4; M+1-42-60); 437 (2; M+1-16-116); 301 (15; M+1-16-42-2x30-32-116)	12β-OAc-GenA-F (**272**)
		570	571 (4; M+1); 553 (26; M+1-18); 511 (23; M+1-18-42); 481 (8; M+1-18-42-30); 467 (4; M+1-18-42-44); 449 (14; M+1-2x18-44-42); 437 (2; M+1-18-44-42-30); 347 (3; M+1-2x18-30-42-44-116); 301 (15; M+1-2x18-30-32-42-130)	12β-OAc-GenA-H (**47**); 12β-OAc-GenA-D (**224**); GA-F (**22**)
		572	531 (5; M+1-42); 513 (15; M+1-18-42); 467 (4; M+1-18-16-42-30); 451 (16; M+1-2x18-42-44); 421 (48; M+1-2x18-42-44-30); 363 (17; M+1-2x18-16-42-116); 315 (7; M+1-42-30-32-154); 301 (15; M+1-14-28-30-42-158)	GenA-K (**223**)
		588	571 (4; M+1-18); 529 (8; M+1-60); 515 (100; M+1-42-32)	MeGA-K (**231**)
		598	515 (100; M+1-14-28-42); 511 (23; M+1-46-42); 467 (4; 46-44-42); 451 (16; M+1-46-42-2x30); 301 (15; M+1-2x18-32-46-44-42-98)	EtGA-F (**228**)
3	9.0	516	517 (100; M+1); 499 (4; M+1-18); 425 (2; M+1-18-44-30)	GenA-C2 (**269**); GA-B (**8**); GA-A (**10**)
		518	519 (6; M+1); 501 (2; M+1-18); 465 (1; M+1-3x18)	GA-C2 (**18**)
		534	517 (100; M+1-18); 499 (4; M+1-2x18); 425 (2; M+1-2x18-44-30)	12βOH-GA-C_2 (**257**)

Peak	R_t/min	MW	Fragmentation	Assigment
3	9.0	554	555 (2; M+1); 519 (6; M+1-2x18); 513 (2; M+1-42); 425 (2; M+1-130)	**285**; **286**
		570	553 (12; M+1-18); 499 (4; M+1-42-30); 425 (2; M+1-18-2x42-44)	GA-M_K (**51**) / GA-P (**249**) / GA-Q (**250**)
4	9.5	472	473 (19; M+1); 437 (5; M+1-2x18); 379 (51; M+1-18-16-2x30); 311 (22; -3x18-30-78)	GN3OL (**67**)
		474	475 (50; M+1); 457 (43; M+1-18); 421 (7; M+1-3x18); 369 (9; M+1-2x18-70); 317 (23; M+1-2x18-30-32-60)	GR3OL-M (**212**)
		484	485 (5; M+1); 423 (3; M+1-18-44); 343 (28; M+1-44-98); 313 (34; M+1-44-30-98)	11α-OH-GA-DM (**247**) / 11β-OH-GA-DM (**248**); GLA-E (**246**)
		500	501 (26; M+1); 483 (9; M+1-18); 457 (43; M+1-44); 421 (7; M+1-2x18-44)	GLA-A (**29**)
		502	503 (22; M+1); 485 (1; M+1-18)	GLA-B (**30**)
		512	513 (75; M+1); 481 (6; M+1-32); 465 (5; M+1-18-30); 437 (5; M+1-32-44); 423 (3; M+1-44-30-16); 421 (7; M+1-18-44-30); 407 (1; M+1-32-44-30); 337 (3; M+1-18-44-16-98)	GenA-D (**220**); GA-E (**21**) / GNPA-A (**31**); GenA-G (**271**)
		514	515 (47; M+1); 497 (41; M+1-18); 481 (23; M+1-18-16); 479 (18; M+1-2x18); 473 (19; M+1-42); 461 (10; M+1-3x18); 453 (3; M+1-18-44); 437 (5; M+1-18-60); 423 (3; M+1-18-44-30); 409 (33; M+1-106); 379 (51; M+1-18-30-2x44); 317 (23; M+1-16-30-152); 311 (22; M+1-16-30-158); 305 (8; M+1-210)	**283**; GenA-B (**219**); GA-AM_1 (**12**); GA-C1 (**17**) / GA-D (**19**); GenA-A (**213**); LA-D (**278**); GA-J (**234**)

Peak	R_t/min	MW	Fragmentation	Assigment
4	9.5	516	517 (31; M+1); 483 (9; M+1-18-16); 481 (6; M+1-2x18); 475 (50; M+1-42); 457 (43; M+1-60); 437 (5; M+1-2x18-44); 415 (32; M+1-60-42); 413 (37; M+1-18-44-42); 409 (33; M+1-18-44-16-30); 407 (43; M+1-2x18-44-30); 349 (5; M+1-2x18-132); 343 (28; M+1-18-44-30-16)	**259**; LA-E2 (**83**); GA-A (**10**)
		518	519 (22; M+1); 501 (15; M+1-18); 483 (9; M+1-2x18); 465 (5; M+1-3x18); 457 (42; M+1-18-44); 409 (33; M+1-2x18-44-30)	GA-C2 (**18**)
		526	527 (67; M+1); 485 (1; M+1-42); 423 (3; M+1-18-44-42)	15α-OAc-GLA-E (**267**)
		528	529 (1; M+1); 511 (26; M+1-18); 485 (1; M+1-44); 481 (5; M+1-18-30); 437 (5; M+1-18-44-30); 423 (1; M+1-44-30-32); 421 (7; M+1-16-18-30-44)	**284**; Elfvingic acid A (**273**)
		530	531 (21; M+1); 513 (75; M+1-18); 437 (5; M+1-18-32-44); 305 (8; M+1-226)	12βOH-GenA-B (**270**)
		532	533 (5; M+1); 515 (47; M+1-18); 497 (41; M+1-2x18); 485 (1; M+1-18-30); 453 (3; M+1-2x18-44); 437 (5; M+1-2x18-44-16)	GA-I (**206**); GA-G (**23**)
		534	517 (31; M+1-18); 487 (30; M+1-18-30); 407 (43; M+1-3x18-44-30)	12βOH-GA-C_2 (**257**)
		548	531 (21; M+1-18); 513 (75; M+1-2x18); 487 (30; M+1-18-44); 457 (43; M+1-18-44-30); 421 (6; M+1-3x18-44-30)	**258**
		568	569 (100; M+1); 551 (1; M+1-18); 465 (5; M+1-18-44-42); 437 (5; M+1-16-116); 421 (7; M+1-30-116); 317 (30; M+1-42-210)	12β-OAc-GenA-F (**272**)
		570	571 (3; M+1); 553 (18; M+1-18); 511 (25; M+1-18-42); 481 (5; M+1-18-42-30); 437 (5; M+1-18-44-42-30)	GA-F (**22**)

Peak	R_t/min	MW	Fragmentation	Assigment
4	9.5	572	573 (36; M+1); 531 (21; M+1-42); 519 (22; M+1-3x18); 513 (75; M+1-18-42); 483 (9; M+1-42-18-30); 477 (10; M+1-3x18-42); 423 (1; M+1-18-16-30-42-44); 421 (7; M+1-2x18-44-42-30); 407 (43; M+1-18-44-42-30-32); 379 (51; M+1-2x18-30-2x42-44); 305 (1; M+1-18-32-42-60-116)	GenA-K (**223**); GA-H (**24**); **260**
		574	575 (9; M+1); 515 (47; M+1-18-42); 513 (75; M+1-18-44); 453 (3; M+1-2x18-42-44); 409 (33; M+1-18-44-42-30-32); 343 (27; M+1-42-2x30-130); 305 (8; M+1-2x18-42-30-32-130)	GA-K (**26**)
		586	587 (20; M+1); 569 (100; M+1-18); 545 (11; M+1-42); 527 (67; M+1-18-42); 511 (26; M+1-32-44); 483 (9; M+1-32-42-30); 465 (5; M+1-18-32-42-30)	MeGA-H (**230**)
		588	589 (9; M+1); 571 (3; M+1-18); 529 (1; M+1-42-18); 515 (47; M+1-42-32); 453 (3; M+1-18-44-42-32); 407 (43; M+1-18-44-42-32-30-16); 305 (8; 2x18-44-42-2x32-30-68)	MeGA-K (**231**)
5	9.9	458	459 (11; M+1); 415 (2; M+1-44); 325 (1; M+1-32-102)	LA-A (**69**)
		510	511 (100; M+1); 467 (5; M+1-44)	GenA-F (**221**)
		512	513 (8; M+1); 495 (3; M+1-18); 407 (1; M+1-32-30-44); 325 (1; M+1-30-158)	GenA-H (**222**); GenA-D (**220**); GA-E (**21**); GenA-G (**271**)
		514	515 (1; M+1); 497 (3; M+1-18); 479 (1; M+1-2x18); 467 (7; M+1-18-30); 453 (1; M+1-18-44); 317 (4; M+1-16-30-152); 305 (1; M+1-210)	**283**; GenA-B (**219**); GA-AM_1 (**12**); GenA-A (**213**); **287**; GA-C1 (**17**) / GA-D (**19**); GA-J (**234**)

Peak	R_t/min	MW	Fragmentation	Assigment
5	9.9	528	529 (23; M+1); 511 (100; M+1-18); 467 (5; M+1-18-44); 319 (1; M+1-16-18-60-116)	**284**; Elfvingic acid A (**273**)
		530	531 (2; M+1); 513 (8; M+1-18); 495 (3; M+1-2x18); 305 (4; M+1-226)	12βOH-GenA-B (**270**); GA-M (**236**) / 12βOH-GA-C1 (**225**); MeGA-B (**15**)
		548	531 (2; M+1-18); 513 (8; M+1-2x18); 467 (5; M+1-2x18-30-16); 319 (1; M+1-3x18-2x30-116)	**258**
		554	513 (8; M+1-42); 511 (100; M+1-44)	**286**
		572	573 (2; M+1); 531 (2; M+1-42); 513 (8; M+1-18-42); 483 (3; M+1-18-42-30)	**260**
		588	529 (23; M+1-18-42); 515 (1; M+1-32-42); 453 (1; M+1-18-32-42-44); 407 (1; M+1-18-32-42-44-16-30); 305 (1; M+1-2x18-2x32-42-44-30-68)	MeGA-K (**231**)
		598	527 (5; M+1-42-30); 515 (1; M+1-14-28-42); 511 (100; M+1-46-42); 467 (5; M+1-46-42-44)	EtGA-F (**228**)
6	10.6	512	513 (100; M+1); 495 (14; M+1-18)	GenA-H (**222**); GenA-D (**220**); GA-E (**21**); GenA-G (**271**)
		514	515 (8; M+1); 497 (1; M+1-18); 443 (1; M+1-42-30)	GenA-B (**219**); GA-AM_1 (**12**); GenA-A (**213**); **287**; GA-C1 (**17**) / GA-D (**19**); LA-D (**278**); GA-J (**234**)

Peak	R_t/min	MW	Fragmentation	Assigment
6	10.6	530	531 (2; M+1); 513 (100; M+1-18); 495 (14; M+1-2x18)	12βOH-GenA-B (**270**); GA-C6 (**233**); GA-M (**236**) / 12βOH-GA-C1 (**225**)
		532	533 (2; M+1); 515 (8; M+1-18); 497 (1; M+1-2x18)	GA-I (**206**); GA-G (**23**)
		548	549 (3; M+1); 531 (9; M+1-18); 513 (100; M+1-2x18)	**258**
		554	513 (100; M+1-42); 511 (4; M+1-44)	**285**; **286**
		572	531 (2; M+1-42); 513 (100; M+1-18-42)	**260**
		588	529 (2; M+1-18-42); 515 (8; M+1-42-32)	MeGA-K (**231**)
		598	527 (1; M+1-42-30); 515 (8; M+1-14-28-42); 511 (4; M+1-46-42)	EtGA-F (**228**)
		616	533 (2; M+1-14-28-42); 531 (9; M+1-42-44); 513 (100; M+1-18-44-42); 511 (3; M+1-18-16-30-42); 497 (1; M+1-2x18-14-28-42); 495 (13; M+1-2x18-44-42)	**261**
7	11.0	512	513 (6; M+1); 495 (4; M+1-18); 303 (1; M+1-210)	GenA-H (**222**); GenA-D (**220**); GenA-G (**271**)
		514	515 (48; M+1); 497 (100; M+1-18); 479 (3; M+1-2x18); 471 (4; M+1-44); 355 (2; M+1-30-130); 303 (1; M+1-212)	**283**; GenA-B (**219**); **287**; GA-C1 (**17**) / GA-D (**19**); GA-J (**234**)
		516	517 (1; M+1); 499 (5; M+1-18); 471 (1; M+1-30-16)	**259**; GenA-C2 (**269**); GA-B (**8**); GA-AM_1 (**12**); GA-A (**10**)
		528	529 (3; M+1); 511 (10; M+1-18); 469 (1; M+1-16-44); 303 (1; M+1-18-2x30-32-116)	**284**; Elfvingic acid A (**273**)
		530	513 (6; M+1-18); 495 (4; M+1-2x18); 469 (1; M+1-18-44); 303 (1; M+1-16-212)	12βOH-GenA-B (**270**); GA-C6 (**233**); GA-M (**236**)

Peak	R_t/min	MW	Fragmentation	Assigment
7	11.0	532	533 (3; M+1); 515 (48; M+1-18); 497 (100; M+1-2x18); 471 (1; M+1-18-44); 303 (1; M+1-16-3x18-30-130)	GA-I (**206**); GA-G (**23**)
		534	517 (1; M+1-18); 499 (5; M+1-2x18); 469 (1; M+1-2x18-30)	12βOH-GA-C_2 (**257**)
		548	549 (1; M+1); 513 (6; M+1-2x18); 469 (1; M+1-2x18-44)	**258**
		554	513 (6; M+1-42); 511 (9; M+1-44); 469 (1; M+1-42-44); 303 (1; M+1-252)	**285**; **286**
		568	551 (15; M+1-18); 509 (1; M+1-18-42); 303 (1; M+1-14-42-210)	12β-OAc-GenA-F (**272**)
		570	571 (1; M+1); 553 (5; M+1-18); 511 (10; M+1-18-42-44); 347 (1; M+1-2x18-30-44-42-116); 303 (1; M+1-16-42-210)	12β-OAc-GenA-H (**47**); 12β-OAc-GenA-D (**224**); GA-F (**22**)
		572	513 (5; M+1-18-42); 469 (1; M+1-18-42-44); 303 (1; M+1-2x18-42-30-32-130)	GenA-K (**223**); GA-H (**24**)
		588	571 (1; M+1-18); 529 (3; M+1-18-42); 515 (48; M+1-18-32); 471 (1; M+1-32-44-42)	MeGA-K (**231**)
		598	527 (3; M+1-42-30); 515 (48; M+1-14-28-42); 511 (10; M+1-46-42)	EtGA-F (**228**)
8	11.4	456	427 (11; M+1-30); 413 (4; M+1-44); 397 (2; M+1-60)	LA-F (**281**)
		458	459 (14; M+1); 397 (2; M+1-18-44); 329 (1; M+1-3x18-44-32)	LA-A (**69**)
		460	461 (4; M+1); 425 (8; M+1-18); 399 (24; M+1-18-44); 381 (2; M+1-2x18-44); 305 (2; M+1-156)	LA-N (**72**)
		478	479 (11; M+1); 449 (1; M+1-30); 413 (4; M+1-2x18-30); 305 (2; M+1-30-44-100)	**276**
		484	467 (16; M+1-18); 449 (1; M+1-2x18); 425 (8; M+1-60); 381 (2; M+1-44-60)	11α-OH-GA-DM (**247**) / 11β-OH-GA-DM (**248**); GLA-E (**246**)
		498	499 (4; M+1); 481 (9; M+1-18); 451 (2; M+1-18-30); 433 (3; M+1-2x18-30)	**285**

Peak	R_t/min	MW	Fragmentation	Assigment
8	11.4	510	511 (28; M+1); 493 (10; M+1-18); 467 (16; M+1-44); 463 (6; M+1-18-30); 449 (1; M+1-18-44); 363 (6; M+1-32-116)	GenA-F (**221**)
		512	513 (12; M+1); 495 (4; M+1-18); 481 (9; M+1-2x16); 465 (4; M+1-18-30); 451 (2; M+1-18-44); 433 (3; M+1-2x18-44)	GenA-H (**222**); GenA-D (**220**); GA-E (**21**); GenA-G (**271**)
		514	515 (1; M+1); 497 (21; M+1-18); 481 (9; M+1-18-16); 479 (11; M+1-2x18); 467 (16; M+1-18-30); 435 (2; M+1-2x18-44); 355 (2; M+1-30-130); 319 (4; M+1-2x18-30-130); 317 (9; M+1-18-2x32-116); 305 (2; M+1-18-16-60-116)	GenA-B (**219**); GenA-A (**213**); **287**; GA-C1 (**17**) / GA-D (**19**)
		516	517 (10; M+1); 499 (4; M+1-18); 483 (4; M+1-18-16); 481 (9; M+1-2x18); 467 (16; M+1-18-32); 451 (2; M+1-2x18-30); 445 (2; M+1-42-30); 413 (4; M+1-18-44-42); 329 (16; M+1-16-30-42-100)	**259**; GenA-C2 (**269**); LA-E2 (**83**); GA-A (**10**)
		528	529 (100; M+1); 511 (28; M+1-18); 467 (16; M+1-18-44); 363 (6; M+1-18-30-32-44-42); 319 (4; M+1-18-2x30-16-116); 307 (3; M+1-2x18-30-156)	**284**; Elfvingic acid A (**273**)
		530	531 (23; M+1); 513 (12; M+1-18); 499 (4; M+1-32); 495 (4; M+1-2x18); 481 (9; M+1-18-32); 451 (2; M+1-2x18-44); 433 (3; M+1-3x18-44); 305 (2; M+1-216)	12βOH-GenA-B (**270**); GA-C6 (**233**); GA-M (**236**) / 12βOH-GA-D (**263**); MeGA-B (**15**)
		532	533 (1; M+1); 515 (1; M+1-18); 497 (21; M+1-2x18); 305 (2; M+1-228)	GA-I (**206**); GA-G (**23**)
		534	535 (1; M+1); 517 (10; M+1-18); 499 (4; M+1-2x18); 425 (8; M+1-2x18-44-30)	12βOH-GA-C_2 (**257**)
		548	549 (1; M+1); 531 (23; M+1-18); 513 (12; M+1-2x18); 467 (16; M+1-2x18-16-30); 319 (4; M+1-3x18-2x30-116)	**258**

Peak	R_t/min	MW	Fragmentation	Assigment
8	11.4	554	555 (3; M+1); 513 (12; M+1-42); 511 (28; M+1-44); 451 (2; M+1-18-42-44); 425 (8; M+1-130)	**285**; **286**
		568	569 (1; M+1); 551 (9; M+1-18); 509 (9; M+1-18-44); 465 (4; M+1-18-44-42); 317 (9; M+1-42-210)	12β-OAc-GenA-F (**272**)
		570	571 (56; M+1); 553 (69; M+1-18); 511 (28; M+1-18-42); 493 (4; M+1-2x18-42); 481 (9; M+1-18-42-30); 467 (16; M+1-18-42-44); 449 (1; M+1-2x18-42-44);	12β-OAc-GenA-H (**47**); 12β-OAc-GenA-D (**224**); GA-F (**22**)
		572	573 (8; M+1); 555 (3; M+1-18); 531 (23; M+1-42); 513 (12; M+1-42-18); 483 (4; M+1-18-30-42); 451 (2; M+1-2x18-44-42); 363 (6; M+1-2x18-16-42-116); 305 (2; M+1-16-154-98)	GenA-K (**223**); GA-H (**24**); **260**
		586	569 (1; M+1-18); 545 (8; M+1-42); 527 (20; M+1-18-42); 483 (4; M+1-32-42-30)	MeGA-H (**230**)
		588	589 (1; M+1); 571 (56; M+1-18); 553 (69; M+1-2x18); 547 (5; M+1-42); 529 (100; M+1-18-42); 513 (12; M+1-32-44); 515 (1; M+1-32-42); 495 (4; M+1-18-32-44); 305 (2; M+1-2x18-2x32-44-42-68-30)	MeGA-K (**231**)
		598	527 (20; M+1-42-30); 515 (1; M+1-14-28-42); 511 (28; M+1-46-42); 467 (16; M+1-46-44-42); 451 (2; M+1-2x30-46-42)	EtGA-F (**228**)-
9	11.7	512	513 (100; M+1); 495 (4; M+1-18); 481 (3; M+1-32); 477 (2; M+1-2x18); 465 (3; M+1-18-30); 451 (2; M+1-18-44); 437 (1; M+1-16-60); 433 (3; M+1-2x18-44); 403 (2; M+1-2x18-44-30); 331 (2; M+1-30-152); 325 (2; M+1-30-158)	GenA-H (**222**); GenA-D (**220**); GA-E (**21**) / GNPA-A (**31**); GenA-G (**271**)
		514	515 (12; M+1); 497 (2; M+1-18); 481 (3; M+1-18-16); 479 (1; M+1-2x18); 471 (3; M+1-44); 467 (1; M+1-18-30); 443 (1; M+1-42-30); 439 (1; M+1-32-44); 437 (1; M+1-18-60); 403 (2; M+1-44-68); 321 (2; M+1-194); 319 (4; M+1-2x18-30-130)	**283**; GenA-B (**219**); GA-AM_1 (**12**); GenA-A (**213**); **287**; GA-C1 (**17**) / GA-D (**19**); LA-D (**278**)

Peak	R_t/min	MW	Fragmentation	Assigment
9	11.7	530	531 (2; M+1); 513 (100; M+1-18); 499 (3; M+1-32); 495 (4; M+1-2x18); 481 (3; M+1-18-32); 469 (3; M+1-18-44); 451 (2; M+1-2x18-44); 437 (1; M+1-18-44-32); 331 (2; M+1-200); 309 (2; M+1-18-16-30-158)	12βOH-GenA-B (**270**); GA-C6 (**233**); GA-M (**236**) / 12βOH-GA-D (**263**); MeGA-B (**15**)
		532	515 (12; M+1-18); 497 (2; M+1-2x18); 471 (3; M+1-18-44); 437 (1; M+1-2x18-60); 403 (2; M+1-130)	GA-I (**206**); GA-G (**23**)
		548	549 (39; M+1); 531 (2; M+1-18); 513 (100; M+1-2x18); 469 (3; M+1-2x18-44); 467 (1; M+1-2x18-16-30); 457 (2; M+1-18-44-30); 319 (4; M+1-3x18-2x30-116)	**258**
		554	555 (24; M+1); 513 (100; M+1-42); 511 (3; M+1-44); 469 (3; M+1-42-44); 451 (2; M+1-18-44-42)	**285**; **286**
		568	569 (1; M+1); 551 (5; M+1-18); 509 (6; M+1-18-42); 465 (3; M+1-18-44-42); 437 (1; M+1-16-116)	12β-OAc-GenA-F (**272**)
		572	573 (3; M+1); 555 (24; M+1-18); 531 (2; M+1-42); 513 (100; M+1-18-42); 469 (3; M+1-18-42-44); 451 (2; M+1-2x18-44-42); 325 (2; M+1-30-60-42-116)	GenA-K (**223**); GA-H (**24**); **260**
		574	575 (2; M+1); 557 (4; M+1-18); 513 (100; M+1-18-44); 471 (3; M+1-18-44-42); 343 (3; M+1-42-2x30-130)	GA-K (**26**)
		586	569 (1; M+1-18); 527 (5; M+1-18-42); 465 (3; M+1-18-32-42-30); 331 (2; M+1-2x18-2x32-44-42-70)	MeGA-H (**230**)
		588	571 (3; M+1-18); 557 (4; M+1-32); 529 (1; M+1-18-42); 515 (12; M+1-32-42); 471 (3; M+1-32-44-42)	MeGA-K (**231**)
		598	599 (1; M+1); 557 (4; M+1-42); 527 (5; M+1-42-30); 515 (12; M+1-14-28-42); 511 (3; M+1-46-42); 467 (1; M+1-46-44-42); 451 (2; M+1-2x30-46-42)	EtGA-F (**228**)
10	11.9	400	401 (5; M+1); 341 (5; M+1-60); 303 (3; M+1-98)	Lucidone-B (**282**)

Peak	R_t/min	MW	Fragmentation	Assigment
10	11.9	438	439 (6; M+1); 421 (4; M+1-18); 309 (2; M+1-18-3x32-16)	LAL-A (**256**)
		440	441 (5; M+1); 423 (4; M+1-18); 309 (2; M+1-2x18-60-36)	GOL-B (**64**)
		454	455 (1; M+1); 401 (5; M+1-3x18); 395 (4; M+1-60); 365 (4; M+1-30-60); 357 (3; M+1-2x18-30-32); 329 (1; M+1-2x18-30-60); 315 (3; M+1-18-30-32-60); 309 (2; M+1-18-44-16-30-38)	LAL-C (**45**); GIOL-F (**63**); GA-Y (**59**)
		456	457 (15; M+1); 439 (6; M+1-18); 421 (4; M+1-2x18); 395 (4; M+1-18-44); 357 (3; M+1-2x18-30-34); 329 (1; M+1-2x18-60-32); 315 (3; M+1-2x18-16-30-60)	L2OL (**43**)
		458	459 (70; M+1); 441 (5; M+1-18); 423 (4; M+1-2x18); 385 (1; M+1-44-30); 303 (3; M+1-156)	LA-A (**69**)
		460	443 (2; M+1-18); 425 (2; M+1-2x18); 387 (4; M+1-44-30); 381 (3; M+1-2x18-44); 357 (3; M+1-44-2x30); 305 (6; M+1-156)	LA-N (**72**)
		474	475 (3; M+1); 457 (15; M+1-18); 439 (6; M+1-2x18); 421 (4; M+1-3x18); 369 (1; M+1-2x18-70); 329 (1; M+1-3x18-2x30-32)	GR3OL-M (**212**)
		478	479 (5; M+1); 369 (1; M+1-2x18-14-60); 305 (6; M+1-30-44-100)	**276**
		484	441 (5; M+1-44); 423 (4; M+1-18-44); 381 (3; M+1-44-60)	GLA-E (**246**)
		486	451 (4; M+1-2x18); 423 (4; M+1-18-16-30); 395 (4; M+1-18-44-30)	**266**
		502	503 (7; M+1); 441 (5; M+1-18-44); 425 (2; M+1-18-60)	GLA-B (**30**)
		510	511 (7; M+1); 463 (2; M+1-18-30); 451 (4; M+1-60); 409 (6; M+1-42-60); 301 (3; M+1-210)	GenA-F (**221**); GA-T-Q (**57**)
		512	513 (31; M+1); 495 (11; M+1-18); 481 (1; M+1-32); 465 (5; M+1-18-30); 451 (4; M+1-18-44); 423 (4; M+1-16-44-30); 421 (4; M+1-18-44-30); 331 (2; M+1-30-152); 303 (3; M+1-210)	GenA-H (**222**); GenA-D (**220**); GA-E (**21**) / GNPA-A (**31**); GenA-G (**271**)

Peak	R_t/min	MW	Fragmentation	Assigment
10	11.9	514	515 (11; M+1); 497 (8; M+1-18); 481 (1; M+1-18-16); 479 (5; M+1-2x18); 455 (1; M+1-18-42); 443 (2; M+1-42-30); 439 (6; M+1-32-44); 423 (4; M+1-18-44-30); 409 (6; M+1-16-30-60); 395 (4; M+1-16-18-44-42); 365 (4; M+1-18-16-116); 351 (4; M+1-18-44-42-60); 319 (3; M+1-2x18-30-130); 305 (6; M+1-210); 303 (3; M+1-212); 301 (3; M+1-16-42-156)	GenA-B (**219**); GA-AM_1 (**12**); GenA-A (**213**); **287**; GA-C1 (**17**) / GA-D (**19**); LA-D (**278**); GA-J (**234**)
		516	517 (1; M+1); 499 (2; M+1-18); 481 (1; M+1-2x18); 475 (3; M+1-42); 457 (15; M+1-60); 455 (1; M+1-18-44); 451 (4; M+1-2x18-30); 409 (6; M+1-18-16-30-44); 395 (4; M+1-18-44-60); 385 (1; M+1-16-116); 347 (2; M+1-14-156); 329 (1; M+1-16-42-30-100); 303 (3; M+1-214); 301 (3; M+1-216)	**259**; GenA-C2 (**269**); GA-B (**8**); LA-E2 (**83**); GA-A (**10**)
		518	519 (6; M+1); 465 (5; M+1-3x18); 457 (15; M+1-18-44); 439 (6; M+1-2x18-44); 409 (6; M+1-2x18-44-30); 395 (4; M+1-18-44-30-32)	GA-C2 (**18**)
		526	527 (8:M+1); 441 (3; M+1-42-44); 423 (4; M+1-42-44-18)	15-OAc-GLA-E (**267**)
		528	529 (1; M+1); 511 (7; M+1-18); 423 (4; M+1-44-30-32); 319 (3; M+1-16-18-2x30-116)	Elfvingic acid A (**273**)
		530	531 (5; M+1); 513 (31; M+1-18); 499 (2; M+1-32); 495 (11; M+1-2x18); 481 (1; M+1-18-32); 455 (1; M+1-32-44); 451 (4; M+1-2x18-44); 439 (6; M+1-18-44-30); 421 (4; M+1-2x18-44-30); 331 (2; M+1-200); 309 (2; M+1-16-18-30-158); 305 (6; M+1-226); 303 (3; M+1-16-212)	12βOH-GenA-B (**270**); GA-C6 (**233**); GA-M (**236**); MeGA-B (**15**)
		532	515 (11; M+1-18); 497 (8; M+1-2x18); 455 (1; M+1-18-60); 305 (6; M+1-228); 303 (3; M+1-16-3x18-30-130)	GA-I (**206**); GA-G (**23**)

Peak	R_t/min	MW	Fragmentation	Assigment
10	11.9	534	535 (2; M+1); 517 (1; M+1-18); 499 (2; M+1-2x18); 455 (1; M+1-2x18-44); 425 (2; M+1-2x18-44-30); 305 (6; M+1-3x18-16-30-130)	12βOH-GA-C_2 (**257**)
		548	549 (15; M+1); 531 (5; M+1-18); 513 (31; M+1-2x18); 457 (15; M+1-18-44-30); 441 (5; M+1-18-44-16-30); 421 (4; M+1-3x18-44-30); 319 (3; M+1-3x18-2x30-116)	**258**
		554	555 (5; M+1); 513 (31; M+1-42); 511 (7; M+1-44); 451 (4; M+1-18-44-42); 439 (6; M+1-42-44-30); 425 (2; M+1-130); 303 (3; M+1-252)	**285**; **286**
		568	569 (100; M+1); 551 (6; M+1-18); 509 (5; M+1-18-42); 465 (5; M+1-18-44-42); 421 (4; M+1-30-116); 303 (3; M+1-14-42-210)	12β-OAc-GenA-F (**272**)
		570	571 (5; M+1); 553 (4; M+1-18); 511 (7; M+1-18-42); 481 (1; M+1-30-60); 347 (2; M+1-2x18-30-44-42-116); 331 (2; M+1-2x18-16-30-44-42-116); 303 (3; M+1-16-42-210); 301 (3; M+1-2x18-30-32-42-130)	12β-OAc-GenA-H (**47**); 12β-OAc-GenA-D (**224**); GA-F (**22**)
		572	573 (4; M+1); 555 (5; M+1-18); 531 (5; M+1-42); 513 (31; M+1-18-42); 511 (7; M+1-18-44); 451 (4; M+1-2x18-44-42); 423 (4; M+1-18-44-42-16-30); 421 (4; M+1-2x18-44-42-30); 409 (6; M+1-2x18-2x42-44); 305 (6; M+1-16-154-98); 303 (3; M+1-130-2x18-42-30-32); 301 (3; M+1-14-28-30-42-158)	GenA-K (**223**); 12β-OAc-GA-D (**264**); GA-H (**24**); **260**
		574	557 (2; M+1-18); 513 (31; M+1-18-44); 409 (6; M+1-18-44-42-30-32); 331 (2; M+1-2x18-44-42-30-32-60)	GA-K (**26**)
		586	569 (100; M+1-18); 545 (3; M+1-42); 527 (1; M+1-18-42); 465 (5; M+1-18-32-42-30); 331 (2; M+1-2x18-42-44-2x32-70)	MeGA-H (**230**)

Peak	R_t/min	MW	Fragmentation	Assigment
10	11.9	588	571 (5; M+1-18); 557 (2; M+1-32); 529 (1; M+1-18-42); 515 (11; M+1-32-42); 305 (M+1-2x18-2x32-44-42-68-30)	MeGA-K (**231**)
		598	557 (2; M+1-42); 527 (1; M+1-42-30); 515 (11; M+1-14-28-42); 511 (7; M+1-42-46); 451 (4; M+1-2x30-46-42); 423 (4; M+1-14-30-46-44-42); 357 (3; M+1-2x18-32-46-44-42-98); 301 (3; M+1-2x18-32-46-44-42-98)	EtGA-F (**228**)
		614	615 (6; M+1); 555 (5; M+1-18-42); 525 (3; M+1-18-42-30); 511 (7; M+1-44-18-42); 481 (1; M+1-44-30-18-42); 451 (4; M+1-18-16-130); 347 (2; M+1-2x18-2x30-42-130)	3βOAc-GA-H (**265**)
11	12.2	514	515 (13; M+1); 497 (1; M+1-18); 467 (1; M+1-18-30)	GenA-A (**213**)
		532	515 (13; M+1-18); 497 (1; M+1-2x18); 471 (1; M+1-18-44)	GA-I (**206**); GA-G (**23**)
		548	549 (1; M+1); 513 (7; M+1-2x18); 487 (1; M+1-18-44); 469 (3; M+1-2x18-44); 467 (1; M+1-2x18-16-30)	**258**
		554	555 (5; M+1); 513 (7; M+1-42); 511 (2; M+1-44); 469 (3; M+1-18-44-42)	**285**; **286**
		568	569 (3; M+1); 551 (2; M+1-18); 509 (14; M+1-60)	12β-OAc-GenA-F (**272**);
		570	571 (52; M+1); 553 (100; M+1-18); 511 (2; M+1-18-42); 509 (13; M+1-18-44); 467 (1; M+1-18-44-42); 301 (1; M+1-16-42-210)	12β-OAc-GenA-H (**47**); 12β-OAc-GenA-D (**224**); GA-F (**22**)
		572	573 (2; M+1); 555 (5; M+1-18); 513 (7; M+1-18-42); 469 (3; M+1-18-44-42); 301 (1; M+1-14-28-30-42-158)	GenA-K (**223**); GA-H (**24**); **260**
		588	571 (52; M+1-18); 515 (13; M+1-32-42); 471 (1; M+1-32-44-42)	MeGa-K (**231**)
		598	527 (11; M+1-42-30); 515 (13; M+1-14-28-42); 511 (2; M+1-46-42); 467 (1; M+1-46-44-42); 301 (1; M+1-2x18-32-46-44-42-98)	EtGA-F (**228**)

Peak	R_t/min	MW	Fragmentation	Assigment
12	12.3	514	515 (100; M+1); 497 (3; M+1-18)	GenA-B (**219**); GA-AM$_1$ (**12**); GenA-A (**213**); **287**; GA-C1 (**17**) / GA-D (**19**) / GA-J (**234**)
		532	515 (100; M+1-18); 497 (3; M+1-2x18)	GA-I (**206**); GA-G (**23**)
		570	553 (5; M+1-18); 511 (2; M+1-18-42)	12β-OAc-GenA-H (**47**); GA-F (**22**)
		598	515 (100; M+1-14-28-42); 511 (2; M+1-46-42)	EtGA-F (**228**)
13	12.5	428	429 (5; M+1); 413 (5; M+1-16); 329 (2; M+1-44-56); 315(2; M+1-16-98)	LA-DM (**217**)
		472	473 (8; M+1); 455 (2; M+1-18); 435 (2; M+1-18-20); 379 (1; M+1-2x18-58)	GN3OL (**67**); LOL-A (**239**)
		478	479 (4; M+1); 413 (5; M+1-2x18-30); 305 (1; M+1-30-44-100)	**276**
		498	499 (54; M+1); 481 (6; M+1-18); 367 (1; M+1-16-116)	**285**
		510	511 (27; M+1); 493 (5; M+1-18); 467 (3; M+1-44)	GenA-F (**221**)
		512	513 (27; M+1); 495 (5; M+1-18); 481 (5; M+1-32); 471 (4; M+1-42); 421 (1; M+1-18-44-30); 379 (1; M+1-18-44-42-30); 303 (4; M+1-210)	GenA-H (**222**); GenA-D (**220**); GA-E (**21**) / GNPA-A (**31**); GenA-G (**271**); GA-X (**251**)
		514	515 (100; M+1); 497 (31; M+1-18); 481 (6; M+1-18-16); 479 (4; M+1-2x18); 473 (8; M+1-42); 471 (4; M+1-44); 467 (3; M+1-18-30); 455 (2; M+1-16-44); 453 (9; M+1-18-44); 443 (2; M+1-42-30); 435 (2; M+1-2x18-44); 379 (2; M+1-18-2x44-30); 321 (1; M+1-194); 317(2; M+1-16-30-152); 305 (1; M+1-210); 303 (4; M+1-212)	**283**; GenA-B (**219**); GA-AM$_1$ (**12**); GenA-A (**213**); **287**; GA-C1 (**17**) / GA-D (**19**); LA-D (**278**); GA-J (**234**)

Peak	R_t/min	MW	Fragmentation	Assigment
13	12.5	516	517 (4; M+1); 499 (54; M+1-18); 483 (1; M+1-18-16); 481 (6; M+1-2x18); 475 (3; M+1-42); 471 (4; M+1-16-30); 467 (3; M+1-18-32); 455 (2; M+1-18-44); 445 (1; M+1-42-30); 413 (5; M+1-18-44-42); 329 (2; M+1-16-42-30-100); 303 (4; M+1-216)	**259**; GenA-C2 (**269**); GA-B (**8**); LA-E2 (**83**); GA-A (**10**)
		528	529 (10; M+1); 511 (27; M+1-18); 485 (4; M+1-44); 467 (3; M+1-18-44); 455 (1; M+1-44-30); 421 (1; M+1-16-18-30-44); 307 (15; M+1-2x18-30-156)	**284**
		530	531 (2; M+1); 513 (27; M+1-18); 499 (54; M+1-32); 495 (13; M+1-2x18); 481 (6; M+1-18-32); 455 (2; M+1-32-44); 421 (1; M+1-2x18-44-30); 305 (1; M+1-226); 303 (4; M+1-16-212)	12βOH-GenA-B (**270**); GA-C6 (**233**); GA-M (**236**) / 12βOH-GA-D (**263**) / 12βOH-GA-C1 (**225**); MeGA-B (**15**)
		532	533 (2; M+1); 515 (100; M+1-18); 497 (31; M+1-2x18); 485 (4; M+1-18-30); 471 (4; M+1-18-44); 455 (2; M+1-18-60); 453 (9; M+1-2x18-44); 305 (1; M+1-228); 303 (4; M+1-16-3x18-30-130);	GA-I (**206**); GA-G (**23**)
		548	549 (2; M+1); 531 (2; M+1-18); 513 (27; M+1-2x18); 487 (4; M+1-18-44); 467 (3; M+1-2x18-16-30); 441 (2; M+1-18-44-16-30); 421 (1; M+1-3x18-44-30)	**258**
		554	555 (8; M+1); 513 (27; M+1-42); 511 (27; M+1-44); 303 (4; M+1-252)	**285**; **286**
		568	569 (2; M+1); 551 (17; M+1-18); 509 (9; M+1-60); 421 (1; M+1-30-116); 317 (2; M+1-42-210); 303 (4; M+1-14-42-210)	12β-OAc-GenA-F (**272**)
		570	571 (11; M+1); 553 (8; M+1-18); 511 (27; M+1-18-42); 481 (6; M+1-18-42-30); 467 (3; M+1-18-44-42); 303 (4; M+1-16-42-210)	**287**; 12β-OAc-GenA-D (**224**); 12β-OAc-GenA-H (**47**); GA-F (**22**)

Peak	R_t/min	MW	Fragmentation	Assigment
13	12.5	572	573 (4; M+1); 555 (8; M+1-18); 531 (2; M+1-42); 513 (27; M+1-18-42); 483 (1; M+1-18-30-42); 471 (4; M+1-42-60); 421 (1; M+1-2x18-44-42-30); 379 (1; M+1-2x18-30-44-2x42); 305 (1; M+1-16-154-98); 303 (4; M+1-2x18-42-32-30-130)	GenA-K (**223**); GA-H (**24**); **260**
		574	575 (19; M+1); 513 (27; M+1-18-44); 471 (4; M+1-18-44-42); 453 (9; M+1-2x18-44-42)	GA-K (**26**)
		588	571 (11; M+1-18); 529 (10; M+1-18-42); 515 (100; M+1-32-42); 471 (4; M+1-32-44-42); 453 (9; M+1-18-32-44-42); 305 (1; M+1-2x18-2x32-44-42-68-30)	MeGA-K (**231**)
		598	527 (1; M+1-42-30); 515 (100; M+1-14-28-42); 511 (27; M+1-46-42); 467 (3; M+1-46-44-42)	EtGA-F (**228**)
14	12.9	440	441 (4; M+1); 423 (7; M+1-18); 363 (10; M+1-18-60)	GOL-B (**64**)
		454	419 (9; M+1-2x18); 363 (10; M+1-2x18-56); 327 (12; M+1-18-16-56-38); 315 (18; M+1-18-30-32-60); 313 (10; M+1-18-2x32-60)	GNO-A (**268**); LAL-C (**45**)
		456	457 (7; M+1); 439 (1: M+1-18); 315 (18; M+1-2x18-16-30-60)	L2OL (**43**)
		458	459 (8; M+1); 441 (4; M+1-18); 423 (7; M+1-2x18); 303 (1; M+1-156)	LA-A (**69**)
		470	471 (5; M+1); 427 (4; M+1-44); 395 (2; M+1-2x16-44); 343 (4; M+1-16-44-68)	7-Oxo-GA-Z (**79**)
		472	473 (1; M+1); 419 (9; M+1-3x18); 361 (2; M+1-3x18-58); 313 (10; M+1-2x18-2x32-60)	GN3OL (**67**); LOL-A (**239**)
		484	469 (1; M+1-16); 467 (2; M+1-18); 449 (3; M+1-2x18); 441 (4; M+1-44); 423 (7; M+1-18-44); 343 (4; M+1-44-98); 327 (12; M+1-16-44-98); 313 (10; M+1-44-30-98); 303 (1; M+1-44-138)	11α-OH-GA-DM (**247**) / 11β-OH-GA-DM (**248**); GLA-E (**246**)

Peak	R_t/min	MW	Fragmentation	Assigment
14	12.9	486	469 (1; M+1-18); 451 (3; M+1-2x18); 423 (7; M+1-18-16-30); 395 (2; M+1-18-44-30); 327 (12; M+1-18-44-68-30)	**266**
		498	499 (8; M+1); 481 (2; M+1-18); 451 (3; M+1-18-30)	**285**
		510	511 (29; M+1); 493 (14; M+1-18); 469 (1; M+1-42); 467 (2; M+1-44); 463 (3; M+1-18-30); 451 (3; M+1-18-42); 449 (3; M+1-18-44); 419 (9; M+1-18-44-30)	GenA-F (**221**); GA-T-Q (**57**)
		512	513 (45; M+1); 495 (33; M+1-18); 481 (2; M+1-32); 465 (1; M+1-18-30); 451 (3; M+1-18-44); 423 (7; M+1-16-44-30); 303 (1; M+1-210)	GenA-H (**222**); GenA-D (**220**); GA-E (**21**) / GNPA-A (**31**); GenA-G (**271**)
		514	515 (100; M+1); 497 (23; M+1-18); 481 (2; M+1-16-18); 479 (22; M+1-2x18); 473 (1; M+1-42); 471 (5; M+1-44); 467 (2; M+1-18-30); 453 (8; M+1-18-44); 443 (1; M+1-42-30); 439 (1; M+1-32-44); 423 (7; M+1-18-44-30); 395 (2; M+1-16-18-44-42); 319 (7; M+1-2x18-44-68-16-32); 303 (1; M+1-212)	**283**; GenA-B (**219**); GA-AM_1 (**12**); GenA-A (**213**); **287**; GA-C1 (**17**) / GA-D (**19**); LA-D (**278**); GA-J (**234**)
		516	517 (7; M+1); 499 (8; M+1-18); 483 (1; M+1-18-16); 481 (2; M+1-2x18); 471 (5; M+1-16-30); 395 (2; M+1-18-44-60); 343 (4; M+1-16-158); 303 (1; M+1-214)	**259**; GenA-C2 (**269**); GA-B (**8**); GA-A (**10**)
		518	483 (1; M+1-2x18); 461 (1; M+1-58); 457 (7; M+1-18-44); 439 (1; M+1-2x18-44); 395 (2; M+1-18-44-30-32)	GA-C2 (**18**)
		526	527 (84; M+1); 441 (4; M+1-42-44); 423 (7; M+1-18-44-42)	15α-OAc-GLA-E (**267**)
		528	529 (6; M+1); 511 (29; M+1-18); 469 (1; M+1-16-44); 467 (2; M+1-18-44); 423 (7; M+1-44-30-32); 363 (10; M+1-18-30-32-44-42)	**284**

Peak	R_t/min	MW	Fragmentation	Assigment
14	12.9	530	513 (46; M+1-18); 495 (34; M+1-2x18); 469 (1; M+1-18-44); 451 (3; M+1-2x18-44); 439 (1; M+1-18-44-30); 303 (1; M+1-16-212)	12βOH-GenA-B (**270**); GA-C6 (**233**); GA-M (**236**) / 12βOH-GA-C1 (**225**) / 12βOH-GA-D (**263**)
		532	533 (2; M+1); 515 (100; M+1-18); 497 (23; M+1-2x18); 471 (5; M+1-18-44); 453 (8; M+1-2x18-44); 303 (1; M+1-16-3x18-30-130)	GA-I (**206**); GA-G (**23**)
		534	535 (9; M+1); 517 (7; M+1-18); 469 (1; M+1-2x18-30)	12βOH-GA-C_2 (**257**)
		548	549 (21; M+1); 513 (46; M+1-2x18); 469 (1; M+1-2x18-44); 467 (2; M+1-2x18-16-30); 457 (7; M+1-18-44-30); 441 (4; M+1-18-44-16-30); 319 (6; M+1-3x18-2x30-116)	**258**
		554	555 (4; M+1); 513 (46; M+1-42); 511 (29; M+1-44); 469 (1; M+1-42-44); 451 (3; M+1-18-44-42); 439 (1; M+1-44-42-30); 395 (2; M+1-30-130); 303 (1; M+1-252)	**285**; **286**
		568	569 (15; M+1); 551 (24; M+1-18); 509 (24; M+1-18-42); 465 (1; M+1-18-44-42); 303 (1; M+1-14-42-210)	12βOAc-GenA-F (**272**)
		570	571 (3; M+1); 553 (17; M+1-18); 511 (29; M+1-18-42); 481 (2; M+1-18-42-30); 467 (2; M+1-18-42-44); 449 (3; M+1-2x18-44-42); 303 (1; M+1-16-42-210)	12βOAc-GenA-H (**47**); 12βOAc-GenA-D (**224**); GA-F (**22**)
		572	573 (3; M+1); 555 (4; M+1-18); 513 (46; M+1-18-42); 483 (1; M+1-18-30-42); 469 (1; M+1-18-42-44); 451 (3; M+1-2x18-44-42); 363 (10; M+1-2x18-42-132); 303 (1; M+1-2x18-30-32-42-130)	GenA-K (**223**); GA-H (**24**); **260**
		574	575 (5; M+1); 557 (1; M+1-18); 513 (46; M+1-18-44); 471 (5; M+1-18-44-42); 453 (8; M+1-2x18-44-42); 343 (4; M+1-42-2x30-130)	GA-K (**26**)

Peak	R_t/min	MW	Fragmentation	Assigment
14	12.9	586	587 (5; M+1); 569 (15; M+1-18); 527 (84; M+1-18-42; 483 (4; M+1-32-42-30); 465 (1; M+1-18-32-42-30)	MeGA-H (**230**)
		588	571 (3; M+1-18); 557 (1; M+1-32); 529 (3; M+1-18-42); 515 (100; M+1-32-42); 471 (5; M+1-32-44-42); 453 (8; M+1-18-32-44-42)	MeGA-K (**231**)
		598	557 (1; M+1-42); 539 (1; M+1-46-14); 527 (84; M+1-42-30); 515 (100; M+1-14-28-42); 511 (29; M+1-46-42); 467 (2; M+1-46-44-42); 451 (3; M+1-2x30-46-42); 423 (7; M+1-14-30-46-44-42)	EtGA-F (**228**)
15	13.3	438	421 (6; M+1-18); 363 (1; M+1-16-60); 359 (2; M+1-16-2x32); 309 (2; M+1-18-16-3x32)	LAL-A (**256**)
		456	421 (6; M+1-2x18); 383 (2; M+1-18-56); 357 (3; M+1-2x18-2x32); 329 (3; M+1-2x18-32-60); 315 (1; M+1-2x18-16-30-60); 311 (2; M+1-2x18-68-42)	L2OL (**43**)
		472	473 (6; M+1); 437 (2; M+1-2x18); 311 (2; M+1-3x18-70-38)	GN3OL (**67**)
		486	487 (2; M+1); 469 (1; M+1-18); 443 (3; M+1-44)	**266**
		512	513 (5; M+1); 495 (1; M+1-18); 465 (4; M+1-18-30); 437 (2; M+1-16-60); 421 (6; M+1-18-44-30); 331 (1; M+1-30-152)	GenA-H (**222**); GenA-D (**220**); GA-G (**21**) / GNPA-A (**31**); GenA-G (**271**)
		514	515 (7; M+1); 497 (3; M+1-18); 479 (1; M+1-2x18); 473 (6; M+1-42); 471 (2; M+1-44); 443 (3; M+1-42-30); 437 (2; M+1-18-60); 409 (3; M+1-106); 383 (2; M+1-16-116); 311 (2; M+1-16-30-158); 305 (1; M+1-210); 301 (3; M+1-16-42-156)	**283**; GenA-B (**219**); GenA-A (**213**); GA-C1 (**17**) / GA-D (**19**); LA-D (**278**); GA-J (**234**)
		516	517 (7; M+1); 499 (1; M+1-18); 471 (2; M+1-16-30); 437 (2; M+1-2x18-44); 409 (3; M+1-18-16-30-44); 383 (2; M+1-18-44-30-42); 347 (2; M+1-14-156); 301 (3; M+1-216)	**259**; GenA-C2 (**269**); GA-A (**10**)

Peak	R_t/min	MW	Fragmentation	Assigment
15	13.3	528	529 (1; M+1); 511 (4; M+1-18); 469 (1; M+1-16-44); 421 (6; M+1-16-18-30-44); 363 (1; M+1-18-30-32-44-42)	**284**
		530	531 (1; M+1); 513 (5; M+1-18); 499 (1; M+1-32); 495 (1; M+1-2x18); 469 (1; M+1-18-44); 437 (2; M+1-18-44-32); 421 (6; 2x18-44-30); 331 (1; M+1-200); 309 (2; M+1-18-16-30-158); 305 (1; M+1-226)	12βOH-GenA-B (**270**); GA-C6 (**233**); GA-M (**236**) / 12βOH-GA-D (**263**) / 12βOH-GA-C1 (**225**); MeGA-B (**15**)
		532	533 (1; M+1); 515 (7; M+1-18); 497 (3; M+1-2x18); 471 (2; M+1-18-44); 437 (2; M+1-2x18-60); 305 (1; M+1-228)	GA-I (**206**); GA-G (**23**)
		534	535 (1; M+1); 517 (7; M+1-18); 499 (1; M+1-2x18); 487 (2; M+1-18-30); 469 (1; M+1-2x18-30); 305 (1; M+1-3x18-16-30-130)	12βOH-GA-C_2 (**257**)
		548	549 (5; M+1); 531 (1; M+1-18); 513 (5; M+1-2x18); 487 (2; M+1-18-44); 469 (1; M+1-2x18-44); 441 (2; M+1-18-44-16-30); 421 (6; M+1-3x18-44-30)	**258**
		568	569 (1; M+1); 551 (2; M+1-18); 509 (100; M+1-18-42); 465 (4; M+1-18-44-42); 437 (2; M+1-16-116); 421 (6; M+1-30-116)	12β-OAc-GenA-F (**272**)
		572	573 (1; M+1); 555 (2; M+1-18); 531 (1; M+1-42); 513 (5; M+1-18-42); 469 (1; M+1-18-44-42); 421 (6; M+1-16-18-30-44-42); 363 (1; M+1-2x18-16-42-116); 305 (1; M+1-16-154-98); 301 (3; M+1-14-28-30-42-158)	GenA-K (**223**); GA-H (**24**); **260**
		574	513 (5; M+1-18-44); 471 (2; M+1-18-44-42); 409 (3; M+1-18-42-44-30-32); 331 (1; M+1-2x18-44-42-30-32-60)	GA-K (**26**)
		586	569 (1; M+1-18); 545 (1; M+1-42); 527 (6; M+1-18-42); 331 (1; M+1-2x18-2x32-44-42-70)	Me-GA-H (**230**)

Peak	R_t/min	MW	Fragmentation	Assigment
15	13.3	588	571 (2; M+1-18); 557 (2; M+1-32); 529 (1; M+1-18-42); 515 (7; M+1-32-42); 471 (2; M+1-32-44-42)	MeGA-K (**231**)
		598	539 (2; M+1-18-42); 527 (6; M+1-42-30); 515 (7; M+1-14-28-42); 511 (4; M+1-46-42); 357 (3; M+1-2x18-14-2x30-46-44-42); 301 (3; M+1-2x18-32-46-44-42-98)	EtGA-F (**228**)
16	13.7	472	457 (49; M+1-16); 381 (1; M+1-2x18-56); 363 (1; M+1-3x18-56); 338 (2; M+1-15-2x18-16-68)	GN3OL (**67**)
		474	475 (2; M+1); 457 (49; M+1-18); 329 (5; M+1-3x18-2x30-32)	GR3OL-M (**212**);
		510	511 (100; M+1); 493 (7; M+1-18); 467 (1; M+1-44); 363 (1; M+1-32-116)	GenA-F (**221**)
		512	513 (14; M+1); 495 (4; M+1-18); 481 (2; M+1-32); 471 (2; M+1-42); 376 (2; M+1-15-18-44-60); 325 (1; M+1-42-130); 303 (2; M+1-210)	GenA-H (**222**); GenA-D (**220**); GA-E (**21**) / GNPA-A (**31**); GenA-G (**271**); GA-X (**251**)
		516	475 (2; M+1-42); 457 (49; M+1-60); 329 (5; M+1-16-30-42-100)	LA-E2 (**83**)
		518	483 (1; M+1-2x18); 457 (49; M+1-18-44)	GA-C2 (**18**)
		528	529 (16; M+1); 511 (100; M+1-18); 467 (1; M+1-18-44); 455 (1; M+1-44-30); 363 (1; M+1-18-30-32-44-42); 336 (1; M+1-15-30-32-116)	**284**
		530	531 (2; M+1); 513 (14; M+1-18); 498 (2; M+1-18-15); 495 (4; M+1-2x18); 481 (2; M+1-18-32); 455 (1; M+1-32-44); 303 (2; M+1-16-212)	12βOH-GenA-B (**270**); GA-C6 (**233**); GA-M (**236**) / 12βOH-GA-C1 (**225**) / 12βOH-GA-D (**263**); MeGA-B (**15**)
		548	549 (2; M+1); 531 (2; M+1-18); 513 (14; M+1-2x18); 457 (49; M+1-18-44-30)	**258**
		554	513 (14; M+1-42); 511 (100; M+1-44); 496 (1; M+1-15-44)	**286**

Peak	R_t/min	MW	Fragmentation	Assigment
16	13.7	568	509 (13; M+1-18-42); 494 (2; M+1-15-18-42); 330 (3; M+1-15-14-210); 303 (2; M+1-14-42-210)	12β-OAC-GenA-F (**272**)
		570	571 (1; M+1); 553 (2; M+1-18); 511 (100; M+1-18-42); 481 (2; M+1-18-42-30); 467 (1; M+1-18-44-42); 303 (2; M+1-16-42-210)	12β-OAc-GenA-H (**47**); GA-F (**22**)
		572	531 (2; M+1-42); 513 (14; M+1-18-42); 496 (1; M+1-15-18-44); 483 (1; M+1-18-30-42); 363 (1; M+1-2x18-16-42-116); 325 (1; M+1-30-42-60-116)	GenA-K (**223**); **260**
		574	557 (1; M+1-18); 513 (14; M+1-18-44); 498 (2; M+1-15-18-44); 471 (2; M+1-18-44-42)	GA-K (**26**)
		586	545 (2; M+1-42); 527 (7; M+1-18-42); 483 (1; M+1-32-42-30)	MeGA-H (**230**)
		588	571 (1; M+1-18); 557 (1; M+1-32); 529 (16; M+1-18-42); 515 (1; M+1-32-42); 498 (2; M+1-15-32-44); 471 (2; M+1-32-44-42)	MeGA-K (**231**)
		598	557 (1; M+1-42); 527 (7; M+1-42-30); 515 (1; M+1-14-28-42); 511 (100; M+1-46-42); 467 (1; M+1-46-44-42); 357 (1; M+1-2x18-14-2x30-46-44-42); 301 (1; M+1-2x18-32-46-44-42-98)	EtGA-F (**228**)
17	14.0	510	511 (100; M+1); 493 (51; M+1-18)	GenA-F (**221**)
		512	513 (11; M+1); 495 (9; M+1-18); 481 (2; M+1-32); 480 (1; M+1-15-18); 471 (2; M+1-42); 436 (1; M+1-18-15-44); 433 (2; 2x18-44); 423 (1: M+1-16-44-30); 421 (2; M+1-18-44-30); 396 (2; M+1-15-42-60)	GenA-H (**222**); GenA-D (**220**); GA-E (**21**) / GNPA-A (**31**); GenA-G (**271**); GA-X (**251**)
		528	529 (2; M+1); 511 (100; M+1-18); 479 (2; M+1-18-32); 453 (2; M+1-32-44); 438 (1; M+1-15-44-32); 435 (1; M+1-18-32-44); 423 (1; M+1-44-30-32); 421 (2; M+1-16-18-30-44)	**284**; MeGA-D (**227**)

Peak	R_t/min	MW	Fragmentation	Assigment
17	14.0	530	531 (1; M+1); 513 (11; M+1-18); 499 (2; M+1-32); 498 (1; M+1-15-18); 495 (9; M+1-2x18); 481 (2; M+1-18-32); 454 (1; M+1-15-18-44); 436 (1; M+1-2x18-15-44); 421 (2; M+1-2x18-44-30)	12βOH-GenA-B (**270**); GA-C6 (**23**); GA-M (**236**) / 12βOH-GA-C1 (**221**) / 12βOH-GA-D (**263**); MeGA-B (**15**)
		548	549 (7; M+1); 531 (1; M+1-18); 513 (11; M+1-2x18); 454 (1; M+1-2x18-15-44); 457 (2; M+1-18-44-30); 421 (2; M+1-3x18-44-30); 308 (3; M+1-2x18-15-16-174)	**258**
		554	513 (11; M+1-42); 511 (100; M+1-44); 496 (3; M+1-15-44)	**286**
		568	569 (2; M+1); 551 (1; M+1-18); 509 (5; M+1-18-42); 494 (33; M+1-15-18-42); 421 (2; M+1-30-116); 317 (1; M+1-42-210)	12β-OAc-GenA-F (**272**)
		570	571 (1; M+1); 538 (1; M+1-15-18); 511 (100; M+1-18-42); 494 (32; M+1-15-18-44); 481 (2; M+1-18-42-30)	12β-OAc-GenA-D (**224**); GA-F (**22**)
		572	573 (2; M+1); 555 (5; M+1-18); 531 (1; M+1-42); 513 (11; M+1-18-42); 496 (3; M+1-15-18-44); 483 (1; M+1-18-42-30); 436 (1; M+1-15-2x18-44-42); 423 (1; M+1-18-44-42-16-30); 421 (2; M+1-2x18-44-42-30); 320 (1; M+1-15-2x18-42-30-130); 316 (2; M+1-15-16-30-42-154); 315 (1; M+1-42-30-32-154)	GenA-K (**223**); GA-H (**24**); **260**
		574	557 (5; M+1-18); 513 (11; M+1-18-44); 498 (1; M+1-15-18-44); 471 (2; M+1-18-44-42); 453 (2; M+1-2x18-44-42)	GA-K (**26**)
		588	571 (1; M+1-18); 557 (5; M+1-32); 529 (2; M+1-18-42); 515 (2; M+1-32-42); 498 (2; M+1-15-32-44); 471 (2; M+1-32-44-42); 453 (2; M+1-18-32-44-42)	MeGA-K (**231**)

Peak	R_t/min	MW	Fragmentation	Assigment
17	14.0	598	557 (5; M+1-42); 527 (1; M+1-42-30); 515 (2; M+1-14-28-42); 511 (100; M+1-46-42); 423 (1; M+1-14-30-46-44-42)	EtGA-F (**228**)
18	14.5	512	513 (22; M+1); 495 (100; M+1-18)	GenA-H (**222**); GenA-D (**220**); GA-E (**21**) / GNPA-A (**31**); GenA-G (**271**)
		514	515 (2; M+1); 497 (6; M+1-18)	GenA-B (**219**); GA-AM_1 (**12**); GenA-A (**213**); **287**; GA-C1 (**17**) / GA-D (**19**); GA-J (**234**)
		530	513 (22; M+1-18); 498 (1; M+1-15-18); 495 (100; M+1-2x18)	12βOH-GenA-B (**270**); GA-M (**236**) / 12β-OH-GA-C1 (**225**) / 12βOH-GA-D (**263**)
		532	515 (2; M+1-18); 497 (6; M+1-2x18)	GA-I (**206**); GA-G (**23**)
		548	549 (4; M+1); 513 (22; M+1-18)	**258**
		554	513 (22; M+1-42); 511 (2; M+1-44); 496 (28; M+1-15-44)	**286**
		572	513 (22; M+1-18-42); 496 (28; M+1-15-18-44)	GenA-K (**223**)
19	14.7	460	461 (7; M+1); 443 (5; M+1-18); 425 (2; M+1-2x18); 387 (3; M+1-44-30); 357 (1; M+1-44-60); 305 (2; M+1-156)	LA-N (**72**)
		510	511 (25; M+1); 493 (9; M+1-18); 478 (3; M+1-15-18); 463 (11; M+1-18-30); 419 (2; M+1-18-44-30); 408 (3; M+1-15-16-44-28); 405 (1; M+1-30-32-44); 392 (1; M+1-15-18-44-42)	GenA-F (**221**)

Peak	R_t/min	MW	Fragmentation	Assigment
19	14.7	512	513 (100; M+1); 495 (74; M+1-18); 481 (1; M+1-32); 480 (2; M+1-15-18); 471 (1; M+1-42); 465 (7; M+1-18-30); 451 (3; M+1-18-44); 437 (2; M+1-32-44); 436 (2; M+1-15-18-44); 410 (2; M+1-15-16-30-42); 379 (2; M+1-18-44-42-30); 337 (6; M+1-18-44-16-98); 303 (1; M+1-210)	GenA-H (**222**); GenA-D (**220**); GA-E (**21**) / GNPA-A (**31**); GenA-G (**271**); GA-X (**251**)
		514	515 (9; M+1); 497 (15; M+1-18); 481 (1; M+1-18-16); 479 (12; M+1-2x18); 471 (1; M+1-44); 455 (3; M+1-16-44); 443 (5; M+1-42-30); 437 (2; M+1-18-60); 436 (2; M+1-15-16-18-30); 422 (2; M+1-15-18-60); 405 (1; M+1-2x18-44-30); 395 (4; M+1-16-18-44-42); 379 (2; M+1-18-30-2x44); 319 (2; M+1-2x18-30-130); 317 (1; M+1-16-30-152); 311 (2; M+1-16-30-158); 305 (2; M+1-210); 303 (1; M+1-212); 301 (7; M+1-16-42-156)	**283**; GenA-B (**219**); GA-AM_1 (**12**); GenA-A (**213**); **287**; GA-C1 (**17**) / GA-D (**19**); LA-D (**278**); GA-J (**234**)
		516	517 (1; M+1); 481 (1; M+1-2x18); 437 (2; M+1-2x18-44); 303 (1; M+1-214); 301 (7; M+1-216)	GA-A (**10**)
		526	527 (6; M+1); 485 (3; M+1-42); 441 (3; M+1-42-44)	15α-OAc-GLA-E (**267**)
		528	529 (1; M+1); 511 (25; M+1-18); 485 (3; M+1-44); 455 (3; M+1-44-30); 332 (3; M+1-15-18-44-2x30-60); 319 (2; M+1-16-18-2x30-116)	**284**
		530	513 (100; M+1-18); 498 (1; M+1-15-18); 495 (74; M+1-2x18); 481 (1; M+1-18-32); 455 (3; M+1-32-44); 451 (3; M+1-2x18-44); 437 (2; M+1-18-44-32); 436 (2; M+1-15-2x18-44); 408 (3; M+1-15-16-18-30-44); 305 (2; M+1-226); 303 (1; M+1-16-212)	12βOH-GenA-B (**270**); GA-C6 (**233**); GA-M (**236**) / 12βOH-GA-C1 (**225**) / 12βOH-GA-D (**263**); MeGA-B (**15**)

Peak	R_t/min	MW	Fragmentation	Assigment
19	14.7	532	533 (7; M+1); 515 (9; M+1-18); 500 (2; M+1-15-18); 497 (15; M+1-2x18); 485 (3; M+1-18-30); 471 (1; M+1-18-44); 456 (2; M+1-15-18-44); 455 (3; M+1-18-60); 437 (2; M+1-2x18-60); 305 (2; M+1-228); 303 (1; M+1-16-3x18-30-130)	GA-I (**206**); GA-G (**23**)
		548	549 (10; M+1); 513 (100; M+1-2x18); 455 (3; M+1-18-2x16-44); 425 (2; M+1-18-44-32-30); 305 (2; M+1-2x18-2x44-2x30-60)	**258**
		554	513 (100; M+1-42); 511 (25; M+1-44); 496 (38; M+1-15-44); 451 (3; M+1-18-44-42); 425(2; M+1-130); 395 (4; M+1-18-130); 303 (1; M+1-252)	**285**; **286**
		568	569 (37; M+1); 509 (25; M+1-18-42); 494 (4; M+1-15-18-42); 465 (7; M+1-18-44-42); 437 (2; M+1-16-116); 345 (2; M+1-14-210); 303 (1; M+1-14-42-210)	12β OAC-GenA-F (**272**)
		570	571 (5; M+1); 553 (4; M+1-18); 538 (2; M+1-15-18); 511 (25; M+1-18-42); 494 (4; M+1-15-18-44); 481 (1; M+1-18-30-42); 437 (2; M+1-18-44-42-30); 405 (1; M+1-18-44-42-30-32); 303 (1; M+1-16-42-210); 301 (7; M+1-16-2x18-30-32-42-130)	12β-OAc-GenA-H (**47**); 12β-OAc-GenA-D (**224**); GA-F (**22**)
		572	513 (100; M+1-18-42); 496 (39; M+1-15-18-44); 478 (3; M+1-15-2x18-44); 451 (3; M+1-2x18-44-42); 436 (2; M+1-15-2x18-44-42); 379 (2; M+1-2x18-30-44-2x42); 316 (6; M+1-15-16-30-42-154); 305 (2; M+1-16-154-98); 301 (7; M+1-2x18-30-32-42-130)	GenA-K (**223**); **260**
		574	557 (3; M+1-18); 513 (100; M+1-18-44); 498 (1; M+1-15-18-44); 471 (1; M+1-18-44-42)	GA-K (**26**)
		586	569 (37; M+1-18); 545 (3; M+1-42); 465 (7; M+1-18-32-42-30)	MeGA-H (**230**)

Peak	R_t/min	MW	Fragmentation	Assigment
19	14.7	588	571 (5; M+1-18); 557 (3; M+1-32); 529 (1; M+1-18-42); 515 (9; M+1-32-42); 498 (1; M+1-15-32-44); 471 (1; M+1-32-42-44); 305 (2; M+1-2x18-2x32-44-42-68-30)	MeGA-K (**231**)
		598	599 (1; M+1); 539 (4; M+1-18-42); 527 (6; M+1-42-30); 515 (9; M+1-14-28-42); 511 (25; M+1-46-42); 451 (3; M+1-46-42-2x30); 357 (1; M+1-2x18-14-2x30-46-44-42); 301 (7; M+1-2x18-32-46-44-42-98)	EtGA-F (**228**)
		614	615 (2; M+1); 511 (25; M+1-18-44-42); 512 (4; M+1-18-15-42-28); 481 (1; M+1-18-44-42-30); 451 (3; M+1-18-16-130); 345 (2; M+1-2x18-30-32-42-130)	3βOAc-GA-H (**265**)
		616	599 (1; M+1-18); 525 (5; M+1-18-42-32); 513 (100; M+1-18-44-42); 511 (25; M+1-18-16-30-42); 495 (74; M+1-2x18-44-42); 481 (1; M+1-18-44-42-32); 451 (3; M+1-2x18-130)	**261**
20	14.9	510	511 (100; M+1); 493 (5; M+1-18); 463 (1; M+1-18-30); 449 (4; M+1-18-44); 323 (1; M+1-32-156)	GenA-F (**221**)
		512	513 (13; M+1); 495 (5; M+1-18); 452 (1; M+1-15-16-30); 433 (2; M+1-2x18-44)	GenA-D (**220**)
		528	511 (100; M+1-18); 421 (1; M+1-16-18-30-44); 336 (1; M+1-15-32-30-116); 319 (1; M+1-18-16-2x30-116);	**284**
		546	547 (11; M+1); 511 (100; M+1-2x18); 493 (5; M+1-3x18);449 (4; M+1-3x18-44); 433 (2; M+1-3x18-44-16); 389 (1; M+1-3x18-44-2x30); 321 (1; M+1-2x18-2x30-130)	GA-N (**237**)
		548	513 (13; M+1-2x18); 487 (1; M+1-18-44); 308 (1; M+1-15-2x18-15-16-174)	**258**
		554	555 (2; M+1); 513 (13; M+1-42); 511 (100; M+1-44); 496 (1; M+1-15-44)	**286**

Peak	R_t/min	MW	Fragmentation	Assigment
20	14.9	570	571 (1; M+1); 553 (6; M+1-18); 511 (100; M+1-18-42); 452 (1; M+1-15-18-44-42)	12β-OAc-GenA-H (**47**); GA-F (**22**)
		572	555 (2; M+1-18); 513 (13; M+1-18-42); 496 (1; M+1-15-18-44); 421 (1; M+1-2x18-44-42-30)	GenA-K (**223**)
21	15.3	498	499 (100; M+1); 367 (1; M+1-132)	**285**
		532	533 (1; M+1); 500 (18; M+1-15-18); 497 (6; M+1-2x18); 485 (1; M+1-18-30); 403 (1; M+1-130)	GA-I (**206**); GA-G (**23**)
		534	535 (8; M+1); 499 (100; M+1-2x18)	12βOH-GA-C_2 (**257**)
		570	571 (1; M+1); 553 (4; M+1-18); 499 (100; M+1-42-30); 485 (1; M+1-42-44); 457 (1; M+1-2x42-30)	GA-Mk (**51**) / GA-P (**249**) / GA-Q (**250**)
22	15.7	568	569 (36; M+1); 551 (100; M+1-18); 509 (1; M+1-18-42)	12β-OAc-GenA-F (**272**)
		570	571 (4; M+1); 553 (7; M+1-18); 511 (1; M+1-18-42)	12β-OAc-GenA-H (**47**); GA-F (**22**)
		612	571 (4; M+1-42); 569 (36; M+1-44); 553 (7; M+1-2x30); 552 (39; M+1-15-16-30); 551 (100; M+1-30-32); 499 (1; M+1-42-30); 495 (1; M+1-32-44-42)	GA-T (**11**)
23	16.1	428	429 (8; M+1); 331 (8; M+1-98); 315 (14; M+1-16-98)	LA-DM (**217**)
		454	437 (5; M+1-18); 331 (8; M+1-16-18-28-30-32); 315 (14; M+1-18-30-32-60)	LAL-C (**45**)
		456	439 (4; M+1-18); 421 (3; M+1-2x18); 315 (14; M+1-2x18-16-30-60); 311 (8; M+1-2x18-42-68)	L2OL (**43**)
		468	469 (5; M+1); 425 (4; M+1-44); 355 (5; M+1-16-44-54); 311 (8; M+1-16-44-98)	GA-DM (**32**)
		484	485 (5; M+1); 469 (5; M+1-16); 441 (3; M+1-44); 425 (4; M+1-60); 410 (16; M+1-15-60); 303 (2; M+1-44-138)	11α-OH-GA-DM (**247**) / 11β-OH-GA-DM (**248**)
		486	469 (5; M+1-18); 405 (3; M+1-18-2x32); 355 (5; M+1-18-16-44-56)	**266**

Peak	R_t/min	MW	Fragmentation	Assigment
23	16.1	512	513 (100; M+1); 495 (7; M+1-18); 465 (6; M+1-18-30); 437 (5; M+1-32-44); 421 (3; M+1-18-44-30); 410 (16; M+1-15-16-42-30); 303 (2; M+1-210)	GenA-H (**222**); GA-E (**21**) / GNPA-A (**31**); GenA-G (**271**); GA-X (**251**)
		528	529 (6; M+1-18); 511 (9; M+1-18); 485 (5; M+1-44); 469 (5; M+1-16-44); 421 (3; M+1-16-18-30-44); 336 (1; M+1-15-30-32-116); 307 (M+1-2x18-30-156)	**284**
		530	513 (100; M+1-18); 499 (10; M+1-32); 498 (1; M+1-15-18); 469 (5; M+1-18-44); 437 (5; M+1-18-32-44); 439 (4; M+1-18-44-30); 421 (3; M+1-2x18-44-30); 331 (8; M+1-200); 305 (4; M+1-226); 303 (2; M+1-16-212)	12βOH-GenA-B (**270**); GA-C6 (**233**); MeGA-B (**15**)
		548	549 (16; M+1); 513 (100; M+1-2x18); 469 (5; M+1-2x18-44); 441 (3; M+1-18-16-44-30); 421 (3; M+1-3x18-44-30)	**258**
		554	513 (100; M+1-42); 511 (9; M+1-44); 469 (5; M+1-42-44); 425 (4; M+1-18-44-68); 303 (2; M+1-252)	**285**; **286**
		568	551 (3; M+1-18); 509 (4; M+1-18-42); 494 (2; M+1-15-18-42); 465 (6; M+1-18-44-42); 437 (5; M+1-16-116); 421 (3; M+1-30-116); 330 (3; M+1-15-14-210); 303 (2; M+1-14-42-210)	12β-OAc-GenA-F (**272**)
		570	571 (6; M+1); 511 (9; M+1-18-42); 437 (5; M+1-18-44-42-30); 405 (3; M+1-18-44-42-30-32); 351 (4; M+1-18-30-42-130); 331 (8; M+1-2x18-16-30-44-42-116); 303 (2; M+1-16-42-210)	12β-OAc-GenA-H (**47**); GA-F (**22**)
		572	513 (100; M+1-18-42); 478 (3; M+1-15-2x18-44); 469 (5; M+1-18-44-42); 421 (3; M+1-2x18-30-44-42); 331 (8; M+1-2x18-2x30-60-44-42); 315 (14; M+1-42-30-32-154); 305 (4; M+1-18-32-60-116)	GenA-K (**223**); GA-H (**24**)
		574	557 (1; M+1-18); 513 (100; M+1-18-44); 498 (1; M+1-15-18-44); 331 (8; M+1-16-42-30-156)	GA-K (**26**)

Peak	R_t/min	MW	Fragmentation	Assigment
23	16.1	586	569 (7; M+1-18); 527 (3; M+1-18-42); 465 (6; M+1-18-32-42-30); 331 (8; M+1-2x18-2x32-44-42-70)	MeGA-H (**230**)
		588	571 (6; M+1-18); 557 (1; M+1-32); 529 (6; M+1-18-42); 515 (4; M+1-32-42); 498 (1; M+1-15-32-44); 305 (4; M+1-2x18-2x32-30-44-42-68)	MeGA-K (**231**)
		598	557 (1; M+1-42); 527 (3; M+1-42-30); 515 (4; M+1-14-28-42); 511 (9; M+1-46-42)	EtGA-F (**228**)
		632	603 (7; M+1-30); 559 (7; M+1-74); 515 (4; M+1-74-44); 514 (52; M+1-15-74-30); 513 (100; M+1-74-16-30); 511 (7; M+1-74-16-32)	BuGA-F (**288**)

Table A3-15 Identification and assignment of the peaks in GL 4W grown in sawdust.

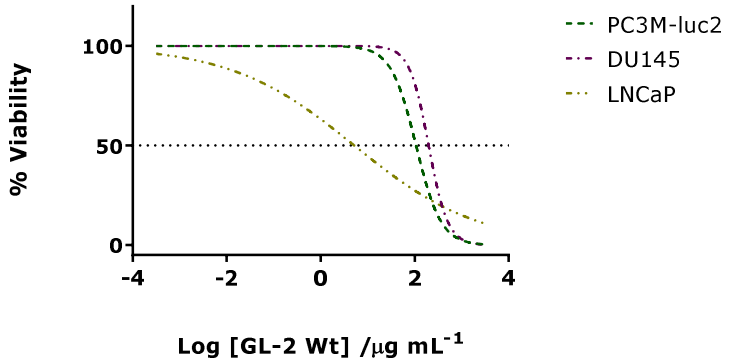
Dose-response curves

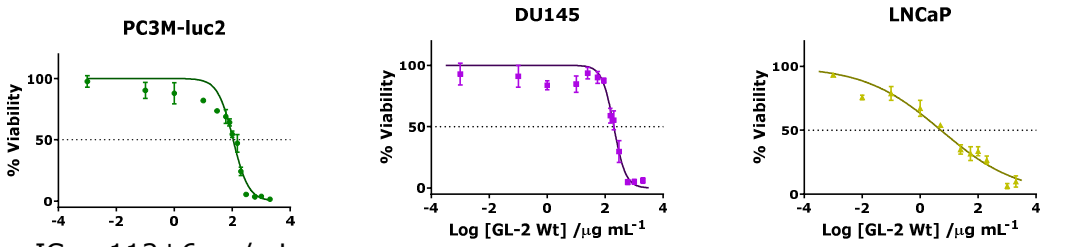
GL extracts ability to inhibit the cell growth was biologically evaluated against three prostate cancer cell-lines: PC3M-luc2, DU145 and LNCaP. The MTT assay was used for this purpose.

GL 2 weeks

Tip

Extraction in ethanol

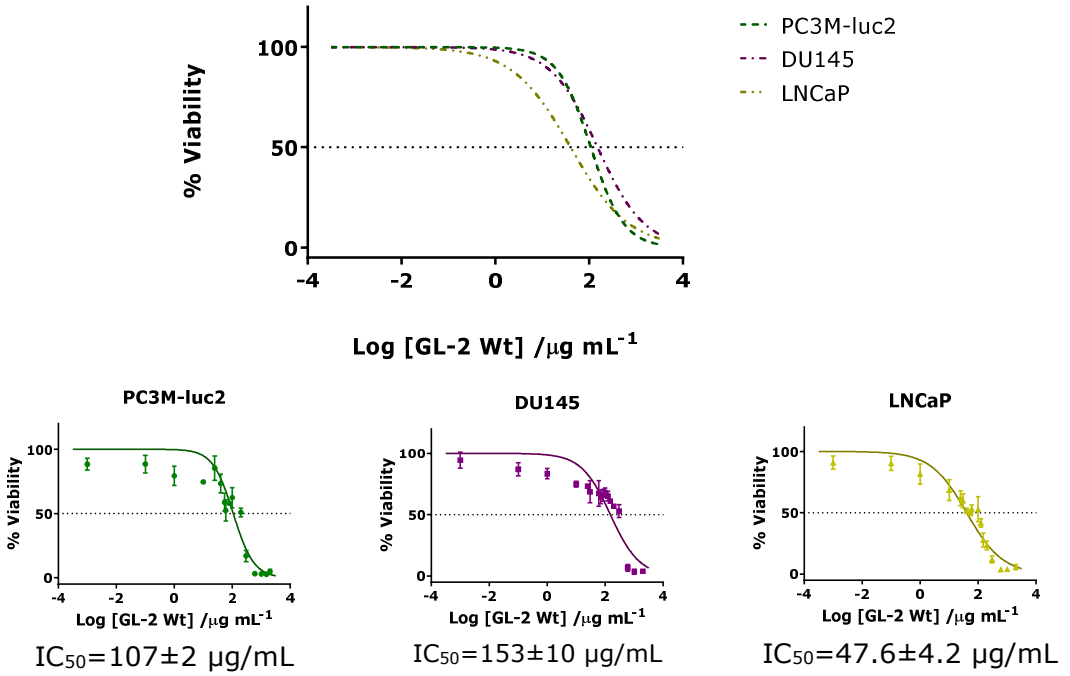




IC_{50}=112±6 µg/mL IC_{50}=192±17 µg/mL IC_{50}=5.74±1.33 µg/mL

Figure A3-22 Dose response curves for prostate cancer cell-lines, PC3M-luc2 (green), DU145 (purple) and LNCaP (gold), treated with the ethanol extract of GL tip harvested at 2 weeks. Extract concentration ranged from 0 to 2000 µg mL^{-1}. Curves are the mean of two experiments each with six replicates. Plates were seeded as follow: PC3M-luc2 at $3x10^4$ cell mL^{-1}·and both DU145 and LNCaP at $4.5x10^4$ cell mL^{-1}. IC_{50} values are indicated as mean ± SD.

Extraction in methanol



IC_{50}=107±2 µg/mL IC_{50}=153±10 µg/mL IC_{50}=47.6±4.2 µg/mL

Figure A3-23 Dose response curves for prostate cancer cell-lines, PC3M-luc2 (green), DU145 (purple) and LNCaP (gold), treated with the methanol extract of GL tip harvested for 2 weeks. Extract concentration ranged from 0 to 2000 µg mL^{-1}. Curves are the mean of two experiments each with six replicates. Plates were seeded as follow: PC3M-luc2 at $3x10^4$ cell mL^{-1}·and both DU145 and LNCaP at $4.5x10^4$ cell mL^{-1}. IC_{50} values are indicated as mean ± SD.

Stalk

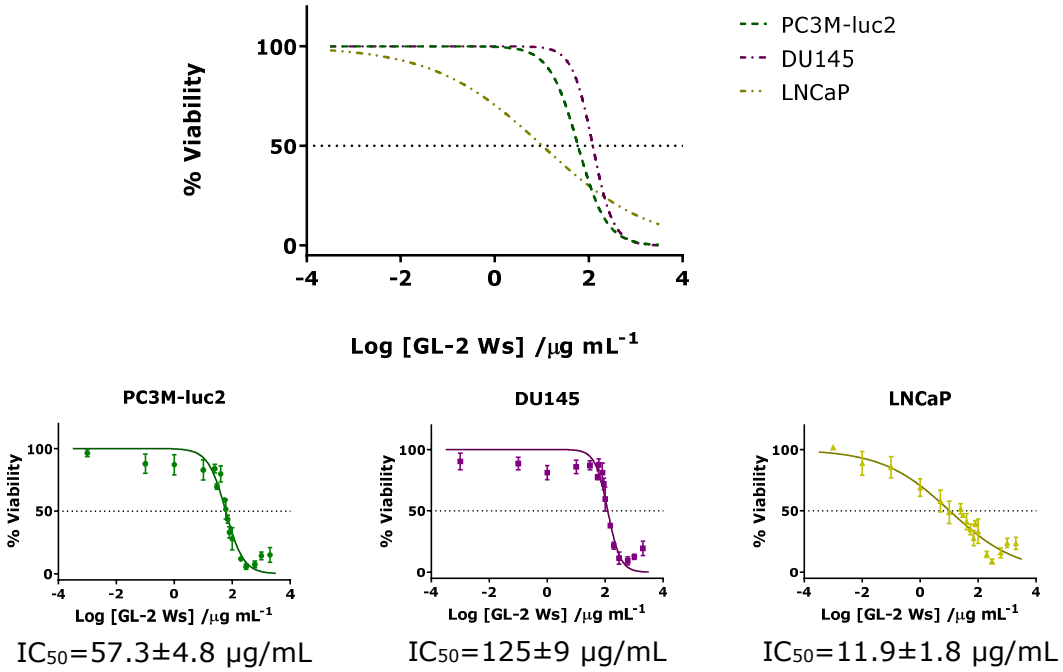
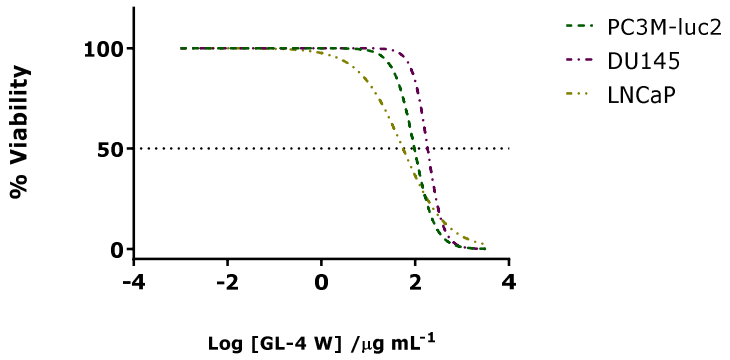
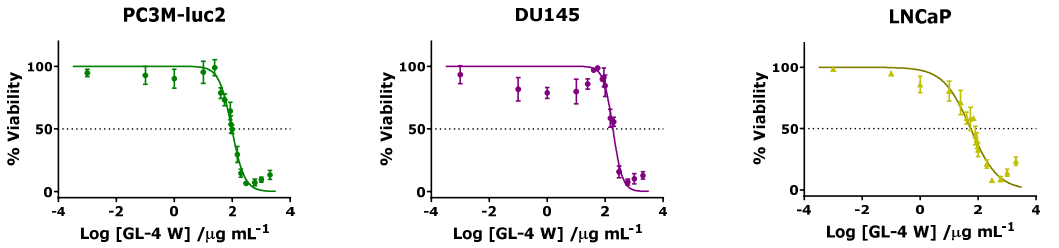


Figure A3-24 Dose response curves for prostate cancer cell-lines, PC3M-luc2 (green), DU145 (purple) and LNCaP (gold), treated with the ethanol extract of GL stalk harvested at 2 weeks. Extract concentration ranged from 0 to 2000 µg mL^{-1}. Curves are the mean of two experiments each with six replicates. Plates were seeded as follow: PC3M-luc2 at $3x10^4$ cell mL^{-1}·and both DU145 and LNCaP at $4.5x10^4$ cell mL^{-1}. IC_{50} values are indicated as mean ± SD.

GL 4 weeks

GL grown in sawdust

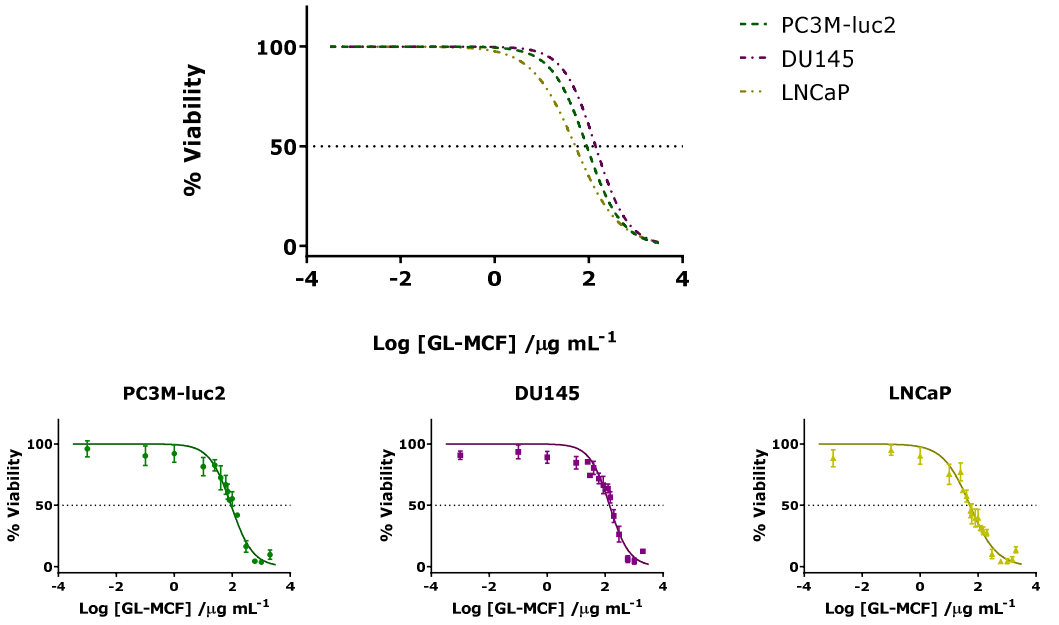




IC_{50}=99.8±7.9 µg/mL IC_{50}=187±10 µg/mL IC_{50}=54.4±5.4 µg/mL

Figure A3-25 Dose response curves for prostate cancer cell-lines, PC3M-luc2 (green), DU145 (purple) and LNCaP (gold), treated with the ethanol extract of GL grown in sawdust and harvested at 4 weeks. Extract concentration ranging from 0 to 2000 µg mL^{-1}. Curves are the mean of two experiments each with 6 replicates. Plates were seeded as follow: PC3M-luc2 at $3x10^4$ cell mL^{-1}·and both DU145 and LNCaP at $4.5x10^4$ cell mL^{-1}. IC_{50} values are indicated as mean ± SD.

GL grown in MCF



IC_{50}=99.2±4.0 µg/mL IC_{50}=154±2 µg/mL IC_{50}=52.7±3.6 µg/mL

Figure A3-26 Dose response curves for prostate cancer cell-lines, PC3M-luc2 (green), DU145 (purple) and LNCaP (gold), treated with the ethanol extract of GL grown in MCF and harvested at 4 weeks. Extract concentration ranged from 0 to 2000 µg mL^{-1}. Curves are the mean of two experiments each with six replicates. Plates were seeded as follow: PC3M-luc2 at $3x10^4$ cell mL^{-1}·and both DU145 and LNCaP at $4.5x10^4$ cell mL^{-1}. IC_{50} values are indicated as mean ± SD.

GL grown in EFB

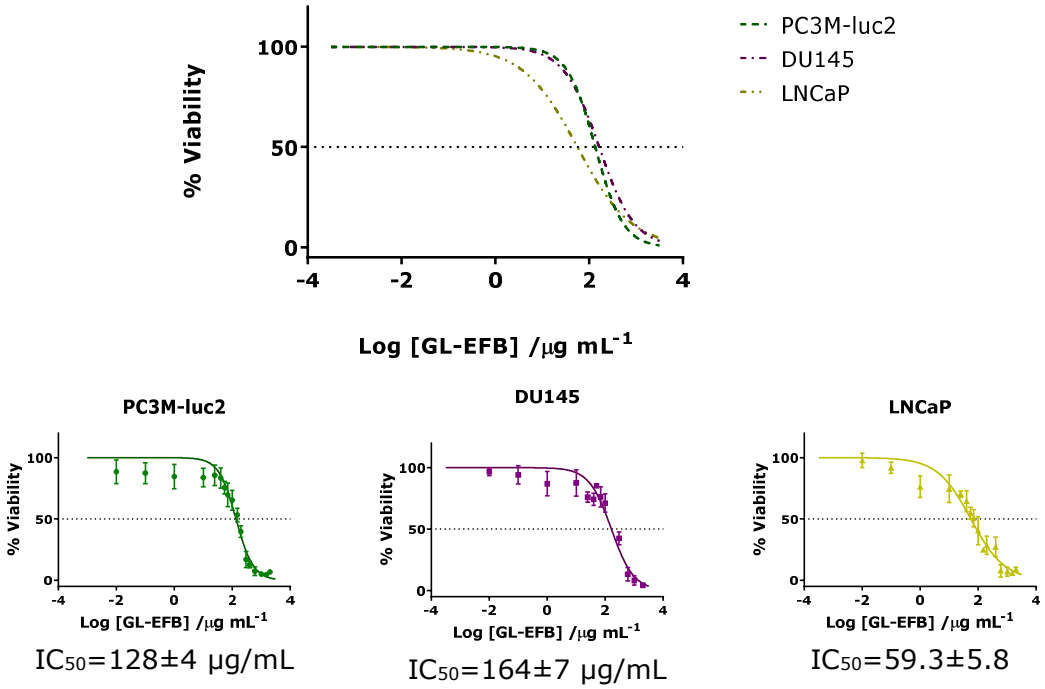


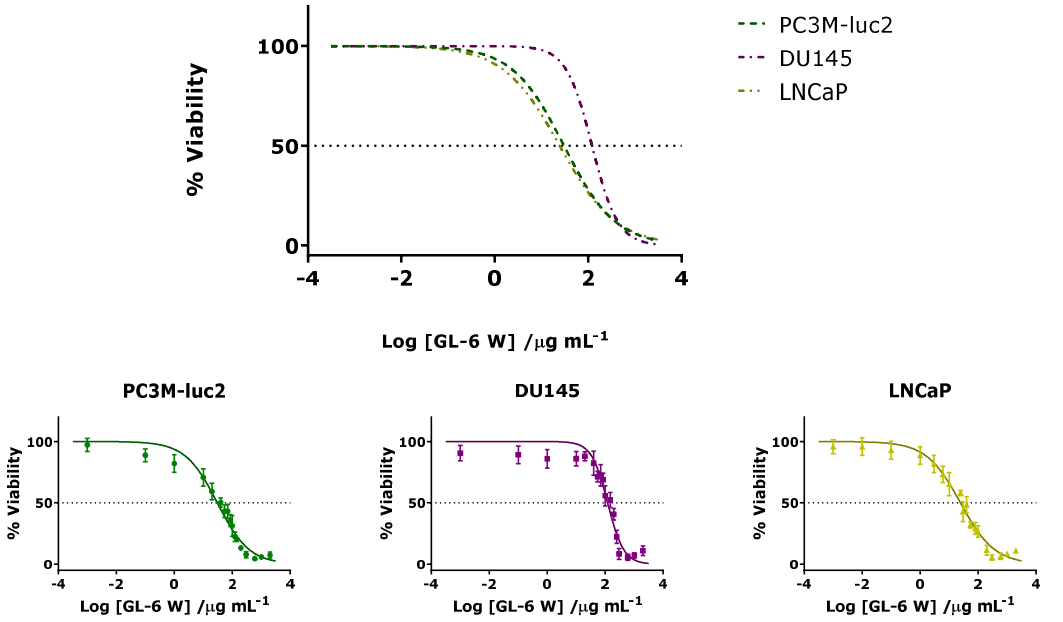
Figure A3-27 Dose response curves for prostate cancer cell-lines, PC3M-luc2 (green), DU145 (purple) and LNCaP (gold), treated with the ethanol extract of GL grown in EFB and harvested at 4 weeks. Extract concentration ranged from 0 to 2000 µg mL^{-1}. Curves are the mean of two experiments each with six replicates. Plates were seeded as follow: PC3M-luc2 at $3x10^4$ cell mL^{-1}·and both DU145 and LNCaP at 4.5 10^4 cell mL^{-1}. IC_{50} values are indicated as mean ± SD.

GL 6 weeks

GL harvested at 6 weeks was extracted with ethanol and chloroform. The antler variety was harvested at 6 weeks and extracted with ethanol.

Extraction in ethanol

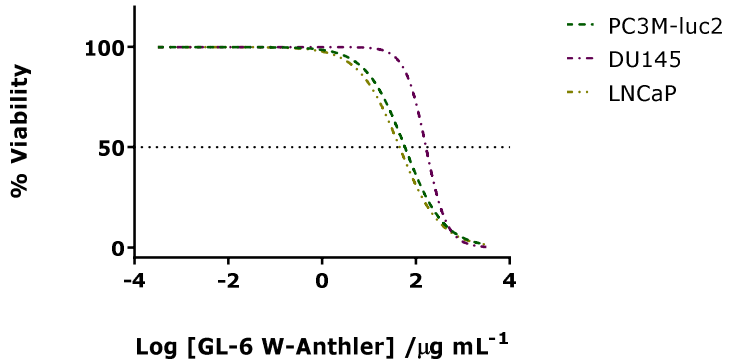
GL (normal)

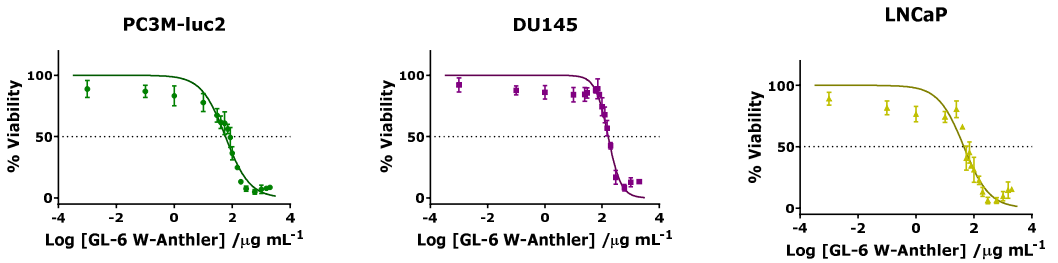


IC_{50}=31.4±4.9 µg/mL IC_{50}=118±8 µg/mL IC_{50}=24.7±4.9 µg/mL

Figure A3-28 Dose response curves for prostate cancer cell-lines, PC3M-luc2 (green), DU145 (purple) and LNCaP (gold), treated with the ethanol extract of GL harvested at 6 weeks. Extract concentration raned from 0 to 2000 µg mL^{-1}. Curves are the mean of two experiments each with six replicates. Plates were seeded as follow: PC3M-luc2 at $3x10^4$ cell mL^{-1}·and both DU145 and LNCaP at 4.5 10^4 cell mL^{-1}. IC_{50} values are indicated as mean ± SD.

GL antler type

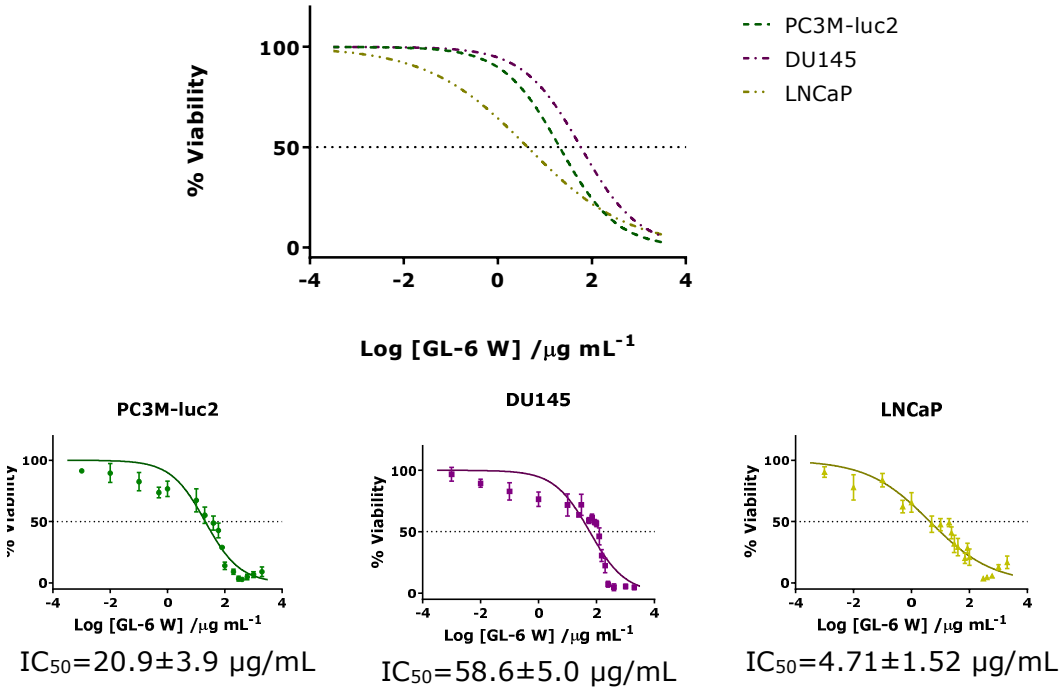




IC_{50}=59.9±2.3 µg/mL IC_{50}=165±2 µg/mL IC_{50}=41.3±5.3 µg/mL

Figure A3-29 Dose response curves for prostate cancer cell-lines, PC3M-luc2 (green), DU145 (purple) and LNCaP (gold), treated with the ethanol extract of GL anthler type harvested at 6 weeks. Extract concentration ranged from 0 to 2000 µg mL^{-1}. Curves are the mean of two experiments each with six replicates. Plates were seeded as follow: PC3M-luc2 at $3x10^4$ cell mL^{-1}·and both DU145 and LNCaP at $4.5x10^4$ cell mL^{-1}. IC_{50} values are indicated as mean ± SD.

Extraction by sonication in chloroform



IC_{50}=20.9±3.9 µg/mL IC_{50}=58.6±5.0 µg/mL IC_{50}=4.71±1.52 µg/mL

Figure A3-30 Dose response curves for prostate cancer cell-lines, PC3M-luc2 (green), DU145 (purple) and LNCaP (gold) were treated with the chloroform extract of GL harvested at 6 weeks. Extracts concentration ranged from 0 to 2000 µg mL^{-1}. Curves are the mean of two independents experiments each with six replicates. Plates were seeded as follow: PC3M-luc2 at $3x10^4$ cell mL^{-1}·and both DU145 and LNCaP at $4.5x10^4$ cell mL^{-1}. IC_{50} values are indicated as mean ± SD.

GL 8 weeks

GL harvested at 8 weeks was extracted with a variety of solvents: ethanol, methanol, dichloromethane, ethyl acetate and water.

Extraction in ethanol

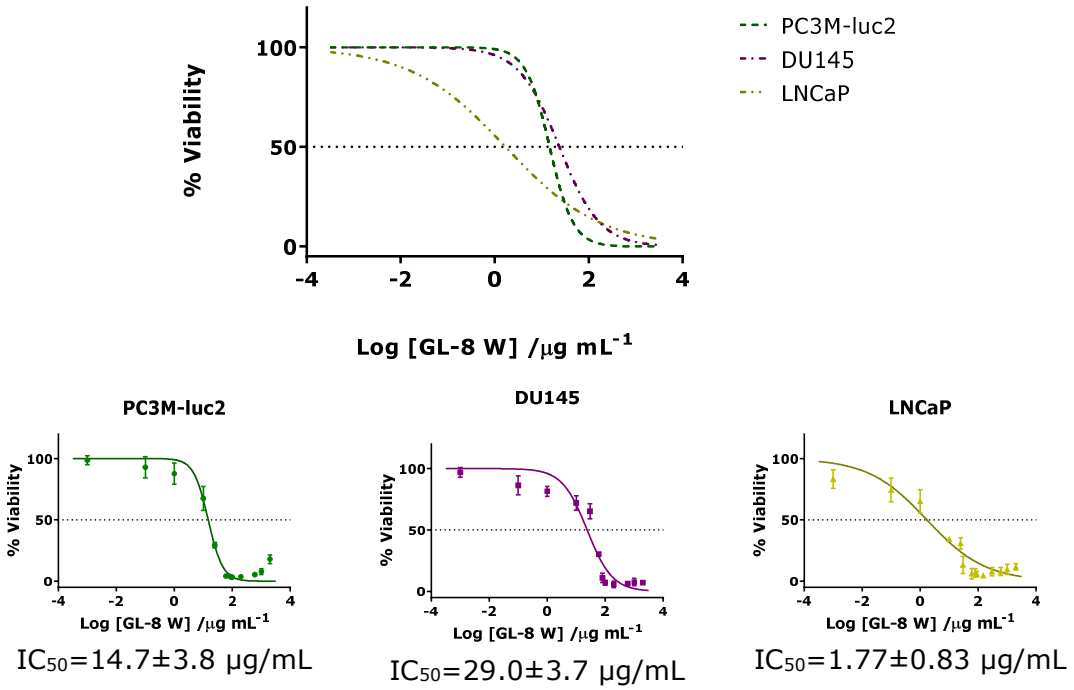
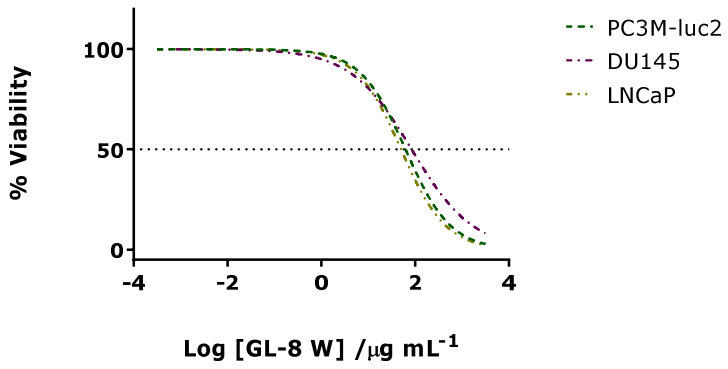
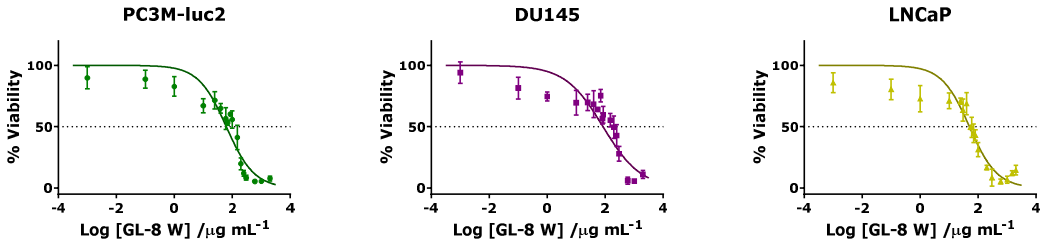


Figure A3-31 Dose response curves for prostate cancer cell-lines, PC3M-luc2 (green), DU145 (purple) and LNCaP (gold), treated with the ethanol extract of GL harvested at 8 weeks. Extract concentration ranged from 0 to 2000 µg mL^{-1}. Curves are the mean of two experiments each with six replicates. Plates were seeded as follow: PC3M-luc2 at $3x10^4$ cell mL^{-1}·and both DU145 and LNCaP at $4.5x10^4$ cell mL^{-1}. IC_{50} values are indicated as mean ± SD.

Extraction in methanol

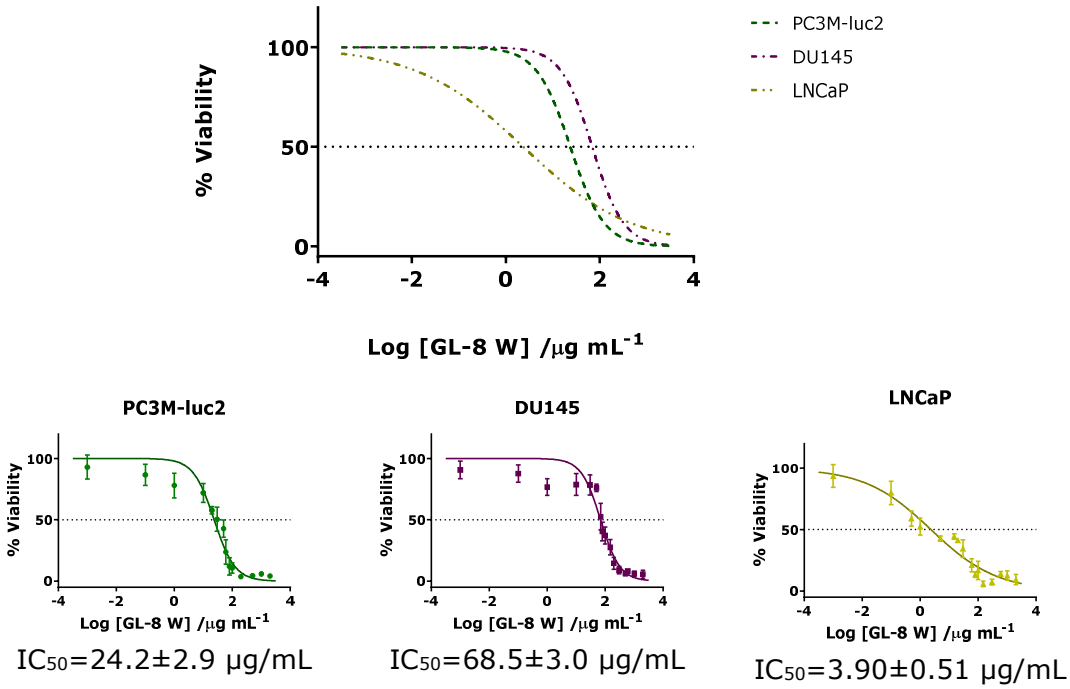




IC_{50}=60.7±3.1 µg/mL IC_{50}=83.0±5.9 µg/mL IC_{50}=51.4±5.6 µg/mL

Figure A3-32 Dose response curves for prostate cancer cell-lines, PC3M-luc2 (green), DU145 (purple) and LNCaP (gold) were treated with the methanol extract of GL harvested at 8 weeks. Extracts concentration ranged from 0 to 2000 µg·mL^{-1}. Curves are the mean of two independents experiments each with six replicates. Plates were seeded as follow: PC3M-luc2 at 3x10^4 cell mL^{-1}·and both DU145 and LNCaP at 4.5x10^4 cell mL^{-1}. IC_{50} values are indicated as mean ± SD.

Extraction in dichloromethane



IC_{50}=24.2±2.9 µg/mL IC_{50}=68.5±3.0 µg/mL IC_{50}=3.90±0.51 µg/mL

Figure A3-33 Dose response curves for prostate cancer cell-lines, PC3M-luc2 (green), DU145 (purple) and LNCaP (gold) were treated with the dichloromethane extract of GL harvested at 8 weeks. Extract concentration ranged from 0 to 2000 µg mL^{-1}. Curves are the mean of two independents experiments each with six replicates. Plates were seeded as follow: PC3M-luc2 at 3x10^4 cell mL^{-1}·and both DU145 and LNCaP at 4.5 10^4 cell mL^{-1}. IC_{50} values are indicated as mean ± SD.

Extraction in ethyl acetate

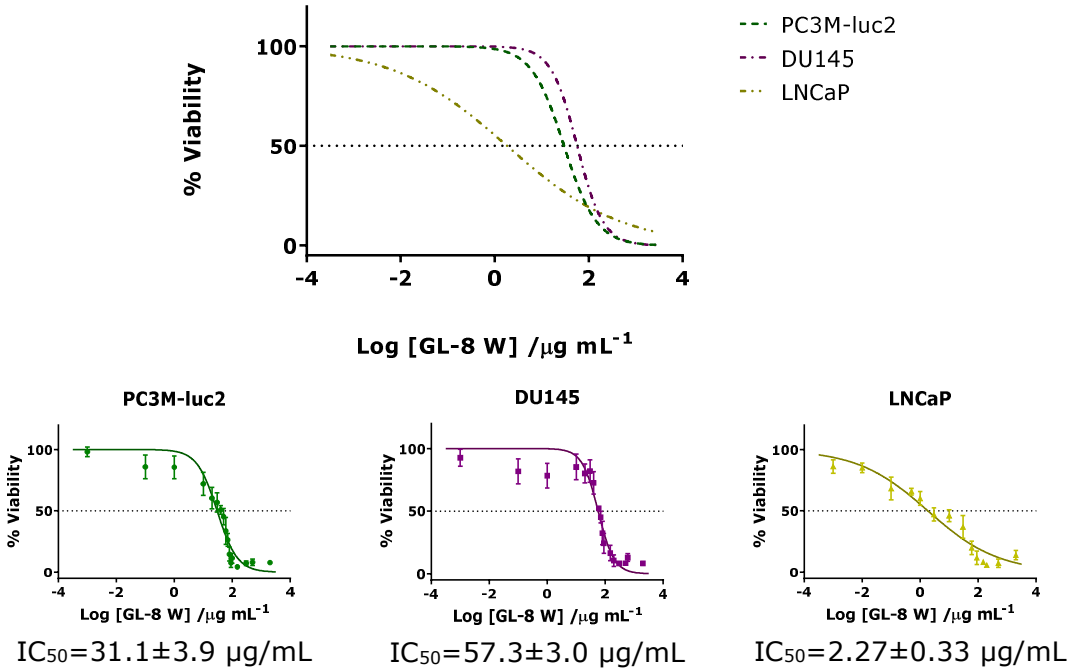


Figure A3-34 Dose response curves for prostate cancer cell-lines, PC3M-luc2 (green), DU145 (purple) and LNCaP (gold) were treated with the ethyl acetate extract of GL harvested at 8 weeks. Extract concentration ranged from 0 to 2000 µg mL^{-1}. Curves are the mean of two independents experiments each with six replicates. Plates were seeded as follow: PC3M-luc2 at $3x10^4$ cell mL^{-1}·and both DU145 and LNCaP at $4.5x10^4$ cell mL^{-1}. IC_{50} values are indicated as mean ± SD.

Extraction in water

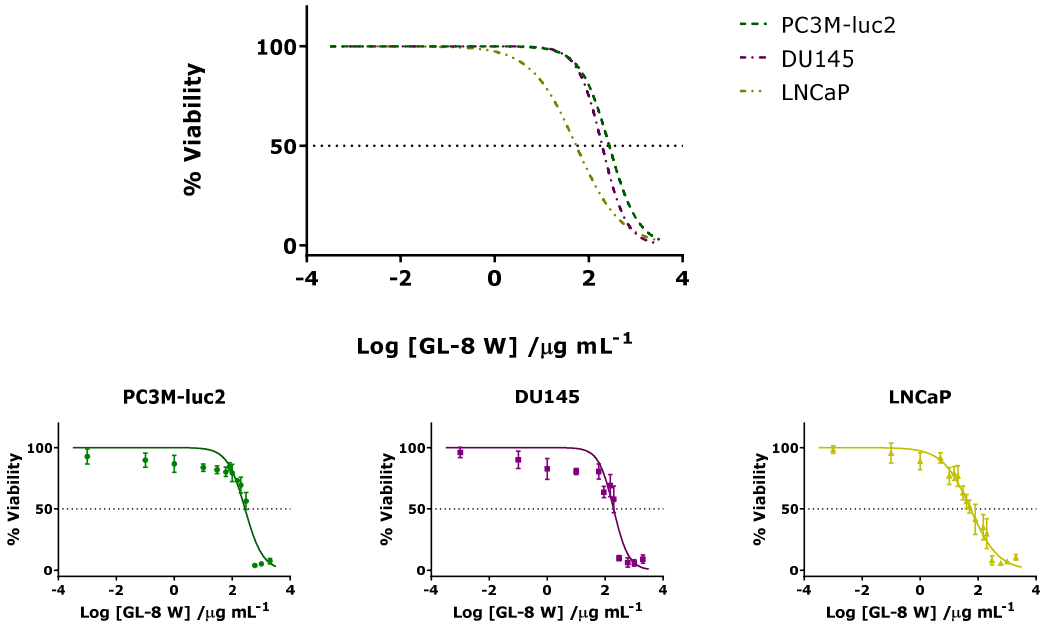


Figure A3-35 Dose response curves for prostate cancer cell-lines, PC3M-luc2 (green), DU145 (purple) and LNCaP (gold) treated with the water extract of GL harvested at 8 weeks. Extracts concentration ranged from 0 to 2000 µg mL^{-1}. Curves are the mean of two independents experiments each with six replicates. Plates were seeded as follow: PC3M-luc2 at $3x10^4$ cell mL^{-1}·and both DU145 and LNCaP at $4.5x10^4$ cell mL^{-1}. IC_{50} values are indicated as mean ± SD.

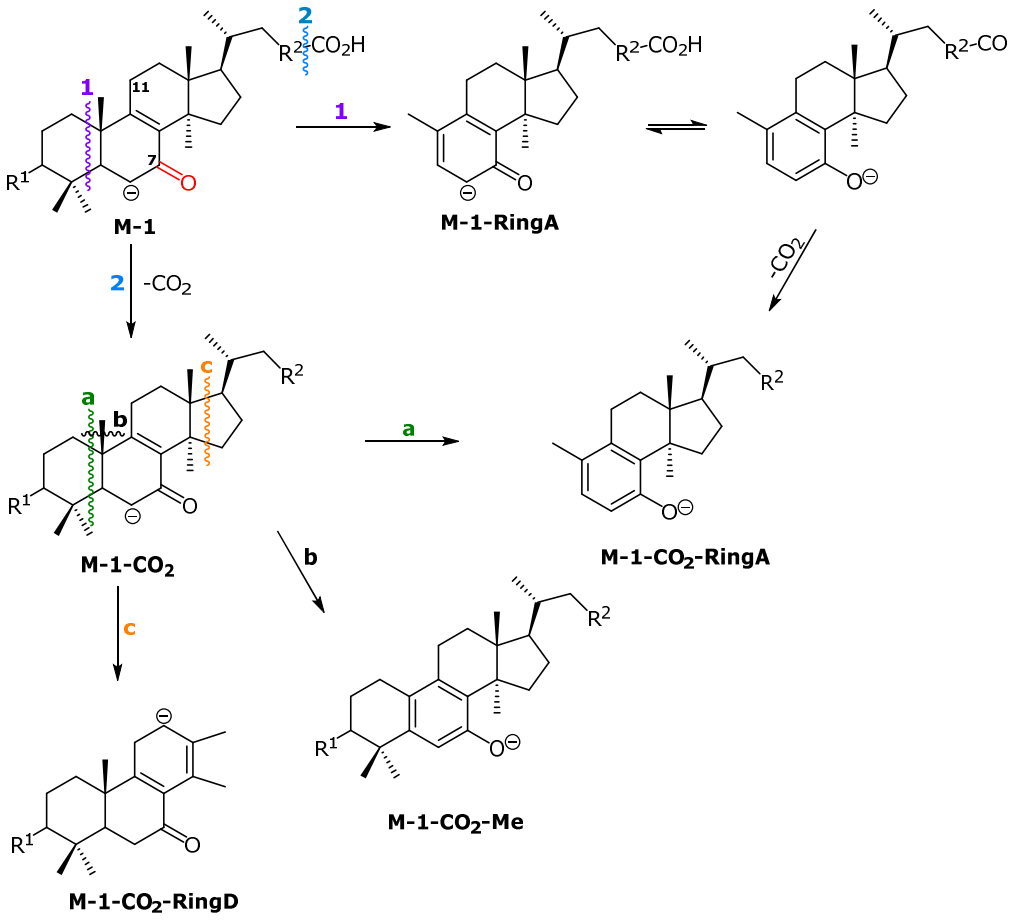
Mass fragmentation rules

Studying the fragmentation of triterpenes could help to identify them by distinguishing among the different isomers. It has been demonstrated that a different substitution pattern in the molecule will generate a different set of fragments.[142, 143]

Triterpenoid acids could be analysed by LC-MS in either positive or negative mode. However, much valuable information could be obtained when the analysis is performed in the negative mode. The positive mode is valuable for detecting the triterpenoid alcohols and aldehydes.

All the discussion that follows refer to the fragmentation observed in the negative mode.[142]

Cleavage of ring A in GA



Scheme A4-1 Cleavage of ring A in GA with C-7 = carbonyl and C-11 ≠ carbonyl.

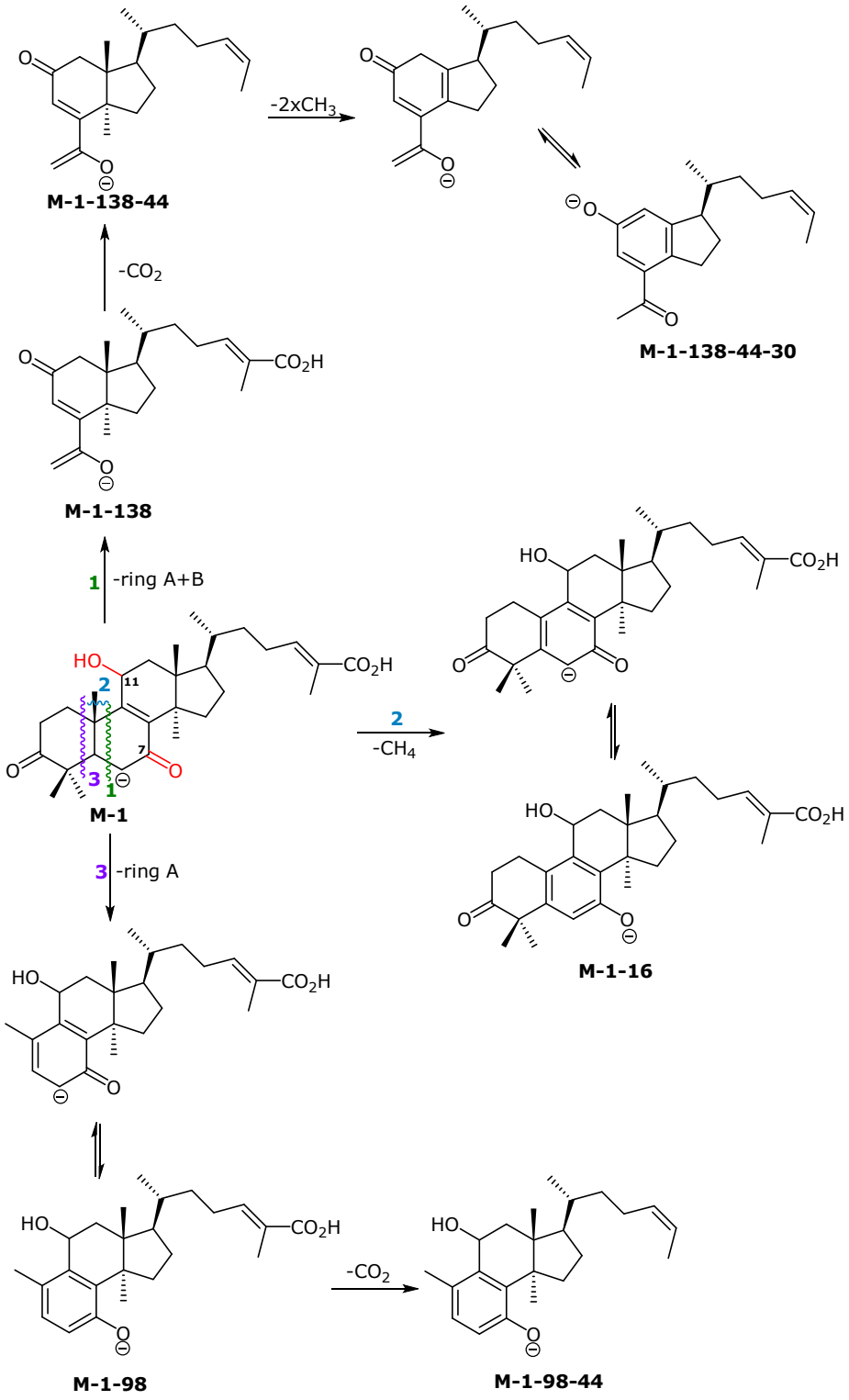
Ring A cleavage is characteristic of GA that possess a carbonyl group at C-7 and either a hydroxyl or hydrogens at C-11. Scheme A4-1 depicts the fragmentation pathway leading to cleavage of ring A. Two competitive routes have been observed. In route 1, highlighted in purple, the first step is the cleavage of ring A followed by decarboxylation. In route 2 (light blue), the decarboxylation step occurs first. This decarboxylated compound **M-1-CO_2** can undergo three further fragmentations, indicated as routes a (green), b (black) and c (orange).

Some examples of GA that undergo cleavage of ring A are: LA-DM (**217**); GA-DM (**32**); 7-Oxo-GA-Z (**79**); MeGA-DM (**78**); 11α-OH-GA-DM (**247**); 11β-OH-GA-DM (**248**) and 7-Oxo-MeGA-Z (**80**).

GA	MW	Fragmentation
217[a]	428	427 (M-1); 411 (M-1-16); 383 (M-1-44); 367 (M-1-60); 329 (M-1-98); 327 (M-1-44-56); 313 (M-1-98-16); 285 (M-1-98-44); 269 (M-1-98-44-16); 245 (M-1-98-84);
32[a]	468	467 (M-1); 423 (M-1-44); 407 (M-1-60); 380 (M-1-15-16-56); 369 (M-1-98); 353 (M-1-44-16-54); 325 (M-1-44-98); 309 (M-1-16-44-98); 285 (M-1-44-70-68)
79[a]	470	469 (M-1); 425 (M-1-44); 409 (M-1-16-44); 393 (M-1-2x16-44); 382 (M-1-15-16-44-56); 365 (M-1-44-60); 353 (M-1-16-44-56); 341 (M-1-16-44-68); 319 (M-1-16-30-44-60); 287 (M-1-18-44-2x60); 267 (M-1-44-60-98)
78[b]	482	481 (M-1); 383 (M-1-98)
247[a]	484	483 (M-1); 467 (M-1-16); 465 (M-1-18); 447 (M-1-36); 439 (M-1-44); 423 (M-1-60); 408 (M-1-15-60); 385 (M-1-98); 345 (M-1-138); 341 (M-1-98-44); 325 (M-1-16-44-98); 311 (M-1-44-30-98); 301 (M-1-138-44); 271 (M-1-138-44-30); 243 (M-1-44-2x98)
248[a]		
80[b]		483 (M-1); 385 (M-1-98)

Table A4-1 Fragmentation for GA with a carbonyl group at C-7 and a different functionality from carbonyl at C-11. Fragmentation of ring A is characteristic for this GA substitution. a Observed fragmentation[142]; b predicted fragmentation.

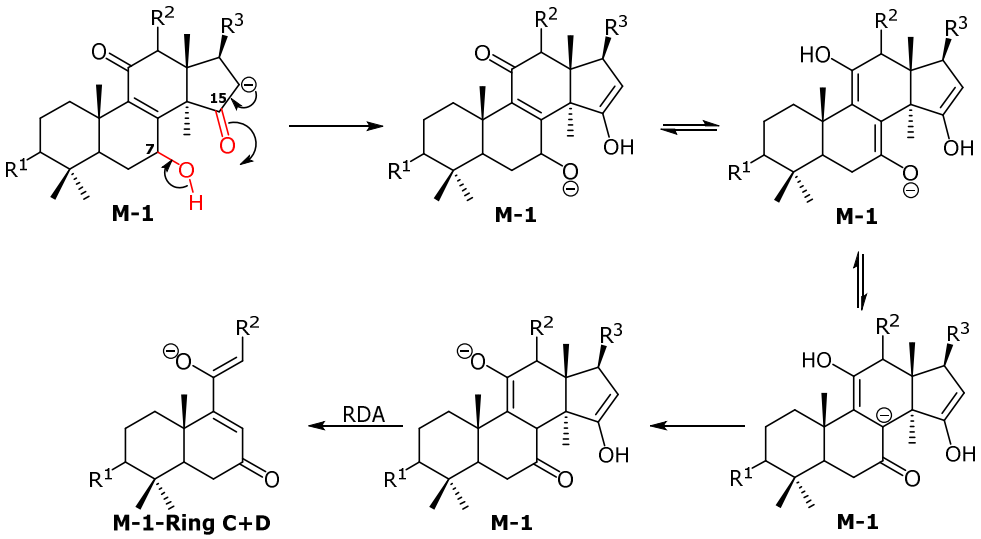
Cleavage of ring B in GA



Scheme A4-2 Fragmentation observed in 7-oxo-11-hydroxy GA derivatives. Three routes followed: **1** (green) rings A+B fragmentation; **2** (blue) methane cleavage to form an aromatic ring B; **3** (purple) ring A cleavage leading to an aromatic ring B.

Cleavage of ring B is characteristic of 7-oxo-11-hydroxy GA derivatives (*e.g.* **247** and **248**) (Scheme A4-2). Three competitive routes have been observed for the fragmentation of this type of GA derivatives, marked as 1 (green), 2 (blue) and 3 (purple) in Scheme A4-2. In route 1 direct cleavage of rings A and B leads to a fragment ion m/z 345 that is subject to further fragmentation. Thus, a sequential loss of carbon dioxide and two methyl radicals to generate the stable aromatic ion m/z 271 is observed. In route 2 the elimination of methane generates the fragment ion m/z 467 with a stable aromatic system on ring B. Whilst, in route 3 ring A is cleaved.

Cleavage of ring C in GA



Scheme A4-3 Fragmentation of ring C in 7-hydroxy-15-oxo GA derivatives. Cleavage is proposed to occur by a retro-Diels-Alder fragmentation (RDA).[142]

Ring C fragmentation is characteristic of 7-hydroxy-15-oxo GA derivatives. A plausible mechanism for this fragmentation is depicted in Scheme A4-3. Ring C cleavage is thought to happen after a retro-Diels-Alder fragmentation (RDA) to generate the highly-stabilised ion **M-1-Ring C+D**. Observed and predicted fragmentation of these type of GA is indicated in Table A4-2.

GA	MW	Fragmentation
Lucidone B (**282**)[a]	400	399 (M-1); 381 (M-1-18); 339 (M-1-60); 301 (M-1-98); 283 (M-1-116); 247 (M-1-152); 149 (M-1-250)
Lucidone A (**215**)[a]	402	401 (M-1); 383 (M-1-18); 359 (M-1-42); 303 (M-1-98); 249 (M-1-152); 193 (M-1-2x42-18-106); 151 (M-1-250)

GA	MW	Fragmentation
LA-A (**69**)[a]	458	457 (M-1); 439 (M-1-18); 421 (M-1-2x18); 395 (M-1-18-44); 383 (M-1-30-44); 323 (M-1-32-102); 301 (M-1-156); 287 (M-1-16-154); 261 (M-1-42-154); 257 (M-1-16-30-154); 247 (M-1-210); 209 (M-1-248); 193 (M-1-16-248); 149 (M-1-210-98)
LA-N (**72**)[a]	460	459 (M-1); 441 (M-1-18); 423 (M-1-2x18); 397 (M-1-18-44); 385 (M-1-30-44); 379 (M-1-2x18-44); 355 (M-1-2x30-44); 331 (M-1-128); 303 (M-1-156); 289 (M-1-170); 287 (M-1-172); 263 (M-1-196); 259 (M-1-200); 249 (M-1-210); 209 (M-1-250); 195 (M-1-264)
MeLA-A (**207**)[b]	472	471 (M-1); 247 (M-1-224); 223 (M-1-248)
LA-B (**216**)[b]	474	473 (M-1); 263 (M-1-210); 209 (M-1-264)
LA-C (**208**)[b]	476	475 (M-1); 265 (M-1-210); 209 (M-1-266)
20OH-LA-N (**73**)[b]		475 (M-1); 249 (M-1-226); 225 (M-1-250)
EtLA-A (**70**)[b]	486	485 (M-1); 247 (M-1-238); 237 (M-1-248)
MeLA-C (**209**)[b]	490	489 (M-1); 265 (M-1-224); 223 (M-1-266)
285[a]	498	497 (M-1); 479 (M-1-18); 449 (M-1-18-30); 435 (M-1-18-44); 431 (M-1-2x18-36); 387 (M-1-110); 365 (M-1-132); 285 (M-1-212); 193 (M-1-304)
GA-β (**34**)[b]	500	499 (M-1); 455 (M-1-44); 249 (M-1-250)
GenA-D (**220**)[a]	512	511 (M-1); 493 (M-1-18); 479 (M-1-2x16); 478 (M-1-15-18); 450 (M-1-15-16-30); 449 (M-1-18-44); 435 (M-1-16-60); 431 (M-1-2x18-44); 405 (M-1-30-32-44); 335 (M-1-18-44-16-98); 329 (M-1-30-152); 301 (M-1-210); 286 (M-1-15-210); 285 (M-1-16-210); 283 (M-1-18-210); 261 (M-1-250); 247 (M-1-264); 172 (M-1-15-60-264); 149 (M-1-98-264)
GenA-G (**271**)[a]		511 (M-1); 493 (M-1-18); 478 (M-1-18-15); 463 (M-1-18-30); 449 (M-1-18-44); 435 (M-1-16-60); 421 (M-1-30-60); 301 (M-1-210); 285 (M-1-16-210)

GA	MW	Fragmentation
GA-C1 (**17**)[a]	514	513 (M-1); 495 (M-1-18); 477 (M-1-2x18); 451 (M-1-18-44); 436 (M-1-15-18-44); 433 (M-1-2x18-44); 418 (M-1-15-2x18-44); 393 (M-1-16-18-44-42); 353 (M-1-30-130); 301 (M-1-212); 285 (M-1-228); 268 (M-1-245); 259 (M-1-254); 247 (M-1-266); 232 (M-1-15-266); 228 (M-1-285); 217 (M-1-30-266); 189 (M-1-18-2x44-248); 149 (M-1-98-266)
GA-D (**19**)[a]		
GA-LM2 (**33**)[b]		513 (M-1); 495 (M-1-18); 469 (M-1-44); 451 (M-1-18-44); 265 (M-1-248); 247 (M-1-266)
GenA-B (**219**)[a]		513 (M-1); 495 (M-1-18); 480 (M-1-15-18); 452 (M-1-15-16-30); 451 (M-1-18-44); 437 (M-1-44-32); 433 (M-1-2x18-44); 407 (M-1-106); 331 (M-1-30-152); 315 (M-1-16-30-152); 303 (M-1-210); 287 (M-1-16-210); 263 (M-1-250); 249 (M-1-264); 241 (M-1-272)
283[a]		513 (M-1); 469 (M-1-44); 451 (M-1-18-44); 436 (M-1-15-18-44); 378 (M-1-15-120); 319 (M-1-194); 303 (M-1-210); 265 (M-1-248); 247 (M-1-266); 233 (M-1-280); 191 (M-1-322); 159 (M-1-354)
287[a]		513 (M-1); 495 (M-1-18); 480 (M-1-15-18); 466 (M-1-15-32); 451 (M-1-18-44); 436 (M-1-15-18-44); 420 (M-1-15-18-60); 409 (M-1-18-44-42); 394 (M-1-15-18-44-42); 331 (M-1-30-152); 317 (M-1-2x18-30-130); 301 (M-1-60-152); 285 (M-1-2x18-30-32-130)
GA-B (**8**)[a]	516	515 (M-1); 497 (M-1-18); 453 (M-1-18-44); 450 (M-1-15-18-32); 409 (M-1-18-88); 393 (M-1-18-44-60); 287 (M-1-228); 249 (M-1-266); 212 (M-1-303); 205 (M-1-310); 189 (M-1-326)
GA-Df (**20**)[b]		515 (M-1); 497 (M-1-18); 453 (M-1-18-44); 265 (M-1-250); 249 (M-1-266)
GA-ε (**37**)[b]		515 (M-1); 497 (M-1-18); 471 (M-1-44); 453 (M-1-18-44); 265 (M-1-250); 249 (M-1-266)

GA	MW	Fragmentation
MeGA-D (**227**)[b]	528	527 (M-1); 495 (M-1-32); 451 (M-1-32-44); 279 (M-1-248); 247 (M-1-280)
GA-M (**236**)[a]	530	529 (M-1); 511 (M-1-18); 467 (M-1-18-44); 449 (M-1-2x18-44); 434 (M-1-15-2x18-44); 406 (M-1-15-16-18-30-44); 287 (M-1-30-212); 263 (M-1-266)
12βOH-GA-D (**263**)[a]		
GA-O (**238**)[b]		529 (M-1); 511 (M-1-18); 467 (M-1-18-44); 281 (M-1-248); 247 (M-1-280)
MeGA-B (**15**)[a]		529 (M-1); 497 (M-1-32); 479 (M-1-18-32); 453 (M-1-32-44); 409 (M-1-32-2x44); 329 (M-1-200); 303 (M-1-226); 288 (M-1-15-226); 263 (M-1-250-16); 249 (M-1-280); 195 (M-1-16-32-44-242); 149 (M-1-280-100)
^{t}BuLA-B (**71**)[b]		529 (M-1); 265 (M-1-264); 263 (M-1-266)
GA-G (**23**)[a]	532	531 (M-1); 513 (M-1-18); 498 (M-1-15-18); 495 (M-1-2x18); 469 (M-1-18-44); 454 (M-1-15-18-44); 451 (M-1-2x18-44); 436 (M-1-15-2x18-44); 301 (M-1-16-3x18-30-130); 265 (M-1-266); 203 (M-1-18-44-266)
GA-I (**206**)[a]		531 (M-1); 513 (M-1-18); 495 (M-1-2x18); 483 (M-1-18-30); 469 (M-1-18-44); 453 (M-1-18-60); 451 (M-1-2x18-44); 435 (M-1-2x18-60); 401 (M-1-130); 382 (M-1-15-44-30-60); 303 (M-1-228); 251 (M-1-280); 249 (M-1-282); 215 (M-1-2x18-280)
GA-η (**39**)[b]		531 (M-1); 513 (M-1-18); 487 (M-1-44); 469 (M-1-18-44); 265 (M-1-266)
MeLA-P (**218**)[b]		531 (M-1); 489 (M-1-42); 307 (M-1-224); 223 (M-1-308)
GA-N (**237**)[b]	546	545 (M-1); 527 (M-1-18); 483 (M-1-18-44); 281 (M-1-264); 263 (M-1-282)
286[a]	554	553 (M-1); 511 (M-1-42); 509 (M-1-44); 494 (M-1-15-44); 467 (M-1-42-44); 449 (M-1-18-42-44); 301 (M-1-252); 263 (M-1-290)

GA	MW	Fragmentation
12β-OAc-GenA-D (**224**)[a]	570	569 (M-1); 551 (M-1-18); 536 (M-1-15-18); 492 (M-1-15-18-44); 465 (M-1-18-44-42); 447 (M-1-2x18-44-42); 414 (M-1-155); 301 (M-1-16-42-210); 288 (M-1-18-263); 263 (M-1-306); 233 (M-1-42-30-264)
GenA-K (**223**)[a]	572	571 (M-1); 553 (M-1-18); 538 (M-1-15-18); 511 (M-1-18-42); 494 (M-1-15-18-44); 476 (M-1-15-2x18-44); 467 (M-1-18-44-42); 434 (M-1-15-2x18-44-42); 419 (M-1-2x18-30-44-42); 405 (M-1-18-44-42-62); 392 (M-1-15-18-44-42-60); 377 (M-1-18-44-42-30-60); 361 (M-1-2x18-16-42-116); 323 (M-1-42-30-60-116); 314 (M-1-15-16-30-42-154); 313 (M-1-42-30-32-154); 303 (M-1-16-154-98); 290 (M-1-15-42-70-154); 289 (M-1-30-154-98); 265 (M-1-306); 231 (M-1-18-16-306); 198 (M-1-2x18-15-16-306)
BuGA-B (**14**)[b]		571 (M-1); 497 (M-1-74); 453 (M-1-74-44); 385 (M-1-74-44-68); 321 (M-1-250); 249 (M-1-322)
GA-K (**26**)[a]	574	573 (M-1); 555 (M-1-18); 511 (M-1-18-44); 496 (M-1-15-18-44); 469 (M-1-18-44-42); 451 (M-1-2x18-44-42); 407 (M-1-18-44-42-30-32); 341 (M-1-42-60-130); 329 (M-1-16-42-30-156); 302 (M-1-15-156-100); 289 (M-1-42-2x30-182); 265 (M-1-308); 235 (M-1-30-308); 185 (M-1-18-30-32-308)
MeGA-K (**231**)[a]	588	569 (M-18); 555 (M-1-32); 527 (M-1-18-42); 513 (M-1-42-32); 496 (M-1-15-32-44); 469 (M-1-32-44-42); 451 (M-1-18-32-44-42); 405 (M-1-16-18-30-32-44-42); 303 (M-1-2x18-30-2x32-44-42-68); 302 (M-1-15-16-2x18-2x32-44-42-68); 290 (M-1-15-2x18-2x30-32-44-42-68); 265 (M-1-42-280)

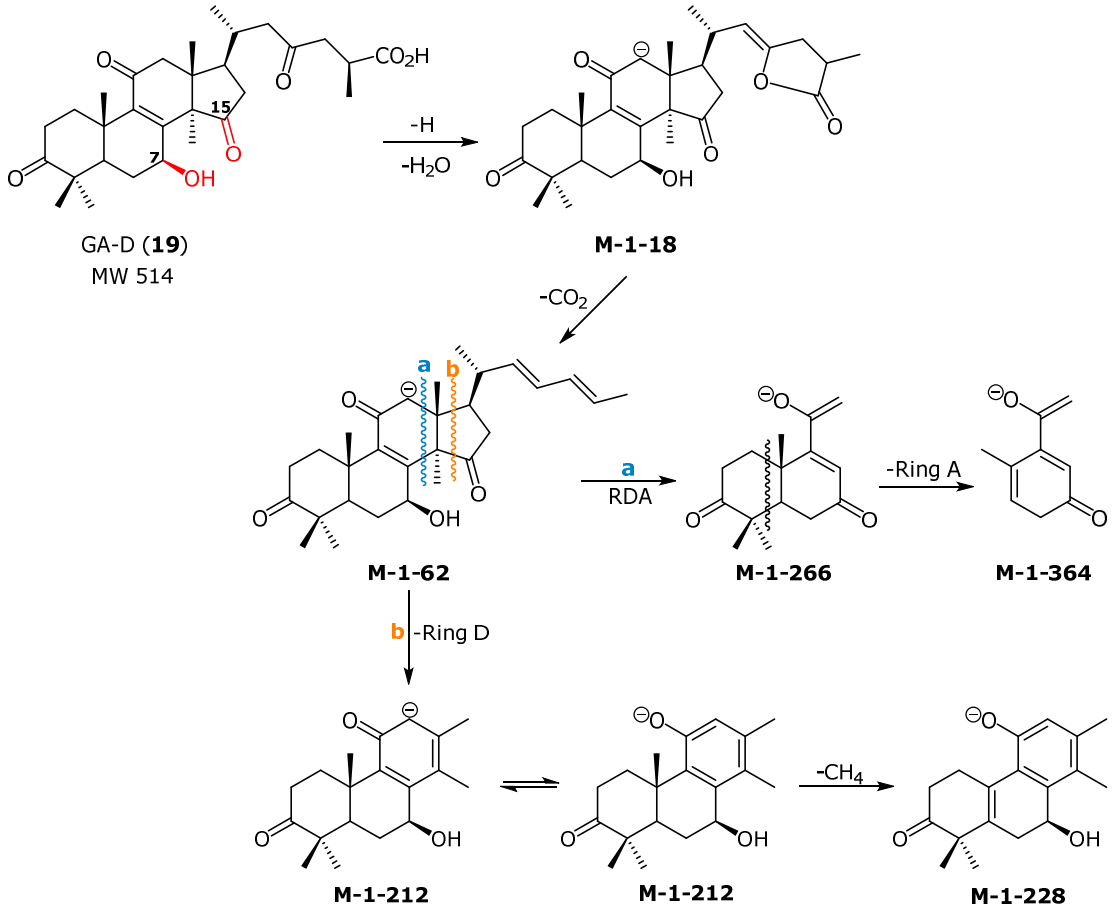
Table A4-2 Fragmentation of GA with C-7 hydroxyl and C-15 carbonyl. **a** Observed fragmentation[142]; **b** predicted fragmentation.

Cleavage of ring D in GA

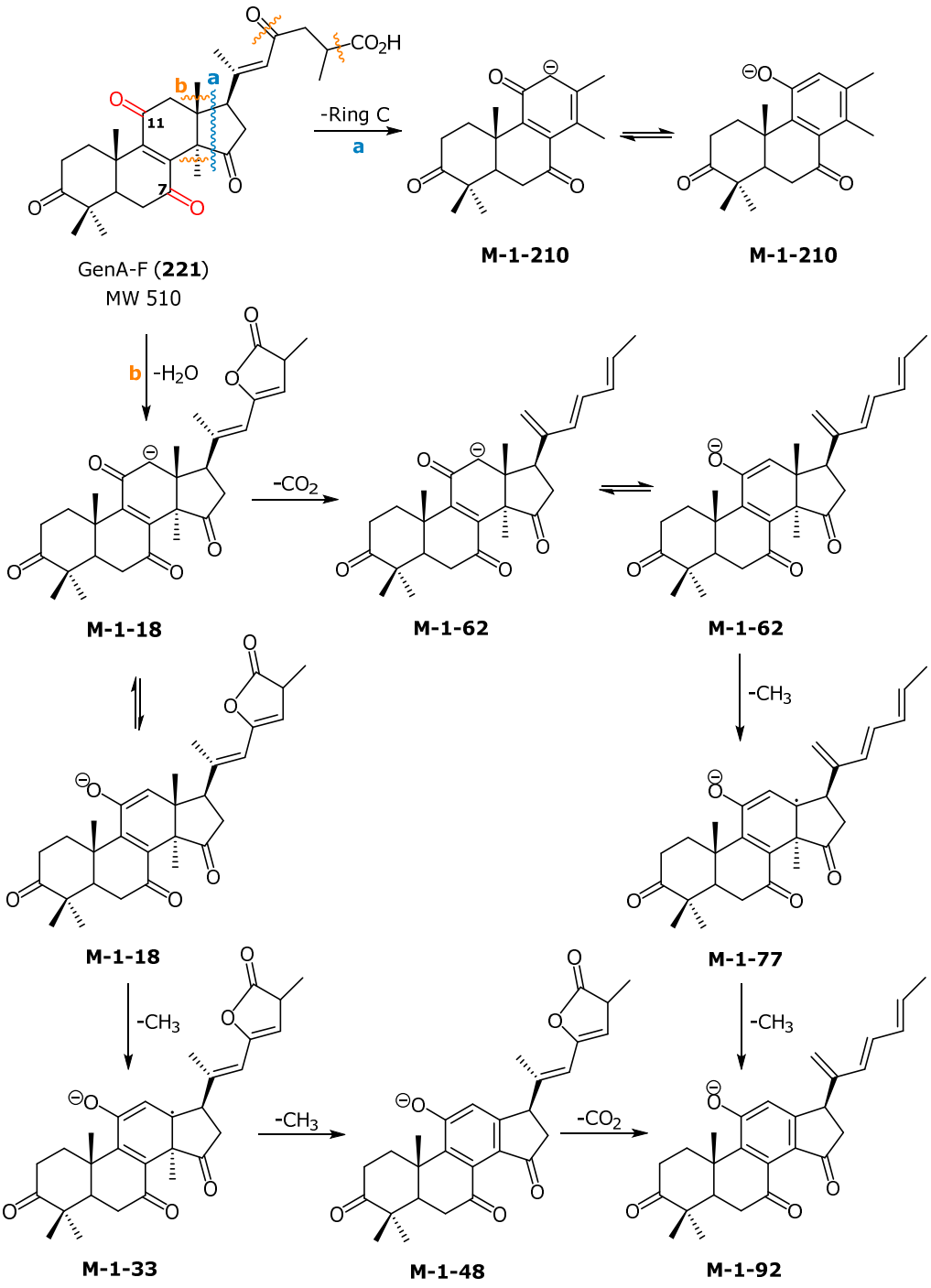
Ring D cleavage is observed in most of the GA. It could be the dominant pathway in GA with 11-oxo-groups. However, it could become the subordinate pathway because of the cleavage of other rings. As an example, fragmentation of GA-D (**19**) is depicted in Scheme A4-4. After water and carbon dioxide loss, ring C (route a) or ring D (route b) could be fragmented.

Loss of the methyl group

Although most of the ions formed follow the even-electron rule, the radical ionic fragment is also observed in the negative ion mode. This fragmentation is predominantly observed in compounds with 7,11-dioxo groups, but also detected in GA with 7,15-dihydroxy-11-oxo groups (Scheme A4-5). Table A4-3 shows the observed and predicted fragmentation of these type of GA.



Scheme A4-4 Fragmentation of GA-D (**19**). **a** Ring C cleavage; **b** ring D cleavage.



Scheme A4-5 Loss of methyl radical in 7,11-dioxo GA.

Fragmentation of the side chain

Depending on the type of side chain (Figure A4-1), four different classes of fragmentation have been observed.

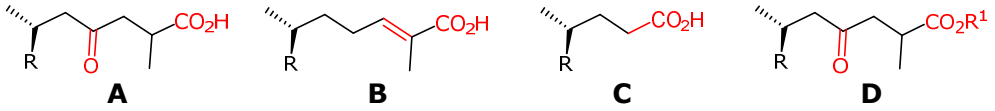


Figure A4-1 Types of side chains. **A** γ-keto acid; **B** α,β-unsaturated acid; **C** saturated acid; **D** γ-keto ester.

GA with side chain A sequentially lose a molecule of water (Δm=18) followed by carbon dioxide (Δm=44). Type B side chain losses carbon dioxide directly from the precursor ion. Type C side chain can lose either carbon dioxide or acetic acid (Δm=60). Type D follows a similar fragmentation as type A, but instead of water the corresponding alcohol is released (Δm=32, R^1=Me; Δm=46, R^1=Et; Δm=74, R^1=Bu) (Scheme A4-6).

GA	MW	Fragmentation
LA-F (**281**)[a]	456	455 (M-1); 437 (M-1-18); 425 (M-1-30); 419 (M-1-2x18); 411 (M-1-44); 395 (M-1-60); 393 (M-1-18-44); 383 (M-1-28-44); 380 (M-1-15-60); 377 (M-1-18-60); 339 (M-1-16-100); 301 (M-1-2x18-16-102); 247 (M-1-2x18-16-156); 245 (M-1-3x18-156); 209 (M-1-18-30-98-100); 207 (M-1-18-30-98-102); 163 (M-1-2x18-30-98-128); 149 (M-1-2x18-16-98-156)
279[a]	458	457 (M-1); 439 (M-1-18); 421 (M-1-2x18); 413 (M-1-44); 397 (M-1-60); 395 (M-1-18-44); 385 (M-1-28-44); 383 (M-1-30-44); 382 (M-1-15-60); 379 (M-1-18-60); 338 (M-1-15-30-74); 303 (M-1-3x18-100); 287 (M-1-2x18-32-102); 249 (M-1-2x18-16-156); 163 (M-1-2x18-30-100-128)
280[a]	460	459 (M-1); 441 (M-1-18); 423 (M-1-2x18); 415 (M-1-44); 397 (M-1-18-44); 300 (M-1-15-16-128); 299 (M-1-32-128); 285 (M-1-16-158); 269 (M-1-32-158); 187 (M-1-16-98-158)
LA-M (**277**)[a]	462	461 (M-1); 443 (M-1-18); 401 (M-1-60); 301 (M-1-60-100); 287 (M-1-30-44-100); 267 (M-1-18-30-44-102)
MeLA-Q (**211**)[b]	474	473 (M-1); 455 (M-1-18); 439 (M-1-18-16); 437 (M-1-2x18); 342 (M-1-15-116); 327 (M-1-30-116); 324 (M-1-15-18-116)

GA	MW	Fragmentation
276[a]	478	477 (M-1); 430 (M-1-15-18-14); 411 (M-1-2x18-30); 367 (M-1-2x18-14-60); 350 (M-1-15-16-2x18-60); 303 (M-1-30-44-100); 288 (M-1-15-30-44-100); 273 (M-1-18-14-44-28-100); 257 (M-1-18-14-16-44-28-100)
MeLA-L (**210**)[b]	488	487 (M-1); 469 (M-1-18); 451 (M-1-2x18); 442 (M-1-15-30); 439 (M-1-18-30); 341 (M-1-30-116); 338 (M-1-18-15-116); 311 (M-1-2x30-116)
GenA-F (**221**)[a]	510	509 (M-1); 491 (M-1-18); 476 (M-1-15-18); 465 (M-1-44); 461 (M-1-18-30); 447 (M-1-18-44); 432 (M-1-15-18-44); 417 (M-1-18-44-30); 406 (M-1-15-16-44-28); 403 (M-1-32-44-30); 390 (M-1-18-15-44-42); 389 (M-1-15-16-44-42); 361 (M-1-32-116); 321 (M-1-32-156); 299 (M-1-210); 277 (M-1-18-98-116); 247 (M-1-18-30-98-116); 236 (M-1-18-15-30-210); 200 (M-1-15-14-98-14)
GA-E (**21**) / GNPA-A (**31**)[a]	512	511 (M-1); 493 (M-1-18); 449 (M-1-18-44); 434 (M-1-15-18-44); 419 (M-1-18-44-30); 401 (M-1-2x18-44-30); 378 (M-1-15-18-14-86); 323 (M-1-30-158); 285 (M-1-14-212)
GenA-G (**271**)[a]		511 (M-1); 493 (M-1-18); 478 (M-1-15-18); 463 (M-1-18-30); 449 (M-1-18-44); 435 (M-1-32-44); 421 (M-1-16-44-30); 301 (M-1-28-182); 285 (M-1-14-212)
GenA-H (**222**)[a]		511 (M-1); 493 (M-1-18); 463 (M-1-18-30); 449 (M-1-18-44); 434 (M-1-15-18-44); 403 (M-1-18-30-16-44); 377 (M-1-18-30-44-42); 301 (M-1-210); 247 (M-1-264); 147 (M-1-100-264)
3-Oxo-GA-ζ (**41**)		511 (M-1); 493 (M-1-18); 467 (M-1-44); 463 (M-1-18-30); 450 (M-1-16-15-30); 449 (M-1-18-44); 434 (M-1-18-15-44)

GA	MW	Fragmentation
LA-D (**278**)[a]	514	513 (M-1-); 471 (M-1-42); 453 (M-1-16-44); 441 (M-1-30-42); 435 (M-1-18-60); 394 (M-1-18-15-60-42); 349 (M-1-18-44-42-60); 299 (M-1-16-42-156); 287 (M-1-42-28-156); 275 (M-1-18-16-2x30-42-102); 257 (M-1-42-30-28-156); 195 (M-1-16-2x30-98-102)
GA-AM$_1$ (**12**)[a]		513 (M-1); 495 (M-1-18); 451 (M-1-18-44); 437 (M-1-32-44); 436 (M-1-18-15-44); 249 (M-1-18-16-100-130)
GA-J (**234**)[a]		513 (M-1); 495 (M-1-18); 451 (M-1-18-44); 436 (M-1-15-18-44); 421 (M-1-18-44-30); 377 (M-1-18-30-2x44); 309 (M-1-16-30-158)
GA-ζ (**38**)[b]		513 (M-1); 495 (M-1-18); 477 (M-1-2x18); 469 (M-1-44); 451 (M-1-18-44); 436 (M-1-15-18-44); 418 (M-1-15-2x18-44); 403 (M-1-2x18-30-44)
GenA-A (**213**)[a]		513 (M-1); 495 (M-1-18); 480 (M-1-18-15); 479 (M-1-18-16); 465 (M-1-18-30); 451 (M-1-18-44); 434 (M-1-15-16-18-30); 433 (M-1-2x18-44); 403 (M-1-2x18-30-44); 381 (M-1-116-16); 363 (M-1-18-16-116); 350 (M-1-18-15-14-116); 301 (M-1-212); 193 (M-1-2x18-32-156-98)
LA-E2 (**83**)[a]	516	515 (M-1); 473 (M-1-42); 455 (M-1-60); 443 (M-1-30-42); 411 (M-1-18-44-42); 386 (M-1-15-28-44-42); 369 (M-1-2x30-44-42); 351 (M-1-18-2x30-44-42); 327 (M-1-16-30-42-100); 302 (M-1-15-2x18-2x30-42-60); 274 (M-1-15-2x18-16-30-42-102); 261 (M-1-2x18-14-2x30-42-102); 196 (M-1-15-2x30-42-100-102)
GA-A (**10**)[a]		515 (M-1); 497 (M-1-18); 479 (M-1-2x18); 435 (M-1-2x18-44); 341 (M-1-16-158); 301 (M-1-214); 299 (M-1-216); 285 (M-1-16-214); 233 (M-1-14-268); 195 (M-1-2x18-30-98-156); 173 (M-1-30-98-214); 151 (M-1-98-266)

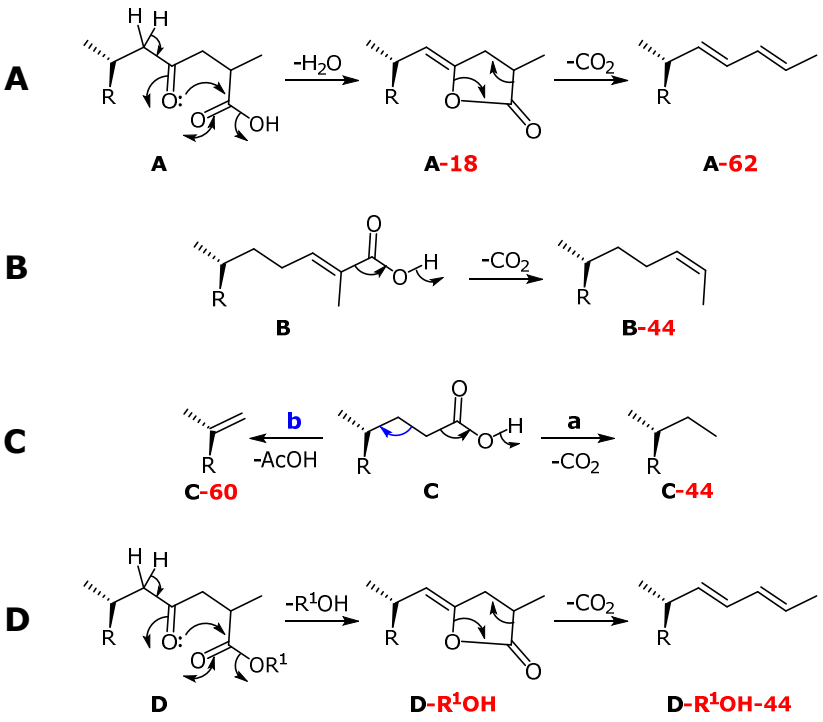
GA	MW	Fragmentation
GA-B9 (**232**)[b]		515 (M-1); 497 (M-1-18); 481 (M-1-18-16); 479 (M-1-2x18); 469 (M-1-16-30); 435 (M-1-2x18-44); 407 (M-1-18-16-30-44); 392 (M-1-2x18-15-28-44)
GA-γ (**35**)[b]		515 (M-1); 497 (M-1-18); 481 (M-1-18-16); 471 (M-1-44); 453 (M-1-18-44); 450 (M-1-15-18-32); 449 (M-1-2x18-30); 435 (M-1-2x18-44)
GA-σ (**36**)[b]		
259[a]		515 (M-1); 497 (M-1-18); 479 (M-1-2x18); 469 (M-1-16-30); 465 (M-1-18-2x16); 449 (M-1-2x18-30); 435 (M-1-2x18-44); 407 (M-1-18-44-30-16); 392 (M-1-2x18-44-28-15); 381 (M-1-18-44-30-42); 285 (M-1-130-100); 255 (M-1-30-130-100)
GenA-C2 (**269**)[a]		515 (M-1); 497 (M-1-18); 481 (M-1-18-16); 453 (M-1-18-44); 435 (M-1-2x18-44); 405 (M-1-2x18-44-30); 383 (M-1-116-16); 345 (M-1-156-14); 287 (M-1-100-114-14); 249 (M-1-18-32-116-100); 193 (M-1-2x18-30-156-100)
GA-C (**16**)[a]	518	517 (M-1); 499 (M-1-18); 481 (M-1-2x18); 463 (M-1-3x18); 455 (M-1-18-44); 437 (M-1-2x18-44); 420 (M-1-3x18-15-28); 407 (M-1-2x18-44-30); 393 (M-1-18-30-32-44); 302 (M-1-18-15-154-28); 287 (M-1-130-100); 273 (M-1-130-100-14)
GA-C2 (**18**)[a]		
12βOH-GA-E (**262**)[a]	528	527 (M-1); 509 (M-1-18); 479 (M-1-18-30); 465 (M-1-18-44); 435 (M-1-18-30-44); 405 (M-1-18-2x30-44)
Elfvingic acid A (**273**)[a]		527 (M-1); 479 (M-1-18-30); 465 (M-1-18-44); 435 (M-1-18-30-44); 421 (M-1-30-32-44); 417 (M-1-2x18-30-44); 317 (M-1-18-16-2x30-116); 301 (M-1-18-2x30-32-116); 299 (M-1-2x18-16-2x30-116)

GA	MW	Fragmentation
284[a]		527 (M-1); 509 (M-1-18); 483 (M-1-44); 467 (M-1-16-44); 465 (M-1-18-44); 453 (M-1-30-44); 436 (M-1-15-32-44); 421 (M-1-30-32-44); 419 (M-1-18-30-44-16); 389 (M-1-18-2x30-44-16); 361 (M-1-18-30-32-44-42); 334 (M-1-15-30-32-116); 317 (M-1-18-2x30-16-116); 305 (M-1-2x18-30-156); 290 (M-1-2x18-15-30-156); 269 (M-1-14-2x30-184)
GA-C6 (**233**)[a]	530	529 (M-1); 511 (M-1-18); 467 (M-1-18-44); 437 (M-1-18-30-44); 419 (M-1-2x18-30-44); 307 (M-1-18-16-30-158); 301 (M-1-16-212); 275 (M-1-2x18-2x30-158); 245 (M-1-18-284); 199 (M-1-18-100-212); 187 (M-1-30-100-212)
GA-θ (**40**)[b]		529 (M-1); 511 (M-1-18); 485 (M-1-44); 467 (M-1-18-44); 455 (M-1-30-44); 437 (M-1-18-30-44); 434 (M-1-15-2x18-44); 407 (M-1-18-2x30-44)
MeGA-A (**13**)[b]		529 (M-1); 511 (M-1-18); 497 (M-1-32); 479 (M-1-18-32); 453 (M-1-32-44); 420 (M-1-18-15-32-44); 405 (M-1-18-30-32-44); 390 (M-1-15-18-30-32-44)
12βOH-GA-C2 (**257**)[a]	534	533 (M-1); 515 (M-1-18); 497 (M-1-2x18); 485 (M-1-18-30); 467 (M-1-2x18-30); 453 (M-1-2x18-44); 423 (M-1-2x18-44-30); 405 (M-1-3x18-44-30); 303 (M-1-3x18-16-30-130); 287 (M-1-3x18-30-32-130)
GA-L (**235**)		533 (M-1); 518 (M-1-18); 497 (M-1-2x18); 467 (M-1-2x18-30); 453 (M-1-2x18-44); 423 (M-1-2x18-30-44); 399 (M-1-18-116)
258[a]	548	547 (M-1); 529 (M-1-18); 511 (M-1-2x18); 485 (M-1-18-44); 470 (M-1-15-18-44); 467 (M-1-2x18-44); 465 (M-1-2x18-16-30); 455 (M-1-18-44-30); 452 (M-1-15-2x18-44); 439 (M-1-18-44-16-30); 419 (M-1-3x18-44-30); 317 (M-1-3x18-2x30-116); 306 (M-1-2x18-15-16-174); 281 (M-1-18-14-2x30-174); 193 (M-1-14-58-282); 165 (M-1-100-282)

GA	MW	Fragmentation
285[a]	554	553 (M-1); 511 (M-1-42); 467 (M-1-15-18-44); 437 (M-1-30-44-42); 423 (M-1-30-14-44-42); 393 (M-1-2x30-14-44-42); 301 (M-1-18-42-192); 235 (M-1-16-2x30-42-2x100)
12β-OAc-GenA-F (**272**)[a]	568	567 (M-1); 549 (M-1-18); 507 (M-1-18-42); 492 (M-1-15-18-42); 474 (M-1-15-2x18-42); 463 (M-1-18-44-42); 435 (M-1-16-116); 419 (M-1-30-116); 343 (M-1-14-210); 328 (M-1-15-14-210); 315 (M-1-42-210); 301 (M-1-14-42-210); 285 (M-1-42-30-210); 243 (M-1-42-14-28-30-210)
12β-OAc-GenA-H (**47**)[a]	570	569 (M-1); 551 (M-1-18); 509 (M-1-18-42); 465 (M-1-18-44-42); 376 (M-1-18-15-14-2x30-42-44); 345 (M-1-2x18-30-44-42-116); 329 (M-1-2x18-16-30-44-42-116); 301 (M-1-16-42-210)
GA-F (**22**)[a]		569 (M-1); 551 (M-1-18); 509 (M-1-18-42); 479 (M-1-18-42-30); 465 (M-1-18-44-42); 450 (M-1-18-15-44-42); 435 (M-1-18-30-44-42); 418 (M-1-15-2x18-14-44-42); 403 (M-1-18-30-32-44-42); 388 (M-1-15-18-30-32-44-42); 349 (M-1-18-30-42-130); 299 (M-1-2x18-30-32-42-130); 257 (M-1-2x18-16-2x30-42-158); 189 (M-1-2x18-16-30-42-158-98)
GA-H (**24**)[a]	572	571 (M-1); 553 (M-1-18); 511 (M-1-18-42); 467 (M-1-18-44-42); 432 (M-1-15-2x18-16-30-42); 421 (M-1-18-16-30-44-42); 377 (M-1-2x18-30-44-2x42); 301 (M-1-2x18-30-32-42-130); 274 (M-1-15-2x18-16-30-42-158)
260[a]		571 (M-1); 529 (M-1-42); 511 (M-1-18-42); 481 (M-1-18-30-42); 449 (M-1-2x18-44-42); 362 (M-1-15-2x18-30-44-2x42); 318 (M-1-2x18-15-30-42-130); 299 (M-1-14-28-30-42-158); 261 (M-1-2x36-14-2x30-42-158); 214 (M-1-15-14-30-42-158-98); 187 (M-1-18-14-16-98-268)

GA	MW	Fragmentation
GA-α (**28**)[b]	574	573 (M-1); 555 (M-1-18); 531 (M-1-42); 513 (M-1-18-42); 511 (M-1-18-44); 496 (M-1-15-18-44); 483 (M-1-18-30-42); 469 (M-1-18-44-42); 341 (M-1-2x30-42-130)
MeGA-F (**229**)[b]	584	583 (M-1); 551 (M-1-32); 541 (M-1-42); 511 (M-1-30-42); 509 (M-1-32-42); 507 (M-1-32-44); 479 (M-1-30-32-42); 465 (M-1-32-42-44)
MeGA-H (**230**)[a]	586	585 (M-1); 567 (M-1-18); 543 (M-1-42); 525 (M-1-18-42); 481 (M-1-32-42-30); 463 (M-1-18-30-32-42); 384 (M-1-15-2x18-2x32-44-42); 329 (M-1-2x18-2x32-44-42-70); 277 (M-1-18-16-2x30-42-172); 186 (M-1-15-16-42-100-226)
EtGA-F (**228**)[a]	598	597 (M-1); 555 (M-1-42); 537 (M-1-18-42); 525 (M-1-42-30); 513 (M-1-14-28-42); 509 (M-1-46-42); 465 (M-1-46-44-42); 449 (M-1-2x30-46-42); 421 (M-1-14-30-46-44-42); 404 (M-1-15-16-30-46-44-42); 355 (M-1-2x18-14-2x30-46-44-42); 299 (M-1-2x18-32-46-44-42-98); 271 (M-1-42-98-186); 257 (M-1-14-42-98-186)
3βOAc-GA-H (**265**)[a]	614	613 (M-1); 595 (M-1-18); 553 (M-1-18-42); 552 (M-1-15-18-28); 523 (M-1-18-30-42); 510 (M-1-18-15-28-42); 509 (M-1-18-44-42); 479 (M-1-18-30-44-42); 465 (M-1-18-130); 449 (M-1-18-16-130); 345 (M-1-2x18-2x30-42-130); 343 (M-1-2x18-30-32-42-130)
261[a]	616	615 (M-1); 597 (M-1-18); 553 (M-1-18-44); 511 (M-1-18-44-42); 509 (M-1-18-16-30-42); 493 (M-1-2x18-44-42); 479 (M-1-18-32-44-42); 467 (M-1-18-130); 449 (M-1-2x18-130)
BuGA-H (**25**)[b]	628	627 (M-1); 585 (M-1-42); 566 (M-1-15-18-28); 555 (M-1-30-42); 553 (M-1-74); 511 (M-1-74-42); 509 (M-1-74-44); 481 (M-1-74-42-30); 467 (M-1-74-44-42)

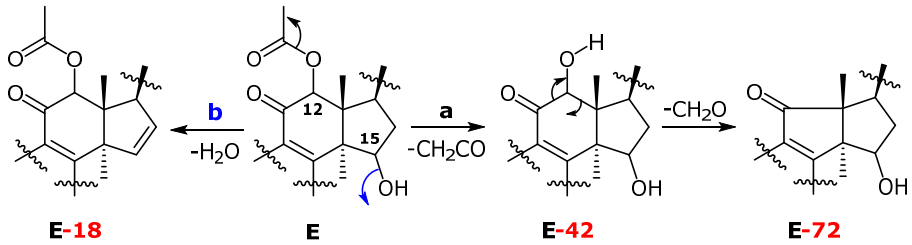
Table A4-3 Fragmentation of GA with 7,11-dioxo and 7,15-dihydroxy-11-oxo groups. a Observed fragmentation[142, 143]; b predicted fragmentation.



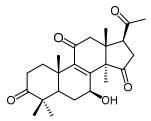
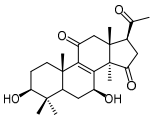
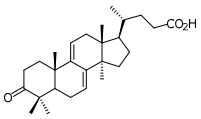
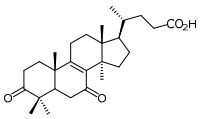
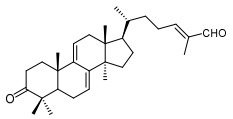
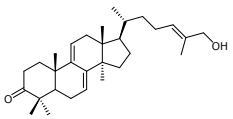
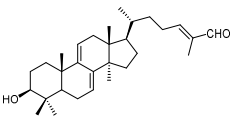
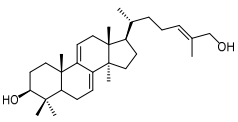
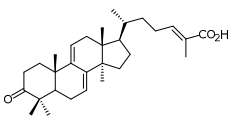
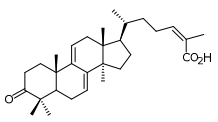
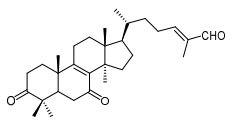
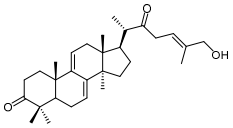
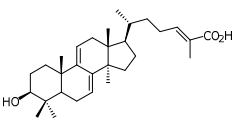
Scheme A4-6 Side chain fragmentation. **A** Type A side chain loses sequentially water and carbon dioxide. **B** Type B side chain loses carbon dioxide. **C** Type C side chain can lose either carbon dioxide (route a) or acetic acid (route b). **D** Type D side chain loses sequentially the corresponding alcohol (R^1=Me, Et, Bu) followed by carbon dioxide.

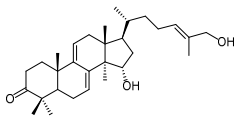
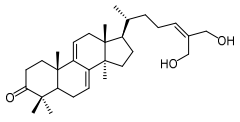
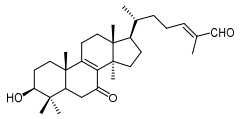
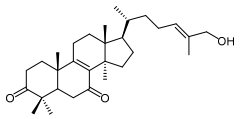
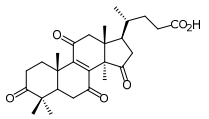
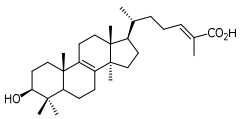
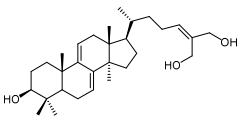
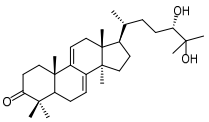
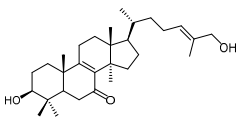
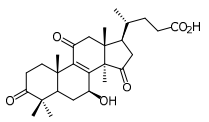
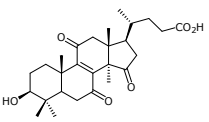
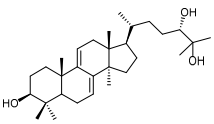
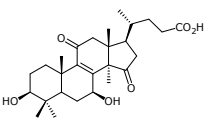
Other fragmentation features

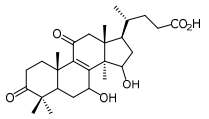
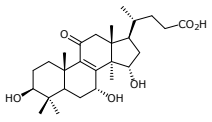
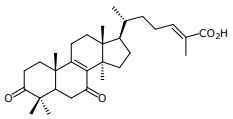
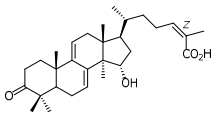
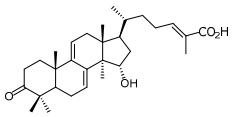
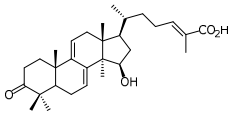
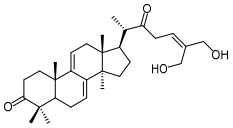
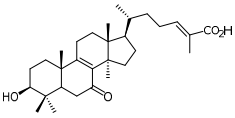
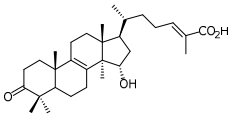
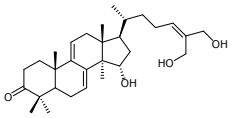
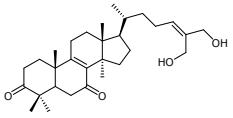
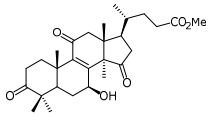
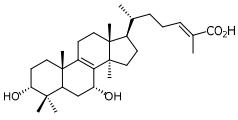
Other fragmentation observed is the loss of CH_2=CO (Δm=42) in acetyloxy derivatives (*i.e.*, formation of **E-42** in Scheme A4-7 (route a)). In the case of C-12 hydroxyl derivatives, the loss a molecule of formaldehyde (Δm=30) has been detected. The elimination of C-15 hydroxyl by loss of water is very easy (Scheme A4-7 (route b)). Finally, the substitution of C-3 or C-12 does not affect the cleavage of the skeleton.[142, 143]

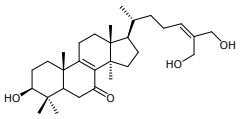
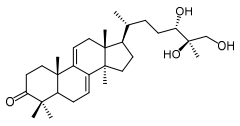
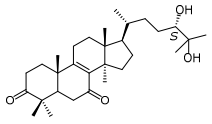
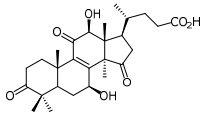
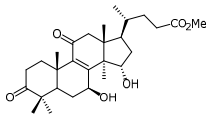
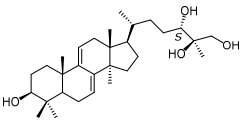
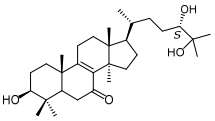
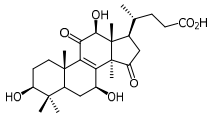
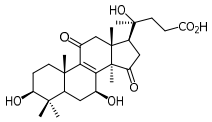
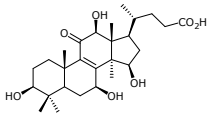
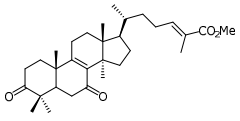
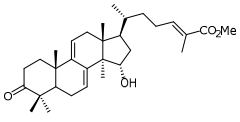
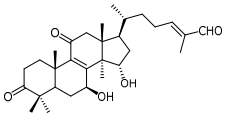


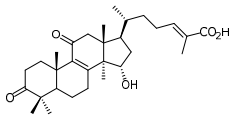
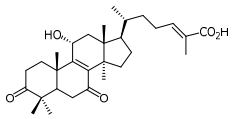
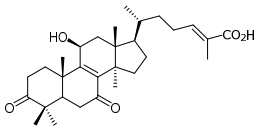
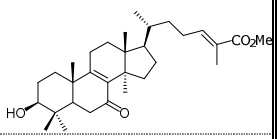
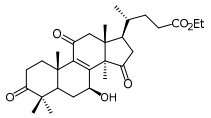
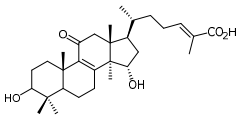
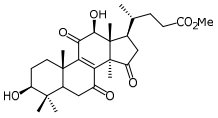
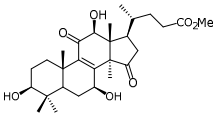
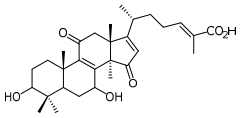
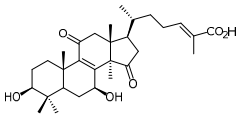
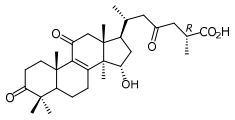
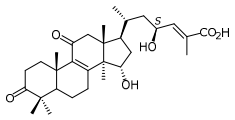
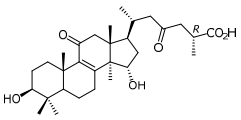
Scheme A4-7 Other fragmentation features. a Loss of -CH_2CO in C-12 acetyloxy compounds that could follow by loss of formaldehyde. b Easy loss of water in C-15 hydroxyl derivatives.

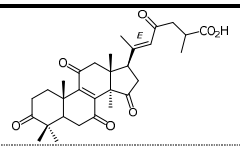
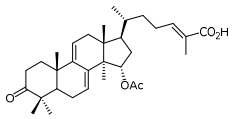
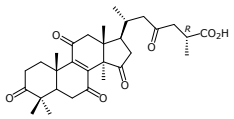
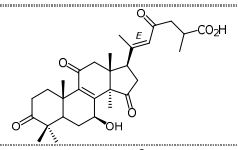
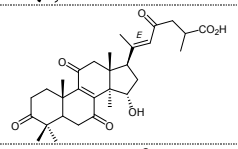
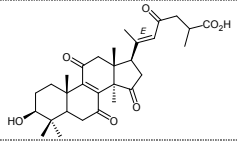
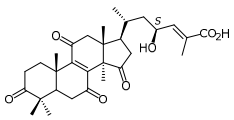
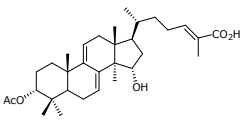
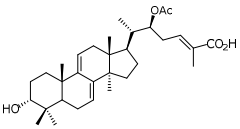
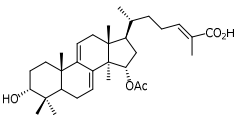
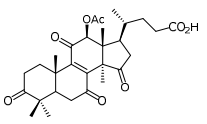
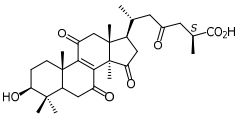
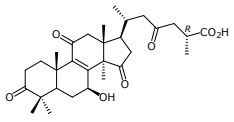
Triterpene	MF	MW	MW+Na	Exact M	Structure
Lucidone-B (**282**)	$C_{24}H_{32}O_5$	400.52	423.22	400.2250	
Lucidone-A (**215**)	$C_{24}H_{34}O_5$	402.53	425.52	402.2406	
LonA (**74**)	$C_{27}H_{40}O_3$	412.61	435.60	412.2977	
LA-DM (**217**)	$C_{27}H_{40}O_4$	428.61	451.60	428.2927	
GAL-A (**275**)	$C_{30}H_{44}O_2$	436.68	459.67	436.3341	
GENONOL (**60**) / GOL-A (**252**)	$C_{30}H_{46}O_2$	438.70	461.69	438.3498	
LAL-A (**256**)	$C_{30}H_{46}O_2$	438.70	461.69	438.3498	
GOL-B (**64**)	$C_{30}H_{48}O_2$	440.71	463.70	440.3654	
GA-S1 (**55**)	$C_{30}H_{44}O_3$	452.68	475.77	452.3290	
GA-S_Z (**56**)	$C_{30}H_{44}O_3$	452.68	475.77	452.3290	
LAL-B (**44**)	$C_{30}H_{44}O_3$	452.68	475.67	452.3290	
22OxoGOL-A (**253**)	$C_{30}H_{44}O_3$	452.68	475.67	452.3290	
GA-Y (**59**)	$C_{30}H_{46}O_3$	454.70	477.69	454.3447	

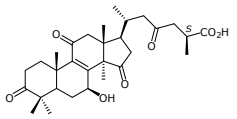
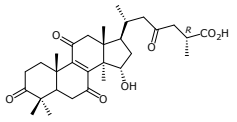
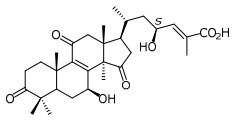
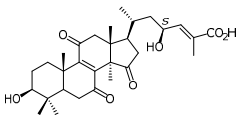
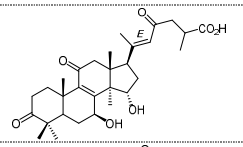
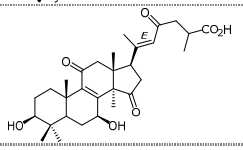
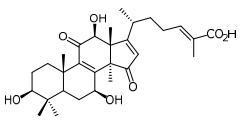
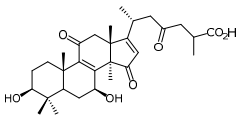
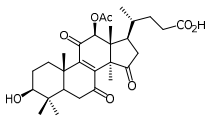
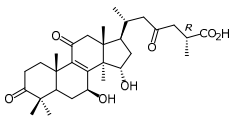
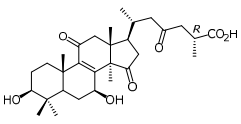
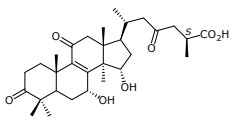
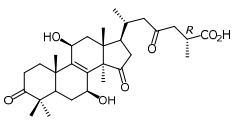
Triterpene	MF	MW	MW+Na	Exact M	Structure
GENON2OL (**61**) / 15α-G2OL-A (**254**)	$C_{30}H_{46}O_3$	454.70	477.69	454.3447	
GIOL-F (**63**)	$C_{30}H_{46}O_3$	454.70	477.69	454.3447	
LAL-C (**45**)	$C_{30}H_{46}O_3$	454.70	477.69	454.3447	
GNO-A (**268**)	$C_{30}H_{46}O_3$	454.70	477.69	454.3447	
LA-F (**281**)	$C_{27}H_{36}O_6$	456.58	479.57	456.2512	
GA-Z (**244**)	$C_{30}H_{48}O_3$	456.71	479.70	456.3603	
G3OL (**205**)	$C_{30}H_{48}O_3$	456.71	479.70	456.3603	
GN2OL (**66**)	$C_{30}H_{48}O_3$	456.71	479.70	456.3603	
L2OL (**43**)	$C_{30}H_{48}O_3$	456.71	479.70	456.3603	
LA-A (**69**)	$C_{27}H_{38}O_6$	458.60	481.59	458.2668	
279	$C_{27}H_{38}O_6$	458.60	481.59	458.2668	
LOL-B (**68**)	$C_{30}H_{50}O_3$	458.73	481.72	458.3760	
LA-N (**72**)	$C_{27}H_{40}O_6$	460.61	483.60	460.2825	

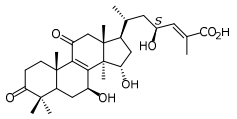
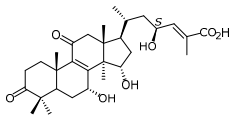
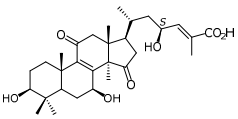
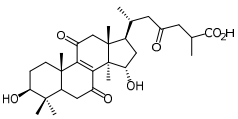
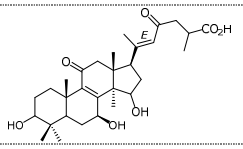
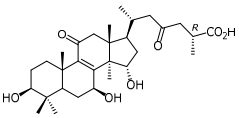
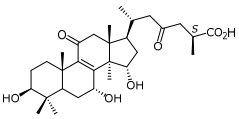
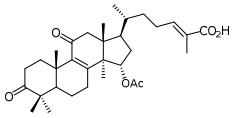
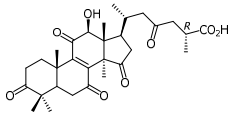
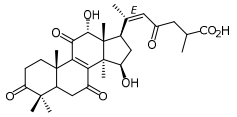
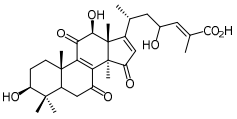
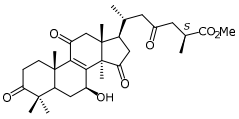
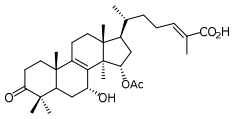
Triterpene	MF	MW	MW+Na	Exact M	Structure
280	$C_{27}H_{40}O_6$	460.61	483.60	460.2825	
LA-M (**277**)	$C_{27}H_{42}O_6$	462.63	485.62	462.2981	
GA-DM (**32**)	$C_{30}H_{44}O_4$	468.68	491.67	468.3240	
15αOH-GA-S$_Z$ (**54**)	$C_{30}H_{44}O_4$	468.68	491.67	468.3240	
GA-TR (**58**)	$C_{30}H_{44}O_4$	468.68	491.67	468.3240	
GA-TR$_1$ (**274**)	$C_{30}H_{44}O_4$	468.68	491.67	468.3240	
22OxoGIOL-F (**255**)	$C_{30}H_{44}O_4$	468.68	491.67	468.3240	
7-OxoGA-Z (**79**)	$C_{30}H_{46}O_4$	470.69	493.68	470.3396	
GA-Ma (**240**)	$C_{30}H_{46}O_4$	470.69	493.68	470.3396	
GIOL-B (**62**)	$C_{30}H_{46}O_4$	470.69	493.68	470.3396	
3-OxoGIOL-E (**82**)	$C_{30}H_{46}O_4$	470.69	493.68	470.3396	
MeLA-A (**207**)	$C_{28}H_{40}O_6$	472.62	495.61	472.2825	
GA-U (**241**)	$C_{30}H_{48}O_4$	472.71	495.70	472.3553	

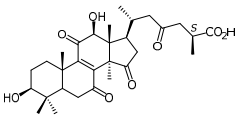
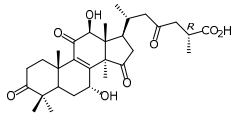
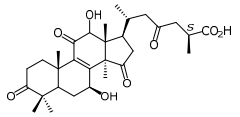
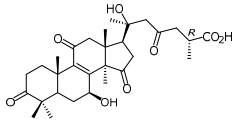
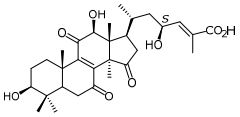
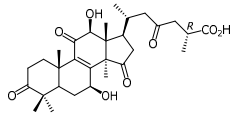
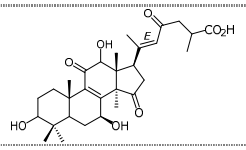
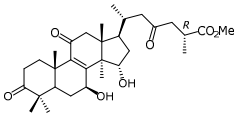
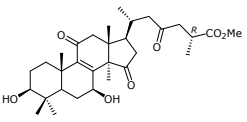
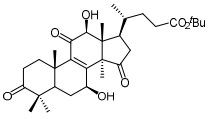
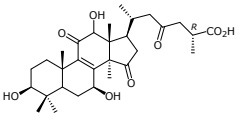
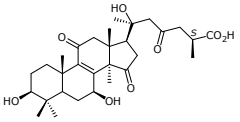
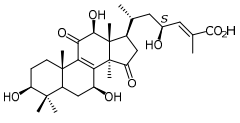
Triterpene	MF	MW	MW+Na	Exact M	Structure
GIOL-E (**48**)	$C_{30}H_{48}O_4$	472.71	495.70	472.3553	
GN3OL (**67**)	$C_{30}H_{48}O_4$	472.71	495.70	472.3553	
LOL-A (**239**)	$C_{30}H_{48}O_4$	472.71	495.70	472.3553	
LA-B (**216**)	$C_{27}H_{38}O_7$	474.59	497.58	474.2618	
MeLA-Q (**211**)	$C_{28}H_{42}O_6$	474.64	497.63	474.2981	
GIOL-A (**65**)	$C_{30}H_{50}O_4$	474.73	497.72	474.3709	
GR3OL-M (**212**)	$C_{30}H_{50}O_4$	474.73	497.72	474.3709	
LA-C (**208**)	$C_{27}H_{40}O_7$	476.61	499.60	476.2774	
20OH-LA-N (**73**)	$C_{27}H_{40}O_7$	476.61	499.60	476.2774	
276	$C_{27}H_{42}O_7$	478.63	501.62	478.2931	
MeGA-DM (**78**)	$C_{31}H_{46}O_4$	482.71	505.70	482.3396	
MeGA-TR (**204**)	$C_{31}H_{46}O_4$	482.71	505.70	482.3396	
LAL-E (**46**)	$C_{30}H_{44}O_5$	484.68	507.67	484.3189	

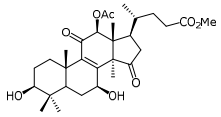
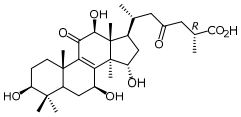
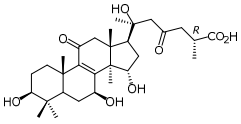
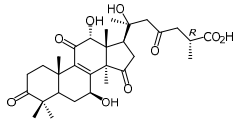
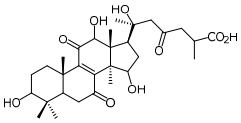
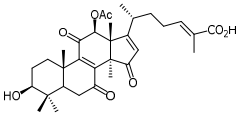
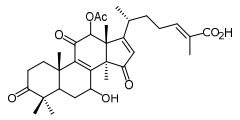
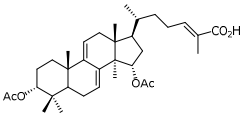
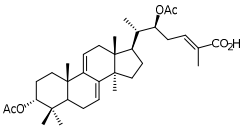
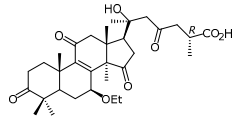
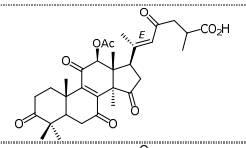
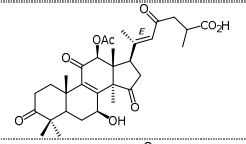
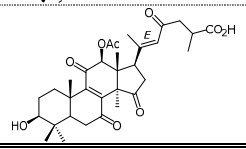
Triterpene	MF	MW	MW+Na	Exact M	Structure
GLA-E (**246**)	$C_{30}H_{44}O_5$	484.68	507.67	484.3189	
11α-OH-GA-DM (**247**)	$C_{30}H_{44}O_5$	484.68	507.67	484.3189	
11β-OH-GA-DM (**248**)	$C_{30}H_{44}O_5$	484.68	507.67	484.3189	
7-Oxo-MeGA-Z (**80**)	$C_{31}H_{48}O_4$	484.72	507.71	484.3553	
EtLA-A (**70**)	$C_{29}H_{42}O_6$	486.65	509.29	486.2981	
266	$C_{30}H_{46}O_5$	486.69	509.68	486.3345	
MeLA-L (**210**)	$C_{28}H_{40}O_7$	488.62	511.61	488.2774	
MeLA-C (**209**)	$C_{28}H_{42}O_7$	490.64	513.63	490.2931	
285	$C_{30}H_{42}O_6$	498.66	521.29	498.2981	
GA-β (**34**)	$C_{30}H_{44}O_6$	500.68	523.67	500.3138	
GLA-A (**29**)	$C_{30}H_{44}O_6$	500.68	523.67	500.3138	
GLA-D (**245**)	$C_{30}H_{44}O_6$	500.68	523.67	500.3138	
GLA-B (**30**)	$C_{30}H_{46}O_6$	502.69	525.32	502.3294	

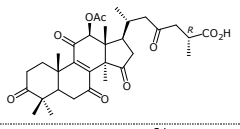
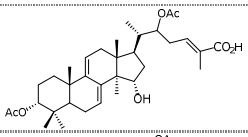
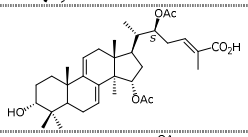
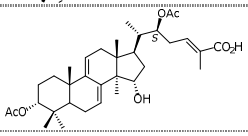
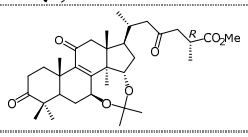
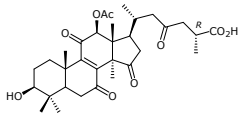
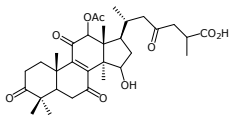
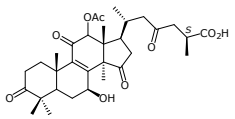
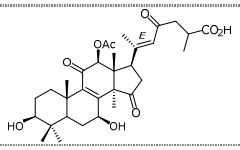
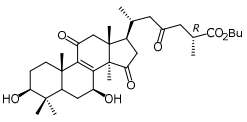
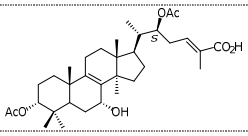
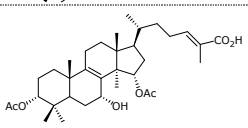
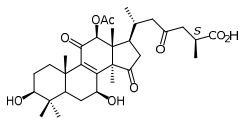
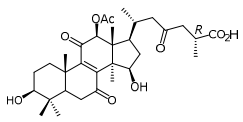
Triterpene	MF	MW	MW+Na	Exact M	Structure
GenA-F (**221**)	$C_{30}H_{38}O_7$	510.63	533.62	510.2618	
GA-T-Q (**57**)	$C_{32}H_{46}O_5$	510.72	533.71	510.3345	
GA-E (**21**); GNPA-A (**31**)	$C_{30}H_{40}O_7$	512.64	535.63	512.2774	
GenA-D (**220**)	$C_{30}H_{40}O_7$	512.64	535.63	512.2774	
GenA-G (**271**)	$C_{30}H_{40}O_7$	512.64	535.63	512.2774	
GenA-H (**222**)	$C_{30}H_{40}O_7$	512.64	535.63	512.2774	
3-Oxo-GA-ζ (**41**)	$C_{30}H_{40}O_7$	512.64	535.63	512.2774	
GA-M_f (**50**)	$C_{32}H_{48}O_5$	512.73	535.72	512.3502	
GA-S (**53**)	$C_{32}H_{48}O_5$	512.73	535.72	512.3502	
GA-X (**251**)	$C_{32}H_{48}O_5$	512.73	535.72	512.3502	
LA-D (**278**)	$C_{29}H_{38}O_8$	514.62	537.61	514.2567	
GA-AM_1 (**12**)	$C_{30}H_{42}O_7$	514.66	537.65	514.2931	
GA-C1 (**17**)	$C_{30}H_{42}O_7$	514.66	537.65	514.2931	

Triterpene	MF	MW	MW+Na	Exact M	Structure
GA-D (**19**)	$C_{30}H_{42}O_7$	514.66	537.65	514.2931	
GA-J (**234**)	$C_{30}H_{42}O_7$	514.66	537.65	514.2931	
GA-LM2 (**33**)	$C_{30}H_{42}O_7$	514.66	537.65	514.2931	
GA-ζ (**38**)	$C_{30}H_{42}O_7$	514.66	537.65	514.2931	
GenA-A (**213**)	$C_{30}H_{42}O_7$	514.66	537.65	514.2931	
GenA-B (**219**)	$C_{30}H_{42}O_7$	514.66	537.65	514.2931	
283	$C_{30}H_{42}O_7$	514.66	537.65	514.2931	
287	$C_{30}H_{42}O_7$	514.66	537.65	514.2931	
LA-E2 (**83**)	$C_{29}H_{40}O_8$	516.63	539.62	516.2723	
GA-A (**10**)	$C_{30}H_{44}O_7$	516.68	539.66	516.3087	
GA-B (**8**)	$C_{30}H_{44}O_7$	516.68	539.66	516.3087	
GA-B9 (**232**)	$C_{30}H_{44}O_7$	516.68	539.66	516.3087	
GA-Df (**20**)	$C_{30}H_{44}O_7$	516.68	539.67	516.3087	

Triterpene	MF	MW	MW+Na	Exact M	Structure
GA-γ (**35**)	$C_{30}H_{44}O_7$	516.68	539.67	516.3087	
GA-δ (**36**)	$C_{30}H_{44}O_7$	516.68	539.67	516.3087	
GA-ε (**37**)	$C_{30}H_{44}O_7$	516.68	539.67	516.3087	
259	$C_{30}H_{44}O_7$	516.68	539.67	516.3087	
GenA**-**C2 (**269**)	$C_{30}H_{44}O_7$	516.68	539.67	516.3087	
GA-C (**16**)	$C_{30}H_{46}O_7$	518.69	541.68	518.3244	
GA-C2 (**18**)	$C_{30}H_{46}O_7$	518.69	541.68	518.3244	
15α-OAc-GLA-E (**267**)	$C_{32}H_{46}O_6$	526.71	549.70	526.3294	
12βOH-GA-E (**262**)	$C_{30}H_{40}O_8$	528.64	551.63	528.2723	
Elfvingic acid A (**273**)	$C_{30}H_{40}O_8$	528.64	551.63	528.2723	
284	$C_{30}H_{40}O_8$	528.64	551.63	528.2723	
MeGA-D (**227**)	$C_{31}H_{44}O_7$	528.69	551.68	528.3087	
GA-V (**242**)	$C_{32}H_{48}O_6$	528.73	551.72	528.3451	

Triterpene	MF	MW	MW+Na	Exact M	Structure
GA-C6 (**233**)	$C_{30}H_{42}O_8$	530.66	553.65	530.2880	
GA-M (**236**)	$C_{30}H_{42}O_8$	530.66	553.65	530.2880	
12βOH-GA-D (**263**)	$C_{30}H_{42}O_8$	530.66	553.65	530.2880	
GA-O (**238**)	$C_{30}H_{42}O_8$	530.66	553.65	530.2880	
GA-θ (**40**)	$C_{30}H_{42}O_8$	530.66	553.65	530.2880	
12βOH-GA-C1 (**225**)	$C_{30}H_{42}O_8$	530.66	553.65	530.2880	
12βOH-GenA-B (**270**)	$C_{30}H_{42}O_8$	530.66	553.65	530.2880	
MeGA-A (**13**)	$C_{31}H_{46}O_7$	530.70	553.69	530.3244	
MeGA-B (**15**)	$C_{31}H_{46}O_7$	530.70	553.69	530.3244	
^{t}BuLA-B (**71**)	$C_{31}H_{46}O_7$	530.70	553.69	530.3244	
GA-G (**23**)	$C_{30}H_{44}O_8$	532.67	555.66	532.3036	
GA-I (**206**)	$C_{30}H_{44}O_8$	532.67	555.66	532.3036	
GA-η (**39**)	$C_{30}H_{44}O_8$	532.67	555.66	532.3036	

Triterpene	MF	MW	MW+Na	Exact M	Structure
MeLA-P (**218**)	$C_{30}H_{44}O_8$	532.67	555.66	532.3036	
12βOH-GA-C_2 (**257**)	$C_{30}H_{46}O_8$	534.69	557.68	534.3193	
GA-L (**235**)	$C_{30}H_{46}O_8$	534.69	557.68	534.3193	
GA-N (**237**)	$C_{30}H_{42}O_9$	546.66	569.65	546.2829	
258	$C_{30}H_{44}O_9$	548.67	571.29	548.2985	
285	$C_{34}H_{42}O_8$	554.68	577.67	554.2880	
286	$C_{34}H_{42}O_8$	554.68	577.67	554.2880	
GA-Me (**49**)	$C_{34}H_{50}O_6$	554.77	577.76	554.3607	
GA-R (**52**)	$C_{34}H_{50}O_6$	554.77	577.76	554.3607	
7-*O*EtGA-O (**27**)	$C_{32}H_{46}O_8$	558.71	581.70	558.3193	
12β-OAc-GenA-F (**272**)	$C_{32}H_{40}O_9$	568.66	591.65	568.2672	
12β-OAc-GenA-D (**224**)	$C_{32}H_{42}O_9$	570.68	593.67	570.2829	
12β-OAc-GenA-H (**47**)	$C_{32}H_{42}O_9$	570.68	593.67	570.2829	

Triterpene	MF	MW	MW+Na	Exact M	Structure
GA-F (**22**)	$C_{32}H_{42}O_9$	570.68	593.67	570.2829	
GA-Mk (**51**)	$C_{34}H_{50}O_7$	570.77	593.77	570.3557	
GA-P (**249**)	$C_{34}H_{50}O_7$	570.77	593.77	570.3557	
GA-Q / GA-P1 (**250**)	$C_{34}H_{50}O_7$	570.77	593.77	570.3557	
MeGA-A acetonide (**75**)	$C_{34}H_{50}O_7$	570.77	593.76	570.3557	
GA-H (**24**)	$C_{32}H_{44}O_9$	572.70	595.69	572.2985	
260	$C_{32}H_{44}O_9$	572.70	595.69	572.2985	
12βOAc-GA-D (**264**)	$C_{32}H_{44}O_9$	572.70	595.69	572.2985	
GenA-K (**223**)	$C_{32}H_{44}O_9$	572.70	595.69	572.2985	
BuGA-B (**14**)	$C_{34}H_{52}O_7$	572.78	595.77	572.3713	
GA-DH (**42**)	$C_{34}H_{52}O_7$	572.78	595.77	572.3713	
GA-W (**243**)	$C_{34}H_{52}O_7$	572.78	595.77	572.3713	
GA-K (**26**)	$C_{32}H_{46}O_9$	574.71	597.70	574.3142	
GA-α (**28**)	$C_{32}H_{46}O_9$	574.71	597.70	574.3142	

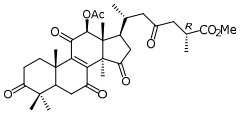
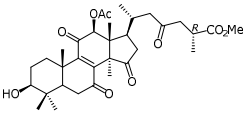
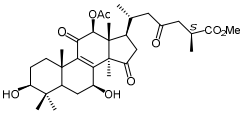
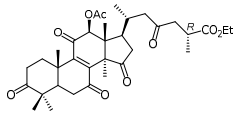
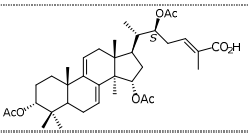
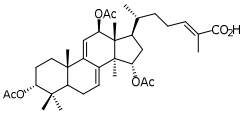
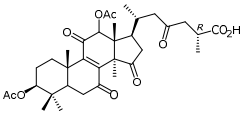
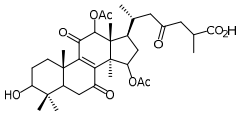
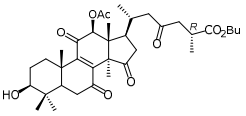
Triterpene	MF	MW	MW+Na	Exact M	Structure
MeGA-F (**229**)	$C_{33}H_{44}O_9$	584.71	607.7	584.2985	
MeGA-H (**230**)	$C_{33}H_{46}O_9$	586.72	609.71	586.3142	
MeGA-K (**231**)	$C_{33}H_{48}O_9$	588.74	611.73	588.3298	
EtGA-F (**228**)	$C_{34}H_{46}O_9$	598.73	621.72	598.3142	
GA-T (**11**)	$C_{36}H_{52}O_8$	612.80	635.79	612.3662	
12βOAc-GA-Me (**81**)	$C_{36}H_{52}O_8$	612.80	635.79	612.3662	
3βOAc-GA-H (**265**)	$C_{34}H_{46}O_{10}$	614.73	637.72	614.3091	
261	$C_{34}H_{48}O_{10}$	616.75	639.31	616.3247	
BuGA-H (**25**)	$C_{36}H_{52}O_9$	628.80	651.79	628.3611	

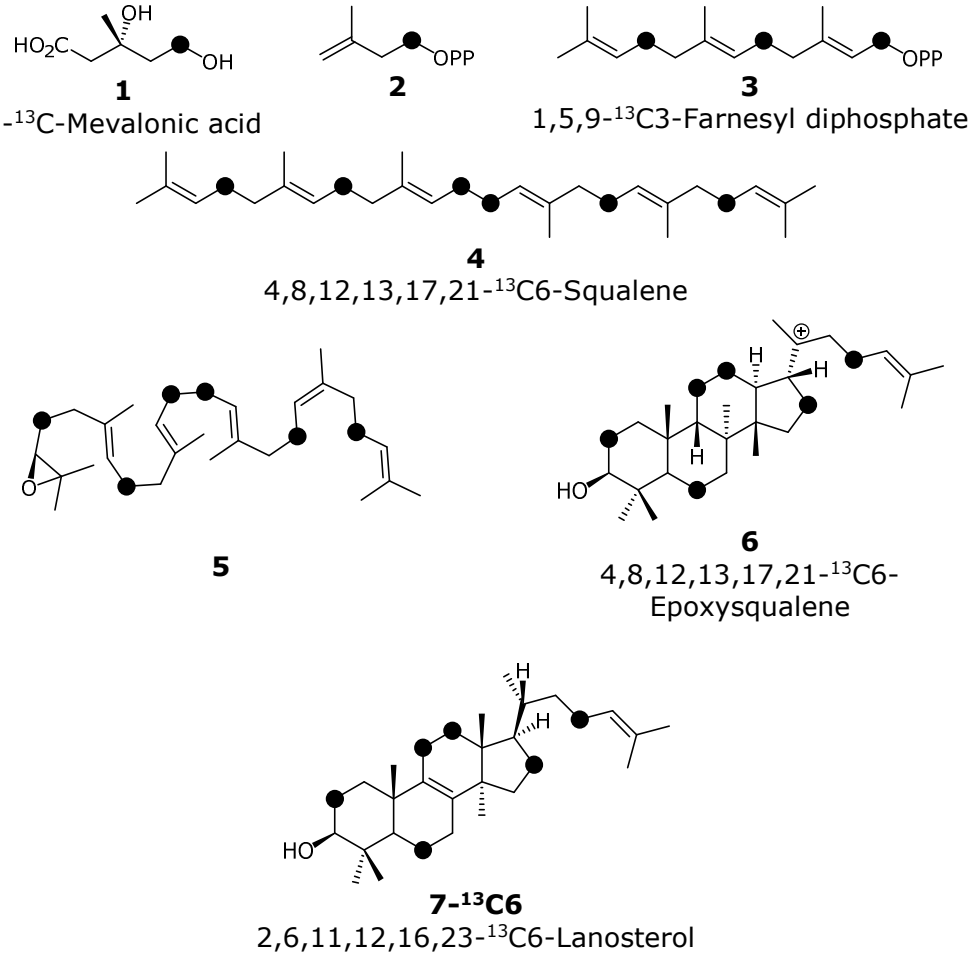
Table A5-1 Triterpenes isolated from GL ordered by molecular weight.[142-143, 159-160] **BuGA** = butyl ganoderdate; **^{t}BuLA** = *tert*-butyl lucidenate; **EtLA** = ethyl lucidenate; **GA** = ganoderic acid; **GAL** = ganoderal; **GenA** = ganoderenic acid; **GENONOL** = ganodermenonol; **GENON2OL** = ganodermenondiol; **GIOL** = ganoderiol; **GLA** = ganolucidic acid; **GN2OL** = ganodermanondiol; **GNO** = ganoderone; **GN3OL** = ganodermanontriol; **GNPA** = ganosporenic acid; **GOL** = ganoderol; **G3OL** = ganodermatriol; **GR3OL** = ganoderitriol; **LA** = lucidenic acid; **LAL** = lucialdehyde; **LonA** = 4,4,14α-trimethyl-5α-chol-7,9(11)-dien-3-oxo-24-oic acid; **LOL** = lucidumol; **L2OL** = lucidadiol; **MeLA** = methyl lucidenate.

Compound numbering index

In this section all the compounds that appear in the Thesis has been ordered numerically by their structure frame. Compounds has been group in Figures. A list of these Figures is given below:

Figure	Compound number
A6-1	**1-7-^{13}C6**
A6-2	**8**, **10**, **12-31**, **192-195**, **206**, **225-238**, **257-265**; **288**
A6-3	**7**, **9**, **32-46**, **78-80**, **87**, **96**, **240-248**, **266-268**
A6-4	**47**, **213**, **219-224**, **269-273**
A6-5	**48**, **82**
A6-6	**11**, **49-64**, **81**, **85**, **183**, **200**, **203-205**, **249-256**, **274-275**
A6-7	**65-68**, **202**
A6-8	**69-73**, **83, 89**, **99**, **106**, **184**, **196-199**, **207-211**, **216-218, 276-281**
A6-9	**74-75**
A6-10	**76-77**
A6-11	**84**, **88**, **97**, **149-150**
A6-12	**86**, **90**
A6-13	**91-93**, **98**, **188**, **212**, **239**
A6-14	**94-95**
A6-15	**100**, **107-110**, **116-117**, **126**, **145-148**, **158**, **174**, **181**, **185**, **189**, **191**
A6-16	**101**, **175-180**
A6-17	**102-104**
A6-18	**105**, **182**
A6-19	**111-115**
A6-20	**118-121**, **201**
A6-21	**122-125**, **131-144**
A6-22	**127-128**
A6-23	**129-130**, **214**
A6-24	**151-157**
A6-25	**159-166**
A6-26	**186-187**
A6-27	**190**
A6-28	**215**; **282**
A6-29	**283-287**

Table A6-1 Relating Figures with compounds.



1
5-^{13}C-Mevalonic acid

2

3
1,5,9-^{13}C3-Farnesyl diphosphate

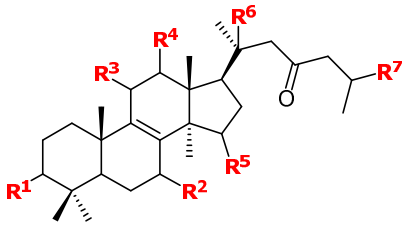
4
4,8,12,13,17,21-^{13}C6-Squalene

5

6
4,8,12,13,17,21-^{13}C6-Epoxysqualene

7-^{13}C6
2,6,11,12,16,23-^{13}C6-Lanosterol

Figure A6-1 Compounds **1**-**7**. Black dots denote ^{13}C.

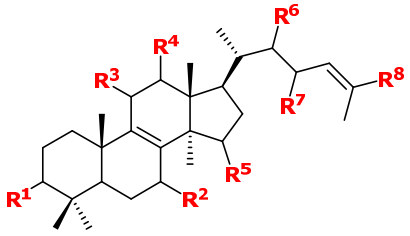


8, 10, 12-31, 192-195, 206, 225-238, 257-265, 288

Nº	Name	R¹	R²	R³	R⁴	R⁵	R⁶	R⁷
8	GA-B	β-OH	β-OH	-C=O	-H	-C=O	-H	*R*-CO_2H
10	GA-A	-C=O	β-OH	-C=O	-H	α-OH	-H	*R*-CO_2H
12	GA-AM_1	β-OH	-C=O	-C=O	-H	-C=O	-H	*S*-CO_2H
13	MeGA-A	-C=O	β-OH	-C=O	-H	α-OH	-H	*R*-CO_2Me
14	BuGA-B	β-OH	β-OH	-C=O	-H	-C=O	-H	*R*-CO_2Bu
15	MeGA-B	β-OH	β-OH	-C=O	-H	-C=O	-H	*R*-CO_2Me
16	GA-C	β-OH	β-OH	-C=O	-H	α-OH	-H	*R*-CO_2H
17	GA-C1	-C=O	β-OH	-C=O	-H	-C=O	-H	*R*-CO_2H
18	GA-C2	β-OH	α-OH	-C=O	-H	α-OH	-H	*S*-CO_2H
19	GA-D	-C=O	β-OH	-C=O	-H	-C=O	-H	*S*-CO_2H
20	GA-Df	-C=O	β-OH	β-OH	-H	-C=O	-H	*R*-CO_2H
21	GA-E	-C=O	-C=O	-C=O	-H	-C=O	-H	*R*-CO_2H
22	GA-F	-C=O	-C=O	-C=O	β-OAc	-C=O	-H	*R*-CO_2H
23	GA-G	β-OH	β-OH	-C=O	-OH	-C=O	-H	*R*-CO_2H
24	GA-H	β-OH	-C=O	-C=O	β-OAc	-C=O	-H	*R*-CO_2H
25	BuGA-H	β-OH	-C=O	-C=O	β-OAc	-C=O	-H	*R*-CO_2Bu
26	GA-K	β-OH	β-OH	-C=O	β-OAc	-C=O	-H	*S*-CO_2H
27	7-OEtGA-O	-C=O	β-OEt	-C=O	-H	-C=O	-OH	*R*-CO_2H
28	GA-α	β-OH	-C=O	-C=O	β-OAc	β-OH	-H	*R*-CO_2H
29	GLA-A	-C=O	-H	-C=O	-H	α-OH	-H	*R*-CO_2H
30	GLA-B	β-OH	-H	-C=O	-H	α-OH	-H	*R*-CO_2H
31	GNPA-A	-C=O	-C=O	-C=O	-C=O	-C=O	-H	*R*-CO_2H
192		β-OAc	-C=O	-C=O	-H	-H	-H	*R*-CO_2H
193		α-OAc	-C=O	-C=O	-H	-H	-H	*R*-CO_2H
194		β-OH	-C=O	-C=O	-H	-H	-H	*R*-CO_2H
195		-C=O	-C=O	-C=O	-H	-H	-H	*R*-CO_2H
206	GA-I	β-OH	β-OH	-C=O	-H	-C=O	-OH	*S*-CO_2H
225	12βOH-GA-C1	-C=O	β-OH	-C=O	β-OH	-C=O	-H	*R*-CO_2H
226	12βOH-GA-E	-C=O	-C=O	-C=O	β-OH	-C=O	-H	*R*-CO_2H
227	MeGA-D	-C=O	β-OH	-C=O	-H	-C=O	-H	*S*-CO_2Me
228	EtGA-F	-C=O	-C=O	-C=O	β-OAc	-C=O	-H	*R*-CO_2Et
229	MeGA-F	-C=O	-C=O	-C=O	β-OAc	-C=O	-H	*R*-CO_2Me
230	MeGA-H	β-OH	-C=O	-C=O	β-OAc	-C=O	-H	*R*-CO_2Me
231	MeGA-K	β-OH	β-OH	-C=O	β-OAc	-C=O	-H	*S*-CO_2Me
232	GA-B9	-C=O	α-OH	-C=O	-H	α-OH	-H	*S*-CO_2H

Nº	Name	R^1	R^2	R^3	R^4	R^5	R^6	R^7
233	GA-C6	β-OH	-C=O	-C=O	β-OH	-C=O	-H	*S*-CO_2H
234	GA-J	-C=O	-C=O	-C=O	-H	α-OH	-H	*R*-CO_2H
235	GA-L	β-OH	β-OH	-C=O	-H	α-OH	-OH	*R*-CO_2H
236	GA-M	-C=O	α-OH	-C=O	β-OH	-C=O	-H	*R*-CO_2H
237	GA-N	-C=O	β-OH	-C=O	α-OH	-C=O	-OH	*R*-CO_2H
238	GA-O	-C=O	β-OH	-C=O	-H	-C=O	-OH	*R*-CO_2H
257	12βOH-GA-C_2	β-OH	β-OH	-C=O	β-OH	α-OH	-H	*R*-CO_2H
258		-OH	-C=O	-C=O	-OH	-OH	-OH	-CO_2H
259		β-OH	-C=O	-C=O	-H	α-OH	-H	-CO_2H
260		-C=O	-C=O	-C=O	-OAc	-OH	-H	-CO_2H
261		-OH	-C=O	-C=O	-OAc	-OAc	-H	-CO_2H
262	12βOH-GA-E	-C=O	-C=O	-C=O	-OH	-C=O	-H	*R*-CO_2H
263	12βOH-GA-D	-C=O	β-OH	-C=O	-OH	-C=O	-H	*S*-CO_2H
264	12βOAc-GA-D	-C=O	β-OH	-C=O	-OAc	-C=O	-H	*S*-CO_2H
265	3βOAc-GA-H	β-OAc	-C=O	-C=O	β-OAc	-C=O	-H	*R*-CO_2H
288	BuGA-F	-C=O	-C=O	-C=O	β-OAc	-C=O	-H	*R*-CO_2Bu

Figure A6-2 Compounds **8**, **10**, **12-31**, **192-195**, **206**, **225-238**, **257-265**, **288**. Bu = butyl; Et = ethyl; Me = methyl; GLA = ganolucidic acid; GNPA = ganosporenic acid; **258** = 3,12,15,20-Tetrahydroxy-7,11,23-trioxolanost-8-en-26-oic acid.

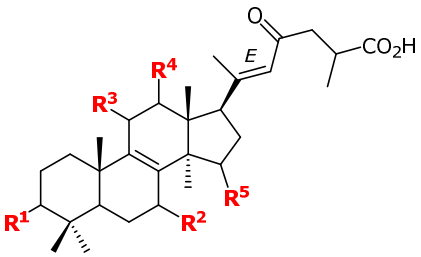


7, **9**, **32-46**, **78-80**, **87**, **96**, **167-173**, **240-248**, **266-268**

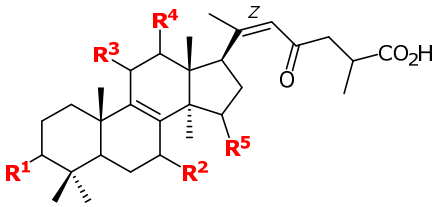
Nº	Name	R^1	R^2	R^3	R^4	R^5	R^6	R^7	R^8
7	Lanosterol	β-OH	-H	-H	-H	-H	-H	-H	-CH_3
9	3-OxoLAN	-C=O	-H	-H	-H	-H	-H	-H	-CH_3
32	GA-DM	-C=O	-C=O	-H	-H	-H	-H	-H	-CO_2H
33	GA-LM2	-C=O	β-OH	-C=O	-H	-C=O	-H	*S*-OH	-CO_2H
34	GA-β	β-OH	β-OH	-C=O	-H	-C=O	-H	-H	-CO_2H
35	GA-γ	-C=O	β-OH	-C=O	-H	α-OH	-H	*S*-OH	-CO_2H
36	GA-δ	-C=O	α-OH	-C=O	-H	α-OH	-H	*S*-OH	-CO_2H
37	GA-ε	β-OH	β-OH	-C=O	-H	-C=O	-H	*S*-OH	-CO_2H
38	GA-ζ	β-OH	-C=O	-C=O	-H	-C=O	-H	*S*-OH	-CO_2H
39	GA-η	β-OH	β-OH	-C=O	β-OH	-C=O	-H	*S*-OH	-CO_2H
40	GA-θ	β-OH	-C=O	-C=O	β-OH	-C=O	-H	*S*-OH	-CO_2H
41	3-Oxo-GA-ζ	-C=O	-C=O	-C=O	-H	-C=O	-H	*S*-OH	-CO_2H
42	GA-DH	α-OAc	α-OH	-H	-H	-H	*S*-OAc	-H	-CO_2H

Nº	Name	R^1	R^2	R^3	R^4	R^5	R^6	R^7	R^8
43	L2OL	β-OH	-C=O	-H	-H	-H	-H	-H	$-CH_2OH$
44	LAL-B	-C=O	-C=O	-H	-H	-H	-H	-H	-CHO
45	LAL-C	β-OH	-C=O	-H	-H	-H	-H	-H	-CHO
46	LAL-E	-C=O	β-OH	-C=O	-H	α-OH	-H	-H	-CHO
78	MeGA-DM	-C=O	-C=O	-H	-H	-H	-H	-H	$-CO_2Me$
79	7-OxoGA-Z	β-OH	-C=O	-H	-H	-H	-H	-H	$-CO_2H$
80	7-Oxo-MeGA-Z	β-OH	-C=O	-H	-H	-H	-H	-H	$-CO_2Me$
87	LAN-Ac	β-OAc	-H	-H	-H	-H	-H	-H	$-CH_3$
96	LAN-MeO	β-OMe	-H	-H	-H	-H	-H	-H	$-CH_3$
167		β-OAc	-OH	-C=O	-H	-H	-H	-H	$-CO_2Et$
168		β-OAc	-C=O	-C=O	-H	-H	-H	-C=O	$-CO_2Et$
169		β-OAc	-C=O	-C=O	-H	-H	-H	-OH	$-CO_2Et$
170		β-OAc	-OH	-C=O	-H	-H	-H	-OH	$-CO_2Et$
171		β-OAc	-C=O	-C=O	-H	-C=O	-H	-C=O	$-CO_2Et$
172		β-OAc	-C=O	-C=O	-H	-OH	-H	-C=O	$-CO_2Et$
173		β-OAc	-C=O	-C=O	-H	-OH	-H	-OH	$-CO_2Et$
240	GA-Ma	-C=O	-H	-H	-H	α-OH	-H	-H	$-CO_2H$
241	GA-U	α-OH	α-OH	-H	-H	-H	-H	-H	$-CO_2H$
242	GA-V	-C=O	α-OH	-H	-H	α-OAc	-H	-H	$-CO_2H$
243	GA-W	α-OAc	α-OH	-H	-H	α-OAc	-H	-H	$-CO_2H$
244	GA-Z	β-OH	-H	-H	-H	-H	-H	-H	$-CO_2H$
245	GLA-D	-C=O	-H	-C=O	-H	α-OH	-H	*S*-OH	$-CO_2H$
246	GLA-E	-C=O	-H	-C=O	-H	α-OH	-H	-H	$-CO_2H$
247	11α-OH-GA-DM	-C=O	-C=O	α-OH	-H	-H	-H	-H	$-CO_2H$
248	11β-OH-GA-DM	-C=O	-C=O	β-OH	-H	-H	-H	-H	$-CO_2H$
266		-OH	-H	-C=O	-H	α-OH	-H	-H	$-CO_2H$
267	15α-OAc-GLA-E	-C=O	-H	-C=O	-H	α-OAc	-H	-H	$-CO_2H$
268	GNO-A	-C=O	-C=O	-H	-H	-H	-H	-H	$-CH_2OH$

Figure A6-3 Compounds **7, 9**, **32**-**46**, **78**-**80**, **87**, **96**, **167**-**173**, **240**-**248**, **266**-**268**. GLA = ganolucidic acid; GNO = ganoderone; LAN = lanosterol; 3-oxo-GA-ζ = 23*S*-hydroxy-3,7,11,15-tetraoxolanost-8,24*E*-dien-26-oic acid; L2OL = lucidadiol; LAL = lucialdehyde; LAN-Ac = lanosterol acetate.



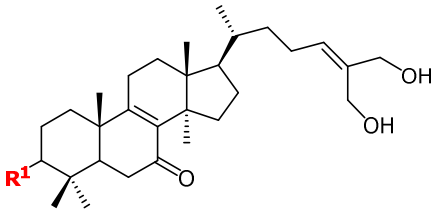
47, **213**, **219**-**224**, **269**-**272**



273

Nº	Name	R^1	R^2	R^3	R^4	R^5	$\Delta^{20,22}$
47	12βOAc-GenA-H	β-OH	-C=O	-C=O	β-OAc	-C=O	*E*
213	GenA-A	-C=O	β-OH	-C=O	-H	α-OH	*E*
219	GenA-B	β-OH	β-OH	-C=O	-H	-C=O	*E*
220	GenA-D	-C=O	β-OH	-C=O	-H	-C=O	*E*
221	GenA-F	-C=O	-C=O	-C=O	-H	-C=O	*E*
222	GenA-H	β-OH	-C=O	-C=O	-H	-C=O	*E*
223	GenA-K	β-OH	β-OH	-C=O	β-OAc	-C=O	*E*
224	12βOAc-GenA-D	-C=O	β-OH	-C=O	β-OAc	-C=O	*E*
269		-OH	β-OH	-C=O	-H	-OH	*E*
270	12βOH-GenA-B	-OH	β-OH	-C=O	-OH	-C=O	*E*
271	GenA-G	-C=O	-C=O	-C=O	-H	α-OH	*E*
272	12βOAc-GenA-F	-C=O	-C=O	-C=O	β-OAc	-C=O	*E*
273	Elfvingic acid A	-C=O	-C=O	-C=O	α-OH	β-OH	*Z*

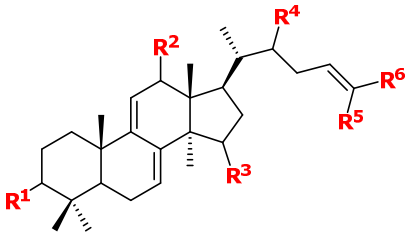
Figure A6-4 Compounds **47**, **213**, **219**-**224**, **269**-**273**. 12β-OAc-GenA-H=12β-acetoxy-3β-hydroxy-7,11,15,23-tetraoxo-lanost-8,20*E*-diene-26-oic acid; GenA = ganoderenic acid.



48, **82**

Nº	Name	R^1
48	GIOL-E	β-OH
82	3-OxoGIOL-E	-C=O

Figure A6-5 Compounds **48**, **82**. GIOL = ganoderiol, 3-OxoGIOL-E = 5α-lanosta-8,24-diene-26,27-dihydroxy-3,7-dione.

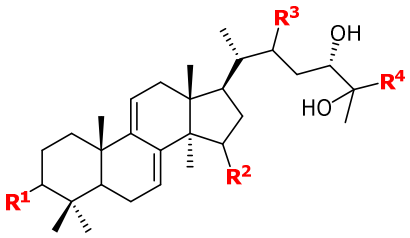


11, 49-64, 81, 85, 183, 200, 203-205, 249-256, 274-275

Nº	Name	R^1	R^2	R^3	R^4	R^5	R^6
11	GA-T	α-OAc	-H	α-OAc	*S*-OAc	$-CH_3$	$-CO_2H$
49	GA-Me	α-OAc	-H	α-OAc	-H	$-CH_3$	$-CO_2H$
50	GA-M_f	α-OAc	-H	α-OH	-H	$-CH_3$	$-CO_2H$
51	GA-Mk	α-OAc	-H	α-OH	-OAc	$-CH_3$	$-CO_2H$
52	GA-R	α-OAc	-H	-H	*S*-OAc	$-CH_3$	$-CO_2H$
53	GA-S	α-OH	-H	-H	*S*-OAc	$-CH_3$	$-CO_2H$
54	15αOH-GA-S_Z	-C=O	-H	α-OH	-H	$-CO_2H$	$-CH_3$
55	GA-S_1	-C=O	-H	-H	-H	$-CH_3$	$-CO_2H$
56	GA-Sz	-C=O	-H	-H	-H	$-CO_2H$	$-CH_3$
57	GA-T-Q	-C=O	-H	α-OAc	-H	$-CH_3$	$-CO_2H$
58	GA-TR	-C=O	-H	α-OH	-H	$-CH_3$	$-CO_2H$
59	GA-Y	β-OH	-H	-H	-H	$-CH_3$	$-CO_2H$
60	GENONOL	-C=O	-H	-H	-H	$-CH_3$	$-CH_2OH$
61	GENON2OL	-C=O	-H	α-OH	-H	$-CH_3$	$-CH_2OH$
62	GIOL-B	-C=O	-H	α-OH	-H	$-CH_2OH$	$-CH_2OH$
63	GIOL-F	-C=O	-H	-H	-H	$-CH_2OH$	$-CH_2OH$
64	GOL-B	β-OH	-H	-H	-H	$-CH_3$	$-CH_2OH$
81	12βOAc-GA-Me	α-OAc	β-OAc	α-OAc	-H	$-CH_3$	$-CO_2H$
85	agnosterol	β-OH	-H	-H	-H	$-CH_3$	$-CH_3$
183		β-OAc	-H	-H	-H	$-CH_3$	$-CO_2Et$
200		α-OAc	-H	-H	-H	$-CH_3$	$-CO_2H$
203		β-OAc	-H	-H	-H	$-CH_3$	$-CH_2OH$
204	MeGA-TR	-C=O	-H	α-OH	-H	$-CH_3$	$-CO_2Me$
205	G3OL	β-OH	-H	-H	-H	$-CH_2OH$	$-CH_2OH$
249	GA-P	α-OH	-H	α-OAc	*S*-OAc	$-CH_3$	$-CO_2H$
250	GA-Q	α-OAc	-H	α-OH	*S*-OAc	$-CH_3$	$-CO_2H$
251	GA-X	α-OH	-H	α-OAc	-H	$-CH_3$	$-CO_2H$
252	GOL-A	-C=O	-H	-H	-H	$-CH_3$	$-CH_2OH$
253	22OxoGOL-A	-C=O	-H	-H	-C=O	$-CH_3$	$-CH_2OH$
254	15α-G2OL-A	-C=O	-H	α-OH	-H	$-CH_3$	$-CH_2OH$
255	22OxoGIOL-F	-C=O	-H	-H	-C=O	$-CH_2OH$	$-CH_2OH$

Nº	Name	R^1	R^2	R^3	R^4	R^5	R^6
256	LAL-A	β-OH	-H	-H	-H	$-CH_3$	-CHO
274	GA-TR_1	-C=O	-H	β-OH	-H	$-CH_3$	$-CO_2H$
275	GAL-A	-C=O	-H	-H	-H	$-CH_3$	-CHO

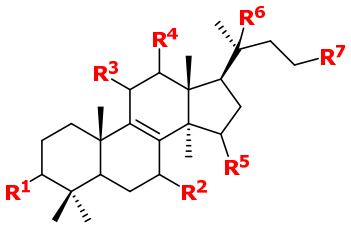
Figure A6-6 Compounds **11**, **49**-**64**, **81**, **85**, **183**, **200**, **203**-**205**, **249**-**256**, **274**-**275**. GAL = ganoderal; GENONOL = ganodermenonol; GENON2OL = ganodermenondiol; 15α,26-dihydroxy-5α-lanosta-7,9,24*E*-triene-26-oic acid; GIOL = ganoderiol; GOL = ganoderol; 12-OAcGA-Me = 3α,12β,15α-triacetoxy-5α-lanosta-7,9(11),24-tiren-26-oic acid; G3OL = ganodermatriol; LAL = lucialdehyde.



65-**68**, **202**

Nº	Name	R^1	R^2	R^3	R^4
65	GIOL-A	β-OH	-H	-H	$-CH_2OH$
66	GN2OL	-C=O	-H	-H	$-CH_3$
67	GN3OL	-C=O	-H	-H	$-CH_2OH$
68	LOL-B	β-OH	-H	-H	$-CH_3$
202		α-OAc	-H	-H	$-CH_3$

Figure A6-7 Compounds **65**-**68**, **202**. GIOL = ganoderiol; GN2OL = ganodermanondiol; GN3OL = ganodermanontriol; LOL = lucidumol.

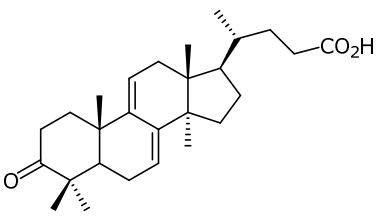


69-**73**, **83**, **89**, **99**, **106**, **184**, **196**-**199**, **207**-**211**, **216**-**218**, **276**-**281**

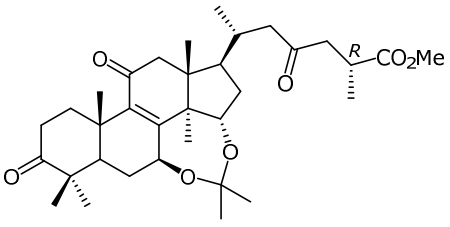
Nº	Name	R^1	R^2	R^3	R^4	R^5	R^6	R^7
69	LA-A	-C=O	β-OH	-C=O	-H	-C=O	-H	$-CO_2H$
70	EtLA-A	-C=O	β-OH	-C=O	-H	-C=O	-H	$-CO_2Et$
71	^{t}BuLA-B	-C=O	β-OH	-C=O	β-OH	-C=O	-H	$-CO_2{}^t$Bu
72	LA-N	β-OH	β-OH	-C=O	-H	-C=O	-H	$-CO_2H$
73	20OH-LA-N	β-OH	β-OH	-C=O	-H	-C=O	-OH	$-CO_2H$
83	LA-E2	β-OH	-C=O	-C=O	β-OAc	-C=O	-H	$-CO_2H$
89		β-OAc	-H	-H	-H	-H	-H	-CHO

Nº	Name	R^1	R^2	R^3	R^4	R^5	R^6	R^7
99		β-OMe	-H	-H	-H	-H	-H	-CHO
106		β-OAc	-H	-H	-H	-H	-H	$-CO_2H$
184		β-OH	-H	-H	-H	-H	-H	$-CO_2H$
196		β-OAc	-C=O	-C=O	-H	-H	-H	$-CO_2H$
197		α-OAc	-C=O	-C=O	-H	-H	-H	$-CO_2H$
198		β-OH	-C=O	-C=O	-H	-H	-H	$-CO_2H$
199		-C=O	-C=O	-C=O	-H	-H	-H	$-CO_2H$
207	MeLA-A	-C=O	β-OH	-C=O	-H	-C=O	-H	$-CO_2Me$
208	LA-C	β-OH	β-OH	-C=O	β-OH	-C=O	-H	$-CO_2H$
209	MeLA-C	β-OH	β-OH	-C=O	β-OH	-C=O	-H	$-CO_2Me$
210	MeLA-L	β-OH	-C=O	-C=O	β-OH	-C=O	-H	$-CO_2Me$
211	MeLA-Q	-C=O	β-OH	-C=O	-H	α-OH	-H	$-CO_2Me$
216	LA-B	-C=O	β-OH	-C=O	β-OH	-C=O	-H	$-CO_2H$
217	LA-DM	-C=O	-C=O	-H	-H	-H	-H	$-CO_2H$
218	MeLA-P	β-OH	β-OH	-C=O	β-OAc	-C=O	-H	$-CO_2Me$
276		β-OH	β-OH	-C=O	β-OH	β-OH	-H	$-CO_2H$
277	LA-M	β-OH	α-OH	-C=O	-H	α-OH	-H	$-CO_2H$
278	LA-D	-C=O	-C=O	-C=O	β-OAc	-C=O	-H	$-CO_2H$
279		β-OH	-C=O	-C=O	-H	-C=O	-H	$-CO_2H$
280		-C=O	-OH	-C=O	-H	-OH	-H	$-CO_2H$
281	LA-F	-C=O	-C=O	-C=O	-H	-C=O	-H	$-CO_2H$

Figure A6-8 Compounds **69**-**73**, **83**, **89**, **99**, **106**, **184, 196-199**, **207**-**211**, **216**-**218**, **276**-**281**. LA = lucidenic acid; Et = ethyl, ^{t}Bu = *tert*-butyl; 20OH-LA = 20-hydroxylucidenic acid.

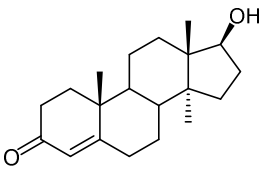


74
LonA

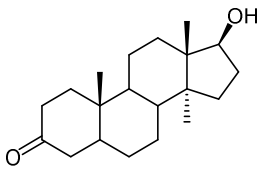


75
MeGA-A acetonide

Figure A6-9 Compounds **74** and **75**. LonA = 4,4,14α-trimethyl-5α-chol-7,9(11)-dien-3-oxo-24-oic acid; Me = methyl.

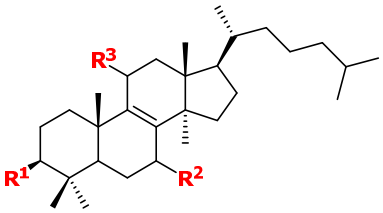


76
Testosterone



77
DHT

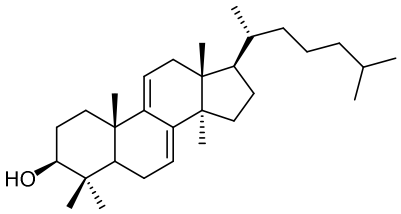
Figure A6-10 Compounds **76** and **77**. DHT = dihydrotestosterene.



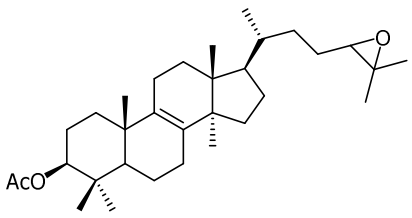
84, **88**, **97**, **149**, **150**

N°	Name	R^1	R^2	R^3
84	DHL	-OH	-H	-H
88	DHL-Ac	-OAc	-H	-H
97	DHL-MeO	-OMe	-H	-H
149		-OAc	-C=O	-C=O
150		-OAc	-O-O*t*Bu	-C=O

Figure A6-11 Compounds **84**, **88**, **97**, **149**-**150**. DHL = dihydrolanosterol; DHL-Ac = dihydrolanosterol acetate; DHL-MeO = dihydrolanosterol methoxide.

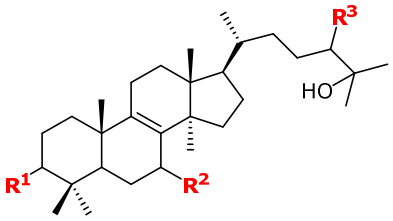


86
Dihydroagnosterol



90

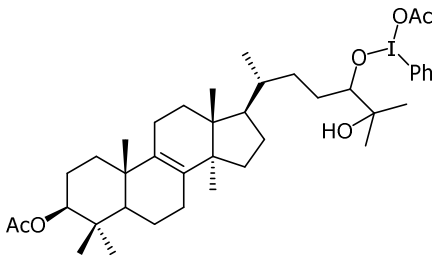
Figure A6-12 Compound **86** and **90**.



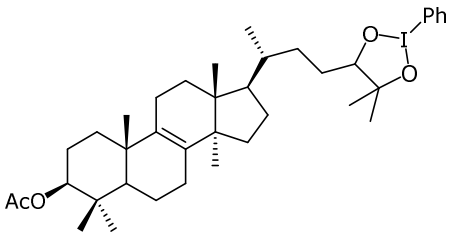
91-**93**, **98**, **188**, **212**, **239**

N°	Name	R^1	R^2	R^3
91		β-OAc	-H	-OH
92		β-OAc	-H	-C=O
93		β-OAc	-H	-Br
98		β-OMe	-H	-OH
188		β-OH	-H	-OH
212	GR3OL-M	β-OH	-C=O	*S*-OH
239	LOL-A	-C=O	-C=O	*S*-OH

Figure A6-13 Compounds **91**-**93**, **98**, **188**, **212**, **239**. GR3OL = ganoderitriol; LOL = lucidumol.

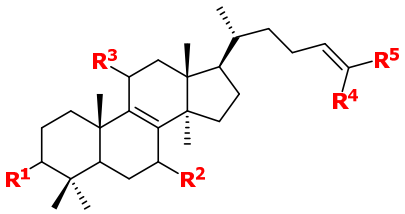


94



95

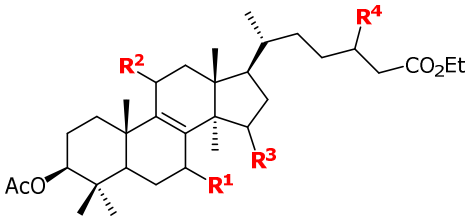
Figure A6-14 Compounds **94** and **95**.



100, **107-110**, **116-117**, **126**, **145-148**, **158**, **174**, **181**, **185**, **189**, **191**

N°	R^1	R^2	R^3	R^4	R^5
100*E*	β-OAc	-H	-H	$-CH_3$	$-CO_2Et$
100Z	β-OAc	-H	-H	$-CO_2Et$	$-CH_3$
107	β-OH	-H	-H	$-CH_3$	$-CO_2H$
108	-C=O	-H	-H	$-CH_3$	$-CO_2H$
109	β-OAc	-H	-H	$-CH_3$	$-CO_2H$
110	α-OAc	-H	-H	$-CH_3$	$-CO_2H$
116	-C=O	-H	-H	$-CH_3$	$-CO_2Et$
117	α-OH	-H	-H	$-CH_3$	$-CO_2Et$
126	α-OAc	-H	-H	$-CH_3$	$-CH_3$
145	β-OAc	-C=O	-C=O	$-CH_3$	$-CO_2Et$
146	β-OH	-C=O	-C=O	$-CH_3$	$-CO_2H$
147	β-OAc	-H	-C=O	$-CH_3$	$-CO_2Et$
148	β-OAc	-O-O^{t}Bu	-C=O	$-CH_3$	$-CO_2Et$
158	β-OAc	-OH	-OH	$-CH_3$	$-CO_2Et$
174	-C=O	-C=O	-C=O	$-CH_3$	$-CO_2H$
181	β-OAc	-OH	-OH	$-CH_3$	$-CO_2Et$
185	β-OH	-H	-H	$-CH_3$	$-CH_2OH$
189	β-OH	-H	-H	$-CH_3$	$-CO_2Me$
191	β-OAc	-C=O	-C=O	$-CH_3$	$-CO_2H$

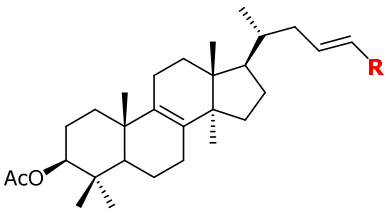
Figure A6-15 Compounds **100**, **107-110**, **116-117**, **126**, **145-148**, **158**, **174**, **181**, **185**, **189**, **191**.



101, **175**-**180**

N°	R^1	R^2	R^3	R^4
101	-H	-H	-H	-OH
175	-C=O	-C=O	-H	-C=O
176	-H	-C=O	-H	-C=O
177	-C=O	-C=O	-C=O	-C=O
178	-C=O	-C=O	-H	-OH
179	-H	-C=O	-H	-OH
180	-O-O^{t}Bu	-C=O	-H	-OH

Figure A6-16 Compounds **101**, **175**-**180**.



102-**104**

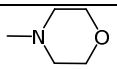
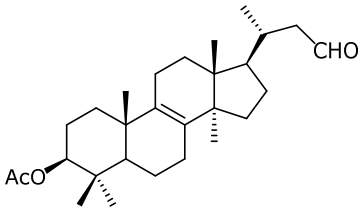
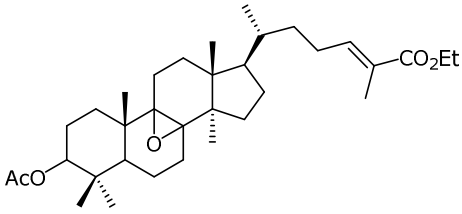
N°	R
102	-N(CH_2Ph)$_2$
103	
104	

Figure A6-17 Enamines **102**-**104**.

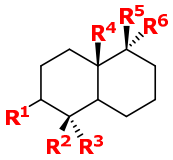


105



182

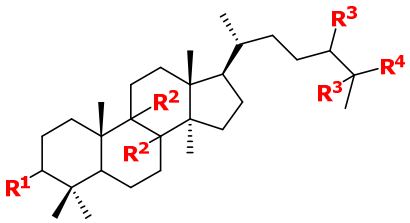
Figure A6-18 Aldehyde **105** and epoxide **182**.



111-115

N°	R^1	R^2	R^3	R^4	R^5-R^6
111	-C=O	$-CH_3$	$-CH_2CH=CH_2$	$-CH_3$	
112	α-OH	$-CH_3$	$-CH_2CH=CH_2$	$-CH_3$	
113	-C=O	-H	-H	-H	-H
114	α-OH	-H	-H	-H	-H
115	β-OH	-H	-H	-H	-H

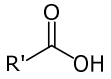
Figure A6-19 Compounds **111**-**115**.



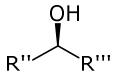
118-121, 201

N°	R^1	R^2	R^3	R^4
118	-OH	-H	-H	$-CH_2OH$
119	-OH	-H	$\Delta^{24, 25}$	$-CO_2Et$
120	-OH	$\Delta^{8, 9}$	-H	$-CO_2Et$
121	-C=O	-H	-H	$-CO_2Et$
201	α-OAc	$\Delta^{8, 9}$	-OH	$-CH_3$

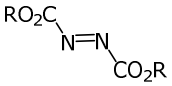
Figure A6-20 Compounds **118**-**121**, **211**.



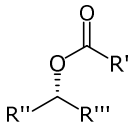
122
Carboxylic acid



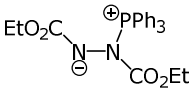
123
2ary Alcohol



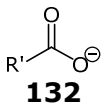
124
DAD
DEAD: R = Et



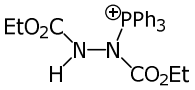
125
Inverted ester



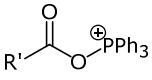
131



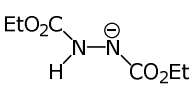
132
Carboxylate



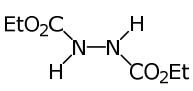
133



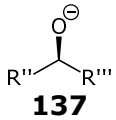
134



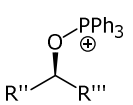
135



136



137
Alcoxide



138

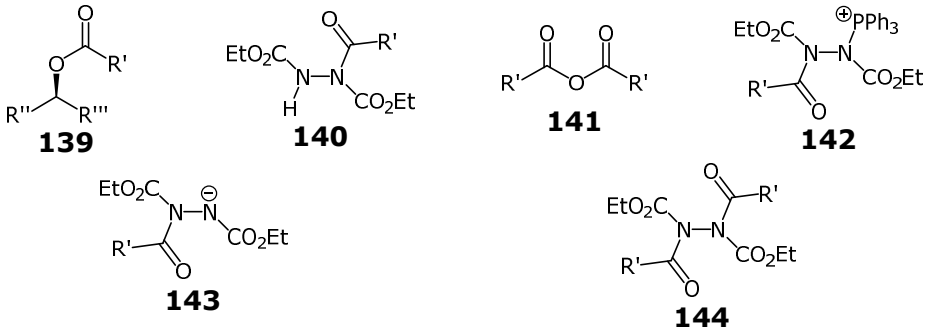
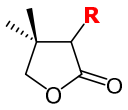
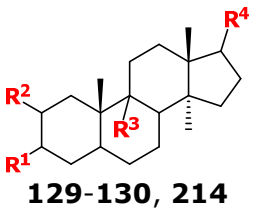


Figure A6-21 Compounds **122**-**125**, **131**-**144**. DAD = Diazodicarboxylate; DEAD = diethylazodicarboxylate.



N°	R
127	β-OH
128	α-OH

Figure A6-22 Compounds **127**-**128**.



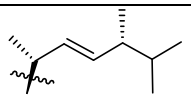
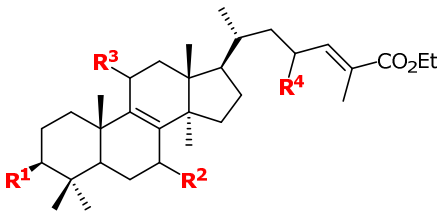
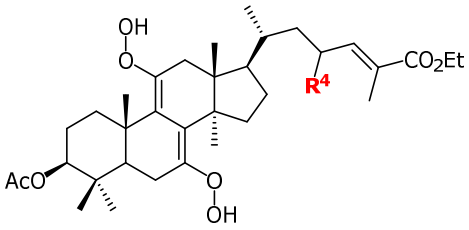
N°	R^1	R^2	R^3	R^4
129	-C=O	-H	-H	β-OH
130	-C=O	-H	-H	α-OPNB
214	α-OH	β-OH	α-OH	

Figure A6-23 Compounds **129**-**130**, **214**. PNB = *para*-Nitrobenzoic acid.



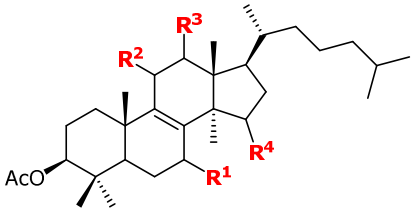
151-155



156-157

N°	R¹	R²	R³	R⁴	MW
151	-OH	-O-OH	-C=O	-H	530
152	-OAc	-O-OH	-H	-H	558
153	-OAc	-O-OH	-C=O	-H	572
154	-OAc	-C=O	-C=O	-O-OH	586
155	-OAc	-C=O	-C=O	-O-O^{t}Bu	642
156	-	-	-	-H	588
157	-	-	-	-O-O^{t}Bu	676

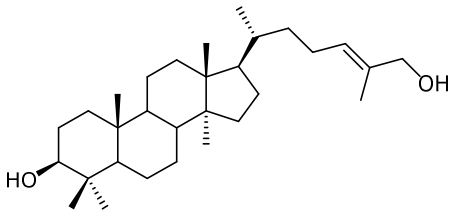
Figure A6-24 Compounds **151**-**157**.



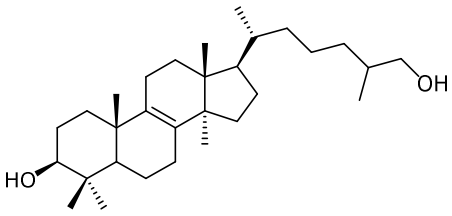
159-166

N°	R¹	R²	R³	R⁴
159	-H	-C=O	-H	-H
160	-OH	-C=O	-H	-H
161	-OH	-OH	-H	-H
162	-C=O	-C=O	-H	-C=O
163	-C=O	-C=O	-H	-OH
164	-OH	-C=O	-H	-OH
165	-C=O	-C=O	-OH	-C=O
166	-C=O	-C=O	-OH	-OH

Figure A6-25 Compounds **159**-**166**.

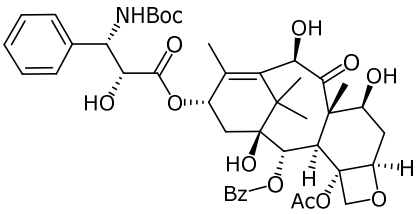


186



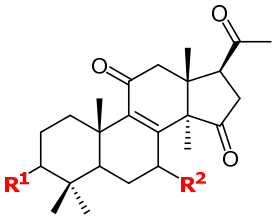
187

Figure A6-26 Compounds **186**-**187**.



190
Taxotere

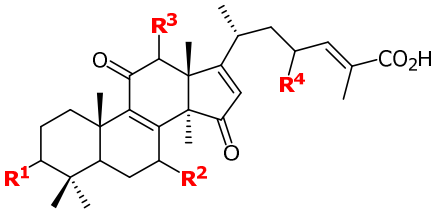
Figure A6-27 Taxotere (**190**).



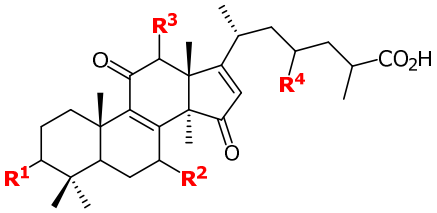
215, **282**

N°	Name	R^1	R^2
215	Lucidone-A	β-OH	β-OH
282	Lucidone-B	-C=O	β-OH

Figure A6-28 Compounds **215** and **282**.



283-**286**



287

N°	R^1	R^2	R^3	R^4
283	β-OH	β-OH	β-OH	-H
284	β-OH	-C=O	β-OH	-OH
285	β-OH	-C=O	β-OAc	-H
286	-C=O	-OH	-OAc	-H
287	-OH	-OH	-H	-C=O

Figure A6-29 Compounds **283**-**287**.